UNIVERSITAT DE BARCELONA

The Iron Regulatory Protein/Iron Responsive Element (IRP/IRE) system: functional studies of new target mRNAs and pathological implications for novel IRE mutations

Sara Luscieti

UNIVERSITAT DE BARCELONA

FACULTAT DE FARMÀCIA I CIÈNCIES DE L'ALIMENTACIÓ

PROGRAMA DE DOCTORAT EN BIOMEDICINA

The Iron Regulatory Protein/Iron Responsive Element (IRP/IRE) system: functional studies of new target mRNAs and pathological implications for novel IRE mutations.

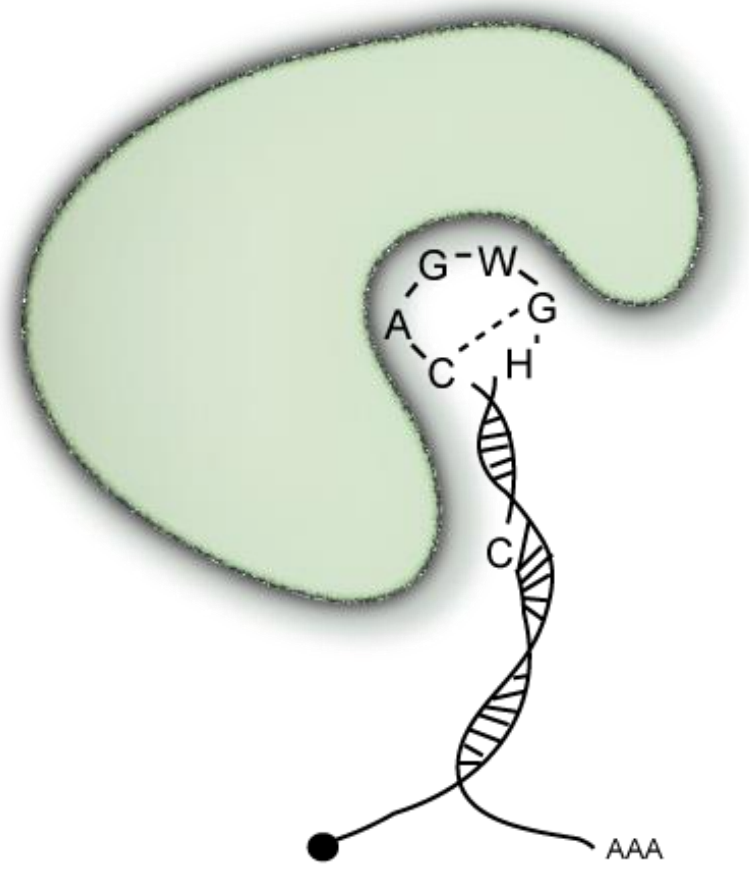

SARA LUSCIETI 2016

UNIVERSITAT DE BARCELONA

FACULTAT DE FARMÀCIA I CIÈNCIES DE L'ALIMENTACIÓ

PROGRAMA DE DOCTORAT EN BIOMEDICINA

The Iron Regulatory Protein/Iron Responsive Element (IRP/IRE) system: functional studies of new target mRNAs and pathological implications for novel IRE mutations.

Memòria presentada per Sara Luscieti per optar al títol de doctor per la

Universitat de Barcelona

Doctoranda: Sara Luscieti

Directora: Mayka Sánchez Fernández

Tutor: Rafael Oliva Virgili

SARA LUSCIETI 2016

SUMMARY

Iron is an essential micronutrient required for many cellular reactions and a tight regulation of its metabolism is therefore crucial for health. Cellular iron homeostasis relies on the coordination of iron uptake, storage and mobilization. These processes are controlled post-transcriptionally by the IRP/IRE regulatory system. The Iron Regulatory Proteins (IRP1 and IRP2) can recognize *cis*-regulatory mRNA motifs termed IREs (Iron Responsive Elements), conserved RNA elements located in the untranslated regions (UTR) of mRNAs that encode for proteins involved in iron metabolism. IRP/IRE interactions regulate the expression of mRNAs encoding for proteins for iron acquisition, storage, utilization and export in response to cellular iron level itself being the interaction of the IRPs with IRE motifs promoted under iron-deficient conditions and abolished in iron-replete conditions. Depending on the location of the IRE, IRPs binding regulates gene expression differentially: IRPs inhibit translation initiation when bound to IREs at the 5' UTR, while IRPs association with 3' IREs stabilizes and protects the mRNA from degradation.

The lack of control of expression of IRE-containing mRNAs is associated in humans with pathological conditions showing the importance of components of the IRP/IRE regulatory system.

In the last decades, significant progress has been made in the iron metabolism field, however, post-transcriptional regulation of gene expression by the IRP/IRE regulatory system has been limited to a small subset of known genes. A genome-wide study carried out by our group to characterize the whole repertoire of mRNAs that can interact with the IRPs, identified 35 novel IRP1 and IRP2 candidate target-genes.

This work focused on the validation and functional characterization of one of this candidates: Profilin2 (Pfn2). Pfn2 is an actin-binding protein involved in the control of cytoskeletal dynamics. We identified a conserved IRE in the 3' UTR of Pfn2 mRNA which is functional in *in vitro* binding studies with IRP1 and IRP2.

Pfn2 mRNA showed preferentially downregulation under iron-excess condition in cell lines and we demonstrated to be regulated by IRPs-mediated stabilization *in vivo*, since Pfn2 mRNA levels are reduced in a mouse model with *Irp1* and *Irp2* gene inactivation.

Moreover, the reduction of cellular free iron levels by Pfn2 overexpression experiments in cell lines, as well as, the misregulation of iron distribution observed in mice knockout for *Pfn2* gene, revealed Pfn2 as a previously unrecognized player in iron metabolism.

In addition, we also contributed to the identification of a functional 3' IRE in human BDH2 mRNA, a protein involved in lipocalin-siderophores iron-trafficking, as well as, in the identification and characterization of two novel L-ferritin IRE mutations (Heidelberg +52G>C and Badalona+36C>U) causative of Hereditary Hyperferritinemia Cataract Syndrome and a novel mutation in ALAS2 IRE demonstrated to be a modifier of clinical severity in a family with Erythropoietic Protoporphyria.

RESUMEN

El hierro es un micronutriente esencial requerido por múltiples reacciones celulares y una regulación adecuada de su metabolismo es fundamental para la salud. La homeostasis celular del hierro está basada en la coordinación de la absorción, el almacenamiento y la movilización de este elemento. Estos procesos son controlados post-transcripcionalmente por el sistema IRP/IRE. Las proteínas reguladoras del hierro (IRP1 e IRP2) reconocen un motivo estructural presente en el ARNm de algunos genes denominado IRE (Iron Responsive Element). El IRE es un motivo conservado y situado en las regiones no traducidas (UTR) de los ARNm de proteínas implicadas en el metabolismo del hierro. Las interacciones IRP/IRE regulan la expresión de los ARNm que codifican proteínas para la adquisición, el almacenamiento, la utilización y la exportación de hierro en respuesta a los niveles celulares de hierro, porque la interacción de las IRPs con los motivos IRE se ve incrementada a niveles bajos de hierro y disminuida en condiciones altas de hierro. Según la localización de los IRE, las IRPs regulan de manera distinta la expresión de sus dianas: las IRPs inhiben la iniciación de la traducción cuando se unen a IREs situados en el 5' UTR, mientras que su asociación con los IREs del 3' UTR estabiliza y protege dicho ARNm de la degradación.

La falta de coordinación de la expresión de genes que contienen IRE está asociada con condiciones patológicas ilustrando la importancia de los componentes del sistema regulador IRP/IRE.

En las últimas décadas se han realizado progresos importantes en el campo del metabolismo del hierro. Sin embargo, la regulación post-transcripcional de la expresión génica por el sistema IRP/IRE se ha limitado a un pequeño subconjunto de genes. Un estudio “genome-wide” llevado a cabo en nuestro grupo para la caracterización global del sistema regulador IRP/IRE dio como resultado la identificación de 35 genes diana que se unen a IRP1 e IRP2. La presente tesis tiene como objetivo general validar y caracterizar funcionalmente una de esas dianas: Profilin2 (Pfn2). Pfn2 es una proteína que une actina y que está involucrada en la regulación de la dinámica del citoesqueleto.

Hemos identificado un IRE localizado en el 3’ UTR del ARNm de Pfn2; el IRE es funcional en estudios *in vitro* para la unión a IRP1 e IRP2. El ARNm de Pfn2 viene preferentemente regulado y reducido en condiciones altas de hierro en líneas celulares y hemos demostrado *in vivo* que es regulado por estabilización mediada de las IRPs, ya que los niveles de ARNm de Pfn2 se encuentran reducidos en ratones a los que los genes de *Irp1* y *Irp2* han sido inactivados. Así mismo, la sobrexpresión de Pfn2 en líneas celulares asociada a una reducción en los niveles de hierro libre, así como la desregulación de la distribución del hierro encontrada en ratones “knockout” para el gen de *Pfn2*; convierten a Pfn2 como un actor nuevo en el metabolismo del hierro.

Por otro lado hemos contribuido tanto a la identificación de un 3’ IRE funcional en el ARNm humano de BDH2, una proteína involucrada en el tráfico de hierro a través del sistema de lipocalinas-sideróforos, como a la identificación de dos nuevas mutaciones en el IRE de la Ferritina L (Heidelberg +52G>C y Badalona+36C>U) responsables del Síndrome Hereditario de Hiperferritinemia con Cataratas y también a la identificación de una nueva mutación en el IRE de ALAS2 que ha demostrado ser un modificador de la importancia clínica de los síntomas en una familia con Protoporfiria Eritropoyética.

TABLE OF CONTENTS

I. LIST OF FIGURES

II. LIST OF TABLES

III. LIST OF ABBREVIATIONS

2,5-DHBA	2,5-dihydroxybenzoic acid
A	adenosine
ABCB7	ATP-binding cassette subfamily B member 7
ACO1 / IRP1	aconitase 1, soluble
ACO2	aconitase 2, mitochondrial
AD	Alzheimer's disease
AHSP	alpha hemoglobin stabilizing protein
ALAS	delta aminolevulinate synthase
APP	amyloid precursor protein
ASGR1 / RHL-1	asialoglycoprotein receptor 1
ATP	adenosine triphosphate
BDH2	3-hydroxybutyrate dehydrogenase, type 2
BMP	bone morphogenetic protein
BOLA3	bolA family member 3
C	cytosine
C/EBPalpha	CCAAT/enhancer-binding protein alpha
CAT	chloramphenicol acetyl transferase
CDC14A	cell division cycle 14A
CDC42	cell division cycle 42
CDK1	cyclin-dependent kinase 1
cDNA	complementary deoxyribonucleic acid
CDS	coding DNA sequence
CHOP	C/EBP homologous protein
CIA	cytosolic assembly machinery
c-MYC	v-myc avian myelocytomatosis viral oncogene homolog
COPD	chronic obstructive pulmonary disease
COXPD19	combined oxidative phosphorylation deficiency 19
CP	ceruloplasmin
CUL1	cullin 1
CyFIP1	cytoplasmic FMR1 interacting protein 1
DMT1 / SLC11A2	divalent metal transporter 1 / solute carrier family 11 (proton-coupled divalent metal ion transporter), member 2
EMSA	electrophoretic mobility shift assay

EPO	erythropoietin
EST	expressed sequence tag
ETC	electron transport chain
FBXL5	F-box and leucine-rich repeat protein 5
FDX1 /FDX2	ferredoxin 1 / ferredoxin 1-like or ferrodoxin 2
FDXR	ferredoxin reductase
Fe	iron
Fe/S	iron-sulfur
FECH	ferrochelatase
FPN1 / SLC40A1	ferroportin-1 / solute carrier family 40 (iron-regulated transporter), member 1
FRDA	Friedreich's ataxia
FTH1	ferritin heavy chain
FTL	ferritin light chain
FTMT	ferritin mitochondrial
FXN	frataxin
G	guanosine
GDF15	growth differentiation factor 15
GLRX5	glutaredoxin 5
GMP	guanosine monophosphate
Gox / Hao1	glycolate oxidase / liver hydroxyacid oxidase 1
Grb2	growth factor receptor-bound protein 2
GTP	guanosine triphosphate
GWAS	genome-wide association studies
H^+	proton
H_2O_2	hydrogen peroxide
HAMP	hepcidin antimicrobial peptide
HFE	hemochromatosis
HFE2 / HJV	hemochromatosis type 2 (juvenile) / hemojuvelin
HH	Hereditary Hemochromatosis
HIF2α / EPAS1	hypoxia inducible factor-2 alpha / endothelial PAS domain protein 1
HML	hereditary myopathy with lactic acidosis
HMOX1	heme oxygenase (decycling) 1
IBA57	IBA57, iron-sulfur cluster assembly homolog
IRE	iron regulatory element
IREB2 / IRP2	iron-responsive element binding protein 2
IRIDA	iron-refractory iron-deficiency anemia

IRP	iron regulatory protein
ISCU	iron-sulfur cluster assembly enzyme
ISD11	iron-sulfur protein biogenesis, desulfurase-interacting protein 11
JAC1 / HSCB	HscB mitochondrial iron-sulfur cluster co-chaperone
JAK	janus kinase
LCN2	lipocalin2
LIP	labile iron pool
LRP1 /CD91	low density lipoprotein receptor-related protein 1
MFRN1/SLC25A37	mitoferrin 1 / solute carrier family 25 (mitochondrial iron transporter), member 37
MFRN2/SLC25A28	mitoferrin 2 / solute carrier family 25 (mitochondrial iron transporter), member 28
MRCKα / CDC42BPA	myotonic dystrophy kinase alpha / CDC42 binding protein kinase alpha
mRNA	messenger ribonucleic acid
NADH	nicotinamide adenine dinucleotide
NDFUS1	75kDa NADH dehydrogenase (ubiquinone) Fe/S protein 1, (NADH-coenzyme Q reductase)
NFS1	NFS1 cysteine desulfurase
NFU1	NFU1 iron-sulfur cluster scaffold homolog
NTBI	non transferrin bound iron
OH^-	hydroxide ion
$^{\bullet}OH$	hydroxyl radical
OMIM	Online Mendelian Inheritance in Man database
PBH	prohibitin
PCR	polymerase chain reaction
PFN2	profilin 2
PPIX	protoporphyrin IX
PtdIns(4,5)P_2	phosphatidylinositol 4,5-diphosphate
pVHL	von Hippel-Lindau tumor suppressor, E3 ubiquitin protein ligase
qPCR	quantitative polymerase chain reaction
RBC	red blood cell
ROCK2	Rho-associated, coiled-coil containing protein kinase 2
ROS	reactive oxygen specie
SCARA5	scavenger receptor class A, member 5
SD	standard deviation
Sdh	succinate dehydrogenase
SDS-PAGE	Sodium Dodecyl Sulphate - PolyAcrylamide Gel Electrophoresis
SEM	standard error of the mean

SKP1	S-phase kinase-associated protein 1
SLC11A2	(see DMT1)
SLC22A17	solute carrier family 22, member 17
SLC25A28	(see MFRN2)
SLC25A37	(see MFRN1)
SLC39A14	(see ZIP14)
SLC39A8	(see ZIP8)
SLC40A1	(see FPN1)
SLC48A1/HRG1	solute carrier family 48 (heme transporter), member 1 / heme responsive gene 1
SMAD	small mother against decapentaplegic
SNP	single nucleotide polymorphism
STAT3	signal transducer and activator of transcription 3
STAT5	signal transducer and activator of transcription 5
STEAP3	STEAP family member 3, metalloreductase
TCA	tricarboxylic acid cycle
TF	transferrin
TFR1	transferrin receptor 1
TFR2	transferrin receptor 2
Timd2	T cell immunoglobulin and mucin domain containing 2
TMPRSS6	transmembrane protease serine 6
TWSG1	twisted gastrulation protein homolog 1
U	uracil
UTR	untranslated region
XLEPP	X-linked Erythropoietic Protoporphyria
XLSA	X-linked sideroblastic anemia
ZIP14 / SLC39A14	Zrt-, Irt-like protein 14 / solute carrier family 39 (zinc transporter), member 14
ZIP8 / SLC39A8	Zrt-, Irt-like protein 8 / solute carrier family 39 (zinc transporter), member 8

1. INTRODUCTION

1.1 Iron biology

1.1.1 Dual nature of iron

Iron is an essential micronutrient for all living beings. It is present as cofactor or as part of prosthetic groups like heme or iron-sulfur (Fe/S) clusters inside proteins involved in a variety of biological processes. Iron-containing protein are implicated in oxygen transport (hemoglobin and myoglobin), citric acid cycle and cellular respiration (Fe/S proteins and cytochromes), antioxidant defense (peroxidase and catalase), DNA/RNA synthesis and nucleotide metabolism (ribonucleotide reductase) and many others metabolic reactions.
The biological relevance of iron is due to its chemical nature; it can easily switch from the reduced form (ferrous, Fe^{2+}) to the oxidized form (ferric, Fe^{3+}). Molecules containing iron can therefore readily accept or donate electrons, making this metal an essential component in vital processes that require electron transfer.
This redox capacity makes iron also potentially toxic because ferrous iron can react with hydrogen peroxide via the Fenton's reaction (Merkofer *et al.* 2006):

$$Fe^{2+} + H_2O_2 \rightarrow Fe^{3+}\ OH^- + {}^{\bullet}\mathbf{OH}$$

giving rise to reactive oxygen species (ROS) that are damaging to cellular structures. ROS promote DNA damage, proteins oxidation and lipids peroxidation eventually leading to cell death and organ dysfunction.
Since both iron excess and iron deficiency are detrimental, the level of free reactive iron must be controlled and limited. If an adequate balance is not achieved, this will have pathological consequences. For instance, iron deficiency leads to anemia, a major world-wide public health problem, and iron overload is toxic and increases the oxidative stress of body tissues leading to inflammation, cell death, systemic organ dysfunction and cancer (Hentze *et al.* 2010).
The dual nature of iron, had led to the evolution of homeostatic mechanisms for a tight regulation of free iron concentrations both at systemic as well as at cellular level.

1.2 Systemic iron homeostasis

1.2.1 Iron distribution and fluxes in the body

An adult human contains around 3-5 g of iron, most of which in erythrocyte hemoglobin (2-3 g) (Hentze *et al.* 2004). Skeletal muscles also contain iron mainly associated to myoglobin, an hemoprotein important for oxygen storage and release during periods of hypoxia (Ordway *et al.* 2004). Liver and spleen are iron-rich organs and the main reservoir of iron for the body. In these tissues iron is stored in liver hepatocytes and liver and spleen specialized macrophages.

Iron is distributed to the tissues through the blood where it is transported bound to the glycoprotein transferrin (TF) in a soluble non-toxic form (Bartnikas 2012). All cells in the body can uptake iron bound to transferrin protein through the ubiquitously expressed transferrin receptor 1 (TFR1) (Thorstensen *et al.* 1990).
Every day 20-25mg of iron move from the blood to peripheral tissues, mainly to the bone marrow to sustain erythroid demand.
Senescent or damaged erythrocytes are phagocyted by macrophages of the reticuloendothelial system present in spleen, liver and bone marrow and iron is recovered and recycled to the blood to keep plasma iron concentration stable (Figure 1.1).

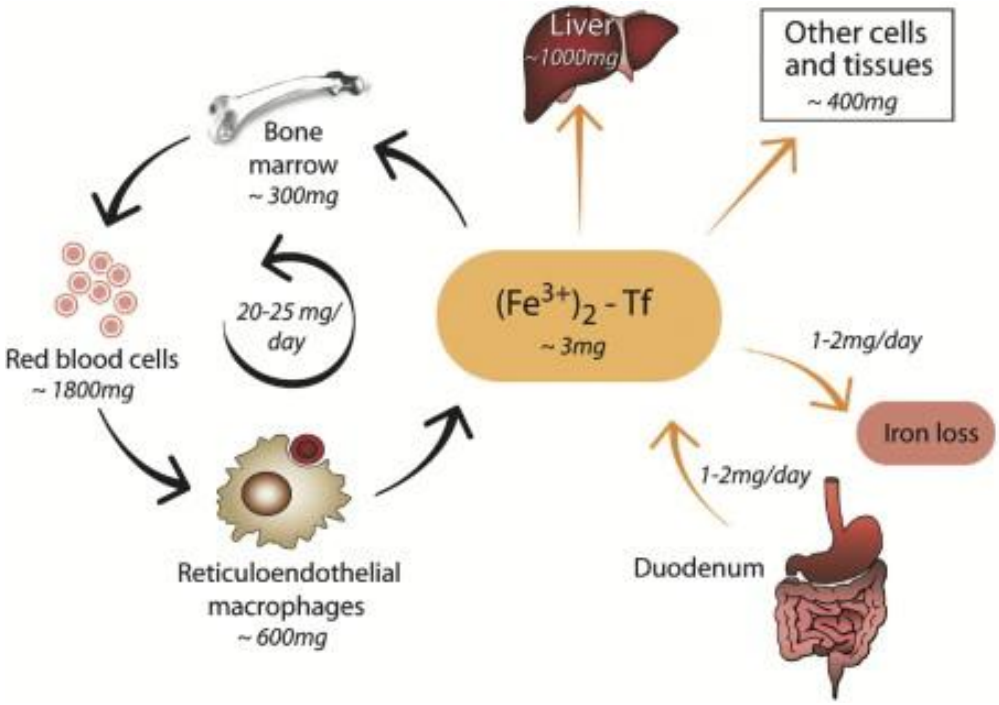

Figure 1.1 Systemic iron homeostasis. Representation of iron cycle in the human body. The key organs/tissues of iron metabolism are represented: duodenum (absorption), red blood cells (utilization), macrophages (recycling), liver (storage). The values of iron content of different organs and the daily fluxes are indicated. Tf: transferrin.
Picture reproduced with permission from Hentze *et al.* 2004.

There is no mechanism for an active iron excretion from the body. Unspecific loss of iron (1-2mg/day) occurs as a consequence of bleedings or desquamation of epithelial surfaces (Green *et al.* 1968). These losses are compensated by dietary iron absorption in the duodenum. Iron excess is stored in liver hepatocytes and spleen macrophages and is readily mobilized if necessary (Figure 1.1).

1.2.2 Regulation of systemic iron homeostasis: hepcidin

For maintaining a correct balance of iron in the body, efficient and coordinated mechanisms that control iron absorption, storage and mobilization are required.
Hepcidin (encoded by the gene *HAMP*) has been demonstrated to be such a regulator. Hepcidin is a small peptide hormone synthesized in large amount by hepatocytes and secreted into the bloodstream, where it circulates free or bound to plasma proteins, and is excreted through the kidney (Park *et al.* 2001; Peslova *et al.* 2009; Itkonen *et al.* 2012). Mature hepcidin peptide (25 amino acids) derives from the cleavage of a larger precursor and contains four disulfide bonds. Hepcidin is produced mainly by the liver, but can also be

produced in lower amount by kidney, heart, pancreas and hematopoietic cells (Kulaksiz *et al.* 2005; Peyssonnaux *et al.* 2006; Merle *et al.* 2007; Kulaksiz *et al.* 2008). Hepcidin was originally identified as a peptide with antimicrobial properties (Krause *et al.* 2000; Park *et al.* 2001) and its role as a key protein in iron metabolism was described later. Hepcidin transcript was found to be upregulated in the liver of iron overloaded mice (Pigeon *et al.* 2001) and mice knockout for the hepcidin gene had a severe iron overload phenotype (Nicolas *et al.* 2001). Hepcidin acts by controlling the membrane levels of its receptor: ferroportin (FPN1) the only known iron exporter. Ferroportin is mainly expressed in duodenum, spleen and liver and mediates the delivery of dietary iron from enterocytes to the bloodstream and the efflux of recycled iron from hepatocytes and spleen macrophages. The binding of hepcidin to ferroportin induces its internalization and lysosomal degradation (Nemeth *et al.* 2004); thus hepcidin produces a systemic response that controls the flow of iron into bloodstream (Figure 1.2). When hepcidin concentration are low, iron enters the blood at high rate, while when hepcidin concentrations are high, ferroportin is degraded and iron is blocked inside enterocytes, macrophages and hepatocytes (Ganz 2011).

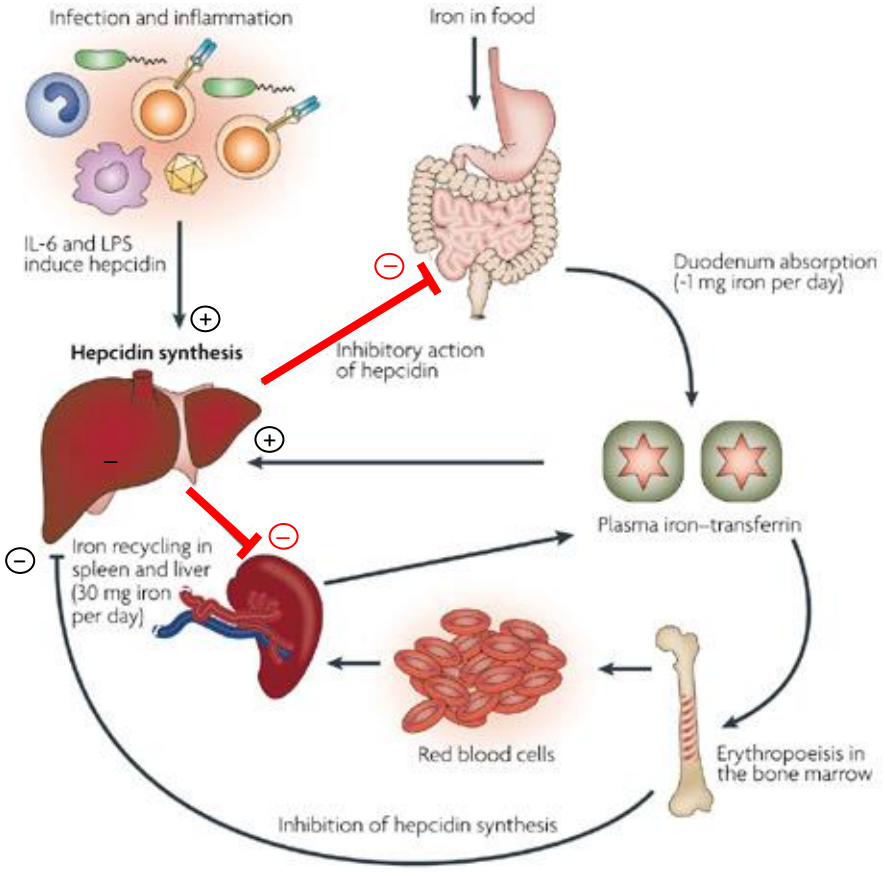

Figure 1.2 Hepcidin regulation of iron uptake and release. Hepcidin blocks ferroportin activity and inhibits iron absorption from the duodenum and iron recycling from macrophages. Hepcidin is produced by the liver in response to increased transferrin saturation levels in the plasma. Hepcidin is also induced by inflammatory stimuli as lipopolysaccharide (LPS) and interleukin-6 (IL-6). If the bone marrow requires extra iron to produce red blood cells, hepcidin synthesis is suppressed. Picture modified from Drakesmith *et al.* 2008.

Hepcidin expression responds to different stimuli. Systemic availability of iron is the main regulator of hepcidin expression as an elevated transferrin saturation in the plasma and high hepatic iron stores activate hepcidin production (Ramos *et al.* 2011).

Hepcidin is also upregulated during inflammatory/infectious states (Armitage *et al.* 2011) so as to reduce available iron indispensable for pathogens growth.

On the other hand, a higher erythroid activity or hypoxia suppresses hepcidin expression (Pak *et al.* 2006; Peyssonnaux *et al.* 2007); this facilitates iron liberation from macrophage and absorption from the diet in order to sustain bone marrow needs (Figure 1.2-1.3).
At molecular level, these extracellular signals are sensed by the hepatocytes through specific receptor molecules on the cell surface; these receptors trigger the activation of signaling cascades that, finally, control the activity of hepcidin promoter (Hentze *et al.* 2010) (Figure 1.3).

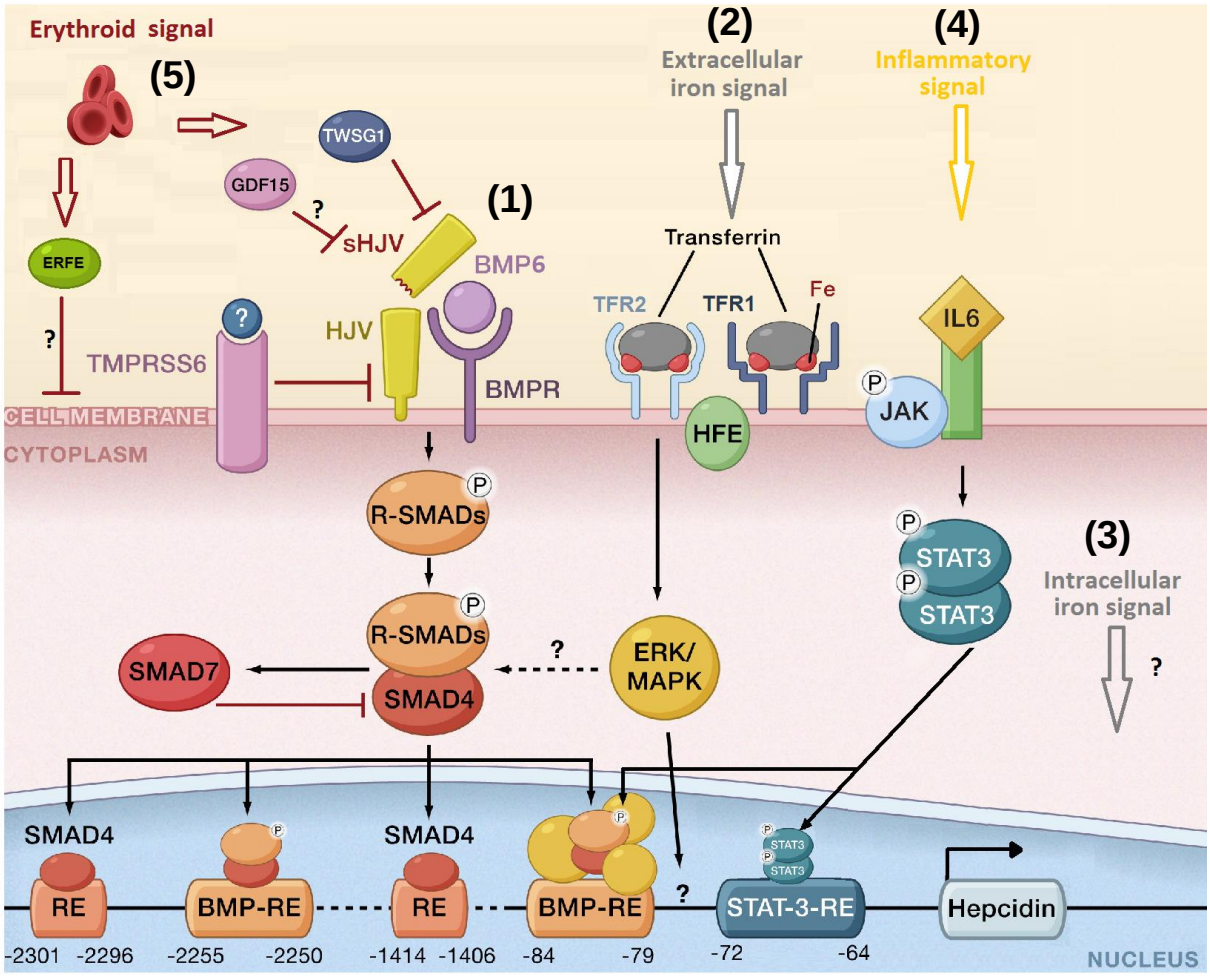

Figure 1.3 Molecular mechanisms for the regulation of hepcidin expression. Hepcidin is transcriptionally regulated by different and antagonist signals. **(1)** The bone morphogenetic proteins (BMP) signaling is the central route for hepcidin stimulation in response to high iron concentration; BMP activates SMAD phosphorylation and translocation to the nucleus where they bind to responsive elements on hepcidin promoter and activate its translation (Babitt *et al.* 2006). Particularly BMP6 has been shown to be responsible of this regulation (Meynard *et al.* 2009), as BMP6 is positively regulated by iron. Hemojuvelin (HJV) is an important BMP co-receptor; it can be cleaved by the protease TMPRSS6, with consequent inhibition of hepcidin expression (Silvestri *et al.* 2008). **(2)** Hepatocytes sense transferrin saturation in the plasma. At high transferrin saturation, HFE bound to TFR1 is displaced and binds to TFR2 (Goswami *et al.* 2006); the HFE/TFR2 complex activates the extracellular signal regulated kinase (ERK) / mitogen activated protein kinase (MAPK) and SMAD signaling. **(3)** High intracellular iron stores are as well able to activate hepcidin expression, but the underlying mechanism has to be elucidated. **(4)** Inflammatory cytokines IL1 and IL6 are also inducers of hepcidin expression. IL6 activates the Janus Kinase (JAK)/signal transducer and activator of transcription (STAT3) signaling pathway, which stimulates STAT3-binding motif close to the transcription site on hepcidin promoter (Fleming 2007). BPM signaling also contributes to the inflammatory response (Wang *et al.* 2005b). Hepcidin is also increased by endoplasmic reticulum stress or by stress-inducible transcription factors CHOP and C/EBPalpha (Oliveira *et al.* 2009; Vecchi *et al.* 2009). **(5)** GDF15 and TWSG1 are factors released by erythroid precursors and have been demonstrated to inhibit the BMP/SMAD pathway for hepcidin activation (Tanno *et al.* 2007; Tanno *et al.* 2009). Recently, a new erythroid hormone, erythroferrone (ERFE) was demonstrated to mediate hepcidin inhibition during stress erythropoiesis independently of the BMP/SMAD pathway (Kautz *et al.* 2014). Picture modified from Hentze *et al.* 2010.

1.2.3 Human diseases caused by hepcidin and ferroportin misregulation

Being hepcidin of central importance in the control of systemic iron homeostasis, ineffective regulation of its expression results in pathological consequences.

Hereditary Hemochromatosis (HH) is an heterogeneous group of autosomal-recessive genetic disorders that affect hepcidin gene itself (*HAMP*, responsible for HH type2B OMIM #613313) or genes encoding for proteins involved in the signaling pathway for hepcidin induction (Barton 2013): *HFE* (responsible for HH type1, OMIM #235200), *HFE2* (hemojuvelin, HJV, responsible for HH type2A, OMIM #602390) or transferrin receptor 2 (*TFR2*, responsible for HH type3, OMIM #604250).

As a result of mutations in these genes, HH patients present inappropriately low levels of hepcidin which lead to an uncontrolled dietary iron absorption and deposit in parenchymal organs such as liver, heart and pancreas. Tissues iron overload can lead to severe complications such as liver cirrhosis and hepatocarcinoma, heart failure, diabetes, hypogonadism and arthritis and needs to be treated with periodic phlebotomies or iron chelating therapies in order to reduce the detrimental excess of iron (Kanwar *et al.* 2013).

Mutations affecting ferroportin, the hepcidin target, are responsible for an autosomal-dominant iron overload disorder called “ferroportin disease” or HH type4 (OMIM #606069) (Pietrangelo 2004). In these cases, loss-of-function mutations decrease membrane concentration of ferroportin on the plasma membrane and, as a result, iron is trapped in macrophages. While gain-of-function mutations make ferroportin resistant to hepcidin-induced degradation and are associated with parenchymal iron loading similar to classical HH (Mayr *et al.* 2010).

Recently, a new gene (*BMP6*) has been associated to an HH variant with autosomal-dominant transmission (Daher *et al.* 2015). *BMP6* mutations lead to reduced hepcidin synthesis and mild to moderate liver iron overload.

In iron-refractory iron-deficiency anemia (IRIDA, OMIM #206200), a genetic disorder caused by mutations in the gene encoding the transmembrane serine protease matriptase-2 (*TMPRSS6*) the phenotype is the opposite. TMPRSS6 inhibits hepcidin production and its defect results in abnormally high levels of hepcidin leading to a severe anemia mostly unresponsive to oral iron therapy (Finberg *et al.* 2008; Melis *et al.* 2008).

1.3 Cellular iron homeostasis

Maintenance of iron homeostasis inside cells require coordinated regulation of iron uptake, utilization and storage in order to assure appropriate iron levels to cellular needs and to avoid iron toxicity. Differing from systemic regulation, cellular iron homeostasis also controls iron excretion (Hentze *et al.* 2010).

1.3.1 Cellular iron uptake

The major route for iron uptake in mammalian cells is the receptor-mediated endocytosis of iron loaded transferrin (Fe_2-TF) from the plasma performed by transferrin receptor 1 protein. Transferrin protein binds two atoms of iron in its ferric state (Fe^{3+}). Fe_2-TF/TFR1 complex is internalized in endosomes in a clathrin-depended way. Reduction of the pH in the endosomes facilitates the release of iron from transferrin (Dautry-Varsat *et al.* 1983). Free iron is then reduced to Fe^{2+} by the metalloprotease STEAP3 (Ohgami *et al.* 2005; Ohgami *et al.* 2006) and it is transported to the cytoplasm by the action of divalent metal ion transporter (DMT1) while the endocytic vesicles are recycled to cell surface, apo-TF released extracellularly and TFR1 is ready for another round of endocytosis (Figure 1.4, upper-left). TFR1 is ubiquitously

expressed but it plays an essential function in maturing erythroblasts where it is expressed at high level to support the huge demand of iron for hemoglobin synthesis. TFR1 gene knockout in mice is early lethal during embryogenesis due to a severe anemia and neurological abnormalities and TFR1 haploinsufficiency also result in an impaired erythropoiesis and a slightly abnormal iron homeostasis (Levy *et al.* 1999). Recently, a new missense mutation in human *TFRC* gene, encoding for TFR1 protein, has been shown to cause a combined immunodeficiency with impaired function of T and B cells (Jabara *et al.* 2016).
Epithelial cells of the kidney utilize a distinct mechanism for TF bound iron uptake through megalin-dependent, cubilin-mediated endocytosis (Kozyraki *et al.* 2001).

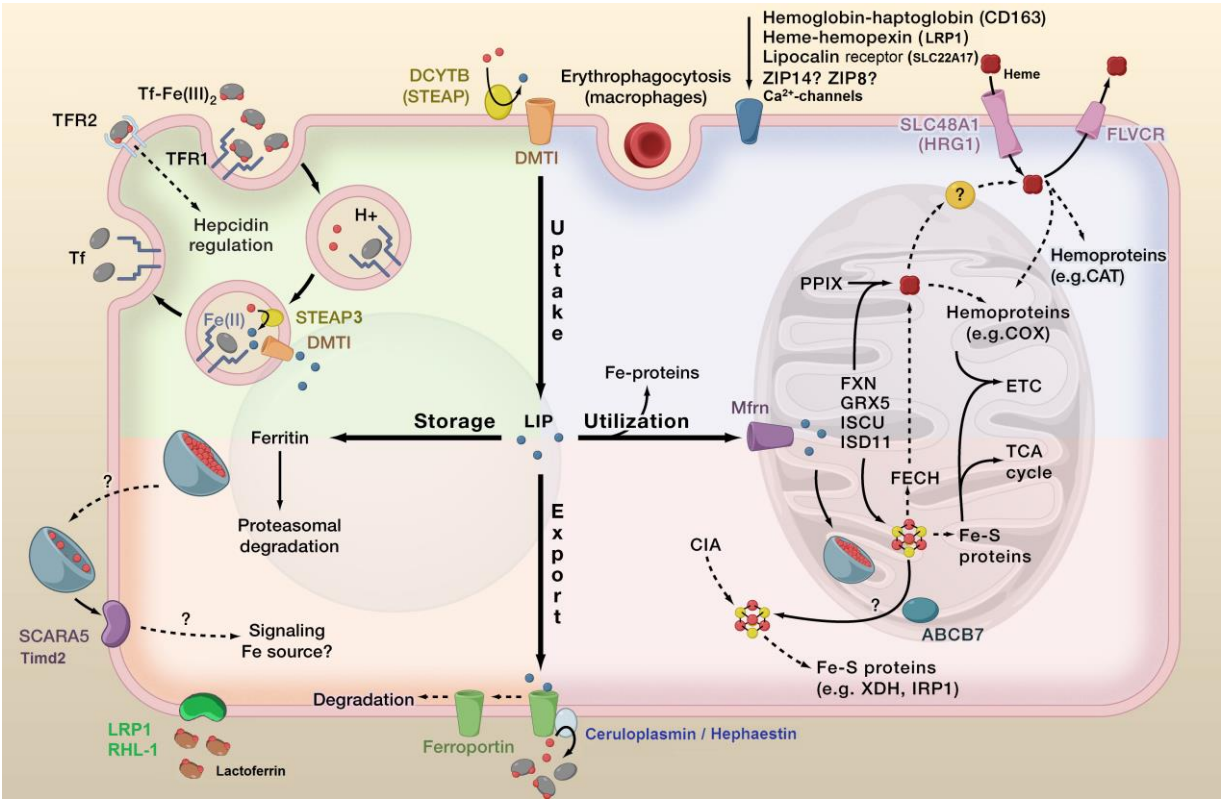

Figure 1.4 Cellular iron trafficking. In the picture are represented the main routes of iron uptake, utilization, storage and export. DCYTB: duodenal cytochrome B; Tf: transferrin; TFR1: transferrin receptor 1; TFR2: transferrin receptor 2; STEAP3: STEAP family member 3, metalloreductase; DMT1: divalent metal ion transporter 1; LIP: labile iron pool; SCARA5: scavenger receptor class A, member 5; Timd2: T cell immunoglobulin and mucin domain containing 2; LRP1: low density lipoprotein receptor-related protein 1; RHL-1: major subunit of the asialoglycoprotein receptor 1; CIA: cytosolic iron-sulfur cluster assembly machinery; XDH: xanthine dehydrogenase; IRP1: iron regulatory protein 1; ABCB7: ATP-binding cassette subfamily B member 7; ETC: electron transport chain; TCA cycle: tricarboxylic acid cycle; FECH: ferrochelatase; FXN: frataxin; GLRX5: glutaredoxin 5; ISCU: iron-sulfur cluster scaffold protein; ISD11: iron-sulfur protein biogenesis, desulfurase-interacting protein 11; Mfrn: mitoferrin; PPIX: protoporphyrin IX; COX: cyclooxygenase; CAT: catalase; FLVCR: feline leukemia virus subgroup receptor-1 (heme exporter); SLC48A1: solute carrier family 48, member 1; ZIP14: solute carrier family 39 (zinc transporter), member 14; ZIP8: solute carrier family 39 (zinc transporter), member 8. Picture modified from Hentze *et al.* 2010.

Hypotransferrinemic (hpx/hpx) mice (Trenor *et al.* 2000), as well as human cases of congenital atransferrinemia (OMIM #209300) (Goldwurm *et al.* 2000), that carry mutations in the transferrin gene and present a strong reduction of plasma levels of transferrin, are severely anemic but develop massive iron overload in non-hematopoietic tissues, such as liver and pancreas. This disease illustrates that there are other ways for iron uptake independent of the transferrin/transferrin receptor 1 cycle.
A fraction of plasma iron circulates not bound to transferrin, heme or ferritin, the so called non-transferrin bound iron (NTBI). NTBI becomes important in iron overload disorders, in which

plasma iron is present in excess of transferrin-binding capacity. NTBI is rapidly taken up by hepatocytes (Zimelman *et al.* 1977) and recently demonstrated also by T lymphocytes (Arezes *et al.* 2013) probably as clearance mechanism of potentially toxic circulating iron. Different transporters have been postulated to be involved in hepatic clearance of NTBI with DMT1 playing an important role in transporting NTBI into cells (Shindo *et al.* 2006). DMT1 therefore has multiple functions in iron metabolism: in all cell types, acting as an endosomal protein involved in iron transfer to the cytosol, in hepatocytes as iron importer on the plasma membrane. DMT1 is also present on the apical membrane of duodenal enterocytes where it is fundamental for absorbing dietary iron. Other candidates for NTBI uptake are two members of the ZIP (ZRT/IRT-like Proteins) family of metal-ion transporters: ZIP14 (SLC39A14, highly expressed in liver, pancreas and heart) and ZIP8 (SLC39A8, highly expressed in placenta and lung) (Pinilla-Tenas *et al.* 2011; Wang *et al.* 2012). Calcium channels may also contribute to iron uptake in cardiomyocytes (Oudit *et al.* 2003) (Figure 1.4).

In addition, iron can be acquired also as heme. How heme is internalized in cells still remains elusive; different transporters have been proposed but, so far, only SLC48A1/HRG1 (solute carrier family 48, member 1) seems reliable (Rajagopal *et al.* 2008). Heme can be also acquired indirectly, as in the case of machrophages that obtain heme via the phagocytosis of senescent red blood cells. Moreover, free heme in the plasma, derived from vascular hemolysis, binds to plasma proteins as haptoglobin or hemopexin and is cleared respectively by macrophages via CD163 receptor or in hepatocytes and other cell types via LRP1/CD91 receptor endocytosis (Kristiansen *et al.* 2001; Hvidberg *et al.* 2005) (Figure 1.4).

Finally, other forms of protein-bound iron uptake through specific receptors have been postulated: serum ferritin can be internalized via SCARA5 (scavenger receptor class A, member 5) receptor in kidney cells or via murine Timd2 (T cell immunoglobulin and mucin domain containing 2) receptor in T and B lymphocytes and in kidney and liver cells (Chen *et al.* 2005; Li *et al.* 2009) (Figure 1.4). Lactoferrin is an iron-binding protein similar to transferrin which is present in body fluids, mainly in milk. Two lactoferrin receptors have been found to be expressed by the liver: low density lipoprotein receptor-related protein 1 (LRP1/CD91) and the RHL-1 subunit of the asialoglycoprotein receptor 1 (Meilinger *et al.* 1995; Bennatt *et al.* 1997) (Figure 1.4).

Recently, Lipocalin2 dependent endocytosis of iron-loaded siderophores through the lipocalin receptor has been reported to be involved in liver iron uptake and regulation of iron trafficking to the mitochondria (Devireddy *et al.* 2005; Devireddy *et al.* 2010).

I will discuss more in depth Lipocalin2-mediated iron trafficking because it is relevant for the results reported in this thesis (see Results and Discussion 3.3 and 3.4.7.4).

1.3.1.1 Lipocalin2-mediated iron trafficking

Siderophores are low molecular weight Fe^{3+}-chelator molecules secreted by microorganisms, such as bacteria and fungi, in order to scavenge iron from the environment, that are then recognized and taken up by active transport mechanisms (Neilands 1995).

Recent findings on human lipocalin2 (LCN2) function have evidenced that siderophores play also an important role in mammalian iron trafficking. Lipocalin2, also known as lipocalin24p3 or neutrophil gelatinase associated lipocalin (NGAL), belongs to lipocalins family of secreted proteins that bind different low molecular weight substrates and carry out different functions (Akerstrom *et al.* 2000). LCN2 has been implicated in anti-microbial and inflammatory response (Liu *et al.* 1995; Goetz *et al.* 2002; Srinivasan *et al.* 2012), renal development (Yang *et al.* 2002) and apoptosis (Devireddy *et al.* 2001).

Several groups have demonstrated that LCN2 can bind iron and deliver it to or remove it from cells (Goetz *et al.* 2002; Yang *et al.* 2002; Devireddy *et al.* 2005). Devireddy and collaborators have demonstrated that LCN2 activity depends on its iron-status. On one hand, iron-containing LCN2 (Holo-LCN2) binds to the cell surface receptor SLC22A17, it is internalized and releases its bound iron, increasing intracellular iron concentration (Figure 1.5A). On the other hand, iron-lacking LCN2 (Apo-LCN2) is internalized, associates with an intracellular siderophore and transfers iron to the extracellular medium, reducing cellular iron concentration (Figure 1.5B).

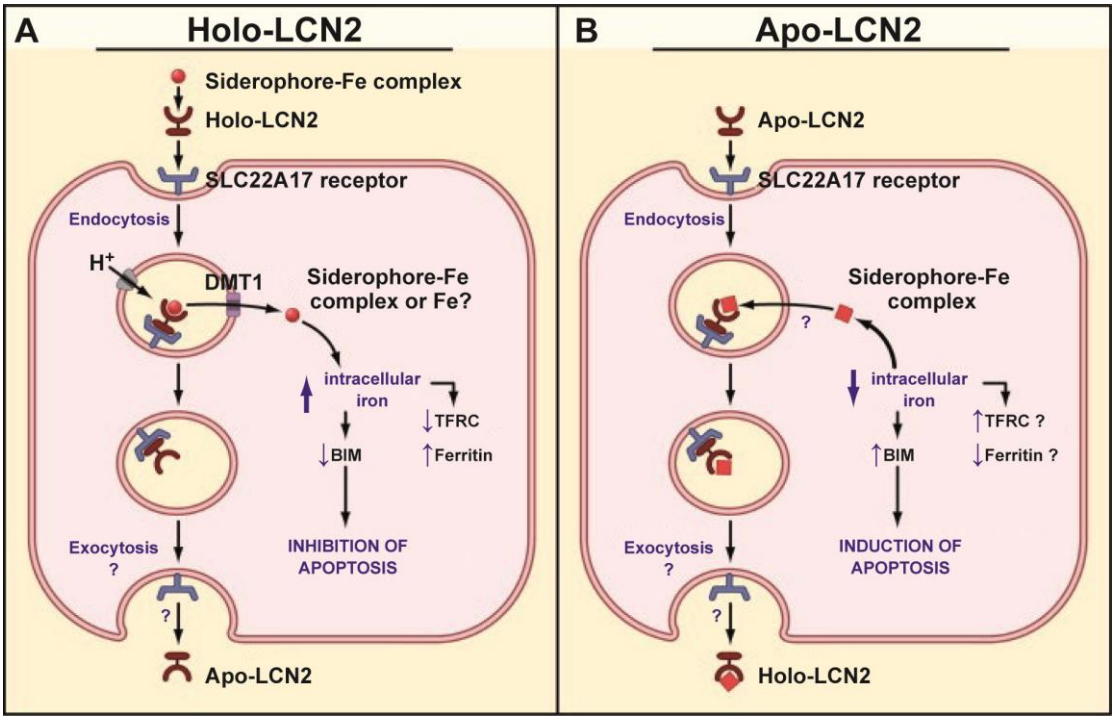

Figure 1.5 Lipocalin2-mediated iron trafficking. (A) Holo-LCN2, loaded with an iron-bound siderophore, donates iron to cells via internalization of the LCN2 receptor, SLC22A17 (Devireddy *et al.* 2005). The mechanism of iron release from the siderophores-LCN2 complex is still unclear, however Yang and collaborators demonstrated that iron release occurs at low pH and that the internalized LCN2 co-localizes with the divalent metal ion transporter DMT1 (Yang *et al.* 2002), suggesting acidification of the endosomes and a possible intervention of DMT1 in the transport of the released iron to the cytosol. Yang and collaborators also showed that LCN2 is not degraded after internalization (Yang *et al.* 2002), suggesting a possible protein recycling to the membrane after iron release. The iron, transferred to the cytoplasm, decreases TFRC expression and an increases ferritin levels. Moreover, iron inhibits apoptosis by reducing the levels of BIM protein, a pro-apoptotic member of the Bcl-2 family (Devireddy *et al.* 2005). **(B)** By contrast, when Apo-LCN2 is internalized, it binds to the endogenous siderophore 2,5-DHBA to form Holo-LCN2, which is subsequently released from the cell by exocytosis. Reduction of intracellular iron concentration results in the upregulation of the pro-apoptotic molecule, BIM, leading to apoptosis (Devireddy *et al.* 2005). Picture modified from Richardson 2005.

Devireddy and colleagues demonstrated the existence of a mammalian siderophores, the 2,5-dihydroxybenzoic acid (2,5-DHBA), analog to the *Escherichia coli* Enterobactin (Devireddy *et al.* 2010) (Figure 1.5B). The mammalian siderophore is biosynthesized by an evolutionary conserved pathway where the 3-hydroxybutyrate dehydrogenase type 2 (BDH2) catalyzes the rate-limiting step (Guo *et al.* 2006; Devireddy *et al.* 2010). BDH2 silencing in mammalian cells, which leads to siderophores depletion, results in cytoplasmic iron accumulation, with elevated levels of reactive oxygen species, whereas the mitochondria are iron-deficient (Devireddy *et al.* 2010). In addition, siderophores-depleted mammalian cells or zebrafish embryos are defective in heme synthesis (Devireddy *et al.* 2010) showing that LCN2-siderophores pathway plays an important role for iron uptake and for the regulation of iron trafficking to the mitochondria.

1.3.2 Cellular iron trafficking and utilization

Independently of the route used for entering the cytosol, only a small fraction of bioactive iron (labile iron pool, LIP) is present in this compartment and, in that case, it is complexed to low molecular weight chelators as citrates, sugars, ascorbate, ADP, ATP or other nucleotides (Petrat *et al.* 2003). Most of the iron traffics to the mitochondria where it is essential for the synthesis of heme and Fe/S cluster groups but the metal itinerary from the cytosol to the mitochondrial matrix is not well understood. Two transporters are present in the mitochondrial inner membrane: mitoferrin1 (Mfrn1/SLC25A37) and mitoferrin2 (Mfrn2/SLC25A28) in erythroid and not erythroid cells, respectively (Shaw *et al.* 2006; Paradkar *et al.* 2009). It is still unknown how iron crosses the mitochondrial outer membrane; potential transporters have been identified (Nilsson *et al.* 2009). The mammalian siderophore 2,5-dihydroxybenzoic acid (2,5-DHBA) has also been demonstrated to be involved in iron delivery to the mitochondria (Devireddy *et al.* 2010). Finally, in erythroblasts, that require huge amount of iron, it may be directly transported from transferrin-containing endosomes to mitochondria via a direct contact between the organelles, the so called “kiss and run” mechanism (Sheftel *et al.* 2007).

Once iron is in the mitochondrial matrix it can be used for heme synthesis, Fe/S synthesis or stored within mitochondrial ferritin (see section 1.3.3) (Figure 1.4 right).

Heme synthesis pathway is represented by a series of 8 reactions that take place both in the cytosol and in the mitochondria; the first and rate-limiting step is catalyzed by the delta-aminolevulinate synthase (ALAS) in the mitochondrial matrix. Two genes for ALAS exist: the ubiquitously expressed ALAS1 and the erythroid-specific ALAS2 (Ponka 1997). The latter is regulated by iron via the iron regulatory proteins (IRPs, see section 1.4.1). In humans, defects of ALAS2 gene are responsible of the genetic disease X-linked sideroblastic anemia (XLSA, OMIM #300751), characterized by ineffective erythropoiesis and iron deposit in the mitochondria (Cotter *et al.* 1992). ALAS2 gain-of-function mutations are also responsible for the X-linked Erythropoietic Protoporphyria (XLEPP, OMIM #300752). The following 4 steps of heme production take place in the cytosol; the coproporphyrinogen III intermediate enters again the mitochondria for being decarboxylated and oxidized to produce protoporphyrin IX (PPIX). Finally, an atom of ferrous iron is inserted in the protoporphyrin ring by the Fe/S enzyme ferrochelatase (FECH). Deficiency in ferrochelatase activity leads to Erythropoietic Protoporphyria (OMIM #177000) characterized by toxic accumulation of protoporphyrins in the tissues (Lamoril *et al.* 1991). It is unknown how heme is exported out of the mitochondrion. Apart from heme production, mitochondrial iron is used for the synthesis of other important inorganic cofactors: the Fe/S clusters. Assembly of Fe/S clusters is assisted by a complex machinery of both mitochondrial a cytosolic proteins; this pathway has been widely studied in the yeast model leading to the identification of more than 20 molecules that have been afterward further studied in higher eukaryotes (Lill *et al.* 2008). Basically, this mitochondrial process can be divided into an initial phase where Fe/S cluster are transiently assembled on a proteic scaffold called ISCU (Agar *et al.* 2000) and subsequently released and transferred to acceptor apoproteins. In this first phase, the cysteine desulfurase complex NFS1-ISD11 liberates organic sulfur from the amino acid L-cysteine while iron seems to be chaperoned by the frataxin protein (FXN) (Gerber *et al.* 2003; Bulteau *et al.* 2004). The nature of the chemical mechanism of Fe/S assembly has not been well clarified but it requires a chain of electron transfer from NADH in which are involved the proteins ferredoxins (FDX1/FDX2) and ferredoxin reductase (FDXR) (Sheftel *et al.* 2010b; Shi *et al.* 2012). Once assembled, the transient Fe/S cluster has to be transferred onto apoproteins; this process is facilitated by “chaperone” molecules as JAC1, Mge1 and glutaredoxin 5 (GLRX5) (Muhlenhoff *et al.* 2003; Lill *et al.* 2008). Proteins using Fe/S groups as cofactor are also present in the cytoplasm and

in the nucleus; a cytosolic assembly machinery (CIA) also exists (Roy *et al.* 2003; Balk *et al.* 2004; Hausmann *et al.* 2005). The CIA components catalyze a similar process to the mitochondrial one, however, the functionality of the mitochondrial assembly machinery is required for the maturation of cytosolic Fe/S proteins. It has been hypothesized that the mitochondrion produces a compound "X", whose nature is not clear, that is exported to the cytosol where is essential for Fe/S cluster proteins maturation. A central role in this transport is played by the mitochondrial inner membrane transporter ABCB7 (Kispal *et al.* 1997). Defects in any of the components of the Fe/S cluster biogenesis machinery not only affect Fe/S containing enzymes but also result in a deregulation of cellular iron homeostasis (Richardson *et al.* 2010). Neurodegenerative and hematological human diseases have been associated with mutations in Fe/S machinery proteins, underlining the central importance of this process for life (see section 1.6.5).

1.3.3 Cellular iron storage: ferritins

Iron not required for cellular needs is either exported from the cells or safely stored within ferritin protein in a not reactive form (Figure 1.4 lower-left). Ferritin are heteropolymers made of 24 subunits of heavy (FTH1) and light (FTL) chains forming a spherical shell surrounding a cavity capable of accommodating up to 4500 atoms of iron as ferric oxohydroxide (Arosio *et al.* 2009). Heavy and light chain show 55% amino acid identity but their 3D structure is extremely conserved. They are ubiquitously expressed but with tissues specific ratio that allows flexibility to adapt to cell needs (Harrison *et al.* 1996); H-rich ferritins are more predominant in heart and brain, L-rich ferritins are more predominant in liver and spleen. The two chains carry out different functions within ferritin protein: FTH1 displays ferroxidase activity by converting the pro-oxidant Fe^{2+} to Fe^{3+}, while FTL helps iron nucleation in the mineral core. Iron can be mobilized from ferritin stores if required; the exact mechanism for iron release from ferritin has not been fully clarified but involves lysosomal and proteasomal pathways (Kidane *et al.* 2006). Ferritin H-subunit is essential for life for its detoxifying properties. Knockout of the *Fth1* gene in mice is embryonic lethal (Ferreira *et al.* 2000) and no mutations in human FTH1 gene have been described apart from a single family case with a mutation in the iron regulatory element (IRE) in the 5' UTR of FTH1 mRNA causing an iron overload syndrome (OMIM #615517). Human mutations in the FTL subunit are responsible for human disorders: neuroferritinopathy, a group of neurodegenerative disorders with brain iron accumulation (OMIM #606159) (Curtis *et al.* 2001; Vidal *et al.* 2004), Hereditary Hyperferritinemia-Cataract Syndrome (HHCS, OMIM #600886) (Beaumont *et al.* 1995) and inherited benign hyperferritinemia without cataracts (Kannengiesser *et al.* 2009; Thurlow *et al.* 2012). Recently, a patient affected by a homozygous loss-of-function mutation in the L-ferritin gene has been described (Cozzi *et al.* 2013), indicating that FTL function is dispensable for life; this patient presented undetectable serum ferritin and idiopathic generalized seizures. Fibroblasts and neurons derived from this patient showed altered iron homeostasis and increased oxidative stress.

A ferritin form, made of L-subunits, partially glycosilated and depleted of iron is present in body fluids: serum, cerebrospinal fluid and synovial fluids. This ferritin form is of clinical relevance, since its concentration could have a direct correlation with the total amount of iron stored in the body and thus it is largely used for the diagnosis of iron-deficient anemias and iron overload (Arosio *et al.* 2009). However, serum ferritin levels are increased also in inflammation, infection, liver diseases, cancer and in response to oxidative stress (Wish 2006). Ferritins play a fundamental detoxifying function in the cell; regulation of the ferritin genes is necessary to provide the correct balance between iron-mediated toxicity and the iron necessary for metabolism. Ferritins expression is mainly regulated by a post-transcriptional

mechanism. This process is mediated by interaction between RNA binding proteins (iron regulatory proteins, IRPs) and a region in the 5′ untranslated region of ferritin H and L mRNA termed iron responsive element (IRE) (see section 1.4.3); in addition, ferritins expression is also transcriptionally controlled (White *et al.* 1988).
A mitochondrial form of ferritin (FTMT) also exists (Arosio *et al.* 2010). FTMT are homopolymers of a nuclear-encoded protein similar to ferritin heavy chain. FTMT levels are increased in sideroblastic anemias, disorders with mitochondrial iron accumulation, suggesting a protective role against iron toxicity in the organelle (Invernizzi *et al.* 2013). In contrast to cytosolic ferritins, FTMT is expressed only in a few tissues as testis, heart, brain, pancreas and kidney (Santambrogio *et al.* 2007) and its expression is not controlled by the IRPs.

1.3.4 Cellular iron export: ferroportin

Iron export eliminates excess of iron that is not needed neither stored by the cells. It can occur in many cell types but it is particularly important in macrophages and duodenal enterocytes that are responsible for maintaining plasma iron level and also in placental cells for the delivery of iron to the fetus during gestation (Hentze *et al.* 2010). As mentioned before, the only known iron exporter in vertebrates is ferroportin. Disruption of ferroportin gene in mice is embryonic lethal due to an impaired transfer of maternal iron to the embryos through the extraembryonic visceral endoderm (Donovan *et al.* 2005). Selective ferroportin inactivation in all embryo tissues apart from extraembryonic visceral endoderm and placenta give rise to viable pups although presenting a severe anemia and iron accumulation in enterocytes, macrophages, and hepatocytes, consistent with the important role of ferroportin in those cell types (Donovan *et al.* 2005). Ferroportin exports iron as Fe^{2+} and, therefore, it acts in the plasma membrane together with a copper-dependent ferroxidase: ceruloplasmin (expressed by all cells types) or hephaestin (expressed mainly in enterocytes) (De Domenico *et al.* 2007).
Apart from ferroportin-mediated release of elemental iron, cells can also export iron bound to ferritin (Leimberg *et al.* 2008) or as heme (Figure 1.4). Feline leukemia virus subgroup receptor-1 (FLVCR1) has been demonstrated to export cytoplasmic heme and is essential for mouse erythroid maturation eliminating toxic excesses of heme. FLVCR1 also mediates heme export from macrophages and liver hepatocytes (Keel *et al.* 2008).

1.4 Regulation of cellular iron homeostasis

The maintenance of iron homeostasis is achieved through a coordinated and balanced expression of proteins involved in iron uptake, export, storage and utilization. Although transcriptional mechanisms have been described in the literature, cellular iron homeostasis is mainly controlled by an iron-sensitive post-transcriptional machinery. This regulatory system is represented by the iron regulatory proteins (IRPs) through their binding to *cis*-regulatory motifs termed iron responsive elements (IRE) located in the 5’ and 3’ untranslated regions (UTR) of target mRNAs (Anderson *et al.* 2012; Joshi *et al.* 2012).

1.4.1 Iron Responsive Elements (IRE)

Iron responsive elements are conserved hairpin structures of 25-30 nucleotides located in the UTR of various mRNAs. A canonical IRE consists of a 6-nucleotides apical loop (5’-CAGWGH-3’; where W stands for A or U and H stands for A, C or U) on a stem of 5 paired nucleotides, an asymmetric bulge with an unpaired cytosine on the 5’ side of the stem, and an additional lower stem of variable length (Addess *et al.* 1997) (Figure 1.6). An exposed AGW pseudotriloop is formed by a base pair between the first and the fifth residue of the loop,

stabilizing the IRE structure. The AGW pseudotriloop and the cytosine bulge are important for the interaction with the iron regulatory proteins (Addess *et al.* 1997; Walden *et al.* 2006).

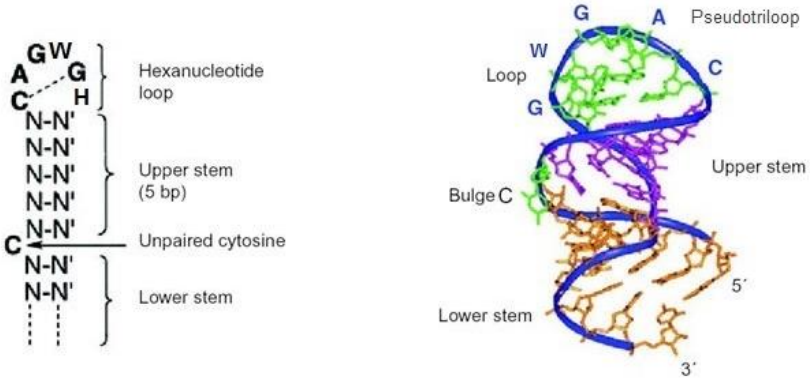

Figure 1.6 Sequence and structure of an iron responsive element. Consensus sequence and secondary structure of a canonical IRE are represented. Picture modified from Rouault 2006.

IREs have been described in mRNAs encoding for proteins involved in iron uptake (TFR1, DMT1), iron storage (FTH1, FTL), heme synthesis (ALAS2), energy metabolism (ACO2, *Drosophila* succinate dehydrogenase, Sdh), oxygen sensing (hypoxia inducible factor-2 alpha, HIF2α), and iron export (FPN) (Sanchez *et al.* 2007; Muckenthaler *et al.* 2008) (Figure 1.7). Other IRE structures have been reported and I discuss them in section 1.7.

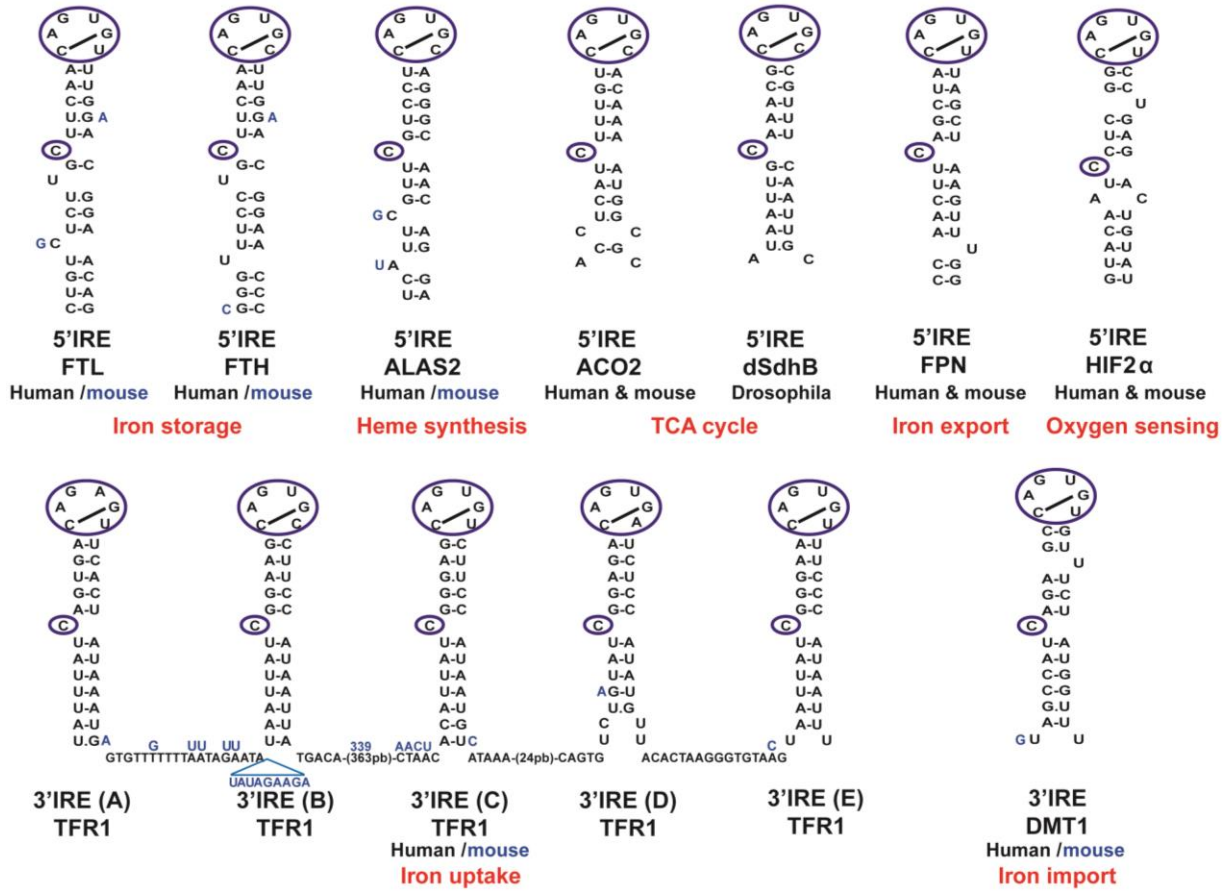

Figure 1.7 Functional IREs. In the picture are represented the IRE secondary structures of the classical, and well-recognized targets of the IRPs. All motifs present a consensus apical loop (5'-CAGWGH-3') and a C-bulge on the 5' strand of the stem (blue circles). mRNAs carrying the IRE in the 5' UTR are shown in the top part of the picture and 3' UTR IREs in the bottom part; the 5 IREs of TFR1 are named from A to E. IREs are well conserved across evolution; in blue are indicated minor sequence differences among human and mouse IREs. In red is indicated the function of the encoded protein. FTL: L-ferritin; FTH: H-ferritin; ALAS2: erythroid-specific delta aminolevulinate synthase; dSdhB: *Drosophila* succinate dehydrogenase B; FPN: ferroportin; HIF2α: hypoxia inducible factor-2 alpha; TFR1: transferrin receptor 1; DMT1: divalent metal ion transporter 1. Picture from Joshi *et al.* 2012.

1.4.2 Iron Regulatory Proteins (IRPs)

Mammalian cells express two different iron regulatory proteins encoded by two different genes: *IRP1* (or *ACO1*) and *IRP2* (or *IREB2*).

IRP1 and *IRP2* are homologous genes, derived by gene duplication and belong to the family of aconitases together with the tricarboxylic acid (TCA) cycle enzyme mitochondrial aconitase (*ACO2*). Aconitases are enzymes that isomerise citrate to isocitrate via a *cis*-aconitate intermediate; a characteristic feature of these enzymes is the presence of a cubane 4Fe-4S cluster in the catalytic site where 3 cytosine residues coordinate 3 iron atoms of the cluster and the forth labile iron interact with the substrate (Beinert *et al.* 1993). IRP1 is a cytosolic aconitase with 30% amino acid sequence identity (100% in the catalytic core) to mitochondrial aconitase, however, the Fe/S cluster of IRP1 is easily lost upon iron depletion (Rouault *et al.* 1992). Resolution of the crystal structure of IRP1 revealed that the structure of IRP1 is very similar to the one of ACO2 (Robbins *et al.* 1989; Dupuy *et al.* 2006). IRP1 is composed of four globular domains with a catalytic site at the interface between domains 1-3 and 4 where the 4Fe-4S cluster is accommodated coordinated by cysteine residues (Figure 1.8A). Disassembly of the Fe/S cluster upon iron depletion induces a switch to an open conformation that allows interaction with the IRE (Walden *et al.* 2006) (Figure 1.8B). RNA binding and aconitase activity of IRP1 are mutually exclusive and the switch between conformations is reversible, making IRP1 a bifunctional protein (Rouault *et al.* 1992).

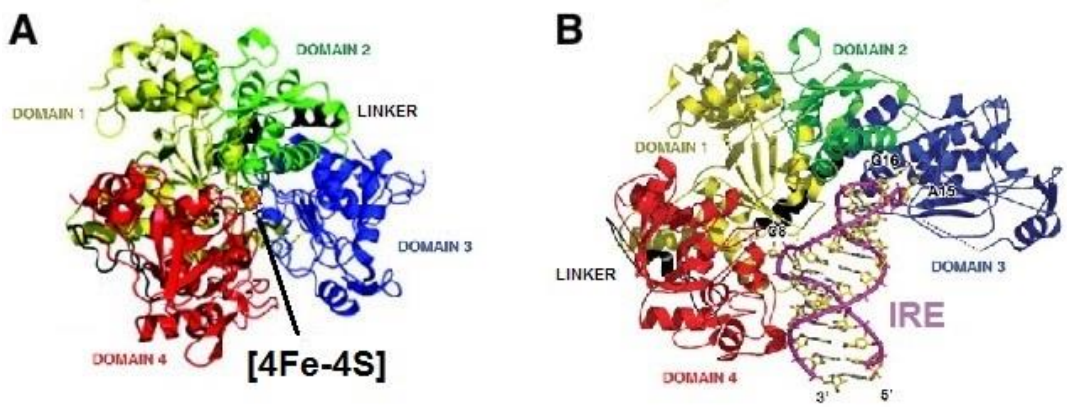

Figure 1.8 Crystal structure of IRP1. (A) Picture shows the crystal structure of IRP1 in its aconitase conformation bound to the Fe/S cluster. Domains 1-3 are compact and are connected to domain 4 by a flexible hinge linker (black). **(B)** Crystal structure of IRP1 in its mRNA binding conformation is represented; loss of the Fe/S cluster induces the switch to an open conformation that can accommodate the IRE. Picture modified from Rouault 2006 and Walden *et al.* 2006.

IRP2 crystal structure has not been yet resolved but has been predicted upon IRP1 structure (Zumbrennen *et al.* 2009). Although sharing 57% amino acidic sequence identity with IRP1, IRP2 does not assemble an Fe/S cluster and does not exhibit aconitase activity (Guo *et al.* 1994). Moreover, IRP2 contains an additional 73 amino acid insertion at the N-terminus of the protein; there role of this domain is not clear, although it was initially thought to be involved in iron-dependent degradation of IRP2 (Iwai *et al.* 1995).

Both IRPs are ubiquitously expressed, however, IRP1 is particularly abundant in kidney, brown fat and liver and IRP2 in brain, intestine, and spleen (Henderson *et al.* 1993; Guo *et al.* 1995; Meyron-Holtz *et al.* 2004).

1.4.3 Post-transcriptional regulation of IRP-target mRNAs

The interaction of the IRPs with IRE motifs is promoted under iron-deficient conditions and abolished in iron-replete cells by different mechanisms (see section 1.4.4). Depending on the

location of the IREs in the untranslated region (UTR) of the target mRNA, the binding of the IRPs differentially regulates its expression. Both IRPs inhibit translation when bound to 5' UTR IREs, as in the case of ferritins and FPN, by preventing the recruitment of the small ribosomal subunit to the mRNA (Muckenthaler *et al.* 1998). Conversely, IRPs binding to multiple 3' UTR IREs, as in the case of TFR1, protects the transcript from endonucleolytic cleavage and degradation (Casey *et al.* 1989) (Figure 1.9).

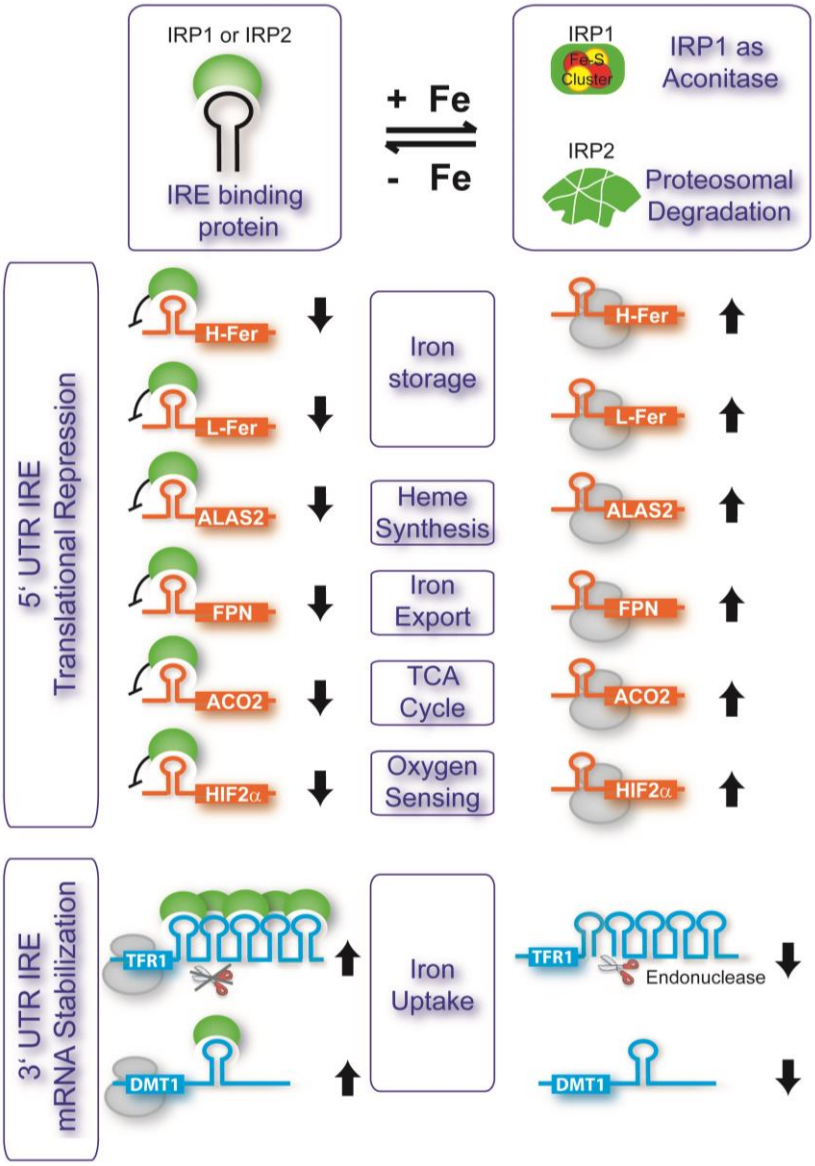

Figure 1.9 IRP/IRE regulatory system. In iron-deficient cells (left), IRP1 and IRP2 bind to *cis*-regulatory IRE motifs on target mRNAs. IRP binding to 5' UTR IRE targets inhibits their translation, whereas IRP interaction with 3' IREs increases mRNA stability. In iron-replete cells (right), IRP/IRE interaction is abolished since IRP1 protein switches to aconitase activity via assembling a cubane Fe/S cluster and IRP2 is degraded by the proteasome. This results in a higher translation of 5' IRE targets and more rapid degradation of 3' IRE mRNAs. Picture modified from Joshi *et al.* 2012.

In iron-deficient conditions, the binding of the IRPs to IREs promotes iron uptake via TF-TFR1 endocytosis and avoids iron storage within ferritin or iron export via FPN, that are not required under such conditions. On the other hand, when cellular iron is high, loss of IRP binding activity reduces iron uptake due to TFR1 mRNA degradation and iron excesses are safely stored and exported by actively translated ferritin and FPN, respectively. Therefore, loss of IRP binding capacity prevents toxic effects that could arise by excess of redox-active free iron (Figure 1.4 and 1.9).

1.4.4 Regulation of IRP activity

Controlling the expression of key proteins of iron uptake, usage, storage and export, the IRPs coordinate cellular of iron fluxes. For an efficient balance of cellular iron homeostasis, IRP activity is coupled to iron status. Cellular iron pools regulate the mRNA binding activity of the two IRPs through distinct mechanisms. Apart from iron itself, various other stimuli have been reported to affect IRPs activity.

1.4.4.1 Regulation of IRP1 activity

As mentioned in section 1.4.2, IRP1 is a bifunctional protein, acting either as IRE binding protein in iron deficiency or as cytosolic aconitase, when it incorporates an Fe/S cluster in iron-replete conditions (Figure 1.9 and 1.10). The "Fe/S switch" is the main mechanism of IRP1 regulation and represents a link between cellular iron status and Fe/S biogenesis. However, the mechanism by which iron deficiency triggers the loss of the cluster is still not clear; *in vitro* studies have shown that the loss of the forth labile iron of the cluster (4Fe/4S → 3Fe/4S) disrupts aconitase activity but is not sufficient to acquire RNA binding activity and that a more profound alteration of the cluster is necessary (Haile *et al.* 1992).
Apart from iron deficiency, reactive oxygen species (ROS) and reactive nitrogen species (RNS) can promote the Fe/S cluster loss (Beinert *et al.* 1996) (Figure 1.10).

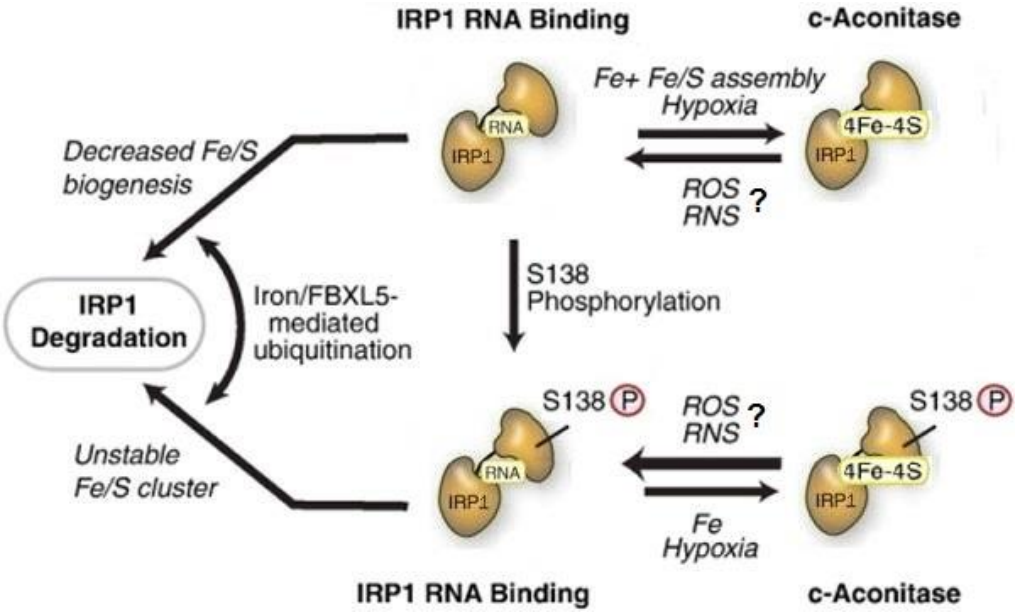

Figure 1.10 Mechanism of IRP1 regulation. IRP1 activity is mainly controlled via assembly/loss of the cubane 4Fe/4S cluster. In the apo-protein form, IRP1 functions as a high affinity IRE-binding protein, while acting as aconitase when the cluster is assembled. The cluster is destabilized by ROS and RNS, while hypoxia favors the aconitase form. IRP1 can also be phosphorylated at serine 138; the phosphorylated protein can assemble the Fe/S cluster, however, this is more sensitive to ROS/RNS-mediated disruption. Iron mediates FBXL5-dependent IRP1 degradation upon serine 138 phosphorylation or when Fe/S biogenesis is defective. FBLX5: F-box and leucine-rich repeat protein 5; c-Aconitase: cytosolic aconitase; ROS: reactive oxygen species; RNS: reactive nitrogen species. Picture modified from Anderson et al. 2012.

Nevertheless, contradictory reports are present in the literature regarding IRP1 regulation by oxidative stress. Exogenous H_2O_2 was shown to convert c-aconitase to the IRP1 IRE-binding form (Hentze *et al.* 1996; Cairo *et al.* 2002; Mueller 2005; Wang *et al.* 2008). However, other studies have shown that IRP1 activation might involve signaling pathways rather than a direct oxidative effect on IRP1 (Pantopoulos *et al.* 1998; Caltagirone *et al.* 2001). On the other hand, several reports have shown that agents or conditions promoting increased cellular H_2O_2 or O_2^- reversibly inactivates IRP1 (Cairo *et al.* 1996; Tacchini *et al.* 1997; Gehring *et al.* 1999).

Consistent with this, increased ferritin levels have been described in cell lines exposed to oxidative stimuli (Cairo *et al.* 2000; Torti *et al.* 2002) raising the hypothesis that IRP1 inactivation, leading to TFR1 downregulation, ferritin upregulation and thus decreased LIP, would be an homeostatic response to prevent further ROS formation. Nitric oxide (NO) promptly reacts with IRP1 4Fe/4S cluster and promotes its complete disassembly converting c-aconitase to IRP1 RNA-binding form (Bouton *et al.* 2003). In addition, protein kinase C can phosphorylate IRP1 at serine 138. Serine 138 phosphomimetic mutants are more sensitive to ROS/RNS-mediated cluster loss and can undergo cluster disassembly even in the absence of disturbing stimuli (Brown *et al.* 1998; Deck *et al.* 2009).
The "Fe/S switch" is the wide accepted mechanism controlling IRP1 activity, supported by the observation that the total levels of c-aconitase/IRP1 protein do not vary in response to iron changes (Haile *et al.* 1992). However, under physiological conditions, IRP1 predominantly exists in the c-aconitase form (Meyron-Holtz *et al.* 2004). In liver, the c-aconitase pool can be up to 100-fold more abundant than the IRE-binding form of IRP1 and severe dietary iron deficiency increases the IRP1 binding pool no more than 4-fold, indicating that only a small portion of c-aconitase is recruited for acting as RNA binding protein (Chen *et al.* 1997). Hence, iron-mediated changes in IRP1 protein levels would not be easily detected by regular techniques. Literature data indicate that IRP1 can be degraded during iron overload or following serine 138 phosphorylation (Neonaki *et al.* 2002; Fillebeen *et al.* 2003). *In vitro* studies using a mutant IRP1 unable to assemble the Fe/S cluster due to artificial mutations of the cluster-ligating cysteines, show an iron-mediated IRP1 degradation (Clarke *et al.* 2006). Moreover, mouse models, as well as *in vitro* studies, where the Fe/S cluster biogenesis is impaired show reduced IRP1 levels (Clarke *et al.* 2006; Fosset *et al.* 2006; Shi *et al.* 2009; Song *et al.* 2009; Sheftel *et al.* 2010b; Shan *et al.* 2012) suggesting that the iron-dependent IRP1 degradation may be a compensatory mechanism to prevent excessive RNA binding activity when the "Fe/S switch" is not effective. These findings are supported by the recent discovery of the FBXL5 ubiquitin ligase that targets IRP2 for degradation, but can potentially act also on IRP1 (Salahudeen *et al.* 2009; Vashisht *et al.* 2009; Moroishi *et al.* 2011).

1.4.4.2 Regulation of IRP2 activity

Unlike IRP1, IRP2 is irreversibly regulated at the level of protein stability in response to iron and oxygen (Figure 1.9 and 1.11). The E3 ligase F-box and leucine-rich repeat protein 5 (FBXL5) was recently identified to be responsible of this regulation (Salahudeen *et al.* 2009; Vashisht *et al.* 2009). FBXL5 is part of an E3 ubiquitin ligase complex (SKP1-CUL1-FXBL5); it confers substrate specificity for IRP2 and contains an iron- and oxygen-binding hemerythrin domain mediating differential FXLB5 stability. In iron-deficient or hypoxic conditions, the di-iron center of the hemerythrin domain is destabilized (Chollangi *et al.* 2012; Shu *et al.* 2012; Thompson *et al.* 2012), which results in FBXL5 degradation and consequently IRP2 stabilization. In iron/oxygen replete conditions, FBXL5 interacts with IRP2 and targets it for proteasomal degradation (Figure 1.11). The lysosomal pathway has been shown to also play a role in IRP2 degradation, but mainly for normal protein turnover, whereas proteasomal degradation is predominant in response to iron (Dycke *et al.* 2008). Oxygen-dependent degradation of IRP2 may also involve the 2-oxoglutarate dependent dioxygenases, which are enzymes that catalyze the hydroxylation of protein substrates targeting them for ubiquitination and proteasomal degradation. Dimethyloxalylglycine, an inhibitor of the 2-oxoglutarate dependent dioxygenases, blocks IRP2 iron-mediated degradation (Hanson *et al.* 2003; Wang *et al.* 2004). The effects of ROS and RNS on IRP2 regulation have also been studied with contradictory results (Kim *et al.* 2004; Wang *et al.* 2005a).

Moreover, IRP2 can be phosphorylated at serine 157, located within the 73 amino acid N-terminal domain, by the action of the cyclin-dependent kinase 1 (CDK1) during G2/M phase of cell cycle and dephosphorylated by the phosphatase CDC14A during mitotic exit (Wallander *et al.* 2008). Previously, a 3' IRE was identified in human CDC14A mRNA (Sanchez *et al.* 2006) (see section 1.7.1.2). IRP2 phosphorylation at serine 157 is not dependent on iron and is associated with reduced IRE binding activity; however, it is still unknown how this contributes to cell cycle regulation. Finally, IRP2 was shown to be a transcriptional target of STAT5 in erythroid cells (Kerenyi *et al.* 2008) and c-MYC in immortalized B cells (Wu *et al.* 1999).

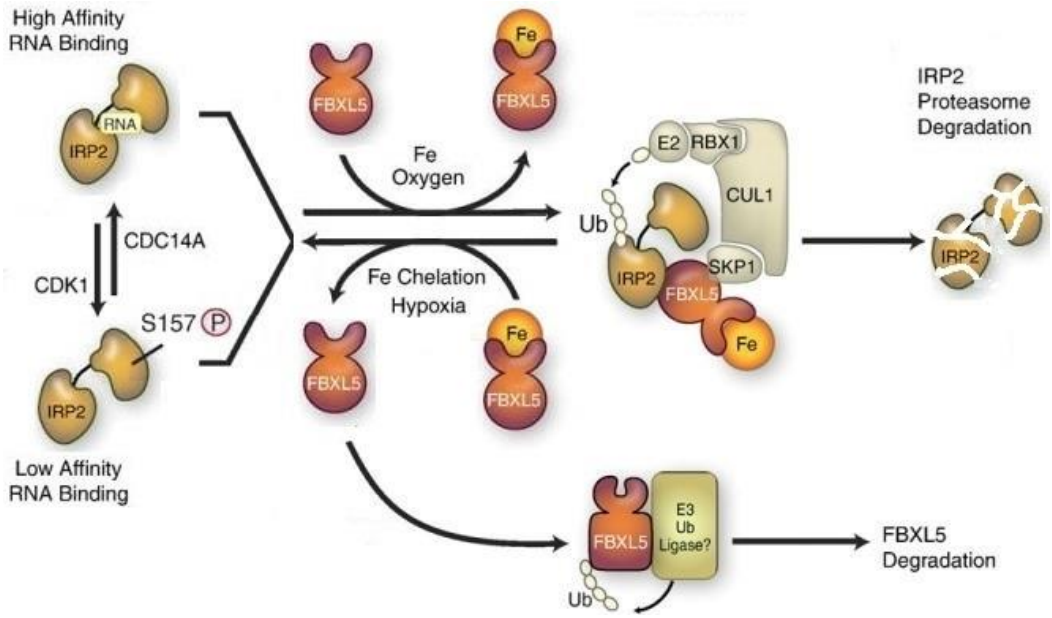

Figure 1.11 Mechanisms of IRP2 regulation. When iron/oxygen are high, the FBLX5 hemerythrin domain binds iron; this produces conformational changes that stabilize FBLX5 protein. FBLX5 binds to IRP2 and associates with the SKP1-CUL1 complex promoting IRP2 ubiquitination and degradation via the proteasome. In low iron and oxygen conditions, FBLX5 is destabilized and targeted for degradation by the action of an unknown ubiquitin ligase; as a consequence IRP2 levels increase. IRP2 can be also phosphorylated at serine 157, independently of iron levels. Serine 157 phosphorylation is associated with reduced IRE binding activity. Both non-phosphorylated and phosphorylated IRP2 undergo iron-dependent FBLX5-mediated degradation. FBLX5: E3 ligase F-box and leucine-rich repeat protein 5; SKP1: S-phase kinase-associated protein 1; CUL1: cullin 1; CDK1: cyclin-dependent kinase 1; CDC14A: cell division cycle 14A. Picture modified from Anderson *et al.* 2012.

1.5 The IRP/IRE regulatory system in physiology

The IRP/IRE regulatory system has been widely studied, demonstrating the central function of IRP regulation not only in the maintenance of cellular iron homeostasis, but also showing important implications in systemic processes as duodenal iron absorption, erythropoiesis and liver iron storage. Most of the knowledge currently available comes from the generation and characterization of mouse models with *Irp1* and *Irp2* gene ablation (Table 1.1).

1.5.1 Mouse models with IRP1 and/or IRP2 deficiency

Inactivation of *Irp1* and *Irp2* genes in mice (double *Irp1* and *Irp2* knockout) leads to embryonic lethality at the blastocyst stage indicating the central role of the IRP/IRE system in early development (Smith *et al.* 2006). On the other hand, mice with single *Irp1* or *Irp2* gene deletion are viable underlining functional redundancy between the two IRPs (LaVaute *et al.* 2001; Meyron-Holtz *et al.* 2004; Galy *et al.* 2005a; Zumbrennen-Bullough *et al.* 2014). However, single *Irp1*-/- or *Irp2*-/- mice display different phenotypes likely due to different subsets of target genes or tissue-specific roles. *Irp1*-/- mice were initially described to lack any

overt phenotype under standard laboratory conditions apart from mild ferritin and Tfr1 dysregulation in kidneys and brown fat where *Irp1* expression is more abundant (Meyron-Holtz *et al.* 2004; Galy *et al.* 2005a). Recently, *Irp1*-/- mice were reported to develop polycythemia, alterations of iron metabolism together with pulmonary hypertension and cardiac hypertrophy (Anderson *et al.* 2013; Ghosh *et al.* 2013; Wilkinson *et al.* 2013). These abnormalities are caused by translational de-repression of Hif2α mRNA which induces expression of erythropoietin (EPO) leading to reticulocytosis, polycythemia, and suppression of hepatic hepcidin mRNA. These data underline the unique and specific regulation exerted by Irp1 on Hif2α mRNA (Zimmer *et al.* 2008). *Irp1*-/- mice die of hemorrhages when placed on an iron-deficient diet (Ghosh *et al.* 2013), but, if fed with a normal diet, polycythemia is corrected after the 10th week of age (Wilkinson *et al.* 2013) explaining why *Irp1*-/- phenotype has not been recognized in the past.

Three distinct strains of *Irp2*-/- mice have been generated by independent groups (LaVaute *et al.* 2001; Galy *et al.* 2005a; Zumbrennen-Bullough *et al.* 2014). All *Irp2*-/- strains develop microcytic hypochromic anemia and erythropoietic protoporphyria associated with altered body iron distribution. Iron content is elevated in the duodenum and liver and correlates with increased ferritin and decreased Tfr1 expression, and is reduced in the spleen together with reduced ferritin expression (Cooperman *et al.* 2005; Galy *et al.* 2005b). Microcytic anemia is associated with normal transferrin saturation and serum iron parameters. It is due to an erythroid-specific iron deficiency, as a consequence of reduced Tfr1 levels, since erythroid precursors are strongly dependent on transferrin-bound iron uptake for heme synthesis. In line with this, mice lacking *Irp2* in hepatocytes, enterocytes and macrophages do not develop anemia (Ferring-Appel *et al.* 2009). The *Irp2*-/- strain generated by LaVaute *et al.* develop late-onset neurodegeneration, neuronal loss and iron overload in the white matter areas of the brain (LaVaute *et al.* 2001). The onset and severity of the neurodegeneration is aggravated in *Irp1*+/- *Irp2*-/- mice (Smith *et al.* 2004). The neuronal defects of both *Irp2*-/- and *Irp1*+/- *Irp2*-/- mice were alleviated by Tempol, a drug able to convert c-aconitase to IRP1 RNA-binding form and thus restoring iron homeostasis by stabilizing Tfr1 mRNA and repressing ferritin synthesis (Ghosh *et al.* 2008). More recently, *Irp2*-/- strain generated by LaVaute *et al.* were reported to have lower motor neuronal degeneration and spinal cord axonopathy that was more severe in *Irp1*+/- *Irp2*-/- mice (Jeong *et al.* 2011). In contrast, *Irp2*-/- mice generated by another strategy (Galy *et al.* 2006) do not display signs of neurodegeneration nor brain iron deposits or mitochondriopathy and only present minor motor coordination and balance defects. A third, independent *Irp2*-/- strain was recently generated confirming the erythropoietic abnormalities of these mice (Zumbrennen-Bullough *et al.* 2014). However, besides marked iron deposition in brain white matter and in oligodendrocytes, no overt signs of neurodegeneration were observed in this third mouse model and only a mild impairment in locomotion, exploration, motor coordination/balance and nociception was described. The discordance of the neurodegenerative phenotype in the three *Irp2*-/- mouse lines may be due to the different targeting strategies used for gene ablation, genetic background or environmental issues.

To study the effects of double IRPs deficiency *in vivo* and overcome the embryonic lethality of double IRP ablation, mouse strains with tissue-specific *Irp1* and *Irp2* deletion have been generated (reviewed in Anderson *et al.* 2012 and Wilkinson *et al.* 2014) proving essential contribution to the comprehension of the role of the IRP/IRE system in key tissues involved in systemic iron metabolism, as discussed in sections 1.5.2-1.5.3-1.5.4.

The different mouse models with global or tissue-specific *Irp1* and/or *Irp2* genetic ablation or activation generated so far are detailed in Table 1.1 (adapted from Wilkinson *et al.* 2014).

Table 1.1 Phenotypic features of mouse models with global or tissue-specific *Irp1* and *I*or *Irp2* genetic ablation/activation. Modified from Wilkinson *et al.* 2014.

Mouse model	Site of modification	Reference	Phenotype	Phenotype reference
Irp1 -/-	Global	(Meyron-Holtz *et al.* 2004; Galy *et al.* 2005a)	Polycythemia, stress erythropoiesis, splenomegaly and increased expression of erythropoietin	(Anderson *et al.* 2013; Ghosh *et al.* 2013; Wilkinson *et al.* 2013)
			Pulmonary hypertension, cardiac hypertrophy and fibrosis. Mice succumb to hemorrhages when fed with iron-deficient diet	(Ghosh *et al.* 2013; Wilkinson *et al.* 2013)
			Increased expression of Dmt1, Fpn1 and DcytB mRNAs in the duodenum	(Anderson *et al.* 2013)
			Misregulation of ferritin and Tfr1 expression in the kidney and brown fat	(Meyron-Holtz *et al.* 2004)
			Efficient inflammatory signaling response to tupertine	(Viatte *et al.* 2009)
			Increased ferroportin expression in splenic macrophages and decreased hepcidin mRNA levels in the liver	(Wilkinson *et al.* 2013)
Irp2-/-	Global	(LaVaute *et al.* 2001; Galy *et al.* 2005a; Zumbrennen-Bullough *et al.* 2014)	Microcytic hypochromic anemia with mild duodenal and hepatic iron overload and splenic iron deficiency	(Cooperman *et al.* 2005; Galy *et al.* 2005b)
			Reduced Tfr1 expression in erythroid precursors	(Cooperman *et al.* 2005; Galy *et al.* 2005b)
			High levels of protoporphyrin IX in erythroid precursors	(Cooperman *et al.* 2005)
			Increased ferritin levels in all tissue	(Cooperman *et al.* 2005)
			Iron overload in neurons and progressive neurodegeneration	(LaVaute *et al.* 2001)
			Efficient inflammatory signaling response to tupertine	(Viatte *et al.* 2009)
			Lower motor neuronal degeneration with spinal cord axonopathy	(Jeong *et al.* 2011)
			Mild neurological and behavioral defects, as well as nociception	(Zumbrennen-Bullough *et al.* 2014)
			Minor performance deficits in specific neurologic tests (coordination, balance)	(Galy *et al.* 2006)
Irp2-/-	Liver-specific	(Ferring-Appel *et al.* 2009)	Mild hepatic iron overload	(Ferring-Appel *et al.* 2009)
Irp2-/-	Intestinal-specific	(Ferring-Appel *et al.* 2009)	Mild duodenal iron overload	(Ferring-Appel *et al.* 2009)
Irp2-/-	Macrophage-specific	(Ferring-Appel *et al.* 2009)	No pathology	(Ferring-Appel *et al.* 2009)
Irp1-/- Irp2-/-	Global	(Smith *et al.* 2006)	Embryonic lethality at the blastocyst stage	(Smith *et al.* 2006)
Irp1+/- Irp2-/-	Global	(Smith *et al.* 2004)	More severe presentation of neuronal pathology than the *Irp2-/-* mice	(Smith *et al.* 2004)
			Neuronal pathology partially rescued by the pharmacological activation of Irp1	(Ghosh *et al.* 2008)
Irp1-/- Irp2-/-	Liver-specific	(Galy *et al.* 2010)	Lethality within 1-2 weeks after birth due to liver failure. Mitochondrial dysfunction	(Galy *et al.* 2010)
Irp1-/- Irp2-/-	Intestinal-specific	(Galy *et al.* 2008)	Growth retardation, early death (within 30 days) due to dehydration. Increased expression of ferritin and ferroportin and decreased expression of Tfr1 and Dmt1	(Galy *et al.* 2008)
Irp1-/- Irp2-/-	Adult ligand- induced intestinal specific	(Galy *et al.* 2013)	Increased expression of ferritin leading to "mucosal block", in spite of increased expression of ferroportin and Dmt1	(Galy *et al.* 2013)
Irp1 gain-of-function due to expression of a constitutive active Irp1 transgene	Global	(Casarrubea *et al.* 2013)	Macrocytic erythropenia due to impaired erythroid differentiation	(Casarrubea *et al.* 2013)
Irp2 gain-of-function due to disruption of *Fbxl5*	Global	(Moroishi *et al.* 2011; Ruiz *et al.* 2013)	Embryonic lethality. Lethality was prevented by simultaneous ablation of *Irp2*	(Moroishi *et al.* 2011; Ruiz *et al.* 2013)
Irp2 gain-of-function due to disruption of *Fbxl5*	Liver-specific	(Moroishi *et al.* 2011)	Hepatic iron overload, steatohepatitis and low hepcidin mRNA levels. Mice succumb to liver failure when fed with high-iron diet	(Moroishi *et al.* 2011)

1.5.2 The IRP/IRE regulatory system in dietary iron absorption

Iron absorption from the diet takes place in the proximal duodenum. Iron is transported across the apical membrane of duodenal enterocytes followed by its translocation through the basolateral membrane into the bloodstream, where is loaded onto apo-transferrin (Muckenthaler *et al.* 2008) (Figure 1.12).

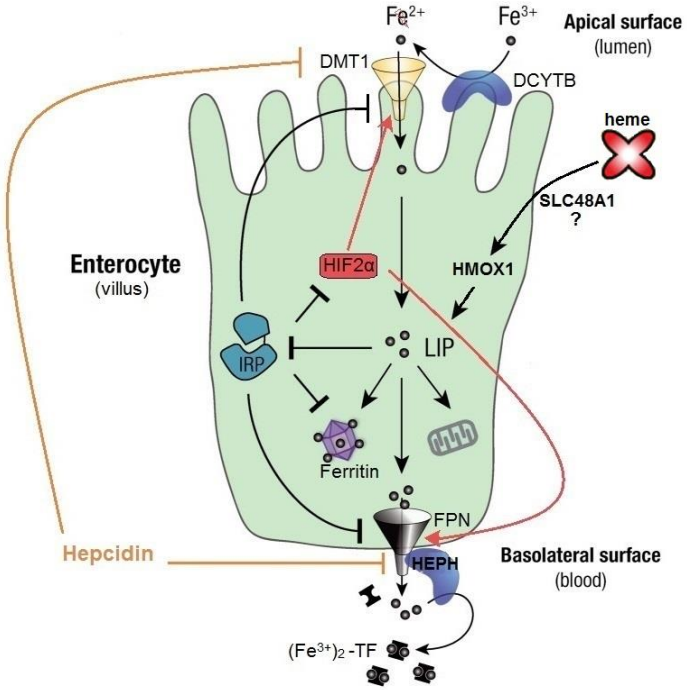

Figure 1.12 The IRP/IRE regulatory system in dietary iron absorption. Two main forms of iron are taken up by duodenal enterocytes: heme and inorganic iron. In diet rich in meat, heme accounts for two-thirds of dietary iron supply; heme is transported by the putative heme-carrier SLC48A1 and then degraded by the action of heme oxygenase to release iron. Transport of inorganic iron requires iron to be converted to its reduced form (Fe^{2+}) either by reducing agent in the lumen of the gut or by the reductase DCYTB. Iron is then transported across the membrane by the DMT1 transporter. Cytoplasmic iron is therefore exported into the bloodstream via the basolateral transporter ferroportin in conjunction with the ferroxidase hephaestin and loaded onto apo-transferrin. Duodenal enterocytes also express ferritin, which limits excessive iron transfer to the circulation (Vanoaica *et al.* 2010) while TFR1 expression is limited to the precursor cells in the crypts that cannot uptake dietary iron (Waheed *et al.* 1999). DMT1: divalent metal ion transporter; DCYTB: duodenal cytochrome B; SLC48A1: solute carrier family 48, member 1; HMOX1: heme oxygenase 1; HIF2α: hypoxia inducible factor-2 alpha; IRP: iron regulatory protein; LIP: labile iron pool; FPN: ferroportin; HEPH: hephaestin. Picture modified from Muckenthaler *et al.* 2008.

As there is no controlled pathway for iron excretion, dietary iron absorption is tightly regulated via a network of transcriptional, post-transcriptional and post-translational mechanisms where the IRP system plays a key role (Figure 1.12).

Liver hepcidin, produced in response to high serum or hepatic iron, inhibits further iron absorption by promoting the degradation of the basolateral transporter ferroportin (Nemeth *et al.* 2004). Hepcidin also induces DMT1 degradation via the proteasome (Chung *et al.* 2009; Brasse-Lagnel *et al.* 2011). Both ferroportin and DMT1 are transcriptionally activated by HIF2α in iron-deficient enterocytes (Mastrogiannaki *et al.* 2009; Shah *et al.* 2009; Taylor *et al.* 2011). DMT1, ferroportin and ferritin are direct targets of the IRP regulatory system (see section 1.4.1 and 1.4.3). IRP activity, activated under iron deficiency, translationally represses ferroportin and stabilizes DMT1 mRNA (Abboud *et al.* 2000; McKie *et al.* 2000; Galy *et al.* 2008).

In addition, both ferroportin (Zhang *et al.* 2009) and DMT1 (Hubert *et al.* 2002) present mRNA isoforms lacking the IRE sequence that can therefore escape IRP regulation. However, in other reports the expression of the IRE-containing variants was found to be predominant over

the non-IRE forms in the duodenum (Canonne-Hergaux *et al.* 1999; Hubert *et al.* 2002; Darshan *et al.* 2011; Galy *et al.* 2013).
Finally, HIF2α mRNA contains a 5' UTR IRE and it is negatively regulated by IRP activity (Sanchez *et al.* 2007). The IRP system can therefore indirectly regulate DMT1 and ferroportin expression by repressing HIF2α. HIF2α function has been demonstrated to be critical for maintaining systemic iron balance since mice with specific *Hif2α* deletion in the gut epithelium show decreased serum and liver iron levels with reduced hepcidin expression (Mastrogiannaki *et al.* 2009).
The characterization of mice with global or intestinal-specific *Irp1* and *Irp2* ablation provided important information on the role or the IRP/IRE system in dietary iron absorption (Anderson *et al.* 2012; Wilkinson *et al.* 2014) (Table 1.1).
Irp1-/- mice display high level of ferroportin and Dmt1 in the duodenum, most probably as a result of Hif2α de-repression (Anderson *et al.* 2013). *Irp2*-/- mice and intestinal-specific *Irp2*-/- present mild duodenal iron overload, with increased ferritin levels but no altered ferroportin or Dmt1 expression (Galy *et al.* 2005b; Ferring-Appel *et al.* 2009). Thus Irp1, and not Irp2, appears to be the main regulator of Dmt1 and ferroportin in the duodenum.
Mice with intestinal-specific inactivation of both *Irp1* and *Irp2* dye shortly after birth due to malabsorption and dehydration (Galy *et al.* 2008) and present altered intestinal structure and mitochondriopathy showing the importance of the IRPs for intestine function and survival. At molecular level, the duodenum presented increased ferritin and ferroportin levels and reduced Dmt1 and Tfr1 expression, as expected in the absence of IRP function. Surprisingly, blood parameters revealed no signs of systemic iron deficiency; it is possible that the increase in ferroportin expression might compensate the reduced uptake.
Adult mice with duodenal-specific tamoxifen-inducible *Irp1* and *Irp2* ablation were also generated (Galy *et al.* 2013). They are viable and present normal intestine architecture, high expression of ferritin and ferroportin, reduced Tfr1 and, unexpectedly upregulation of Dmt1 expression in contrast to what observed in pups with constitutive Irp1 and Irp2 intestine-specific ablation (Galy *et al.* 2008). These data suggest that the IRP system might regulate Dmt1 expression in young mice but not in adult life. Nevertheless, these mice show defective iron absorption besides the high expression of the iron importer Dmt1 and the basolateral transported ferroportin. This phenotype was attributed to a "mucosal block" effect exerted by ferritin upregulation, sequestering iron and impeding the delivery to the bloodstream in accordance with other studies showing the importance of ferritin in iron absorption (Ferreira *et al.* 2000; Vanoaica *et al.* 2010).

1.5.3 The IRP/IRE regulatory system in liver function

The liver is the major storage site for iron and also expresses a complex range of molecules involved in the regulation of iron homeostasis. Hepatocytes are the principal site of production and secretion of the serum iron transporter transferrin, the ferroxidase ceruloplasmin and, most importantly, the systemic regulator of iron homeostasis, hepcidin (Graham *et al.* 2007; Muckenthaler *et al.* 2008). The liver also expresses molecules (HFE, TFR2, HJV, etc.) that sense changes in body iron status to adjust the synthesis of hepcidin (Figure 1.3). The liver plays therefore a central function in iron metabolism.
Mice with global or liver-specific *Irp2* deletion present hepatic iron overload with increased ferritin expression (Galy *et al.* 2005b; Ferring-Appel *et al.* 2009). On the other side, conditional inactivation of both *Irp1* and *Irp2* in hepatocytes is lethal to mice within 2 weeks after birth (Galy *et al.* 2010). These mice showed profound liver damage, internal bleeding, hepatic steatosis and apoptosis. Besides reduced level of hepatic hepcidin, there was no sign of

systemic iron dysfunction. At molecular level, hepatocytes presented a pattern of expression typical of IRP loss: augmented ferritin and ferroportin expression and reduced Tfr1 and Dmt1 levels. As a consequence of this increased iron storage and export together with reduced iron uptake, IRP-deficient hepatocytes suffer severe iron starvation; accordingly, total and mitochondrial non-heme iron content were strongly reduced compared with control mice. Mitochondria require high amount of iron for the synthesis of Fe/S clusters and heme, essential cofactors for a number of proteins including complexes of the electron transport chain and the TCA cycle. Mitochondriopathy is the major pathological feature of IRPs deficient hepatocytes; mitochondria appear swollen, with abnormal cristae structure. Mitochondrial iron deficiency correlates with reduced activity of respiratory complexes, TCA enzymes, ferrochelatase as well as the cytosolic Fe/S enzyme xanthine dehydrogenase. The defect of mitochondrial energy metabolism, secondary to iron deficiency, is presumably the cause of the hepatic failure in liver-specific Irp1 and Irp2 knockout mice (Galy *et al.* 2010).

The importance of the IRP/IRE system for liver function and viability has been further highlighted by a more recent mouse model with *Fbxl5* gene ablation (Moroishi *et al.* 2011; Ruiz *et al.* 2013). FBXL5 is involved in IRP2 (and possibly apo-IRP1) degradation and *Fbxl5* inactivation determines a secondary increase in Irp2 expression (see section 1.4.4.2). Global *Fbxl5*-/- mice die during embryogenesis, associated with iron overload and oxidative stress in the embryos. Interestingly, viability is restored by simultaneous deletion of the *Irp2*, but not *Irp1*, gene showing that Irp2 upregulation plays a major role in the lethal phenotype caused by *Fbxl5* deletion (Moroishi *et al.* 2011). Mice with liver-specific ablation of *Fbxl5* are viable but develop steatosis, oxidative stress and mitochondriopathy in hepatocytes. Increased IRP activity was associated with augmented Tfr1 levels and iron overload and these mice died with acute liver failure when fed a high-iron diet (Moroishi *et al.* 2011).

Taken together, these studies point up the importance of the IRP/IRE system in liver physiology to secure an adequate iron balance and, in particular, adequate iron supply to the mitochondria for the synthesis of heme and Fe/S proteins necessary for energy metabolism.

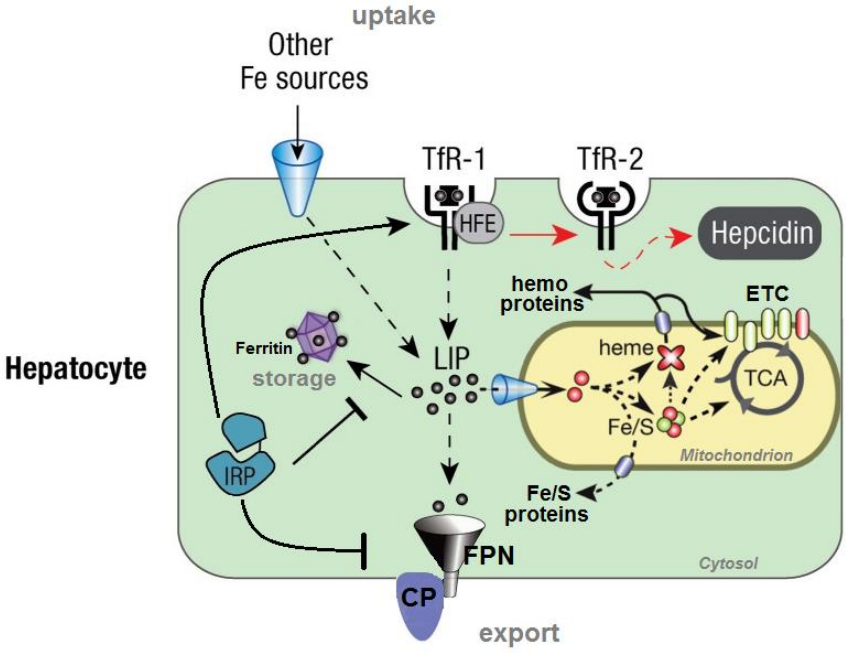

Figure 1.13 IRP/IRE regulatory system in liver function. The IRP/IRE system vitally influences liver function. By controlling cellular iron uptake, efflux, and storage, IRPs secure sufficient cytosolic iron availability for mitochondrial import and subsequent utilization for Fe/S and heme biosynthesis. ETC: electron transport chain; TCA: tricarboxylic acid cycle; Fe/S: iron sulfur cluster; FPN: ferroportin; CP: ceruloplasmin; LIP: labile iron pool; IRP: iron regulatory protein; TFR1: transferrin receptor 1; TFR2: transferrin receptor 2. Picture modified from Muckenthaler *et al.* 2008 and Galy *et al.* 2010.

1.5.4 The IRP/IRE regulatory system in erythropoiesis

An adult human produces about 2 millions red blood cells (RBC) per second; thus the bone marrow daily needs big amount of iron to sustain heme synthesis (Muckenthaler *et al.* 2008). To ensure an efficient supply of iron to the bone marrow, iron metabolism and erythropoietic activity are coordinated by regulatory loops where the IRP/IRE system is involved at different points.

As discussed in section 1.2.2, an increased erythropoietic activity stimulates iron absorption via suppression of hepcidin production and consequent upregulation of intestinal iron uptake and release from reticulo-endothelial macrophages (Figure 1.14).

The maturation of erythroid cells is stimulated by the hormone erythropoietin. EPO is produced by the kidney and to a smaller extent in the liver and it is transcriptionally activated during hypoxia (Franke *et al.* 2013). EPO transcription is mainly regulated by the hypoxia inducible factor-2 alpha. In normoxia, HIF2α is hidroxylated by the action of prolyl-hydroxilases (PHD, iron-dependent enzymes) and degraded by the proteasome. In hypoxic or low iron conditions, PDH activity is reduced, which turns into HIF2α stabilization, translocation to the nucleus, heterodimerization with the constitutively expressed HIF1β and activation of the EPO promoter (Franke *et al.* 2013) (Figure 1.14). As a result, erythroid proliferation and maturation is promoted to increase blood oxygen binding capacity in response to low oxygen tension. Besides being regulated by oxygen levels, HIF2α carries a 5' UTR IRE and it is controlled by the IRPs (Sanchez *et al.* 2007). IRP activation under in iron deficiency can therefore reduce HIF2α and, consequently, EPO levels (Figure 1.14). IRP control can limit RBC production when iron availability is low to avoid the generation of hypocromic microcytic erythrocytes. The characterization of Irp1-/- mice has demonstrated that IRP1 and not IRP2 controls HIF2α translation; Irp1-/- mice display typical signs of HIF2α activation: increased EPO production which leads to polycythemia and splenomegaly due to extramedullar erythropoiesis (Anderson *et al.* 2013; Ghosh *et al.* 2013; Wilkinson *et al.* 2013) (see section 1.5.1 and Table 1.1). Nevertheless, the phenotype of *Irp2*-/- mice, which present hypochromic microcytic anemia (Cooperman *et al.* 2005; Galy *et al.* 2005b) underlines that IRP2 has also an important role but probably in other aspects of erythropoiesis. However, when Irp2 deficiency is limited to hepatocytes, enterocytes or macrophages, mice do not develop hematological defects (Ferring-Appel *et al.* 2009) indicating the microcytic anemia of *Irp2*-/- mice is likely due to a local defect in RBC precursors.

Developing RBCs are strongly dependent on transferrin-bound iron uptake to sustain heme synthesis. The importance of the TF-TFR1 cycle is highlighted by mouse models with transferrin (Trenor *et al.* 2000) or Tfr1 deficiency (Levy *et al.* 1999). Hypotransferrinemic mice suffer severe hypochromic microcytic anemia and parenchymal iron overload indicating that non-erythroid organs can uptake iron via alternative pathways, while RBCs are more dependent on transferrin-bound iron. DMT1 is involved in the transfer of iron from the endocytic vesicles to the cytoplasm and Dmt1 mutant mice also display impaired iron uptake in RBC precursors (Fleming *et al.* 1998). TFR1 and DMT1 are both IRPs target and are stabilized by IRPs binding via 3' UTR IREs. Consistently, the erythrocytes of *Irp2*-/- mice show decreased Tfr1 expression as well as high ferritin levels in the bone marrow (Cooperman *et al.* 2005; Galy *et al.* 2005b) indicating an insufficient iron uptake. *Irp2*-/- mice also present erythropoietic protoporphyria (Cooperman *et al.* 2005) due to de-repression of Alas2, augmented heme biosynthesis in the absence of adequate iron supply which results in the accumulation of toxic protoporphyrin IX (Figure 1.14). Taken together these data indicate that IRP2 acts as the major regulator of TFR1 and ALAS2 mRNA in RBCs. However, the anemia of *Irp2*-/- mice is more severe when also one allele of *Irp1* gene is inactivated (Smith *et al.*

2004) and Irp1 activation secondary to Fe/S biogenesis defect was demonstrated to cause Alas2 repression and anemia in human patients and in a zebrafish model of sideroblastic anemia (Wingert *et al.* 2005; Camaschella *et al.* 2007; Ye *et al.* 2010) indicating that IRP1 is also involved in the control of erythroid TFR1 and ALAS2 (see section 1.6.5.3 and Figure 1.14).

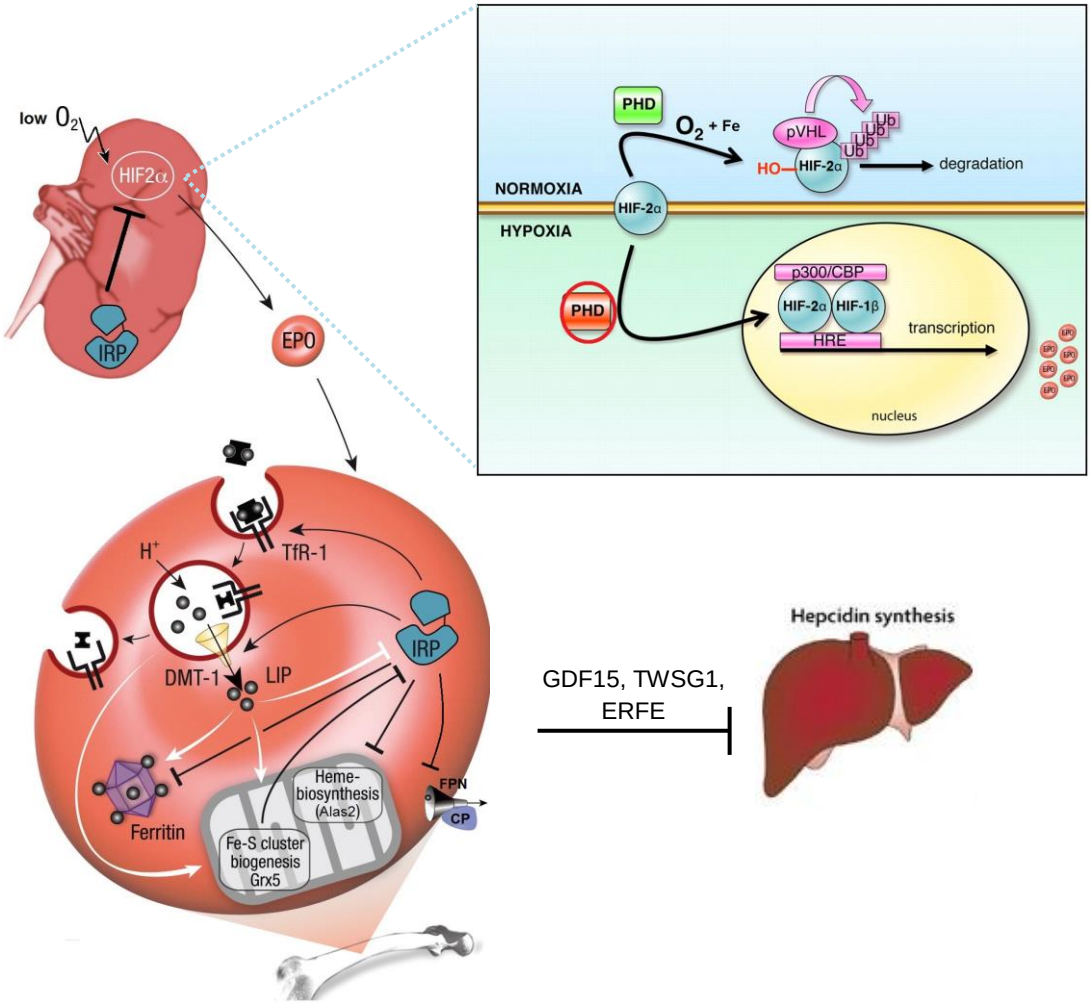

Figure 1.14 The IRP/IRE regulatory system in erythropoiesis. The IRP system influences bone marrow erythropoiesis by controlling the expression of HIF2 that transcriptionally activates the production of the erythropoietin hormone in the kidney. IRPs also coordinate TFR1, ferritin, DMT1 and FPN expression in developing erythroblasts to guarantee adequate iron supply for hemoglobin production. HIF2α: hypoxia inducible factor-2 alpha; EPO: erythropoietin; PHD: prolyl-hydroxilases; pVHL: von Hippel-Lindau E3 ubiquitin ligase; HRE: hypoxia responsive element; IRP: iron regulatory protein; LIP: labile iron pool; GDF15: growth differentiation factor 15; ERFE: erythroferrone; TWSG1: twisted gastrulation protein homolog 1; Grx5: glutaredoxin 5; ALAS2: erythroid-specific delta aminolevulinate synthase; DMT1: divalent metal ion transporter; TFR1: transferrin receptor 1; FPN: ferroportin; CP: ceruloplasmin. Picture modified from Muckenthaler *et al.* 2008 and Balligand *et al.* 2009.

Finally, the iron exporter ferroportin is also expressed in erythrocytes (Zhang *et al.* 2009) and it is regulated by the IRPs via its 5' IRE (Abboud *et al.* 2000) as well as subjected to hepcidin-mediated degradation (Zhang *et al.* 2011). Interestingly, in erythrocytes and enterocytes alternative splicing produces a ferroportin isoform lacking the IRE that can bypass IRP control. FPN1B, the isoform that does not contain the IRE, is preferentially expressed in early stages of erythroid differentiation (Zhang *et al.* 2009) possibly representing a feedback mechanism to avoid toxic iron accumulation when the rate of iron uptake exceed mitochondrial utilization. During terminal differentiation stages, when the request of iron for heme synthesis is unusually high, the IRE variant FPN1A is the predominant FPN mRNA (Zhang *et al.* 2009) and it is expected to be repressed by the IRP activity to limit iron export.

In maturing erythroblasts, the IRP system has a vital function coordinating the synthesis of ferritin, TFR1, ALAS2 and ferroportin to guarantee efficient production of hemoglobin. However, a study on primary murine erythroid progenitors has demonstrated that during terminal differentiation the expression of IRE-containing mRNA escape IRP control: the coordinated ferritin and Alas2 expression is uncoupled and high Tfr1 mRNA levels persist even in the presence of high iron (Schranzhofer *et al.* 2006). To explain this unexpected findings, the authors suggested that in maturing erythroblasts massive mRNA transcription may lead to an excess of IRE sites over available IRP molecules (Schranzhofer *et al.* 2006).

1.6 The IRP/IRE network in human disease

To date there are no reports of mutations directly affecting IRP1 or IRP2 genes responsible for pathological conditions; however, several human diseases have been linked to a disturbed IRP/IRE regulation (Table 1.2).

1.6.1 Hereditary Hyperferritinemia-Cataract Syndrome (HHCS)

Hereditary Hyperferritinemia-Cataract Syndrome (OMIM #600886) was first described in 1995 as an autosomal dominant disease characterized by a combination of high serum ferritin levels with early-onset bilateral cataract and the absence of iron overload (Beaumont *et al.* 1995; Bonneau *et al.* 1995; Girelli *et al.* 1995). HHCS is due to mutations in the IRE of L-ferritin subunit that impair IRP interaction leading to an uncontrolled synthesis of the L-ferritin subunit that deposits in the lens and cause cataracts formation. HHCS is inherited as an autosomal dominant trait in all reported families and few cases have been described with *de novo* mutations (Arosio *et al.* 1999; McLeod *et al.* 2002; Craig *et al.* 2003; Hetet *et al.* 2003; Hernandez Martin *et al.* 2008; Cao *et al.* 2010; Munoz-Munoz *et al.* 2013). Homozygous mutations are very unusual in HHCS (Alvarez-Coca-Gonzalez *et al.* 2010; Giansily-Blaizot *et al.* 2013; Luscieti *et al.* 2013).

To date, 37 different mutations affecting FTL IRE have been described; they include point mutations and deletions of different size (Luscieti *et al.* 2013) (Figure 1.15).

HHCS patients have a marked phenotypic variability with regard to ocular involvement, serum ferritin levels and the age of onset of the cataract. This is related to the different impact of each mutation on IRP binding: mutations affecting the most important IRE structural motifs, such as the hexanucleotide loop or the C-bulge area, are detected in patients with more elevated serum ferritin levels compared to those patients with mutations affecting the base pairing of the upper or lower stem of the IRE (Allerson *et al.* 1999). However, even between relatives sharing the same mutations, differences in the phenotype may exist, suggesting that other genetic or environmental factors may play a role in the development of clinical symptoms (Girelli *et al.* 2001). The geographical distribution of HHCS patients is worldwide; global prevalence of the disease has not been clearly defined; however, it has been estimated to be 1 in 200000 in the Australian population (Craig *et al.* 2003). Cataracts appearance early in age is the only clinical feature of this disease and is treated by surgery. Thus, HHCS is not a life-threatening disease; however, differential diagnosis with the iron overload Hereditary Hemochromatosis (HH) is of great importance in the clinical practice. Both diseases share high levels of serum ferritin as biochemical hallmark; because of this, some HHCS patient can be misdiagnosed and subjected to unnecessary liver biopsies and/or repeated phlebotomies that are contraindicated in the treatment of HHCS.

I have contributed to the identification of two new mutations in the L-ferritin IRE in two families with HHCS. In our publication we also study the functional consequences of these mutations (see Results and Discussion 3.1 and Luscieti *et al.* 2013).

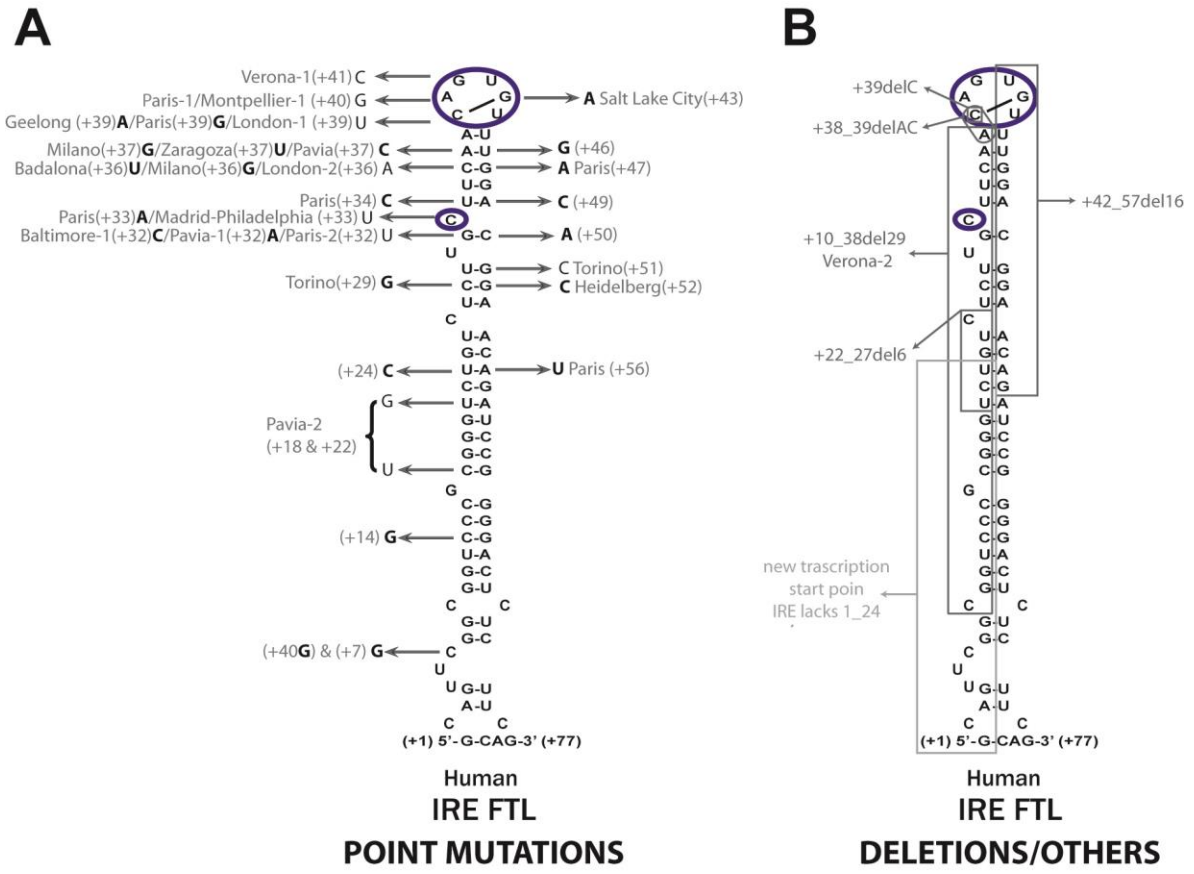

Figure 1.15 HHCS mutations. In the picture is represented the structure of the IRE of human FTL: reported point mutations **(A)** and deletions **(B)** causative of HHCS are indicated. Location of the mutations is based on NM_000146.3 GenBank reference sequence. Picture modified from Luscieti et al. 2013. .

1.6.2 Autosomal dominant iron overload syndrome

An autosomal dominant iron overload syndrome (OMIM #615517) has been described in only one Japanese family (Kato *et al.* 2001). The affected subject presented high serum ferritin levels, increased transferrin saturation and iron deposits in the liver and bone marrow. An heterozygous point mutation in the IRE of H-ferritin (NM_002032.2; c.[-164A>T];[=]) (Figure 1.16) was found to segregate with the symptoms of the disease in this family. Opposite to L-ferritin IRE mutations, electrophoretic mobility shift assay (EMSA) analysis revealed that the mutated IRE had a higher binding affinity to the IRPs compared to wild-type FTH1 IRE. H-ferritin expression was found to be reduced in the liver of the patient, consistent with a strong translational repression via IRPs, while L-ferritin levels were increased. Expression of FTH1 carrying the mutated IRE in COS-1 cells showed lower iron incorporation within ferritin despite an increased total cellular iron uptake. This results are consistent with a mouse model knockout for Fth1 gene that showed early embryonic lethality due to massive iron deposition (Ferreira *et al.* 2000) and suggested that the decrease in H-subunit not only impaired iron uptake into the ferritin molecule but also caused iron accumulation in the cytosol, possibly due to the decrease in ferroxidase activity. However, this report remains the only described case of a mutation affecting the IRE of the H-ferritin subunit and in a larger study of subjects with abnormally high serum ferritin and iron levels FTH1 IRE pathologic mutations were not found (Cremonesi *et al.* 2003a).

1.6.3 Mutations in ferroportin IRE

A mutation close to the 5' IRE of ferroportin gene was reported in a Japanese patient presenting with typical phenotypic pattern of Hereditary Hemochromatosis (HH): iron overload in liver and spleen, chronic hepatitis, impaired glucose tolerance, and skin pigmentation with high serum iron levels, serum ferritin and transferrin saturation (Liu *et al.* 2005). The mutation in FPN 5' UTR (NM_014585.5; c.[-188A>G];[=]) is present in heterozygous state in the patient but absent in the patient's healthy children, suggesting an autosomal dominant pattern of inheritance compatible with Hereditary Hemochromatosis type 4. No mutations were identified in any of the classical HH causative genes. Nevertheless a new gene (*BMP6*) has been recently identified as a cause of dominant HH (Daher *et al.* 2015) and this gene was not studied in that family.

The change described by Liu *et al.* is located seven nucleotides downstream FPN IRE and may affect IRP recognition (Figure 1.16); however, this was not experimentally demonstrated. An irradiation-induced mouse model, with a microdeletion in ferroportin promoter region, altering the transcription start site and eliminating the IRE has been described (Mok *et al.* 2004). Heterozygous mice present erythropoietin-dependent polycythemia while homozygous mice show hypochromic microcytic anemia.

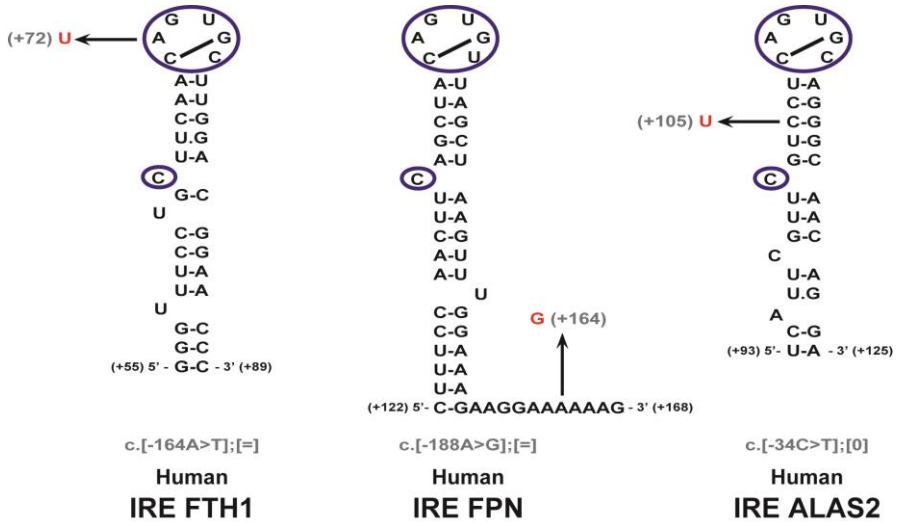

Figure 1.16 Other IREs described mutations. The IRE structures present in the 5' UTR of FTH1, FPN and ALAS2 mRNAs are represented. Arrows indicate the nucleotide changes reported in literature cases (Kato *et al.* 2001; Liu *et al.* 2005; Lee *et al.* 2009). Nucleotide position is based on the following GenBank reference sequences: NM_002032.2 (FTH1), NM_ 014585.5 (FPN) and NM_000032.4 (ALAS2).

1.6.4 Mutation in ALAS2 IRE

ALAS2 gene is located on the X-chromosome and encodes for the first a rate-limiting enzyme of heme biosynthetic pathway (see section 1.3.2). ALAS2 mutations cause 2 different disease: X-linked Sideroblastic Anemia (XLSA) and X-linked Erythropoietic Protoporphyria (XLEPP). XLSA is caused by loss-of-function mutations located in the coding region or promoter region that result in diminished enzyme activity leading to reduced protoporphyrin IX synthesis, accumulation of iron, and insufficient hemoglobin levels. These patients clinically present with moderate to severe sideroblastic anemia, and iron overload secondary to chronic ineffective erythropoiesis (OMIM #300751).

On the other hand, gain-of-function mutations of ALAS2, located in the C-terminal part of the protein, are causative of Erythropoietic Protoporphyria (OMIM #300752) characterized by severe photosensitivity associated with decreased iron stores.

A patient with a point mutation in the IRE of ALAS2 has been described by Lee and collaborators (Lee *et al.* 2009). The patient is a 55 years old man with a history of chronic hepatitis C infection and presented with typical Hemochromatosis symptoms: hepatic cirrhosis, cardiomyopathy, arrhythmia, hypogonadism, diabetes and bronzed skin color. However, no mutations were found in the classical genes associated with of HH (here *BMP6* was also not tested) and there was no family history of Hemochromatosis. The patient carries an hemizygous point mutation located in the upper stem of ALAS2 IRE (NM_000032.4; c.[-34C>T];[0]) (Figure 1.16). Gel retardation assays showed that the mutated IRE exhibits slightly lower affinity to the IRPs compared to wild type IRE. The authors predicted that this would result in disregulated levels of ALAS2 expression, possibly with increased heme production. High levels of ALAS2 or heme might cause a more rapid progression from proliferating erythroid precursors to terminal differentiation driving increased erythropoiesis and iron uptake. Since a healthy brother of the proband was hemizygous for the ALAS2 IRE mutation but negative for hepatitis C infection, it is presumable that this alteration in ALAS2 IRE alone does not lead to the iron overload phenotype but may be important when associated with additional risk factors such as hepatitis C infection.
I have contributed to the identification of a new mutation in ALAS2 IRE in a patient with Erythropoietic Protoporphyria (see Results and Discussion 3.2).

1.6.5 IRPs deregulation upon Fe/S cluster defects

As mentioned in section 1.4.2, IRP1 is a bifunctional protein and its activity as aconitase depends on the assembly of a cubane Fe/S cluster in the catalytic site. Fe/S cluster formation and assembly is therefore critical for the regulation of IRP1 activity.
Genetic defects that impair components of the mitochondrial pathway for Fe/S cluster synthesis result in a decreased activity of mitochondrial and cytoplasmic Fe/S proteins and mitochondrial iron accumulation (Sheftel *et al.* 2010a). As a consequence of this reduced availability of Fe/S cluster, IRP1 is constitutively activated as an IRE binding protein leading to a pathogenic deregulation of cellular iron homeostasis (Table 1.2).

1.6.5.1 Friedreich's ataxia (FRDA)

Freidreich’s ataxia (OMIM #229300) is a neurodegenerative disease characterized by spinocerebellar ataxia, hypertrophic cardiomyopathy and increased incidence of diabetes (Parkinson *et al.* 2013). It is an autosomic recessive disorder (prevalence 1 in 50000) with onset in the late infancy or preadolescent age. The evolution of the pathology leads to a progressive loss of movement coordination and, in a variable time lapse of 10-15 years, FRDA patients need to use a wheelchair and to be assisted in daily activities. Communicative ability is also compromised while cognitive skills are intact. Cardiomyopathy is present in 75% of patient and leads to premature death due to heart failure or arrhythmia (Puccio *et al.* 2002). FRDA is commonly caused (in 95-98% of the cases) by a homozygous GAA triplet expansion in the first intron of frataxin gene (*FXN*). This expansion causes a reduction of FXN mRNA synthesis and, consequently, of FXN protein in the mitochondria. The number of GAA repetitions vary from 100 to more than 1000 in FRDA patients while healthy individuals carry less than 35 repetitions. It has been described a correlation between the number of repetitions and the severity and age of onset of the disease (Patel *et al.* 2001).
Although the exact physiological function of frataxin is not known, different experimental evidences have suggested its involvement in Fe/S cluster biogenesis, iron binding-sequestration and response to oxidative stress (Puccio *et al.* 2002). FXN has been demonstrated to be able to oligomerize and bind iron working as an iron-storage protein in the

mitochondria and as a chaperone in Fe/S biogenesis (Cavadini *et al.* 2002). In yeast, deletion of the homologous gene of FXN, Yfh1, impairs the activity of Fe/S enzymes, causes mitochondrial DNA damage, mitochondrial iron accumulation and increased sensitivity to oxidative stress (Muhlenhoff *et al.* 2002). Silencing of human *FXN* in HeLa cells results in a similar phenotype with reduction of growth, inhibition of aconitase activity, reduction of cytosolic iron content and ferritin levels without alteration of mitochondrial iron content (Zanella *et al.* 2008). Lymphoblasts and fibroblasts of FRDA patients have also evidence of cytosolic iron depletion and iron loading within the mitochondria (Li *et al.* 2008).

In this scenario of Fe/S cluster reduced availability, IRP1 is converted to its IRE-binding form. Moreover, the cytosolic iron deficiency stabilizes IRP2 protein, further contributing to IRE-binding activity (Li *et al.* 2008). IRPs activation promotes cellular iron uptake by stabilizing TFR1; iron trafficked to the mitochondria cannot be used for Fe/S cluster synthesis because of FXN deficiency and thus creating a pathological vicious cycle.

Global *Fxn* gene deletion in mice leads to early embryonic lethality, while models of conditional deletion in striated muscles or neuro/cardiac muscle tissues reproduced the symptoms and signs of FRDA patients such as cardiac hypertrophy, sensory neurons dysfunction, decreased activity of Fe/S cluster containing enzymes and iron accumulation in the mitochondria (Puccio *et al.* 2001).

1.6.5.2 Sideroblastic anemia with spinocerebellar ataxia (ASAT)

Sideroblastic anemia with spinocerebellar ataxia is another disease affecting the Fe/s cluster pathway. ASAT (OMIM #301310) is a very rare disease (only 5 affected families have been described worldwide) with a recessive X-linked transmission pattern. Hemizygous affected males present with spinocerebellar ataxia evident from early infancy accompanied by severe cerebellar hypoplasia. The ataxia has been described to be either non-progressive or slowly progressive. Hyperreflexia and mild learning disability is also present in these patients (Bekri *et al.* 1993). In addition, ASAT patients present a mild anemia independent of transfusions. The anemia is characterized by hypochromic, microcytic erythrocytes with high levels of free protoporphyrin IX and a characteristic iron accumulation in bone marrow erythroblasts (ringed sideroblasts). Heterozygous females develop only the hematological signs of the disease but do not show neurological involvement. ASAT is caused by missense mutations in *ABCB7* gene; this gene encodes for a transporter belonging to the family of ATP-binding cassette (ABC) transporters and is located in the inner mitochondrial membrane where is involved in Fe/S clusters export from the mitochondria to the cytosol (see section 1.3.2). ABCB7 is highly expressed in bone marrow as well as in the cerebellum.

Yeast mutant deleted of the *ABCB7* homologous gene, *Atm1*, shows reduced activity of Fe/S cluster enzymes, iron accumulation in the mitochondria and increased oxidative stress (Kispal *et al.* 1997). Similarly, silencing of the human *ABCB7* in HeLa cells produced an important iron accumulation in the mitochondria of these cells and showed reduced proliferation, impairment of aconitase activity, induction of TFR1 and reduced ferritin levels due to an increased IRP1 RNA binding activity, while the activity of mitochondrial Fe/S proteins was not affected (Cavadini *et al.* 2007).

In mice, knockout of *Abcb7* gene is lethal at embryonic stage as it is the conditional deletion of this gene in different tissues. The only viable *Abcb7* knockout was obtained in liver (Pondarre *et al.* 2006) indicating a minor role of ABCB7 in this organ or the existence of redundant mechanisms. Liver *Abcb7* knockout mice showed iron deposition in periportal hepatocytes but this iron is not stored in the mitochondrial compartment. The activity of mitochondrial Fe/S enzymes was only marginally altered, whereas the activity of cytosolic Fe/S proteins was

strongly reduced including cytosolic aconitase with consequent augment of IRP1 mRNA binding, overexpression of TFR1 but also mild increase in ferritin content. However, parallel to an increased IRP1 binding activity, IRP1 protein levels were reduced suggesting an iron-dependent, cluster-independent mechanism of regulating IRP1 protein. IRP2 binding activity and protein levels were upregulated in the liver of *Abcb7* knockout mice. Alteration of ABCB7 function leads therefore to a loss of cellular iron homeostasis similar to what observed for FXN deficiency.

1.6.5.3 Sideroblastic anemia due to GLRX5 defect

GLRX5 is a protein with redox activity involved in the biogenesis of Fe/S clusters. The yeast mutant deleted for *Grx5* gene presents defects of Fe/S cluster enzymes, iron accumulation and signs of oxidative stress, common phenotypes to impaired Fe/S cluster biogenesis (Rodriguez-Manzaneque *et al.* 2002).

A zebrafish mutant lacking Glrx5 expression, called *"shiraz"*, presents hypochromic anemia lethal at 7-10 days after fertilization (Wingert *et al.* 2005). In the *shiraz* mutant, it has been demonstrated that the defect of Fe/S cluster pathway activates mRNA binding activity of IRP1. The hypochromic anemia observed in the animal, could be therefore explained by an impaired heme synthesis due to ALAS2 translational block as a result of IRP1 binding to the 5' UTR IRE in ALAS2 mRNA. Expression of an ALAS2 mRNA lacking the IRE sequence in the *shiraz* mutant leads to a complete rescue of the phenotype, this rescue is not possible if an ALAS2 mRNA containing the IRE is expressed.

A patient with hypochromic microcytic anemia due to a quantitative GLRX5 defect was described by Camaschella and collaborators (Camaschella *et al.* 2007) (OMIM #205950); the patient presented with mild anemia, hepatosplenomegaly, low number of ringed sideroblasts and iron overload. Surprisingly, the anemia was worsened by blood transfusions but improved with iron chelation. Sequencing analysis identified an homozygous change in exon 1 of *GLRX5* gene (NM_016417.2; c.[294A>G];[294A>G]); this substitution does not alter the amino acid sequence but, being located at the edge of the exon1, interferes with the correct splicing and leads to low levels of GRLX5 expression. Similarly to the *shiraz* phenotype, lymphoblastoid cell lines derived from the patient and compared to cell lines obtained from control subjects showed a higher iron incorporation, reduced aconitase activity, increased TFR1 and reduced ferritin content, compatible with the observed increase in IRP1 binding activity. Less IRP2 degradation was hypothesized to occur in the patient because of low-heme content, further contributing to the IRP activity. This might explain the reason why, surprisingly, iron chelation improve patient's anemia. Chelation therapy will redistribute iron to the cytosol, which might decrease IRP2 excess, improving heme synthesis.

GLRX5 is highly expressed in early erythroid precursors of the bone marrow. *GLRX5* knockdown in the erythroid K562 cell line showed IRP1 activation as mRNA binding protein and increased IRP2 levels as a consequence of cytosolic iron depletion. Decreased ALAS2 levels, attributable to IRP-mediated translational repression, were observed together with a marked reduction in ferrochelatase levels (Ye *et al.* 2010). Interestingly, the expression of the iron exporter ferroportin was increased in cells derived from the affected patient, perhaps contributing to the iron deficiency observed in the cytosol of patient's cells (Ye *et al.* 2010). Erythroblasts express both high levels of IRP-repressible ALAS2 and non-IRP-repressible ferroportin 1b (Cianetti *et al.* 2005); this unique combination of IRP-targets likely accounts for the tissue-specific phenotype of human GLRX5 deficiency. The discovery of this disease established a previously unknown connection between heme biosynthesis and Fe/S cluster biogenesis. Recently a second case of GLRX5 defect has been described. A Chinese patient

affected by sideroblastic anemia was found to be compound heterozygous for 2 missense mutations in the *GLRX5* gene (Liu *et al.* 2013).

In addition, 3 patients presenting with a mitochondrial dysfunction syndrome and characterized by normal development with childhood-onset spastic paraplegia, spinal lesion, and optic atrophy were shown to be carrier of a single in-frame amino acid deletion in *GRLX5* exon1 (Baker *et al.* 2014). GLRX5 protein levels were shown to be unchanged but *in silico* predictions showed that the mutation might affect the binding with the Fe/S cluster at GLRX5 active site. Patients were deficient in lipoylation of mitochondrial proteins but cellular iron metabolism, and respiratory chain activity were unaffected.

1.6.5.4 Hereditary myopathy with lactic acidosis (HML) and others mitochondrial diseases

Hereditary myopathy with lactic acidosis (HML) (OMIM #255125) is a rare autosomal recessive muscular disorder found in different families of northern Swedish descent. It is characterized by exercise intolerance with muscle tenderness, cramping, dyspnea, and palpitations. Biochemical features include lactic acidosis and, rarely, rhabdomyolysis. The disease appears in childhood and has a chronic course with exacerbations and remissions. HML is caused by intronic mutations in *ISCU* gene inducing aberrant mRNA splicing and reduced levels of functional protein (Mochel *et al.* 2008; Olsson *et al.* 2008). ISCU aberrant splicing occurs specifically in the skeletal muscle, while mRNA is normally processed in other tissues. The expression of the muscle-specific MyoD1 transcription factor has been linked to this altered splicing, explaining the tissue specific pattern of the disease (Crooks *et al.* 2012). ISCU is as scaffold protein assisting Fe/S cluster formation in the mitochondrion. ISCU deficiency impairs Fe/S cluster synthesis and leads to decreased activity of mitochondrial and cytosolic Fe/S cluster proteins and abnormal IRP activation, as described before for FRDA and ASAT patients.

A distinct case of an adolescent onset, autosomal recessive mitochondrial myopathy, associated with recurrent episodes of myoglobinuria and lactic acidosis has been described by Spiegel and collaborators (Spiegel *et al.* 2013). Genetic study identified an homozygous mutation in *FDX2* gene coding for Fe/S cluster biogenesis protein ferredoxin. The mutation disrupts the ATG initiation site of translation resulting in severe reduction of FDX2 content in the patients' muscles and fibroblasts mitochondria together with reduced activity of Fe/S cluster enzymes.

Recessive mutations affecting the cysteine desulfurase *NFS1* (Farhan *et al.* 2014) or the cysteine desulfurase associated protein *ISD11* (Lim *et al.* 2013) are also causative of mitochondrial disorders with defects of Fe/S cluster enzymes.

A rare mitochondrial disorder characterized by lactic acidemia, hypotonia, respiratory chain complex II and III deficiency, multisystem organ failure, and abnormal mitochondria was reported to affect three related children of a Mennonite community (Farhan *et al.* 2014). Exome sequencing identified an homozygous missense mutation in *NFS1* gene and NFS1 transcript and protein levels were markedly reduced in the patients' tissues.

Massively parallel sequencing of mitochondrial genes identified an homozygous mutation in *ISD11* gene in a patient with deficiency of complexes I, II and III in muscle and liver (Lim *et al.* 2013). The same mutation was found in a more severely affected cousin who presented an important lactic acidosis and died short after birth. *In vitro* studies showed that the mutated ISD11 was unable to complement ISD11 deletion in yeast consistent with a defect in the early step of Fe/S cluster biogenesis.

IRP activity studies have not been realized in the reported patients with *FDX2*, *NFS1* and *ISD11* mutations. However, being those proteins implicated in early steps of the Fe/S cluster biosynthesis, IRP1 and IRP2 IRE-binding activities are expected to be increased similarly to what is observed for *FXN*, *ABCB7*, *GLRX5* and *ISCU* mutations.
Additional mitochondrial dysfunction syndromes are caused by mutations affecting other Fe/S cluster assembly-associated proteins: the scaffold protein NFU1 (Seyda *et al.* 2001; Cameron *et al.* 2011; Navarro-Sastre *et al.* 2011), the reductase BOLA3 (Cameron *et al.* 2011; Haack *et al.* 2013) and IBA57 (Ajit Bolar *et al.* 2013). However, *in vitro* and patients' studies showed that these proteins are involved in late steps of Fe/S cluster maturation, mainly affecting respiratory complexes and lipoate-containing enzymes but not cytosolic Fe/S cluster proteins and therefore not altering IRP activity and iron homeostasis (Cameron *et al.* 2011; Navarro-Sastre *et al.* 2011; Sheftel *et al.* 2012; Baker *et al.* 2014).

Table 1.2 Human disorders causatively linked to defects of the IRP/IRE system.

Human disease	Gene	Phenotype	Inheritance	OMIM	Reference
Hereditary Hyperferritinemia-Cataract Syndrome (HHCS)	*FTL*: point mutations and deletions in the IRE that impair IRP binding	Elevated serum ferritin in the absence of iron overload or inflammation. Tendency to the development of bilateral cataract in early age	AD	#600886	(Beaumont *et al.* 1995; Bonneau *et al.* 1995; Girelli *et al.* 1995); other papers reported several other mutations
Autosomal dominant iron overload syndrome	*FTH1*: point mutation in the IRE that increases IRP binding	Reduction of FTH1 expression leading to an iron overload syndrome similar to Hereditary Hemochromatosis	AD	#615517	(Kato *et al.* 2001)
Hemochromatosis with mutation of ferroportin gene	*FPN*: point mutation located 7 nucleotides downstream the IRE, not demonstrated effect on IRP binding	Phenotype similar to Hereditary Hemochromatosis	AD?	-	(Liu *et al.* 2005)
Severe iron overload syndrome	*ALAS2*: hemizygous point mutation in the IRE that slightly impairs IRP binding	Severe Hemochromatosis phenotype in the presence of hepatitis C infection	iron overload risk factor	-	(Lee *et al.* 2009)
Friedreich's ataxia (FRDA)	*FXN*: GAA triplet expansion (in 97% of the cases) or point mutations leading to FXN deficiency and Fe/S cluster biogenesis defect	Spinocerebellar ataxia with cardiomyopathy	AR	#229300	(Campuzano *et al.* 1996; Delatycki *et al.* 1999)
Sideroblastic anemia and spinocerebellar ataxia (ASAT)	*ABCB7*: missense mutations	Spinocerebellar ataxia and mild sideroblastic anemia	XR	#301310	(Allikmets *et al.* 1999)
Autosomal recessive pyridoxine-refractory sideroblastic anemia	*GLRX5*: point mutation affecting splicing and leading to GLRX5 deficiency and Fe/S cluster biogenesis defect	Sideroblastic anemia with hepatosplenomegaly and iron overload	AR	#205950	(Camaschella *et al.* 2007; Liu *et al.* 2013)
Hereditary myopathy with lactic acidosis (HML)	*ISCU*: missense mutation altering mRNA splicing resulting in reduced levels of ISCU protein and Fe/S cluster biogenesis defect	Myopathy with lactic acidosis characterized by childhood onset of exercise intolerance with muscle tenderness, cramping, dyspnea, and palpitations	AR	#255125	(Mochel *et al.* 2008)
Mitochondrial myopathy	*FDX2*: point mutation disrupting the ATG initiation translation site resulting in severe reduction of FDX2 and Fe/S cluster biogenesis defect	Depleted skeletal muscle energy production manifesting by recurrent episodes of myoglobinuria or progressive muscle weakness	AR	-	(Spiegel *et al.* 2014)
Infantile mitochondrial complex II/III deficiency	*NFS1*: missense mutation	Mitochondrial complex II/III deficiency, lactic acidemia, hypotonia, multisystem organ failure and abnormal mitochondria	AR	-	(Farhan *et al.* 2014)
Combined oxidative phosphorylation deficiency 19 (COXPD19)	*ISD11*: missense mutation close to exon-intron boundary probably leading to ISD11 deficiency and Fe/S cluster biogenesis defect	Respiratory distress, hypotonia, and severe lactic acidosis in the newborn period. Combined oxidative phosphorylation deficiency, including complexes I, II, III and Fe/S-containing proteins	AR	#615595	(Lim *et al.* 2013)

1.6.6 Other pathological implications of the IRPs

Genome-wide association studies (GWAS) have associated IRP2 single nucleotide polymorphisms (SNPs) with Alzheimer's disease (AD) (Coon *et al.* 2006); however, these findings need to be confirmed in a larger population and the functional significance of these SNPs needs to be clarified. A role for altered iron metabolism in the pathogenesis of Alzheimer's disease has been suggested by several reports. Brain regions exhibiting extensive senile plaque lesions show iron accumulation; iron is thought to be involved in the generation of an excess of reactive radical species, leading to the observed cell and tissue damage (Lovell *et al.* 1998). However, it is still not clear if iron accumulation is a cause or a consequence of the disease. Interestingly, histological analysis of brains from AD patients showed altered distribution of IRP2, which co-localizes with the AD pathologic hallmarks: the intracellular neurofribillary tangles of hyperphosphorylated Tau protein and senile plaques composed of extracellular deposits of beta-amyloid peptides. In addition, an mRNA motif able to bind *in vitro* to IRP1 has been identified in the mRNA of the amyloid precursor protein (APP) (Rogers *et al.* 2002). APP processing is aberrant in AD patients giving rise to beta-amyloid peptides that accumulate in senile plaques. Moreover, APP has been shown to acts as a neuronal ferroxidase, contributing to iron export together with FPN and inhibition of APP ferroxidase activity results in neuronal iron accumulation (Duce *et al.* 2010).

More recent GWAS showed association between IRP2 polymorphisms and susceptibility to chronic obstructive pulmonary disease (COPD) (DeMeo *et al.* 2009; Chappell *et al.* 2011); IRP2 expression was altered in the lungs of COPD patients and was hypothesized to contribute to iron accumulation in the lungs of these patients.

IRP1 binding activity was found to be increased in Parkinson's disease (Faucheux *et al.* 2002) and polymorphisms of both IRP1 and IRP2 have been linked to age-related macular degeneration (Synowiec *et al.* 2012).

IRPs have been also involved in cancer biology. In nude mice, tumor xenografts overxpressing IRP1 showed a suppression of tumors growth (Chen *et al.* 2007). Intriguingly, IRP2 overexpression had tumorigenic properties that were attributed to the IRP2 specific 73 amino acid domain (Maffettone *et al.* 2010). In both cases, TFR1 and ferritins levels were similarly regulated; however, IRP1 or IRP2 overexpressing xenografts showed different gene-expression profiles suggesting that the opposite effect exerted on tumors growth could be due to IRP1 or IRP2 specific regulation of a different subset of genes. IRP1 polymorphisms have been associated with cutaneous malignant melanoma (Yang *et al.* 2010) and IRP2 gene is located within a lung cancer associated locus (Hansen *et al.* 2010; Fehringer *et al.* 2012).

1.7 Expanding the IRP regulon

In the last decade, several studies evidenced that the IRP/IRE regulatory network is wider than previously thought. Apart from previously described and widely studied IREs found in the mRNAs of TFR1, FTH1, FTL, FPN, DMT1, ACO2, ALAS2, HIF2α and dSdhB (Figure 1.7, section 1.4.1), different groups have reported other IREs or IRE-like structures in mRNAs related or *a priori* not related with iron metabolism. However, not in all cases, evidence of the IRP regulation of these transcripts was clearly demonstrated.

1.7.1 Other IRE structures

1.7.1.1 MRCKα: one IRE at 3' UTR

Computational analysis of UTR databases identified an IRE motif in the 3' UTR of human myotonic dystrophy kinase alpha (MRCKα; official name: CDC42 binding protein kinase alpha, CDC42BPA) (Cmejla *et al.* 2006). MRCKα is a serine/threonine kinase that acts as a downstream effector of the small Rho GTPase CDC42, involved in cytoskeletal reorganization. MRCKα protein is well conserved in different species, however the IRE hairpin is unique to humans (Figure 1.17). Direct and competitive EMSA experiments showed that MRCKα IRE is able to interact *in vitro* with IRP1 and IRP2 from cell lysates. Moreover, MRCKα mRNA showed an iron-dependent regulation: MRCKα mRNA was upregulated by iron chelation and stabilization experiments showed longer mRNA half-life in iron-deficient conditions, as would be expected for an IRE located in 3′UTR. However and unlike TFR1, MRCKα mRNA seems to be regulated only by iron deficiency.

1.7.1.2 CDC14A: one IRE at 3' UTR

A 3' UTR IRE was identified in a splice variant of the cell division cycle 14A mRNA (CDC14A) (Sanchez *et al.* 2006). CDC14A encodes a phosphatase, ortholog of the yeast Cdc14 which is involved in the dephosphorylation of several targets closely related to cell cycle, during mitotic exit and initiation of DNA replication; however, relatively little is known about the function of CDC14A in higher eukaryotes.

CDC14A IRE was identified together with the one of HIF2α mRNA (see section 1.4.1) through predicted computational analysis and biochemical experiments. mRNA clones corresponding to IRE-like motifs were spotted on a home-made microarray: the IronChip, a platform covering ~500 genes involved in iron metabolism and connected pathways (Muckenthaler *et al.* 2003a; Muckenthaler *et al.* 2003b). IRP1/mRNA complexes were immunopurified from different human cell lines and mouse tissues and IRP-interacting mRNA were identified on the IronChip. CDC14A IRE (Figure 1.17) is conserved in different species but not in mouse. Additionally, database analysis revealed four splicing variants for CDC14A mRNA with the IRE motif included only in two of them. Human CDC14A IRE efficiently binds to both IRP1 and IRP2 in *in vitro* competitive EMSA experiments. Furthermore, CDC14A-IRE mRNA was upregulated by iron chelation, whereas the levels of the CDC14A-non-IRE variants remain unchanged. Still, iron-deficiency regulation on CDC14A was cell specific and iron supplementation showed no effect (Sanchez *et al.* 2006).

Iron scarcity was shown to arrest cells in G1/S phase (Le *et al.* 2002), therefore, CDC14A upregulation by IRPs upon iron deficiency might play a role in the iron chelation-induced cell cycle arrest (Sanchez *et al.* 2006). Interestingly, it has been shown that CDC14A can dephosphorylate IRP2. IRP2 is phosphorylated during G2/M phase with consequent reduction of IRP-binding activity, whereas its CDC14A-dependent dephosphorylation during mitotic exit, restores IRP2 RNA-binding activity (Wallander *et al.* 2008).

1.7.1.3 Hao1/Gox: one IRE at 3' UTR

An IRE-like motif was found in the 3' UTR of mouse glycolate oxidase (Gox; official name: liver hydroxyacid oxidase 1, Hao1) (Kohler *et al.* 1999). Glycolate oxidases are enzyme that participate in glyoxylate cycle for energy production in plants, bacteria and fungi. Gox identification in this report was the first evidence of a functional glycolate oxidase enzyme in vertebrate. Mouse Gox was shown to be specifically expressed in the liver.

The approach leading to Gox identification as a possible IRPs partner consisted in a selection of IRE-containing mRNAs on an IRP1 affinity chromatography column; bound mRNAs were then used to construct a cDNA library that was subsequently screened in gel shift experiments. Gox IRE is conserved only in mouse and differs from the canonical structure by a mismatch (A:A) in the upper stem (Figure 1.17). This IRE-like sequence exhibits strong binding to both IRPs in competitive EMSA experiments performed at room temperature, but the interaction was lost at 37°C. Gox IRE, cloned at the 5' of a reporter construct, did not confer iron-dependent regulation of the reporter's expression. However, Gox mRNA levels were strongly upregulated by iron supplementation. The authors concluded that Gox IRE is not functional within cells and that Gox upregulation upon iron treatment might be due to alternative mechanisms.

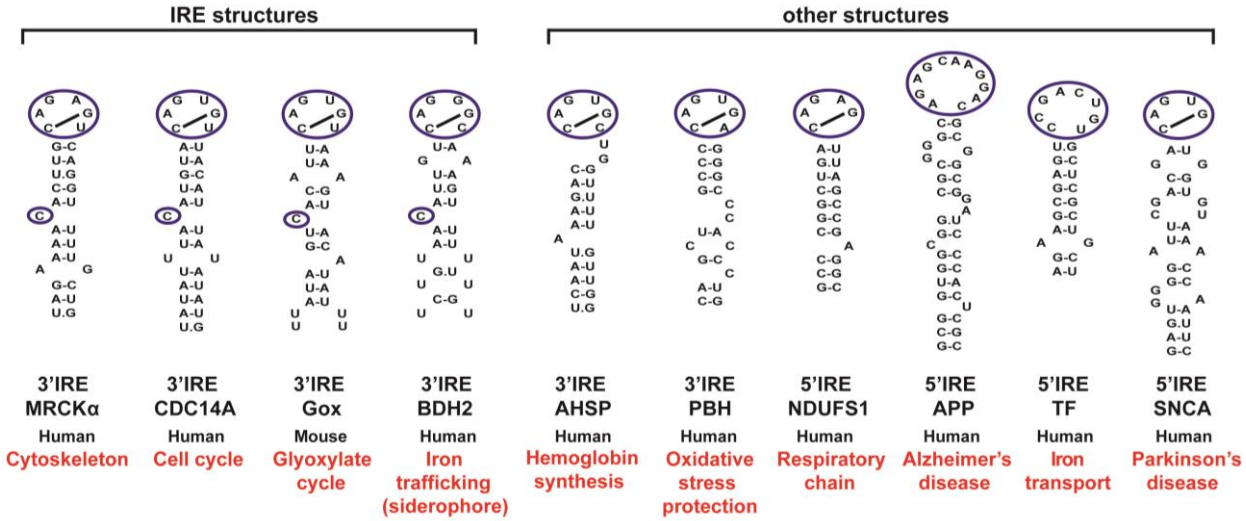

Figure 1.17 Other IREs and IRE-like structures. The picture shows IRE motifs (left) and other IRE-like structures (right) reported in the literature. Important structural elements of an IRE such as the apical loop and the cytosine-bulge are indicated by blue circles. Notice that not all the reported motifs conserve the canonical structure. The function of the encoded protein is indicated in red. MRCKα: myotonic dystrophy kinase alpha; CDC14A: cell division cycle 14A; Gox: glycolate oxidase; AHSP: alpha hemoglobin stabilizing protein; PBH: prohibitin; NDUFS1: 75kDa NADH dehydrogenase Fe/S protein 1; APP: amyloid precursor protein; TF: transferrin; SNCA: alpha synuclein. Picture modified from Joshi *et al.* 2012.

1.7.1.4 BDH2: one IRE at 3' UTR

The 3-hydroxybutyrate dehydrogenase (BDH2) catalyzes a rate-limiting step in the biogenesis of mammalian siderophores, small iron binding molecules that facilitate iron transport. An IRE structure was identified in the 3' UTR of human BHD2 mRNA and demonstrated to confer iron-dependent regulation on BDH2 at mRNA and protein level (Liu *et al.* 2012). We contributed to this work; for more details see section 3.3 in Results and Discussion.

1.7.1.5 AHSP: one IRE-like motif at 3' UTR

An IRE-like motif was predicted in the 3' UTR of the alpha hemoglobin stabilizing protein (AHSP) mRNA (dos Santos *et al.* 2008). AHSP is a chaperon protein binding and stabilizing the α-globin chain during hemoglobin synthesis.

The predicted IRE-like motif is conserved among primates and diverges significantly from the canonical structure by presenting an A-bulge, instead of a C-bulge and having to additional unpaired nucleotides (UG) at the 3' end of the hexanucleotide apical loop (Figure 1.17). Noticeably, other reports support the *in vitro* functionality of IRE structures with a bulged

nucleotide different than cytosine (Meehan *et al.* 2001). AHSP IRE poorly binds to IRP1 and IRP2 in direct and competitive EMSA experiments. Besides its structural diversity, AHSP mRNA co-immunoprecipitated with IRP1 or IRP2 protein in HeLa cells, while an IRE-mutated version did not. Furthermore, iron supplementation considerably inhibited the co-immumoprecipitation. In addition, mRNA half-life measurements showed increased AHSP mRNA half-life upon iron chelation, compatible with an IRP-mediated stabilization. The induction of AHSP production via IRP interactions may provide a compensatory mechanism to stabilize excess apo α-globin during iron deficiency (dos Santos *et al.* 2008).

1.7.1.6 PBH: one IRE-like motif at the CDS-3' UTR boundary

An IRE-like motif was found in the nuclear-encoded mitochondrial protein, prohibitin (PBH) (Artal-Sanz *et al.* 2009). Prohibitin function is not well understood. It is able to oligomerize and bind iron and was demonstrated to have protective activity against oxidative stress suggesting that PHB may be involved in the storage of intracellular iron similar to ferritin and may play an important role in cellular iron homeostasis.
Sequence analysis revealed an atypical IRE-like motif with a longer upper stem at a very unique location, at the junction of coding and non-coding region at the 3' end of human PBH mRNA. PBH was reported to be iron regulated; iron supplementation increases PBH protein levels whereas iron chelation reduces them. However, the regulation observed in response to iron changes does not correspond to the one expected for a 3' UTR IRE and no other data regarding the functionality of the PBH IRE are available.

1.7.1.7 NDFUS1: one IRE-like motif at 5' UTR

NDFUS1 encodes for the 75-kDa Fe/S cluster-containing subunit of mitochondrial complex I. An atypical IRE-like structure was predicted in the 5' UTR of human NDFUS1 mRNA (Lin *et al.* 2001). This structure does not contain a C-bulged nucleotide and the apical loop is constituted of 5 nucleotides instead of 6 (Figure 1.17). NDFUS1 protein levels are increased by iron supplementation and decreased upon iron chelation whereas mRNA levels are minimally affected, in accordance with a conventional 5' IRE post-transcriptional regulation. EMSA experiments showed that the IRE-like motif was able to interact with a cytoplasmic protein different than IRP1 or IRP2; this interaction could be competed by H-ferritin IRE and was found to be modified by cellular iron status. This report suggests therefore the existence of a novel iron regulatory protein, whose nature needs further characterization.

1.7.1.8 APP: one atypical IRE-like motif at 5' UTR

The amyloid precursor protein (APP) is a membrane protein known for being the precursor of the beta amyloid peptide involved in the etiopathogenesis of Alzheimer's disease. A very atypical IRE structure was found in the 5' UTR of human APP mRNA immediately upstream of an IL1 acute box domain (Rogers *et al.* 2002). This structure does not contain a cytosine-bulge and the apical loop is composed of 11 nucleotides (Figure 1.17), however, folding free energy estimations indicate a very stable configuration. APP protein levels were shown to be iron modulated in neuroblastoma cell lines: they diminish upon iron chelation and increase upon iron supplementation while APP mRNA levels are unaffected. Likewise, three different reporter assays showed that APP 5' UTR induces downregulation of the reporter gene expression under iron deficiency conditions while iron confers a significant increase of reporter expression. These data suggested a regulation similar to the ferritin 5' UTR IRE. Gel-shift

assays showed that APP IRE is able to interact with recombinant IRP1 or cell lysate and, when specifically mutated, loses this capability. However, contrary to an increased IRP binding during iron deficiency, it was observed that APP IRE interaction with cell extracts from iron chelated cells was reduced compared to the binding in no iron manipulated conditions. Moreover, APP IRE-IRP binding was increased upon IL1 stimulation, indicating that other factors may be involved in APP iron-mediated regulation.

1.7.1.9 TF: one atypical IRE-like motif at 5' UTR

Transferrin (TF) is a glycoprotein that transports iron in the blood and delivers to peripheral cells. Evidence that the human transferrin (TF) is regulated by iron at the level of translation was also reported (Cox *et al.* 1993). Transgenic mice which carry a chimeric gene composed of the human TF 5' UTR fused to the chloramphenicol acetyl transferase (CAT) reporter gene showed suppression of the reporter expression after intraperitoneal injections of iron while CAT mRNA levels remained unchanged suggesting a post-transcriptional regulation.
Analysis of the TF 5' UTR revealed a potential IRE-like hairpin-loop structure lacking the C-bulge and presenting a larger apical loop (Figure 1.17). The predicted folding energy showed a very stable conformation. Binding assays, performed using liver cytoplasmic extracts, showed a TF 5' UTR RNA/protein complex that migrated similarly to the ferritin IRE/protein complex. The binding was reduced when using cytoplasmic extracts coming from iron treated mice, what it is compatible with a reduced IRP binding activity in iron-replete condition. Competitive band shift assays showed that H-ferritin IRE can efficiently compete this binding. Moreover, a mutated version of the TF 5' UTR, with specific deletion of the putative IRE sequence, was not able to compete for protein binding.
Remarkably, Cox and collaborators, as well as previous reports (Lane 1966; Morgan *et al.* 1983), showed that iron loading decreases TF expression, while iron deficiency leads to an increased TF expression. The modulation of TF expression in response to iron is therefore opposite to what expected for a 5' UTR IRE-containing mRNA. Nevertheless, a definitive proof that IRPs bind to TF mRNA have not been shown.

1.7.1.10 SNCA: one bioinformatically predicted IRE-like motif at 5' UTR

α-synuclein (SNCA) is a protein involved in Parkinson's disease. An atypical IRE-like motif was bioinformatically predicted in the 5' UTR of the human α-synuclein mRNA (Friedlich *et al.* 2007); however, functional validation of this binding element is still pending.

1.7.2 Genome wide screening for novel IRPs target mRNAs

To systematically define the entire IRP/IRE regulatory network on a genome-wide scale, my supervisor, Dr. Mayka Sánchez, developed a strategy to specifically immunoprecipitate IRP-mRNA complexes followed by a microarray analysis of the co-immunoprecipitated mRNAs (Sanchez *et al.* 2011).
Total RNA from 5 different mouse tissues (duodenum, liver, brain, spleen, and bone marrow) was incubated with recombinant IRP1 or IRP2 and RNA-protein complexes were immunoprecipitated with specific antibodies. Genome-wide identification of the immunoprecipitated mRNAs was achieved using Affymetrix microarrays and the results were normalized and analyzed using 2 independent microarray mathematical algorithms (RMA + MAS5). Microarray data analysis revealed 44 mRNAs that bind to both IRP1 and IRP2 in at least one tissue (Figure 1.18).

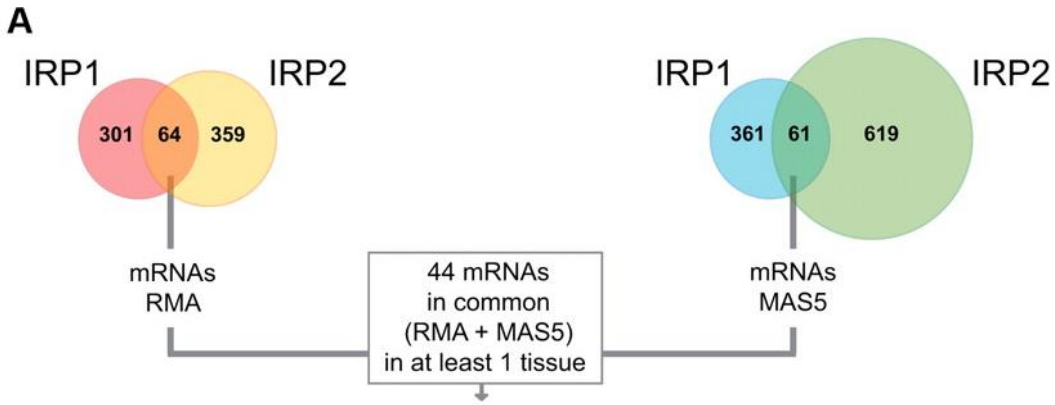

B

Gene Symbol	IRP1 Duodenum	IRP1 Liver	IRP1 Bone Marrow	IRP1 Spleen	IRP1 Brain	IRP2 Duodenum	IRP2 Liver	IRP2 Bone Marrow	IRP2 Spleen	IRP2 Brain	IRE motif Position	IRE motif Species
Ftl1	■	■	■	■	■	■	■	■	■	■	5´	*Mm/Hs*
Tfrc	■	■	■	■	■	■	■	■	■	■	3´	*Mm/Hs*
Lrpap1	■	■	■	■	■	■	■	■	■	■	3´	*Mm*
Slc40a1	■	■	■	■	■	■	■		■	■	5´	*Mm/Hs*
Aco2	■	■	■	■	■	■	■		■	■	5´	*Mm/Hs*
Ftl2	■	■	■	■	■		■	■	■		5´	*Mm/Hs*
Slc11a2	■	■	■	■	■	■	■		■		3´	*Mm/Hs*
0610007L01Rik	■	■	■	■	■	■	■		■		n.d.	
Ccdc45	■	■	■	■	■	■	■		■		n.d.	
Epas1	■	■	■	■	■	■	■		■		5´	*Mm/Hs*
Cxcl16	■	■	■	■	■	■	■		■		3´	*Mm*
Fxyd5	■	■	■	■	■	■			■		5´	*Hs*
Ormdl1	■	■	■	■	■	■	■				3´	*Hs*
Gyg	■	■	■	■	■				■		CDS	*Mm/Hs*
Garnl1	■		■	■	■	■	■	■	■	■	5´-CDS	*Mm*
Egr2	■		■	■	■	■	■	■	■	■	CDS	*Mm*
A430093A21Rik		■	■	■	■	■	■		■	■	CDS	*Mm*
Alas2		■	■	■	■		■		■	■	5´	*Mm/Hs*
Fth1		■	■	■	■			■	■	■	5´	*Mm/Hs*
Pfn2	■	■	■	■		■	■		■		n.d.	
8430410A17Rik	■		■	■	■				■	■	CDS	*Mm*
Trp53inp2	■	■	■	■	■	■	■				3´	*Hs*
Kcnf1	■		■		■	■		■	■	■	3´	*Mm*
Hao1		■	■		■		■			■	3´	*Mm*
Mkrn1	■	■			■	■	■				n.d.	
Gstm6	■	■			■	■	■				3´	*Mm*
Pdcl3			■	■		■	■		■	■	n.d.	
AI45035/Pex12	■				■	■			■	■	n.a.	*Mm*
Arfip2	■				■	■			■	■	n.d.	
BC051227				■	■	■			■		CDS	*Mm*
Ppp1r1b	■				■	■				■	5´	*Mm*
Gstt3	■	■				■	■				CDS	*Mm*
D5Ertd255e			■	■				■	■		n.d.	
Dlg2			■		■				■	■	CDS/3´	*Mm/Hs*
Lnx1	■				■	■					n.d.	
Lsm12		■		■					■		n.d.	
Pabpc4l		■		■					■		CDS	*Mm*
4930579E17Rik		■			■					■	3´	*Mm*
Dhx32	■			■		■					n.d.	
Ankrd29				■		■			■	■	3´	*Hs*
Dirc2					■	■	■			■	n.d.	
Nr4a3				■					■	■	5´	*Hs*
2010107G12Rik	■					■					CDS	*Mm*
Pyroxd1	■					■					CDS	*Hs*

Figure 1.18 Novel IRP1 and IRP2 candidate target mRNAs. (A) Number of positively detected mRNAs found to interact with both IRP1 and IRP2 obtained from the analysis with RMA and MAS5 algorithms. **(B)** In the table are listed the 44 mRNAs common targets of IRP1 and IRP2. Red and black squares indicate respectively positive or negative enrichment in the immunoprecipitated fraction compared to the mock immunoprecipitation (no IRP1 or IRP2 recombinant protein added) in 2 independent replicas. In green are indicated the 9 well-known IRE-containing mRNAs, also detected in the microarray and considered as positive experimental controls. Predicted IRE motifs using the SIREs program in mouse or human databases and their positions in the mRNA are indicated. 5': 5' UTR; 3': 3' UTR; CDS: coding region; *Hs*: *Homo sapiens*; *Mm*: *Mus musculus*. Picture from Sanchez *et al.* 2011.

Among these 44 mRNAs, all 9 well-known IRE-containing mRNAs (Ftl1, Ftl2, Fth1, Tfrc, Slc40a1, Slc11a2, Alas2, Aco2, and Epas1) were detected, thus confirming the *bona fide* of the method.
Hence, 35 novel mRNAs that bind both IRP1 and IRP2 were identified using this screening approach (Figure 1.18). In addition, the microarray data detected 101 mRNAs that exclusively interact with IRP1 and 113 specific IRP2-binding mRNAs in at least one tissue, underlining the concept that IRP1 and IRP2 can regulate different subsets of target mRNAs.
Bioinformatic prediction for IRE motifs was carried out using a newly developed software called SIREs (Searching for IREs) (Campillos *et al.* 2010). SIRES analysis revealed IRE-like structures in most of the mRNA candidates located either in the 5' UTR, in the 3' UTR or, and for the first time, IRE structures were also detected in the coding region (Sanchez *et al.* 2011).

1.7.3 A novel IRP-target mRNA candidate: Profilin2

My thesis focused in the validation and characterization of one on these 35 novel IRP-target RNAs: Profilin2 (see Results and Discussion 3.4). Here I will discuss available literature data concerning Profilin2 structure and function.

1.7.3.1 Profilin2: structure and function

Profilin2 (Pfn2) belongs to the profilins family. Profilins are small actin-binding proteins whose structure is very conserved from bacteria to higher eukaryotes besides poor sequence homology among members of the family (Witke 2004). Structurally and functionally profilins consist of three domains: an actin-binding domain, a poly-L-proline binding domain and a phosphatidylinositol phosphates binding domain (Witke 2004) (Figure 1.19).
In mammals, four different profilin genes have been characterized: Pfn1 is expressed everywhere except for skeletal muscle and it is essential for cell viability (Witke *et al.* 1998; Witke *et al.* 2001), Pfn2 is expressed predominantly in the central nervous system and at lower levels in skeletal muscle, uterus and kidney (Witke *et al.* 1998) while Pfn3 and Pfn4 are mostly restricted to the testis (Behnen *et al.* 2009). Pfn1 and Pfn2 share 65% amino acid identity while Pfn3 and 4 are less conserved and have different binding properties (Witke 2004; Behnen *et al.* 2009).
In addition, Pfn2 transcript can be alternatively spliced at the C-terminus producing a minor isoform: Pfn2b (Di Nardo *et al.* 2000; Lambrechts *et al.* 2000). The major transcript Pfn2a and the minor isoform Pfn2b differ significantly in respect to tissue specificity, subcellular localization as well as binding properties. Pfn2b lacks actin-binding activity and the affinity to poly-L-proline ligands is greatly reduced whereas, contrary to Pfn2a, Pfn2b binds to tubulin protein (Di Nardo *et al.* 2000; Lambrechts *et al.* 2000).
Although Pfn1 and Pfn2 are structurally very similar, proteomics experiments have shown that they bind different sets of proteins in mouse brain (Witke *et al.* 1998). In particular, Profilin2 interacts with ligands involved in signal transduction, membrane trafficking and vesicles recycling such as ROCK2, synapsins, CyFIP1 and dynamin1. Dynamin1 is the main component of the Profilin2 complex, it binds directly and with high affinity to Pfn2 and they co-localize in vesicular structures in the cell body, axons and dendrites (Witke *et al.* 1998). The binding of actin and dynamin1 to Pfn2 is mutually exclusive (Gareus *et al.* 2006). Dynamin1 is a neuron-specific GTPase involved in endocytosis and membrane trafficking. Dynamin1 forms a spiral around to the neck of budding vesicles that extends lengthwise and constricts through GTP hydrolysis promoting the scission of the nascent vesicles from the cell membrane or from the membrane of cellular compartments (Roux *et al.* 2006).

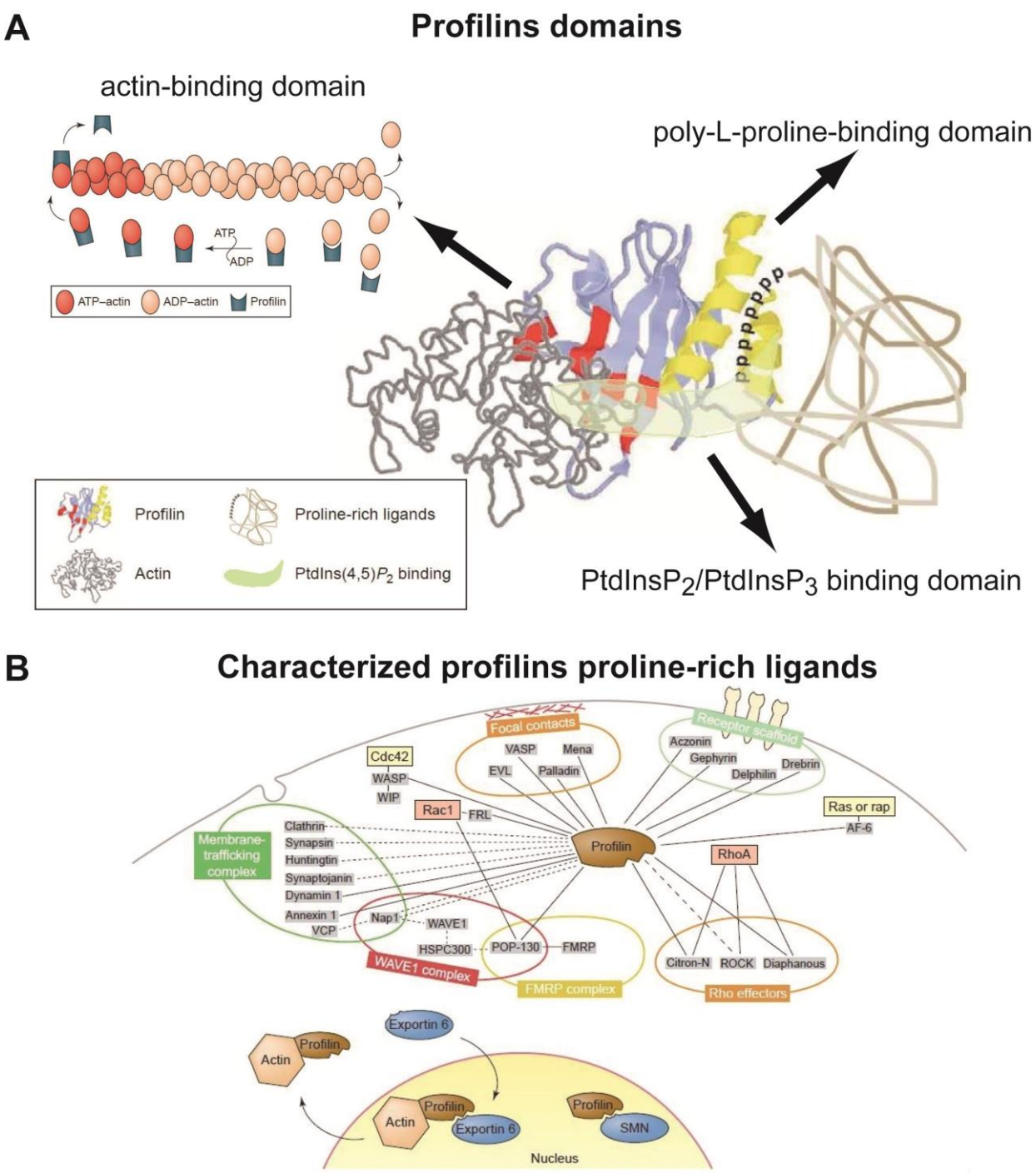

Figure 1.19 Profilins family structure and functions. (A) Actin filaments consist of ATP-actin that is slowly converted to ADP-actin by the ATPase activity of actin; ATP filaments are protected from depolymerisation, while ADP filaments are easily disassembled. Profilin binds to actin in a 1:1 complex, it facilitates ADP-ATP exchange on G-actin and promotes filaments elongation providing ATP-actin monomers to the growing end of the filament (Witke 2004). The phosphatidylinositol (PtdInsP_2) binding region overlaps with the actin and poly-L-proline binding sites and was shown to have a regulatory role to both actin (Lassing *et al.* 1985; Goldschmidt-Clermont *et al.* 1990) and poly-L-proline binding (Lambrechts *et al.* 1997). Profilins might also play an important role in signal transduction, since can bind PtdInsP_2 with high affinity and inhibit its cleavage by the non-tyrosine-phosphorylated form of the phospholipase-Cγ (Goldschmidt-Clermont *et al.* 1991). **(B)** Finally, the poly-L-proline-binding domain interacts with a variety of proline-rich ligands. In yeast, mutations of the poly-L-proline binding site are lethal, suggesting that ligand-binding is an essential property of profilins (Lu *et al.* 2001). More than 50 ligands were characterized from different organisms including proteins involved in nuclear export, endocytosis and transcription factors. Although only some of these interactions have been demonstrated to have a physiological significance, they show unexpected links of profilins function to pathways not directly related to actin polymerization. Proteins found to interact with profilins are grouped according their subcellular localization or functional characteristics. Black lines indicate direct interactions; dashed lines indicate potentially direct interactions. Picture modified from Witke 2004.

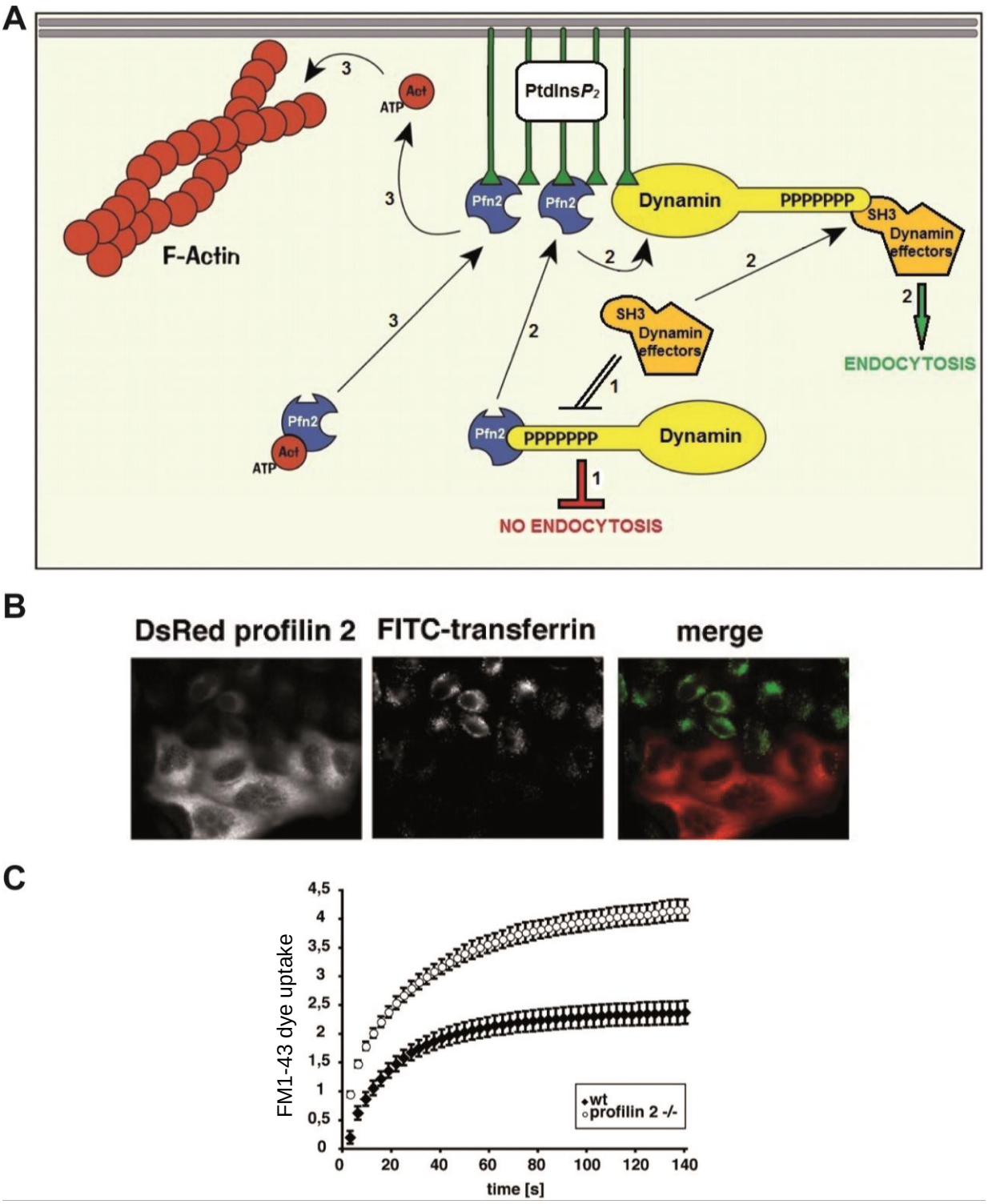

Figure 1.20 Profilin2 is a negative regulator of endocytosis. **(A)** Schematic representation of Pfn2 regulation on dynamin1 activity proposed by Gareus and collaborators. (1) Pfn2 is normally bound to actin or alternatively to the proline-rich domain of dynamin1. Pfn2 sequesters the binding site on dynamin1 for Grb2, amphiphysin, endophilin and possibly other proteins containing SH3 domains. Blocking the binding of these dynamin-effectors, Pfn2 inhibits the endocytosis process. (2) Both Pfn2 and dynamin1 have been demonstrated to bind PtdInsP_2 (Gieselmann *et al.* 1995; Zheng *et al.* 1996) and membrane phosphoinositides have been recognized as spatial organizer of actin polymerization as well as endocytosis (Takenawa *et al.* 2001). Gareus and collaborators demonstrated that PtdInsP_2 can disrupt the interaction between Pfn2 and dynamin1 (Gareus *et al.* 2006). Local increase of PtdInsP_2 concentration in the membrane was proposed as the signal that induces the dissociation of Pfn2 from dymanin1, allowing the binding of SH3 dynamin-effectors and permitting endocytosis. (3) PtdInsP_2 also release G-actin from the profilactin complex and makes monomeric actin available for filament elongation (Lassing *et al.* 1985; Goldschmidt-Clermont *et al.* 1990; Gareus *et al.* 2006). **(B)** Data of Gareus and collaborators showing the inhibition

of transferrin uptake in HeLa cells overexpressing DsRed-Pfn2. Cells transfected with DsRed-Pfn2 are visible in the red channel (left panel). Cells were treated with FITC-labeled transferrin and cells that have taken up transferrin are visible in the green channel (central panel). The merged image (right panel) shows that cells overexpressing Pfn2 take up significantly less transferrin compared to untransfected cells, not expressing Pfn2. **(C)** Data of Gareus and collaborators showing the kinetic of membrane uptake measured using FM1-43 dye in cultured cortical neurons isolated from wild-type mice (filled symbol) or from Pfn2 knockout mice (clear symbol). FM1-43 dye becomes florescent upon insertion into lipid membrane, while it is non-fluorescent in aqueous phase. The graph shows that neurons lacking Pfn2 present a 2-fold higher membrane uptake compared to control neurons. Picture modified from Gareus *et al.* 2006.

Profilin2 binding to dynamin1 is nucleotide-dependent; in total brain lysates the binding of dynamin1 to Pfn2-Sepharose is inhibited by GTP-γ-S, ATP, while GMP has no effect, indicating that dynamin1 in its GTP form does not bind Pfn2 or that another protein regulates the binding in a nucleotide-dependent manner (Witke *et al.* 1998).
Moreover, Profilin2 binding site on the proline-rich region of dynamin1 overlaps with the docking sites for other ligands such as the growth factor receptor-bound protein 2 (Grb2), amphiphysin and endophilin (Grabs *et al.* 1997; Okamoto *et al.* 1997; Slepnev *et al.* 1998; Schmidt *et al.* 1999; Takei *et al.* 1999). The binding of the dynamin-effectors Grb2, amphiphysin and endophilin is important to stimulate the GTPase activity of dynamin1 (Gout *et al.* 1993) and for the assembly and recruitment of the endocytic machinery to the membrane (Takei *et al.* 1999). Gareus and collaborators demonstrated that Pfn2 competes for the binding to dynamin1 with the dynamin-effectors Grb2, amphiphysin and endophilin (Gareus *et al.* 2006) (Figure 1.20A). Pfn2 binding with high affinity to dynamin1 result in dynamin1 sequestration; Pfn2 appears therefore to act as a **negative regulator of endocytosis**. *In vitro* studies corroborates this hypothesis since exogenous expression of Pfn2 in HeLa cells causes a reduced receptor-mediated endocytosis and ablation of Pfn2 expression in neurons increases membrane uptake (Gareus *et al.* 2006) (Figure 1.20B-C). Specifically the authors demonstrated that the overexpression of Pfn2 (in red, Figure 1.20B) **inhibits transferrin uptake** in HeLa cells.
While Pfn1 gene inactivation is lethal in mice at initial stages of embryonic development (Witke *et al.* 2001), Pfn2 deletion is viable but results in a severe neurological phenotype (Pilo Boyl *et al.* 2007). Mice lacking Pfn2 are hyper-reactive and show increased locomotion and exploratory behavior in novel environment compared to control mice. This phenotype correlates with increased synaptic excitability and higher neurotransmitter vesicles exocytosis in glutamatergic neurons of the cortico-striatal pathway. Most probably, in the brain of these mice, the absence of Pfn2 impairs actin polymerization in the synapses, which is important for providing a barrier function to limit further vesicle exocytosis after depolarization (Morales *et al.* 2000; Shupliakov *et al.* 2002), resulting in an increased synaptic vesicles release. However, also actin-independent activities of Pfn2 can contribute to vesicle exocytosis (Gareus *et al.* 2006). Pfn2 appears therefore to also negatively regulate vesicles exocytosis.

2. MATERIALS AND METHODS

2.1 Materials

2.1.1 Chemicals and reagents

Reagent	Company
2,2,2-Tribromoethanol	Sigma Aldrich
2′,7′-Dichlorofluorescin diacetate	Sigma Aldrich
3,3'-Diaminobenzidine - DAB	Sigma Aldrich
5,6-Dichlorobenzimidazole 1-β-D-ribofuranoside - DRB	Sigma Aldrich
96 Well Polystyrene Cell Culture Microplates, black	Greiner Bio-One
Acrylamide	Electran
Agarose	Lonza
Aminoallyl-ATTO680-UTP	Jena Bioscience
Ammonium iron(III) citrate	Sigma Aldrich
Ammonium persulfate - APS	Sigma Aldrich
Ammonium sulfate - $(NH_4)_2SO_4$	Sigma Aldrich
Antibiotic-Antimycotic (100X), liquid	Life Technologies
Bathophenanthrolinedisulfonic acid disodium salt trihydrate	Sigma Aldrich
Bio-Rad Protein Assay Dye Reagent Concentrate	Bio-Rad
Bovine serum albumin - BSA	Sigma Aldrich
Bromophenol blue - BPB	Sigma Aldrich
Calcein AM	Life Technologies
Chloroform	Merck
cOmplete, EDTA-free Protease Inhibitor Cocktail Tablets	Roche
Deferoxamine mesylate - DFO	Sigma Aldrich
Deoxynucleotides set - dNTPs	Fisher Scientific
Dimethyl sulfoxide - DMSO	Sigma Aldrich
Dithiothreitol - DTT	Sigma Aldrich
DMEM - Ham's F12, without L-glutamine	BioWest
DMEM high glucose with pyruvate, without L-glutamine	BioWest
DMEM, with 4mM L-glutamine, without bicarbonate, without phenol red	Sigma Aldrich
Doxycycline hyclate	Sigma Aldrich
Dual-Luciferase Reporter Assay System	Promega
Entellan mounting medium	Merck

Ethanol absolute	Merck
Ethidium bromide	Merck
Ethylenediaminetetraacetic acid - EDTA	Sigma Aldrich
Fetal Bovine Serum, qualified, E.U.-approved, South America origin	Life Technologies
Fetal calf serum	PAA
G418 disulfate salt	Sigma Aldrich
GFX PCR DNA and Gel Band Purification kit	GE Healthcare
Giemsa solution	Sigma Aldrich
Glutaraldehyde 50% solution	Sigma Aldrich
Glycerol	Sigma Aldrich
Glycine	Sigma Aldrich
Hemin from porcine	Sigma Aldrich
Heparin sodium	Serva
HEPES	Sigma Aldrich
Hydrochloric acid 37% - HCl	Merck
hydrogen peroxide 30%(w/w) - H_2O_2	Sigma Aldrich
Iron atomic spectroscopy standard concentrate 1.00 g Fe	Sigma Aldrich
L-ascorbic acid	Sigma Aldrich
L-ascorbic acid	Sigma Aldrich
L-Glutamine 200mM (100X), liquid	Life Technologies
Lipofectamine LTX and PLUS Reagents	Life Technologies
Luminata Forte Western HRP substrate	Millipore
Luminol	Sigma Aldrich
Magnesium sulfate - $MgSO_4$	Sigma Aldrich
May-Grünwald solution	Sigma Aldrich
Methanol	VWR
Methylthiazolyldiphenyl-tetrazolium bromide	Sigma Aldrich
Mowiol mounting medium	Sigma Aldrich
NN-Methylenebisacrylamide	Electran
NNNN-Tetramethylethylenediamine - TEMED	Sigma Aldrich
Nucleospin plasmid mini DNA purification kit	Macherey-Nagel
Opti-MEM R Reduced-Serum Medium	Life Technologies
Paraformaldehyde - PFA	Sigma Aldrich
Paraplast Plus	Sigma Sigma Aldrich
p-Coumaric acid	Sigma Aldrich
Phenol-chloroform-isoamyl alcohol mixture (25:24:1)	Sigma Aldrich
Pierce BCA Protein Assay kit	Thermo Scientific
Polyethylenimine - PEI	Polysciences Inc
Polyvinylidene fluoride membrane – PVDF	Millipore

Potassium chloride -KCl	Merck
Potassium dihydrogen phosphate - KH_2PO_4	Merck
Potassium ferrocyanide - potassium hexacyanoferrate (II) trihydrate	Sigma Aldrich
Precision Plus Protein Dual Color Standards	Bio-Rad
Probenecid	Sigma Aldrich
Propanol-2	Merck
PureYield Plasmid Midiprep System	Promega
Random primers	Life Technologies
rATP, rGTP, rCTP, rUTP ribonucleoside triphosphate monomers	Sigma Aldrich
RPMI 1640, without L-glutamine	BioWest
Sodium acetate - CH_3COONa	Calbiochem
Sodium azide	Merck
Sodium chloride - NaCl	Merck
Sodium dodecyl sulphate - SDS	Merck
Sodium phosphate dibasic - Na_2HPO_4	Merck
Superfrost Plus Microscope Slides	Thermo Scientific
Thiazolyl Blue Tetrazolium Bromide - MTT	Sigma Aldrich
Thioglycolic acid 70% (w/w) solution	Sigma Aldrich
Trichloroacetic acid - TCA	Sigma Aldrich
TRIReagent	Life Technologies
TRIS base	Calbiochem
Tris-Borate-EDTA (TBE) buffer (5x)	Conda
Triton X100	Merck
Tween 20	Fisher
Xylene	Merck
β-Mercaptoethanol	Sigma Aldrich

2.1.2 Enzymes and antibodies

Enzymes used in this study:

Enzyme	**Company**
ApaI	New England Biolabs
BamHI	New England Biolabs
DpnI	New England Biolabs
EcoRI	New England Biolabs
GoScript Reverse Transcriptase	Promega
HgaI	New England Biolabs
HindIII	New England Biolabs
iTaq Universal SYBR Green Supermix 2x	Bio-Rad
KpnI	New England Biolabs

MEGAscript T7 kit	Life Technologies
MseI	New England Biolabs
NheI	New England Biolabs
Pfu DNA polymerase	EMBL Heidelberg core facility
Quick Ligation kit (T4 DNA ligase)	New England Biolabs
RNasin Ribonuclease Inhibitor	Promega
RQ1 RNase-Free DNase	Promega
SacI	New England Biolabs
T7 RNA polymerase	EMBL Heidelberg core facility
XbaI	New England Biolabs

Antibodies used for Western blotting:

Primary	Source	Dilution	Secondary	Company	Dilution
Ferritin	Novus Biologicals	1:750	α-rabbit-HRP conjugated	Cell Signaling Technology	1:3000
FPN	home made[1]	1:1000	α-rabbit-HRP conjugated	Cell Signaling Technology	1:3000
IRP1	home made[2]	1:1000	α-rabbit-HRP conjugated	Cell Signaling Technology	1:3000
IRP2	home made[3]	1:1000	α-rabbit-HRP conjugated	Cell Signaling Technology	1:3000
Pfn2	home made[4]	1:1000	α-rabbit-HRP conjugated	Cell Signaling Technology	1:3000
S6 ribosomal protein	Cell Signaling Technology	1:1000	α-rabbit-HRP conjugated	Cell Signaling Technology	1:3000
TFR1	Zymed	1:2000	α-mouse-HRP conjugated	Cell Signaling Technology	1:3000
α-tubulin	Sigma Aldrich	1:20000	α-mouse-HRP	Cell Signaling Technology	1:5000
β-actin	Sigma Aldrich	1:10000	α-mouse-HRP conjugated	Cell Signaling Technology	1:5000

[1] polyclonal antibody raised against the C-terminus of mouse Fpn, kind gift of Prof. Kostas Pantopoulos, McGill University, Montreal

[2] polyclonal antibody raised against full-length human IRP1-his tagged protein, kind gift of Dr. Bruno Galy, EMBL, Heidelberg

[3] polyclonal antibody raised against the N-terminus 73aa domain of mouse Irp2, kind gift of Dr. Bruno Galy, EMBL, Heidelberg

[4] polyclonal antibody raised against the C-terminus of mouse Pfn2a, kind gift of Dr. Pietro Pilo Boyl, University of Bonn

2.1.3 Buffers and solutions

All solutions were prepared with MilliQ water (Millipore).

Buffer	Composition
Cytoplasmic lysis buffer (CLB) - for EMSA	25mM TRIS/HCl pH 7.4 40mM KCl 1% Triton X100 1x cOmplete, EDTA-free protease inhibitor cocktail (at use)

DNA loading buffer (6x)	10mM TRIS/HCl pH 8.0 1mM EDTA 50% glycerol 0.1% bromophenol blue
ECL solution - for Western blotting	100mM TRIS/HCl pH 8.5 0.8mM luminol 0.2mM p-Coumaric acid store at 4°C protected from light 0.009% H_2O_2 (at use)
In vitro transcription buffer (5x)	200mM TRIS/HCl pH 8.0 40mM $MgCl_2$ 250mM NaCl 10mM spermidine
Luria Bertani broth (LB) pH 7.0 - bacterial culture medium	10g tryptone 5g yeast extract 10g NaCl adjust pH to 7.0 and autoclave (1.5% agar - added for plates) adjust pH to 7.0 and autoclave cool down to ~50°C and add 100µg/ml ampicillin or 30µg/ml kanamycin
Lysis buffer - for protein extraction	20mM TRIS/HCl pH 8.0 1mM EDTA 100mM NaCl 10% glycerol 0.5% NP40 1x cOmplete, EDTA-free protease inhibitor cocktail (at use)
PBS buffer pH 7.4	137mM NaCl 2.7mM KCl 8mM Na_2HPO_4 1.46mM KH_2PO_4 adjust pH to 7.4
PCR buffer (10x)	200mM TRIS/HCl pH 8.8 100mM $(NH_4)_2SO_4$ 100mM KCl 1% Triton X100 20mM $MgSO_4$ (at use)
Running buffer pH 8.3 (10x) - for Western blotting	250mM TRIS 1.92M glycine 0.1% SDS

SDS loading buffer (5x) - for Western blotting	110mM TRIS/HCl pH 6.8 20% glycerol 3.8% SDS 8% β-Mercaptoethanol 0.01% bromophenol blue
TBS buffer	50mM TRIS/HCl pH 7.4 150mM NaCl
TBST buffer pH 8.0-8.4 (10x)	0.6M TRIS/HCl pH 8.0-8.4 1.5M NaCl 5% Tween 20
Transfer buffer pH 8.3 (1x)	25mM TRIS 192mM glycine 20% methanol

2.1.4 Instruments

Instrument	Company
ABI PRISM 7900HT Sequence Detection System	Applied Biosystems
BZ-9000 Microscope	Keyence
Centrifuge FRESCO21	Thermo Scientific
Electrophoresis power supply ECPS 3000/150	Pharmacia
FluorChemHD2	Alpha Innotech
Fluorimeter SPECTRAMax GEMINI EM	Molecular Devices
GelDoc XR System	Bio-Rad
Horizontal electrophoresis chamber	EMBL Heidelberg
Leica VT1200 Vibratome	Leica Biosystems
Luminometer Centro LB960	Berthold Technologies
Mini Trans-Blot Electrophoretic Transfer Cell	Bio-Rad
Mini-PROTEAN Tetra Cell	Bio-Rad
Nanodrop 1000	Thermo Scientific
Odyssey Infrared Imaging System	LI-COR
Peristaltic pump	Pharmacia
Rotary Microtome Leica RM2245	Leica Biosystems
Spectrophotometer SPECTRAMax 340PC	Molecular Devices
Spectrophotometer Ultrospec 3100pro	Amersham Biosciences
Termomixer compact	Eppendorf
Thermal cycler 2720	Applied Biosystems
TissueRuptor	Qiagen

2.1.5 PCR primers

All primers were purchased from Invitrogen and diluted in H_2O to a 100μM working solution.

Table 2.1 Primers sequences

Gene	Specie	Sequence (5'→ 3')	Use
Abcb7	*Mm*	CGAGCCAGAGTTGCCATCTC CATGAAAGGAACCACAATATTCATG	qPCR
Aco2	*Mm*	GTACCATCAACCATCCACTGTGA AAATAATACACTTCCTGGTTTATGTCCTT	qPCR
ADARB1	*Hs*	CCACACAAGGACAGGAGAGTC CAGCCTTGGAATTGAATTGG	qPCR gene dosage
ALAS2	*Hs*	CTCATTCGTTCGTCCTCAGTGCAGGGCAACAGGAT CTAGATCCTGTTGCCCTGCACTGAGGACGAACGAATGAGGTAC	to clone ALAS2 IRE WT (KpnI/XbaI)
ALAS2	*Hs*	CTCATTCGTCCGTCCTCAGTGCAGGGCAACAGGAT CTAGATCCTGTTGCCCTGCACTGAGGACGGACGAATGAGGTAC	to clone ALAS2 IRE MUT (KpnI/XbaI)
Asgr1 / RHL-1	*Mm*	CAGGGAAGTAGTGTGGGAAGAAA CAGTAGCAAACTGGAGTGATCTTCA	qPCR
Cd163	*Mm*	TGATAATTTCGAAGAAGCCAAAGTT TGGGATTTCTCCTCCAACCA	qPCR
Cd91 / Lrp1	*Mm*	TGTGGATGAGCATACCATCAACA GCCAGTCGATTGCCATCTG	qPCR
Cp	*Mm*	CTGGCACTGAAGAAAAGAAACTTATTT CCTTCTTATATTTTCTTCCAATACGATCT	qPCR
Dmt1- IRE	*Mm*	AGCTAGGGCATGTGGCACTCT ATGTTGCCACCGCTGGTATC	qPCR
Dmt1-not IRE	*Mm*	GTGGTGGCTGCAGTGGTTAGCG GCGGTCAGTCCCAGGCGGTACG	qPCR
Dnm1	*Mm*	TGTGTGGACATGGTTATCTCG CACAATTCGCTCCATCTCCT	RT-PCR
DNM1	*Hs*	CCGAGAACCGTGTCTCAAGT GCTCCATCTCCTCCCGTAG	RT-PCR
Exoc6 / Sec15l1	*Mm*	TGGAGATGTACAGTAAGCTGAAGGA CACATTCTCTAGCTGTTCCATTGTTT	qPCR
Flvcr1a	*Mm*	CCGTCGCCTCGGTATGG CACTAAAACAGGTGGCAACAAAAA	qPCR (Chiabrando *et al.* 2012)
Flvcr1b	*Mm*	TCGCTTCCTATTGACAGCTATTAACA CACTAAAACAGGTGGCAACAAAAA	qPCR (Chiabrando *et al.* 2012)
Fpn1	*Mm*	GGGTGGATAAGAATGCCAGACTT GTCAGGAGCTCATTCTTGTGTAGGA	qPCR
Fth1	*Mm*	TGGAACTGCACAAACTGGCTACT ATGGATTTCACCTGTTCACTCAGATAA	qPCR
FTL	*Hs*	TTCCAGGGATTGGGTTTCTAATT TCACTTCCTCATCTAGGAAGTGAGTCT	qPCR gene dosage
FTL	*Hs*	GTCAACAGCCTGGTCAATTTGTAC CGCAGCTGGAGGAAATTAGG	qPCR gene dosage
FTL	*Hs*	CGGTCCCGCGGGTCTGTCTCTTGCTTCAACAGTGTTTGGACGGAACAGATCCGGGGACTT CTAGAAGTCCCCGGATCTGTTCCGTCCAAACACTGTTGAAGCAAGAGACAGACCCGCGGGACCGGTAC	to clone IRE WT (KpnI/XbaI)
FTL	*Hs*	CGGTCCCGCGGGTCTGTCTCTTGCTTTAACAGTGTTTGGACGGAACAGATCCGGGGACTT CTAGAAGTCCCCGGATCTGTTCCGTCCAAACACTGTTAAAGCAAGAGACAGACCCGCGGGACCGGTAC	to clone IRE Badalona MUT (KpnI/XbaI)
FTL	*Hs*	CGGTCCCGCGGGTCTGTCTCTTGCTTAAACAGTGTTTGGACGGAACAGATCCGGGGACTT CTAGAAGTCCCCGGATCTGTTCCGTCCAAACACTGTTTAAGCAAGAGACAGACCCGCGGGACCGGTAC	to clone IRE London2 MUT (KpnI/XbaI)
FTL	*Hs*	CGGTCCCGCGGGTCTGTCTCTTGCTTGAACAGTGTTTGGACGGAACAGATCCGGGGACTT CTAGAAGTCCCCGGATCTGTTCCGTCCAAACACTGTTCAAGCAAGAGACAGACCCGCGGGACCGGTAC	to clone IRE Milano MUT (KpnI/XbaI)
FTL	*Hs*	CGGTCCCGCGGGTCTGTCTCTTGCTTCAAAGTGTTTGGACGGAACAGATCCGGGGACTT CTAGAAGTCCCCGGATCTGTTCCGTCCAAACACTTTGAAGCAAGAGACAGACCCGCGGGACCGGTAC	to clone IRE MUT ΔC loop (KpnI/XbaI)
FTL	*Hs*	CGGTCCCGCGGGTCTGTCTGTTGCTTCAACAGTGTTTGGACGGAACAGATCCGGGGACTT CTAGAAGTCCCCGGATCTGTTCCGTCCAAACACTGTTGAAGCAACAGACAGACCCGCGGGACCGGTAC	to clone IRE Torino MUT (KpnI/XbaI)

FTL	*Hs*	CGGTCCCGCGGGTCTGTCTCTTGCTTCAACAGTGTTTGGACGCAACAGATCCGGGGACTT CTAGAAGTCCCCGGATCTGTTGCGTCCAAACACTGTTGAAGCAAGAGACAGACCCGCGGG ACCGGTAC	to clone IRE Heidelberg MUT (KpnI/XbaI)
Ftl1	*Mm*	CGTGGATCTGTGTCTTGCTTCA GCGAAGAGACGGTGCAGACT	qPCR
GAPDH	*Hs*	GCTCCCACCTTTCTCATCC CTGCAGCGTACTCCCCAC	qPCR gene dosage
Hamp1	*Mm*	ATACCAATGCAGAAGAGAAGG AACAGATACCACACTGGGAA	qPCR (Casarrubea *et al.* 2013)
Hamp1	*Mm*	CCTATCTCCATCAACAGATG AACAGATACCACACTGGGAA	qPCR
Hcp1	*Mm*	GAATGGTGGTCTTTGCGTTTG ACAGGCGTCGTGACCAATG	qPCR
Hfe	*Mm*	CACTGCCACCGCGTTCA CTCAGCACGGCGACTCTCA	qPCR
Hif-2α	*Mm*	ACCCCGAGGAGCTACTTGGA GTTTGGCTAGCATCCGGTACTG	qPCR
Hmox1	*Mm*	AGAGCCGTCTCGAGCATAGC TCTCGGCTTGGATGTGTACCT	qPCR
HPRT1	*Hs*	GAACGTCTTGCTCGAGATGTGA TCCAGCAGGTCAGCAAAGAAT	qPCR gene dosage
Irp1	*Mm*	GAGACTGGGCAGCCAAAGG CGACCTGTGAGTCCCAGAGAGT	qPCR
Irp2	*Mm*	TGTTGTATTTGGGAGACTCTGTCACT TCATTACCTCTTCGAGCTCCATAA	qPCR
L19	*Hs/Mm*	ACCCCAATGAGACCAATGAAAT CAGCCCATCTTTGATGAGCTT	qPCR
L1PA (LINE)	*Hs*	AAAAAGTCAGGAAACAACAGGTG TCCCACCAACAGTGTAAAAGTG	qPCR gene dosage
Lcn2 / Lipocalin24p3	*Mm*	TTCCGGAGCGATCAGTTCC TTTTTTCTGGACCGCATTGC	qPCR
Lrpap1	*Mm*	GCTGCTGGAGG AGAAGACCAA TCTGGTCCTCAGAGCTCATTGTG	qPCR
Lrpap1- IRE	*Mm*	CTGCTTCTGGAGCAGATCTCTAGTC ACCGCATCTAAGTTTGTAGCTTGAG	qPCR
Mon1a	*Mm*	GTGACTGGTACCCTCGGTAGGT GCATGTCAGCAGCCATCTTTT	qPCR
PFN2	*Hs*	TGGCAACATAATTGCAGCAC GATTGTACAACCGGCACCTT	qPCR (IRE)
Pfn2	*Mm*	GGGAAGGGGGCATGCCAAGT AGACTGTACACCGGCACCTTGCT	qPCR (IRE)
Pfn2	*Mm*	CCGGAATTCAAAACATATGAACTCGCTTTATACCTGAAG CCCAAGCTTACTAGATGAGCCAAGGAAATGCTCCAAAGT	to clone fragment A (EcoRI/HindIII)
Pfn2	*Mm*	CCGGAATTCTCTTTTCAGCACTTTGGAGCATTTCCTT CCCAAGCTTAATAGTCTGTCCCAAGTGCAGTCACTGTATTA	to clone fragment B (EcoRI/HindIII)
Pfn2	*Mm*	CCGGAATTCTTACTTTTTAATACAGTGACTGCACTTGGGAC CCCAAGCTTTGGACACACTCCAGATGGTTATGTTGG	to clone fragment C (EcoRI/HindIII)
Pfn2	*Mm*	CCGGAATTCGATATTAGGTATCCCAACATAACCATCTGGAG CCCAAGCTTTATCCACAATGCCCAAACAATAGAAGCA	to clone fragment D EcoRI/HindIII)
Pfn2	*Mm*	CCGGAATTCACATTCTAGTATTGCTTCTATTGTTTGGGCAT CCCAAGCTTGGGCCCTCGAGGGATACTCTAG	to clone fragment E (EcoRI/HindIII)
Pfn2	*Mm*	CTGGGGAAGGGGGCATGCCAGTTGGGCATCACTTCG CGAAGTGATGCCCAACTGGCATGCCCCCTTCCCCAG	mutagenesis ΔA IRE loop
PFN2	*Hs*	CCGGAATTCTTGCCCAATGGATCATTTGTATGTTAACC CCCAAGCTTGGAAGACTAAATGAGCCAAGTAAATGCTC	to clone Hs fragment A
PFN2	*Hs*	GGAGGGGGCATGCCAGTTGGGCATCACTTTGTC GACAAAGTGATGCCCAACTGGCATGCCCCCTCC	mutagenesis ΔA IRE loop

Pfn2	*Mm*	CGGAAGGGGGCATGCCAAGTTGGGCATCACTTCGTCTT CTAGAAGACGAAGTGATGCCCAACTTGGCATGCCCCCTTCCGGTAC	to clone Pfn2 IRE WT (KpnI/XbaI)
PFN2	*Hs*	CGGGAGGGGGCATGCCAAGTTGGGCATCACTTTGTCTT CTAGAAGACAAAGTGATGCCCAACTTGGCATGCCCCCTCCCGGTAC	to clone PFN2 IRE WT (KpnI/XbaI)
Pfn2	*Mm*	CGGAAGGGGGCATGCCAGTTGGGCATCACTTCGTCTT CTAGAAGACGAAGTGATGCCCAACTGGCATGCCCCCTTCCGGTAC	to clone Pfn2 IRE MUT ΔA loop (KpnI/XbaI)
PFN2	*Hs*	CGGGAGGGGGCATGCCAGTTGGGCATCACTTTGTCTT CTAGAAGACAAAGTGATGCCCAACTGGCATGCCCCCTCCCGGTAC	to clone PFN2 IRE MUT ΔA loop (KpnI/XbaI)
Pfn2	*Mm*	GGTCTAGACTGCTAGGCAGACTGTTAAGTATTAGGGG GGTCTAGAGGGCCCTCGAGGGATACTCTAG	to clone 3' UTR (XbaI)
Pfn2	*Mm*	GAAACTGGGGAAGGGGGCATGCCGGCATCACTTCGTCTTAGCAGTTAGTGG CCACTAACTGCTAAGACGAAGTGATGCCGGCATGCCCCCTTCCCCAGTTTC	mutagenesis Δ apical loop
Pfn2	*Mm*	CCGCCATTGTCGGCTACTGC	RT-PCR- isoform studies E1Af (Lambrechts *et al.* 2000)
Pfn2	*Mm*	CTGGATCTGGTTCGGTTGTG	RT-PCR- isoform studies E1Bf (Lambrechts *et al.* 2000)
Pfn2	*Mm*	GGCAAAATATGATAGTCAAGCTGTTG	RT-PCR- isoform studies 004-for
Pfn2	*Mm*	ACAGACTAACAACCATCTATCCCACAGC	RT-PCR- isoform studies 003-rev
Pfn2	*Mm*	CGTACAGAGGCATGCACT	RT-PCR- isoform studies E4r (Lambrechts *et al.* 2000)
Pfn2	*Mm*	GAAAAGACCGGGAAGGTTTCTTTACCAACG	3' RACE forward
Pfn2	*Mm*	TGGGGAGCCAACATACAACGTTGCTGTTGG	3' RACE for forward nested primer
Pfn2a	*Mm*	CACAATGGACATCCGGACAA TTTTGCCATTGAGTATGCCTTCT	qPCR
PFN2A	*Hs*	AGCTGGTAGAGTCTTGGTCTTTGTAAT TTGCCATTGAGTATGCCTTCTTATT	qPCR
PFN2B	*Hs*	GGACATCCGGACAAAGAGTCAA TCCCATGACTATAACCAATGCTCTAC	qPCR
Pfn2b	*Mm*	GCCGGGAGAGCATTGGT TTATGATGCCAGATAAAGGTTGGTT	qPCR
Scara5	*Mm*	TGTGGGTATCTTCATCTTAGCAGTG AGTCAGCGCCTTCAAGTCATC	qPCR
Slc22a17 / 24p3R	*Mm*	TCACCACCAATGCCATCG AGCCCCAAGGTCAGCAGC	qPCR
Slc25a37 / Mfrn1	*Mm*	TGTACCCGGTGGACTCCGT CTTGTATACCGGGCTTTGGG	qPCR
Slc25a38 / Mfrn2	*Mm*	GCATTGCGTGATGTACCCG TGGGTCAGGCTGTAGGCTCT	qPCR
Slc39a14 / Zip14	*Mm*	GCCAAGCGCCATTGAAGTAT CGCTGGCCCCCATGA	qPCR
Slc39a8 / Zip8	*Mm*	AGCAGGGAGCGCTGGAC GAGAAACCATGAAGAGAAAAGATGTCT	qPCR
Slc48a1	*Mm*	GGACGGTGGTCTACCGACAA CCTCCAGTAATCCTGCATGTACAT	qPCR
Steap3	*Mm*	CAATCTGGCTGTGAAGCAGG TCCAGACTTCTTCCTCAGCCC	qPCR
Tbp	*Mm*	CTTCGTGCAAGAAATGCTGAATAT CGTGGCTCTCTTATTCTCATGATG	qPCR
Tfr1	*Mm*	CCCATGACGTTGAATTGAACCT GTAGTCTCCACGAGCGGAATA	qPCR
Tfr1	*Mm*	CCCATGACGTTGAATTGAACCT GTAGTCTCCACGAGCGGAATA	qPCR
Tfr2	*Mm*	GTACAACGTGCGCATCATGAG GTCTACCAGGGCACCCAAAGT	qPCR

Timd2	*Mm*	GGACTATATGTTGGAAGTTAAACCAGAA AAATAGTTGTGGGTCTTCCTGTAGCT	qPCR
Trf	*Mm*	AGGCGCATTCAAGTGTCTGA CAGCCTTCTCCGGCAAGA	qPCR
β-actin	*Mm*	GCTTCTTTGCAGCTCCTTCGT ACCAGCGCAGCGATATCG	qPCR

2.1.6 Plasmid constructs

Table 2.2 Plasmid vectors

Insert	Gene	Specie	Backbone	Use
ALAS2 IRE MUT	*ALAS2*	*Hs*	pI12-CAT (Gray *et al.* 1993)	EMSA
ALAS2 IRE WT	*ALAS2*	*Hs*	pI12-CAT (Gray *et al.* 1993)	EMSA
Fth1 5' UTR at 5' of luciferase CDS	*Fth1*	*Mm*	pCIF (Sanchez *et al.* 2007)	luciferase assay
Fth1 5' UTR MUT ΔC IRE loop at 5' of luciferase CDS	*Fth1*	*Mm*	pCIF (Sanchez *et al.* 2007)	luciferase assay
FTH1 full length clone	*Fth1*	*Mm*	pCMV6 Kana/Neo (OriGene)	EMSA / overxpression
FTH1 full length clone MUTΔC IRE loop	*Fth1*	*Mm*	pCMV6 Kana/Neo (OriGene)	EMSA / overxpression
FTH1 IRE MUT ΔC apical loop	*FTH1*	*Hs*	pI12-CAT (Gray *et al.* 1993)	EMSA
FTH1 IRE WT	*FTH1*	*Hs*	pI12-CAT (Gray *et al.* 1993)	EMSA
FTL IRE Badalona MUT	*FTL*	*Hs*	pI12-CAT (Gray *et al.* 1993)	EMSA
FTL IRE Heidelberg MUT	*FTL*	*Hs*	pI12-CAT (Gray *et al.* 1993)	EMSA
FTL IRE London2 MUT	*FTL*	*Hs*	pI12-CAT (Gray *et al.* 1993)	EMSA
FTL IRE Milano MUT	*FTL*	*Hs*	pI12-CAT (Gray *et al.* 1993)	EMSA
FTL IRE MUT ΔC IRE loop	*FTL*	*Hs*	pI12-CAT (Gray *et al.* 1993)	EMSA
FTL IRE Torino MUT	*FTL*	*Hs*	pI12-CAT (Gray *et al.* 1993)	EMSA
FTL IRE WT	*FTL*	*Hs*	pI12-CAT (Gray *et al.* 1993)	EMSA
HIF2α 5' UTR at 5' of luciferase CDS	*EPAS1*	*Hs*	pCIF (Sanchez *et al.* 2007)	luciferase assay
HIF2α 5' UTR MUT ΔC IRE loop at 5' of luciferase CDS	*EPAS1*	*Hs*	pCIF (Sanchez *et al.* 2007)	luciferase assay
IRP1-HIS	*IRP1*	*Hs*	pT7-7 (EMBL)	recombinant protein expression
IRP2-HIS	*IRP2*	*Hs*	pET16b (EMBL)	recombinant protein expression
Pfn2 3' UTR at 3' of luciferase CDS	*Pfn2*	*Mm*	pGL3-PGK-luc (Promega)	luciferase assay
Pfn2 3' UTR MUT Δ apical loop at 3' of luciferase CDS	*Pfn2*	*Mm*	pGL3-PGK-luc (Promega)	luciferase assay
Pfn2 fragment A	*Pfn2*	*Mm*	pCMV6 XL5 (OriGene)	EMSA
PFN2 fragment A	*PFN2*	*Hs*	pCMV6 XL5 (OriGene)	EMSA
Pfn2 fragment A MUT ΔA IRE loop	*Pfn2*	*Mm*	pCMV6 XL5 (OriGene)	EMSA
PFN2 fragment A MUT ΔA IRE loop	*PFN2*	*Hs*	pCMV6 XL5 (OriGene)	EMSA
Pfn2 fragment B	*Pfn2*	*Mm*	pCMV6 XL5 (OriGene)	EMSA
Pfn2 fragment C	*Pfn2*	*Mm*	pCMV6 XL5 (OriGene)	EMSA
Pfn2 fragment D	*Pfn2*	*Mm*	pCMV6 XL5 (OriGene)	EMSA
Pfn2 fragment E	*Pfn2*	*Mm*	pCMV6 XL5 (OriGene)	EMSA
Pfn2 full length clone	*Pfn2*	*Mm*	pCMV6 Kana/Neo (OriGene)	overexpression

Pfn2 fused at C-terminus with mCherry	*Pfn2*	*Mm*	pmCherry-N1 (Clontech)	overexpression
Pfn2 IRE inside HIF2α 5' UTR at 5' of luciferase CDS	*Pfn2*	*Mm*	pCIF (Sanchez *et al.* 2007)	luciferase assay
Pfn2 IRE MUT ΔA IRE loop inside HIF2α 5' UTR at 5' of luciferase CDS	*Pfn2*	*Mm*	pCIF (Sanchez *et al.* 2007)	luciferase assay
Pfn2 IRE WT	*Pfn2*	*Mm*	pI12-CAT (Gray *et al.* 1993)	EMSA
PFN2 IRE WT	*PFN2*	*Hs*	pI12-CAT (Gray *et al.* 1993)	EMSA
Pfn2 IRE WT MUT ΔA IRE loop	*Pfn2*	*Mm*	pI12-CAT (Gray *et al.* 1993)	EMSA
PFN2 IRE WT MUT ΔA IRE loop	*PFN2*	*Hs*	pI12-CAT (Gray *et al.* 1993)	EMSA

2.2 Methods

2.2.1 Cell biology

Cell culture, treatments and transfections

Cells were cultured in DMEM Dulbecco's Modified Eagle medium (HeLa, 293T, Hepa1-6, RAW264, J774, LTK, NIH3T3), DMEM-F12 medium (AML12) and RPMI 1640 medium (H1299) supplemented with 10% fetal bovine serum, 2mM L-Glutamine, 100 units/ml of penicillin, 100µg/ml of streptomycin and 0.25 µg/ml of Fungizone anti-mycotic (Life Technologies). NIH3T3 cells were cultured in 10% fetal calf serum instead of bovine serum.
For modulation of iron levels, the cells were treated with 100µM desferrioxamine (DFO), an iron chelator, or with 100µM Hemin or 300µM ferric ammonium citrate/100µM L-ascorbic acid (Sigma Aldrich), as source of iron, for the indicated periods of time.
When necessary, cell viability was assessed by MTT assay (Mosmann 1983). $2x10^4$ cells/well in 96-well plates were incubated with 0.5mg/ml MTT (Methylthiazolyldiphenyl-tetrazolium bromide, Sigma Aldrich) in complete medium for 3h at 37°C. MTT is reduced by mitochondrial dehydrogenases of living cells to produce dark purple formazan crystal. Medium was gently removed, crystal were solubilized in 200µl DMSO and quantified measuring the absorbance at 545nm using a SPECTRAMax 340PC spectrophotometer (Molecular Devices).
For transient transfection with plasmid DNA cells were seeded at a density of 10^5 cells/well in 12-well plates and the day after were transfected with 2µg of plasmid DNA and 6.6µl (6 equivalents) of polyethylenimine (PEI, Polysciences Inc) cationic polymer (Boussif *et al.* 1995). Alternatively, cells were transfected using Lipofectamine LTX and PLUS reagents (Life Technologies) following the manufacturer's recommended procedure.
All transfection mixes were prepared in Opti-MEM medium (Life Technologies) and incubated with the cells for 10h in Opti-MEM medium and then changed with complete culture medium. For the establishment of stable transfected cell lines, cells transfected with plasmid carrying neomycin resistance were selected for 3 weeks by 750µg/ml G418 treatment and single clones were isolated and characterized.

Analysis of mRNA stability

IRE sequences present in the 3' UTR of Tfr1 confer mRNA stabilization upon IRP biding in iron-deficient conditions. To test IRP-mediated mRNA stabilization of Pfn2 mRNA, NIH3T3 cells were treated with 100µM DFO, 100µM Hemin or left untreated (control) for 16h and, after that, 30µg/ml of the transcription inhibitor DRB (5,6-dichloro-1β-1-ribofuranosylbenzimidazole) was added. Cells were collected at various time points (0, 2, 4, 6, 8 and 10h) and mRNA levels of Pfn2, Tfr1 and actin were measured by qPCR and normalized to L19 levels. For each

condition, the zero hour DRB-treatment time point was set as 100%. mRNA half-life (t½) was calculated according to the method described by Chen and collaborators (Chen *et al.* 2008): the decay rate constant (*k*) was obtained from the slope of a semi-logaritmic plot of the %RNA as a function of time using a one phase exponential decay analysis in GraphPad Prism software. The half-life was then calculated using the equation: $t_{½} = \ln 2/k$

Luciferase reporter assays

To directly test the iron-dependent post-transcriptional regulation conferred by the newly identified Pfn2 3' UTR IRE a luciferase reporter system was used.
HeLa cells were seeded at a density of 10^5 cells/well in 12-well plates and, 24h later, transiently transfected with 900ng of pCIF luciferase reporter constructs. For normalization of the experiments, 60ng of pCMV-Renilla luciferase plasmid were co-transfected to correct for differences in transfection efficiency. Cells were transfected using PEI polymer as described before and, 24h later, were incubated with medium containing either 100μM DFO, 100μM hemin or no reagent for 16h. Firefly and Renilla activities were determined using the Dual-Luciferase Reporter Assay System (Promega) according to the manufacturer's instructions in a Centro LB960 microplate luminometer (Berthold Technologies).

Labile iron pool (LIP) assays

Cytosolic iron pool was measured by the fluorescent Calcein-AM method (Epsztejn *et al.* 1997) modified as follow. Cells were washed and incubated with 0.5μM Calcein-AM in DMEM (without bicarbonate and phenol red)/20mM HEPES pH 7.2-7.4 for 15 min at 37°C. Cells were washed and baseline calcein fluorescence was read for 15 min (ex=485nm, em=538nm) in a SPECTRAMax GEMINI EM fluorimeter (Molecular Devices). After stabilization of the baseline, 50μM DFO was added to chelate extracellular iron and fluorescence monitored for further 10 min. Finally, 50μM of the fast permeating iron chelator SIH (salicylaldehyde isonicotinoyl hydrazone, kind gift of Prof. Prem Ponka, McGill University, Montreal) was added and fluorescence measured for 10 additional minutes. Calcein-AM is taken up and hydrolysed by cellular esterases to give fluorescent calcein; fluorescence is quenched following chelation of low-mass labile iron. The strong permeating iron chelator SIH induces fluorescence de-quenching by removing calcein-bound iron and releasing calcein; the increase in fluorescence is proportional to the amount of chelatable cellular iron. The following formula was used for LIP calculation: ΔF= mean F_{norm}SIH – mean F_{norm}DFO where $F_{norm}=F_{(t)}/F_{t0}$.

ROS detection

Cells were seeded in 96-well plate at a density of $2x10^4$ cells/well the day before and then loaded with 50μM 2′,7′-Dichlorofluorescin diacetate (DCFDA, Sigma Aldrich) for 1h at 37°C in culture medium. After diffusion in to the cell, DCFDA is deacetylated by cellular esterases to a non-fluorescent compound, which is later oxidized by ROS into 2',7'-dichlorofluorescein (DCF). DCF is a highly fluorescent compound and was detected after washing of the cells in PBS using in a SPECTRAMax GEMINI EM fluorimeter (ex=485nm, em=538nm); fluorescence intensity is directly proportional to ROS production.

2.2.2 Animals handling, treatments and measurements

Animals were kept on constant light/dark cycle and food was supplied *ad libitum*. Animal handling was in accordance with the University of Bonn guidelines. Mice were sacrificed at 8-10 months of age by cervical dislocation and pieces of tissues were flash-frozen in liquid nitrogen for subsequent RNA, protein and iron quantification studies.

Blood hematological and biochemical studies

For blood collection, mice were briefly warmed under an infrared lamp and heparinized or EDTA blood was collected from tail vein followed by heat cauterization to stop the bleeding. Plasma was obtained by centrifugation of heparinized blood samples at 4500 rpm for 10 min at 4°C and collection of the supernatant.

Bone marrow was obtained from femur bones. The femur were cleaned, the heads removed with a scalpel and the bone marrow was flushed out using a syringe and PBS.

Blood hematological profiles were assessed at the Department of Hematology of the University Hospital of Bonn. Plasma iron and transferrin saturation were measured in collaboration with Dunja Ferring-Appel (Hentze group, EMBL, Heidelberg) using Iron (SFBC) and Iron U.I.B.C. kits (BIOLABO) according to the manufacturer's instructions.

Other biochemical parameters were measured at the Claude Bernard Institute Chemistry Laboratory in Paris using an Olympus 400 analyser.

Blood and bone marrow smears were stained with the May Grünwald-Giemsa method for evaluation of cellular subpopulations under microscope.

Perls Prussian Blue staining for iron

9-11 months old mice were used for histological staining of ferric iron with the Perls Prussian Blue coloration (Culling *et al.* 1985).

Animals were intraperitoneally anesthetized with 2,2,2-Tribromoethanol at the dose of 0.25mg/g of weight and then thoracotomized. A needle was inserted in the heart left ventricle to perfuse the fixatives and the right autricle was incised to let flush out blood and fixatives. All perfusions were initiated within 4 min after thoracotomy and at a flux rate of 2ml/min using a peristaltic pump (Pharmacia). Solutions were perfused in the following order:

- 20ml pre-washing solution: 10mM HEPES, 0.9% NaCl, 0.2% sodium heparin (pH 7.4)
- 20ml pre-fixative solution: 10mM HEPES, 0.9% NaCl, 1% glutaraldehyde, 4% PFA (pH 7.4)
- 50ml fixative/staining solution: 4% PFA, 1% potassium ferrocyanide and in 0.9% NaCl (pH~1.0, pH is obtained adding HCl to 1% final concentration immediately before use)
- 15ml post-washing solution: 0.9% NaCl

Liver, spleen, duodenum, kidney and brain were collected and post-fixed in 10ml of 10mM HEPES, 0.9% NaCl, 4% PFA for 48h at 4°C and washed 3 times with TBS buffer.

Liver, spleen, duodenum and kidney were dehydrated by passing through a series of increasing ethanol concentrations (50%, 70%, 80%, 96%, 100%), xylene and paraffin embedded prior to microtome cutting with a thickness of 7µm using a Rotary Microtome Leica RM2245 (Leica Biosystems). Slices were placed on Superfrost slides (Thermo Scientific) in 10% ethanol on a 42°C plate and let dry and further dried over night at 42°C.

Slides were afterward deparaffinized and rehydratated by incubation with xylene and decreasing ethanol series (96%, 90%, 80%, 70%, 50%) and finally in H_2O.

To intensify the staining, the slides were treated with 0.5% potassium ferrocyanide, 0.5%HCl in 0.9% NaCl for 30 min at RT, washed 3 times with TBS and the coloration was enhanced by additional DAB treatment as follow: 0.3% H_2O_2, 0.065% sodium azide in TBS treatment for 15 min, washing 3 times with TBS, 0.025% DAB, 0.005% H_2O_2 in TRIS/HCl pH 7.4 treatment for 30 min, washing 3 times with TBS, slides dehydration and mounting using Entellan mounting medium (Merck).

Brain was processed differently after post-fixation. It was sagittally cut in 20µm thick slices in ice-cold PBS using a Leica VT1200 Vibratome (Leica Biosystems) and slices were treated with an additional 0.5% potassium ferrocyanide incubation as previously described. After DAB

enhancing and washes brain sections were mounted on microscope slides using Mowiol mounting medium (Sigma Aldrich).

In all cases, images were acquired in bright field using the BZ-9000 Microscope (Keyence).

Quantification of non-heme or total iron content in mouse tissues

Non-heme iron content was measured using the bathophenanthroline colorimetric method (Torrance *et al.* 1968; Patel *et al.* 2002). Tissues were dried at 45ºC for 3 days, weighted and digested for 48 hours at 65ºC in 10% TCA/10% HCl (1ml per 100mg of dried material for liver, kidney, lung, heart and skeletal muscle, 6ml per 100mg for duodenum and 9ml per 100mg of spleen) to allow deproteinisation of non-heme iron. 200µl of diluted extracts (1:20 for spleen, 1:10 for liver, kidney, lung, heart and 1:5 for duodenum and skeletal muscle) were added to 1ml of chromogen solution: 0.01% bathophenanthrolinedisulfonic acid, 0.1% thioglycolic in 7M sodium acetate. The thioglycolic acid permits ferric iron reduction to ferrous iron that can then react with bathophenanthrolinedisulfonic acid and form a colored complex. After 10 min of incubation, the absorbance at 535nm was measured using a spectrophotometer Ultrospec 3100pro (Amersham Biosciences). Samples non-heme iron content was determined by interpolation with a standard curve obtained measuring known concentrations of iron atomic spectroscopy standard (Sigma Aldrich). The total amount of non-heme iron was expressed as µg iron/g of dried material.

Alternatively, for brain sections (olfactory bulb, cortex, corpus striatum, hippocampus, cerebellum and midbrain) and bone marrow samples, total iron content was determined by atomic emission spectrometry in collaboration with Dr. Lucía Gutiérrez (Instituto de Ciencia de Materiales de Madrid, ICMM-CSIC, Madrid) as described in (Gutierrez *et al.* 2009). Briefly, samples were lyophilised for 24h in a LyoQuest (Telstar) freeze-drier. Dried samples were weighted and acid digested for the elemental analysis by adding 65% HNO_3 (w/v) and heating up to 95ºC during 1h. After that, samples were allowed to cool down to room temperature and 30% H_2O_2 (w/v) was added and heated up to 95ºC during 1h. Quantitative determination of iron was analyzed by Inductively Coupled Plasma Atomic Emission Spectroscopy (ICP-AES) in an Optima 2100 DV (Perkin Elmer). Samples iron content was obtained by interpolation from a standard curve and normalized to the weight of dried material.

Transmission Electron Microscopy (TEM) and Energy Dispersive X-ray Spectroscopy (EDS)

After dissection, hippocampal and spleen samples were cut into small ~1mm^3 pieces and placed in fixative solution (4% paraformaldehyde and 2.5% glutaraldehyde in PBS) for 2h at room temperature. Fixative was then exchanged with fresh one and fixation was further carried on overnight at 4°C. Samples were then washed with PBS and post-fixed with 1% osmium tetroxide in 0.8 % potassium ferrocyanide for 60 min at 4°C. Samples were again washed in water and then dehydrated in graded acetone solutions (20, 30, 50, 70, 90, 100%) for 15 min each at 4°C. Infiltration was performed gradually through Epon resin: acetone solutions (50 % Epon overnight, 75 and 90 % of Epon for 3h each, 100% Epon overnight and 100% Epon for 1h, all at room temperature). Samples were embedded in Epon resin and polymerised at 60 °C for 48 h. Ultra-thin sections (40-60 nm) were collected on Formvar-coated gold grids. TEM micrographs were taken on a JeolJem 1010 transmission electron microscope operated at 100 kV.

Tissue iron analysis was performed on a JEOL JEM 3000F microscope operated at 300 kV in STEM (Scanning Transmission Electron Microscopy) mode. Energy Dispersive X-ray Spectroscopy (EDS) data was combined with STEM imaging using an Oxford Instruments INCA detector (Oxford Instruments NanoAnalysis) to map the presence of iron.

2.2.3 Molecular biology and biochemistry

RNA extraction

Total RNA was extracted with TRIReagent (Invitrogen) according to the manufacturer's instructions. Briefly, cell pellets or small pieces of mouse tissues were lysed in 1ml of TriReagent in eppendorf tubes and then incubated at room temperature for 10 min. For mouse tissues, the sample was homogenised using a TissueRuptor (Qiagen). 200µl of chloroform was added, and the tubes were vigorously shaken and incubated at room temperature for 10 additional minutes. The samples were centrifuged at 12000 x g rpm for 15 min at 4°C. The aqueous phase was removed an extracted again with 500µl of chloroform centrifuged at 12000 x g for 15 min at 4°C. The aqueous phase was precipitated by addition of 500µl of isopropanol and incubated at -20°C to favor RNA precipitation. RNA was collected by centrifugation at 12000 x g for 15-30 min at 4°C. The supernatant was removed and the RNA pellet was washed with 75% ethanol, air dried and re-dissolved in MilliQ water. The RNA concentration and purity was determined by measuring the absorbance at 260nm and 280nm using a Nanodrop 1000 (Thermo Scientific) and the samples stored at -80°C.

cDNA synthesis

1µg of total RNA was treated with RQ1 RNase-Free DNase (Promega) and reverse transcribed with random primers (Life Technologies) and GoScript Reverse Transcriptase (Promega) following the manufacturer's instructions. For subsequent qPCR analysis, a negative control reaction (without reverse transcriptase) was added to each experiment in order to evaluate the contribution of genomic DNA contaminants to the amplification of each target sequence. cDNA was stored at -20°C.

Polymerase chain reaction (PCR)

PCR amplification was routinely used for cloning purposes, site-directed mutagenesis, screening of bacterial colonies, semi-quantitative studies of gene expression by Reverse Transcription Polymerase Chain Reaction (RT-PCR). The PCR reaction was performed in 1x PCR buffer, 0.3mM dNTPs mix (Fisher Scientific), 0.5µM of the forward and reverse primers and 0.1µl of high fidelity Pfu DNA polymerase (EMBL Heidelberg core facility) and 50ng of DNA template in a final volume of 25µl. The reaction was run on a Thermal cycler 2720 (Applied Biosystems) in the following conditions: 95°C 5 min, (95°C 30s, 60°C 30s, 72°C 30s) x 30 cycles, 72°C 7 min. Annealing temperature and number of cycles were optimized for each amplification. All primers are listed in Table 2.1. After amplification, if required, the PCR product was purified using the GFX PCR DNA and Gel Band Purification kit (GE Healthcare).

Quantitative polymerase chain reaction (qPCR)

As template for the qPCR reaction, the cDNA generated starting from 1µg of total RNA was diluted 1:4 before use. The reaction mix contained 5µl of iTaq Universal SYBR Green Supermix 2x (Bio-Rad), 0.3µM of the forward and reverse primers and 1µl of cDNA in a total volume of 10µl. The qPCR was run on an ABI PRISM 7900HT Sequence Detection System (Applied Biosystems) in the following themocycling conditions: 95°C 2 min, (95°C 15s, 60°C 1 min) x 40 cycles. Relative quantification analysis was performed using the RQ manager software (Applied Biosystems); for each target gene, the level of expression was calculated as average of the triplicates normalized against the mRNA levels of 2 housekeeping mRNAs (L19, TBP and/or β-actin) and calibrated to a reference sample. All primers are listed in Table 2.1.

Restriction digestion of DNA

Digestion with restriction enzymes was routinely used for cloning purposes or for linearization of plasmid vectors to be used for *in vitro* transcription of RNA probes for EMSA.

The desired amount of DNA (PCR product or plasmid vector) was incubated in 1x of the appropriate reaction buffer and 10 units of restriction enzyme/µg DNA, supplemented with BSA to the recommended concentration if required and incubated at 37°C (or recommended temperature) for 2h. Efficiency of digestion was checked by agarose gel electrophoresis. If necessary for the following application, the digestion product was purified using the GFX PCR DNA and Gel Band Purification kit (GE Healthcare).

Agarose DNA electrophoresis

Typically, a 2% agarose gel was used for electrophoretic separation of PCR fragments while a 1% agarose gel was used for analysis of plasmid DNA or RNA quality control.

The desired amount of agarose was boiled in 1x TBE buffer until complete dissolution, cooled down, added of 0.5µg/ml ethidium bromide solution and then poured in an horizontal electrophoresis chamber with combs (EMBL, Heidelberg) and let solidify. The DNA was prepared in 1x DNA loading buffer, separated electrophoretically at 90V along with a molecular weight marker. The image was acquired using the GelDoc XR System (Bio-Rad).

Cloning strategies

For cloning purposes, the sequence of interest was PCR-amplified with specific primers carrying restriction sites, the PCR reaction was purified using the GFX PCR DNA and Gel Band Purification kit (GE Healthcare) and then digested with the corresponding restriction enzymes. Alternatively, for sequences shorter than 70bp, as in the case of the cloning of IRE sequences, the cloning insert was obtained by annealing of complementary primers corresponding to the sequence of interest and carrying restriction sites.

The inserts thus obtained were introduced into the desired plasmid vectors, digested with the same restriction enzymes and gel purified, using the Quick Ligation kit (New England Biolabs) according to the manufacturer's protocol. Generally, 2µl of the ligation reaction were heat-shock transformed into competent TOP10 bacterial cells (Invitrogen).

For site-directed mutagenesis purposes, 50ng of the wild-type template plasmid vector were PCR-amplified using complementary primers carrying the desired change to introduce in the following settings: 95°C 30s, (95°C 3s, 55°C 1 min, 68°C 10 min) x 16 cycles, 68°C 10 min. The template DNA was eliminated by enzymatic digestion with DpnI, which is specific for methylated DNA and 2µl of the digestion reaction were heat-shock transformed into TOP10 competent bacteria.

TOP10 transformed cells were plated onto LB plates with 100µg/ml amplicillin or 30µg/ml kamicin. Colonies were grown in LB broth with antibiotics, plasmid DNA extracted using the Nucleospin plasmid mini DNA purification kit (Macherey-Nagel) according to the manufacturer's instructions and the presence of the correct insert verified by Sanger sequencing (GATC Biotech, Konstanz).

All primers used for cloning purposes are listed in Table 2.1.

Non-radioactive competitive electrophoretic mobility shift assay (EMSA)

Direct or competitive EMSAs were used to assess *in vitro* binding of RNA sequences to recombinant IRP1 or IRP2 proteins. Competitive EMSAs are a modification of a classical band shift assay implying more stringent binding conditions. A non-radioactive version of classical EMSA was set up based on the paper of Köhn and colleagues (Kohn *et al.* 2010).

In these experiments a fluorescent-labeled probe corresponding to the FTH1-IRE sequence was incubated with IRP1 or IRP2 protein and increasing amounts of non-labeled competitor RNA sequences; if the non-labeled sequence interacts with the IRP protein, it would compete for the binding with the FTH1-IRE probe, eliminating the signal of the shifted band.
Firstly, *in vitro* transcription reactions were performed to synthesize RNA probes for EMSA. For the synthesis of the ATTO680-labeled probe, 2µg of XbaI-linearized I12CAT plasmid, containing the FTH1 IRE, downstream to a T7 promoter, was used as template. The *in vitro* transcription reaction was performed in 1x *in vitro* transcription buffer, 0.33mM rATP, rCTP, rGTP, 3.3µM rUTP, 20µM aminoallyl-ATTO680-rUTP (Jena Bioscience), 30mM DTT, 20 units RNasin Ribonuclease Inhibitor (Promega), 1µl of T7 RNA polymerase (EMBL Heidelberg core facility) and incubated at 37°C for 4h. The non-labeled competitors corresponding to the sequences to test for IRP binding were *in vitro* transcribed using the MEGAscript T7 kit (Life Technologies) following the manufacturer's protocol.
The newly synthesized RNA were purified by phenol/chloroform/isoamyl alcohol extraction, precipitated with 1/10 volume 3M sodium acetate pH 5.2 and 2.5 volumes of ethanol to remove the unincorporated nucleotides and quantified using a Nanodrop 1000 (Thermo Scientific).
For EMSAs 50ng of FTH1-IRE labeled probe were mixed with increasing molar excess (1x, 2x, 5x, 10x, 20x, 40x, 80x) of unlabeled competitors, heated at 95°C for 3 min and chilled on ice. As positive and negative control of the experiments a wild type FTH1-IRE competitor and a mutant version bearing a C deletion in the IRE loop, not interacting with the IRP (Gray *et al.* 1996), were used. The binding reaction was performed incubating 125ng of recombinant IRP1 or IRP2 protein in CLB buffer with the probes mixture 15 min at room temperature. Non-specific interactions were competed by addition of 50µg sodium heparin and further 10 min incubation. 1µl of 80% glycerol loading buffer was added and the reaction loaded on a 5% native acrylamide (60:1 acrylamide:bisacrylamide) gel. Electrophoretic separation of the RNA-protein complexes was carried out at 100V for 30 min in a Mini-PROTEAN Tetra Cell (Bio-Rad) and images acquired using the Odyssey Infrared Imaging System (LI-COR) and bands corresponding to IRP/IRE complexes were quantified using the Odyssey V3.0 software.

Total protein extraction from cultured cells or mice tissues

Cells grown in adhesion were washed with ice-cold PBS and then scraped in the appropriate volume of ice-cold Lysis buffer. For mouse tissues, the samples were homogenised in the appropriate volume of ice-cold Lysis buffer using a TissueRuptor (Qiagen). Homogenized samples were incubated on ice for 30 min and then centrifuged 12000 x g for 10 min at 4°C. The supernatant was transferred to a new tube and protein concentration was quantified using the Bio-Rad protein assay reagent (Bio-Rad) or the Pierce BCA Protein Assay kit (Themo Scientific) as described in the manufacturer's directions. A series of dilutions of known concentration of bovine serum albumin were read as a reference standard curve. Protein extracts were stored at -80°C.

Western blotting

Equal amounts of total protein extracts (10-50µg) were prepared, SDS protein loading buffer was added to final 1x concentration and heat denatured at 95°C for 5 min; heat denaturation step was avoided when FPN protein need to be detected. Protein extracts were then separated on SDS-PAGE along with molecular weight standard (Bio-Rad) in running buffer 1x. SDS-PAGE consisted of 4% stacking and 10%, 12% or 15% separating gels according to the procedure described by Laemmli (Laemmli 1970). Following electrophoresis, proteins were electroblotted in transfer buffer at 20V overnight at 4°C onto polyvinylidene fluoride (PVDF)

membrane (Millipore) pre-activated by a short incubation in methanol. The membrane was subsequently blocked with 5% dry fat-free milk in TBST for 30 min at room temperature. Incubation with primary antibody in 1x TBST/5% milk was performed for 3h at room temperature or overnight at 4°C. After 3 washes with 1x TBST, the membrane was incubated for 1h at room temperature with appropriate secondary antibody coupled to horseradish peroxidase in 1x TBST/5% milk. Primary and secondary antibodies used and the relative dilutions are indicated in the section 2.1.2. After 3 washes with 1x TBST, the secondary antibody was detected using a home-made ECL solution or Luminata Forte Western HRP substrate (Millipore) and acquired with the FluorChemHD2 imaging system (Alpha Innotech). For control of protein loading, membranes were also probed for β-actin, α-tubulin or S6 ribosomal protein endogenous controls. Relative protein expression was assessed by densitometric analysis of signal intensity using the AlphaEaseFC software (Alpha Innotech).

2.2.4 Statistical analysis

Data are shown as mean values ± SD (SEM in the case of mouse parameters). Statistical analysis was performed using two-tailed unpaired Student's t test using GraphPad Prism software and P values <0.05 were considered statistically significant.
In particular: * 0.01> P value >0.05, ** 0.001> P value >0.01, *** P value < 0.001.

3. RESULTS AND DISCUSSION

3.1 Novel mutations in the L-ferritin IRE are causative of Hereditary Hyperferritinemia-Cataract Syndrome (HHCS)

The results here exposed were published in the peer-reviewed journal *Orphanet Journal of Rare Diseases* with impact factor: 3.958 (see Annex I)
Orphanet J Rare Dis. 2013 Feb 19;8:30. doi: 10.1186/1750-1172-8-30. PMID: 23421845
"Novel mutations in the ferritin-L iron-responsive element that only mildly impair IRP binding cause hereditary hyperferritinaemia cataract syndrome"
Luscieti S, Tolle G, Aranda J, Campos CB, Risse F, Morán É, Muckenthaler MU, Sánchez M.
See section 1.6.1 for an introduction of HHCS disease.

3.1.1 Clinical data of two family cases of HHCS

I studied two family cases presenting a history of high serum ferritin levels and juvenile bilateral cataract.

Pedigree 1
The proband (IV:1, Figure 3.1A and Table 3.1) is a 19 year old man of German-Romanian origin, who was referred to the medical doctor due to fatigue and concentration problems. He showed high serum ferritin levels with normal serum iron and transferrin saturation. He presented with cataracts since the age of 16 and has not undergone surgery. He does not present any other clinical signs. No evidence for acute or chronic inflammation was detected and his liver functional tests and abdominal morphology at ecographic inspection were normal. The father (III:2) presents with similar biochemical findings showing elevated serum ferritin and clinical symptoms with cataracts detected also at the age of 16 (Table 3.1). The paternal grandmother (II:2) and a great-aunt (II:4) had also suffered from cataracts (Figure 3.1A).

Pedigree 2
The proband (III:2, Figure 3.1B and Table 3.1) is a 54 year old woman of Spanish origin presenting a 10-year history of hyperferritinemia with no sign of iron overload. Serum iron, transferrin saturation and liver functional tests were normal. The patient presents no evidence of hepatitis, cirrhosis, diabetes, inflammatory diseases, metabolic syndrome or neoplasia. She has suffered from bilateral cataracts since she was 18 years old and underwent surgery at the age of 39. The proband has one sister (III:4) and a cousin (III:9) presenting similar clinical features with hyperferritinemia and juvenile bilateral cataract (Table 3.1). No evidence of elevated serum ferritin was found in four other sisters of the proband. A deceased maternal uncle (II:4) had suffered from hyperferritinemia and cataract reported as an adult. Notice that the proband's parents (II:1 and II:2) were first cousins. The father (II:1) had suffered from cataracts which required surgical correction in adult age. The proband's daughter (IV:1) has no visual impairment and normal serum ferritin, however, this fact has to be considered

together with a concomitant iron-deficient anemia (Table 3.1). The two sons (IV:2 and IV:3) of the other affected sister (III:4) have moderately elevated serum ferritin levels but no documented visual impairments yet (Table 3.1).

Clinical and biochemical data of these families is presented below in Table 3.1.

Table 3.1 Clinical and biochemical values of the affected subjects of the two HHCS families studied

	Pedigree 1		Pedigree 2						
Characteristic	**IV:1**	**III:2**	**III:2**	**III:4**	**III:9**	**IV:1**	**IV:2**	**IV:3**	**Normal values**
Age at diagnosis (years)	19	40	54	53	48	27	27	25	
Sex	M	M	F	F	M	F	M	M	
Cataract diagnosis (years)	**16**	**16**	**20**	**17**	**20**	-	-	-	
Cataract surgery (years)	-	-	**39**	-	-	-	-	-	
Hb (g/dl)	15.6	15	13.2	13.1	15.3	13.4	14.3	14.7	14.6 – 17.8 ♂ 12.1 – 15.9 ♀
MCV (fl)	80.9	80,6	92.3	96	94.1	91.3	85.1	83.4	79 – 99
CRP (mg/L)	4	-	<5	-	4	<5	<5	-	5 – 10
Serum iron (µg/dl)	127	111	74	56	79	37	124	243	37 – 170
TIBC (µg/dl)	-	-	361	-	342	372	327	424	250 – 450
Serum ferritin (ng/ml)	**1290**	**1260**	**719**	**534**	**952**	**239**	**303**	**447**	20 – 250 ♂ 15 – 150 ♀
Transferrin (mg/dl)	291	300	252	-	-	260	229	296	200 – 360
Transferrin saturation (%)	31	25	20	-	23.1	10	38	57	20 – 50 ♂ 15 – 50 ♀
ALT (mU/ml)	-	-	28	17	35	21	38	14	14 – 36
AST (mU/ml)	27	33	35	20	40	20	30	30	9 – 52

The following abbreviations were used: Hb, hemoglobin; MCV, mean corpuscular volume; CRP, C-reactive protein; ALT, alanine aminotransferase; AST, aspartate aminotransferase.

3.1.2 Molecular genetic studies

3.1.2.1 Identification of two novel mutations in L-ferritin IRE

Sequencing of exon 1 of L-ferritin (*FTL*) in the two families revealed the presence of two previously undescribed variations in the IRE sequence.

In pedigree 1, a G>C change was detected at position +52 of the IRE lower stem (NM_000146.3; c.[-148G>C]) in heterozygous state (Figure 3.1A and C and Figure 3.4A). Sequencing analysis in pedigree 2 showed a C>U change at position +36 of the upper stem of *FTL* IRE (NM_000146.3; c.[-164C>T]). Interestingly, the mutation was found to be present in homozygous state in two members of this family (the proband, III:2 and her sister, III:4), while other affected members (III:9, IV:1, IV:2 and IV:3) carry the change in heterozygous state (Figure 3.1B and D and Figure 3.4A). Notice that Hereditary Hyperferritinemia-Cataract Syndrome is an autosomal dominant disease and one single mutation is enough to develop the clinical and biochemical symptoms of this disease (see section 3.1.2.4).

In according with the traditional nomenclature for *FTL* IRE mutations I refer, from now on, to these mutation as the “Heidelberg +52G>C” and the “Badalona+36C>U”, respectively.

Moreover, the sequencing of the complete *FTL* gene (coding region and exon-intron boundaries) did not reveal any other pathological change (Table 3.2).

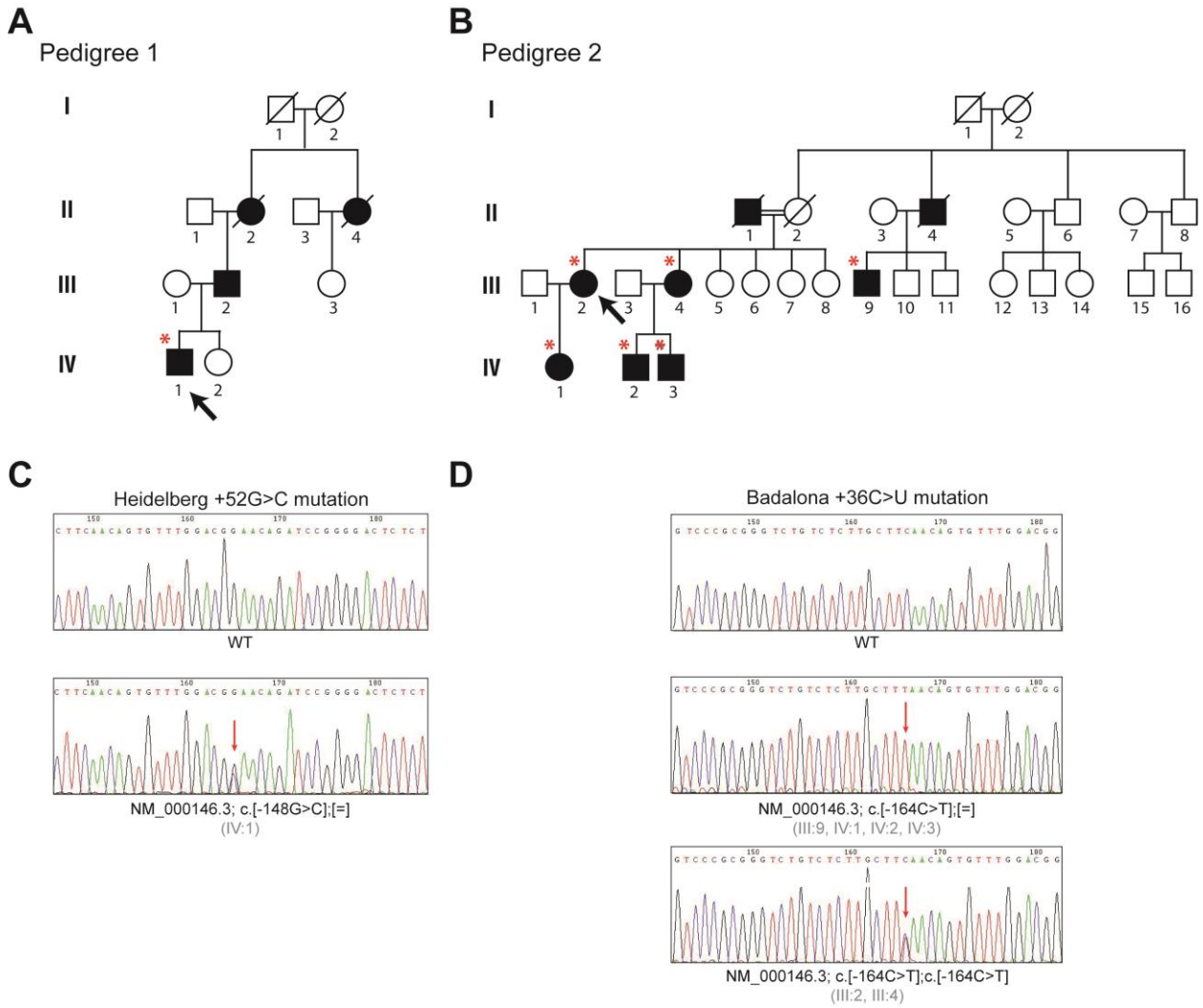

Figure 3.1 Two family cases of HHCS. (A, B) Pedigree trees of the two families studied: squares indicate males and circles females. Filled symbols indicate affected members and barred symbols indicate deceased subjects. Asterisks indicate subjects characterized at the molecular level. **(C, D)** Chromatograms of partial *FTL* IRE sequences where mutations are located; the nucleotide position that is altered is indicated by arrows. WT denotes wild type sequence according to reference sequence NM_000146.3.

Table 3.2 Searching for mutations in *FTL* and *HFE* genes

	Pedigree 1		**Pedigree 2**					
Gene	**IV:1**	**III:2**	**III:2**	**III:4**	**III:9**	**IV:1**	**IV:2**	**IV:3**
***FTL* (NM_000146.3) gene sequencing**								
exon 1	[c.-148G>C]; [=] Heidelberg +52G>C	not tested	[c.-164C>T]; [c.-164C>T] Badalona +36C>U	[c.-164C>T]; [c.-164C>T] Badalona +36C>U	[c.-164C>T]; [=] Badalona +36C>U	[c.-164C>T]; [=] Badalona +36C>U	[c.-164C>T]; [=] Badalona +36C>U	[c.-164C>T]; [=] Badalona +36C>U
exon 2	rs2230267 c.[362T>C]; c.[362T>C] L55L +/+	not tested	not tested	rs2230267 c.[362T>C]; c.[362T>C] L55L +/+	not tested	not tested	not tested	not tested
exon 3	–	not tested	not tested	–	not tested	not tested	not tested	not tested
exon 4	–	not tested	not tested	–	not tested	not tested	not tested	not tested
***HFE* (NM_000410.3) gene sequencing:**			**Hemochromatosis strip assay kit, testing for C282Y, H63D and S65C in HFE gene:**					
exon 2	–	not tested	H63D +/-	–	H63D +/+	S65C +/-	–	–
exon 4	–	not tested						

3.1.2.2 Screening of in Hereditary Hemochromatosis genes

Affected members of both pedigrees did not present signs of iron overload; however, further genetic testing was performed to exclude Hereditary Hemochromatosis as the cause of the hyperferritinemia in these patients. The most common variations associated with Hereditary Hemochromatosis type 1 (C282Y, H63D and S65C) were tested either by the sequencing of exon 2 and 4 of *HFE* gene or using specific commercial reactive strips. Hemochromatosis type 1 was excluded by the results for all the subjects analyzed (Table 3.2).
In addition, the proband IV:1 from pedigree 1 was tested for mutations in the *SLC40A1* gene and negative results excluded also Hemochromatosis type 4.

3.1.2.3 Validation of the Heidelberg and Badalona mutations

To exclude the possibility that the changes found in the two pedigrees are common polymorphisms, 50 control subjects were tested for the presence of the Heidelberg or Badalona mutations by PCR-Restriction Fragment Length Polymorphism (PCR-RFLP), as the +52G>C and +36C>U changes introduce a HgaI and a MseI recognition site, respectively (Figure 3.2A and B). Both changes were absent in 50 control subjects, further supporting their causative role for the disease (Figure 3.2C and D).

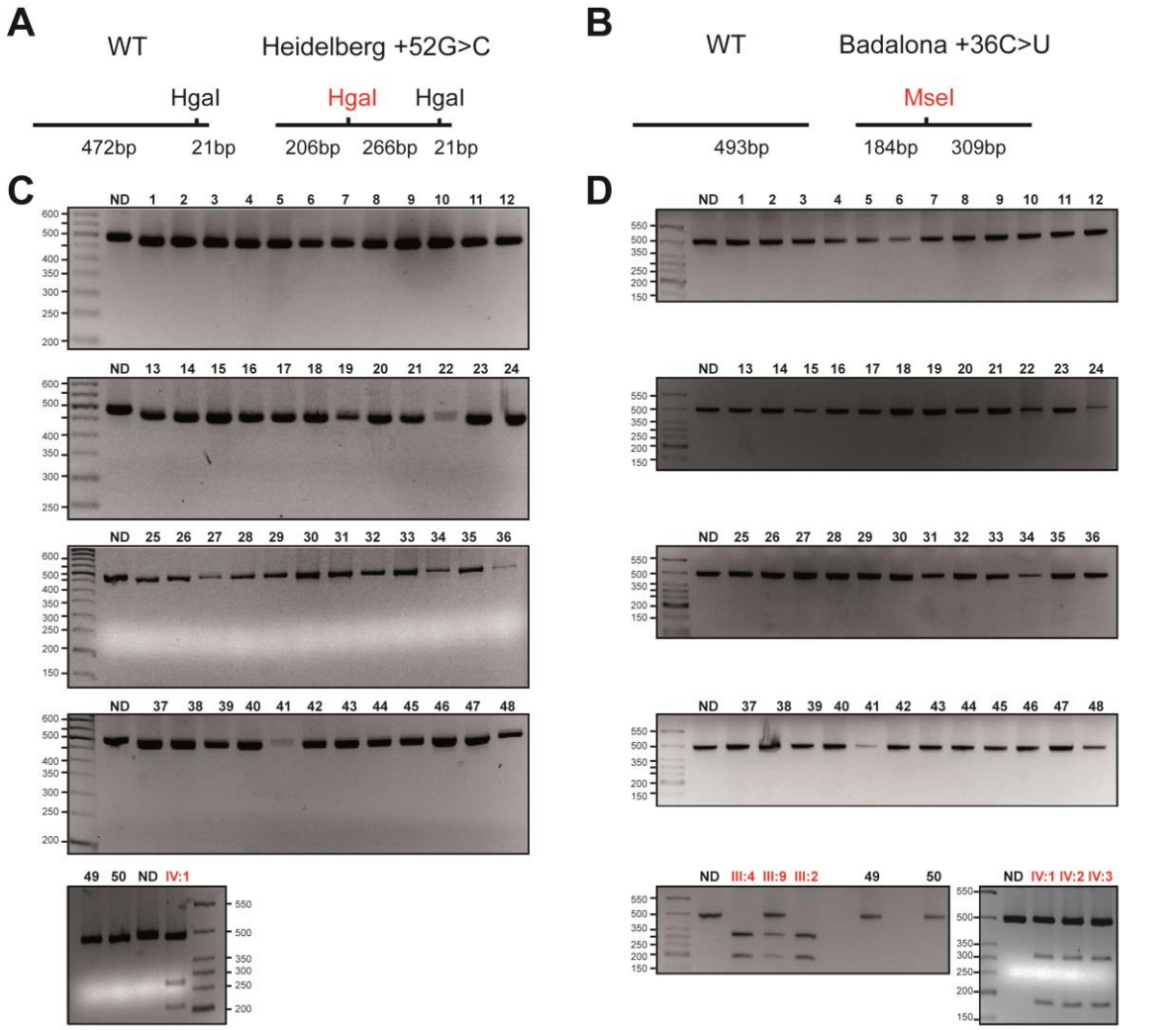

Figure 3.2 PCR-RFLP for the Heidelberg and Badalona mutations. *FTL* exon1 was PCR-amplified from DNA samples of 50 healthy controls and then digested with HgaI or MseI restriction enzymes. **(A, B)** Graphic representation of the expected length of the fragments after HgaI or MseI digestion in the absence (WT) or presence of the Heidelberg or Badalona mutation. **(C, D)** Digestions were run on agarose gels. Numbers from 1 to 50 indicate the samples from healthy controls. Samples from the affected patients of pedigree 1 and 2 are indicated in red. WT: wild type; ND: not digested.

3.1.2.4 Homozygosity of the Badalona mutation

Hereditary Hyperferritinemia-Cataract Syndrome (HHCS) is an autosomal dominant disease and the causative mutation is normally present at heterozygous state. Homozygous mutations are very unusual with only one case reported previously (Alvarez-Coca-Gonzalez *et al.* 2010). In pedigree 2, the mutation Badalona +36C>U was found to be present in homozygous state in two subjects (III:2 and III:4 Figure 3.1B and D). This can be easily explained by the consaguineity between the parents of the homozygous subjects (II:1 and II:2), that are first cousins. To confirm this genotype, we performed additional studies to exclude that the homozygosity of the mutation was not arisen from technical problems, like from an "allele dropout" mechanism. An allele dropout could be due to the presence of a polymorphism in one of the two alleles within the sequence where PCR primers hybridize, resulting in the no amplification of that allele and in a false homozygosity. To rule out this possibility, the results were checked using a different set of primers and the homozygosity of the two patients was observed again and therefore confirmed (data not shown).

Moreover, a possible co-inheritance of the +36C>U mutation together with a large *in trans* deletion was also evaluated with gene dosage studies by qPCR. I amplified DNA samples from healthy controls (2N content) using two different sets of primers covering exon 1 of *FTL* gene, in order to calculate a 2N confidence interval with a 95% confidence. The results of the patients from pedigree 2 fall in between the confidence interval indicating that all the patients carry two copies of the *FTL* gene (Figure 3.3 upper) and thus confirming that the Badalona +36C>U mutation is present at homozygous state in the subjects III:2 and III:4. As internal control of the sensitivity of the method I have checked two additional genes: an unrelated gene *GAPDH* (2N) and *HPRT1,* a gene located on the X chromosome and therefore allowing to differentiate the 1N or 2N content between males and females. As expected, *GAPDH* showed 2N content in all the subjects from pedigree 2 and qPCR results for *HPRT1* correctly identified the male subjects with 1N content (III:9, IV:2 and IV:3 Figure 3.3 lower).

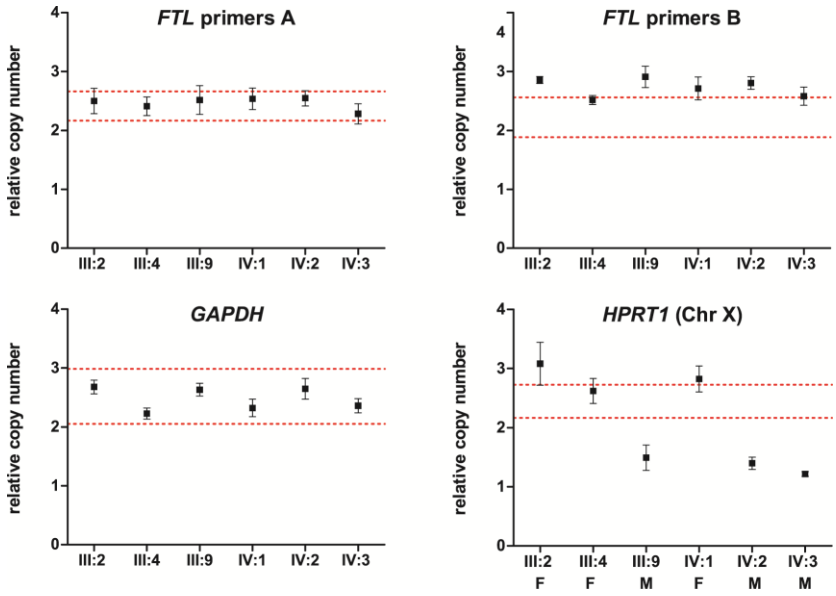

Figure 3.3 Gene dosage studies. The graphs represent the results of allele dosage studies by qPCR. Two sets of primers covering *FTL* exon1 (primers A and primers B) were used and two control genes were amplified: *GAPDH* (2N) and *HPRT1* (1N in males or 2N in females). Results were normalized against *ADARB1* and *L1PA* (LINE sequence) reference genes. To interpret the qPCR results, DNA samples from 17 female controls were also amplified in order to calculate a 2N content 95% confidence interval for each gene. This interval (indicated by the red lines) represents the estimated range of values which is likely to include the true value from an unknown sample with a 95% of confidence. If the qPCR normalized value, calculated for the patients from pedigree 2, falls within this interval is considered as 2N content; if it falls below the interval is considered as 1N content. Experiments were done in triplicate and means ± SD are shown. Chr X: chromosome X; F: female; M: male.

3.1.3 Functional test: binding affinity of the mutated IREs to IRP1 and IRP2

HHCS causative mutations in the IRE of L-ferritin impair the interaction with IRP1 and IRP2 protein, leading to an uncontrolled overproduction of the L-ferritin subunit that deposits in the lens and causes cataracts formation (see section 1.6.1).
I therefore further examined if the IRE structure and the IRP-IRE interaction are affected by the Heidelberg and Badalona mutations.

3.1.3.1 Biocomputational folding analysis

For the Heidelberg mutation, the change of a guanosine to a cytosine at position +52 in FTL IRE is expected to disrupt the base pairing with the cytosine at position +29 (Figure 3.4A).
However, this is not obvious for the Badalona +36C>U mutation. In fact, the substitution of a cytosine by an uracil at position +36 is not expected, *a priori*, to alter the base pairing with the guanosine at positin +47 in the IRE structure (Figure 3.4A), since both C-G or U-G base pairs are possible at RNA level. For this mutation, I performed computational RNA folding predictions of the WT and mutated sequences using the RNAfold WebServer (ViennaRNA Web Services, Institute for Theoretical Chemistry, University of Vienna). The results show that the presence of the Badalona mutation disturbs the base-pairing within the IRE (see color change in Figure 3.4B) and increases the minimum free energy of the folding (-31.60 kcal/mol for the wild type IRE versus -29.50 kcal/mol for the mutated IRE).

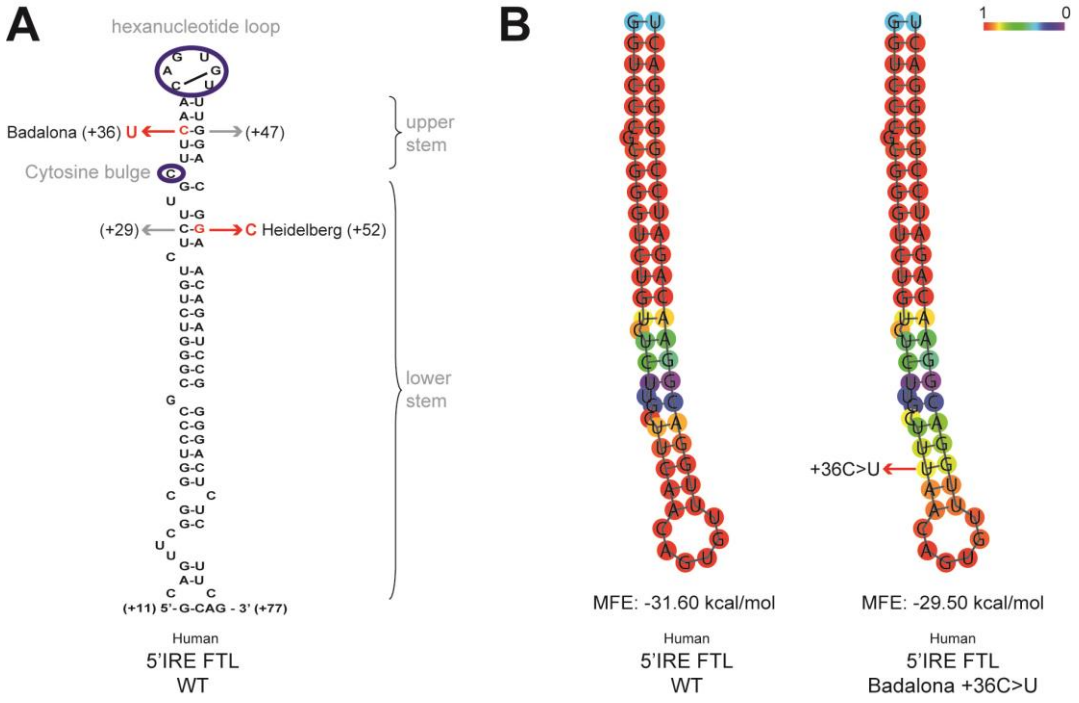

Figure 3.4 Structure of the L-ferritin IRE. (A) Representation of the canonical structure of FTL IRE. The most important structural parts are shown: the hexanucleotide apical loop, the cytosine bulge and the upper and lower stems. The position of the nucleotides altered by the Heidelberg and Badalona mutations are indicated in red. **(B)** RNAfold WebServer folding predictions of the FTL IRE wild type (left) or the Badalona +36C>U change (right). Color scale indicates the probability of base-pairing from 1 (high, red) to 0 (low, blue). MFE: minimum free energy.

3.1.3.2 Electrophoretic mobility shift assays (EMSAs)

For both mutations I next examined the ability of the mutated IRE to interact *in vitro* with recombiant IRP1 or IRP2 by electrophoretic mobility shift assays (EMSAs).
Plasmids for generating EMSA probes were constructed from I-12.CAT plasmid (Gray *et al.* 1993) by replacing FTH1 IRE with annealed synthetic oligonucleotides corresponding to the sequences of FTL IRE WT (nucleotides 11-68 in NM_000146.3) or the mutated versions:

Heidelberg +52G>C and Badalona +36C>U (Figure 3.5A). In addition, I generated plasmids to include proper controls in the EMSAs: a C deletion in the hexanucleotide loop (+39ΔC, negative control), the Torino +29C>G mutation (Bosio *et al.* 2004), that is the counterpart of the Heidelberg +52G>C change (Figure 1.15A and 3.5A) and the Milano +36C>G mutation (Cremonesi *et al.* 2003b) and the London2 +36C>A (Mumford *et al.* 1998), two variations at the same position as the Badalona +36C>U mutation (Figure 1.15A and 3.5A). DNA templates were linearized with XbaI and used for *in vitro* transcription. The obtained fluorescent labeled RNA probes were directly incubated with recombinant IRP1 or IRP2 protein and the IRE-IRP complexes resolved on acrylamide gels (Figure 3.5B and C).

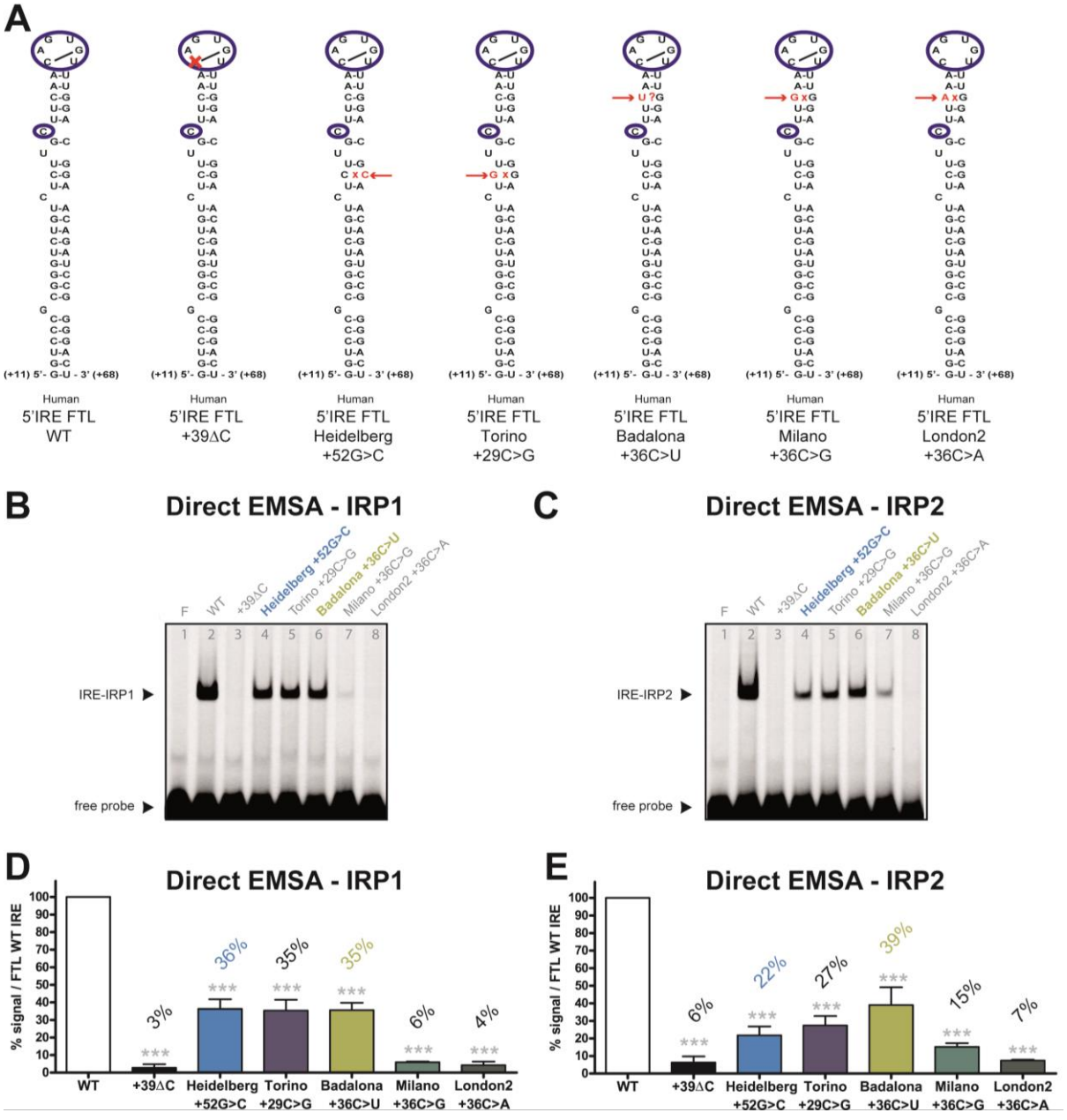

Figure 3.5 Direct EMSAs of WT and mutants FTL IRE with recombinant IRP1 and IRP2. (A) Graphic representation of the FTL IRE motifs (nucleotides 11-68 in NM_000146.3) wild type, the Heidelberg or Badalona mutants and other control mutants, used for the synthesis of RNA probes. **(B, C)** One representative EMSA showing fluorescent labeled RNA probes corresponding to the FTL IRE wild type (lanes 1-2), the mutations +39ΔC (lane 3), Heidelberg +52G>C (lane 4), Torino +29C>G (lane 5), Badalona +36C>U (lane 6), Milano +36C>G (lane 7) and London2 +36C>A (lane 8) that were incubated with recombinant IRP1 (panel B) or IRP2 (panel C) and the IRE-IRP complexes resolved on acrylamide gels. **(D, E)** Quantification of the signals was performed using the Odyssey Infrared Imaging System (LI-CORE Biosciences) and compared to the signal of WT FTL IRE, set as 100%. Means ± SD of at least three independent experiments. WT: wild type; F: free probe.

As expected, almost no binding occurs when using a non-functional IRE structure (+39ΔC, Figure 3.5B-E, lanes 3). The Heidelberg +52G>C and Badalona +36C>U mutations behave similarly and show a reduction of the binding capacity for both IRP1 and IRP2 (Figure 3.5B-E, lanes 4 and 6). The Heidelberg mutation shows a 65% reduction of the binding to IRP1 and nearly an 80% reduction of the binding to IRP2 while the Badalona mutation shows a 65% reduction of the binding to IRP1 and a 60% reduction of the binding to IRP2. A similar effect was observed with the Torino +29C>G control mutation (Figure 3.5B-E, lanes 5), showing also a ~70% reduction of the binding to both IRPs. The Milano +36C>G and the London2 +36C>A control mutations have a stronger effect reducing drastically its binding to both IRPs (Figure 3.5B-E, lanes 7-8) with a ~95% reduction for IRP1 and an 85-95% reduction for IRP2.

I also checked the binding to the IRPs of the Heidelberg +52G>C and Badalona +36C>U changes in more stringent conditions by competitive EMSAs (Figure 3.6). In these experiments, a fluorescent-labeled probe corresponding to the wild type FTL IRE sequence is incubated with increasing amounts of non-labeled competitor RNA sequences corresponding to the FTL IRE wild type or the mutated sequences in study. If the non-labeled sequence interacts with the IRP protein, it would compete for the binding and displace the labeled FTL IRE probe, reducing the signal of the shifted band.

As expected, no competition was observed for the +39ΔC IRE control, not even at the highest molar concentration of competitor RNA (Figure 3.6A-D, lanes 9-14 compared to 3-8), indicating that the +39ΔC IRE is not functional. The Heidelberg +52G>C mutation showed a reduced, although not totally abolished, capacity to compete with the FTL WT probe and behaved similar to its corresponding counterpart control, the Torino +29C>G change (Figure 3.6A-D, lanes 17-22 and 23-28 compared to 3-8).

The Badalona +36C>U mutation showed only a slight but significant reduction in the efficiency of competition when compared to the wild type unlabeled competitor (Figure 3.6 A-D, lanes 31-36 compared to 3-8). In contrast, its corresponding controls, the Milano +36C>G and London2 +36C>A changes, are almost inefficient in competing with the wild type labeled probe (Figure 3.6A-D lanes 37-42 and 45-50 compared to 3-8), indicating that the mutations Milano +36C>G and London2 +36C>A practically totally abolish the binding capacity of the IRE. In contrast the Badalona mutation is partially functional and does not strongly affect the binding *in vitro* to the IRPs as the Milano and London2 mutations; however the Badalona mutation is still causative of the disease.

Similar results were obtained in all EMSAs experiments either using recombinant IRP1 or IRP2 (Figure 3.6A-B and C-D). Both direct and competitive EMSAs indicate that the functionality of L-Ferritin IREs is as follow:

100% wild type > Badalona >> Torino = Heidelberg >> Milano > London2 > +39ΔC 0%

3.1.4 Phenotype/genotype correlation in HHCS

Our extensive analysis of all HHCS cases described in the literature demonstrates that serum ferritin levels correlate with the position of the mutation in the L-ferritin IRE (Figure 3.7). Mutations affecting the most important IRE structural elements, such as the hexanucleotide loop or the C-bulge area are detected in patients with more elevated serum ferritin levels compared to those patients with mutations affecting the base pairing of the upper or lower stem of the IRE (Figure 3.7).

Consistently, our cases with mutations in the upper stem (Badalona mutation) and lower stem (Heidelberg mutation) of the IRE also show intermediate serum ferritin levels (<1300 ng/ml, Table 3.1).

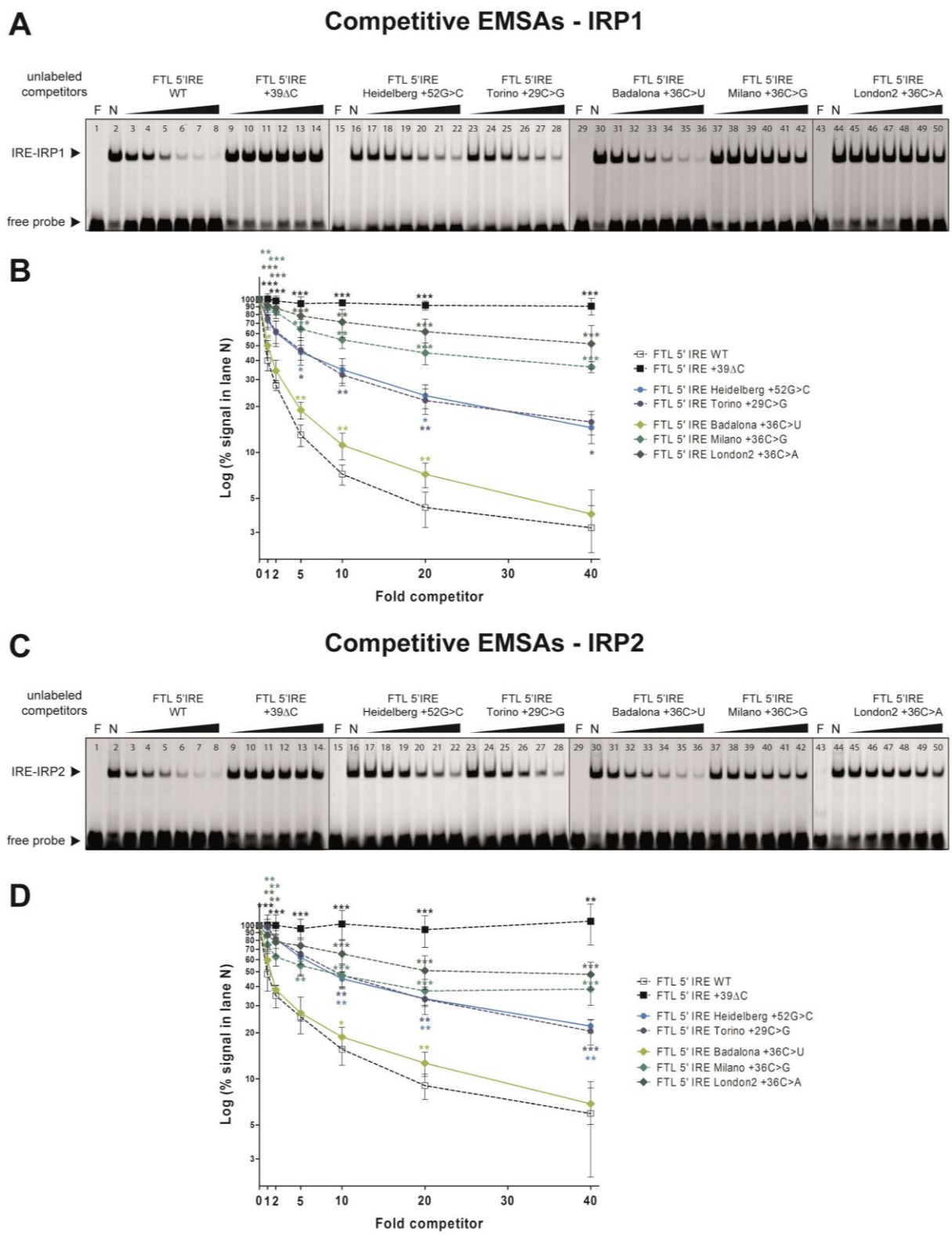

Figure 3.6 Competitive EMSAs of WT and mutants FTL IRE with recombinant IRP1 and IRP2. (A, C) Florescent-labeled FTL IRE wild type probe was incubated with increasing molar excess (1x, 2x, 5x, 10x, 20x and 40x) of unlabeled competitors corresponding to the FTL IRE wild type sequence (lanes 3-8), or the mutants +39ΔC (lanes 9-14), Heidelberg +52G>C (lanes 17-22), Torino +29C>G (lanes 23-28), Badalona +36C>U (lanes 31-36), Milano +36C>G (lanes 37-42) and London2 +36C>A (lanes 45-50). Samples were incubated with recombinant IRP1 (panel A) or IRP2 (panel C) and complexes resolved on acrylamide gels. (B, D) Quantification of the signals of the shifted bands was performed using Odyssey Infrared Imaging System (LI-CORE Biosciences) and compared to the intensity of the signal in lane N, set as 100%. Means ± SD of at least three independent experiments. Statistical analysis compares the signal given by the mutated IRE sequences to the signal given by the WT IRE unlabeled competitor, at each molar concentration. WT: wild type; F: free probe; N: no competitor added.

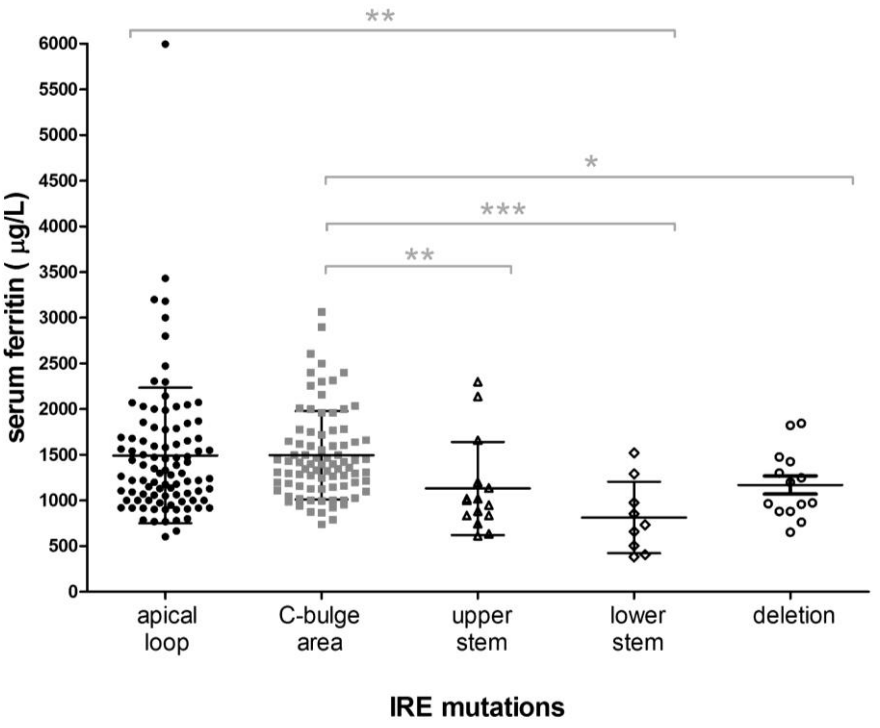

Figure 3.7 Phenotype-genotype correlation in all described HHCS patients. Serum ferritin levels (y-axis) are reported against the position of the IRE mutation in FTL IRE (x-axis). Patients with mutations affecting the apical loop or the C-bulge area present higher serum ferritin levels compared to the ones with mutations in the upper or lower stems.

3.1.5 Discussion

This work has been published in the peer-reviewed journal *Orphanet Journal of Rare Diseases* (Luscieti *et al.* 2013). With this work, we report two novel mutations (Heidelberg +52G>C and Badalona +36C>U) in the L-ferritin IRE causing HHCS in two families. Unexpectedly for an autosomal dominant disease, one of these families carries the mutation in a homozygous state in some affected subjects. Within this family there is a tendency for correlation between the genotype of the subjects and the clinical severity of the disease. However, this correlation is not perfect due to associated factors (age, sex, particular clinical history) that make difficult comparison between subjects. Therefore, we confirm that, as previously reported, a phenotype/genotype correlation in HHCS is difficult to establish due to concomitant pathologies, clinical penetrance and the fact that serum ferritin levels are influenced by sex and age and are subjected to inter and intra-individual variability.

By *in vitro* assays we show that these mutations mildly impair IRP-IRE binding; however this minor disturbance is sufficient for biochemical and clinical symptoms to occur in the patients. As previously demonstrated by others we also confirm a tendency for a correlation between the position of the IRE mutation and the ferritin levels in this disease.

Moderate hyperferritinaemia is a common feature found in the adult population and it can be attributed to different factors including metabolic disease, liver dysfunction, neoplasia, infection and inflammation. Some of these cases could be due to the rare genetic disease HHCS. Therefore, proper tests are important for a correct diagnosis for hyperferritinemia and to avoid unnecessary phlebotomy treatment in the case of HHCS.

3.2 A mutation in the ALAS2 IRE is a modifier of clinical severity in Erythropoietic Protoporphyria

The results exposed here are in preparation for publication in collaboration with the group of Dr. Hervé Puy (INSERM U773, University Paris Diderot).

Porphyrias are a group of genetically distinct disorders, each resulting from a partial deficiency of a specific enzyme in the heme biosynthetic pathway (see Introduction 1.3.2). Mutations that cause porphyria have been identified in all the genes of the heme biosynthetic pathway, except for the ubiquitous isoform of the first enzyme of heme synthesis (*ALAS1*). Porphyrias are inherited as autosomal dominant, autosomal recessive or X-linked traits (Balwani *et al.* 2012). Erythropoietic protoporphyria (EPP) is one type of porphyria. EPP is a rare haematological disorder, characterized by protoporphyrin (PP) accumulation in erythrocytes and other tissues resulting in mild microcytic anemia, acute skin photosensitivity and, rarely, in severe liver disease. The majority of the patients with EPP have autosomal dominant EPP (OMIM #177000) due to a partial deficiency of ferrochelatase (FECH*)*, the last enzyme of the heme biosynthetic pathway. FECH is an inner membrane mitochondrial enzyme that catalyzes the insertion of ferrous iron into protoporphyrin IX to form heme and FECH deficiency in EPP patients causes free protoporphyrins accumulation. In many EPP patients, the clinical expression requires the coinheritance of a *FECH* mutation, that abolishes or markedly reduces FECH activity, *in trans* to an hypomorphic *FECH* allele (rs2272783, NM_000140.3; c.[315-48T>C]), carried by about 11% of western Europeans (Gouya *et al.* 2006). Rare cases of *FECH* autosomal recessive inheritance have been described, counting for about the 4% of EPP patients (Gouya *et al.* 2006). Few EPP patients have been reported to harbour gain-of-function mutations in the last exon of the erythroid isoform of delta-aminolevulinic synthase (*ALAS2*) (Whatley *et al.* 2008). EPP due to *ALAS2* mutations is inherited as an X-linked trait and shows a distinct biochemical feature with a high level of free but also Zinc protoporphyrins (XLEPP, OMIM #300751). Increased ALAS2 activity results in the overproduction and accumulation of free protoporphyrin IX. Moreover, as the FECH enzyme is functional in those patients, all the available Fe2+ is used in the production of heme causing the FECH enzyme to use Zn2+ in its place with a consequent accumulation of Zinc protoporphyrin. Nevertheless, about 5% of the families with erythropoietic protoporphyria are negative for mutations in *FECH* or *ALAS2* genes.

3.2.1 Clinical data of the EPP family

Pedigree 3

A 18 year old Caucasian girl (III:2, Figure 3.8A) was referred to the French Center of Porphyria because of acute photosensitivity suggesting EPP. A high level of free PPIX and ZnPP in erythrocytes confirms the diagnosis (Table 3.3). Iron metabolism parameters (serum iron, serum ferritin and transferrin saturation) were compatible with iron deficiency. FECH enzyme activity was found to be normal. The father and one uncle of the proband presented with free PPIX and ZnPP accumulation in erythrocytes associated with mild-absent photosentivity (II:4 and II:2, Figure 3.8A and Table 3.3).

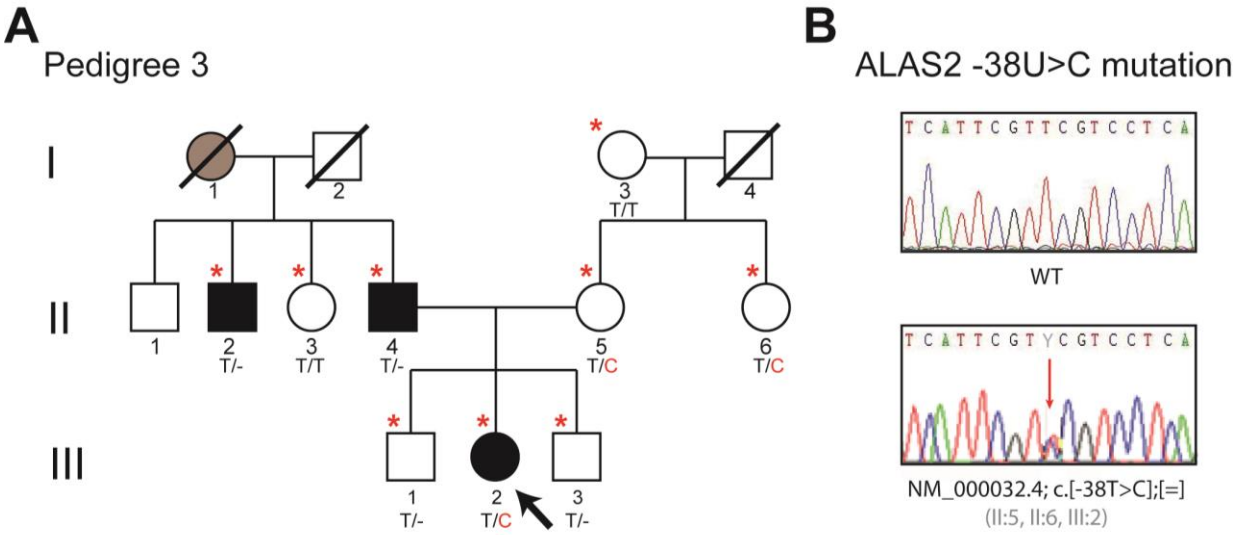

Figure 3.8 Family case of EPP. (A) Pedigree tree of the family studied: squares indicate males and circles females. Filled black symbols indicate affected members, gray symbols indicate unaffected carriers and barred symbols indicate deceased subjects. Asterisks indicate subjects characterized at the molecular level. **(B)** Chromatograms of partial *ALAS2* IRE sequences where mutations are located; the nucleotide position that is altered is indicated by arrows. WT denotes wild type sequence according to reference sequence NM_000032.4.

Table 3.3 Clinical and biochemical values of the affected subjects of the EPP studied family

	Pedigree 3			
Characteristic	**III:2**	**II:4**	**II:2**	**Normal values**
Age at diagnosis (years)	18	-	-	
Sex	F	M	M	
Photosensitivity	**acute**	mild	mild	
Total porphyrins (nmol/L)	**936**	**52**	**54**	0 – 15
Erythroid protoporphyrins (nmol/L RBC):	**140925**	**26664**	**30426**	<1500
- Free PPIX (%)	71	38	33	
- ZnPP (%)	**29**	**62**	**67**	
Hb (g/dl)	12	15.9	15.5	14.6 – 17.8 ♂ 12.1 – 15.9 ♀
FECH activity (nmol/mg prot. h)	3.6	-	4.4	>3.5
Serum iron (µgl/dL)	**22**	111	139	37 – 170
Serum ferritin (ng/ml)	**5**	171	196	20 – 250 ♂ 15 – 150 ♀
Transferrin saturation (%)	**5**	32	31	20 – 50 ♂ 15 – 50 ♀
Transferrin receptor (mg/L)	3.95	2.6	2.54	2.2 – 5.0 ♂ 1.9 – 4.4 ♀

The following abbreviations were used: PPIX, Protoporphyrin IX; ZnPP, Zinc protoporphyrin; Hb, hemoglobin; FECH, ferrochelatase.

3.2.2 Molecular genetic studies

Sequencing analysis of EPP causative genes in patient III:3 showed no punctual or large *FECH* gene mutation, accordingly with normal FECH activity showed by biochemical tests (Table 3.3). Moreover the proband did not harboured the *FECH* low-expressed allele rs2272783, NM_000140.3; c.[315-48T>C].

Sequencing of *ALAS2* gene revealed an heterozygous U>C change at position -38 in the 5' UTR of ALAS2 mRNA, in the lower stem of ALAS2 IRE (NM_000032.4; c.[-38T>C];[=]) (Figure 3.8B and Figure 3.8A). The mutation is absent of the 6500 exome sequencing in the Exome Variant Server database, excluding the possibility of being a neutral polymorphism. However, *ALAS2* sequencing in other subjects of the family showed that the mutation did not cosegregrate with protoporphyrins accumulation, as the subjects II:4 and II:2 carry a WT *ALAS2* genotype (Figure 3.8A). The proband inherited the -38U>C change from the mother (II:5, Figure 3.8A) that presents ZnPP levels in the upper-normal range.

A linkage study allowed to exclude *ALAS2* gene as the causative gene for EPP in this family (studies done by Dr. Hervé Puy laboratory).

The -38U>C change, found in ALAS2 IRE, is not the primary cause of EPP in subject III:2 of this family. However, it is thought to be a modified of EPP in this family, increasing the severity of the disease in the proband (III:2), comparing with her father and uncle (II:4 and II:2) that do not present overt clinical symptoms.

Work done by Dr. Hervé Puy laboratory, combining linkage analysis in the family and exome sequencing studies, has identified a new gene responsible for EPP and mutated in the paternal branch of this family (work under progress). The combination of the mutation in that gene with the -38U>C *ALAS2* mutation explains the clinical severity of patient III:2.

3.2.3 Binding affinity of the mutated ALAS2 IRE to IRP1 and IRP2

To test the functional consequence of the -38U>C change in *ALAS2* IRE, I studied the binding affinity of this IRE toward recombinant IRP1 or IRP2 by competitive electrophoretic mobility shift assays (EMSAs).

3.2.3.1 Competitive electrophoretic mobility shift assays

Plasmids for generating EMSA probes were constructed from I-12.CAT plasmid (Gray *et al.* 1993) by replacing FTH1 IRE with annealed synthetic oligonucleotides corresponding to the sequences of ALAS2 IRE WT (nucleotides 93-125 in NM_000032.4) or the mutated version carrying the -38U>C change (Figure 3.9A). In addition, positive and negative controls were also included, corresponding to the wild type FTH1 IRE (nucleotides 60-85 in NM_002032.2) and a C deletion in the FTH1 IRE hexanucleotide apical loop (+71ΔC, Figure 3.9A), known to disrupt IRPs binding. DNA templates were linearized with XbaI and used for *in vitro* transcription in competitive EMSAs. A fluorescent-labeled FTH1 WT IRE probe was mixed with increasing amounts of non-labeled competitor RNA corresponding to the FTH1 IRE WT or +71ΔC, ALAS2 IRE WT or ALAS2 -38U>C constructs, incubated with recombinant IRP1 or IRP2 protein and the IRE-IRPs complexes resolved on acrylamide gels (Figure 3.9B and C). As expected the FTH1 WT positive control showed efficient competition, while its corresponding negative control, the FTH1 +71ΔC is not able to compete with the FTH1 WT probe (Figure 3.9B-E, lanes 3-8 and 9-14).

The ALAS2 -38U>C mutation also showed a totally abolished ability to compete for IRP binding against the FTH1 WT probe, when compared to the WT ALAS2 IRE sequence (Figure 3.9C-E lanes 17-22 and 23-28). Therefore, this mutation abolishes the ALAS2 IRE functionality. Similar results were obtained in all EMSAs experiments either using IRP1 or IRP2 recombinant protein (Figure 3.9B-E).

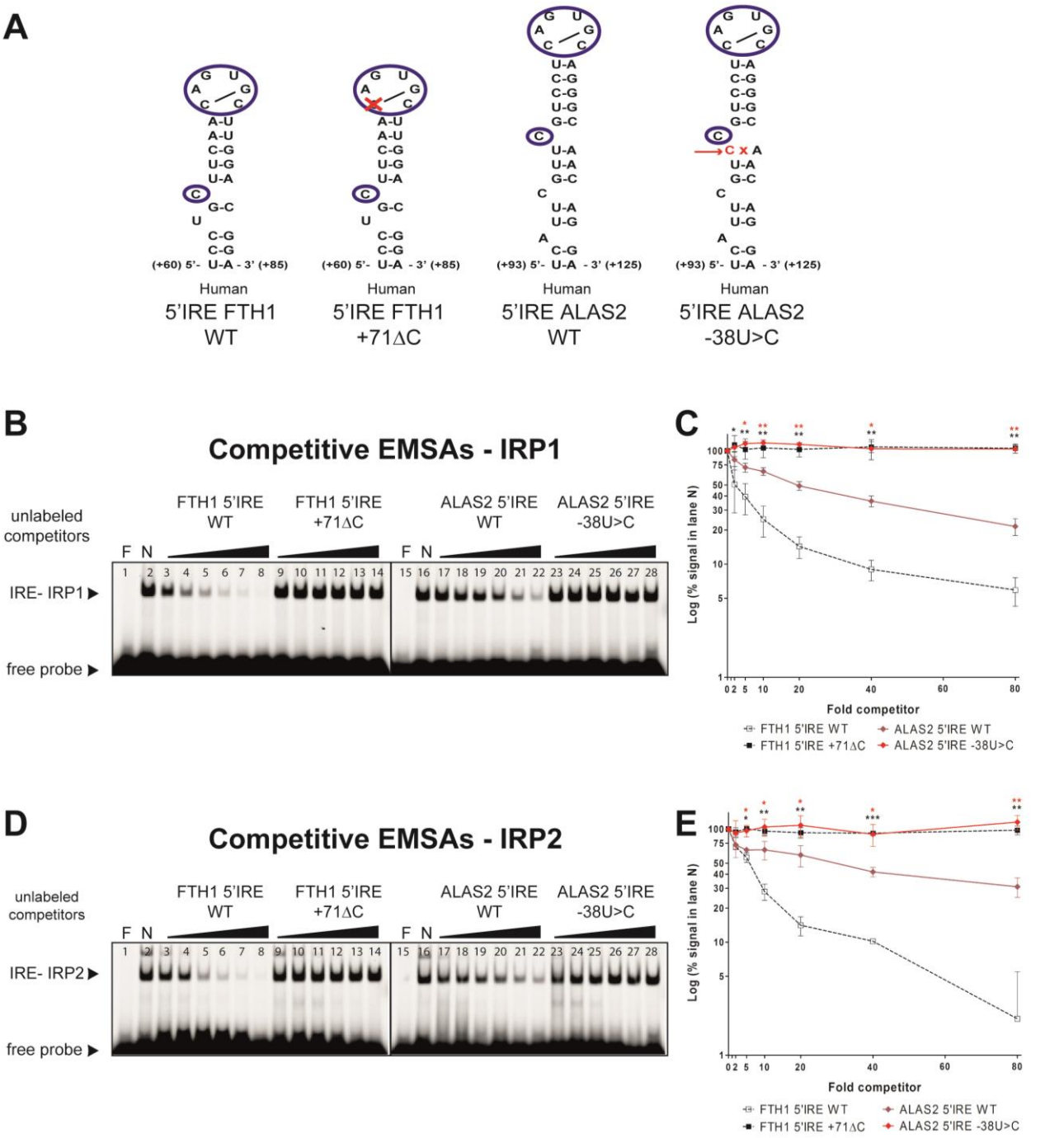

Figure 3.9 ALAS2: competitive EMSAs. (A) Graphic representation of the FTH1 IRE sequences (nucleotides 60-85 in NM_002032.2) wild type or +71ΔC, ALAS2 IRE sequence (nucleotides 93-125 in NM_000032.4) wild type or the -38U>C mutant, used for the synthesis of RNA probes in competitive EMSAs experiment **(B, C)** Florescent-labeled FTH1 IRE wild type probe was incubated with increasing molar excess (2x, 5x, 10x, 20x, 40x and 80x) of unlabeled competitors corresponding to the FTH1 IRE wild type sequence (lanes 3-8), or the mutants +71ΔC (lanes 9-14), ALAS2 IRE wild type sequence (lanes 17-22) or the ALAS2 -38U>C mutation (lanes 23-28). Samples were incubated with recombinant IRP1 (panel B) or IRP2 (panel C) and resolved on acrylamide gels. **(D, E)** Quantification of the signals of the shifted bands was performed using the Odyssey Infrared Imaging System (LI-CORE Biosciences) and compared to the signal in lane N, set as 100%. Means ± SD of at least three independent experiments. Statistical analysis compares the signal given by the mutated IRE of FTH1 and ALAS2 sequences to the signal given by the corresponding WT IRE sequences, at each molar concentration. WT: wild type; F: free probe; N: no competitor added.

3.2.4 Discussion

Approximately 5% of EPP patients do not present mutations in *FECH* or *ALAS2* genes. Here we report a French family with EPP in which the clinical severity of the proband is due to a combination of a mutation in a new gene together with a novel mutation in the *ALAS2* IRE (NM_000032.4; c.[-38T>C];[=]).

The -38U>C mutation in *ALAS2* IRE abolishes IRP1 and IRP2 binding affinity, what will impair ALAS2 mRNA regulation in response to iron levels. Under iron deprivation conditions, IRPs will not repress ALAS2 mRNA translation with consequent overproduction of ALAS2 protein. This will result in a gain-of-function effect similarly to what happens in X-linked EPP due to gain-of-function mutations in *ALAS2* gene (XLEPP, OMIM #300751). However, the *ALAS2* change is not the causative mutation of EPP in this family, since the mother of the proband, that also carries the mutation at heterozygous state, is unaffected and only presents ZnPP levels in the upper-normal range. We hypothesize that the presence of this *ALAS2* variant in the proband, together with a paternal defect in a different gene (ongoing work of the group of Dr. Hervé Puy) works as a modifier of disease severity, triggering the clinical manifestations in the proband compared with her mild affected relatives (father and uncle that present protoporphyrins accumulation but do not develop overt clinical symptoms).

3.3 Identification of a functional 3' IRE in human 3-hydroxybutyrate dehydrogenase (BDH2) mRNA

We have collaborated with the group of Dr. Laxminarayana Devireddy (Case Western Reserve University, Cleveland) with fruitful discussion and in assisting with protocols and reagents in the identification of a functional 3' IRE in the human 3-hydroxybutyrate dehydrogenase (BDH2) mRNA.
Those results were published in the peer-reviewed journal *Journal of Molecular Medicine* with impact factor: 4.768 (see Annex II)
J Mol Med. 2012 Oct;90(10):1209-21. doi: 10.1007/s00109-012-0899-7. PMID: 22527885
"Siderophore-mediated iron trafficking in humans is regulated by iron"
Liu Z, Lanford R, Mueller S, Gerhard GS, Luscieti S, Sanchez M, Devireddy L.

As described before (see Introduction 1.3.1.1), mammalian siderophores have been recently shown to play an important role in cellular iron uptake and iron trafficking to the mitochondria (Devireddy *et al.* 2005; Devireddy *et al.* 2010). BDH2 is the reductase that catalyzes the rate-limiting step in the biogenesis of the mammalian siderophore 2,5-dihydroxybenzoic acid (2,5-DHBA). BDH2 silencing in cell lines or in zebrafish, with consequent 2,5-DHBA deficiency, results in an abnormal iron accumulation in the cytoplasm and iron deficiency in the mitochondria (Devireddy *et al.* 2010).

3.3.1 BDH2 mRNA has a 3' Iron Responsive Element (IRE)

Using our own developed software for IRE prediction, the SIREs Web Server (Searching for IREs, http://ccbg.imppc.org/sires/) (Campillos *et al.* 2010), an IRE-like motif was identified in the 3' UTR of the human BDH2 mRNA (Figure 3.10A-B).

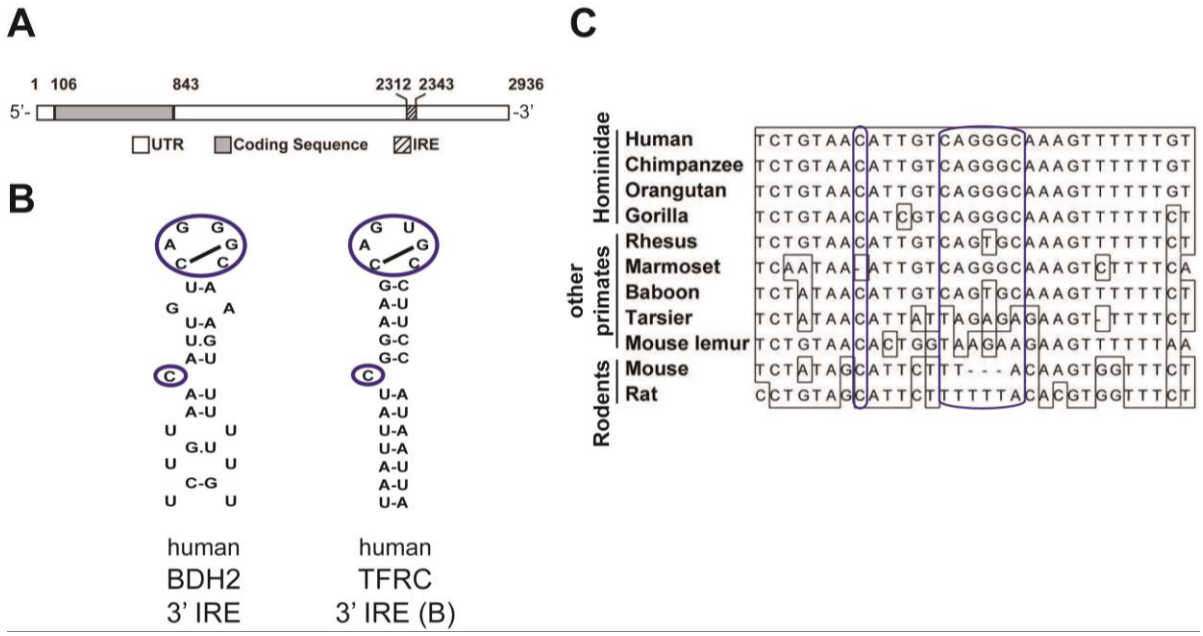

Figure 3.10 BDH2 3' Iron Responsive Element. (A) Position of the IRE identified in the 3' UTR of human BDH2 mRNA. Gray box indicates the coding sequence and white boxes indicate the 5' and 3' UTRs. Numbers indicate nucleotides position of the highlighted elements. **(B)** Illustration of the IRE motifs in BDH2 and TFRC mRNAs. **(C)** Alignment of BDH2 3' UTR sequence in different species. The C-bulge and the 6-nucleotides apical loop are boxed in blue. Figure modified from Liu *et al.* 2012.

BDH2 3' IRE presents a hexanucleotide apical loop, with the 1st and the 5th nucleotides pairing (C-G) to form a pseudotriloop, an upper and lower stem and an unpaired C bulge at the 5' side of the stem, although showing some structural differences with classical IREs. BDH2 IRE 6-nucleotides apical loop (CAGGGC) differs from the consensus sequence (CAGWGH, where W stands for A or U and H stands for A, C or U, see Introduction 1.4.1). In the BDH2 IRE the pseudotriloop sequence is AGG instead of AGU or AGA, however, this non-canonical apical motif has been previously shown to be able to bind IRPs *in vitro* by SELEX (Butt *et al.* 1996). Moreover, BDH2 IRE upper stem is made of 4-paired nucleotides with one mismatch (GxA), similar to the IRE of Gox (Kohler *et al.* 1999) (see Figure 1.17).

Sequence alignment of BDH2 3' UTR in different species showed that the BDH2 IRE is conserved only among Hominidae (human, chimpanzee and orangutan) but not in other primates, or lower species (Figure 3.10C).

3.3.2 BDH2 3' IRE binds to IRP1 and IRP2

3.3.2.1 Binding of human BDH2 IRE to the IRPs, tested by EMSAs

The binding of the 3' IRE-like element identified in the human BDH2 mRNA to IRP1 or IRP2 protein was assessed by electrophoretic mobility shift assays (EMSAs) (Figure 3.11). A 100bp region of BDH2 mRNA, including the IRE wild type or with nucleotide substitutions in the apical loop (MT1 construct) or in the upper stem (MT2 construct) were cloned in pcDNA3.1 vector (Invitrogen). As positive control, a 60bp region of human TFRC mRNA, containing the wild type TFRC IRE B was also cloned in pcDNA3.1 vector (Figure 3.11A). The plasmid constructs above mentioned, were used for the *in vitro* transcription of radiolabeled RNA probes that were incubated with increasing amounts of recombinant IRP1 or IRP2 protein or a combination of both IRPs. The RNA-IRPs complexes were then resolved on acrylamide gels and visualized by autoradiography (Figure 3.11B). As expected, the positive control TFRC IRE B WT probe, binds to both IRPs (Figure 3.11B right panel). The human BDH2 IRE WT also binds to both recombinant IRP1 and IRP2 (Figure 3.11B left panel), and so does the mutant MT1 with nucleotide substitutions in the IRE loop, that are predicted to affect the formation of the pseudotriloop (Figure 3.11A and B left panel). On the contrary the BDH2 IRE mutant MT2, with substitutions in the upper stem region that open and disrupt the stem, shows no binding to recombinant IRP1 or IRP2 (Figure 3.11A and B right panel).

IRPs interaction was also assessed under more stringent conditions by competitive EMSAs using recombinant IRP1 or IRP2 protein (Figure 3.11C). In these experiments, a radiolabeled BDH2 IRE WT probe was incubated with increasing molar excess of unlabeled competitor RNAs corresponding to the BDH2 IRE wild type, or the MT1 or MT2 mutants or the TFRC wild type IRE B. If the non-labeled sequence interacts with the IRP protein, it would compete for the binding and displace the labeled BDH2 IRE probe, reducing the signal of the shifted band. The addition of increasing molar excess of wild type BDH2 IRE inhibited the binding of the radiolabeled probe to both IRP1 and IRP2 in a dose-dependent manner (Figure 3.11C left and central panel). The addition of the MT1 BDH2 IRE mutant also reduces the binding of the radiolabeled BDH2 WT probe to both IRPs (Figure 3.11C left and central panel). On the other hand, the MT2 BDH2 IRE mutant is not able to compete for IRPs binding at all the tested concentrations of unlabeled competitor (Figure 3.11C right panel). As expected, the TFRC IRE B WT positive control shows efficient competition for IRP1 and IRP2 binding (Figure 3.11C left and central panel).

In conclusion, EMSAs showed that BDH2 3' IRE binds *in vitro* to recombinant IRP1 and IRP2.

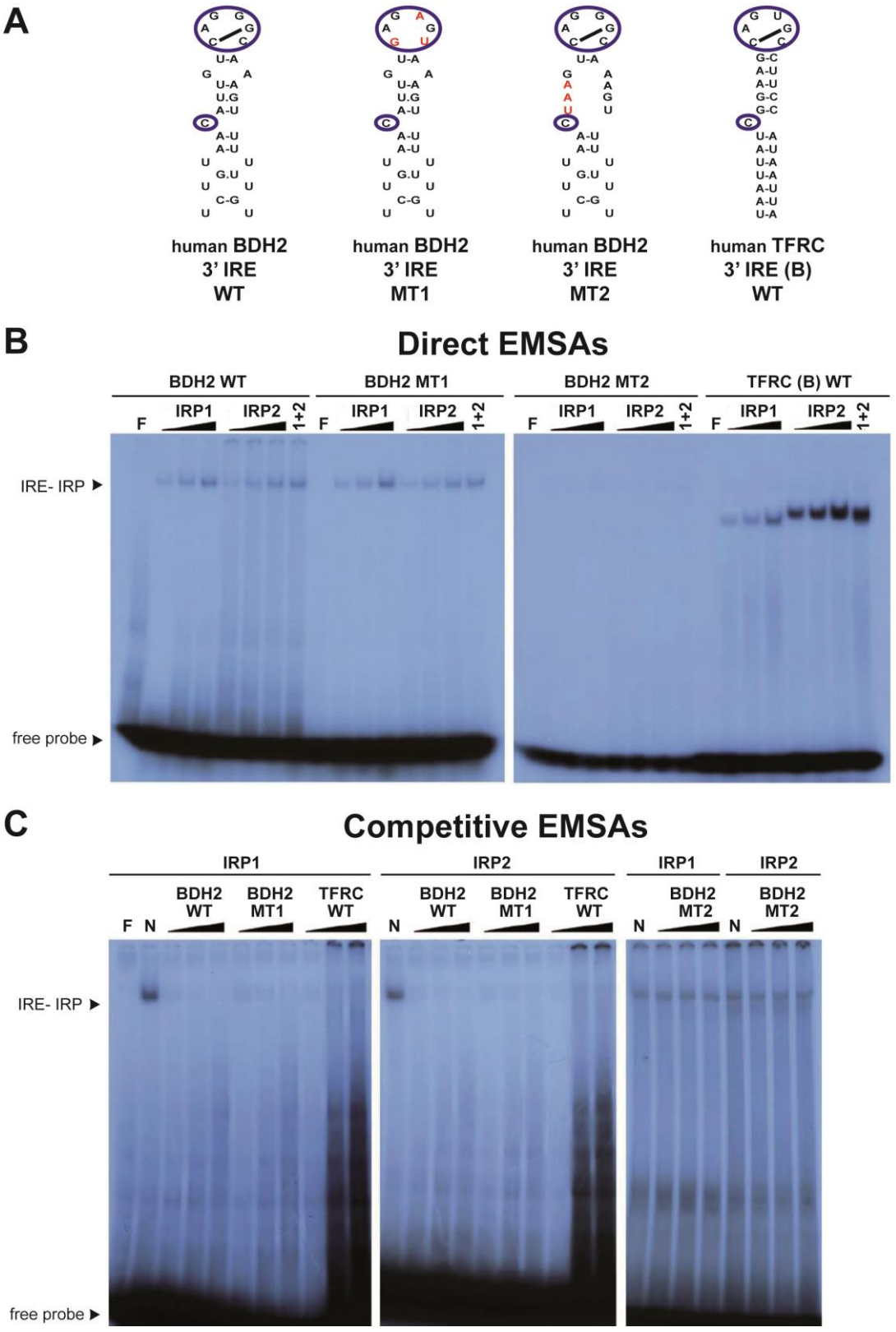

Figure 3.11 BDH2 3' IRE binds to IRPs *in vitro* (A) Schematic representation of the human BDH2 IRE wild type, the BDH2 MT1 and MT2 IRE mutants and the TFRC IRE B, used for *in vitro* transcription of RNA probes in EMSAs. Mutant nucleotides are indicated in red. **(B)** Direct EMSAs: radiolabeled RNA probes corresponding to a 100bp human BDH2 region containing the wild type IRE or the MT1 or MT2 mutant IREs or a 60bp TFRC region containing the IRE B, were incubated with increasing amounts of recombinant IRP1 or IRP2 protein. The RNA-protein complexes were resolved on acrylamide gels and visualized by autoradiography. **(C)** Competitive EMSAs: the specificity of interaction between human BDH2 IRE and IRPs was assessed using a radiolabeled hBDH2 WT IRE probe and an increasing molar excess of unlabeled competitor BDH2 WT, MT1, MT2, or TFRC B IRE RNAs. WT: wild type; F: free probe; N: no competitor added. Picture modified from Liu *et al.* 2012.

3.3.2.2 BDH2 mRNA co-immunoprecipitates with IRP1 and IRP2

To prove that BDH2 3' IRE binds to IRP1 and IRP2 in an *in vivo* setting, endogenous IRP1 and IRP2 were immunoprecipitated with specific antibodies from MCF-10A cells or from MCF-10A cell treated for 16h with 100μM DFO (Deferoxamine, iron chelator) or 100μM Hemin (source of iron) and BDH2 and TFRC mRNAs in the immunoprecipitates were quantified by qPCR (Figure 3.12).

Human BDH2 mRNA co-immunoprecipitated together with IRP1 or IRP2 protein. Iron supplementation with Hemin treatment reduced the co-immunoprecipitation of BDH2 mRNAs with both IRPs, while iron chelation with DFO treatment enhanced it (Figure 3.12A).

TRFC mRNA was quantified as positive control and was similarly immunoprecipitated together with both IRPs (Figure 3.12A).

Similar results were obtained in 293T cells stably expressing FLAG-IRP1 or FLAG-IRP2, where IRP1 and IRP2 were immunoprecipitated using an anti-FLAG antibody (Figure 3.12B).

The above data therefore suggest that BDH2 mRNA associates with IRP1 and IRP2 in cells.

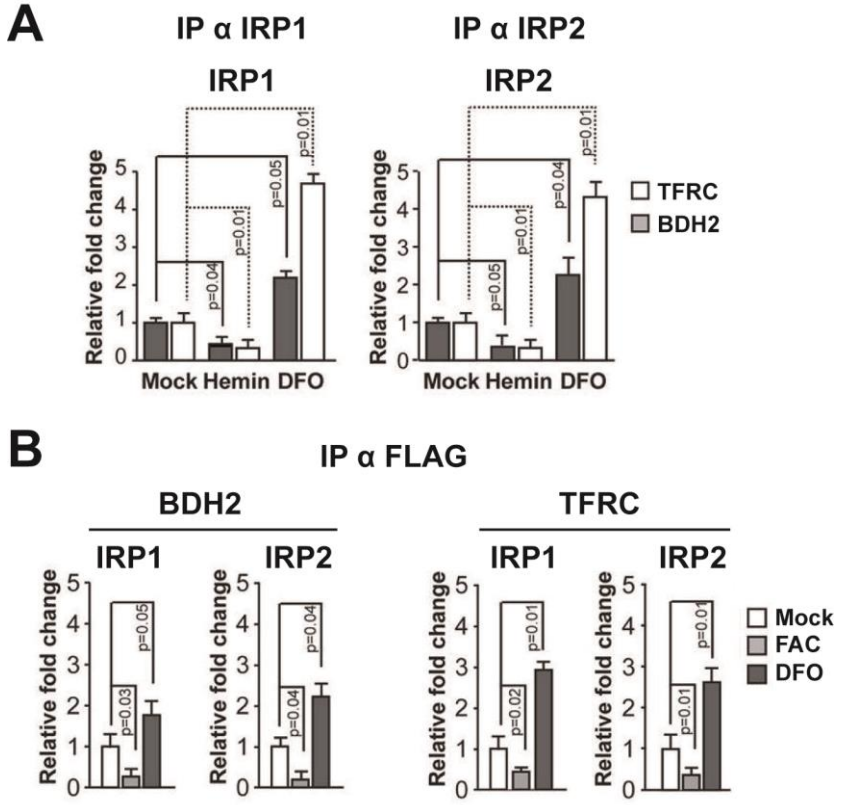

Figure 3.12 BDH2 mRNA co-immunoprecipitates with IRP1 and IRP2. (A) MCF-10A cells were treated with 100μM Hemin, 100μM DFO or left untreated (Mock) for 16h. Endogenous IRP1 or IRP2 were precipitated from cells lysates using specific anti-IRP1 and anti-IRP2 antibodies and G Sepharose beads. BDH2 and TFRC mRNAs were quantified in the immunoprecipitates by qPCR. (B) 293T cells stably expressing FLAG-IRP1 or FLAG-IRP2 were treated with 100μM FAC, 100μM DFO or left untreated for 16h. Exogenous FLAG-IRPs were precipitated from cell lysates using anti-FLAG antibody coated beads and BDH2 and TFRC mRNAs were quantified in the immunoprecipitates by qPCR. In each case, results were normalized to BDH2 or TFRC mRNA levels in untreated Mock cells (set as 1), means ± SD of at least three independent experiments. Picture from Liu *et al.* 2012.

3.3.3 BDH2 mRNA expression is regulated by iron

BDH2 mRNAs holds a 3' UTR IRE that was shown to be functional in *in vitro* and in cell lines binding studies. 3' UTR IREs, as in the case of TFRC, are regulated by increased mRNA stabilization upon IRP binding in low iron conditions, while loss of IRP binding favors TFRC mRNA degradation in iron-replete conditions (see Introduction 1.4.3).

3.3.3.1 Regulation of BDH2 levels with DFO and Hemin treatments

To study the response of BDH2 mRNA to iron levels, different human cell lines were treated with a source of iron (Hemin or ferric ammonium citrate, FAC) or with an iron chelator (Deferoxamine, DFO) (Figure 3.13). In particular, MCF-10A, HeLa (epithelial cells), Huvec (endothelial cells) and K562 (hematopoietic cells) were treated with 100μM Hemin or FAC or with 100μM DFO for 16h and BDH2 and TFRC mRNAs expression was analyzed by qPCR (Figure 3.13A).

As expected, TFRC mRNA levels were downregulated by Hemin or FAC treatment and upregulated by DFO treatment in all the cells analyzed. Similarly, BDH2 mRNA levels were also reduced by iron supplementation with Hemin or FAC and increased by iron chelation with DFO in all cell lines (Figure 3.13A). The iron-regulation of BDH2 was also confirmed at protein level in MCF-10A cells (data not shown).

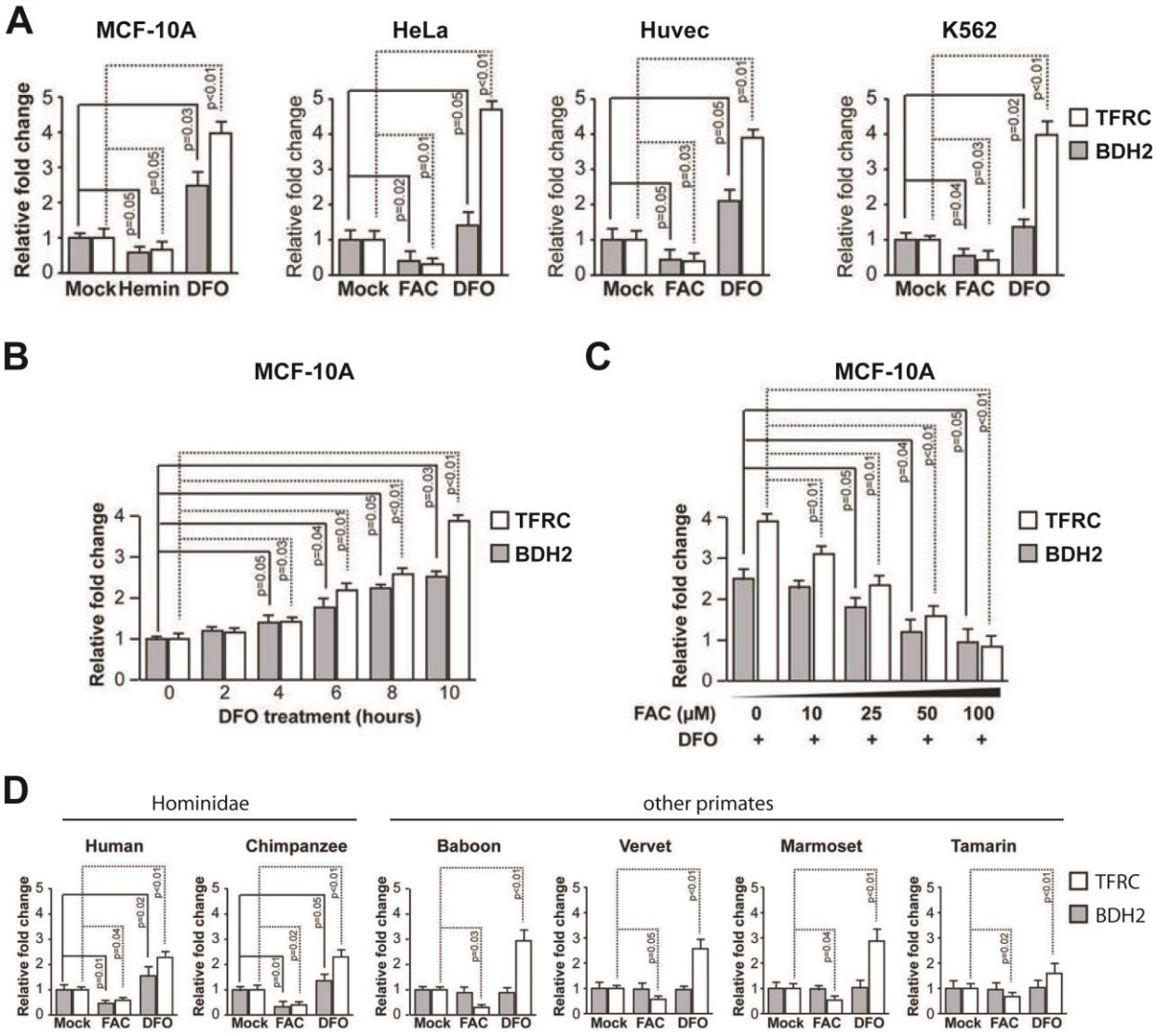

Figure 3.13 BDH2 mRNA is iron-regulated. (A) MCF-10A, HeLa, Huvec and K562 human cells were treated with 100μM Hemin, 100μM FAC, 100μM DFO or left untreated (mock) for 16h and BDH2 and TFRC mRNA expression was analyzed by qPCR. **(B)** MCF-10A cells were treated with 100μM DFO for 2-4-6-8 and 10 hours and BDH2 and TFRC mRNA expression was analyzed by qPCR. **(C)** MCF-10A cells were treated with 100μM DFO together with increasing concentrations of FAC (10-25-50 and 100μM) and BDH2 and TFRC mRNA expression was analyzed by qPCR. **(D)** Transformed human and primates liver cell lines were treated with 100μM FAC, 100μM DFO or left untreated for 16h and BDH2 and TFRC mRNA expression was analyzed by qPCR. In all cases, BDH2 and TFRC levels were normalized to β-actin or eukaryotic translation initiation factor 2B mRNA levels and compared to untreated cells (set as 100%). Means ± SD of at least three independent experiments. Picture from Liu *et al.* 2012.

Time course experiments in MCF-10A cells with 2-4-6-8 and 10h of DFO treatment showed that BDH2 mRNA, similarly to TFRC mRNA, increases progressively in time (Figure 3.13B). Moreover, MCF-10A were treated with 100μM DFO together with increasing concentrations of FAC showed that iron supplementation reversed the DFO-induced augment of BDH2 and TFRC mRNA levels (Figure 3.13C).

Hence, BDH2 mRNA and protein present an iron-dependent regulation, similar to TFRC regulation, and compatible with an IRP-mediated stabilization of a 3' IRE.

As mentioned before, BDH2 IRE sequence is conserved only among primates belonging to the Hominidae family (Figure 3.10C). BDH2 mRNA iron-regulation was therefore tested in liver cell lines derived from human or other primates (Figure 3.13D). BDH2 mRNA was decreased by FAC treatment and increased by DFO only in human or chimpanzee derived liver cell lines, while no regulation was observed in liver cell lines derived from lower primates (baboon, vervet, marmoset or tamarin), where the BDH2 IRE sequence is not conserved (Figure 3.13D). On the other hand, TFRC mRNA levels were regulated by iron levels in all cell types (Figure 3.13D).

Consistent with this, in MIMCD and FL15.12 mouse cell lines no regulation was observed for Bdh2 mRNA in response to iron chelation or supplementation while the positive control Tfrc mRNA is reduced by FAC and increased by DFO treatment, as expected (data not shown). These data suggest therefore that the iron-regulation of human BDH2 mRNA and protein in response to the iron status is mediated by the 3' IRE-like motif in human BDH2 mRNA.

3.3.3.2 BDH2 expression in Hemochromatosis samples

BDH2 iron-regulation was also tested in liver samples obtained from Hemochromatosis patients (Figure 3.14). Patients with Hereditary Hemochromatosis are characterized by iron overload in parenchymal organs, particularly in the liver (see Introduction 1.2.3).

BDH2 and TFRC mRNA levels were assessed by qPCR in liver samples from Hemochromatosis patients and from normal controls. The cohort of subjects used for qPCR studies is detailed in Figure 3.14C. Patients are grouped according to their HFE genotype, being the C282Y and H63D mutations in HFE gene the most common changes associated with Hemochromatosis type 1 disease.

TFRC positive control mRNA was, as expected, decreased in the liver of Hemochromatosis patients versus healthy controls (Figure 3.14B). Likewise, BDH2 mRNA expression was also found slightly reduced in the liver of Hemochromatosis patients compared to control subjects (Figure 3.14A).

BDH2 downregulation in iron-overloaded Hemochromatosis livers was also examined at protein level by histological studies (Figure 3.14D-E). BDH2 and TFCR protein were detected by immunohistochemistry in liver sections from Hemochromatosis patients (HH1-5) and normal subjects (Normal 1-4). Genetic and biochemical data of the subjects used for histological studies are detailed in Figure 3.14E. Iron overload in Hemochromatosis livers was confirmed by the Perls Prussian Blue staining for ferric iron (Figure 3.14D, blue staining).

TFRC protein was found to be reduced in the livers of Hemochromatosis patients compared to normal controls, as expected in a context of iron excess in HH patients (Figure 3.14D, brow staining). Similarly, BDH2 protein was also diminished in Hemochromatosis patients compared to normal controls (Figure 3.14D, brown staining).

In conclusion, BDH2 mRNA and protein show an iron-dependent regulation compatible with a 3' IRE regulation in patients liver cells as well as in human cultured cell lines.

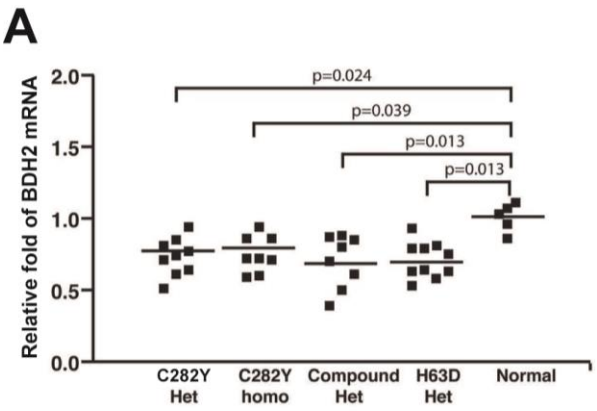

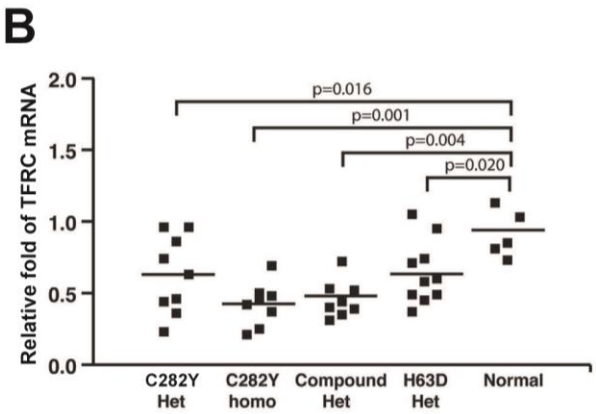

C

Order	Age	Gender	Genotype	Iron	IBC	TF saturation (%)	Ferritin µg/L
1	52	Female	C282Y Het	153	264	58	56.7
2	52	"	"	132	337	39	51.1
3	65	"	"	78	315	25	30.3
4	55	Male	"	69	307	22	123.5
5	47	Female	"	134	308	44	60.6
6	69	Male	"	86	245	35	169.4
7	32	Female	"	88	333	26	107.9
8	54	"	"	116	311	37	158.5
9	54	"	"	N/D	N/D	34.7	1048
10	35	Male	C282Y Homo	106	284	37	499.7
11	40	"	"	106	349	30	111.9
12	33	Female	"	70	406	17	52.4
13	40	"	"	88	282	31	77.4
14	43	"	"	145	379	38	108
15	39	"	"	69	379	18	88.9
16	57	"	"	51	269	19	261.6
17	54	Male	"	N/D	N/D	99.7	1234
18	53	Female	Compound Het	88	255	35	51.7
19	27	"	"	51	344	15	65.3
20	35	"	"	51	324	16	84.6
21	41	"	"	41	370	11	51.4
22	33	"	"	59	366	16	26.4
23	41	"	"	67	309	22	260.1
24	29	"	"	75	395	19	18.9
25	53	Male	"	N/D	N/D	N/D	724
26	57	Female	H63D Het	60	356	17	104.5
27	35	"	"	N/D	N/D	N/D	33.2
28	42	Male	"	113	266	42	220.1
29	55	Female	"	46	349	13	34.4
30	61	"	"	40	303	13	55.7
31	43	"	"	75	281	27	88.4
32	54	"	"	43	319	13	43.9
33	41	Male	"	93	394	24	102.9
34	35	Female	"	74	331	22	74.1
35	47	"	"	57	412	14	13.7
36	72	"	Normal	85	384	22	73.5
37	41	"	"	49	337	15	49.3
38	48	"	"	71	343	21	41
39	46	"	"	76	273	28	52.3
40	44	"	"	85	357	24	16.2

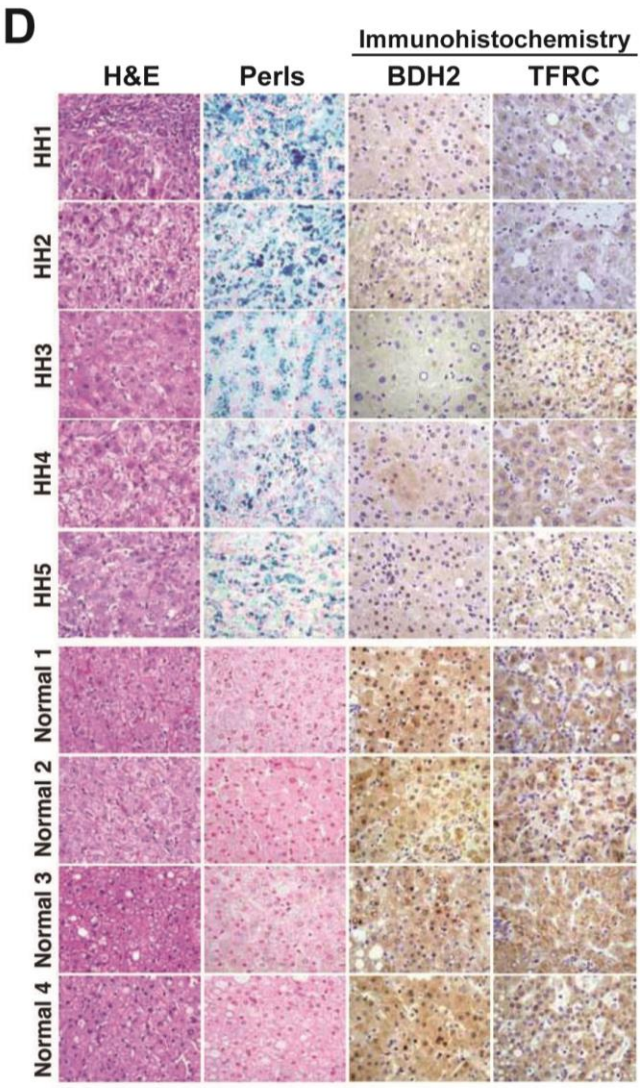

E

Order	Age	Gender	Genotype	Hepatic Iron index	Iron	TF saturation (%)	Ferritin µg/L
1	50	Male	C282Y Homo	5.35	151	97	3425
2	66	Female	"	4.32	194	84	574
3	51	Male	"	4.66	N/D	90	1030.3
4	38	"	C282Y Het	2.35	N/D	74	423.5
5	42	"	"	2.1	98	74	460.6
6	59	Male	Normal	1.2	85	25	109.2
7	42	Female	"	1	39	26	89.9
8	54	"	"	1.3	51	27	58.5
9	44	Male	"	1.12	N/D	24.7	108.8

Figure 3.14 BDH2 mRNA and protein are reduced in the liver from Hemochromatosis patients. BDH2 **(A)** or TFRC **(B)** mRNA levels were analyzed by qPCR in liver samples from normal subjects or Hemochromatosis patients. Hemochromatosis patients are grouped according to their C282Y and H63D HFE genotype. BDH2 and TFRC mRNA levels were normalized to RPL13 ribosomal protein mRNA levels. **(C)** The table shows the age, gender, C282Y/H63D HFE genotype and iron biochemical parameters (serum iron, transferrin saturation and serum ferritin levels) of the cohort of subjects used for qPCR studies **(D)** Liver sections from Hemochromatosis patients (HH 1-5) or normal subjects (Normal 1-4) were immunostained for BDH2 and, as positive control, also for TFRC (brown staining). Iron deposits in Hemochromatosis patients are evidenced by Perls Prussian Blue staining (blue staining). Hematoxylin-eosin (H&E) staining shows liver architecture. **(E)** The table shows for the cohort of subjects used in histological studies: age, gender, C282Y HFE genotype, iron biochemical parameters (serum iron, transferrin saturation and serum ferritin levels) and hepatic iron index (mmol iron/gram of liver/year; if >1.9 it is suggestive of HH). N/D: not determined; iron: serum iron; IBC: iron binding capacity; TF: transferrin. Picture from Liu *et al.* 2012.

3.3.3.3 IRP1 and IRP2 mediate BDH2 mRNA iron dependent regulation

To examine the role of the IRPs in the iron-dependent regulation of BDH2 mRNA, IRP1 and IRP2 expression was silenced in HeLa cells by siRNA technology.

IRP1 or IRP2 silencing or the silencing of both IRPs was achieved by transfecting HeLa cells firstly with shRNA specific for IRP1 or IRP2 and then resistant stable clones were transiently transfected with siRNA specific for IRP1 or IRP2 or both. The efficiency of the silencing was analyzed by qPCR, showing almost complete depletion of IRP1 and/or IRP2 expression (Figure 3.15A).

IRP1 silenced cells, IRP2 silenced cells or IRP1 and IRP2 silenced cells were then treated with 100μM Hemin, 100μM DFO or left untreated for 16h and BDH2 and TFRC expression was analyzed by qPCR (Figure 3.15B-C). Compared to control cells transfected with scrambled siRNA, where BDH2 and TFRC mRNA are reduced after iron supplementation with Hemin and increased after iron chelation with DFO, cells silenced for both IRP1 and IRP2 completely loss BDH2 and TFRC iron dependent-regulation in response to Hemin and FAC treatment (Figure 3.15B-C). The single IRP1 silencing of single IRP2 silencing has intermediate effects, partially abrogating the modulation of BDH2 and TFRC in response to Hemin and FAC (Figure 3.15B-C).

The data shown allow therefore concluding that IRP1 and IRP2 are necessary for iron-dependent regulation of BDH2 mRNA.

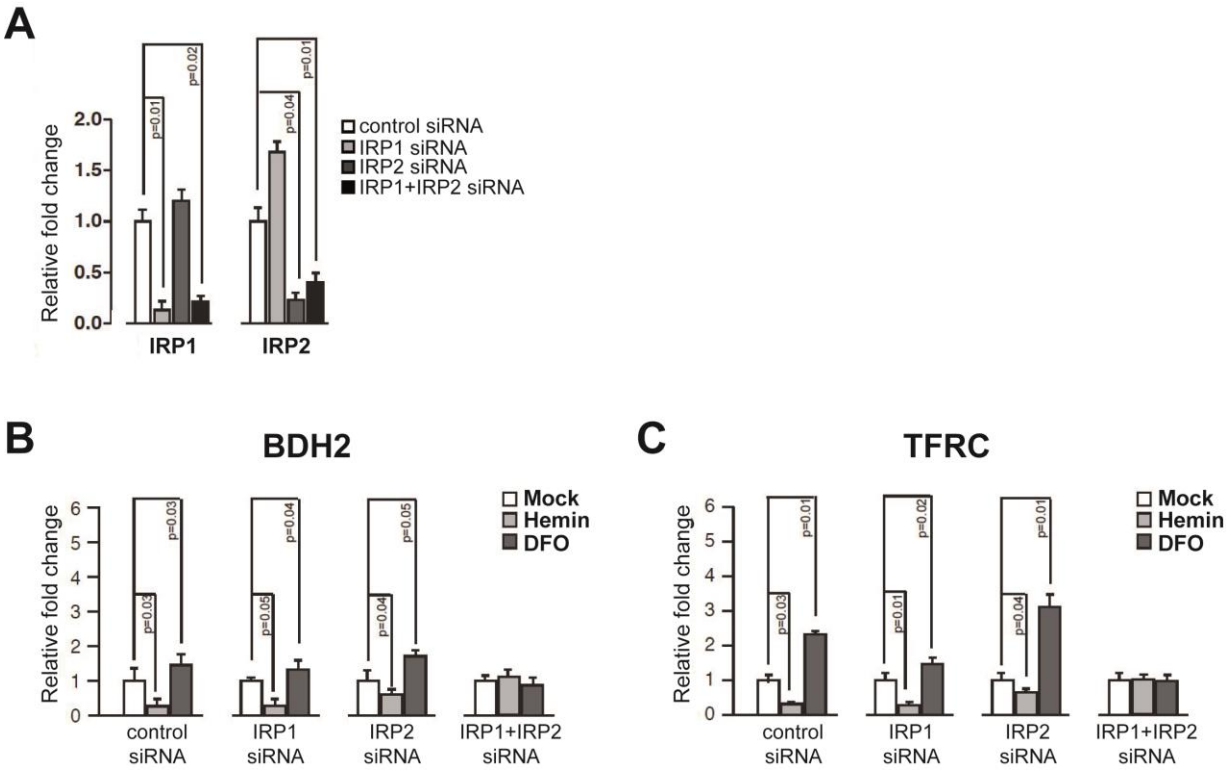

Figure 3.15 Silencing of IRP1 and IRP2 abrogates iron-dependent regulation of BDH2 mRNA. (A) HeLa cells were initially transfected with an empty vector (control) or with vectors expressing shRNAs specific for IRP1 or IRP2. G418 resistant clones were then transfected with a Dharmacon SMARTpool siRNAs specific for IRP1 and IRP2 or a scrambled siRNA (control). The efficiency of IRP1 and IRP2 silencing was evaluated by qPCR. IRP1 and IRP2 mRNA levels were normalized to β-actin mRNA and compared to control siRNA transfected cells (set as 1), means ± SD of at least three independent experiments. BDH2 **(B)** and TFRC **(C)** mRNA levels were quantified by qPCR in HeLa cells transfected with control, IRP1, IRP2 or IRP1+IRP2 siRNAs as described above and then treated with 100μM Hemin or 100μM DFO for 16h. BDH2 and TFRC mRNA levels were normalized to β-actin mRNA and compared in each group to untreated cells (Mock, set as 1), means ± SD of at least three independent experiments. Picture from Liu *et al.* 2012.

3.3.4 Post-transcriptional regulation of BDH2 mRNA

3.3.4.1 human BDH2 IRE and 3' UTR confer iron-dependent regulation onto a reporter gene

Luciferase reporter experiments were used to further demonstrate that the observed regulation of BDH2 mRNA and protein levels in response to iron concentrations is mediated by BDH2 3' IRE (Figures 3.16-3.17).

Different luciferase reporter constructs were generated based on the pGL4.13 vector (Promega) containing a Firefly luciferase cDNA driven by a SV40 early enhancer/promoter (Figure 3.16A).

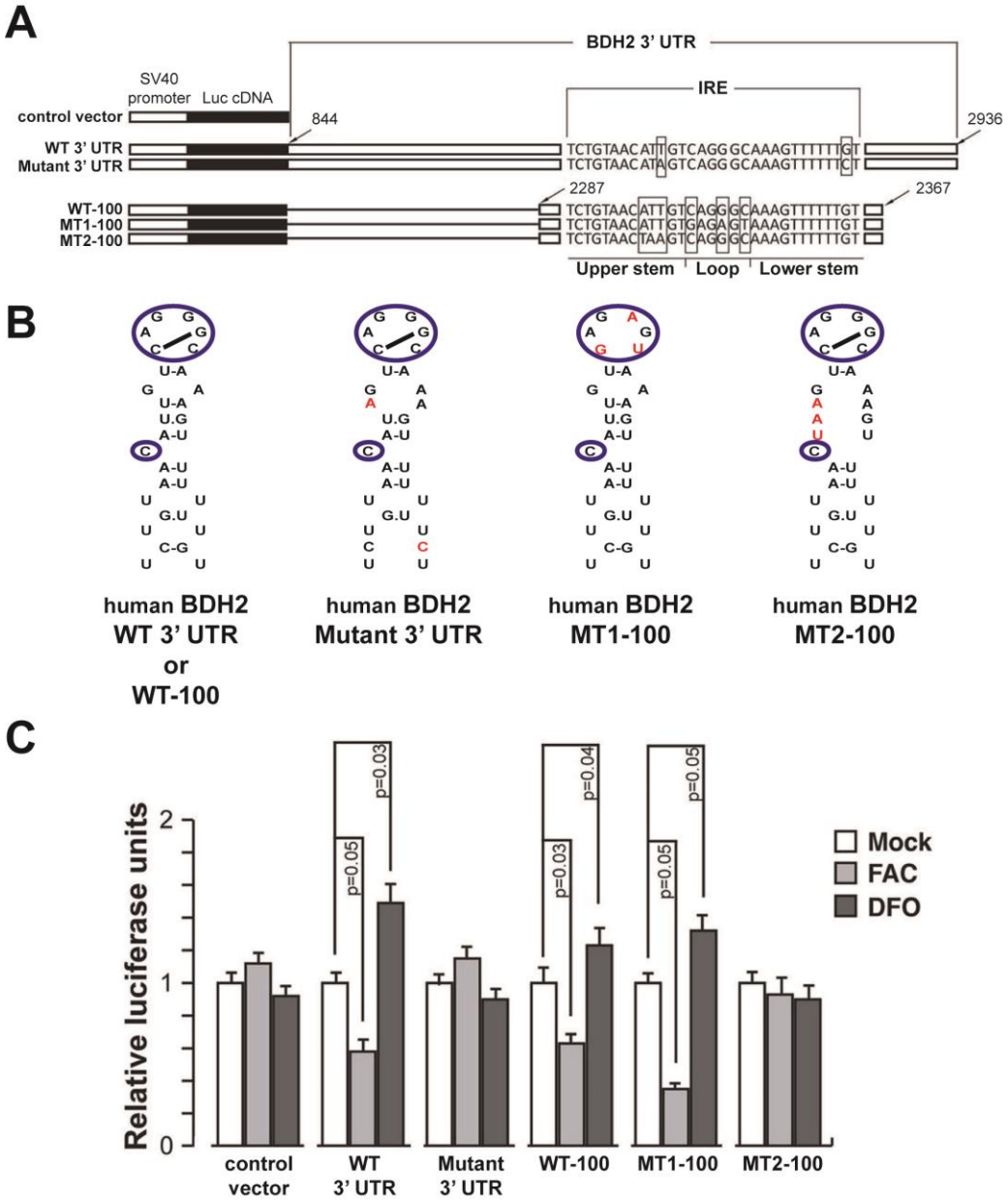

Figure 3.16 BDH2 3' IRE luciferase reporter experiments. (A) Schematic representation of the luciferase reporter constructs based on pGL4.13 vector. Black box indicates the Firefly luciferase coding sequence. The white box at the 5' of the luciferase cDNA indicates the SV40 promoter. The white box at the 3' of the luciferase cDNA indicates the WT or mutant 3' UTR or the 100bp IRE-containing fragment of human BDH2 mRNA. Mutant nucleotides are boxed. **(B)** Graphic representation of the IRE motifs contained in the luciferase reporter constructs. Mutant nucleotides are indicated in red. **(C)** MCF-10A cells were transfected with the luciferase reporter constructs shown and luciferase activity was measured under standard conditions (Mock) or after 16h 100μM FAC of 100μM DFO treatment. Data are represented as Firefly luciferase light units after normalization to Renilla luciferase measurements, means ± SD of at least three independent experiments. Picture from Liu *et al.* 2012.

A ~2kb fragment containing the human BDH2 3' UTR was PCR-amplified and inserted downstream of the luciferase cDNA to obtain the BDH2 WT UTR construct. The BDH2 Mutant UTR construct, with nucleotide substitutions in the IRE upper and lower stems, was obtained by site-directed mutagenesis (Figure 3.16A-B). MCF-10A or HeLa cells were transiently transfected with the Firefly luciferase reporter constructs described above or with the empty pGL4.13 luciferase vector as control. A Renilla luciferase vector was transfected in parallel for normalization of the results to differences in transfection efficiency. After transfection, the cells were treated with 100μM FAC, 100μM DFO or left untreated for 16h and Firefly and Renilla luciferase activities were measured using the Dual-Luciferase Reporter Assay kit (Promega). In cells transfected with the WT UTR construct, the luciferase activity was reduced by iron supplementation with FAC and increased by iron chelation with DFO compared to cells transfected with the control vector, where iron regulation is absent (Figure 3.16C). Nucleotide substitutions in the IRE stem abolished the iron regulation in cells expressing the Mutant UTR construct (Figure 3.16C).

In addition, to demonstrate that the regulation of luciferase expression is actually mediated by the BDH2 3' IRE sequence, luciferase reporter constructs containing a 100bp fragment of BDH2 UTR including the wild type BDH2 IRE (WT-100) or with nucleotide substitutions to disrupt the pseudotriloop or the upper stem of the BDH2 IRE (MT1-100 or MT2-100, respectively) were also generated based on pGL4.13 vector (Figure 3.16A-B). Cells transfected with the WT-100 construct also showed reduced luciferase activity with FAC and increased luciferase activity with DFO (Figure 3.16C). The MT1-100 mutant in the pseuditriloop, that was previously shown to still bind to IRP1 and IRP2 in EMSA experiments (see section 3.3.2.1), also showed iron-dependent regulation of luciferase expression while the MT2-100 mutant in the upper stem and not interacting with the IRPs in EMSA experiments (see section 3.3.2.1) totally abolished luciferase iron-mediated regulation (Figure 3.16C).

To further confirm these results, the 100bp fragment containing the wild type IRE or the MT1 functional mutant were cloned at the 5' of the luciferase cDNA in pGL4.13 vector (Figure 3.17A) and showed to confer iron-dependent regulation similar to a 5' IRE mRNA regulation: increased luciferase activity with FAC and reduced luciferase activity with DFO (Figure 3.17B). In conclusion, luciferase reporter experiments demonstrated that the BDH2 3' IRE is able to confer iron-dependent regulation to an exogenous mRNA.

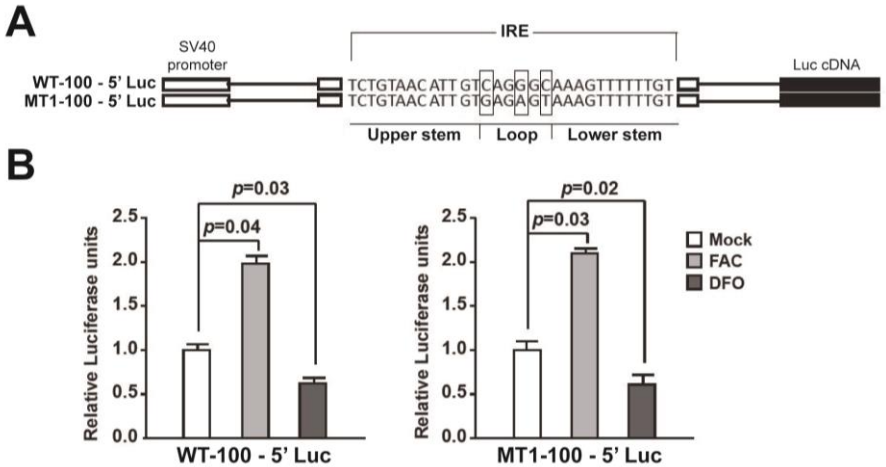

Figure 3.17 BDH2 5' IRE luciferase reporter experiments. (A) Schematic representation of the luciferase reporter constructs based on pGL4.13 vector. Black box indicates the Firefly luciferase cDNA. The white box indicates the SV40 promoter and the WT or mutant 100bp IRE-containing fragment of human BDH2 mRNA. Mutant nucleotides are boxed. **(B)** MCF-10A cells were transfected with the luciferase reporter constructs shown and luciferase activity was measured under standard conditions (Mock) or after 16h 100μM FAC of 100μM DFO treatment. Data are represented as Firefly luciferase light units after normalization to Renilla luciferase measurements, means ± SD. Picture from Liu *et al.* 2012.

3.3.4.2 BDH2 mRNA stability via IRPs and its 3' UTR

Iron-dependent regulation of mRNAs containing 3' UTR IREs, as in the case of TFRC, is mediated by mRNA stabilization upon IRPs binding during iron deficiency (Mullner *et al.* 1989). Conversely, in iron-replete conditions, IRPs binding is prevented, resulting in an increased mRNA degradation (see Introduction 1.4.3).
The role of BDH2 3' IRE in BDH2 mRNA modulation in response to iron levels was therefore examined by mRNA stabilization studies (Figure 3.18).

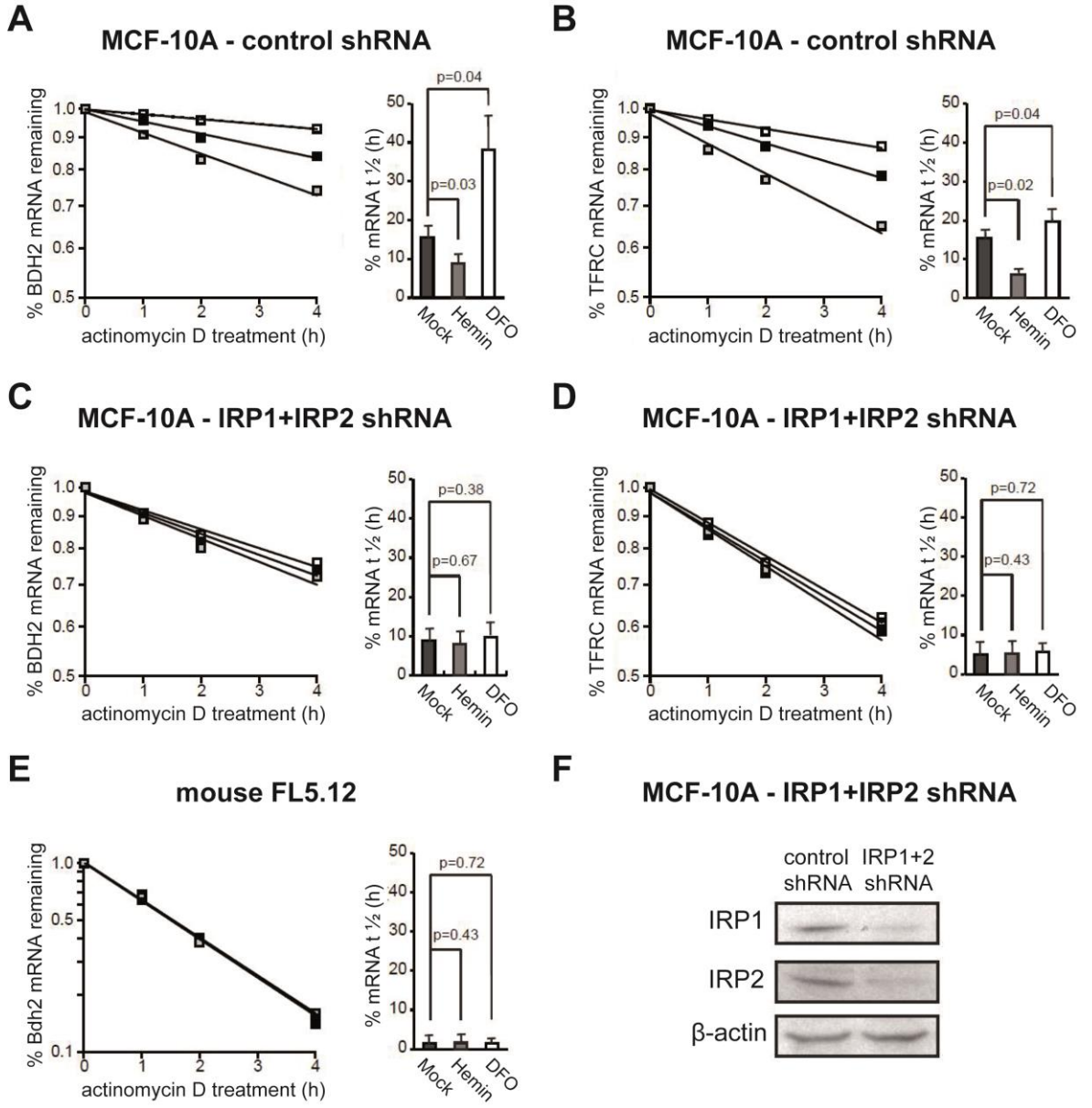

Figure 3.18 BDH2 3' IRE mediates iron-dependent stabilization of BDH2 mRNA. MCF-10A cells were stably transfected with control scrambled shRNA **(A, B)** or with shRNAs specific for IRP1 and IRP2 **(C, D)**. Stable clones were then treated with 100μM Hemin (light grey) or 100μM DFO (white) or left untreated (Mock, dark grey) for 16h. 5μg/ml of Actinomycin D was then added to inhibit transcription and cells were collected at 0, 1, 2 and 4 hours after Actinomycin D addition. BDH2 **(A, C)** and TFRC **(B, D)** mRNAs levels were analyzed at each time point by qPCR. Results were normalized to RPL13 ribosomal protein mRNA levels. For each condition, the zero hour time point was set as 100%. Mean of at least three independent experiments. The graphs show for BDH2 and TFRC the mRNA half-life (t½ or time required to fall 50% of its initial value) calculated in control conditions, iron supplementation or iron deficiency conditions. **(E)** Mouse FL5.12 were treated with 100μM Hemin or 100μM DFO or left untreated (Mock) for 16h. 5μg/ml of Actinomycin D was then added to inhibit transcription and cells were collected at 0, 1, 2 and 4 hours for the analysis of Bdh2 mRNA levels by qPCR as described above. **(F)** The efficiency of IRP1 and IRP2 silencing in MCF-10A cells transfected with control or IRP1+IRP2 shRNAs was evaluated by Western blotting. β-actin was monitored in parallel for normalization. Picture from Liu *et al.* 2012.

MCF-10A cells were stably transfected with a control scrambled shRNA or with shRNAs specific for IRP1 and IRP2 to induce the silencing of both IRPs. The efficacy of the silencing was evaluated by Western blotting, confirming the downregulation of both IRP1 and IRP2 (Figure 3.18F). Stable clones were treated with 100μM Hemin, 100μM DFO or left untreated for 16 hours and then the transcription inhibitor Actinomycin D was added. The cells were collected at 0, 1, 2 and 4 hours of Actinomycin D treatment and the rate of BDH2 and TFRC mRNAs decay was analyzed by qPCR (Figure 3.18A-D).
In control shRNA expressing cells, iron supplementation with Hemin destabilizes BDH2 and TFRC mRNAs, shortening mRNA half-life compared to untreated cells. By contrast, iron chelation with DFO stabilizes BDH2 and TFRC mRNAs prolonging mRNA half-life compared to untreated cells. (Figure 3.18A-B).
BDH2 and TFRC mRNA half-life was strongly reduced in the absence of IRPs expression in cells transfected with IRP1+IRP2 shRNAs (Figure 3.18C-D versus A-B). Moreover, in IRP1 and IRP2 silenced cells, no changes in mRNA stability were observed by Hemin or DFO treatment (Figure 3.18C-D).
In addition, Bdh2 mRNA stability was also studied in the mouse pro-B lymphocyte FL5.12 cell line, where the IRE motif is not present in Bdh2 3' UTR (see section 3.3.1). No destabilization or stabilization effect was observed upon iron supplementation or iron chelation in FL5.12 cells (Figure 3.18E), thus excluding the possibility that BDH2 mRNA is regulated by iron via an IRE-independent mechanism.
We can conclude that, similarly to TFRC, BDH2 mRNA expression is post-transcriptionally regulated by iron via mRNA stabilization upon IRPs binding and that BDH2 regulation is mediated by the IRE sequence in BDH2 3' UTR.

3.3.5 BDH2 regulation is important for maintaining mitochondrial iron homeostasis

All the data presented above suggest that the newly identified 3' IRE in BDH2 mRNA confers an iron-dependent regulation to BDH2 mRNA expression.
BDH2 is the rate-limiting enzyme in the siderophore biosynthetic pathway and previous studies from Dr. Devireddy group showed that BDH2 silencing results in siderophore depletion and leads to mitochondrial iron deficiency in yeast, cell lines and zebrafish embryos (Devireddy *et al.* 2010), underlining the importance of the siderophore pathway for mitochondrial iron delivery (see Introduction 1.3.1.1).
It has been therefore hypothesized that the biological relevance of the iron-dependent regulation of BDH2 expression resides in the control of siderophore iron trafficking to the mitochondria. In particular, it was hypothesized that, in iron-replete conditions, reduced IRPs activity downregulates BDH2 mRNA expression, with consequently reduction of siderophore levels. This, in turn would reduce iron delivery to the mitochondria, preventing a detrimental mitochondrial iron overload in an iron-excess context (Figure 3.19A).
To test this hypothesis, liver cell lines derived from human and chimpanzee (carrying a functional 3' IRE in BDH2 mRNA) or tamarin (lacking a functional 3' IRE in Bdh2 mRNA) were treated with 100μM Hemin to induce cytosolic iron excess and cytosolic and mitochondrial iron content were measured using iron-sensitive fluorescent dyes (Figure 3.19B). In detail, Calcein-Green (Cal-G) is specific for the cytosolic compartment and rhodamine B-[(1,10-phenanthrolin-5-yl)aminocarbonyl]benzyl ester (RPA) for the mitochondrial compartment; iron binding to those dyes results in fluorescence quenching.
Hemin treatment increases, as expected, the cytosolic labile iron pool in all the three liver cell lines, as shown by the decreased Cal-G fluorescence in Hemin treated cells compared to control cells (Figure 3.19).

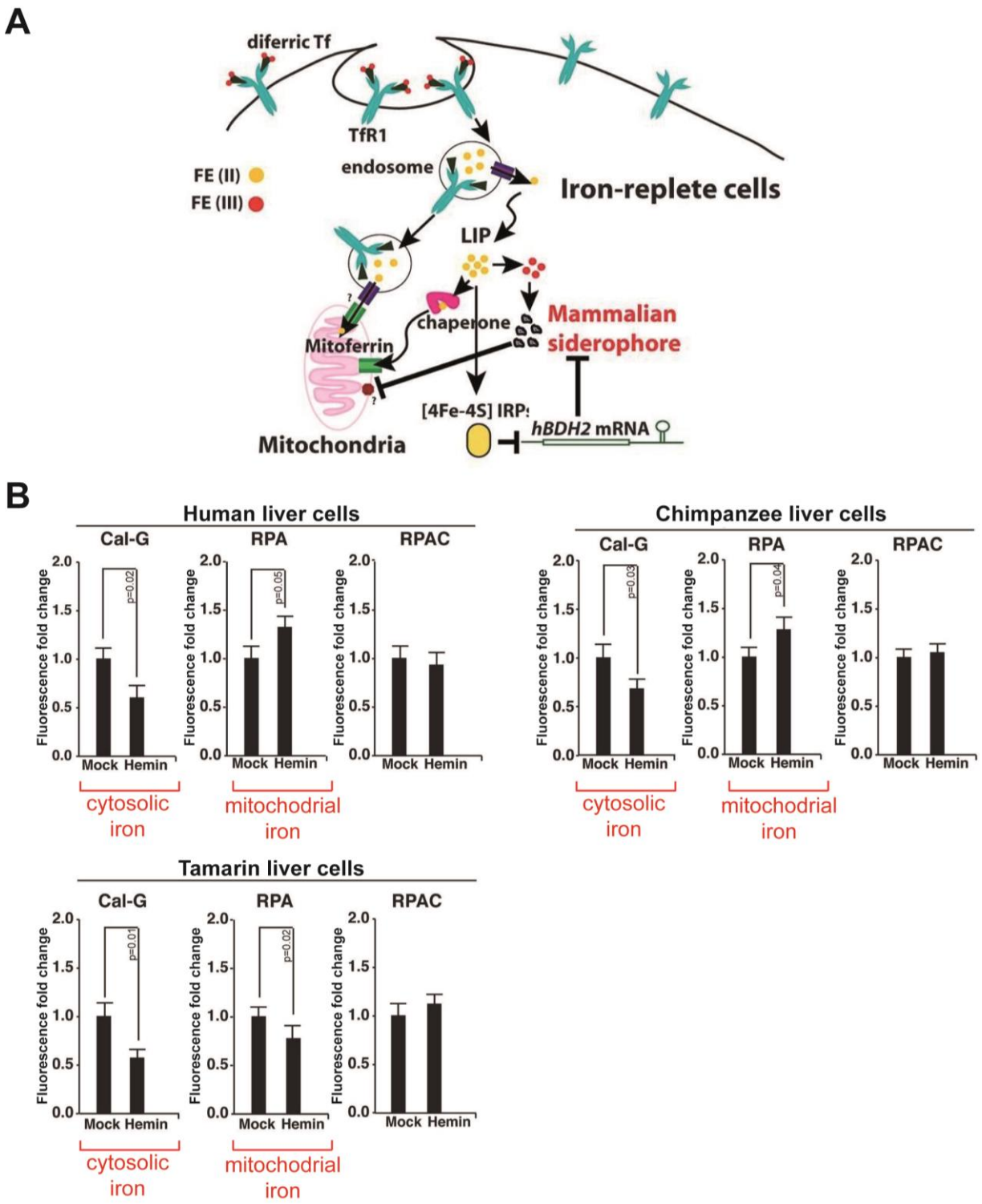

Figure 3.19 Iron regulation of BDH2 expression controls mitochondrial iron homeostasis. (A) Proposed model for iron regulation of siderophore-mediated iron trafficking. In standard conditions, part of the cytosolic iron pool is in the form of siderophore-bound iron, which is important for iron delivery to the mitochondrial compartment. In iron-replete conditions, BDH2 mRNA destabilization and degradation results in reduced siderophore levels and, consequently, reduction of mitochondrial iron content. **(B)** Cytoplasmic and mitochondrial iron content was measured in liver cell lines derived from human, chimpanzee (carrying a 3' UTR IRE in BDH2 mRNA) or tamarin (lacking the 3' UTR IRE) after iron supplementation with 100μM Hemin and compared to untreated (Mock) cells. Labile iron pools were measured using iron-sensitive fluorescent probes: Calcein-Green (Cal-G) for the cytosolic compartment and rhodamine B-[(1,10-phenanthrolin-5-yl)aminocarbonyl]benzyl ester (RPA) for the mitochondrial compartment. Iron binding to these compounds results in fluorescence quenching; the intensity of fluorescence detected is therefore inversely proportional to iron levels. As control, rhodamine B-[(phenanthren-9-yl)aminocarbonyl]benzyl (RPAC) was used. RPAC, similarly to RPA is targeted to the mitochondria but its fluorescence is not responsive to iron levels. Picture from Liu *et al.* 2012.

However, despite cytosolic iron excess, the mitochondria of Hemin treated human or chimpanzee liver cells showed reduced iron content compared to untreated cells, as indicated by the increased RPA fluorescence (Figure 3.19B).
These data support the idea that BDH2 downregulation, secondary to mRNA destabilization in iron-replete condition, diminishes siderophore iron trafficking to the mitochondria, preventing mitochondrial iron overload. This idea is further supported by the observation that in tamarin liver cells, lacking a functional Bdh2 3' IRE, the mitochondrial free iron pool is increased by Hemin treatment in parallel to cytosolic iron pool (Figure 3.19B).

3.3.6 Discussion

In this work published in Liu *et al.* 2012 we describe a novel and functional 3' UTR IRE in human BDH2 mRNA, which is conserved only among primates of the Hominidae family. The 3' IRE confers iron-dependent regulation to BDH2 mRNA in cultured cell lines as well as in liver samples from Hemochromatosis patients.
We also demonstrated that the mechanism of post-transcription regulation of BDH2 mRNA expression is mediated by mRNA stabilization upon IRPs binding, similar to TFRC mRNA regulation.
Altogether, this regulatory feedback on BDH2 mRNA expression will allow to control the siderophore-mediated iron trafficking to the mitochondria in response to iron levels, preventing mitochondrial iron overload in iron-replete conditions.

3.4 A novel IRP-target mRNA: Profilin2

The results exposed here are in preparation for submission to Blood Journal.

As introduced in section 1.7, in the last 20 years, different groups have reported new IRE-containing mRNAs using different approaches, evidencing that the IRP/IRE regulatory network is wider than previously thought. A recent genome-wide screening was carried out by our group in order to identify the whole repertoire of mRNAs that can interact with the IRPs (Sanchez *et al.* 2011). Using this approach, 35 novel mRNAs that bind to both IRP1 and IRP2 were identified as well as a number of IRP1 or IRP2-specific targets (see Introduction 1.7.2). Ongoing work in the laboratory focuses on the functional characterization of these novel mRNAs to demonstrate their post-transcriptional regulation via the binding of the IRPs and to discover and connect known and new cellular functions that need to respond to changes in iron metabolism. Among these 35 new IRP1 and IRP2-binding mRNAs I have focused on the one encoding for Profilin2 (Pfn2).
As mentioned in the introduction (see section 1.7.3), Pfn2 binds to monomeric actin and plays a role in the control of actin polymerization. Moreover, Pfn2 acts as a negative regulator of endocytosis, associating with the proline-rich domain of dynamin1, inhibiting the binding of other ligands, such as Grb2, endophilin and amphiphysin, and thus interfering with the assembly of the endocytic machinery.

3.4.1 Pfn2 mRNA immunoprecipitates together with IRP1 and IRP2

As explained previously, 35 new IRP1 and IRP2 candidate target-mRNAs were identified in a high-throughput genome-wide approach (Sanchez *et al.* 2011). Profilin2 mRNA was selected for further investigations as 3 independent Affymetrix microarray probes corresponding to Pfn2 mRNA were positively detected after RNA immunoprecipitation with IRP1 and IRP2 in multiple tissues: duodenum, liver, spleen, and bone marrow, but not in brain (Figure 1.18).
We further validated Affimetrix data by qPCR analysis in samples from liver, spleen and brain where IRP1-mRNPs were immunoprecipitated (Figure 3.20).

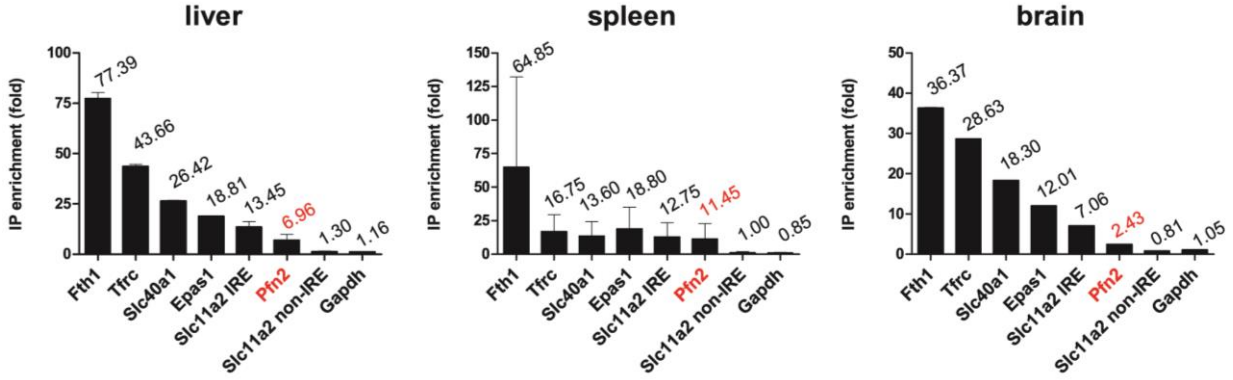

Figure 3.20 Specific enrichment of Pfn2 mRNA in IRP1 immunoprecipitated fractions. IRP/IRE mRNPs were isolated using anti-IRP1 antibody, recombinant IRP1 and mRNAs from different mouse tissues (Sanchez *et al.* 2011). The specificity of IRP1/IRE mRNP isolation was tested by qPCR analysis of immunoprecipitated (IP) liver, spleen and brain samples versus mock IP reactions (no recombinant IRP1 added). Fold enrichment is indicated for Pfn2 mRNA as well as for positive IRE-containing mRNA controls (Fth1, Tfrc, Slc40a1, Epas1 and the IRE isoform of Slc11a2) and negative non-IRE-containing mRNAs (non-IRE Slc11a2 or Gapdh). qPCR absolute quantification; values are reported as means ± SD.

Pfn2 mRNA was detected specifically enriched, together with known IRE-containing mRNAs used as controls, in the immunoprecipitated (IP) fraction compared to the mock IP reaction (where no recombinant IRP1 was added) in all the tissues analyzed, with a different fold of enrichment depending on the tested tissue (Figure 3.20). To note that a 2.43-fold enrichment was also detected in brain, tissue that was apparently negative in Affymetrix experiments, probably due to the lower sensitivity of the arrays compared to the qPCR detection.
These results validate Pfn2 as a good interactor of both IRPs.

3.4.2 Pfn2 has an atypical and conserved 3' Iron Responsive Element (IRE)

When we analyzed Pfn2 mRNA using available bioinformatics tools for IRE prediction (RNAAnalyzer, and UTRScan), we were not able to identify any canonical IRE motif.
Recently, with the collaboration of the bioinformatics unit at IMPPC (Dr. Ildefonso Cases), Dr. Mayka Sanchez developed a new web server for IRE prediction: the SIREs Web Server 1.0 (Searching for IREs, http://ccbg.imppc.org/sires/) (Campillos *et al.* 2010). This new software is improved compared to currently available programs, as it is able to predict both classical IREs but also non-classical IRE motifs such as the ones present in DMT1 and HIF2α mRNAs (Sanchez *et al.* 2007) that present an unpaired nucleotide in the upper stem (Figure 1.7), as well as atypical IREs containing non-canonical apical motifs that have been previously shown to be able to bind IRPs *in vitro* by SELEX (Butt *et al.* 1996; Henderson *et al.* 1996). However, not even using this improved tool we were able to find an IRE-like structure in Pfn2 mRNA.
I then tried to experimentally identify the IRP-binding element of Pfn2 mRNA using a new and non-radioactive method. We have established a new and non-radioactive electrophoretic mobility shift assay (EMSA) methodology to study IRP-RNA interactions based on the paper of Köhn and colleagues (Kohn *et al.* 2010) (see Materials and Methods 2.2.3; this non-radioactive method was also used for the results shown in section 3.1 and 3.2).
The full length mouse Pfn2 mRNA (OriGene cDNA clone) was linearized, *in vitro* transcribed and used as non-labeled competitor in competitive EMSA against a fluorescently-labeled probe corresponding to the IRE of human FTH1 (nucleotides 60-85 in NM_002032.2) (Gray *et al.* 1993). Competitive EMSAs, using recombinant IRP1 protein, showed that the full length Pfn2 mRNA but not a version truncated in its 3' region, by XcmI digestion, was able to efficiently compete with the FTH1 IRE probe for the binding to IRP1 (Figure 3.21A and D, lane 2 versus lanes 3 and 4), suggesting that the RNA element responsible for IRP interaction is located within Pfn2 3' UTR region after the XcmI site.
To further identify the IRP-RNA binding element in Pfn2 mRNA, we have cloned 5 overlapping and truncated portions of the 3' end of Pfn2 mRNA (approximately 260bp in length each, overlapping 40bp) and tested them by the same competitive EMSA (Figure 3.21A). Only one of those fragments, fragment A, was able to specifically compete with the FTH1 probe for IRP1 binding, with a similar competition degree as the Pfn2 full length mRNA does (Figure 3.21D, lane 5). By narrowing down the mRNA fragment involved in IRP binding, it was now possible to perform a closely folding analysis, using RNAfold WebServer (ViennaRNA Web Services, Institute for Theoretical Chemistry, University of Vienna), that identified an atypical IRE motif (nucleotides 1025-1060 in NM_019410.3) (Figure 3.21B).
Similar to other IREs, the Pfn2 3' IRE presents a 5-paired upper stem and an unpaired C bulge at the 5' side of the stem, but differs from a canonical IRE by an atypical sequence in the hexanucleotide apical loop (AAGUUG), being the canonical sequence (CAGWGH, see Introduction 1.4.1 and Figure 1.6). Nevertheless, the 1st and the 5th nucleotides in the apical loop (adenosine and uracil) can still pair allowing the formation of an AGU pseudotriloop, as it happens in canonical IREs (Figure 3.21C).

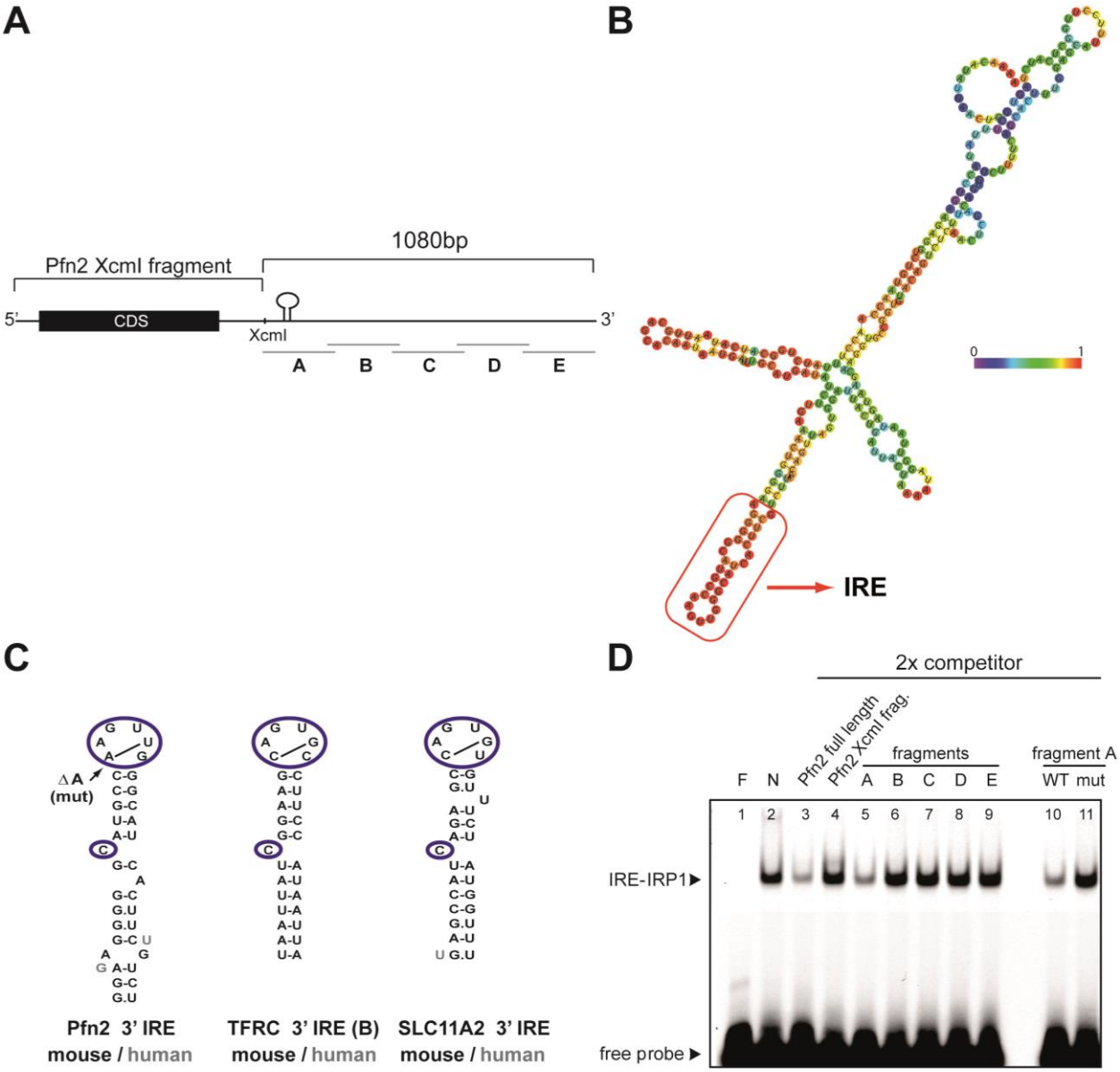

E

H. sapiens	NM_002628.4	GGGAGGGGG C AUGCC AAGUUG GGCAUCACUUUGUCU
G. gorilla gorilla	XM_004037838.1	GGGAGGGGG C AUGCC AAGUUG GGCAUCACUUUGUCU
P. troglodytes	XM_516998.4	GGGAGGGGG C AUGCC AAGUUG GGCAUCACUUUGUCU
T. syrichta	XM_008065605.1	GGGAGGGAG C AUGCC AAGUUG GGCAUCACUUUGUCU
A. melanoleuca	XM_002923453.1	GGGAGGGGG C AUGCC AAGUUG GGCAUCACUUUGUCU
P. tigris	XM_007086379.1	GGGAGGGGG C AUGCC AAGUUG GGCAUCACUUUGUCU
C. lupus	XM_005634653.1	GGGAGGGGG C AUGCC AAGUUG GGCAUCACUUUGUCU
L. weddellii	XM_006733254.1	GGGAGGGGG C AUGCC AAGUUG GGCAUCACUUUGUCU
B. acutorostrata	XM_007188124.1	GGGAGGGGG C AUGCC AAGUUG GGCAUCACUUUGUCU
B. taurus	NM_001128197.1	GGGAGGGGG C AUGCC AAGUUG GGCAUCACUUUGUCU
S. scrofa	XM_003358607.2	GGGAGGGGG C AUGCC AAGUUG GGCAUCACUUUGUCU
C. hircus	XM_005675579.1	GGGAGGGGG C AUGCC AACUUG GGCAUCACUUUGUCU
M. musculus	NM_019410.3	GGAAGGGGG C AUGCC AAGUUG GGCAUCACUUCGUCU
R. norvegicus	NM_030873.1	GGAAGGGGG C AUGCC AAGUCG GGCAUCACUUCGUCU
J. jaculus	XM_004655975.1	GGGGAGGGG C AUGCC AAGUUG GGCAUCACUUUGUCU
T. chinensis	XM_006149725.1	GGGAGGGGG C AUGCC AAGUUG GGCAUCACUUUGUCU
O. princeps	NM_004597698.1	GGGAGGGGG C AUGCC AAGUUG GGCAUUACAUUGUCU
C. cristata	XM_004674910.1	GGGAGGGGG C AUGCC AAGUUG GGCAUCUCUUUGUCU
Conservation		** ** * * ***** **** * ***** * * ****

Figure 3.21 Pfn2 3' Iron Responsive Element. (A) Schematic representation of Pfn2 mRNA. Coding region (CDS, black box), Pfn2 XcmI fragment and fragments A to E and location of the IRE are shown. **(B)** Folding prediction of mouse Pfn2 fragment A using RNAfold WebServer (ViennaRNA Web Services, Institute for Theoretical Chemistry, University of Vienna). Color scale indicates the probability of base-pairing from 1 (high, red)

to 0 (low, blue). The IRE structure detected in Pfn2 mRNA is boxed. **(C)** Illustration of the mouse and human 3' IRE motifs in Pfn2, Tfrc and Slc11a2 mRNAs (nucleotide variations in the human sequences are highlighted in gray). Notice the sequence differences in the apical loop. The arrow indicates the deletion of the first adenosine (ΔA mut) of the apical loop, used as mutant construct. **(D)** Competitive EMSAs using fluorescent FTH1-IRE labeled probe and 2x fold molar excess of unlabeled competitors: full length mouse Pfn2 cDNA or fragments (XcmI fragment, A to E fragments). WT: wild type; mut: fragment A containing a single deletion of the first adenosine in the 6-nucleotides apical loop. One representative experiment is shown. **(E)** Sequence alignment showing phylogenic conservation of Pfn2 IRE among higher eukaryotes, principally primates, higher mammals and plants. 100% conserved residues are indicated with an asterisk. The C-bulge and the 6-nucleotides apical loop are boxed.

The presence of this atypical apical loop (AAGUUG) makes that predictions with SIREs program failed in identifying the IRE in Pfn2 mRNA, since this combination was not allowed in the program. Knowing that this atypical IRE is functional (see below data), we have implemented the SIREs bioinformatics program to be able to detect this motif (now named motif 19 in the SIREs Web Server version 2.0). Therefore, our experimental data allow us to improve our bioinformatics program in the prediction of additional non-classical IREs.

We further confirmed the identified IRE motif as a *bona-fide* IRP-binding element by site-directed mutagenesis of mouse Pfn2 fragment A. A single point mutation (ΔA mut: deletion of the first adenosine in the IRE hexanucleotide apical loop AAGUUG, Figure 3.21C) completely abrogates the competition in EMSAs (Figure 3.21D lanes 10-11).

Additionally, sequence alignment analysis of Pfn2 mRNA 3' region in several species (ClustalO, EMBL-EBI Web Services) showed that the IRE motif is well conserved among higher eukaryotes (Figure 3.21D).

Hence, we tested for IRP1 binding to the human PFN2 sequence. The mouse and human IRE minimal sequences (nucleotides 1025-1060 in NM_019410.3 and nucleotides 1072-1107 in NM_053024.3, respectively) were cloned using synthetic oligonucleotides in I-12.CAT plasmid and used for *in vitro* transcription of unlabeled RNAs in competitive EMSAs against the fluorescently-labeled human FTH1 IRE probe (Figure 3.22).

We found that the human WT IRE sequence is also able to bind recombinant IRP1, but with lower affinity compared to the mouse IRE sequence, shown by a 70% residual signal at 80x fold molar excess of unlabeled competitor compared to the 36% residual signal given by the mouse WT IRE sequence at the same fold molar excess (Figure 3.22A). In both cases the introduction of the ΔA mutation in the first nucleotide of the apical loop, completely abolishes the competition (Figure 3.22A, lane 6 versus 5 and lane 8 versus 7).

We also demonstrate that the IRP1-IRE competitive binding is dose dependent either when using mouse fragment A (Figure 3.22B) or the IRE minimal sequences as unlabeled competitors (Figure 3.22C). A more efficient competition was observed for the longer sequence of mouse fragment A compared to the shorter mouse IRE minimal sequence, as fragment A reduces signal to a 25% at 10x fold molar excess, while the mouse IRE sequence reaches only a 36% residual signal at 80x fold molar excess (Figure 3.22B and D).

Analogous results were obtained in competitive EMSAs when recombinant IRP2 protein was used instead of IRP1 (Figure 3.22D). However, in these *in vitro* settings, the binding of Pfn2 fragment A or IRE sequences to IRP2 appears weaker compared to the binding to IRP1 (Figure 3.22A-C versus D).

In all experiments, unlabeled competitors corresponding to the FTH1 IRE WT and mutant ΔC in the first nucleotide of the apical loop (not interacting with the IRP) (Gray *et al.* 1993) were used as positive and negative controls, respectively.

In summary, we proof that the mouse and the human Pfn2 3' IRE are functional *in vitro*.

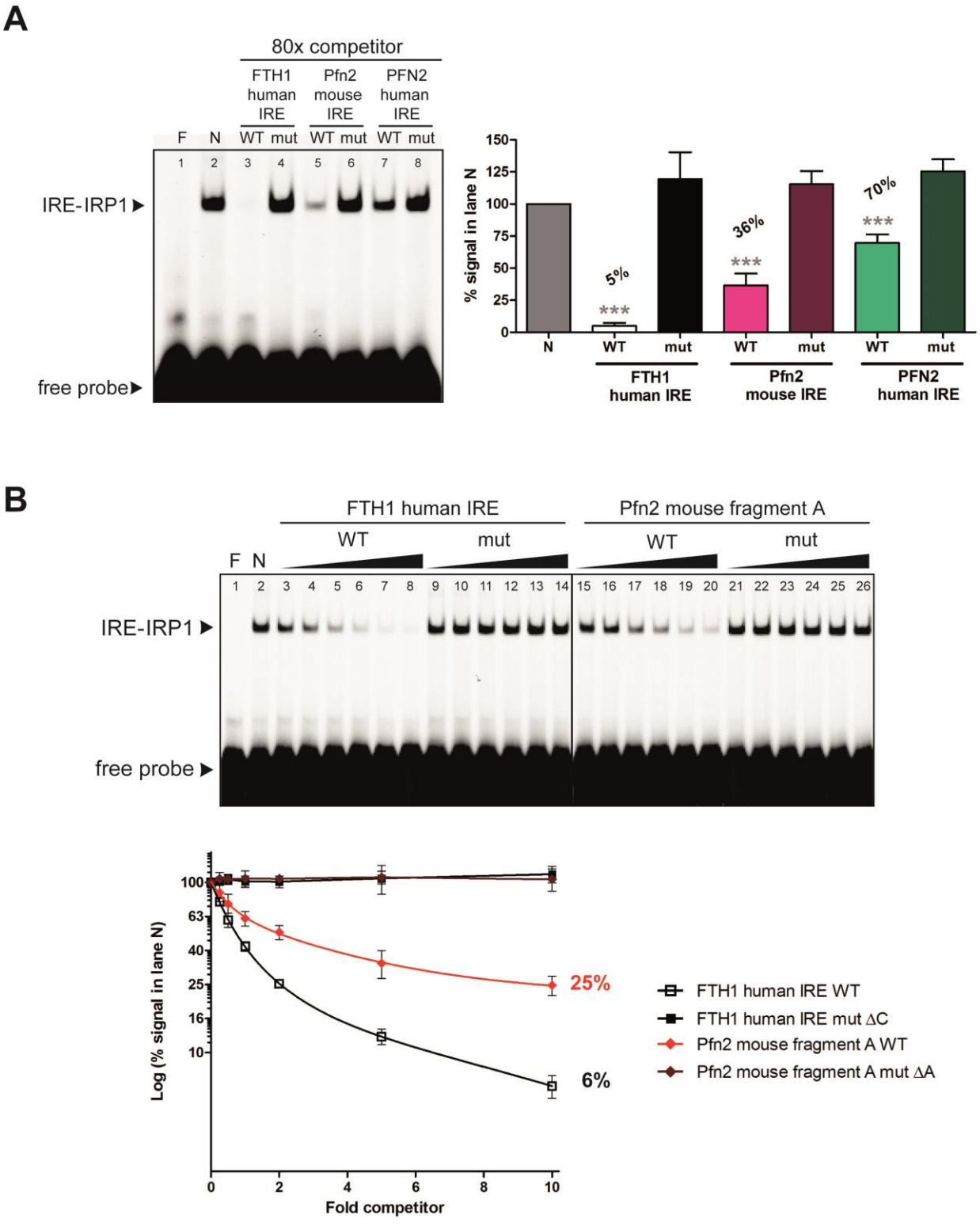

Figure 3.22 Competitive EMSAs with mouse and human Pfn2 IRE. (A) Binding of Pfn2 IRE sequences. Competitive EMSAs using recombinant IRP1, fluorescently-labeled human FTH1 IRE probe and 80x fold molar excess of unlabeled competitors: human FTH1 IRE WT or ΔC mutant (nucleotides 60-85 in NM_002032.2), mouse (nucleotides 1025-1060 in NM_019410.3) or human (nucleotides 1072-1107 in NM_053024.3) Pfn2 IRE sequences WT or ΔA mutant. **(B)** Dose dependent competition of Pfn2 fragment A in IRP1 competitive EMSAs. FTH1 IRE labeled-probe was incubated with increasing molar excess (0.25x, 0.5x, 1x, 2x, 5x and 10x) of unlabeled competitor RNAs: WT and ΔC mutant FTH1 IRE, WT or ΔA mutant mouse Pfn2 fragment A (nucleotides 921-1181 in NM_019410.3).

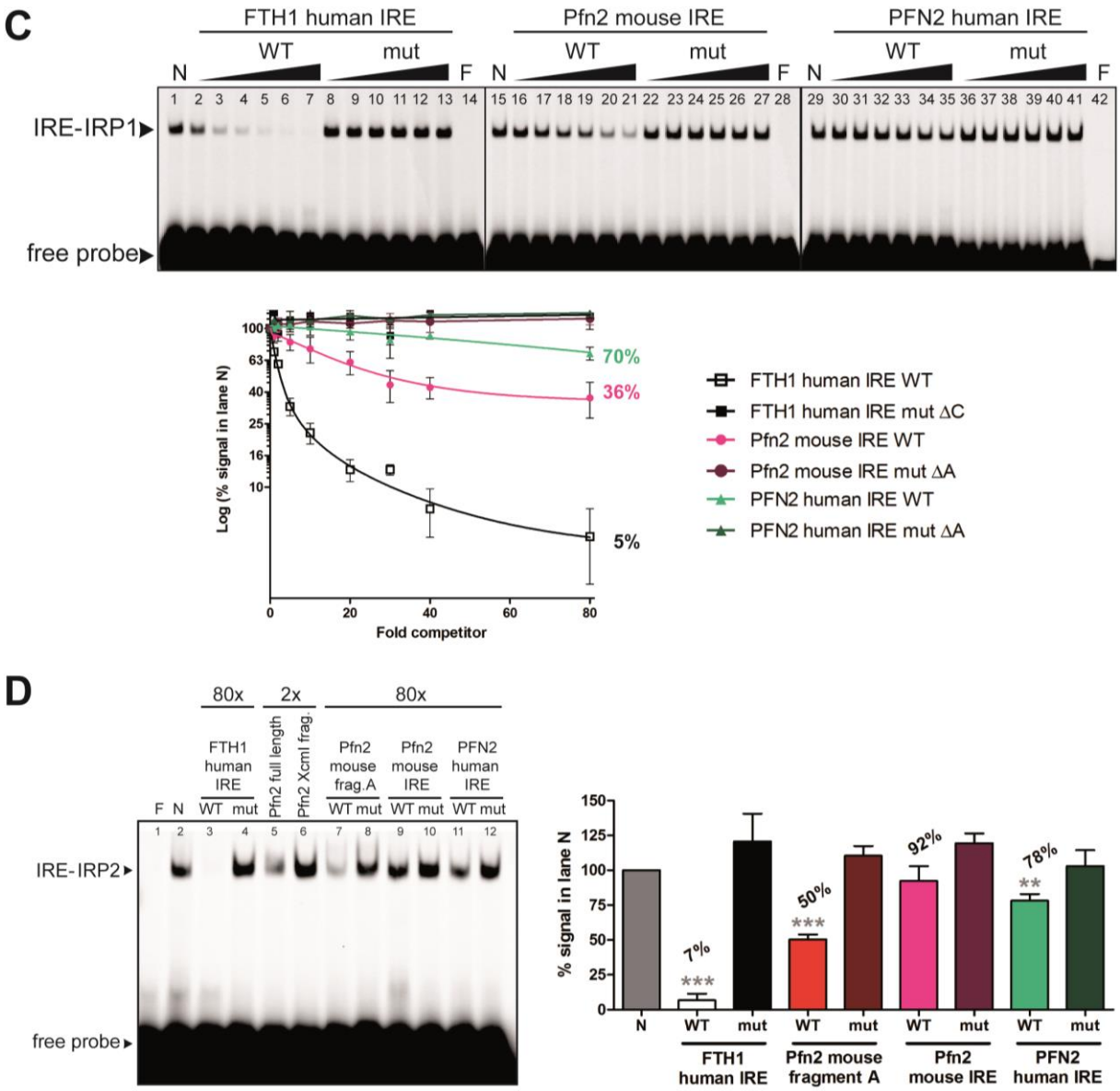

Figure 3.22 Competitive EMSAs with mouse and human Pfn2 IRE. (C) Dose dependent competition of Pfn2 IRE sequences in IRP1 competitive EMSAs. FTH1 IRE labeled-probe was incubated with increasing molar excess (1x, 5x, 10x, 20x, 40x and 80x) of unlabeled competitor RNAs: human FTH1 IRE WT or ΔC mutant, mouse and human Pfn2 IRE sequences WT or ΔA mutant. **(D)** Binding of Pfn2 IRE by recombinant IRP2 in competitive EMSAs using fluorescently-labeled human FTH1 IRE probe and an increasing molar excess (2x or 80x) of unlabeled competitor RNAs: FTH1 IRE WT or ΔC mutant, mouse Pfn2 full length clone and fragment resulting from XcmI digestion, mouse Pfn2 fragment A WT and ΔA mutant and mouse or human Pfn2 IRE sequences WT or mutant. In all cases, the intensity of the shifted signal was quantified using Odyssey Infrared Imaging System (LI-CORE Biosciences). Quantified data, compared to the signal in lane N (taken as 100%), are represented. Means ± SD of at least three independent experiments are shown. F: free probe; N: no competitor added; WT: wild type; mut: mutant (deletion of the first nucleotide of the IRE apical loop).

3.4.3 Post-transcriptional regulation of Pfn2 mRNA in cell lines

As shown above, we demonstrated that Pfn2 mRNA has a functional IRE located at the 3' UTR. For TFRC mRNA, that has 5 IREs in its 3' UTR, it has been demonstrated that it is regulated by increased mRNA stabilization upon IRP binding in low iron conditions. On the other hand, when cellular iron is high, loss of IRP binding favors TFRC mRNA degradation (see Introduction 1.4.3). To study if a similar regulation takes places with Pfn2 mRNA, we examined the post-transcriptional regulation of Pfn2 mRNA in response to changes in iron status or IRPs activity in different cell lines or in mouse tissues (see section 3.4.4).

3.4.3.1 Regulation of Pfn2 mRNA levels in cell lines after DFO and Hemin treatments

To study the response of Pfn2 mRNA to iron levels, we treated cultured cell lines with an iron chelator (Deferoxamine, DFO) or with a source of iron (Hemin).
Mouse cell lines of different origin were used: NIH3T3 (embryonic fibroblasts), RAW264 (macrophages), Hepa1-6 (hepatoma cells) and AML12 (hepatocytes). Moreover, as Pfn2 is physiologically highly expressed in the central nervous system (Witke *et al.* 1998), we also tested the human neuroblastoma SKNBE cell line (Supp. Figure 6.2).
Cells were treated for 10h with 100µM DFO, 100µM Hemin or left untreated and Pfn2 mRNA and protein levels were monitored by qPCR and Western blotting (Figure 3.23 and 3.24, respectively). As positive control we measured in parallel Tfrc and, in some cases, Slc11a2 levels. Tfrc and Slc11a2 mRNAs also bear 3' IREs, five IREs in the case of Tfrc and one single IRE in the case of Slc11a2.
qPCR results showed that, while Tfrc mRNA was, as expected, upregulated by iron chelation with DFO and downregulated by iron loading with Hemin in all the cell lines tested (Figure 3.23A right panel), Pfn2 mRNA levels did not respond to iron stimuli in the same way (Figure 3.23A left panel). Only for Hepa1-6 cells we observed a statistically significant change in Pfn2 expression: Pfn2 mRNA is a 25% reduced after 10h Hemin treatment compared to untreated cells (Figure 3.23A left panel), which is compatible with a 3' IRE regulation. Unexpectedly, Pfn2 mRNA was also a 25%reduced by DFO in Hepa1-6 cells (Figure 3.23A left panel).

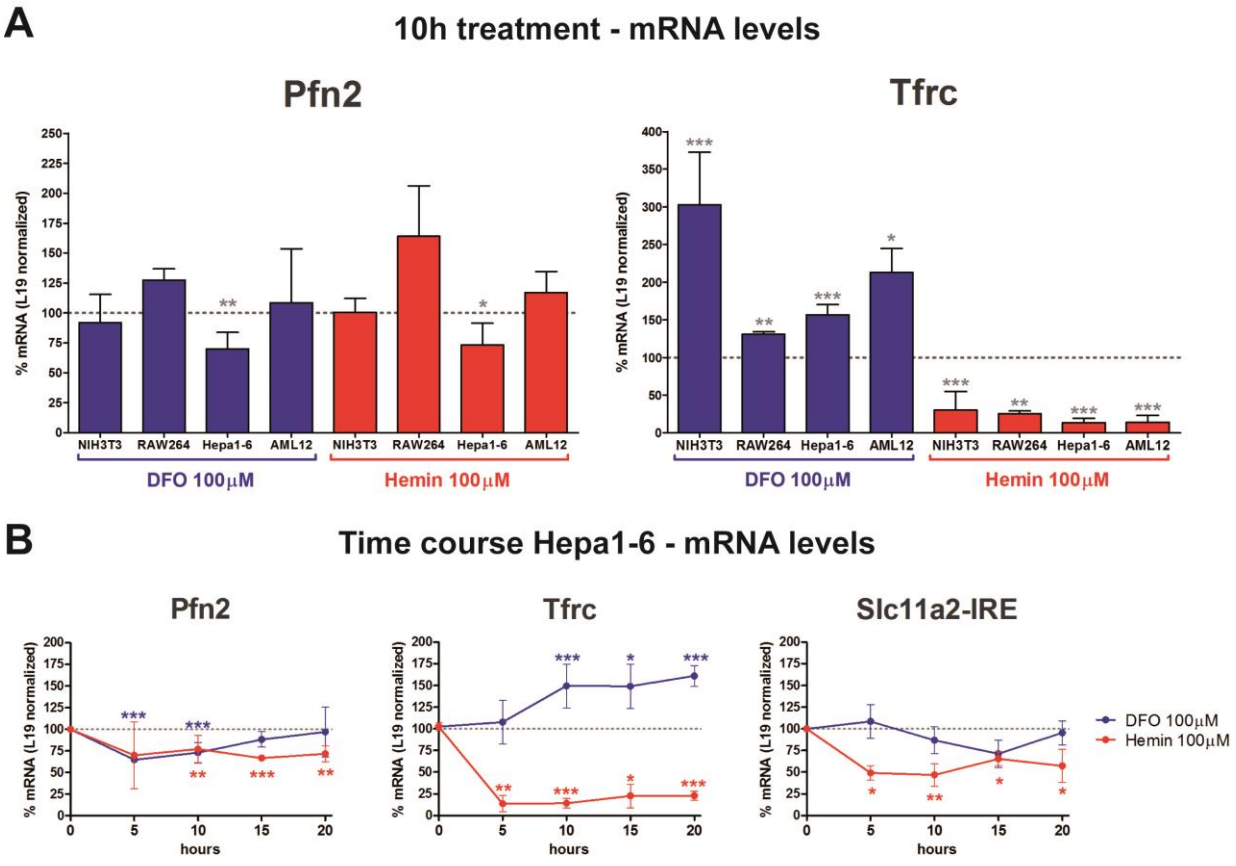

Figure 3.23 Testing of Pfn2 mRNA levels after iron treatment (DFO/Hemin). (A) NIH3T3, RAW264, Hepa1-6 and AML12 cell lines were treated for 10h with 100µM DFO, 100µM Hemin or left untreated and Pfn2 and Tfrc levels monitored by qPCR. Results were normalized against L19 expression and compared to untreated cells (set as 100% and indicated by the gray dashed lines). Means ± SD of at least three independent experiments are shown. **(B)** Hepa1-6 cells were treated for 5-10-15 and 20h with 100µM DFO, 100µM Hemin or left untreated and the mRNA levels of Pfn2, Tfrc and Slc11a2-IRE isoform were monitored by qPCR. Results were normalized against L19 expression and compared to untreated cells (set as 100% and indicated by the gray dashed lines) at each time point. Means ± SD of at least three independent experiments are shown.

We further studied Pfn2 mRNA regulation in Hepa1-6 cells doing a time course experiment at 5-10-15 and 20 hours with 100μM DFO or 100μM Hemin (Figure 3.23B). Once again Pfn2 showed a 25% reduction in mRNA levels after hemin treatment that starts at 5h of treatment and keeps stable in time, while DFO treatment induces an initial downregulation of Pfn2 mRNA at 5-10 hours of treatment but goes back to normal levels at 15-20 hours (Figure 3.23B, left panel).
Tfrc control mRNA was strongly upregulated by DFO treatment and downregulated by Hemin treatment at most time points Figure 3.23B, central panel). The IRE isoform of Slc11a2 also showed a ~40-50% reduction after hemin treatment, stable at all the time points, while there was no upregulation after DFO treatment (Figure 3.23B, right panel), similar to the behavior observed for Pfn2 mRNA.
Therefore, we can conclude that Pfn2 mRNA, similar to Slc11a2 mRNA is selectively downregulated by iron supplementation with Hemin in particular cell lines (Hepa1-6).
Pfn2 expression after 10h treatment with 100μM DFO or 100μM Hemin was also checked at protein level by Western blotting in NIH3T3, RAW264, AML12 and Hepa1-6 mouse cell lines and human SKNBE neuroblastoma cells (Figure 3.24).
In all experiments, TFRC and/or H- and L-Ferritin protein levels were monitored in parallel as positive controls of the effectiveness of the iron chelation or iron supplementation treatments.

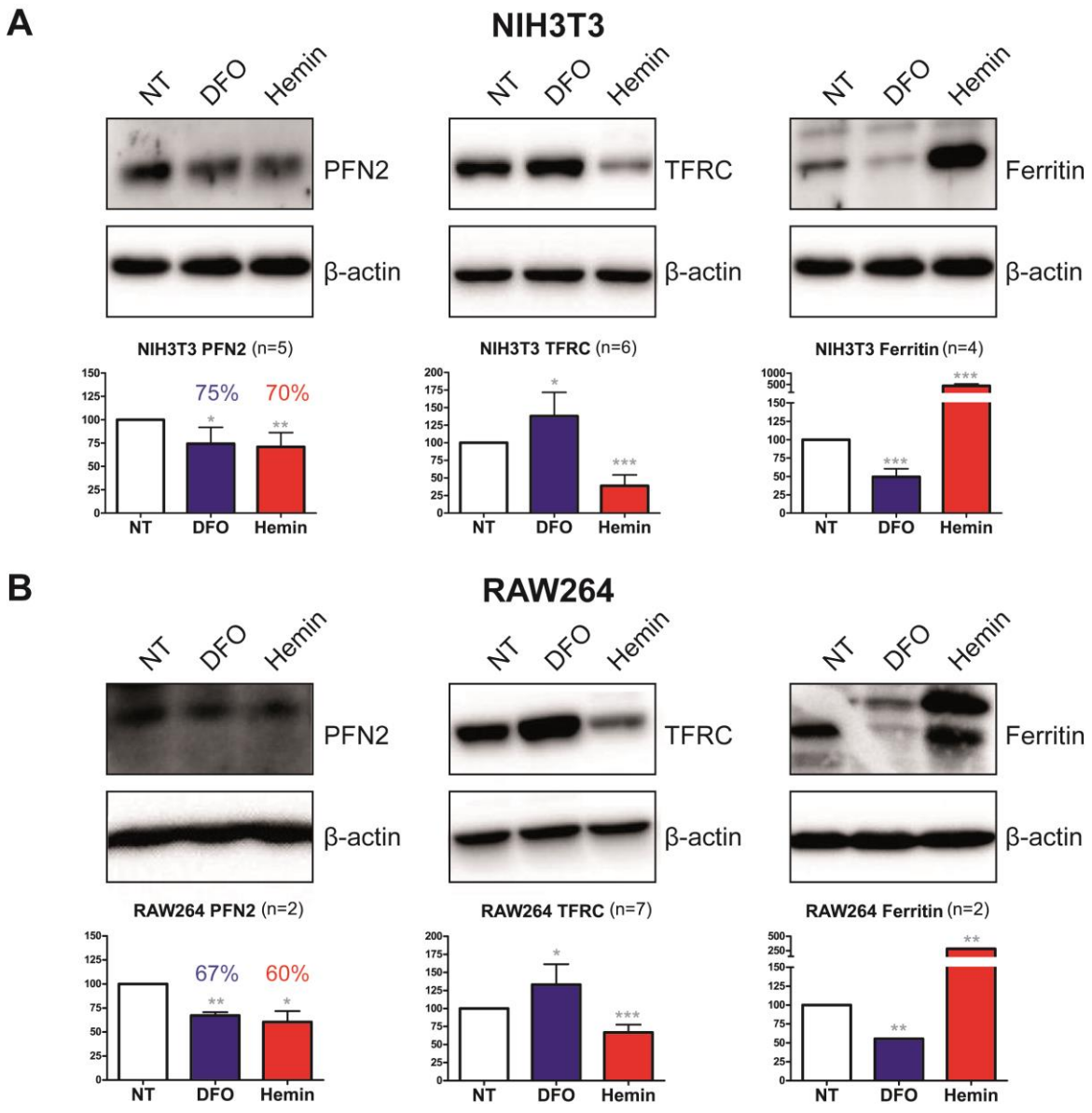

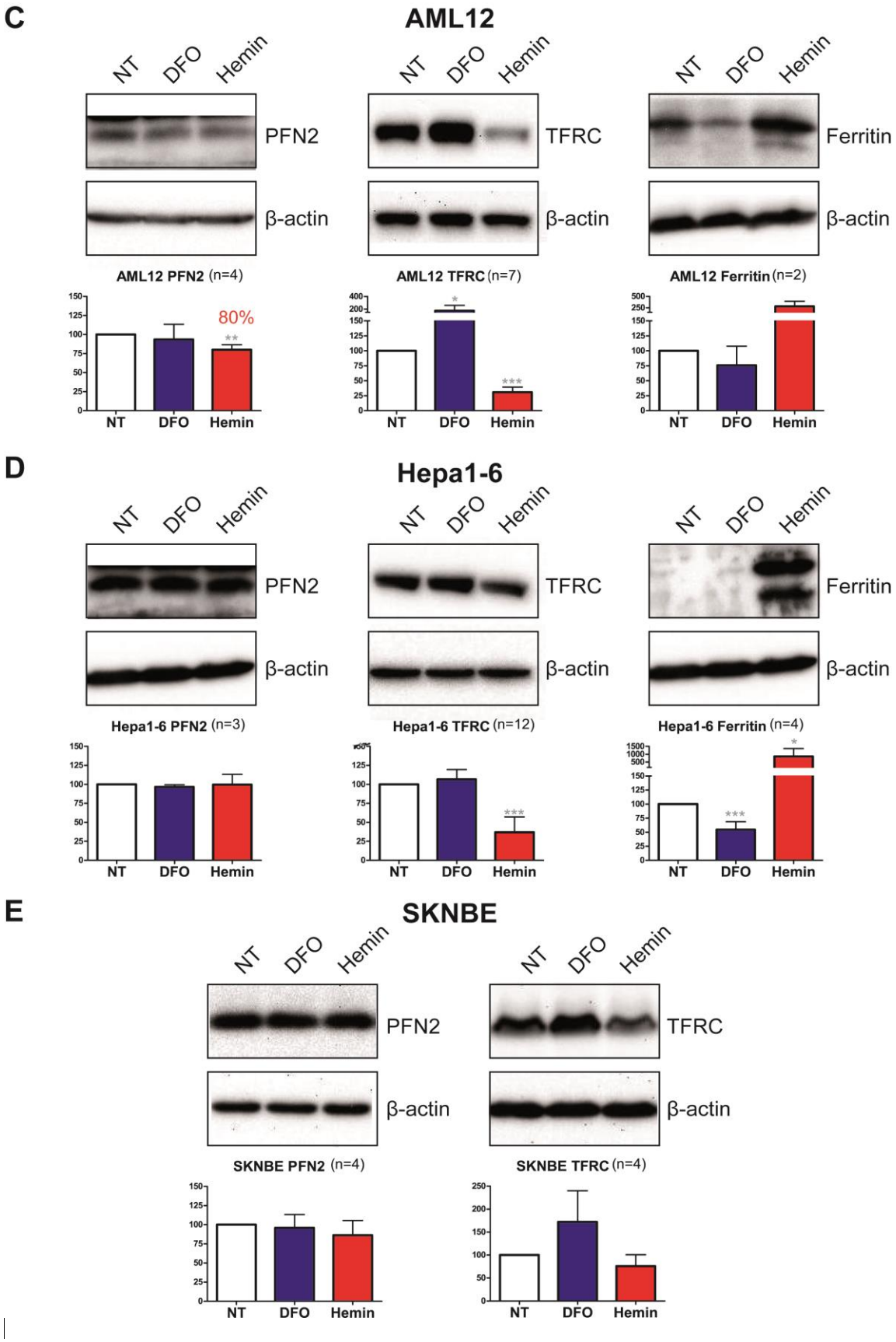

Figure 3.24 Testing of PFN2 protein levels after iron treatment (DFO/Hemin). NIH3T3 **(A)**, RAW264 **(B)**, AML12 **(C)**, Hepa1-6 **(D)** or human neuroblastoma SNKBE cells **(E)** were treated for 10h with 100μM DFO, 100μM Hemin or left untreated and the protein levels of PFN2 (left), TFRC (center) and H- and L-ferritin (right) were analyzed. In all cases, the levels of β-actin were monitored in parallel for normalization. The intensity band signals was quantified using the AlphaEaseFC software (Alpha Innotech) and data were normalized to the signal of not treated cells (NT), set as 100%. Means ± SD of n independent experiments.

As expected, Western blotting experiments showed that TFRC protein levels were increased by iron chelation with DFO and reduced by iron supplementation with Hemin and that, on the other hand, H- and L-Ferritin protein levels were reduced after DFO treatment and increased after Hemin treatment (Figure 3.24) in all the cell lines analyzed, although showing a different degree of regulation depending on the cell line.
The analysis of Pfn2 protein levels showed that in NIH3T3, Pfn2 was reduced a 30% by iron supplementation with Hemin, but, unexpectedly, it was also reduced a 25% by iron chelation with DFO (Figure 3.24A). A similar modulation was also observed in RAW264 and AML12 cells: in RAW264 it was 40% reduced by Hemin and 33% reduced by DFO (Figure 3.24B) and in AML12 it was 20% reduced by Hemin and unchanged after DFO treatment (Figure 3.24C). No apparent regulation in PFN2 protein levels was observed for Hepa1-6 or the neuronal SKNBE cells in response to iron stimuli (Figure 3.24D and E), despite for Hepa1-6 cells we have previously observed a reduction in mRNA levels after either Hemin or DFO treatments (Figure 3.23A left panel).
Thus, we observed a significant downregulation of PFN2 protein levels in NIH3T3, RAW264 and AML12 cells after Hemin treatment, as it happens for TFRC. This is consistent with an enhanced mRNA degradation of a 3' IRE-containing mRNA during iron supplementation, due to the lack of IRPs binding in these conditions. However, no raise in PFN2 protein levels was observed after DFO treatment, as it is expected to happen if mRNA stabilization of Pfn2 3' IRE takes place; on the contrary, iron chelation results in a slight reduction of PFN2 protein in NIH3T3 and RAW264 cells.

3.4.3.2 Pfn2 mRNA stability studies

As mentioned before, the 5 IREs in the 3' UTR of TFRC mRNA were shown to mediate mRNA stabilization upon IRP binding during iron deficiency (Mullner *et al.* 1989). To study a possible mRNA stabilization effect by the IRPs also on Pfn2 mRNA, we measured Pfn2 mRNA half-life in mouse NIH3T3 cells under control conditions, iron-deficient or iron-excess conditions after the addition of the transcription inhibitor 5,6-dichloro-1β-1-ribofuranosylbenzimidazole (DRB) (Harrold *et al.* 1991).
NIH3T3 cells were treated with 100μM DFO, 100μM Hemin or left untreated for 16h. Subsequently, 30μg/ml DRB was added and cells were collected at different time points (0-2-4-6-8 and 10h) for the analysis of Pfn2, Tfrc and β-actin mRNA decay by qPCR (Figure 3.25). Tfrc mRNA half-life, compared with untreated cells (t½=15h), is detectably prolonged following DFO treatment (t½=25h) and strongly shortened after Hemin treatment (t½=6.4h).
On the other hand, the changes observed in Pfn2 mRNA turnover under the same conditions did not show a similar behavior (Figure 3.25). Whereas Pfn2 mRNA half-life is reduced after iron supplementation with Hemin (untreated cells t½=37.1h versus Hemin treated cells t½=11.6h), we unexpectedly observed that iron chelation treatment with DFO dramatically reduced Pfn2 mRNA half-life in NIH3T3 cells (untreated cells t½=37.1h versus DFO treated cells t½=5.8h) (Figure 3.25).
The mRNA turnover of β-actin, an unrelated non-IRE-containing mRNA, was also monitored as negative control of the experiments and it showed no significant differences in the rates of mRNA decay among untreated cells and DFO or Hemin treated cells with ~30-60h t½ values, evidencing the high stability of β-actin mRNA (Figure 3.25).
According with these experiments, in iron supplementation conditions with Hemin, when IRPs do not bind to IRE motifs, Pfn2 mRNA is more rapidly degraded (as happens with Tfrc mRNA). However, in iron deficient conditions with the iron chelator DFO, the IRPs binding to Pfn2 mRNA does not result in increasing mRNA stabilization (as occurs for Tfrc mRNA) but it

seems that even accelerates Pfn2 mRNA degradation. Similar discordant mRNA stability findings were also found with other IRP-target mRNAs, as for CDC14A mRNA (Sanchez *et al.* 2006), where a regulation was observed only under iron chelation with DFO but not with iron supplementation by Hemin treatment.

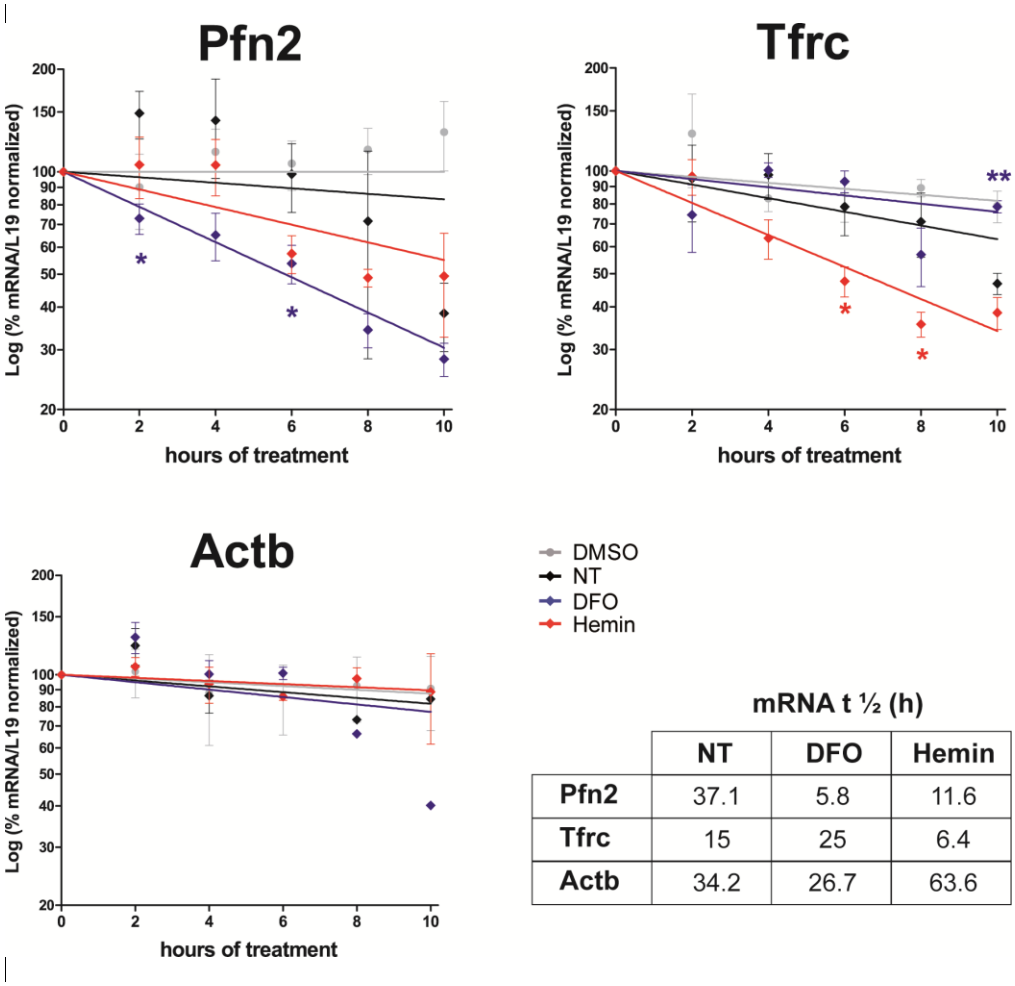

mRNA t ½ (h)

	NT	DFO	Hemin
Pfn2	37.1	5.8	11.6
Tfrc	15	25	6.4
Actb	34.2	26.7	63.6

Figure 3.25 mRNA half-life determination for Pfn2 mRNA. Pfn2, Tfrc and β-actin (Actb) mRNA turnover rates were analyzed in NIH3T3 mouse cells in control conditions (black lines), iron deficiency conditions (DFO, blue lines) and iron supplementation conditions (Hemin, red lines). Cells were treated with 100μM DFO, 100μM Hemin or left untreated for 16h. Subsequently, 30μg/ml DRB was added to inhibit transcription. Alternatively, the same amount of DMSO used for DRB solubilization was added to untreated cells (gray lines) in order to exclude that the changes in mRNA level could be attributable to DMSO by itself. Cells were collected at different time points (0-2-4-6-8 and 10h) after DRB addition and the rate of mRNA decay of Pfn2, Tfrc and β-actin mRNAs was analyzed by qPCR. qPCR data were normalized to L19 mRNA levels and, for each condition, the zero hour DRB treatment time point was set as 100%. The table shows, for Pfn2, Tfrc and β-actin mRNAs, the half-life (t½ or time required for degrading 50% of the existing mRNA molecules) calculated in control conditions, iron deficient or iron replete conditions. Means ± SD of 6 independent experiments are shown. DMSO: dimethyl sulfoxide; NT: untreated cells.

3.4.3.3 Regulation of a Pfn2 IRE luciferase reporter

Following, we performed luciferase reporter experiments to test for Pfn2 regulation in response to iron in a more sensitive setting.

A Pfn2 IRE-luciferase reporter vector was generated, as well as proper experimental controls. I took advantage of a protocol already established by my supervisor Dr. Mayka Sánchez and previously used to demonstrate the iron-dependent modulation mediated by the IRE motif in HIF2α 5' UTR (Sanchez *et al.* 2007). The pCIF-HIF2α WT vector, described in the publication of 2007, contains the Firefly luciferase coding sequence fused at the 5' end with the complete 5' UTR of human HIF2α mRNA (Figure 3.26A left). This construct showed iron-dependent

regulation of luciferase expression and was used as positive control in all experiments (Sanchez *et al.* 2007). An additional H-ferritin positive control construct was generated from the pCIF-HIF2α WT vector by replacing the HIF2α 5' UTR for a portion of the 5' UTR of mouse H-ferritin (pCIF-Fth1 WT). Alternatively, to test for Pfn2 3' IRE regulation, the pCIF-HIF2α WT vector was modified by replacing the HIF2α IRE for the mouse Pfn2 3' IRE inside the 5' UTR of human HIF2α present in the original plasmid (pCIF-HIF2α-IRE Pfn2 WT) (Figure 3.26A left). A mutated version of each construct carrying a non-functional IRE motif was also analyzed. In detail, we used the previously described HIF2α 5' UTR mutant vector (pCIF-HIF2α mut), carrying a deletion of the first nucleotide in HIF2α IRE apical loop (ΔC), known to blunt IRP-IRE interaction (Sanchez *et al.* 2007) as well as analogous mutants generated for Fth1 (ΔC) and Pfn2 (ΔA) constructs (pCIF-Fth1 mut and pCIF-HIF2α-IRE Pfn2 mut) (Figure 3.26A right). HeLa cells were transiently transfected with each of the above mentioned constructs together with a Renilla luciferase plasmid for normalization. Cells were subsequently treated with 100μM DFO, 100μM Hemin or left untreated and Firefly and Renilla activities were measured in cell lysates using the Dual-Luciferase Reporter Assay System (Promega). Cellular toxicity or variability in transfection efficiency were normalized by plotting the Firefly measures as a ratio relative to the Renilla readouts (Figure 3.26B).

Luciferase quantifications showed that, in cells transfected with the wild type HIF2α or Fth1 control constructs, the normalized luciferase activity was reduced by iron chelation with DFO and slightly but significantly increased by iron supplementation with Hemin (Figure 3.26B, 1-3 and 7-9), confirming before published results (Sanchez *et al.* 2007) and indicating translational repression of luciferase reporter upon IRP binding to a functional 5' UTR IRE in iron-deficient conditions. However, for the mouse Pfn2 IRE reporter construct, the luciferase activity was unchanged under control, iron-deficient or iron-replete conditions (Figure 3.26B, 13-15). Notably, as was previously reported for the HIF2α constructs (Sanchez *et al.* 2007), the luciferase activity of cells transfected with the mutant constructs was 2 up to 5-fold higher compared to cells transfected with constructs containing wild type IREs (Figure 3.26B 1-3 versus 4-6, 7-9 versus 10-12 and 13-15 versus 16-18).

This difference implies that the wild type luciferase constructs are strongly repressed compared to the mutant ones, reflecting an efficient IRP interaction with the wild type sequences. Remarkably, this was also observed for the mouse Pfn2 IRE reporter constructs (Figure 3.26B 13-15 versus 16-18).

To figure out if the lack of modulation observed for the wild type Pfn2 3' IRE construct could be attributable to the artificial position of the mouse Pfn2 3' IRE inside the 5' UTR of HIF2α mRNA, we also generated additional reporter constructs for Pfn2. In detail, a portion of mouse Pfn2 3' UTR (fragment A, see Figure 3.21) containing the wild type or ΔA mutated IRE was cloned at the 5' end of the luciferase coding sequence, completely replacing the 5' UTR of HIF2α. However, no modulation of luciferase activity after DFO or Hemin treatment was observed neither with those constructs (data not shown).

In another set of experiments Pfn2 3' IRE was placed in a more natural position at the 3' end of the luciferase reporter gene. In this case, the entire mouse Pfn2 3' UTR or a portion of the 3' UTR (region after XcmI site, see Figure 3.21), both of which carrying the wild type or ΔA mutated IRE were cloned at the 3' end of luciferase in the pGL3-PGK-luc plasmid (Promega). These luciferase assay experiments with Pfn2 3' UTR cloned at the 3' side of the luciferase coding sequence were inconclusive because we realized that the empty vector used, pGL3-PGK-luc, was itself modulated by iron treatments, invalidating our results (data not shown).

In summary, our results indicate that neither the Pfn2 IRE clone nor fragment A of Pfn2 are able to confer iron-regulation (translational repression by DFO and increased translation by Hemin treatment) when artificially cloned at the 5' side of a luciferase reporter gene.

However, the higher luciferase levels/activity measured in cells transfected with the mutant Pfn2 constructs suggests that the wild type Pfn2 constructs are efficiently repressed by the Iron Regulatory Proteins (IRPs).

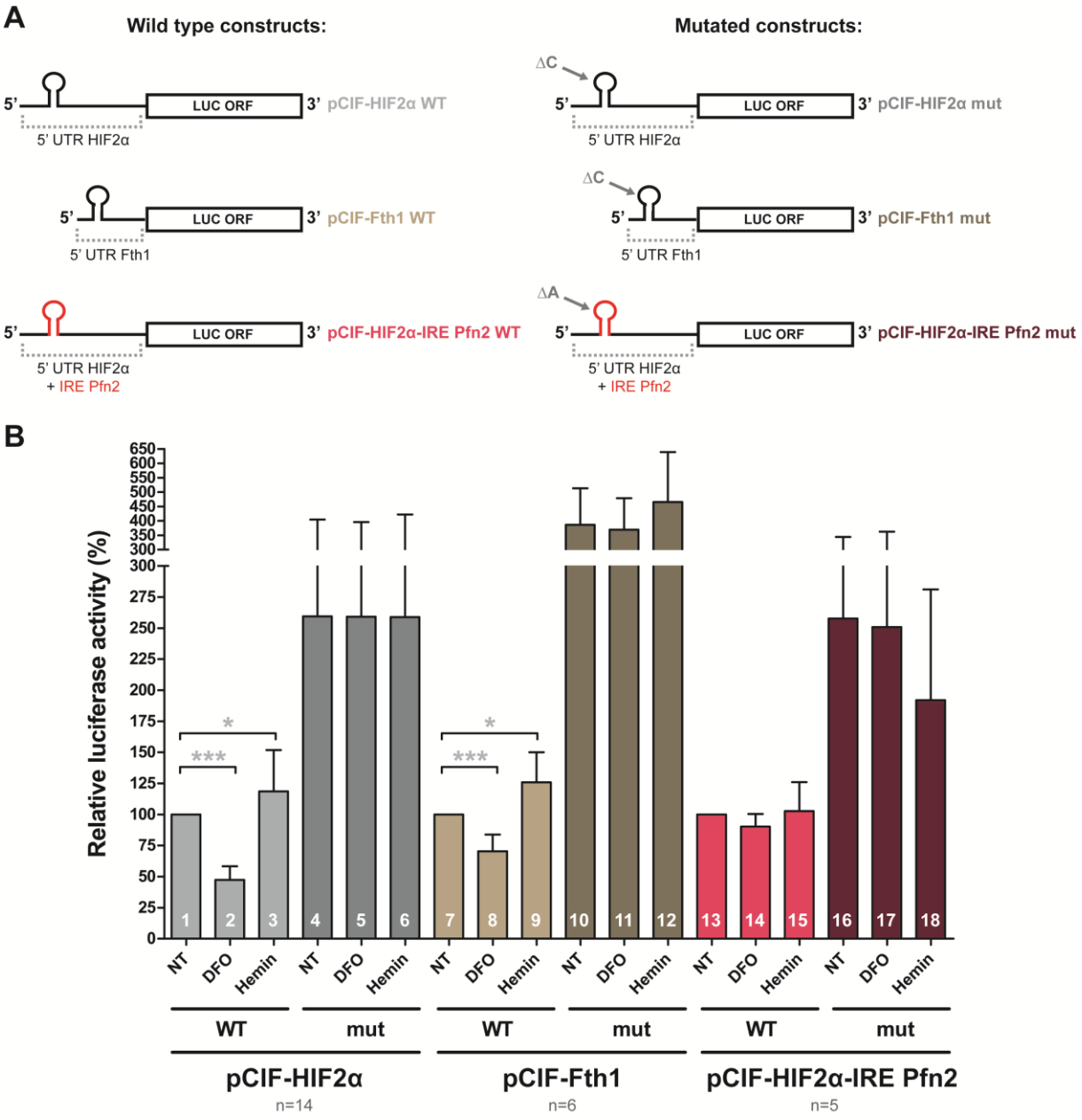

Figure 3.26 Pfn2 IRE luciferase reporter assay. (A) Schematic representation of the luciferase reporter constructs based on the pcDNA3-Luc vector (Sanchez *et al.* 2007). The reporter constructs carry the Firefly luciferase coding sequence (LUC ORF) fused at the 5' of the LUC ORF with the complete 5' UTR of human HIF2α (pCIF-HIF2α) or a portion (nt 59-223 in NM_010238.2) of the 5' UTR of mouse Fth1 (pCIF-Fth1) or, for testing Pfn2 IRE regulation, the 5' UTR of human HIF2α in which HIF2α IRE was replaced for mouse Pfn2 3' IRE (pCIF-HIF2α-IRE Pfn2). A mutated version (mut) of each construct was generated by deleting the first nucleotide of the IRE apical loop (ΔC for HIF2α and Fth1 IREs and ΔA for Pfn2 IRE), mutations that are expected to blunt IRP-IRE interaction. The above mentioned wild type and mutated luciferase constructs were transiently transfected in HeLa cells together with a Renilla luciferase plasmid in order to normalize for transfection efficiency. 24h after transfection, cells were treated for 16h with 100μM DFO, 100μM Hemin or left untreated and Firefly and Renilla luciferase activities were determined using a Dual-Luciferase Reporter Assay System (Promega) in a Centro LB960 microplate luminometer (Berthold Technologies). **(B)** The graph shows relative Firefly luciferase activities, normalized to Renilla luciferase counts. For each construct-group, the values obtained for not treated cells (NT) were set as 100%. Means ± SD of (n) independent experiments are shown. LUC ORF: luciferase open reading frame; WT: wild type; mut: mutant (deletion of the first nucleotide of the IRE apical loop).

3.4.3.4 PFN2 regulation in H1299 cells overexpression a constitutively active IRP1

To further explore the interaction and IRP-mediated regulation on the 3' IRE of Pfn2 mRNA, we tested endogenous PFN2 levels in human H1299 cells overexpressing a constitutively active IRP1 mutant (kind gift of Dr. Kostas Pantopoulos, McGill University, Montreal) (Wang *et al.* 2002) (Figure 3.27). This H1299 stable clone expresses a human IRP1 mutant in which the cysteine at position 437 was substituted for a serine (C437S). Cysteine 437 is critical for the coordination of the Fe/S cluster and its replacement generates an IRP1 protein unresponsive to iron perturbations and constitutively active in its IRE-binding form (Hirling *et al.* 1994). H1299 cells conditional expresses the IRP1 C437S mutant (referred as IRP1 mut) under the control of a tetracycline-inducible expression system (Tet-Off, Clontech) to avoid the toxic effects associated with a sustained IRP1 expression (Hirling *et al.* 1994; DeRusso *et al.* 1995). The H1299 IRP1 mut clone was grown in medium containing 1µg/ml Doxycycline (a tetracycline derivate) and IRP1 mut expression was activated upon Doxycycline removal from the medium (-Dox). H1299 IRP1 mut cells kept under Doxycycline treatment (+Dox) were used as reference control. In -Dox cells, IRP-binding activity reaches its maximum levels at 5 days after the induction (Wang *et al.* 2002). Coinciding with the peak of maximum IRP-binding activity, the cells were treated for 16h with 100µM DFO, 100µM Hemin or left untreated and PFN2 and TFRC protein levels were evaluated by Western blotting under the different iron-conditions (Figure 3.27A right). Moreover, to control for unspecific effects due to Doxycycline treatment itself, PFN2 and TFRC levels were also checked in H1299 parental cells (not containing the IRP1 mut gene) that were subjected to the same treatments (Figure 3.27A left). High levels of IRP1 mut transgene expression are clearly appreciable in -Dox H1299 IRP1 mut clone compared to the same cells kept under Doxycycline (+Dox) (Figure 3.27 bottom-right). As expected and confirming published data (Wang *et al.* 2002), the augmented IRP-binding activity in IRP1 mut overexpressing cells increases TFRC protein levels (Figure 3.27A right, TFRC lane 9 versus 8 and lane 13 versus 12 and Figure 3.27C). This effect was appreciable in untreated cells (100% to 130% TFRC protein increase) and even more evident in Hemin treated cells (40% to 70% TFRC protein increase), while no significant difference was observed among DFO treated cells expressing or not the IRP1 mut transgene (Figure 3.27C). These observations fit the regulatory model of IRP-mediated stabilization of TFRC mRNA. This stabilizatory effect was not detected in H1299 parental cells, thus confirming that the observed phenotype is specifically mediated by IRP1 mut overexpression, although a minimal increase of TFRC protein in NT -Dox (110%) versus NT +Dox cells (100%) was measured (Figure 3.27C).

The quantification of PFN2 protein levels under the same conditions showed, in some but not all experiments, a trend to increased PFN2 protein levels when IRP1 mut expression was induced (Figure 3.27A right, PFN2 lane 11 versus 10 and lane 13 versus 12). However, this data were not always reproducible and overall results indicate that PFN2 protein levels were apparently not affected by the perturbation of IRP activity in H1299 IRP1 mut overexpressing cells (Figure 3.27B).

Analogous results were observed from the quantification of TFRC and PFN2 mRNA levels by qPCR (data not shown).

A possible reason for the inconsistency in our observations could be found in cell culture conditions variability and, in line with this, Wang and collaborators also reported that H1299 IRP1 mut cells grown in particular cell density or serum concentration conditions were able to overcome IRP1 C437S-mediated regulation on H- and L-ferritin mRNAs (Wang *et al.* 2002). On the other hand, as a cell-specific IRP-regulation has been reported for DMT1 (another mRNA with a single IRE at the 3' UTR) (Wardrop *et al.* 1999; Hubert *et al.* 2002); it might be

possible that the regulation of PFN2 by the IRPs is restricted to certain cell lines and not happening in H1299 (human lung carcinoma) cells.
Moreover, our *in vitro* EMSA experiments indicated that the binding of the human PFN2 3' IRE to IRP1 and IRP2 proteins is weaker compared to the mouse IRE (see section 3.4.2); it is therefore likely that the human PFN2 mRNA is not responsive to IRP regulation to the same extent as murine Pfn2 mRNA.
In conclusion, we took advantage of human H1299 cells stably overexpressing an IRP1 mutant constitutively active as IRE-binding protein to study PFN2 3' IRE regulation in response to changes of IRP-binding activity. While an increased IRP-binding mediates TFRC mRNA stabilization and consequent increase of TFRC protein levels, no similar effect was definitely observed for PFN2 mRNA and protein levels.

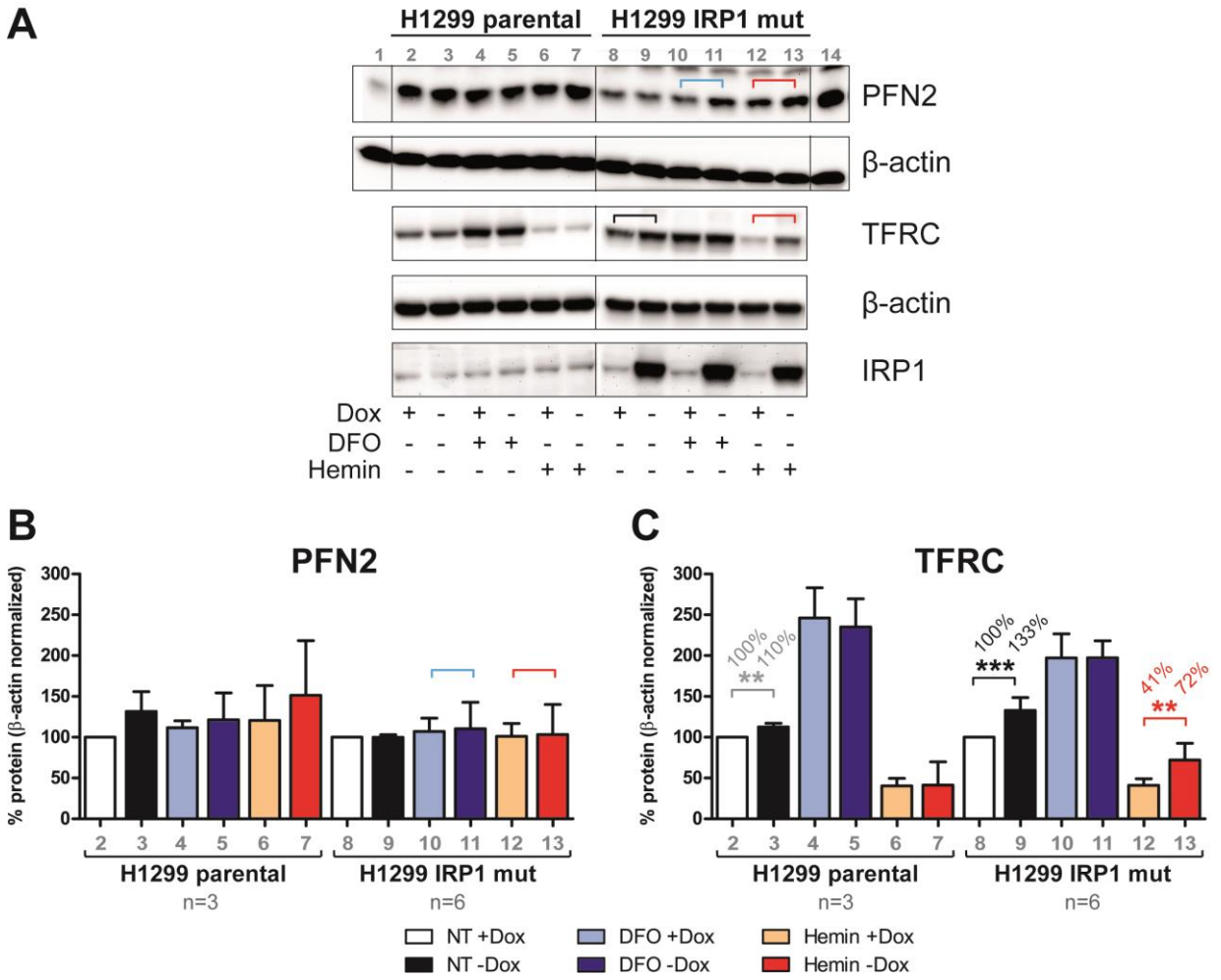

Figure 3.27 PFN2 protein levels in cells overexpressing the IRP1 C437S mutant. (A) A human lung H1299 stable Tet-Off clone expressing human IRP1 C437S mutation (IRP1 mut), known to confer to IRP1 constitutively RNA-binding activity (Wang *et al.* 2002), was used to test for PFN2 regulation upon perturbation of IRP activity. Cells were grown in medium containing 1µg/ml Doxycycline to prevent transgene expression and IRP1 mut expression was activated upon Doxycycline removal from the medium (-Dox). 5 days after induction, cells were treated for 16h with 100µM DFO, 100µM Hemin or left untreated and PFN2 and TFRC protein levels were analyzed by Western blotting. As control, parental H1299 cells, not carrying the IRP1 mut transgene, were subjected to the same treatments. One representative gel is shown: H1299 parental cells (lanes 2-7), H1299 IRP1 mut clone (lanes 8-13), Hek293T control cells (lane 1) and Hek293T cells transfected with a mouse Pfn2 plasmid (lane 14), as control of PFN2 band specificity. Western blotting quantification of PFN2 **(B)** and TFRC **(C)** expression under the above mentioned conditions is represented in the graphs. Data were normalized against β-actin expression and compared to the signal of untreated cells (NT +Dox, set as 100%). Means ± SD of (n) independent experiments are shown. NT: untreated cells; Dox: Doxycycline.

3.4.4 Post-transcriptional regulation of Pfn2 mRNA in mouse tissues

As we could not identify a clear pattern of regulation for Pfn2 mRNA in response to changes of iron levels in our *in vitro* cellular settings, we further tested if Pfn2 mRNA is modulated *in vivo*, either in mice with altered levels of iron in the diet or in genetically modified mouse models with disturbed Irp1 and Irp2 expression.

3.4.4.1 Pfn2 mRNA levels in mice treated with an iron-deficient diet

In order to test the *in vivo* regulation of Pfn2 mRNA in response to changes of iron levels, C57BL/6 mice were made iron-deficient by consuming a low iron diet for three weeks, starting at weaning age. Littermate mice receiving an iron-normal diet were used as control-group. Pfn2 mRNA levels were measured by qPCR in liver, spleen and duodenum samples from control and iron-deficient mice (Figure 3.28).

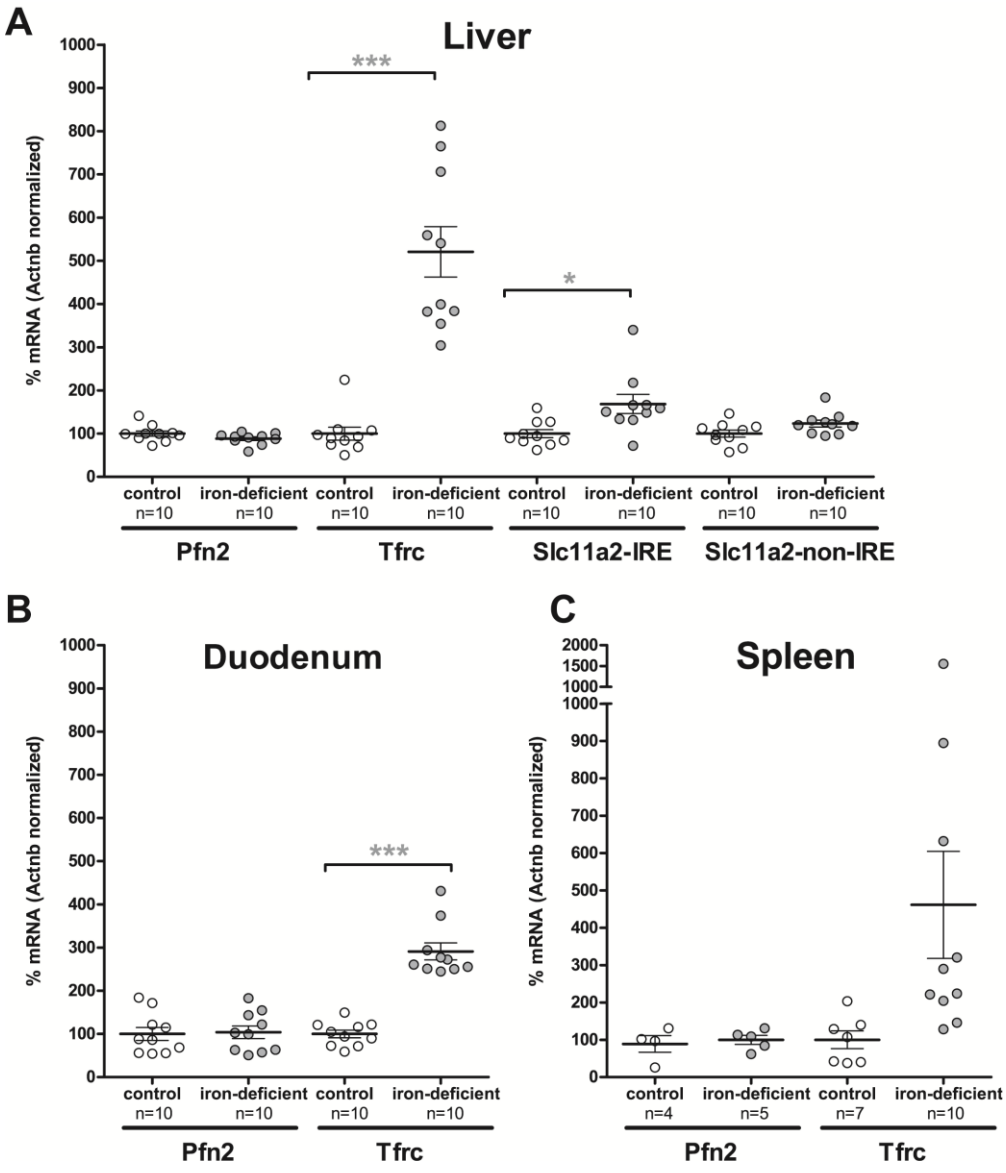

Figure 3.28 Effect of low dietary iron on Pfn2 mRNA levels. mRNA levels of Pfn2 were quantified by qPCR in liver **(A)**, duodenum **(B)** and spleen **(C)** samples from C57BL/6 mice fed for 3 weeks, starting after weaning, with an iron-deficient (<10mg/kg) diet (C1038, Altromin) or a control iron-adequate diet (C1000, Altromin). As positive control, the mRNA levels of other 3' UTR IRE-containing mRNAs, as Tfrc and Slc11a2-IRE and non-IRE isoforms, were quantified in parallel. Results were normalized against β-actin expression and compared to control mice fed with an iron-adequate diet (set as 100%). Means ± SEM are shown. Sample size (n) is indicated.

As control, mRNA levels of other 3' UTR IRE-containing mRNAs, as Tfrc and Slc11a2-IRE and non-IRE isoforms, were also measured. Confirming previously reported data (Dupic *et al.* 2002), liver, spleen and duodenum samples from iron-deficient mice showed upregulated levels of Tfrc mRNA compared to control mice. Tfrc induction is remarkable, although showing different degrees of upregulation among the three tissues (ranging from 3-5 and up to 8-10 folds, Figure 3.28). Additionally, Slc11a2 mRNA quantification in liver samples showed a selective ~2-fold upregulation of the IRE isoform of Slc11a2, while the non-IRE isoform levels are unchanged between iron-deficient and iron-normal mice (Figure 3.28A).

The quantification of Pfn2 mRNA levels in liver, spleen and duodenum samples did not show changes in the expression of Pfn2 transcript between control and iron-deficient mouse groups (Figure 3.28).

These results confirm that dietary manipulation of body iron stores in mice influences the expression of IRE-containing mRNAs. Nevertheless, while iron deficiency upregulates the expression of the 3' IRE-transcripts Tfrc and Slc11a2-IRE, under these tested conditions, Pfn2 mRNA levels are not altered in mice subjected to iron-deficient diet.

3.4.4.2 IRPs exert a positive effect on Pfn2 mRNA levels *in vivo*

To study the *in vivo* effect of IRPs activity on Pfn2 mRNA expression, we took advantage of two mouse models: mice with a moderate gain-of-Irp1-function (Irp1*) (Casarrubea *et al.* 2013) characterized by an increased IRP-binding activity and mice with intestinal-specific *Irp1* and *Irp2* ablation in adult stage (Galy *et al.* 2013), where IRP-binding is abrogated.

A mouse model carrying a gain-of-Irp1-function was recently generated by Casarrubea and collaborators (Casarrubea *et al.* 2013). Those mice systemically express an *Irp1* mutant transgene (referred as *Irp1**) carrying amino acid substitutions in key cysteine residues required for the assembly of the Fe/S cluster (Clarke *et al.* 2006). Irp1* escapes Fe/S cluster-mediated regulation and it is therefore constitutively active in its RNA-binding form. Irp1* transgenic mice are characterized by altered expression of IRP-targets, abnormal body iron distribution and macrocytic erythropenia due to impaired erythroid differentiation (Casarrubea *et al.* 2013).

An increased IRE-binding activity in Irp1* mice is expected to repress 5' UTR IRE mRNAs and stabilize 3' UTR IRE targets. We therefore tested Pfn2 mRNA and protein expression in brain samples from Irp1* and wild type littermate mice (kind gift of Prof. Matthias Hentze and Dr. Bruno Galy, EMBL, Heidelberg) (Figure 3.29). The *Irp1** transgene is ubiquitously expressed in those mice, however, we tested for the brain tissue as Pfn2 is known to be highly expressed in the central nervous system (see Introduction 1.7.3.1 and Supp. Figure 6.2).

mRNA levels of Pfn2 and of other control 3' IRE mRNAs Tfrc, Slc11a2-IRE and non-IRE isoform were quantified by qPCR. While Tfrc mRNA levels were ~2-fold upregulated in Irp1* mice, as expected, Pfn2 mRNA expression was found to be unchanged between wild type and Irp1* mice (Figure 3.29A). Remarkably, neither the IRE and non-IRE isoform of Slc11a2 mRNA showed altered expression in Irp1* mice compared to controls (Figure 3.29A).

The quantification of protein levels by Western blotting confirmed that the expression of PFN2 is similar between wild type and Irp1* mice, whereas TFRC levels are 2-fold upregulated in Irp1* mice (Figure 3.29B).

Thus, an increased IRE-binding activity in the brain of Irp1* mice is not associated either with Pfn2 or Slc11a2-IRE mRNA upregulation and a 2-fold increase was observed only for Tfrc mRNA and protein levels.

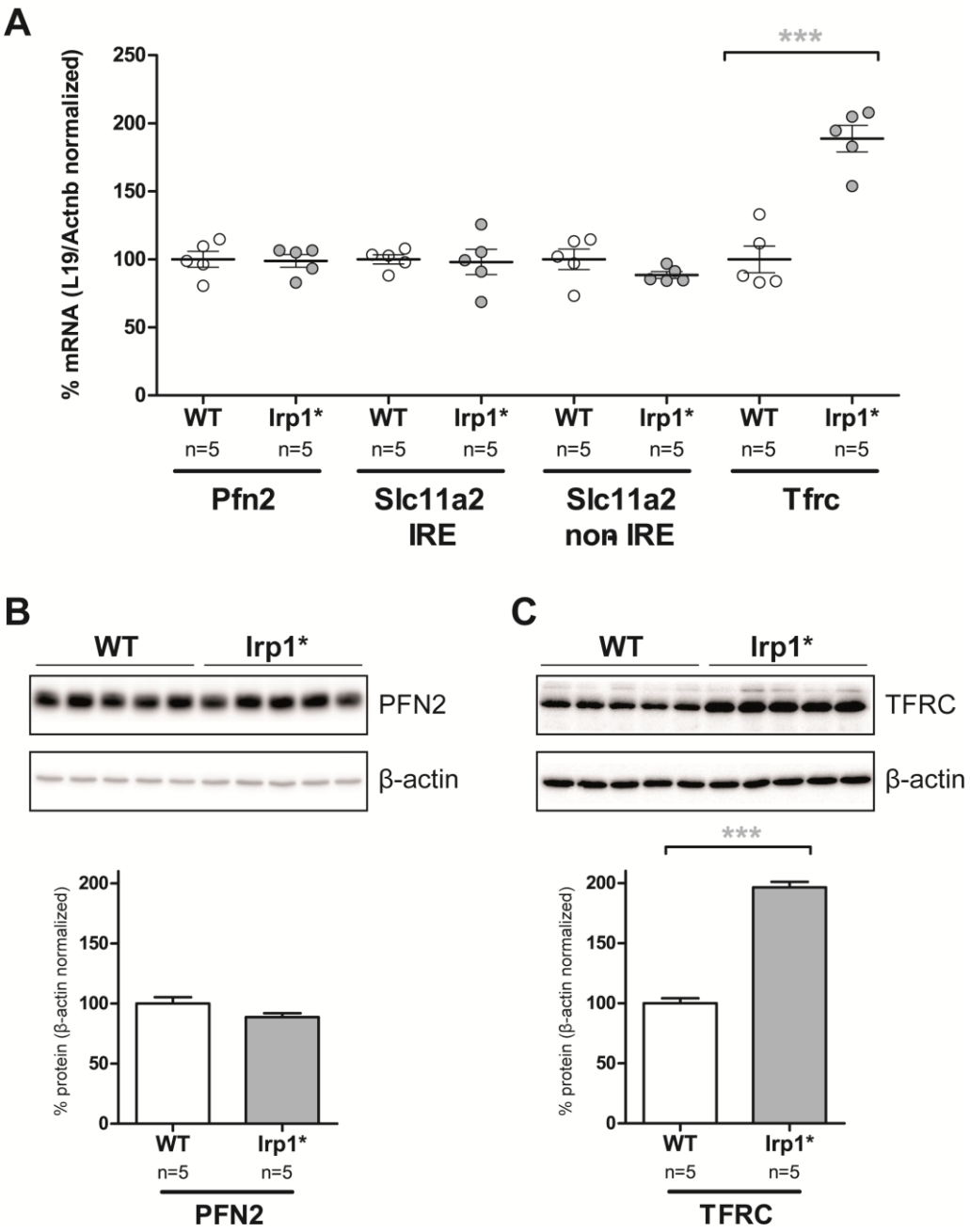

Figure 3.29 Pfn2 expression in the brain of Irp1* transgenic mice. (A) mRNA levels of Pfn2, Slc11a2-IRE, Slc11a2-non-IRE isoforms and Tfrc were quantified by qPCR in brain samples from transgenic mice expressing a constitutively active Irp1 in its IRE-binding form (Irp1*). Results were normalized against β-actin expression and compared to control wild type mice (set as 100%). Means ± SEM are shown. Sample size (n) is indicated. **(B)** Protein levels of PFN2 and TFRC were quantified by Western blotting in the same samples. The levels of β-actin were monitored in parallel for normalization. The intensity of band signals was quantified using the AlphaEaseFC software (Alpha Innotech). Graphs represents normalized data to β-actin. Means ± SEM are shown. Sample size (n) is indicated.

A possible explanation for these observations may reside in the low-grade expression of the *Irp1** transgene. Indeed, Casarrubea and collaborators reported that the *CRE/Lox* strategy for generating the Irp1* mice employed a promoter-less *Irp1** transgene resulting in moderate levels of IRP1* protein, with the purpose to avoid the toxic effects that were previously demonstrated for IRP1 overexpression in cell lines (DeRusso *et al.* 1995).

Our data show that this moderate Irp1* expression effectively stabilizes Tfrc mRNA, containing 5 IREs in its 3' UTR, but it is not sufficient for stabilizing mRNAs carrying a single 3' UTR IRE

as the one of Slc11a2. The absence of Slc11a2 upregulation in Irp1* mice was also reported in the paper of Casarrubea and coworkers for duodenum samples (Casarrubea *et al.* 2013). Similarly to Slc11a2, Pfn2 also has a single 3' IRE and we cannot exclude that its lack of regulation in the brain of Irp1* mice can be attributable to the low-level Irp1* expression.

Casarrubea and collaborator also described a considerable inter-individual and tissue-dependent variability in the effect of *Irp1** transgene on IRP-targets expression. A tissue-specific response to Irp1* activation or a different degree of Irp1* gain-of-function in different tissues, or even IRP-independent mechanisms may also account for this variability or lack of regulation.

Pfn2 expression was also analyzed in mice with intestinal-specific knockout for both *Irp1* and *Irp2* genes (Galy *et al.* 2013). Since global double *Irp1* and *Irp2* deficiency is lethal to mice at embryonic stage (Smith *et al.* 2006), several mouse strains with tissue-specific *Irp1* and *Irp2* deletion have been generated by Dr. Bruno Galy (EMBL, Heidelberg) to overcome the lethality of double IRP ablation (see Introduction 1.5.1). In detail, in the mice characterized in the publication of Galy and collaborators of 2013, *Irp1* and *Irp2* knockout was obtained specifically in the intestinal mucosa using a *CRE/Lox* strategy inducible by tamoxifen administration to mice in the adult stage. Those mice are viable and present normal intestine architecture, but showed decreased iron absorption combined with iron retention in the intestinal mucosa (Galy *et al.* 2013).

In order to assess for Pfn2 mRNA regulation in the absence of IRP activity, we quantified Pfn2 mRNA levels in duodenum samples from double *Irp1* and *Irp2* knockout mice as well as from control mice sacrificed 3 or 5 weeks after IRP ablation induced by tamoxifen treatment (kind gift of Prof. Matthias Hentze and Dr. Bruno Galy, EMBL, Heidelberg) (Figure 3.30).

Mice carrying floxed *Irp1* and *Irp2* genes plus the *CRE* recombinase transgene were injected with 1mg tamoxifen on 5 consecutive days to trigger IRP ablation, while control littermates were given the vehicle only (CRE oil). Additional control mice were: mice missing the *CRE* recombinase transgene treated with oil (no CRE oil) or tamoxifen (no CRE tamoxifen) in order to control for potential effects of tamoxifen treatment or of the *CRE* transgene *per se*.

qPCR quantifications showed that Pfn2 mRNA levels were decreased in duodenal samples from mice with intestinal *Irp1* and *Irp2* deficiency with a ~20% reduction at 3 weeks after IRP ablation by tamoxifen treatment and a ~25% reduction at 5 weeks after treatment (Figure 3.30A and B left). As positive control, Tfrc mRNA expression was also assessed and was expectedly found to be reduced (to ~40% and 45% of control levels at 3 and 5 weeks after treatment respectively) (Figure 3.30A and B right).

These observations indicate that, similarly to Tfrc mRNA, the lack of IRP activity results in an *in vivo* reduction of Pfn2 mRNA levels, as expected for a 3' IRE-containing mRNA controlled by IRP stabilization.

In addition, neither tamoxifen alone (no CRE oil versus no CRE tamoxifen mice), nor the presence of the *CRE* recombinase *per se* (no CRE oil versus CRE oil mice) did affect Pfn2 or Tfrc expression (Figure 3.30), further supporting the idea that Pfn2 mRNA downregulation in tamoxifen-treated CRE mice is mediated by the lack of IRP stabilizing effect.

Overall, although we could not observe an upregulation of Pfn2 expression in Irp1* gain-of-function mice, Pfn2 mRNA levels were significantly reduced in duodenal samples from mice with *Irp1* and *Irp2* intestinal-specific ablation, suggesting that IRPs exert a positive effect on Pfn2 mRNA expression *in vivo*.

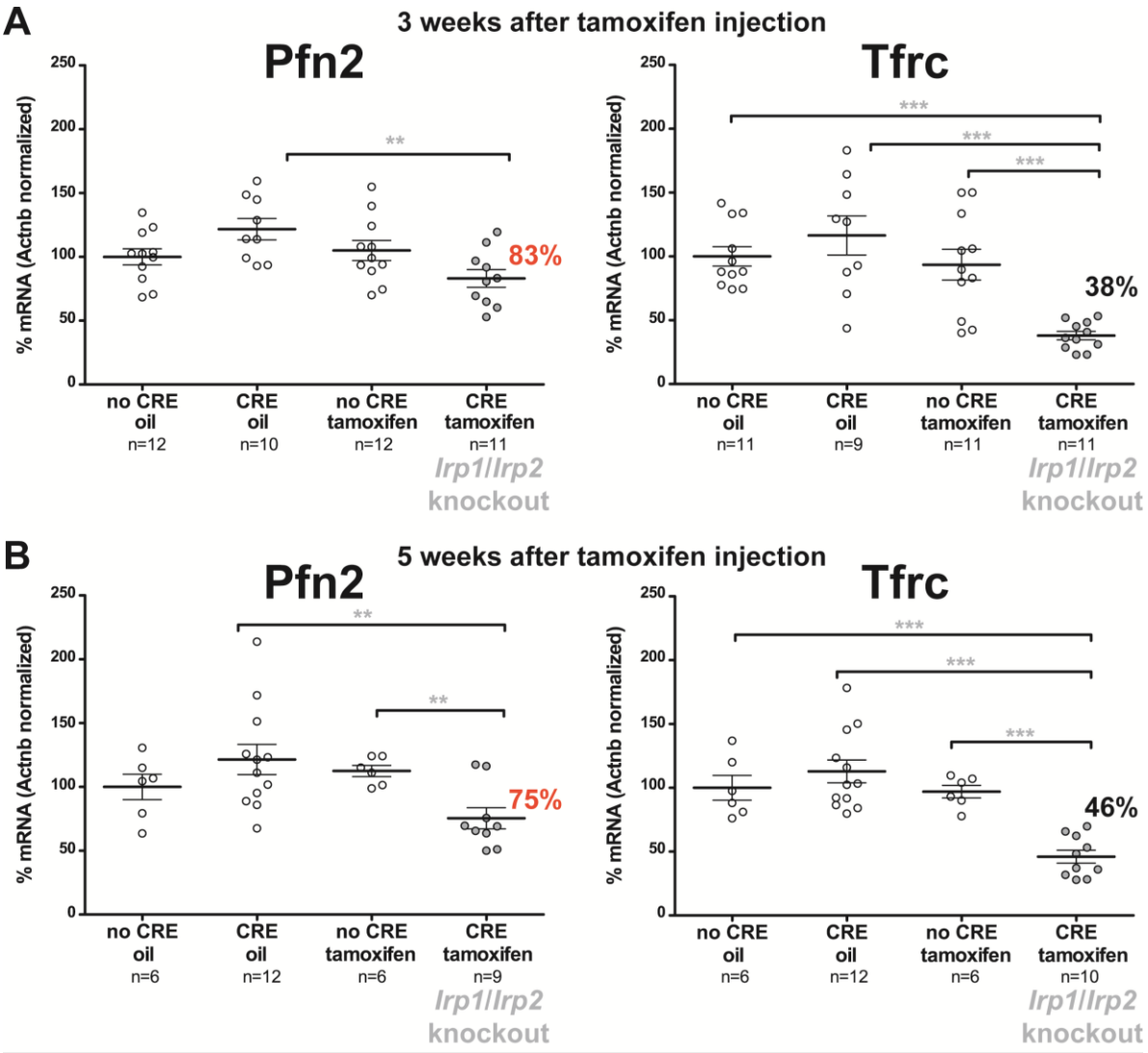

Figure 3.30 Pfn2 expression in duodenum-specific Irp1 and Irp2 knockout mice. Irp1 and Irp2 deficiency was obtained using the CRE/Lox technology in a tamoxifen-inducible system in the intestinal mucosa (Galy *et al.* 2013). The mice carry floxed *Irp1* and *Irp2* alleles plus a tamoxifen-dependent *CRE* recombinase transgene under the control of the *Villin* promoter in the gut epithelium. 10-12 weeks old males were given intraperitoneally 1mg tamoxifen/animal/day on 5 consecutive days (10mg/ml solution in sunflower seed oil:ethanol 9:1) to trigger Irp1 and Irp2 ablation (CRE tamoxifen) in the intestine. Control mice were not transgenic treated with oil (no CRE oil) or tamoxifen (no CRE tamoxifen) or CRE mice receiving the vehicle only (CRE oil). Mice were sacrificed 3 weeks **(A)** or 5 weeks **(B)** after the last tamoxifen injection. Pfn2 and Tfrc mRNA levels were quantified by qPCR in duodenum samples from those mice. Results were normalized against β-actin expression and calibrated to control mice treated with oil (no CRE oil, set as 100%). Means ± SEM are shown. Sample size (n) is indicated.

3.4.5 IRE and non-IRE Pfn2 mRNA isoforms

For SLC11A2 and ferroportin mRNAs additional non-IRE-containing isoforms have been described (Hubert *et al.* 2002; Zhang *et al.* 2009). Previously in literature and databases several isoforms for Pfn2 mRNA have been also described (Di Nardo *et al.* 2000; Lambrechts *et al.* 2000; ENSEMBL database Release 71, April 2013) (Figure 3.31A).

In order to explore if these isoforms excluded the IRE sequence and how this can influence our previous qPCR data we have performed 3' Rapid Amplification of cDNA Ends (3' RACE) experiments in samples from mouse brain and liver. Isoform-specific semiquantitative RT-PCRs were done in mouse brain and liver samples as well as in NIH3T3 and Hepa1-6 mouse cell lines to determine the expression levels of different isoforms described in literature or in databases (Figure 3.31).

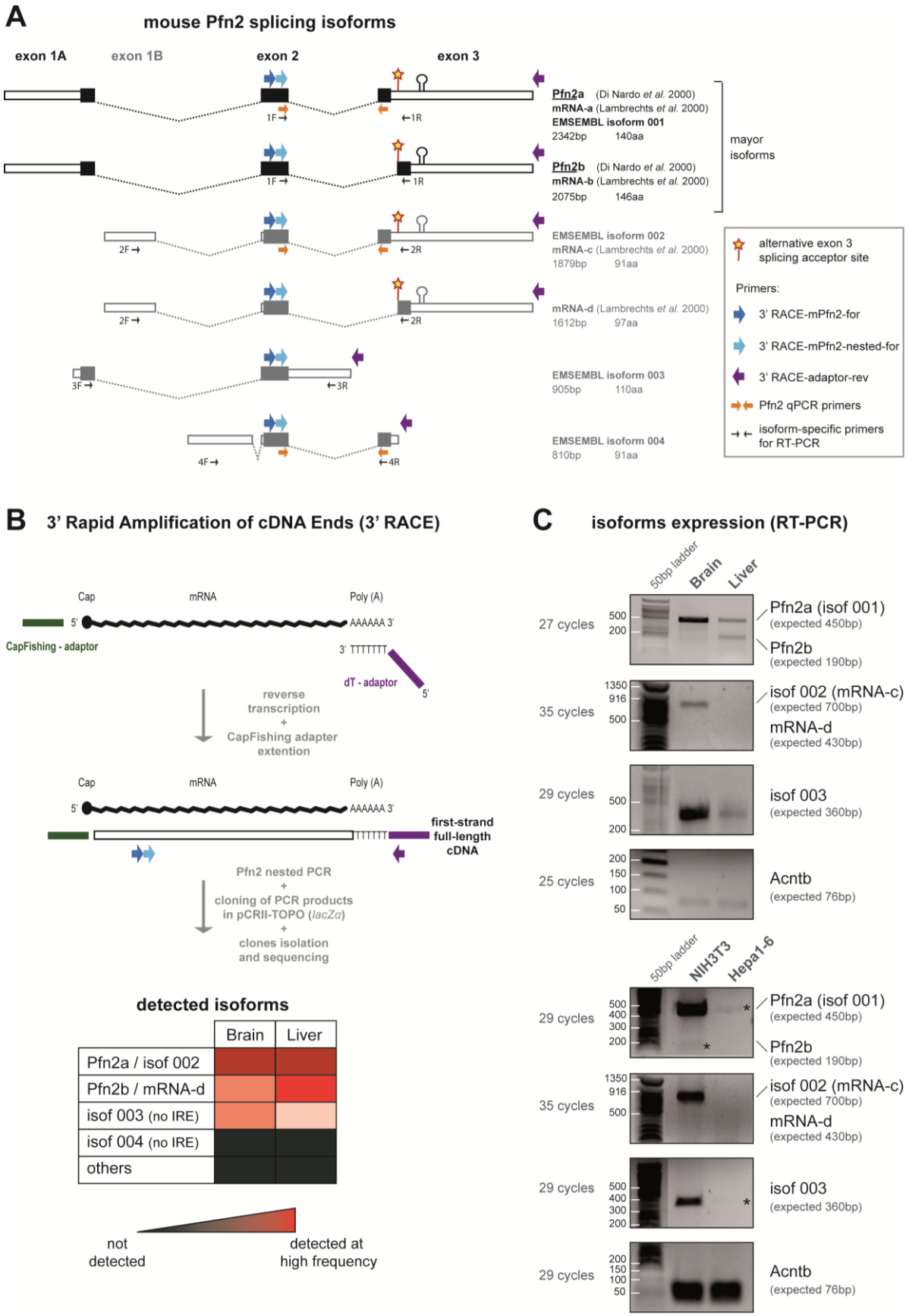

Figure 3.31 Mouse Pfn2 alternative isoforms detected by 3' RACE and RT-PCR. (A) Representation of mouse Pfn2 alternative splicing isoforms described in EMSEMBL database: isoform 001 (Pfn2a/mRNA-a), isoform 002 (mRNA-c), isoform 003 and isoform 004 plus the isoforms Pfn2b (mRNA-b) and mRNA-d reported by Di Nardo *et al.* 2000 and Lambrechts *et al.* 2000. The mayor expressed isoforms and coding for functional PFN2 protein, Pfn2a and Pfn2b, are shown in black, while the other isoforms, coding for truncated and likely non-functional proteins are

shown in gray. Boxes indicate exon sequences (clear boxes indicate the UTRs and filled boxes indicate the coding regions) and dashed lines connect splicing sites. The length of the cDNA sequences and of the corresponding encoded proteins are indicated for each isoform. Arrows show the annealing regions for primers used in 3' RACE, RT-PCR and qPCR experiments and primers are detailed in the figure legend. **(B)** Graphic representation of the 3' RACE experimental steps performed using the CapFishing kit (Seegene). Total RNA from brain or liver mouse samples was firstly reverse transcribed using an oligo-dT-adaptor primer introducing at the 3' end of the obtained cDNA an exogenous unique sequence. The CapFishing adaptor was then added to select for Cap-containing mRNAs and PCR-extend them. The so obtained first-strand full-length cDNA was then used as template for a 2-step nested PCR specific for Pfn2 transcripts using forward primers annealing on Pfn2 exon 2 (blue arrows) and a reverse primer annealing on the dT-adaptor (purple arrow). PCR products were cloned in pCRII-TOPO vector (Invitrogen) and about 50 different clones were sequenced. Sequencing results are summarized in the bottom table showing the Pfn2 isoforms that were detected and an approximated frequency of detection indicated by the color-scale. **(C)** To better quantify the relative abundance of Pfn2 isoforms, isoform-specific PCR primers were designed for RT-PCR experiments: Pfn2a and Pfn2b specific primers, allowing to distinguish Pfn2a (isof 001/mRNA-a) (expected amplification 450bp) from Pfn2b (mRNA-b) isoform (expected amplification 190bp); isof 002 and mRNA-d specific primers, allowing to distinguish isof 002 (mRNA-c) (expected amplification 700bp) from mRNA-d isoform (expected amplification 430bp) as well as specific primers for isof 003 (expected amplification 360bp) or isof 004 (expected amplification 520bp). RT-PCRs were performed on cDNA from brain or liver mouse tissues and from NIH3T3 or Hepa1-6 cells with 25, 27, 29 or 35 PCR cycles of amplification according the case. The identity of the PCR products was confirmed by direct sequencing. β-actin mRNA was also amplified (expected amplification 76bp) for calibration and RNA quality control. One representative image is shown. Asterisks indicate faint bands detected. Cap: mRNA capping modification at 5' end; bp: base pairs; aa: amino acids; F: forward primer; R: reverse primer.

Four different transcripts are described for mouse Pfn2 mRNA in EMSEMBL database (Release 71, April 2013): isoforms 001, 002, 003 and 004 (Figure 3.31A). The longest isoform 001, also referred as Pfn2a or mRNA-a, is the one coding for the functional PFN2a protein of 140 amino acids (Uniprot identifier: Q9JJV2-1) (Figure 3.31A in black). For the other isoforms 002 and 004, containing an open reading frame starting at exon 2, or for the incomplete isoform 003 there is no evidence that those transcripts result in functional proteins (Figure 3.31A in grey).

In addition, in 2000, two different publications by Di Nardo *et al.* and Lambrechts *et al.* reported at the same time the existence of a second functional protein-coding transcript referred as Pfn2b (Di Nardo *et al.* 2000) or mRNA-b (Lambrechts *et al.* 2000). Pfn2b isoform has a different exon 2-exon 3 splicing, utilizing an alternative exon 3 acceptor site located 267 nucleotides downstream the one of Pfn2a isoform (Figure 3.31A in black). The resulting PFN2b protein of 146 amino acids (Uniprot identifier: Q9JJV2-2) is identical to PFN2a up to residue 108 but has a different C-terminus in which the last 32 amino acid residues (VLVFVMGKEGVHGGGLNKKAYSMAKYLRDSGF_PFN2a) are replaced for 38 different ones (ALVIVMGKEGVHAGTINKKTYELALYLKRSVTNLYLAS_PFN2b), conferring to PFN2b distinct binding properties and subcellular localization (Di Nardo *et al.* 2000).

Moreover, Lambrechts and colleagues also described the existence of an alternative exon 1B (Lambrechts *et al.* 2000). Exon 1B alternative splicing combined with the two possible splicing sites at exon 3 gives rise to the isoforms mRNA-c (corresponding to the isoform 002 of ENSEMBL database) and mRNA-d. As stated before, those transcripts have a shorter open reading frame, starting at exon 2, and likely they result in non-functional proteins.

The 3' IRE motif that we have identified in the Pfn2 mRNA is contained in the isoforms Pfn2a (isof 001/mRNA-a), Pfn2b (mRNA-b), isoform 002 (mRNA-c) and mRNA-d, but not in the isoforms 003 and 004.

To investigate the presence of additional non-IRE Pfn2 isoforms, we characterized the 3' end of mouse Pfn2 expressed transcripts in brain and liver tissues by 3' RACE experiments using the Seegene CapFishing cDNA isolation kit (Figure 3.31B). Total RNA was reverse transcribed to obtain a first strand cDNA, introducing at 5' and 3' ends adaptor sequences that could be targeted by PCR primers. Pfn2 transcripts were then selectively amplified by nested

PCR using two different primers annealing on exon 2, common to all Pfn2 isoforms, and a reverse primer annealing to the 3' adaptor sequence (Figure 3.31A-B). PCR products were cloned in pCRII-TOPO vector and clones characterized by Sanger sequencing.
Sequencing results showed that, for brain, the preferentially detected isoform is Pfn2a or isoform 002, as the portion amplified by the 3' RACE PCR is indistinguishable in the two transcripts. Isoform Pfn2b or mRNA-d (also indistinguishable) and the non-IRE isoform 003 were also detected at lower frequency, while no isoform 004 or any other alternative transcript were detected despite extensive clones sequencing (Figure 3.31B). Similar results were obtained for liver, showing the major presence of isoform Pfn2a, undistinguishable from isoform 002. Isoform Pfn2b, indistinguishable from mRNA-d, was also detected at relative higher frequency than in brain, and, at lower frequency, isoform 003 (Figure 3.31B).
To test the expression levels of the different Pfn2 transcripts, we performed semiquantitative RT-PCR in brain and liver mouse tissues or in NIH3T3 (embryonic fibroblasts) and Hepa1-6 (hepatoma) mouse cell lines (Figure 3.31C). We designed RT-PCRs allowing to distinguish between Pfn2a and Pfn2b isoform or between isoform 002 and mRNA-d, according to the length of the amplification product, as well as specific RT-PCRs selectively targeting the isoforms 003 or 004.
Initially, all PCRs were performed at 25 amplification cycles and, in those conditions, we could clearly detect only isoform Pfn2a in brain samples or in NIH3T3 cells (data not shown). At 25 PCR cycles, no amplification products were detectable for isoforms Pfn2b, 002, mRNA-d, 003 or 004 neither in mouse tissues or cell lines (data not shown), indicating that Pfn2a is the major expressed isoform.
In detail, additional RT-PCRs with increased number of PCR cycles confirmed the findings previously published by Di Nardo *et al.* 2000 and Lambrechts *et al.* 2000. The RT-PCR specifically targeting Pfn2a and Pfn2b transcripts showed that Pfn2 is highly expressed in brain samples and in NIH3T3 cells, where Pfn2a is the major transcript and Pfn2b is barely detectable at 27-29 PCR cycles (Figure 3.31C). In liver samples, Pfn2 expression is overall lower compared to the brain and Pfn2a and Pfn2b transcripts are almost equally represented. In Hepa1-6 cells on the other hand, we could only barely detect Pfn2a isoform indicating that Pfn2 is generally much lower expressed in Hepa1-6 compared to NIH3T3 cells (Figure 3.31C). Amplification of isoform 003 was detectable at 29 PCR cycles and for isoform 002 at 35 cycles and both isoforms were predominantly detected in brain and NIH3T3 cells, while in liver samples or in hepatoma Hepa1-6 cells we observed only a faint amplification for isoform 003 and no amplification for isoform 002 (Figure 3.31C).
No amplification was obtained for isoform 004 nor for mRNA-d in none of the tissues or cell lines analyzed that were tested under different primer annealing temperature or cycling PCR conditions (Figure 3.31C). This further reinforces the assumption, given by previous 3' RACE data, that isoform 004 is not or extremely low expressed. According to these results, the mRNA-d isoform described in the publication by Lambrechts *et al.* 2000 is also not expressed in the brain and liver tissue or in NIH3T3 and Hepa1-6 cells; indeed Lambrechts and collaborators also reported a tissue specific mRNA-d detection in kidney samples but not in brain samples (Lambrechts *et al.* 2000).
To sum up, our 3' RACE and RT-PCR results confirmed previously reported data by Di Nardo *et al.* 2000 and Lambrechts *et al.* 2000, showing that Pfn2a is the main Pfn2 isoform in the brain, while in other tissues the ratio between Pfn2a and Pfn2b mRNAs varies and, for example, in liver is about 1:1. We also detected in brain samples and NIH3T3 cells the expression of isoform 002 and of the non-IRE-containing isoform 003, though semiquantitative RT-PCR showed that those transcripts are very low represented compared to the Pfn2a mRNA. No isoform 004 or mRNA-d expression was observed.

In conclusion, we have detected very low levels of expression of isoform 003 (Pfn2 non-IRE isoform) in brain and liver sample and in NIH3T3 or Hepa1-6 cells and no expression of isoform 004 or any additional unpublished Pfn2 transcript. However, isoform 003 is not amplified with the primers that we use for qPCR detection of Pfn2 that are primers specifics for the A isoform of Pfn2 mRNA, the major expressed isoform that includes the IRE.

3.4.6 Effects of Pfn2 function on cellular iron homeostasis

3.4.6.1 Pfn2 overexpression in cell lines alters cellular iron levels

So far, we have examined IRP-mediated regulation on Pfn2 IRE, by measuring changes in Pfn2 mRNA and protein levels in response to modulation of iron status or IRP activity.

As all the well-recognized IRP-target mRNAs encode for proteins involved in the control of iron homeostasis, we investigated Pfn2 effects on intracellular iron levels and the formation of reactive oxygen species (ROS) by Pfn2 overexpression in HeLa and Hepa1-6 cells (Figure 3.32). The cytoplasmic labile iron pool (LIP) was measured using the calcein-AM method and the formation of ROS was assayed using the 2',7'-dichlorofluorescin diacetate method.

HeLa cells were transiently transfected with the pCMV6-Kan/Neo vector containing the mouse Pfn2 wild type cDNA and LIP levels were measured 48h after transfection. As controls for modulation of the LIP, we also transfected the mouse H-Ferritin cDNA (Fth1) or, alternatively, we treated the cells with the iron chelator desferrioxamine (DFO) or with ferric ammonium citrate (FAC) as a source of iron.

Transient overexpression of Pfn2 wild type cDNA in HeLa cells reduced the labile iron pool to ~57% of control cells transfected with the empty vector (Figure 3.32A). A similar reduction was observed for the transient transfection of the iron-storage protein Fth1 or the use of the iron chelator DFO, our positive experimental controls (Figure 3.32A).

Stable clones overexpressing the wild type mouse Pfn2 cDNA were obtained by G418 selection in HeLa and Hepa1-6 cells (Figure 3.32B). In stable Pfn2 overexpressing clones we also detected a reduction of the LIP to ~50% of control cells levels in Hepa1-6 cells and to ~75% of control cells levels for HeLa cells (Figure 3.32B).

Overexpression of Pfn2 in HeLa cells was previously shown to inhibit transferrin endocytosis (Gareus *et al.* 2006) and this effect as endocytosis inhibitor is dependent on dynamin1 binding (see Introduction 1.7.3). LIP reduction by Pfn2 overexpression in HeLa cells is compatible with a reduced iron-transferrin uptake due to dynamin1 sequestration (Figure 3.32D).

Iron is a pro-oxidant metal, thus, complementary to LIP determinations, we also measured the levels of reactive oxygen species (ROS), after transient overexpression of mouse Pfn2 in HeLa cells (Figure 3.32C). As control, HeLa cells were also transfected with the mouse H-ferritin (Fth1) cDNA or treated with the iron chelator DFO. ROS levels were measured 48h after transfection following a pre-treatment with H_2O_2 to induce ROS generation.

In control cells, transfected with an empty vector, H_2O_2 treatment alone increased more than 2-fold ROS levels (Figure 3.32C). The overexpression of mouse Pfn2 reduced ROS generation in cells exposed to H_2O_2 (~120%) to a similar extent as transient transfection of Fth1 or the use of the iron chelator DFO (Figure 3.32C). The observed reductions in ROS generation are in agreement with the reduced free iron levels detected by LIP determinations after Pfn2 or Fth1 overexpression or after iron chelation by DFO treatment.

Thus, the overexpression of Pfn2 reduced the labile iron pool (LIP) and, concordantly, the reactive oxygen species (ROS) levels. Pfn2 excess by overexpression may result in dynamin1 sequestration with consequent inhibition of endocytosis including iron-loaded transferrin uptake by Tfrc-mediated endocytosis (Figure 3.32D).

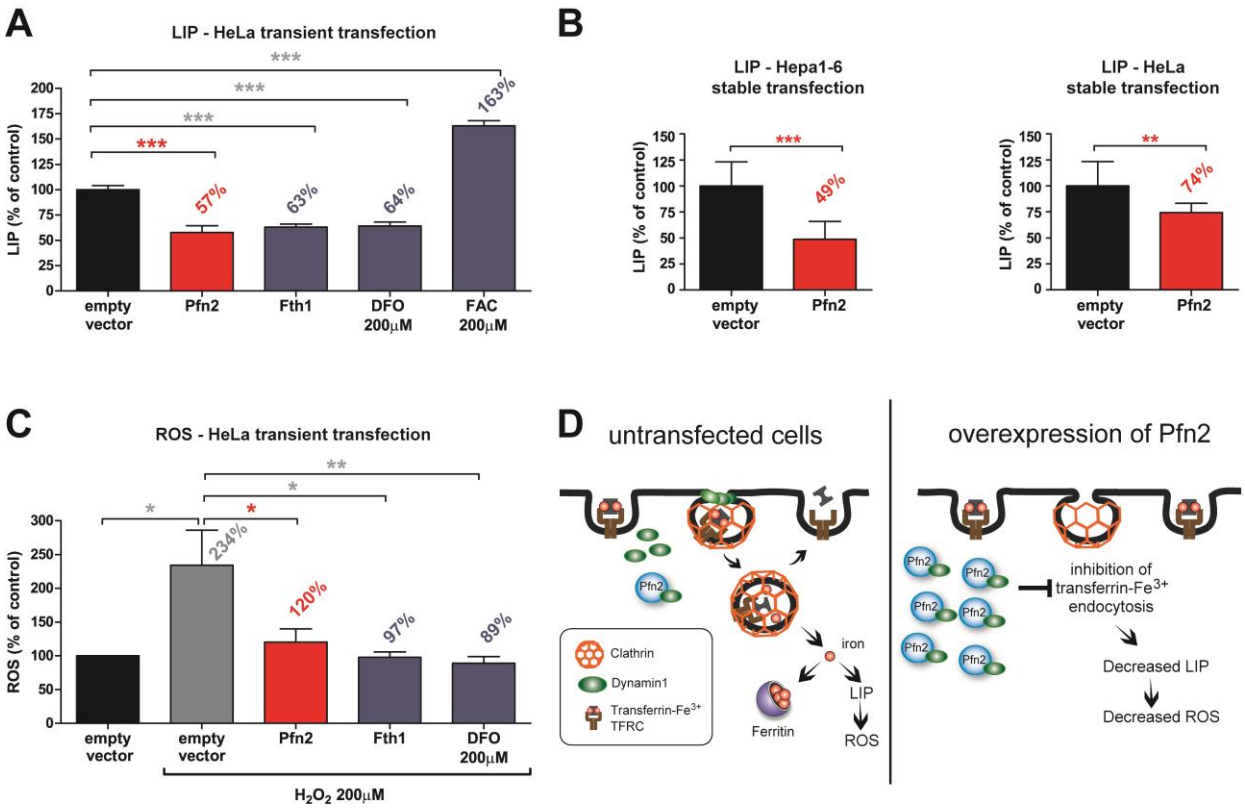

Figure 3.32 Labile iron pool and reactive oxygen species levels in cell lines overexpressing Pfn2. (A) HeLa cells were transiently transfected with pCMV6-Kan/Neo empty vector (OriGene) or pCMV6-Pfn2 vector. As control, cells were also transfected with pCMV6-Fth1 vector or cells transfected with the empty vector were additionally iron-deprived by 200µM DFO treatment or iron-loaded by 200µM FAC treatment for 16h. Cytoplasmic labile iron pool (LIP) was measured by the calcein-AM method 48h after transfection. Data were normalized to cells transfected with the empty vector, set as 100%. Means ± SD are shown. **(B)** Stable Hepa1-6 and HeLa clones overexpressing the wild type mouse Pfn2 were obtained by 750µg/ml G418 selection for 3 weeks. Single clones were isolated and LIP was measured and normalized to cells stably transfected with the pCMV6 empty vector, set as 100%. Means ± SD are shown. **(C)** Reactive oxygen species (ROS) levels were measured using the 2',7'-dichlorofluorescin diacetate method in HeLa cells transiently transfected with pCMV6-Kan/Neo empty vector, pCMV6-Pfn2 or pCMV6-Fth1 vectors or in cells transfected with the empty vectors and treated with 200µM DFO for 16h. ROS levels were assayed 48h after transfection following a pre-treatment with 200µM H_2O_2 to induce ROS generation. ROS quantifications were normalized to cells transfected with the empty vector and not treated with H_2O_2, set as 100%. Means ± SD are shown. **(D)** Predicted schematic model of Pfn2 effect on iron-transferrin uptake. In untransfected cells (left), endogenous Pfn2 binds to dynamin1 but the residual free pool of dynamin1 is allowed to interact with the cellular endocytosis machinery and iron-transferrin/TFRC endocytosis can normally take place. In Pfn2 overexpressing cells (right), Pfn2 excess sequester the dynamin1 protein pool and consequently impedes the binding of dynamin1 to the downstream endocytosis effector-proteins, blocking endocytosis and reducing iron-transferrin uptake via TFRC, cellular LIP and ROS levels.

3.4.6.2 Pfn2 overexpression or silencing in hFPN-GFP overexpressing cells

The maintenance of cellular iron balance is also dependent on cell surface expression of the iron exporter ferroportin (FPN). In addition, hepcidin-mediated internalization of ferroportin seems to also occur through clathrin/dynamin-dependent endocytosis and hepcidin-ferroportin complex internalization was inhibited by the transfection of a dominant-negative dynamin mutant, lacking of GTPase activity (Fernandes *et al.* 2009). Since Pfn2 acts as a negative regulator of endocytosis via sequestration of dynamin1, we addressed if Pfn2 overexpression or silencing in cell lines affects FPN membrane trafficking (Figure 3.33 and 3.34).

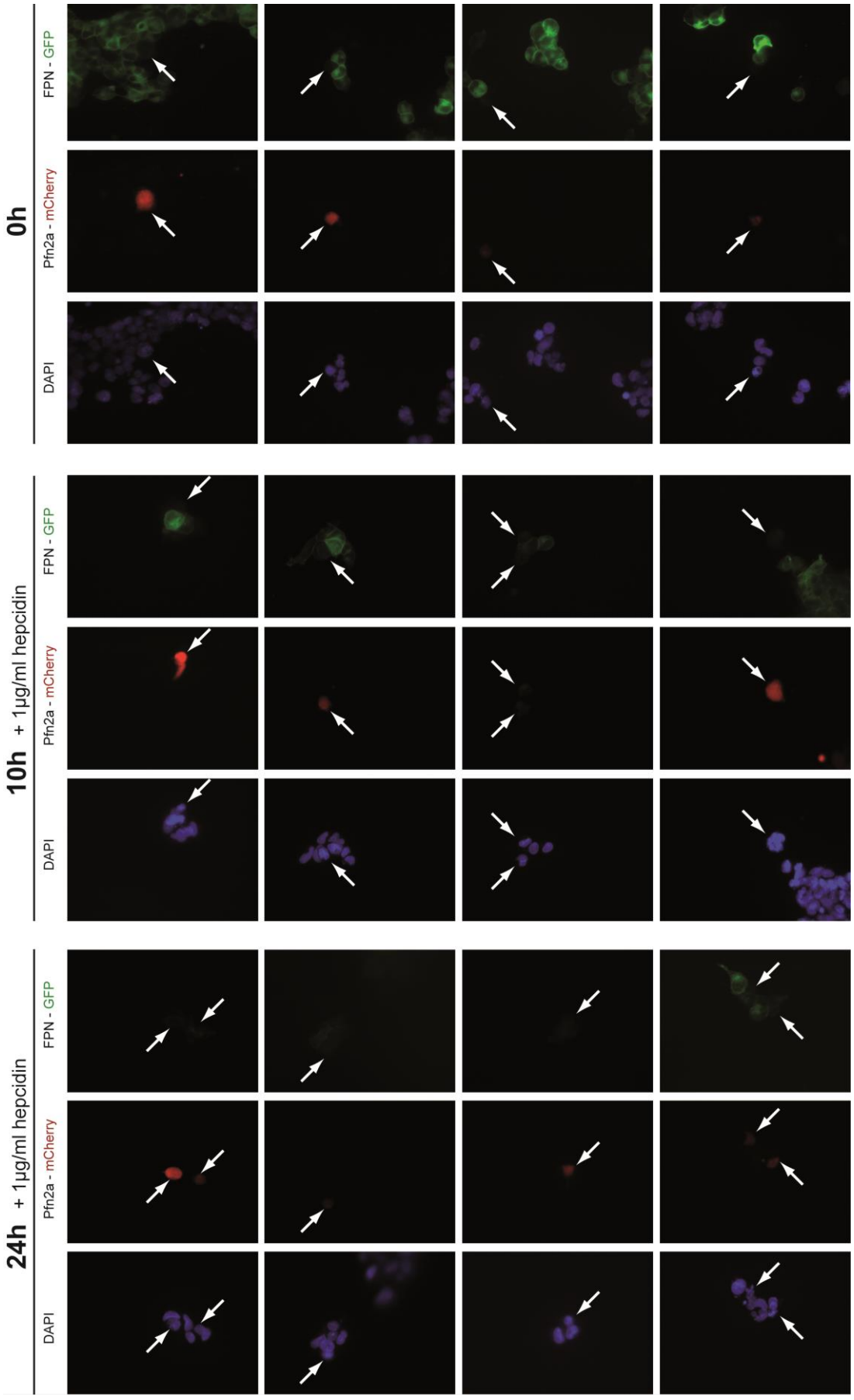

Figure 3.33 Overexpression of mouse Pfn2-mCherry in hFPN-GFP Hek293 cells. hFPN-GFP Hek293 cells were transiently transfected with a mouse Pfn2-mCherry fusion protein plasmid (pmCherry-N1, Clontech). 24h after

transfection, cells were treated for 16h with 20ng/ml of Doxycycline to induce hFPN-GFP expression. After that, the cells were exposed to 1µg/ml of recombinant hepcidin to trigger FPN internalization and degradation. Cells were analyzed by fluorescent microscopy at steady state (0h, cells not exposed to hepcidin treatment) or after 10h o 24h of hepcidin treatment. Epifluorescence images were acquired using a Leica DMI6000B microscope equipped with Leica Application Suite V3 analysis software. FPN-GFP protein is visualized in the green channel, Pfn2-mCherry protein in the red channel and cells nuclei by DNA-DAPI staining in the blue channel. Arrows point the same cells in each of the three different channels.

We took advantage of an already published FPN-GFP reporter system: the T-REx hFPN-GFP Hek293 cells (kind gift of Prof. Elizabeta Nemeth, University of California) (Qiao *et al.* 2012). This cell clone stably expresses a tetracycline-inducible human Ferroportin fused at the C-terminus with the green fluorescent protein (GFP). By fluorescent microscopy observation, the hFPN-GFP fusion protein localizes at the plasma membrane and, after exposition to hepcidin, undergoes internalization and degradation as does the endogenous FPN protein, allowing us to follow and evaluate FPN membrane trafficking (Supp. Figure 6.1A).

We overexpressed by transient transfection the mouse Pfn2 cDNA fused at the C-terminus with the red-fluorescent mCherry protein in Hek293 hFPN-GFP cell line. 24h after transfection, hFPN-GFP expression was induced by 20ng/ml Doxycycline addition to the cell medium for 16h. After FPN-GFP induction, the cells were treated with 1µg/ml of recombinant hepcidin peptide to trigger FPN internalization and degradation and analyzed by epifluorescent microscopy at the 0h time point (no hepcidin) or 10h and 24h after hepcidin addition. hFPN-GFP protein is visible in the green channel, while cells that also overexpress Pfn2-mCherry by transient transfection are visible in the red channel (Figure 3.33).

We observed that cells positively expressing mouse Pfn2 (red fluorescence) show absence of FPN expression (green fluorescence), even before to the exposure to hepcidin (Figure 3.33). This indicates that the overexpression of Pfn2 in Hek293 cells T-REx hFPN-GFP interferes with the expression of FPN by a yet not-known mechanism.

However, we cannot completely exclude the occurrence of a promoter competition phenomenon between the pmCherry-N1 plasmid used for transient expression of Pfn2 and the integrated vector controlling FPN-GFP expression.

We performed complementary experiments by silencing endogenous human PFN2 in Hek293 hFPN-GFP cells using the siRNA technology (Figure 3.34).

Hek293 cells were subjected to two consequent siRNA transfections using 20pmol of a PFN2-specific siRNA or, as control, with a scrambled-sequence siRNA. The efficiency of PFN2 silencing was evaluated by Western blotting 48h after the second transfection, showing a ~75% reduction of PFN2 endogenous levels (Supp. Figure 6.1C). After induction of hFPN-GFP expression by Doxycycline treatment, cells were treated with 1µg/ml recombinant hepcidin and ferroportin endocytosis and degradation was analyses at 5-10 and 24h after exposure to hepcidin (Figure 3.34).

These experiments showed that the silencing of human PFN2 in Hek293 hFPN-GFP cells has no apparent effect on ferroportin expression or trafficking to the membrane, as scrambled or PFN2 siRNA transfected cells exhibit similar cytoplasmatic and membrane staining pattern in steady state conditions before the addition of hepcidin (Figure 3.34, 0h). FPN-GFP internalization and degradation after hepcidin binding also proceeds without appreciable differences in scrambled siRNA cells versus PFN2 silenced cells (Figure 3.34, 5-10-24h).

In conclusion, overexpression of Pfn2 in Hek293 T-REx hFPN-GFP cells seems to block FPN expression and the reduction of PFN2 by siRNA in these cells does not show any gross effect on FPN expression and localization, although PFN2 ablation is not complete.

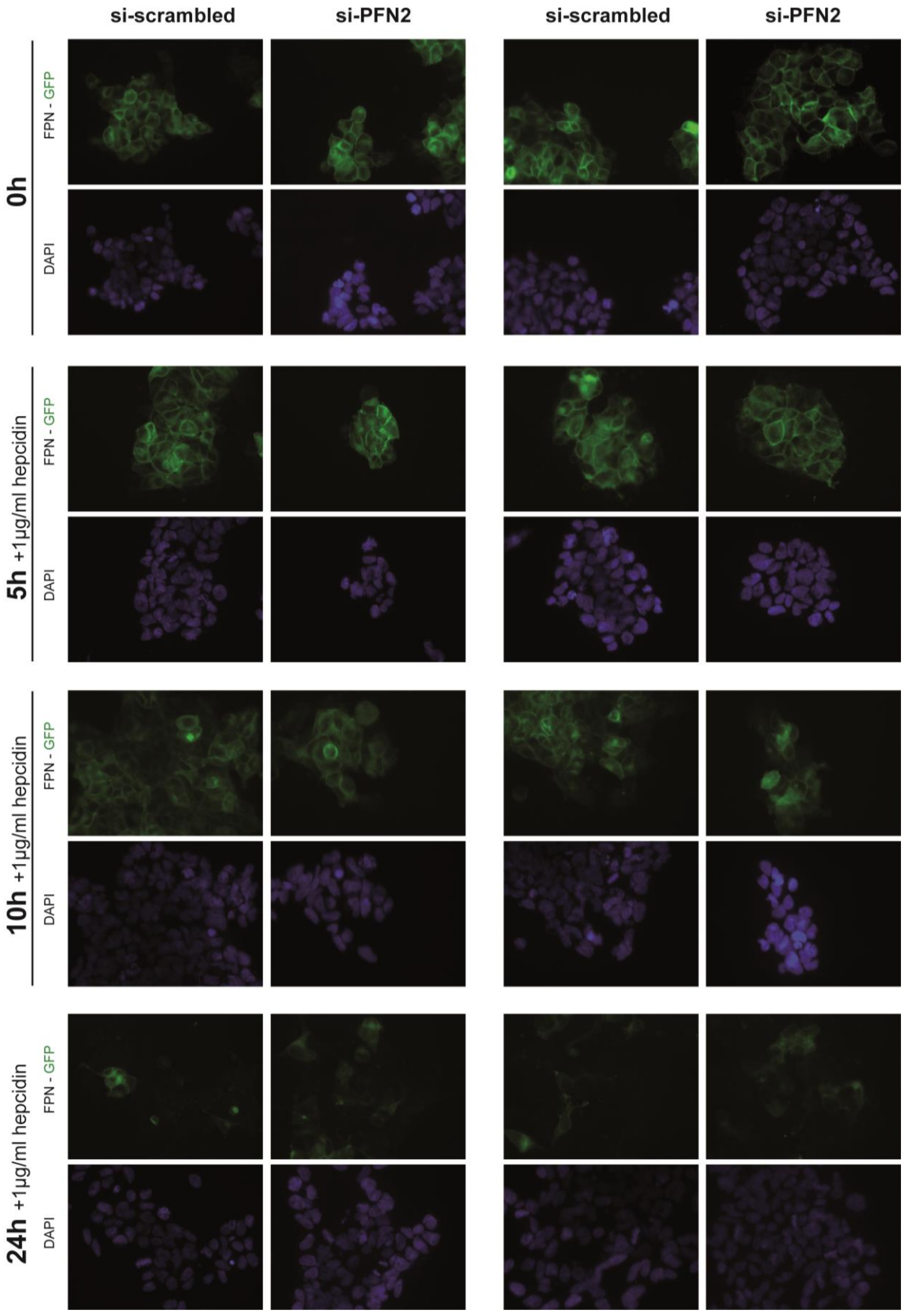

Figure 3.34 PFN2 silencing in Hek293 hFPN-GFP cells. Hek293 cells were subjected to two consequent siRNA transfections (day 1 and day 3) using 20pmol of a PFN2-specific siRNA (Silencer® Select, Ambion) or, as control, with a scrambled-sequence siRNA. hFPN-GFP expression was induced by 20ng/ml Doxycycline treatment for 16h in order that the end of the Doxycycline treatment coincided with the 48h after the second siRNA transfection. Cells

were then treated with 1µg/ml hepcidin and ferroportin internalization and degradation was followed at 5-10 and 24h after hepcidin treatment by epifluorescent microscopy. Images were acquired using a Leica DMI6000B microscope equipped with Leica Application Suite V3 analysis software. FPN-GFP protein is visualized in the green channel and cells nuclei by DNA-DAPI staining in the blue channel.

3.4.7 Effects of Pfn2 deficiency on systemic iron homeostasis

A mouse model knockout for the Profilin2 gene has been generated by the group of Prof. Walter Witke (Institute of Genetics, University of Bonn). *Pfn2*-/- mice were reported to show a complex neurological phenotype characterized by increased exploratory and novelty-seeking behavior with increased locomotion, phenotype that was postulated to arise from a neuronal hyper-excitability due to increased synaptic vesicles exocytosis (Pilo Boyl *et al.* 2007). However, no studies have been done addressing Pfn2 potential implication in iron metabolism. In view of our findings that pointed out Pfn2 mRNA as a novel IRP-target mRNA, it was of particular interest to explore systemic iron homeostasis in the Pfn2 knockout mice. We therefore started a collaboration with the group of Prof. Walter Witke and I spent four months in his laboratory working with *Pfn2* knockout mice to evaluate the consequences of Pfn2 deficiency on systemic iron metabolism.

3.4.7.1 *Pfn2* KO mice present normal hematological parameters

In the body, the iron is mainly utilized by red blood cells for the synthesis of hemoglobin. To evaluate if Pfn2 deficiency affects erythropoiesis, we collected blood and bone marrow samples from 7-9 months old Pfn2 knockout (KO) and wild type (WT) males and analyzed blood cells profiles as well as serum iron parameters.
Analysis of hematological parameters on peripheral blood did not show significant difference in red blood cells count, volume indexes or hemoglobin content between Pfn2 KO mice and their wild type littermates (Table 3.4).

Table 3.4 Hematologic and plasma iron parameters of *Pfn2* knockout versus wild type mice.

	***Pfn2* WT (n)**	***Pfn2* KO (n)**
WBC (x10^3/µl)	9.2 ± 0.9 (6)	10.5 ± 1.7 (6)
RBC (x10^6/µl)	9.5 ± 0.2 (6)	9.3 ± 0.4 (6)
Hb (g/dL)	13.9 ± 0.4 (6)	13.8 ± 0.7 (6)
Ht (%)	46.1 ± 1.3 (6)	45.4 ± 2.3 (6)
MCV (fL)	48.1 ± 0.5 (6)	48.9 ± 0.4 (6)
MCH (pg)	14.5 ± 0.1 (6)	14.8 ± 0.1 (6)
MCHC (g/dL)	30.3 ± 0.2 (6)	30.2 ± 0.2 (6)
PLT (x10^3/µl)	842.2 ± 50.5 (6)	908.4 ± 117.5 (6)
Plasma iron (µmol/L)	16.02 ± 1.46 (8)	18.34 ± 1.92 (8)
Transferrin saturation (%)	38.78 ± 5.08 (8)	40.51 ± 3.30 (8)
Transferrin (g/L)	2.40 ± 0.22 (8)	2.46 ± 0.25 (9)
Ferritin (ng/L)	277.80 ± 24.74 (8)	264.80 ± 23.32 (9)

Results are given as means ± SEM. The sample size (n) is indicated. The following abbreviations were used: WBC, white blood cell; RBC, red blood cell; Hb, hemoglobin; Ht, hematocrit; MCV, mean corpuscular volume; MCH, mean corpuscular hemoglobin; MCHC, mean corpuscular hemoglobin concentration; PLT, platelet.

No significant differences were observed also from the determination of plasma iron indexes as plasma iron concentrations, ferritin and transferrin levels or the transferrin saturation index (Table 3.4).
Moreover, peripheral blood or bone marrow smears were analyzed after May Grünwald-Giemsa staining for the identification of different cellular sub-populations with no remarkable differences among WT and KO mice (data not shown).
Iron content in the bone marrow was either evaluated by Perls Prussian Blue staining on bone marrow smears, or more accurately measured by atomic emission spectrometry (Figure 3.35 and 3.36B) and was similar in wild type and Pfn2 deficient mice.
Thus, we concluded that, in steady state conditions, *Pfn2* KO mice do not present hematological abnormalities.

3.4.7.2 Abnormal iron distribution in Pfn2 deficient mice

We performed enhanced Perls Prussian Blue histological staining for iron on 5 and 9-11 months old Pfn2 KO or WT male animals (Figure 3.35). We analyzed tissues relevant for iron metabolism such as duodenum, the site of iron absorption; liver, a site of iron storage; spleen, a major site of iron recycling; bone marrow, the primary site of erythropoiesis; as well as brain and kidney, due to the physiologic high expression of Pfn2 in those tissues (Supp. Figure 6.2).

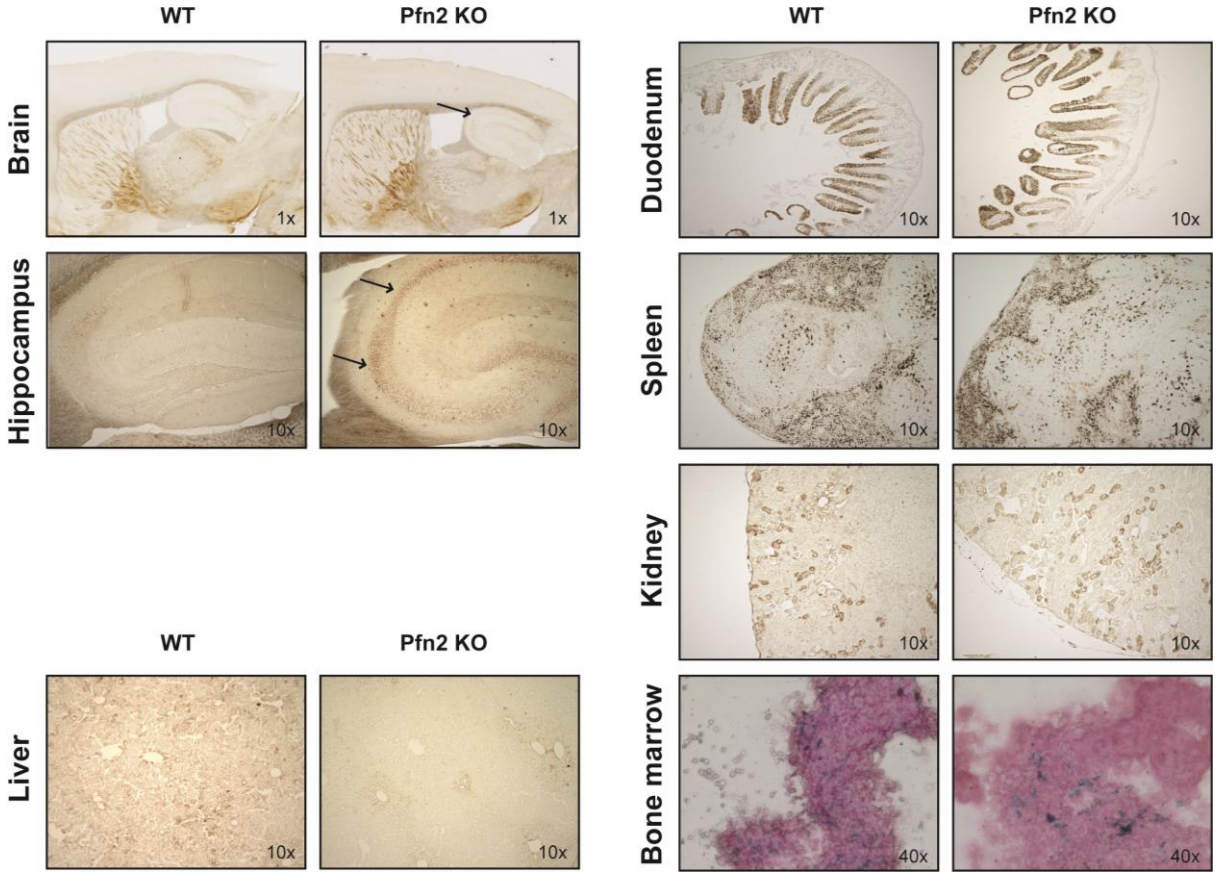

Figure 3.35 Iron staining in Pfn2 KO and wild type mice tissues. Tissue iron distribution in Pfn2 KO or WT mice was analyzed by Perls Prussian Blue staining for ferric iron. 9-11 months old mice were anesthetized and perfused with fixative and potassium ferrocyanide staining solution. After processing of the organs, slices were additionally treated with potassium ferrocyanide and the staining enhanced by DAB treatment (brown staining). Alternatively, bone marrow samples were obtained from femur bones flushing of not perfused mice. Bone marrow smears were methanol-fixed and treated with potassium ferrocyanide for iron staining (blue staining) and cell cytoplasm was counterstained with eosin (pink staining). Images were acquired in bright-field using a BZ-9000 Microscope (Keyence) at different magnifications. WT: wild type; KO: knockout; DAB: 3,3'-Diaminobenzidine.

While no consistent differences in iron distribution were observed in duodenum, spleen, bone marrow or kidney (Figure 3.35, right panels), we detected a noticeable pattern of iron accumulation in particular brain areas, such as the CA1 and CA2 (Cornu Ammonis) areas of the hippocampus (Figure 3.35A, left upper panels, pointed by arrows). This phenotype was more pronounced in 9-11 months old mice compared to 5 months old mice (data not shown). Surprisingly, livers of Pfn2 knockout mice were devoid of their iron storage capacity, as can be seen by the almost lack of iron staining in the liver of mutant mice compared to wild type mice (Figure 3.35A, left bottom panels).

We have to underline that the Perls Blue staining is not a quantitative technique and it is difficult to evaluate moderate differences in iron content, especially in tissues with heterogeneous iron distribution, as brain, spleen or bone marrow.

To further investigate tissue iron content in Pfn2 KO mice, we have therefore performed quantitative iron measurements on different tissues from 7-9 months old Pfn2 KO and WT mice (Figure 3.36A-C).

Non-heme iron content was determined using the bathophenanthroline spectrophotometric method for liver, spleen, duodenum, kidney, lung, heart and skeletal muscle (Figure 3.36C-D). Due to the physiological heterogeneous distribution of iron in the brain, we proceeded studying iron content by dissecting different brain parts (olfactory bulb, striatum, hippocampus, cortex, cerebellum and midbrain) and total iron content was alternatively quantified by atomic emission spectrometry (Figure 3.36A). Bone marrow samples, obtained from the flushing of femur bones were also quantified by atomic emission spectrometry (Figure 3.36B). Measurements by atomic emission methodology was preferred to bathophenanthroline method due to the small size of certain brain sections (olfactory bulb, striatum) or bone marrow samples that might negatively affect the quantification accuracy by the bathophenanthroline method.

Perls Prussian Blue staining showed that iron content was increased in discrete areas of the brain in Pfn2 KO mice compared to WT littermates (Figure 3.35). Confirming previous histological observations, total iron content was increased in the hippocampus (120%) as well as in the olfactory bulb (170%) and midbrain (130%), areas where Pfn2 levels are physiologically highest (unpublished results from Dr. Walter Witke group), whereas iron levels were unchanged in other brain regions (striatum, cortex and cerebellum).

On the other hand, non-heme iron quantifications confirmed the decrease in liver iron content detected by Perls Prussian Blue staining in Pfn2 KO mice, showing a ~30% reduction (Figure 3.36C). These results were further confirmed in younger mice of 2-3 weeks of age, indicating that the hepatic iron shortage is present in Pfn2 KO mice since early age (Figure 3.36D.

In other organs (duodenum, kidney, lung, heart and skeletal muscle) no significant differences of non-heme iron content were observed between wild type and Pfn2 KO mice (Figure 3.36C).

Raw quantification results showed a broad dispersion of iron measurements in spleen samples, which is likely attributable to the physiological very high iron content of the splenic tissue (about 10 times greater compared to other tissues); however, we could not detect statistically significant differences between Pfn2 KO and WT mice (Figure 3.36C).

Finally, the mean of bone marrow total iron content measured by atomic emission spectrometry was higher in Pfn2 KO mice but this difference is not statistically significant compared to WT mice due to the wide spread of the data (Figure 3.36B).

In conclusion Pfn2 deficient mice display signs of iron mismanagement with abnormal body iron distribution. In the brain, iron accumulates in the olfactory bulb, hippocampus and midbrain. Surprisingly, the livers of Pfn2 knockout mice present a reduction in non-heme iron levels and this hepatic iron deficiency was confirmed to occur also in younger mice, suggesting that the phenotype is intrinsic to Pfn2 absence.

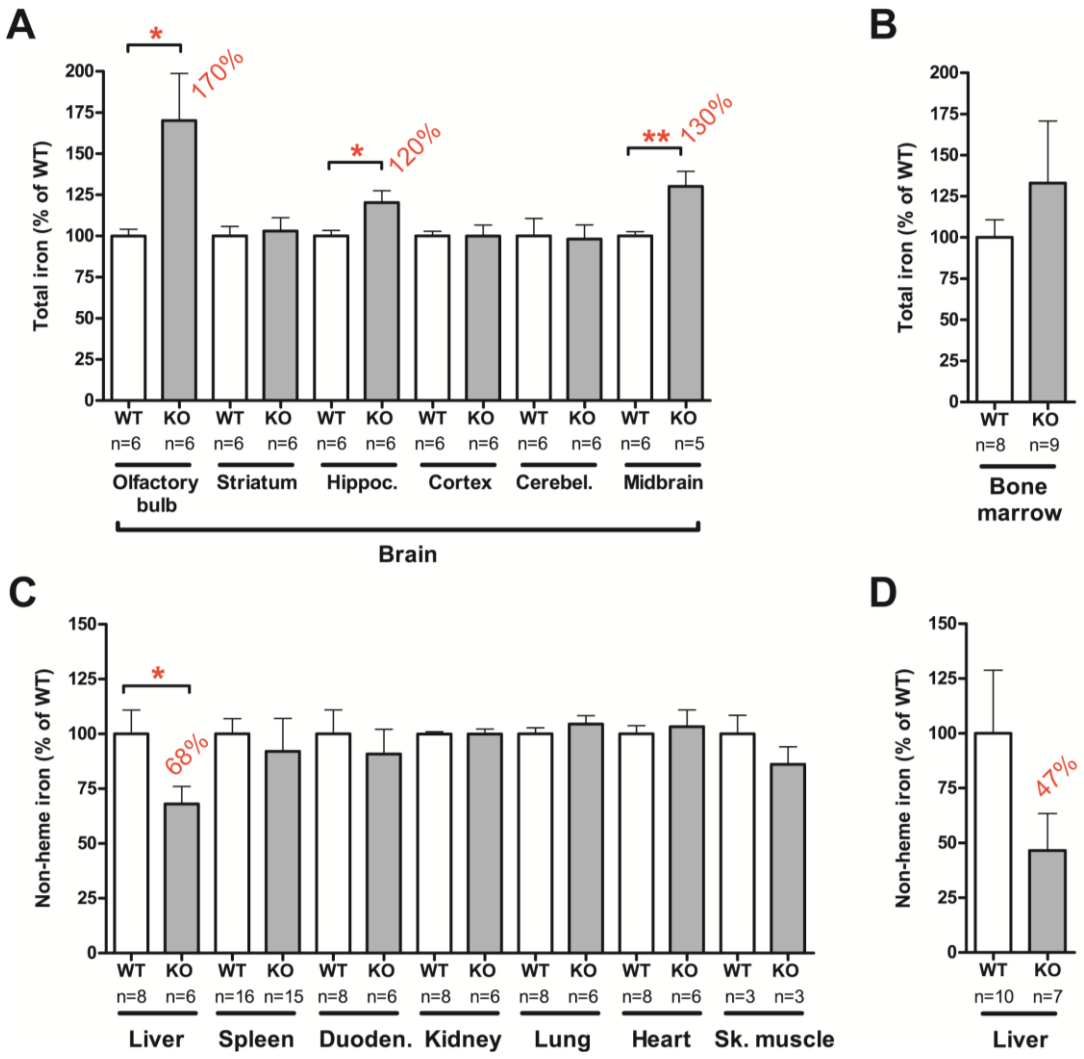

Figure 3.36 Determination of tissues iron content in Pfn2 KO and wild type mice. Atomic emission spectrometry determination of total iron content in brain sections **(A)** or bone marrow samples **(B)** from 7-9 months old male Pfn2 KO and WT mice. Data were normalized as µg iron/g of dry tissue, for brain and bone marrow samples. Alternatively, non-heme iron content was measured using the bathophenanthroline chromogen method in liver, spleen, duodenum, kidney, lung, heart and skeletal muscle from 7-9 months old **(C)** or 2-3 weeks old **(D)** Pfn2 KO and WT mice. Data were normalized as µg iron/g of dry tissue. In all cases, measures are given as means ± SEM compared to wild type mice, set as 100%. The sample size (n) is indicated.

3.4.7.3 Brain iron metabolism in Pfn2 knockout mice

To better understand the iron accumulation in the brain of Pfn2 deficient mice, we studied in the different brain sections the expression of mRNAs encoding for proteins involved in iron homeostasis: H- and L-ferritin (Fth1, Ftl), transferrin receptor 1 (Tfrc), divalent metal transporter 1 (Slc11a2) IRE and non-IRE isoforms, ferroportin (Slc40a11) and the iron regulatory proteins 1 and 2 (Aco1, Ireb2). Protein levels of H- and L-ferritin and transferrin receptor 1 were also monitored by Western blotting (Figure 3.37).

In the hippocampus we did not observe statistically significant changes in mRNA expression of iron-related genes, however, ferritin protein levels detected by Western blotting were surprisingly reduced in Pfn2 KO samples despite the iron accumulation detected in this area. H-ferritin was strongly reduced to a 49% of control levels and L-ferritin also showed a trend to decrease, although not reaching statistical significance (Figure 3.37A).

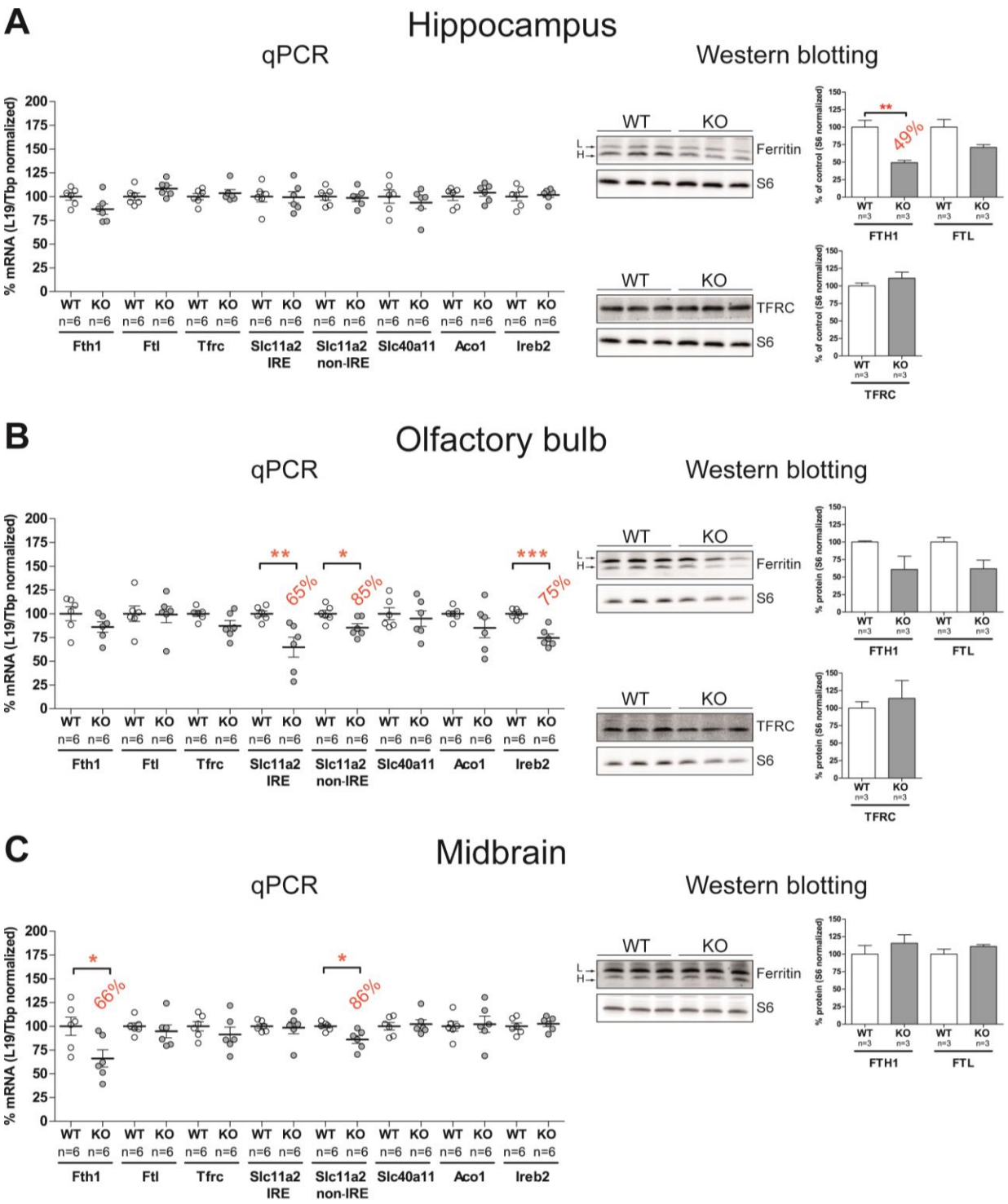

Figure 3.37 Brain expression of iron-related genes. The expression of iron-related genes was analyzed at mRNA level by qPCR (left panels) and protein level by Western blotting (right panels) in different brain areas from WT and Pfn2 KO 7-9 months old mice: hippocampus **(A)**, olfactory bulb **(B)** and midbrain **(C)**. For qPCR experiments, Fth1, Ftl, Tfrc, Slc11a2-IRE and non-IRE isoforms, Slc40a11, Aco1 and Ireb2 mRNAs expression was normalized against L19 ribosomal protein and TATA box binding protein (Tbp) expression and compared to wild type mice (set as 100%). Means ± SEM are shown. Sample size (n) is indicated. For Western blotting experiments, H- and L-ferritin and, in some cases transferrin receptor expression were monitored. S6 ribosomal protein levels were used for normalization. Bands intensity was analyzed using the AlphaEaseFC software (Alpha Innotech). Graphs represent quantified data, compared to the signal of WT mice samples (set as 100%). Means ± SEM are shown. The samples size (n) is indicated. The following abbreviations were used: Fth1: H-ferritin; Ftl: L-ferritin; Tfrc: transferrin receptor 1; Slc11a2 (Dmt1): divalent metal transporter 1; Slc40a11 (Fpn1): ferroportin; Aco1 (Irp1): iron regulatory protein 1; Ireb2 (Irp2): iron regulatory protein 2; WT: wild type mice; KO: Pfn2 knockout mice; L: L-ferritin subunit; H: H-ferritin subunit.

In the olfactory bulb of Pfn2 KO mice, which also presented an increased iron content, we detected a 25% reduced expression of Irp2/Ireb2 (Figure 3.37B). Moreover, the iron transporter Dmt1, encoded by *Slc11a2* gene was also downregulated: the IRE isoform was 35% downregulated, possibly as a consequence of the reduced IRP-activity, but also the non-IRE isoform showed a slight 15% reduction (Figure 3.37B). We interpret these results, as a compensatory feedback to the iron-excess in the olfactory bulb of Pfn2 KO mice, reducing Irp2 mRNA synthesis presumably associated with Irp2 protein degradation via the proteasomal pathway and Irp1 switch to its aconitase form to reduce IRP-activity with consequent destabilization of the 3' IRE in Dmt1 mRNA, and the downregulation of this iron uptake transporter. However, despite the iron accumulation detected, other classical IRP-target were not consequently modulated, Tfrc levels were unchanged and H- and L-ferritin showed an unexpected trend to reduction, similarly to what observed for the hippocampus, although not reaching statistical significance (Figure 3.37B).

In the midbrain, which also showed increase iron content in Pfn2 KO mice, we observed a ~35% reduction in Fth1 mRNA levels, however, this reduction that was not reflected at protein level and the expression levels of other iron-related genes were not altered (Figure 3.37C).

In other brain regions (striatum, cortex and cerebellum), where iron quantifications were comparable among WT and Pfn2 KO mice, no remarkable alteration of iron-related genes expression was observed (Supp. Figure 6.5).

Hence, in the hippocampus of Pfn2 deficient mice we have shown a strong ferritins downregulation despite the iron accumulation detected by iron quantification experiments and Perls staining, raising thus the question of where and in which form is this iron excess stored.

To further investigate the nature of iron deposits in the hippocampus we performed Transmission Electron Microscopy (TEM) studies in collaboration with Dr. Lucía Gutiérrez (ICMM-CSIC, Madrid). TEM analysis revealed the presence of electron-dense aggregates in hippocampus sections of Pfn2 deficient mice, structures that were not detected in WT mice (Figure 3.38A, only Pfn2 knockout samples are shown). At higher magnifications, lamellae structures were appreciable within these aggregates, suggesting that the iron accumulates in the mitochondria (Figure 3.38A-B white arrows). However, not all the mitochondria presented with aggregates; within the same section we could detect mitochondria without aggregates, mitochondria with few electron-dense spots and mitochondria almost full of these electron-dense particles (data not shown).

The presence of iron inside these structures was assessed directly on tissues sections combing elemental analysis by Energy Dispersive X-ray Spectroscopy (EDS) and Scanning Transmission Electron Microscopy (STEM) imaging which allows to spatially map at high resolution the presence of iron. EDS scanning confirmed the presence of iron in hippocampus aggregates (Figure 3.38B).

To further analyze the morphology of the aggregates of the hippocampus we compared them to the well-characterized iron deposits of the spleen (Figure 3.38C). Spleen shows iron accumulation in the form of ferritin, as isolated particles randomly dispersed in the cytoplasm (Figure 3.38C, arrow 3) or dense hemosiderin-like deposits (Figure 3.38C, arrow 4).

The morphology of the hippocampal aggregates is clearly different from ferritin or hemosiderin deposits: in the hippocampus we could detect both isolated particles (Figure 3.38C arrow 1) as well as clustered aggregates (Figure 3.38C arrow 2). However, examination of these structures at higher magnification (Figure 3.38C right bottom corners) showed that the electron-dense cores in hippocampus mitochondria are smaller when compared to the isolated iron cores corresponding to ferritin of spleen samples observed at the same magnification, suggesting thus that iron in the hippocampus is accumulated a non-ferritin form. Iron hippocampus deposits appeared as heterogeneous, showing the coexistence of isolated

particles, consistent with iron storage in a protein form, where a protein shell prevents contact of the iron cores, together with smaller particles with no separation between iron cores, indicating the lack of a protein shell.

We therefore tested whether the mRNA expression of Frataxin (Ftx), a mitochondrial iron-binding protein, was altered in Pfn2 deficient mice, however, qPCR results showed no different Ftx mRNA levels between Pfn2 KO and WT mice (Figure 3.38D). We haven't tested for the expression mitochondrial ferritin, another mitochondrial iron storage protein.

In conclusion, the hippocampus of Pfn2 KO mice showed an increased iron content, associated with a surprising ferritin protein downregulation. Iron was detected in heterogeneous aggregates within mitochondrial structures and aggregates morphology is different from typical deposits of ferritin or hemosiderin, indicating that iron is accumulated in a different form within this tissue.

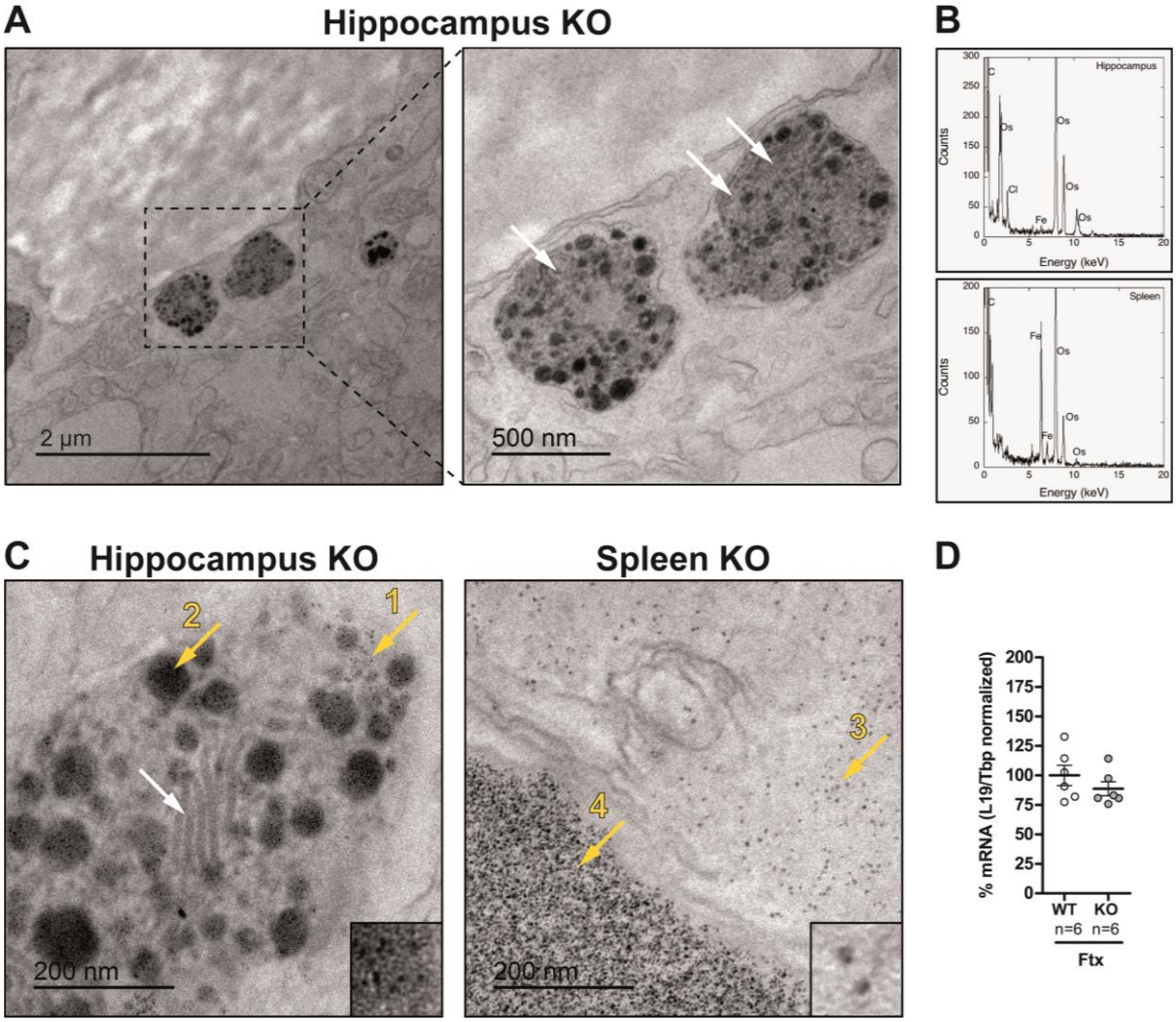

Figure 3.38 Characterization of iron deposits in the hippocampus. (A) Transmission electron micrograph of the hippocampus from 9 months old Pfn2 KO mice. Different magnifications are shown. For TEM experiments, unstained sections were used to avoid the problem of heavy metal clusters that can be mistaken for ferritin deposits. **(B)** TEM images of hippocampus and spleen at the same magnification for comparison of the aggregates morphology. Lamellae structures are highlighted by white arrows. Iron aggregates of different morphology are highlighted by yellow arrows: mitochondrial isolated particles (1), mitochondrial clustered aggregates (2), cytoplasm dispersed ferritin shells (3) and hemosiderin aggregates (4). **(C)** Iron accumulation in electron-dense areas has been tested by Energy Dispersive X-ray Spectroscopy to map the presence of iron in the hippocampus and in spleen, used as positive control. **(D)** qPCR analysis of frataxin (Ftx) mRNA expression in WT and Pfn2 KO mice. Results were normalized to L19 and Tbp expression and compared to WT animals (set as 100%). Means ± SEM are shown. The sample size (n) is indicated.

3.4.7.4 Hepatic iron metabolism in Pfn2 knockout mice

As shown previously in section 3.7.2, the livers of Pfn2 knockout mice are deprived of their iron storage content, contrasting with brain iron accumulation.

As demonstrated by the hepatic iron overload present in patients with atransferrinemia (Goldwurm *et al.* 2000) and by other evidences, liver iron uptake is mediated by other mechanisms independent of the transferrin/transferrin receptor iron uptake.

We have further analyzed the mRNA and protein expression levels of molecules involved in iron homeostasis in the livers of Pfn2 KO mice (Figure 3.39).

H- and L-ferritin protein levels checked by Western blotting were similarly decreased by ~40% in Pfn2 KO mice (Figure 3.39), mirroring the reduction of iron content in liver (Figure 3.36C-D). H-ferritin mRNA levels were unchanged in Pfn2 KO versus WT littermates (Figure 3.39), suggesting a post-transcriptional regulation of protein expression in iron deficient conditions by the IRPs. However, the reduction of L-ferritin chain was also observed at mRNA level (Figure 3.39, ~20% decrease), and therefore, both transcriptional and post-transcriptional regulation may determine the reduction in protein levels observed for the L-subunit. Transferrin receptor C mRNA and protein levels were not significantly modified (Figure 3.39).

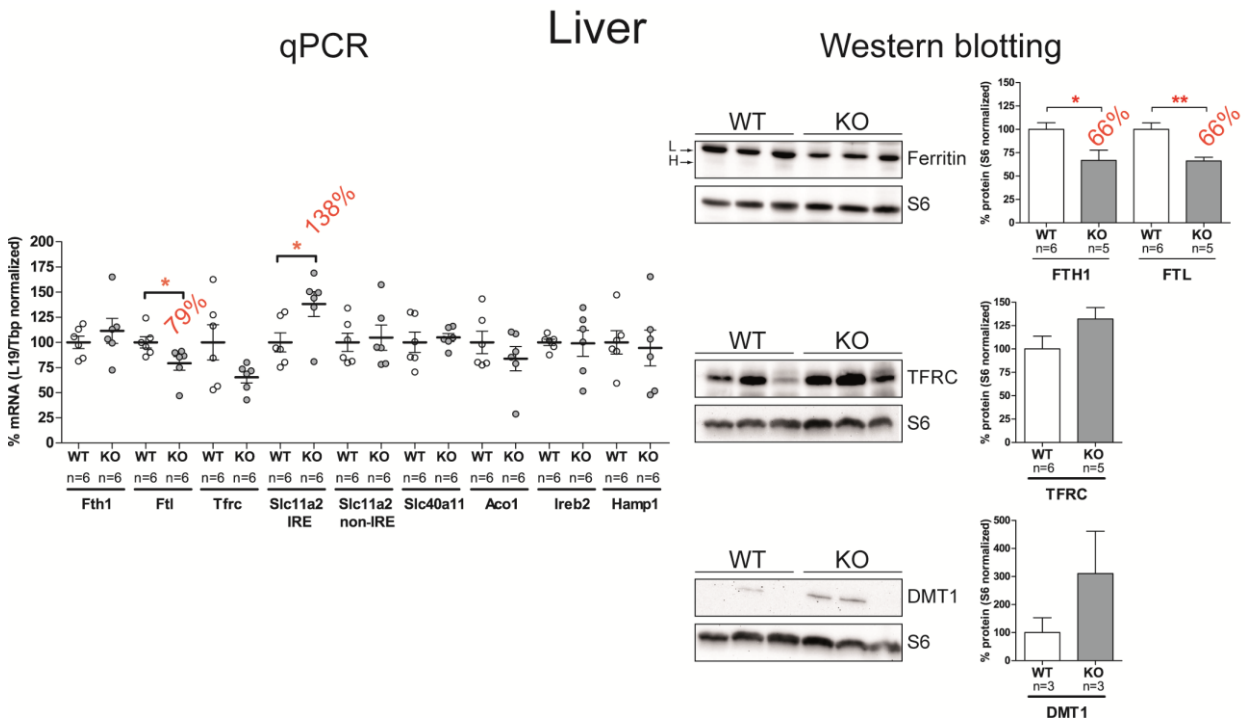

Figure 3.39 Liver expression of iron-related genes. The expression of iron-related genes was analyzed at mRNA level by qPCR (left panel) and protein level by Western blotting (right panels) in liver samples from WT and Pfn2 KO 7-9 months old mice. For qPCR experiments, Fth1, Ftl, Tfrc, Slc11a2-IRE and non-IRE isoforms, Slc40a11, Aco1, Ireb2 and Hamp1 mRNAs expression was normalized against L19 ribosomal protein and TATA box binding protein (Tbp) expression and compared to WT mice (set as 100%). Means ± SEM are shown. Sample size (n) is indicated. For Western blotting experiments, H- and L-ferritin, transferrin receptor C and DMT1 protein levels were monitored. S6 ribosomal protein levels were used for normalization. Band intensity was analyzed using the AlphaEaseFC software (Alpha Innotech). Graphs represent quantified data, compared to the signal of WT mice (set as 100%). Means ± SEM are shown. The samples size (n) is indicated. The following abbreviations were used: Fth1: H-ferritin; Ftl: L-ferritin; Tfrc: transferrin receptor 1; Slc11a2 (Dmt1): divalent metal transporter 1; Slc40a11 (Fpn1): ferroportin; Aco1 (Irp1): iron regulatory protein 1; Ireb2 (Irp2): iron regulatory protein 2; Hamp1: hepcidin antimicrobial peptide; WT: wild type mice; KO: Pfn2 knockout mice; L: L-ferritin subunit; H: H-ferritin subunit.

In the liver, iron uptake is also dependent on the expression of the iron transporter DMT1, encoded by the *Slc11a2* gene (see Introduction 1.3.1). qPCR results showed a specific upregulation of the Slc11a2 IRE-containing mRNA isoform in the liver of Pfn2 KO mice to ~140% of WT mice levels (Figure 3.39). The expression of the non-IRE Slc11a2 isoform was unchanged, suggesting that the specific IRE-isoform upregulation could be mediated by increased IRP binding activity under iron deficient conditions. Increased Slc11a2-IRE mRNA expression was reflected at protein level, although not reaching statistical significance (Figure 3.39).
The mRNA expression of other iron-related genes including, Slc40a1/Fpn, Aco1/Irp1 and Ireb2/Irp2 was not altered in Pfn2 knockout mice (Figure 3.39).
To evaluate a potential systemic response to the liver iron scarcity, we measured hepatic mRNA levels of the iron-regulator hormone hepcidin (Hamp1). We found hepatic Hamp1 levels to be inappropriately unchanged in Pfn2 KO mice (Figure 3.39) as liver iron deficiency should reduce hepcidin mRNA levels in order to increase iron uptake and restore iron deposits.
We measured by atomic emission spectrometry iron levels in the urine of Pfn2 KO mice and found no differences between KO and WT mice (Supp. Figure 6.4), what excluded that liver iron stores are lost as a consequence of an abnormal iron excretion by urine in Pfn2 KO mice.

To obtain more insight into the unexpected liver iron deficiency in Pfn2 KO mice we performed genome-wide expression array analysis using the Affymetrix GeneChip Mouse Gene 2.0 ST platform in 3 wild type and 3 Pfn2 KO mice (Table 3.5).
Overall, microarray data from the liver of Pfn2 KO mice revealed very few changes in the expression profile, with 20 genes upregulated by more than 2 folds and 28 genes downregulated by more than 2 folds compared with WT controls (Table 3.5), representing a 0.06% and a 0.08%, respectively, of the tested transcriptome.
Functional classification of the top regulated genes showed predominantly enzymes of the cytochrome P450 family, phase-II conjugating enzymes, peroxisome lipids transporters and lipid-modifying enzymes (Table 3.5).

Table 3.5 Top regulated genes in Affymetrix microarray of liver samples from Pfn2 KO and WT mice.

Affy ID	Gene Symbol	Description	GO function	Log FC	FC	P Value
Upregulated genes:						
17232215	Moxd1	monooxygenase, DBH-like 1	catecholamine metabolism / oxidoreductase activity	3.23	9.38	0.00339
17478195	Gm15700	predicted gene 15700	---	2.90	7.44	0.01528
17449372	Ugt2b38	UDP glucuronosyltransferase 2 family, polypeptide B38	metabolic process / glucuronosyltransferase activity	2.58	5.97	0.00067
17491205	Saa1	serum amyloid A 1	acute-phase response / cholesterol metabolic process	2.49	5.61	0.00946
17359918	Elovl3	elongation of very long chain fatty acids (FEN1/Elo2, SUR4/Elo3, yeast)-like 3	fatty acid elongation / transferase activity	1.40	2.65	0.00079
17408315	Hsd3b5	hydroxy-delta-5-steroid dehydrogenase, 3 beta- and steroid delta-isomerase 5	steroid biosynthetic process / oxidoreductase activity	1.36	2.56	0.00881
17414512	Mup-ps5	major urinary protein, pseudogene 5	---	1.32	2.50	0.00455
17288876	Arrdc3	arrestin domain containing 3	temperature homeostasis / beta-3 adrenergic receptor binding	1.29	2.44	0.03486
17403108	Adh6-ps1	alcohol dehydrogenase 6 (class V), pseudogene 1	---	1.26	2.39	0.00040
17478730	Gabrb3	gamma-aminobutyric acid (GABA) A receptor, subunit beta 3	GABAergic transmission / ion channel	1.24	2.37	0.00265
17449355	Ugt2b37	UDP glucuronosyltransferase 2 family, polypeptide B37	metabolic process / glucuronosyltransferase activity	1.18	2.27	0.00435
17404245	Cyp7b1	cytochrome P450, family 7, subfamily b, polypeptide 1	bile acid biosynthetic process / oxidoreductase activity	1.18	2.26	0.00012

Affy ID	Gene Symbol	Description	GO function	Log FC	FC	P Value
17491193	Saa3	serum amyloid A 3	acute-phase response	1.16	2.23	0.00524
17313583	Cyp2d9	cytochrome P450, family 2, subfamily d, polypeptide 9	oxidation-reduction process / oxidoreductase activity	1.14	2.21	0.01838
17383892	Lcn2	lipocalin 2	iron binding / transporter activity	1.11	2.16	0.03910
17472404	Gm22036	ncrna:misc_RNA, ENSMUSG00000087904 gene	---	1.06	2.09	0.00015
17445565	Gm15611	predicted gene 15611	---	1.05	2.07	0.03356
17371427	Dhrs9	dehydrogenase/reductase (SDR family) member 9	androgen metabism / alcohol dehydrogenase (NAD) activity	1.04	2.06	0.00007
17400549	Gm20634	predicted gene 20634	nucleosome assembly / DNA binding	1.02	2.02	0.01617
17477016	Gm24938	ncrna:miRNA, ENSMUSG00000076180 gene	---	1.00	2.00	0.01977
Downregulated genes:						
17397990	Mme	membrane metallo endopeptidase	metabolic process / endopeptidase activity	-3.10	-8.57	0.00001
17365410	Cyp17a1	cytochrome P450, family 17, subfamily a, polypeptide 1	steroid biosynthetic process / oxidoreductase activity	-2.84	-7.16	0.00185
17438062	Nipal1	NIPA-like domain containing 1	magnesium transport / transport activity	-2.69	-6.44	0.00023
17320652	Abcd2	ATP-binding cassette, sub-family D (ALD), member 2	fatty acid beta-oxidation / ATPase activity	-2.54	-5.83	0.00823
17247208	Igfbp1	insulin-like growth factor binding protein 1	regulation of cell growth / insulin-like growth factor binding	-2.11	-4.32	0.00149
17271907	Gm11695	predicted gene 11695	---	-2.11	-4.31	0.00002
17280062	Lpin1	lipin 1	fatty acid catabolic process / transcription coactivator activity	-1.99	-3.98	0.00024
17415979	Lepr	leptin receptor	cholesterol metabolism, eating behaviour / signaling activity	-1.94	-3.83	0.00008
17258220	Slc16a5	solute carrier family 16 (monocarboxylic acid transporters), member 5	transport / symporter activity	-1.58	-2.99	0.00001
17277152	Acot3	acyl-CoA thioesterase 3	fatty acid metabolic process / acyl-CoA hydrolase activity	-1.51	-2.84	0.00002
17371374	Cers6	ceramide synthase 6	ceramide biosynthetic process / sphingosine N-acyltransferase activity, DNA binding	-1.35	-2.55	0.00276
17548238	Gm3601	predicted gene 3601	---	-1.27	-2.42	0.00425
17475360	Cyp2b10	cytochrome P450, family 2, subfamily b, polypeptide 10	xenobiotic, steroid metabolic process / oxidoreductase activity	-1.27	-2.41	0.02680
17548717	Gm3601	predicted gene 3601	---	-1.27	-2.41	0.00419
17491699	Mir344d-2	microRNA 344d-2	---	-1.25	-2.38	0.01142
17257591	Snord104	small nucleolar RNA, C/D box 104	---	-1.24	-2.36	0.00055
17335338	Gm22146	ncrna:misc_RNA, ENSMUSG00000088022 gene	---	-1.20	-2.30	0.00406
17342868	LOC100862287	uncharacterized LOC100862287	---	-1.20	-2.29	0.00866
17229036	Fmo2	flavin containing monooxygenase 2	organic acid, NADP metabolic process / oxidoreductase activity	-1.17	-2.25	0.00138
17429632	Mfsd2a	major facilitator superfamily domain containing 2A	transport	-1.16	-2.23	0.00441
17364932	Got1	glutamate oxaloacetate transaminase 1, soluble	aspartate, glutamate metabolic process / transaminase activity	-1.10	-2.14	0.00051
17527332	Nrg4	neuregulin 4	growth factor activity	-1.09	-2.13	0.00411
17478819	E030018B13Rik	RIKEN cDNA E030018B13 gene	---	-1.09	-2.12	0.01741
17545225	Gm25107	ncrna:snoRNA , ENSMUSG00000084421 gene	---	-1.07	-2.10	0.00217
17449710	Cxcl9	chemokine (C-X-C motif) ligand 9	chemotaxis	-1.05	-2.07	0.02850
17459591	St3gal5	ST3 beta-galactoside alpha-2,3-sialyltransferase 5	protein glycosylation / sialyltransferase activity	-1.03	-2.04	0.00430
17428766	Plk3	polo-like kinase 3	cell cycle checkpoint / p53 binding, protein kinase activity	-1.02	-2.02	0.00096
17232235	Ctgf	connective tissue growth factor	ossification, angiogenesis / growth factor activity	-1.01	-2.02	0.01955
17449989	Rasgef1b	RasGEF domain family, member 1B	GTPase signal transduction / guanyl-nucleotide exchange factor activity	-1.01	-2.01	0.01281

Logarithmic and decimal fold change (FC) of Pfn2 KO (n=3) versus control mice (n=3). Regulated genes (>2 or <2 fold change) with a P value <0.05 are shown. GO function: Gene Ontology Consortium biological process / molecular function annotations.

An interesting finding was that among the top upregulated genes we found Lipocalin2 to be 2.16 fold upregulated in the liver of Pfn2 KO mice (Table 3.5).
We have validated microarray expression data by qPCR using 6 WT and 6 Pfn2 KO mice (Figure 3.40) and lipocalin2 mRNA increase in the livers of Pfn2 deficient mice was confirmed, showing a considerable ~10 folds induction (Figure 3.40A), although results did not reach statistical significance due to the high dispersion of the data.
Lcn2 is a protein that binds bacterial and mammalian siderophores, which are high-affinity iron chelators. Besides its role in limiting iron availability to pathogens in the setting of bacterial infection, Lcn2-siderophore complexes can also deliver iron to cells or chelate intracellular iron and export it outside the cell. Lcn2 has been reported to be involved in liver iron uptake and regulation of iron trafficking to the mitochondria (see Introduction 1.3.1.1).
Affymetrix microarray data were further analyzed using the Ingenuity Pathway Analysis program (IPA, Qiagen) for the identification of causal networks and significantly affected pathways (Kramer *et al.* 2014).
IPA results indicated that the most affected pathways and functions in the livers of Pfn2 deficient mice were related to “Nicotine Degradation”, “Xenobiotic Metabolism Signalling”, “Lipid Metabolism”, “Liver Hyperplasia/Hyperproliferation”, “Small Molecules Biochemistry” and “Molecular Transport”.
In addition to conventional microarray analysis, we did Upstream Regulator analysis in IPA program what allows the identification of transcriptional regulators that can explain the observed gene expression changes in a dataset. This analysis in IPA predicted a complex activation/inactivation pattern of diverse transcription factors involved in fatty acid and bile acid metabolism and xenobiotic detoxification; however, the predicted activation/inactivation scores yielded by the program were overall relatively low, indicating weak modulations (Table 3.6).

Table 3.6 Top Upstream Regulators detected by IPA analysis of microarray data in liver samples from Pfn2 KO and WT mice.

Upstream regulator	Description	GO function	Activation Z-score	Prediction	Overlap P value	Nº targets
RORA	RAR-related orphan receptor alpha	lipids, steroids and xenobiotics metabolism / ligand-dependent nuclear receptor	---	---	2.04E-17	18
RORC	RAR-related orphan receptor gamma	lipids, steroids and xenobiotics metabolism / ligand-dependent nuclear receptor	---	---	5.56E-17	17
POR	P450 (cytochrome) oxidoreductase	fatty acids, cholesterol metabolism, apoptosis / oxidoreductase activity	0,896	---	2.61E-12	15
PPARA	peroxisome proliferator activated receptor alpha	positive regulator of fatty acids oxidation, negative regulator of cholesterol storage, response to insulin / ligand-dependent nuclear receptor	0,178	---	7.20E-12	19
GPD1	glycerol-3-phosphate dehydrogenase 1	carbohydrate metabolic process, g lycerol-3-phosphate metabolic process / glycerol-3-phosphate dehydrogenase (NAD+) activity	---	---	1.12E-09	10
SLC25A13	solute carrier family 25 (mitochondrial carrier, adenine nucleotide translocator), member 13	amino acid transmembrane transport, ATP biosynthetic process / mitochondrial inner membrane transporter	---	---	1.38E-09	10
NR1I2 (PXR)	nuclear receptor subfamily 1, group I, member 2	xenobiotic metabolic process, steroid hormone signaling / ligand-dependent nuclear receptor	-0,290	---	1.48E-09	11
CEBPA	CCAAT/enhancer binding protein (C/EBP), alpha	response to nutrients, organic cyclic compound, adipose cell differentiation / transcription factor complex	-0,406	---	1.51E-09	15
AHR	aryl-hydrocarbon receptor	response to xenobiotics, stress, organic cyclic compound, cell cycle/ ligand-dependent nuclear receptor	-1,387	---	4.94E-09	14
LEP	leptin	response to dietary excess, glucose, lipid, cholesterol metabolism, response to insulin / growth factor, hormone activity	-0,470	---	1.60E-08	17
NR1I3 (CAR)	nuclear receptor subfamily 1, group I, member 3	steroid hormone signaling / ligand-dependent nuclear receptor	-1,233	---	1.88E-07	8

Upstream regulator	Description	GO function	Activation Z-score	Prediction	Overlap P value	Nº targets
IL6	interleukin 6	positive regulation of inflammatory response, regulator of cell proliferation, positive regulator of MAPK, STAT signalling / cytokine, growth factor activity	0,247	---	4.90E-07	12
ACOX1	acyl-Coenzyme A oxidase 1, palmitoyl	fatty acid oxidation, positive regulation of cholesterol homeostasis / acyl-CoA, palmitoyl-CoA oxidase activity	1,584	---	6.63E-07	9
TNF	tumor necrosis factor	regulator of T cell proliferation, positive regulator of NF*k*B signalling / cytokine activity	-0,848	---	1.15E-06	18
CYP19A1	cytochrome P450, family 19, subfamily a, polypeptide 1	androgen metabolic process / oxidoreductase activity	-0,700	---	2.55E-06	6
SRD5A1	steroid 5 alpha-reductase 1	lipid, steroid metabolic process / dehydrogenase activity	---	---	6.56E-06	3
RELA	v-rel reticuloendotheliosis viral oncogene homolog A	positive regulation of proliferation, inflammation response, positive regulator of NF*k*B signalling, negative regulator of insulin receptor signalling / transcription factor complex (Nf*k*B)	-0,152	---	7.78E-06	9
PPARG	peroxisome proliferator activated receptor gamma	positive reregulation of fatty acid oxidation, negative regulator of proliferation inflammation / ligand-dependent nuclear receptor	0,095	---	7.98E-06	11
NR5A2	nuclear receptor subfamily 5, group A, member 2	cholesterol homeostasis, bile acid metabolism / ligand-dependent nuclear receptor	-2,183	Inhibited	8.02E-06	6

Upstream regulators are listed according to the overlap P value in IPA, which indicates a significant overlap of dataset genes to known targets controlled by a transcriptional regulator. GO function: Gene Ontology Consortium biological process / molecular function annotations. Activation Z-score and Prediction infer the activation state of the predicted transcriptional regulators (activated z>0; inhibited z<0). Nº targets indicates the number of downstream targets found to be modulated in our array dataset.

To further complete and validate microarray mRNA expression data we analyzed by qPCR additional genes known by literature reports to be involved in iron uptake and trafficking (Figure 3.40A-C).

The additional genes include: the cytochrome P450 oxidoreductase (Por), essential for electron transfer to hepatic P450 enzymes. Lipocalin2 (Lcn2) and its receptor Slc22a17 involved in siderophores iron-trafficking. Bone morphogenetic protein 6 (Bmp6), the key controller of hepcidin expression and molecules involved in BMP signaling: hemochromatosis (Hfe), transferrin receptor 2 (Tfr2) and hemojuvelin (Hjv). ZIP family ion-transporters involved in NTBI iron uptake (Zip14 and Zip8). Ceruloplasmin (Cp) and STEAP family member 3 (Steap3) metalloreductases required to reduce iron and allow its transport via Dmt1. Molecules involved in mitochondrial iron trafficking as the two mitochondrial iron importers mitoferrin1 and 2 (Mfrn1, Mfrn2), the Fe/S mitochondrial exporter (Abcb7) and the Fe/S TCA enzyme (Aco2). The 5' IRE containing hypoxia inducible factor-2 alpha (Hif2α). The iron transporter in bloodstream, transferrin (Tfr) and the chemokine (Ccl2), controlling the transcription of transferrin receptor. Molecules involved in lactoferrin internalization, the low density lipoprotein receptor-related protein 1 (Lrp1) and the asialoglycoprotein receptor 1 (Asgr1). Molecules involved in vesicles trafficking reported to affect iron homeostasis as MON1 homolog A secretory trafficking associated (Mon1a), involved in the trafficking of ferroportin to the plasma membrane or exocyst complex component 6 (Sec15L1), reported to interfere with transferrin receptor exocytosis. Molecules related to heme/hemoglobin transport and metabolism as the heme importers (Slc48a1 and Slc46a1), although the latter was originally identified as heme transporter but later emerged to be a folate transporter. The hemoglobin/haptoglobin scavenger receptor (Cd163). The mitochondrial and plasma membrane heme transporters (Flvcr1a and Flvcr1b) and the non-selective heme exporter (Abcg2). Heme oxigenase (HO) that catalyzes heme degradation. Receptors involved in ferritin uptake (Scara5 and Timdt2) or autophagic degradation of ferritin (Ncoa4).

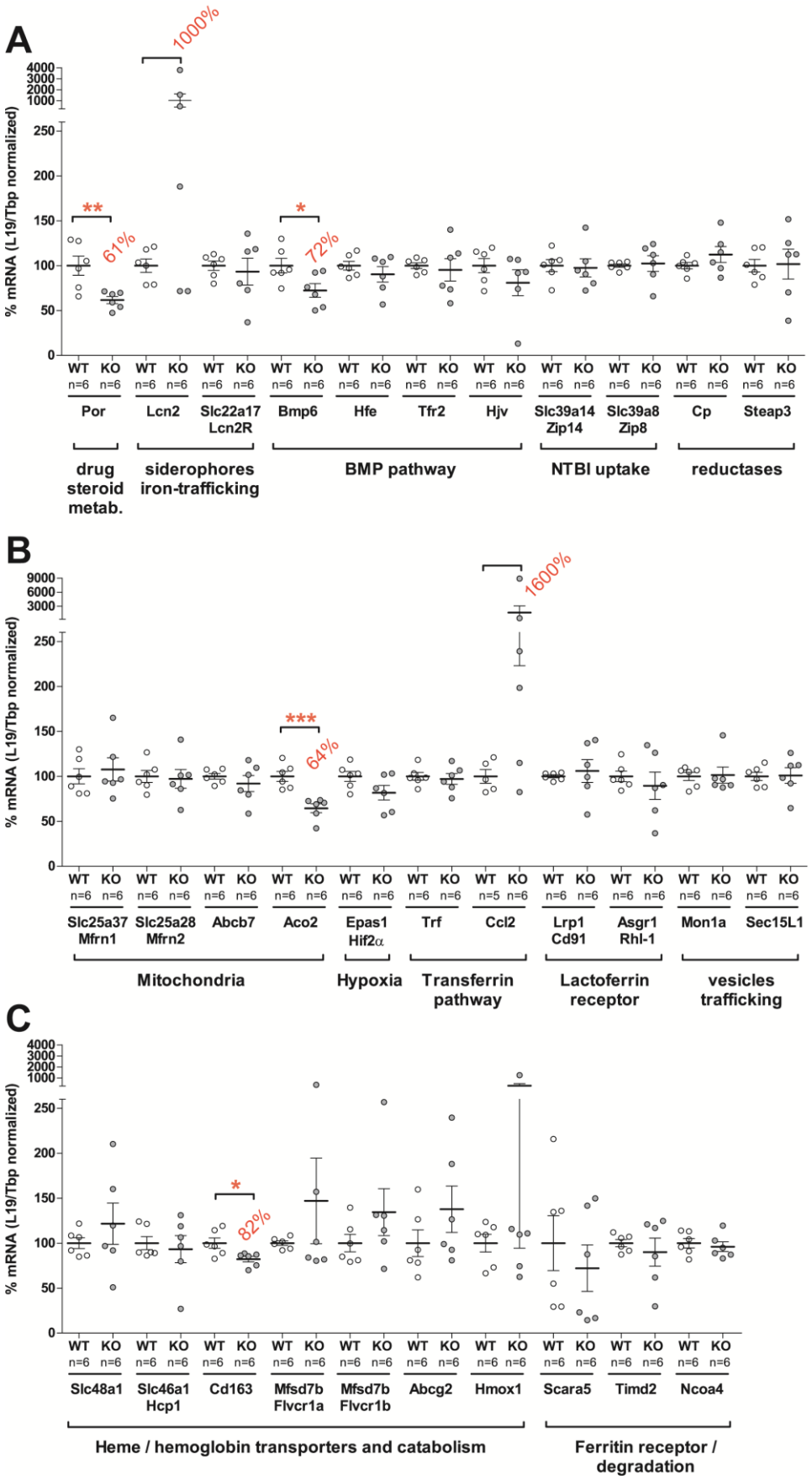

Figure 3.40 Expression analysis of iron-related genes in Pfn2 KO liver samples. We analyzed by qPCR in liver samples from Pfn2 KO mice and WT littermates the expression levels of a set of iron-related genes. mRNAs expression was normalized against L19 ribosomal protein and TATA box binding protein (Tbp) expression and compared to WT mice (set as 100%). Means ± SEM are shown. Sample size (n) is indicated.

We validated the reduction of mRNA levels seen by microarray in the cytochrome P450 oxidoreductase (Por) mRNA, showing a ~40% drop (Figure 3.40A). Por function is essential for hepatic drug and steroid metabolism by providing electron transfer from NADPH to all cytochrome P450 enzymes (Riddick *et al.* 2013).
In line with liver iron deficiency of Pfn2 KO mice, we detected a ~30% reduction of Bmp6 mRNA in Pfn2 KO mice (Figure 3.40A). Bmp6 gene is regulated by iron levels, being upregulated under iron-loaded conditions and reduced by iron deficiency (Kautz *et al.* 2008).
We detected mitochondrial aconitase (Aco2) mRNA levels a ~40% reduced in the livers of Pfn2 KO mice (Figure 3.40B), indicating a negative transcriptional regulation. In addition, we can hypothesize that an increased IRP binding activity in the liver iron-deprived setting would further inhibit Aco2 translation via its 5' UTR IRE. We have not tested it directly, but we can speculate that the livers of Pfn2 KO present reduced mitochondrial aconitase activity, thus possibly indicating a mild impairment of mitochondrial energy metabolism.
We found Ccl2 mRNA to be ~16 folds induced in the liver of Pfn2 KO mice (Figure 3.40B), although data are very spread and the results did not reach statistical significance. Ccl2 is a monocyte chemotactic cytokine that has been studied in a number of pathological conditions characterized by monocyte infiltration (Gerard *et al.* 2001), being either induced or repressed by different stimuli (Deshmane *et al.* 2009). A recent report identified Ccl2 as a critical suppressor of transferrin receptor 1 mRNA expression (Muckenthaler *et al.* 2011).
We also detected a mild ~20% reduction of the hemoglobin/haptoglobin scavenger receptor Cd163 in the liver of Pfn2 KO mice (Figure 3.40C).

In conclusion, the hepatic iron deficiency in Pfn2 KO mice is accompanied by a concordant modulation of IRP-targets, as shown by the reduction of H- and L-ferritin protein levels and the increase of Dmt1 levels, although Tfrc mRNA and protein levels were not significantly altered (Figure 3.39). Accordingly with iron deficiency, we detected reduced Bmp6 mRNA levels, however this did not result in a change in Hamp1 expression, possibly indicating the coexistence of opposite signals acting on Hamp1 promoter. Liver expression data suggest that the IL6 pathway is mildly activated in Pfn2 KO mice with increase of some IL6-targets (Saa1, Saa3), and this could possibly explain the inappropriate normal levels detected for hepcidin. This sustained production of hepcidin in the liver even under low-iron conditions would contribute to the hepatic iron depletion.
Finally, we also found a strong induction of Lcn2 and Ccl2 mRNAs (Figure 3.40). We cannot exclude that Lcn2 and Ccl2 upregulation might be induced by a low-grade chronic inflammatory signal, however, we interpret the over-production of Lcn2, together with the IRP-mediated upregulation of Dmt1 mRNA protein levels, as a liver compensatory feedback to re-establish its depleted iron stores by increasing the expression of the Dmt1 iron transporter and enhancing iron uptake through the Lcn2 pathway.

3.4.7.5 Splenic and other tissues iron metabolism in Pfn2 knockout mice

The origin of the hepatic iron deficiency in Pfn2 knockout mice could be found in an iron mismanagement outside the hepatic tissues; for example by a hepcidin-mediated duodenal iron absorption blockage, an increased iron requirement of the bone marrow or a disturbance in spleen iron re-circularization.
To better understand systemic iron distribution in Pfn2 KO mice, we have further analyzed the mRNA and protein expression levels of molecules involved in iron homeostasis in other tissues: spleen, duodenum, kidney, heart, lung and skeletal muscle (Figure 3.41 and Supp. Figure 6.6).

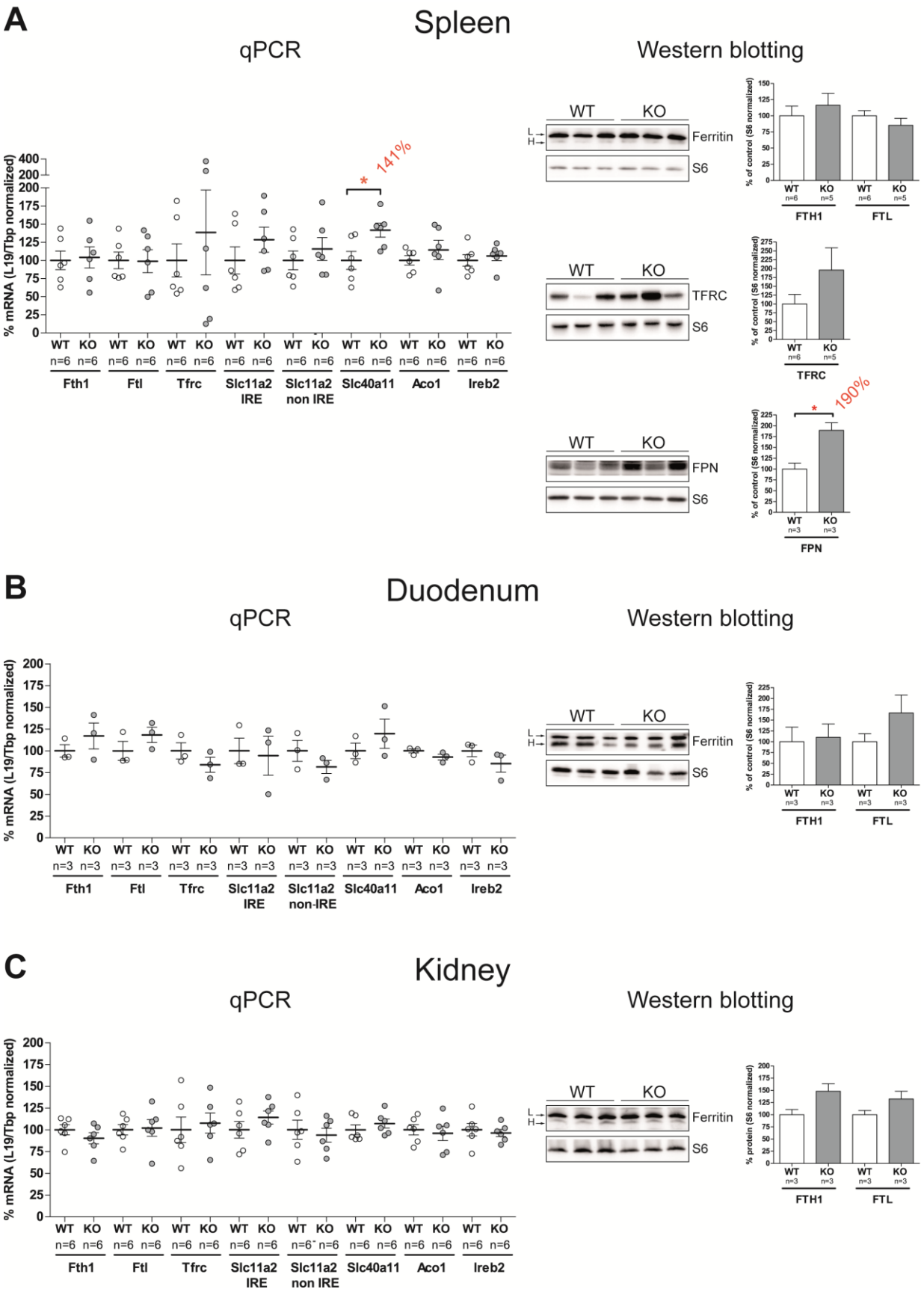

Figure 3.41 Tissue expression of iron-related genes. The expression of iron-related genes was analyzed at mRNA level by qPCR (left panels) and protein level by Western blotting (right panels) in spleen **(A)**, duodenum **(B)** and kidney **(C)** samples from WT and Pfn2 KO 7-9 months old mice. For qPCR experiments, Fth1, Ftl, Tfrc, Slc11a2-IRE and non-IRE isoforms, Slc40a11, Aco1 and Ireb2 mRNAs expression was normalized against L19 ribosomal protein and TATA box binding protein (Tbp) expression and compared to wild type mice (set as 100%).

Means ± SEM are shown. Sample size (n) is indicated. For Western blotting, H- and L-ferritin and, for spleen sample, also Tfrc and Fpn levels were monitored. S6 ribosomal protein was monitored for normalization. Bands intensity was analyzed using the AlphaEaseFC software (Alpha Innotech). Graphs represent quantified data, compared to the signal of WT mice (set as 100%). Means ± SEM are shown. The samples size (n) is indicated. The following abbreviations were used: Fth1: H-ferritin; Ftl: L-ferritin; Tfrc: transferrin receptor 1; Slc11a2 (Dmt1): divalent metal transporter 1; Slc40a11 (Fpn1): ferroportin; Aco1 (Irp1): iron regulatory protein 1; Ireb2 (Irp2): iron regulatory protein 2; WT: wild type mice; KO: Pfn2 knockout mice; L: L-ferritin subunit; H: H-ferritin subunit.

In the spleen, we did not detect any significant difference in the amount of ferritins between wild type and Pfn2 KO (Figure 4.41A), neither at mRNA or protein levels. Tfrc mRNA and protein levels showed a non-statistical significant trend to upregulation, due to the great variability of the data (Figure 4.41A).
Importantly, we found ferroportin levels to be increased both at mRNA levels (~140% increase) and protein level (~190% increase) in the spleen of Pfn2 KO mice compared to control littermates (Figure 4.41A).
Iron-related gene expression studies by qPCR in other tissues as duodenum (the site of iron absorption) or kidney (expressing high levels of Pfn2) as well as other tissues (heart, lung or skeletal muscle) did not reveal any additional significant alteration (Figure 3.41B-C and Supp. Figure 6.6). No differences between WT and Pfn2 KO mice was observed in ferritin protein levels in duodenum or kidney (Figure 3.41B-C).
Spleen total iron content was found to be not different between WT and Pfn2 KO mice (Figure 3.36) and the increased levels of ferroportin production in the spleen of Pfn2 KO mice probably indicates a need for increasing iron export, mainly to sustain erythropoiesis, and could be an attempt to restore liver iron store levels that are mainly replenished by the excess of iron released from senescent erythrocytes degradation by splenic macrophages.

3.4.8 Discussion

Cellular iron maintenance involves the coordination of iron uptake, utilization, and storage and posttranscriptional regulation of gene expression by the IRP/IRE regulatory system plays a central role in the control of cellular and systemic iron homeostasis.
Besides the well-known IREs in TFRC, FTH1, FTL, FPN, DMT1, ACO2, ALAS2, HIF2α and dSdhB mRNAs, in the last decade, several studies have reported other IREs or IRE-like structures in mRNAs directly related or not with iron metabolism, showing that the IRP/IRE regulatory network is wider than previously thought.
We have formerly identified the mouse Profilin2 (Pfn2) mRNA as a novel candidate IRP-target mRNA in a genome-wide screening approach aimed at detecting mRNAs that can interact with both IRP1 and IRP2 protein (Sanchez *et al.* 2011).
My thesis focused in the validation and functional characterization of Profilin2 as a novel IRP-target mRNA.
First of all we have identified an IRE structure located in the 3' UTR of mouse Pfn2 mRNA by *in vitro* EMSA experiments. Pfn2 IRE showed positive interaction with both IRP1 and IRP2 proteins and the specificity of the interaction was confirmed by mutagenesis of Pfn2 IRE sequence. The IRE motif in Pfn2 mRNA presents all the structural features of an IRE, although it differs in the hexanucleotide apical loop (AAGUUG) from the IRE consensus sequence (CAGWGH, where W stands for A or U and H stands for A, C or U); this atypical loop is still functional as it maintains the key base pairing among the first and fifth nucleotide of the loop.
The corresponding human PFN2 IRE was also functional in EMSAs, although showing a weaker binding compared to the mouse sequence. Alignment analysis of the 3' UTR region of

Pfn2 in different species indicated that the IRE sequence is well conserved among higher eukaryotes, further supporting the functional value of the IRE motif in Pfn2 mRNA.

A 3' IRE-containing mRNA is expected to be stabilized and upregulated by IRP binding under iron-deficient conditions and downregulated under iron-replete conditions, when IRP binding does not occur. We therefore tested in cell lines for Pfn2 mRNA regulation in response to changes of iron levels by iron chelation (DFO) or iron supplementation (Hemin) treatments. Pfn2 mRNA was reduced by iron supplementation with Hemin in some cell lines but not in others and no upregulation of Pfn2 mRNA was observed after iron chelation by DFO.

mRNA stabilization studies using the RNA transcription inhibitor DRB indicate that, in NIH3T3 cells, Pfn2 mRNA is not stabilized under iron deficient conditions using DFO; on the contrary, Pfn2 mRNA is very rapidly degraded, opposite to what one would expect by IRP stabilization of a 3' IRE mRNA (as in the case of Tfrc). Therefore, other IRP independent mechanism should account for this observation.

However, in iron supplementation conditions by Hemin it is observed a faster mRNA degradation than in control conditions what is in agreement with a lack of IRP binding and stabilization (Figure 3.25). Both Pfn2 mRNA degradation under iron depleted and iron rich conditions are reflected at protein level in NIH3T3 cells (Figure 3.24).

Contrasting to the ubiquitous iron regulation of the TFRC mRNA, a cell-specific regulation has been reported for DMT1 mRNA (Wardrop *et al.* 1999; Hubert *et al.* 2002) as well as a selective iron regulation was described for other IRE-containing mRNAs as MRCKα or CDC14A which showed regulation only by the iron deficiency stimulus and not by the iron supplementation stimulus (Cmejla *et al.* 2006; Sanchez *et al.* 2006). It is possible that a cell-specific or culture-specific conditions may affect Pfn2 mRNA regulation.

Moreover, as the IRPs are also regulated by other stimuli rather than iron, we cannot exclude that the regulation of Pfn2 by IRPs may integrate multiple and opposing signals as in the case of the regulation of HIF2α, ferroportin or DMT1 (Qian *et al.* 2011; Taylor *et al.* 2011).

However, while *in vitro* cell culture studies failed to unambiguous demonstrate an iron-dependent regulation on Pfn2 mRNA, *in vivo* studies on the other hand showed that Pfn2 mRNA levels were significantly reduced in duodenum samples from mice with intestine-specific Irp1 and Irp2 tamoxifen-inducible knockout. This is compatible with Pfn2 mRNA destabilization in the absence of IRP binding, indicating therefore that the IRPs exert a positive effect on Pfn2 mRNA expression.

Classical well-known IRP-target mRNAs encode for molecules involved in the regulation of iron balance, trafficking and storage. We therefore asked if Pfn2 function plays also a role in iron metabolism.

Profilin2 belongs to the Profilins family of actin-binding proteins essential for regulating cytoskeletal dynamics, moreover, an additional role as regulator of membrane trafficking was reported for Pfn2 in mouse brain (Gareus *et al.* 2006). Pfn2 associates to dynamin1, binding to the C-terminal proline-rich domain in dynamin1 and thus competing with the binding of dynamin1 downstream-effectors, interfering with the assembly of the endocytic machinery: Pfn2 acts therefore as a negative regulator of endocytosis (Gareus *et al.* 2006).

Transferrin is internalized through the classic receptor-mediated endocytosis pathway involving clathrin-coated pits as well as dynamin (van der Bliek *et al.* 1993) and Pfn2 overexpression was shown to inhibit transferrin uptake in HeLa cells while Pfn2 deficiency in neurons associated with increased endocytosis and membrane recycling (Gareus *et al.* 2006). We showed that Pfn2 overexpression in HeLa and Hepa1-6 cells reduces the labile iron pool and reactive oxygen species content, likely interfering with the internalization of the transferrin-transferrin receptor complex with consequent reduction of iron uptake (Figure 3.32).

FPN internalization and degradation after hepcidin binding is also dependent on dynamin function since FPN internalization was suppressed by the treatment with a dynamin inhibitor or by the overexpression of a dominant-negative dynamin mutant (Fernandes *et al.* 2009).
We have analyzed Pfn2 effect on FPN trafficking in Hek293 T-REx hFPN-GFP cell model by Pfn2 overexpression or silencing experiments. The overexpression of Pfn2-mCherry in Hek293 T-REx hFPN-GFP cells seems to block FPN expression, however, we cannot exclude the occurrence of a promoter competition phenomenon not allowing us draw any conclusive hypothesis. An effect of Pfn2 function on FPN membrane trafficking or internalization is plausible, however, further studies are necessary to address this question.
Moreover, in collaboration with the group of Prof. Walter Witke (Institute of Genetics, University of Bonn) we could explore systemic iron metabolism in a mouse model knockout for the *Pfn2* gene.
Mice with constitutive ablation of Pfn2 display normal red blood cell and plasma iron parameters. However, these mice present with a striking iron mismanagement pattern, showing iron accumulation in particular brain regions (hippocampus, olfactory bulb and midbrain) and an important reduction of the liver iron storage (Figure 3.35 and 3.36).
In particular, the pattern of iron accumulation in the hippocampus of Pfn2 KO mice is more pronounced in the pyramidal cell layer suggesting that there are iron deposits within the cell bodies of pyramidal excitatory neurons. As mentioned before, Pfn2 was demonstrated to act as a negative regulator of endocytosis (Gareus *et al.* 2006); iron accumulation in those brain areas could be therefore attributable to an increased uptake of iron-loaded transferrin in the absence of Pfn2 inhibitory control (Figure 3.42). This hypothesis is further strengthened by the observation that iron deposits occur exactly in areas where Pfn2 physiological expression is higher in wild type mice (e.g., the pyramidal layer of the hippocampus).

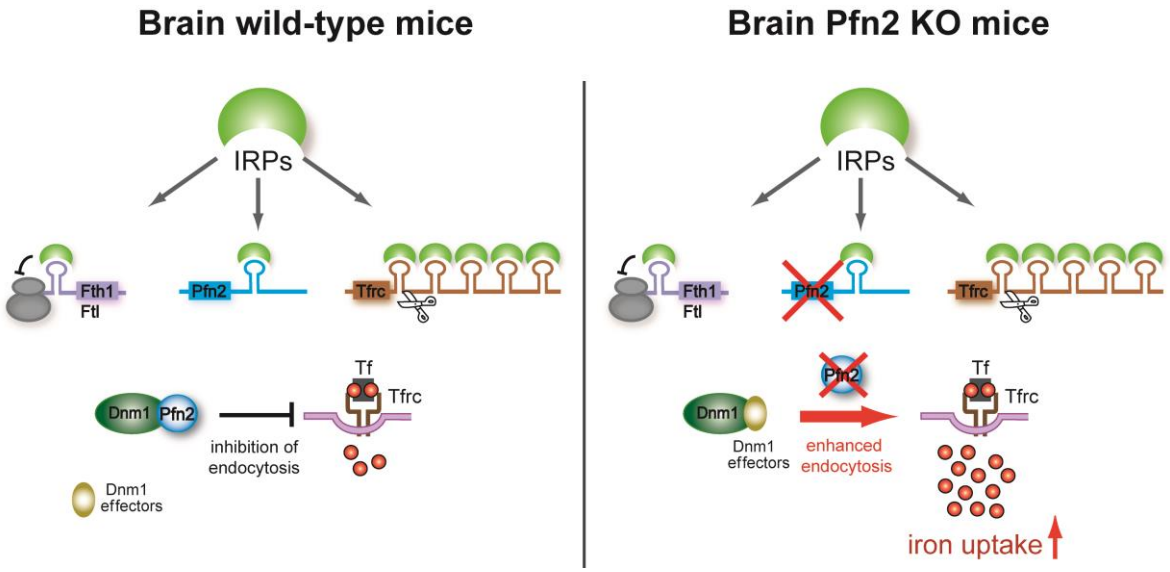

Figure 3.42 Model for brain iron accumulation in Pfn2 KO mice. In our model arrows indicate activation and flat lines indicates inhibition. The following abbreviations were used: Fth1: H-ferritin; Ftl: L-ferritin; Pfn2: profilin2; Tfrc: transferrin receptor; Tf: transferrin; Dnm1: dynamin1.

Iron accumulation in the hippocampus was associated with an unexpected downregulation of the H- and L-subunits of the iron storage protein ferritin. TEM studies showed that the iron deposits seem to be contained within membrane organelles that were identified as mitochondria, based on the presence of lamellae structures (Figure 3.38). In Pfn2 KO mice hippocampal iron accumulation inside mitochondria occurs in a non-classical form: these deposits are completely different from the typical ferritin or hemosiderin deposits observed in

liver or spleen tissues (Figure 3.38) (Cohen *et al.* 2010) but also differ from other mitochondrial iron deposits observed in the frame of neurodegenerative disease for example in the heart tissue of a mouse model for Friedreich ataxia (Whitnall *et al.* 2012).

The behavioral phenotype of Pfn2 knockout mice was related to Pfn2 function in controlling vesicles exocytosis and presynaptic excitability. The deletion of Pfn2 leads to increased glutamate release in neocortical glutamatergic neurons and hyperstimulation of the basal ganglia, which correlates with the hyperactivity and increased novelty-seeking behavior in the mutant mice (Pilo Boyl *et al.* 2007).

Iron is essential for brain metabolism because of its role in energy metabolism and because it is a cofactor for many enzymes involved in neurotransmitters synthesis, and myelination (Hare *et al.* 2013). Both iron deficiency and excess have detrimental effects on the brain: dietary iron deficiency is related with cognitive impairment (Youdim 2008) and, on the other hand, excess of pro-oxidant iron has been associated with several neurodegenerative diseases as Alzheimer's disease or Parkinson's disease or genetic disorders such as Friedreich ataxia, aceruloplasminemia or neuroferritinopathy (Altamura *et al.* 2009; Schipper 2012).

Since there is no overt neurodegenerative or ataxia phenotype in Pfn2 KO mice, we could assume that the amorphous iron aggregates inside the mitochondria in Pfn2 mutant mice are presumably inert. Further investigations are needed to clarify the role of the perturbed cellular iron handling in the brain of Pfn2 deficient mice in relation with its phenotypic effects.

On the other hand, the livers of Pfn2 deficient mice showed an important depletion of its iron stores. The hepatic iron deficiency in Pfn2 KO mice likely activates IRP-binding activity with the consequent observed reduction of H- and L-ferritin levels and upregulation of Dmt1 in order to reestablish the depleted iron stores. Despite the plausible IRP-activation, Tfrc levels remained unchanged (Figure 3.43) probably by compensatory signals (i.e. mRNA reduction by Ccl2 upregulation, see below).

Microarray data indicated that in the liver of Pfn2 KO mice only mild changes of gene expression occur with the most affected genes being Cyp450 and phase-II enzymes. Interpretation of transcriptional changes using the Ingenuity Pathway Analysis software suggested for an activation of fatty acids and bile salts pathways in the liver of Pfn2 KO mice. Cyp450 proteins utilize heme-iron as a cofactor for their enzymatic activity and dietary iron deficiency was previously demonstrated to reduce the activity of Cyp450 enzymes and of the cytochrome P450 oxidoreductase (Por) in rat liver (Dhur et al. 1989). Cyp450 enzymes are involved in xenobiotics and fatty acids metabolism but also steroid biosynthesis, and bioactive metabolites production (vitamin D and retinoic acid metabolites). We hypothesized that a mild impairment of Cyp450 function, secondary to iron shortage, would result in the accumulation of bioactive intermediates that are sensed by nuclear receptors (Ppraα, Pxr, Ahr, Car) leading to their activation/inactivation and the consequent transcriptional changes which, finally, result in the detected expression remodeling of phase-I and phase-II enzymes and predicted by the IPA software as an increase in fatty acids and bile acids metabolism (Figure 3.43).

In line with our data, several works in the literature reported that dietary iron deficiency modulates lipid metabolism in rats liver and alter the mRNA expression of Cyp450 enzymes (Stangl *et al.* 1998; Kamei *et al.* 2010).

Microarray results also evidenced increased expression of lipocalin2 (Lcn2) probably as a compensatory mechanism to increase iron uptake via the lipocalin pathway (Figure 3.43).

Ccl2 cytokine mRNA levels were also induced in the liver of Pfn2 KO mice. Ccl2 levels were previously shown to be iron-sensitive as Ccl2 levels are reduced in Hfe knockout mice and Hemochromatosis patients and negatively correlate with liver iron levels at diagnosis in Hemochromatosis patients (Muckenthaler et al. 2011). Ccl2 was also demonstrated to be a critical suppressor of transferrin receptor mRNA expression in human cells (Muckenthaler et

al. 2011) and thus Ccl2 activation in Pfn2 KO mice livers could help to explain why Tfrc levels are not upregulated despite the iron deficiency of the liver (Figure 3.43).
The mRNA levels of the iron-sensitive Bmp6 were also found to be reduced in the liver of Pfn2 KO mice, in accordance with the iron deficiency. However, the expression of the Bmp6-target and systemic iron-regulating hormone hepcidin (Hamp1) was unexpectedly unchanged in the liver of Pfn2 KO mice, possibly suggesting the co-existence of opposite signals acting on Hamp1 promoter (Figure 3.43). On one hand the reduced Bmp6 levels in the livers of Pfn2 KO mice is expected to decrease hepcidin production (Meynard *et al.* 2009), however, we hypothesized that a positive signal is, on the other hand, activating Hamp1 promoter, sustaining hepcidin production to normal WT levels.
We hypothesized that this positive signal could be inflammation since microarray data showed the presence two acute phase proteins (Saa1 and Saa3, Table 3.5) among the top regulated genes and IPA Upstream Regulator analysis predicted a mild activation of the IL6 pathway in Pfn2 KO mice (Table 3.6), however, other positive and negative acute phase reactants were not coordinately expressed and other inflammatory mediators (Tnf, Nf*k*b, Table 3.6) resulted inactivated by IPA predictions. We therefore hypothesized the presence of a low-grade chronic inflammatory signal in the liver of Pfn2 KO mice that could be responsible for the sustained Hamp1 production despite the hepatic iron deficiency (Figure 3.43).

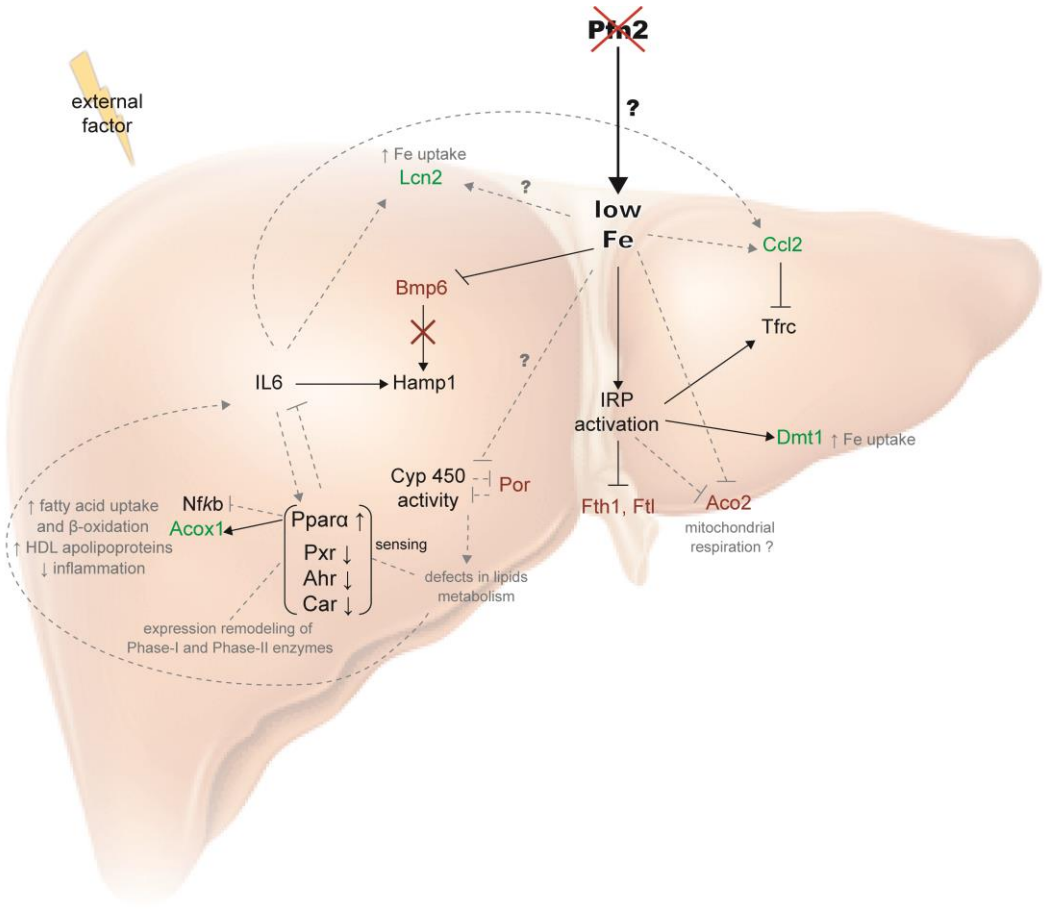

Figure 3.43 Model for gene expression regulation in the liver of Pfn2 KO mice. In our model, molecules whose expression at mRNA or protein levels is increased in Pfn2 KO mice versus WT mice are indicated in green and molecules whose expression is reduced are indicated in red. Arrows: activation; flat lines: inhibition; plain lines: high plausible causal relationship; dashed lines: uncertain/hypothesized causal relationship. The following abbreviations were used: Pfn2: profilin2; Lcn2: lipocalin2; Tfrc: transferrin receptor C; Ccl2: C-C motif chemokine ligand 2; Fth1: H-ferritin; Ftl: L-ferritin; Aco2: aconitase 2; Bmp6: bone morphogenetic protein 6; Hamp1: hepcidin; IL6: interleukin 6; Pparα: peroxisome proliferator activated receptor alpha; Pxr: pregnate X receptor; Ahr: aryl-hydrocarbon receptor; Car: androstane receptor; Nf*k*b: nuclear factor kappa B; Acox1: acyl-Coenzyme A oxidase 1, palmitoyl.

Lcn2 is also an acute phase protein and its activation has been associated with inflammation and tissue injury (Liu *et al.* 1995; Borkham-Kamphorst *et al.* 2011) as well as Ccl2 activation is associated with the inflammatory state (Gerard *et al.* 2001); we cannot therefore exclude that Lcn2 and Ccl2 upregulation in Pfn2 KO mice might be induced by a chronic mild inflammation.
Finally, aconitase2 mRNA expression was also found to be reduced in the expression arrays, possibly implying an impairment of mitochondrial respiratory function in the liver of Pfn2 KO mice (Figure 3.43).

In conclusion, Pfn2 knockout mice present with iron accumulation in discrete brain areas and, on the other hand, these mice display a non-anemic iron-deficient phenotype, as shown by the reduction in the hepatic iron stores (Figure 3.44).
Pfn2 expression in liver is physiologically low in wild type mice (Supp. Figure 6.2) and microarray data did not reveal major alterations in this tissue in the absence of Pfn2 function. The expression changes observed by microarrays, qPCRs and Western blotting in the liver of Pfn2 KO mice (e.g., Ferritin, Dmt1, Lcn2, Bmp6, Cyp450 enzymes) appeared to be a consequence rather than the cause of the iron deficiency.
We hypothesized therefore that the hepatic manifestations of global Pfn2 deficiency likely reflects a systemic defect in iron metabolism.
Urinary iron quantifications demonstrated that the hepatic iron is not lost due to an abnormal excretion in the urines.

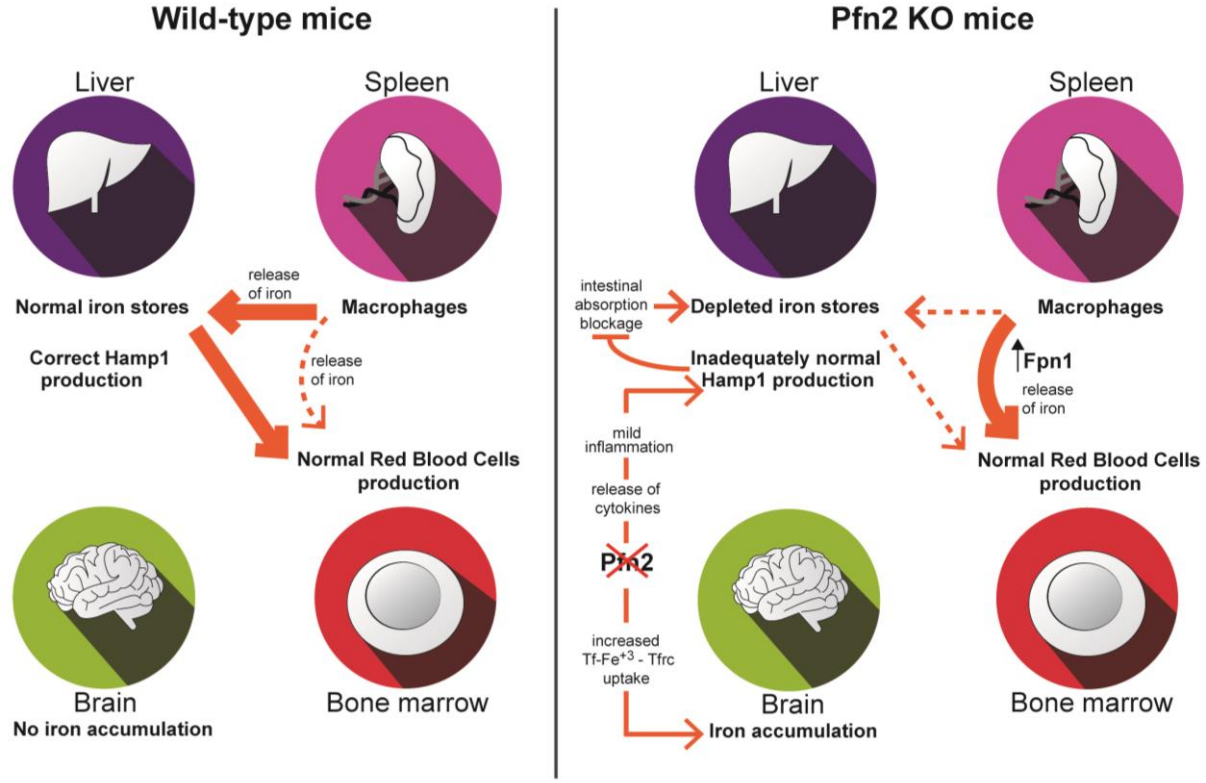

Figure 3.44 Model for systemic iron distribution and homeostasis in WT versus Pfn2 KO mice.

The reduction of the liver iron storage capacity could be also attributed to a reduced iron absorption by an hepcidin-mediated duodenal iron absorption blockage (Figure 3.44). Hepcidin mRNA levels are inappropriately normal in the livers of Pfn2 KO mice despite the low iron levels, which should downregulate Hamp1 production in order to increase dietary iron absorption. Iron content in Pfn2 knockout duodenal samples was comparable to wild type mice and no additional alteration in the mRNA expression of iron-related genes or ferritin

protein levels were detected in duodenum samples from Pfn2 KO mice. Further studies to evaluate duodenal iron metabolism and the rate of iron absorption (direct measurements of iron absorption using radioactive iron) are therefore necessary to answer the question whether the sustained production of Hamp1 in the livers Pfn2 KO mice is responsible for a mild blockage of intestinal iron absorption.
Finally, we observed an upregulation of ferroportin mRNA and protein levels in spleen samples from Pfn2 KO mice, suggesting an increased need for iron release from the spleen stores. We hypothesized that the iron released from the spleen is used to sustain normal erythropoiesis but not to replenish liver iron stores (Figure 3.44).
As body iron stores are reduced in Pfn2 deficient mice, we believe that challenging those mice with erythropoietic stimuli (bleeding, phenylhydrazine treatment, iron deficiency diet) will result in more severe iron phenotype compromising red blood cell production and showing hematological alterations (microcytic anemia).

In summary, our studies indicate that Pfn2 is a previously unrecognized player in iron metabolism. Pfn2 mRNA has a 3' functional and conserved IRE which showed preferentially downregulation under iron-excess conditions by Hemin treatment in cell lines and that we demonstrated to be regulated by IRP-mediated stabilization *in vivo*. Moreover, the reduction of cellular LIP by Pfn2 overexpression experiments in cell lines as well as the misregulation of iron distribution observed in mice knockout for *Pfn2* gene revealed the impact of Pfn2 function on iron homeostasis.

4. CONCLUSIONS

4.1 Work done on novel L-ferritin IRE mutations in Hereditary Hyperferritinemia-Cataract Syndrome (HHCS) published as Luscieti *et al.* 2013 OJRD

4.1.1 We identified two novel mutations (Heidelberg +52G>C and Badalona+36C>U) in two families with HHCS (Pedigrees 1 and 2, section 3.1.1).

4.1.2 The Badalona mutation was found in homozygosis, this is unexpected and unusual for an autosomal dominant disease where mutations in heterozygous state are enough to develop the disease.

4.1.3 Functional assays by *in vitro* EMSAs show the new mutations mildly impair IRP-IRE binding, specially the Badalona mutation that conserves ~40% of its capacity to bind the IRPs. However, this minor disturbance is sufficient for biochemical and clinical symptoms to occur in the patients.

4.1.4 We report a revised update of all mutations in HHCS (see table S2 in Luscieti *et al.* 2013) and performed phenotype/genotype correlation studies. A total of 37 mutations (31 point mutations and 6 deletions) have been described as causative for HHCS.

4.1.5 We confirm that a phenotype/genotype correlation in HHCS is difficult to establish due to concomitant pathologies, clinical penetrance and the fact that serum ferritin levels are influences by sex and age and are subjected to inter and intra-individual variability.

4.1.6 Rare HHCS cases could be responsible for cases of unexplained hyperferritinemia. Therefore, an easy genetic study (sequencing of L-ferritin exon 1) would reveal those cases resolving them and avoiding unnecessary phlebotomy treatments in HHCS cases.

4.2 Work done on novel mutation in ALAS2 IRE as a modifier of clinical severity in Erythropoietic Protoporphyria (EPP)

4.2.1 Work done in collaboration with Dr. Hervé Puy laboratory reveals that EPP is caused by the combination of a mutation in a new gene (work on progress, pending publication) together with a new ALAS2 IRE mutation (NM_000032.4; c.[-38T>C];[=]) in a French family with a female proband presenting a severe phenotype of EPP.

4.2.2 The -38T>C ALAS2 IRE mutation is unable to bind IRP1 and IRP2 *in vitro* in EMSAs. This will de-repress ALAS2 mRNA regulation by the IRPs, increasing ALAS2

production and contributing to the clinical presentation of the disease with increase of ZnPP similar as in XLEPP.

4.2.3 The ALAS2 IRE mutation is a modifier of the clinical severity of the EPP disease in this proband.

4.3 Work done on the identification of a functional 3' IRE in human BDH2 mRNA

4.3.1 Human BDH2 mRNA has a 3' IRE that is conserved in Hominidae but not in other species.

4.3.2 BDH2 IRE can bind *in vitro* and in cell lines (MCF-10A and 293T) to IRP1 and IRP2.

4.3.3 BDH2 mRNA expression is regulated by iron similarly as TFRC mRNA in different cell lines as well as in liver transformed cell lines derived from human and chimpanzee. No iron regulation is observed in liver cell lines derived from other primates or in mouse cell lines, where BDH2 IRE is not conserved.

4.3.4 BDH2 mRNA and protein levels are reduced in liver samples from iron-overloaded Hereditary Hemochromatosis patients. This regulation is compatible with a 3' IRE IRP-mediated regulation.

4.3.5 Iron dependent regulation of BDH2 mRNA was demonstrated to be mediated by IRP1 and IRP2 in HeLa cells using shRNA and siRNA technology.

4.4.6 Human BDH2 IRE and 3' UTR confer iron-dependent regulation onto a heterologous gene (shown by luciferase reporter assays in MCF-10A and HeLa cells).

4.4.7 mRNA stabilization studies in MCF-10A cell lines demonstrate that BDH2 mRNA expression is post-transcriptionally regulated by iron via mRNA stabilization upon IRPs binding. BDH2 mRNA regulation is mediated by its 3' IRE.

4.3.8 Iron regulation of BDH2 expression will control mitochondrial iron homeostasis preventing mitochondrial iron overload in iron-replete conditions.

4.4 Work done on Profilin2 as a novel IRP-target mRNA

4.4.1 Mouse Profilin2 (Pfn2) mRNA immunoprecipitates together with IRP1 and IRP2 in multiple mouse tissues.

4.4.2 Pfn2 has an atypical 3' IRE (motif 19) that is conserved among higher eukaryotes.

4.4.3 Competitive EMSAs shown that human and mouse Pfn2 IRE are functional for binding *in vitro* to IRP1 and IRP2.

4.4.4 Our experimental EMSA data allow us to improve our bioinformatics IRE prediction program (SIREs) in the prediction of one additional non-classical IRE (named as motif 19).

4.4.5 Pfn2 mRNA and protein levels are downregulated by iron supplementation with Hemin in some cell lines but not in others, similar as the regulation observed for Slc11a2 mRNA that also contains a single 3' IRE. No upregulation by DFO was observed neither for Pfn2 nor for Slc11a 2 in Hepa1-6 cells.

4.4.6 mRNA stabilization studies in NIH3T3 do not reflect post-transcriptional IRP-mediated stabilization on Pfn2 mRNA by DFO treatment. However, in iron supplementation conditions by Hemin it is observed a faster mRNA degradation than in control conditions what is in agreement with a lack of IRP binding and stabilization.

4.4.7 Pfn2 3' IRE or 3' UTR do not confer iron-dependent regulation to a heterologous luciferase reporter gene in HeLa cells. However, reporter constructs carrying a non-functional Pfn2 IRE at the 5' of the luciferase CDS display overall higher luciferase activity compared to wild type constructs, implying that wild type constructs expression is strongly repressed and thus reflecting an efficient IRP interaction.

4.4.8 Pfn2 protein levels are unchanged by increased IRP activity in H1299 cells with an overexpression of an IRP1 form constitutively active in the RNA-binding form.

4.4.9 Pfn2 mRNA levels are not modulated *in vivo* in response to low iron diet. Mice fed an iron-deficient diet show upregulation of Tfrc (in liver, duodenum and spleen) and Slc11a2-IRE mRNAs (in liver) but not Pfn2 mRNA.

4.4.10 Pfn2 mRNA is positively regulated by the IRPs *in vivo* in mice models with altered IRP-binding activity. While we could observe neither Pfn2 nor Slc11a2-IRE mRNA upregulation in the IRP1* gain of function mice, and only a 2-fold increase was observed for Tfrc mRNA, Pfn2 mRNA levels were significantly decreased (25% reduction) in duodenal samples from mice with tamoxifen-inducible intestinal *Irp1* and *Irp2* deficiency. These results indicate that the lack of IRPs results in an *in vivo* reduction of Pfn2 mRNA levels, as expected for a 3' IRE-containing mRNA controlled by IRP stabilization.

4.4.11 3' RACE and RT-PCR experiments exclude the expression of alternative non-IRE-containing Pfn2 transcripts that could explain the not clear regulation of Pfn2 mRNA in response to changes of iron status observed in cell lines after DFO or Hemin treatment.

4.4.12 Transient or stable overexpression of Pfn2 cDNA reduces labile iron pool (LIP) and reactive oxygen species (ROS) levels in HeLa and Hepa1-6 cells. These experiments demonstrate that the modulation of Pfn2 levels affects intracellular iron content and associates for the first time Pfn2 function to iron homeostasis.

4.4.13 The overexpression of Pfn2-mCherry in Hek293 T-REx hFPN-GFP cells seems to block FPN expression, however, we cannot exclude the occurrence of a promoter competition phenomenon. On the other hand, human PFN2 depletion by siRNA does not alter ferroportin membrane trafficking or ferroportin internalization and degradation in response to hepcidin binding in Hek293 T-REx hFPN-GFP cell line.

4.4.14 Mice with constitutive ablation of Pfn2 gene display normal red blood cell and plasma iron parameters. However, these mice present with a striking iron mismanagement pattern, showing iron accumulation in particular brain regions (olfactory bulb, hippocampus, and midbrain) and an important reduction of the liver iron storage capacity.

4.4.15 Iron accumulation in the hippocampus is unexpectedly associated with reduced H- and L-ferritin protein levels. TEM studies of the hippocampus showed the presence of electron-dense aggregates containing iron within the mitochondria of Pfn2 KO mice. The morphology of those aggregates is different from spleen ferritin or hemosiderin deposits, suggesting that iron accumulates in a different form in the tissue.

4.4.16 The iron deficiency of the liver in Pfn2 KO mice is accordingly accompanied by reduced H- and L- ferritin protein levels and increase of Dmt1-IRE isoform mRNA levels and protein levels, suggesting IRP-binding activation under low-iron conditions.
We interpret the upregulation of Dmt1 as a liver compensatory feedback signal to re-establish the iron stores by increasing the expression of the iron transporter.

4.4.17 Microarray and qPCR expression analysis of liver samples from Pfn2 KO shows overall few gene expression changes. Differentially regulated genes are phase-I and phase-II metabolizing enzymes suggesting for an increased fatty acids oxidation and bile acids production in Pfn2 KO mice.
Importantly, Lcn2 mRNA levels were found to be strongly induced in the liver of Pfn2 KO mice, probably as a compensatory mechanism of the liver to increase iron uptake via the lipocalin pathway.
Bmp6 mRNA levels were reduced in the liver of Pfn2 KO mice in concordance with low iron levels.
Hamp1 mRNA levels were found to be inadequately normal despite the low iron content in the liver of Pfn2 KO mice.
Liver expression changes indicate a mild activation of IL6 pathway, what suggest a possible mild chronic inflammation in Pfn2 KO mice. This signal could explain the abnormal normal levels of hepcidin, indicating that the inflammatory activation signal, possibly by IL6, overtakes the downregulating signal that low iron levels should have on hepcidin expression.

4.4.18 mRNA and protein levels of Fpn are upregulated in the spleen of Pfn2 KO mice.

4.4.19 We hypothesized that in Pfn2 KO mice, the released splenic iron is used for maintaining normal hematopoiesis but not for replenishing liver iron stores.

5. BIBLIOGRAPHY

Abboud, S., et al. (2000). "A novel mammalian iron-regulated protein involved in intracellular iron metabolism." J Biol Chem 275(26): 19906-19912.

Addess, K. J., et al. (1997). "Structure and dynamics of the iron responsive element RNA: implications for binding of the RNA by iron regulatory binding proteins." J Mol Biol 274(1): 72-83.

Agar, J. N., et al. (2000). "IscU as a scaffold for iron-sulfur cluster biosynthesis: sequential assembly of [2Fe-2S] and [4Fe-4S] clusters in IscU." Biochemistry 39(27): 7856-7862.

Ajit Bolar, N., et al. (2013). "Mutation of the iron-sulfur cluster assembly gene IBA57 causes severe myopathy and encephalopathy." Hum Mol Genet 22(13): 2590-2602.

Akerstrom, B., et al. (2000). "Lipocalins: unity in diversity." Biochim Biophys Acta 1482(1-2): 1-8.

Allerson, C. R., et al. (1999). "Clinical severity and thermodynamic effects of iron-responsive element mutations in hereditary hyperferritinemia-cataract syndrome." J Biol Chem 274(37): 26439-26447.

Allikmets, R., et al. (1999). "Mutation of a putative mitochondrial iron transporter gene (ABC7) in X-linked sideroblastic anemia and ataxia (XLSA/A)." Hum Mol Genet 8(5): 743-749.

Altamura, S., et al. (2009). "Iron toxicity in diseases of aging: Alzheimer's disease, Parkinson's disease and atherosclerosis." J Alzheimers Dis 16(4): 879-895.

Alvarez-Coca-Gonzalez, J., et al. (2010). "The hereditary hyperferritinemia-cataract syndrome: a family study." Eur J Pediatr 169(12): 1553-1555.

Anderson, C. P., et al. (2012). "Mammalian iron metabolism and its control by iron regulatory proteins." Biochim Biophys Acta 1823(9): 1468-1483.

Anderson, S. A., et al. (2013). "The IRP1-HIF-2alpha axis coordinates iron and oxygen sensing with erythropoiesis and iron absorption." Cell Metab 17(2): 282-290.

Arezes, J., et al. (2013). "Non-transferrin-bound iron (NTBI) uptake by T lymphocytes: evidence for the selective acquisition of oligomeric ferric citrate species." PLoS One 8(11): e79870.

Armitage, A. E., et al. (2011). "Hepcidin regulation by innate immune and infectious stimuli." Blood 118(15): 4129-4139.

Arosio, C., et al. (1999). "Hereditary hyperferritinemia cataract syndrome: a de novo mutation in the iron responsive element of the L-ferritin gene." Haematologica 84(6): 560-561.

Arosio, P., et al. (2009). "Ferritins: a family of molecules for iron storage, antioxidation and more." Biochim Biophys Acta 1790(7): 589-599.

Arosio, P., et al. (2010). "Cytosolic and mitochondrial ferritins in the regulation of cellular iron homeostasis and oxidative damage." Biochim Biophys Acta 1800(8): 783-792.

Artal-Sanz, M., et al. (2009). "Prohibitin and mitochondrial biology." Trends Endocrinol Metab 20(8): 394-401.

Babitt, J. L., et al. (2006). "Bone morphogenetic protein signaling by hemojuvelin regulates hepcidin expression." Nat Genet 38(5): 531-539.

Baker, P. R., 2nd, et al. (2014). "Variant non ketotic hyperglycinemia is caused by mutations in LIAS, BOLA3 and the novel gene GLRX5." Brain 137(Pt 2): 366-379.

Balk, J., et al. (2004). "The hydrogenase-like Nar1p is essential for maturation of cytosolic and nuclear iron-sulphur proteins." EMBO J 23(10): 2105-2115.

Balwani, M., et al. (2012). "The porphyrias: advances in diagnosis and treatment." Hematology Am Soc Hematol Educ Program 2012: 19-27.

Bartnikas, T. B. (2012). "Known and potential roles of transferrin in iron biology." Biometals 25(4): 677-686.

Barton, J. C. (2013). "Hemochromatosis and iron overload: from bench to clinic." Am J Med Sci 346(5): 403-412.

Beaumont, C., et al. (1995). "Mutation in the iron responsive element of the L ferritin mRNA in a family with dominant hyperferritinaemia and cataract." Nat Genet 11(4): 444-446.

Behnen, M., et al. (2009). "Testis-expressed profilins 3 and 4 show distinct functional characteristics and localize in the acroplaxome-manchette complex in spermatids." BMC Cell Biol 10: 34.

Beinert, H., et al. (1993). "Aconitase, a two-faced protein: enzyme and iron regulatory factor." FASEB J 7(15): 1442-1449.

Beinert, H., et al. (1996). "Aconitase as Ironminus signSulfur Protein, Enzyme, and Iron-Regulatory Protein." Chem Rev 96(7): 2335-2374.

Bekri, S., et al. (1993). "X-Linked Sideroblastic Anemia and Ataxia."

Bennatt, D. J., et al. (1997). "Isolated rat hepatocytes bind lactoferrins by the RHL-1 subunit of the asialoglycoprotein receptor in a galactose-independent manner." Biochemistry 36(27): 8367-8376.

Bonneau, D., et al. (1995). "Bilateral cataract and high serum ferritin: a new dominant genetic disorder?" J Med Genet 32(10): 778-779.

Borkham-Kamphorst, E., et al. (2011). "Induction of lipocalin-2 expression in acute and chronic experimental liver injury moderated by pro-inflammatory cytokines interleukin-1beta through nuclear factor-kappaB activation." Liver Int 31(5): 656-665.

Bosio, S., et al. (2004). "C29G in the iron-responsive element of L-ferritin: a new mutation associated with hyperferritinemia-cataract." Blood Cells Mol Dis 33(1): 31-34.

Boussif, O., et al. (1995). "A versatile vector for gene and oligonucleotide transfer into cells in culture and in vivo: polyethylenimine." Proc Natl Acad Sci U S A 92(16): 7297-7301.

Bouton, C., et al. (2003). "Iron regulatory proteins as NO signal transducers." Sci STKE 2003(182): pe17.

Brasse-Lagnel, C., et al. (2011). "Intestinal DMT1 cotransporter is down-regulated by hepcidin via proteasome internalization and degradation." Gastroenterology 140(4): 1261-1271 e1261.

Brown, N. M., et al. (1998). "Novel role of phosphorylation in Fe-S cluster stability revealed by phosphomimetic mutations at Ser-138 of iron regulatory protein 1." Proc Natl Acad Sci U S A 95(26): 15235-15240.

Bulteau, A. L., et al. (2004). "Frataxin acts as an iron chaperone protein to modulate mitochondrial aconitase activity." Science 305(5681): 242-245.

Butt, J., et al. (1996). "Differences in the RNA binding sites of iron regulatory proteins and potential target diversity." Proc Natl Acad Sci U S A 93(9): 4345-4349.

Cairo, G., et al. (1996). "Superoxide and hydrogen peroxide-dependent inhibition of iron regulatory protein activity: a protective stratagem against oxidative injury." FASEB J 10(11): 1326-1335.

Cairo, G., et al. (2000). "Iron regulatory proteins in pathobiology." Biochem J 352 Pt 2: 241-250.

Cairo, G., et al. (2002). "The iron regulatory proteins: targets and modulators of free radical reactions and oxidative damage." Free Radic Biol Med 32(12): 1237-1243.

Caltagirone, A., et al. (2001). "Modulation of cellular iron metabolism by hydrogen peroxide. Effects of H2O2 on the expression and function of iron-responsive element-containing mRNAs in B6 fibroblasts." J Biol Chem 276(23): 19738-19745.

Camaschella, C., et al. (2007). "The human counterpart of zebrafish shiraz shows sideroblastic-like microcytic anemia and iron overload." Blood 110(4): 1353-1358.

Cameron, J. M., et al. (2011). "Mutations in iron-sulfur cluster scaffold genes NFU1 and BOLA3 cause a fatal deficiency of multiple respiratory chain and 2-oxoacid dehydrogenase enzymes." Am J Hum Genet 89(4): 486-495.

Campillos, M., et al. (2010). "SIREs: searching for iron-responsive elements." Nucleic Acids Res 38(Web Server issue): W360-367.

Campuzano, V., et al. (1996). "Friedreich's ataxia: autosomal recessive disease caused by an intronic GAA triplet repeat expansion." Science 271(5254): 1423-1427.

Canonne-Hergaux, F., et al. (1999). "Cellular and subcellular localization of the Nramp2 iron transporter in the intestinal brush border and regulation by dietary iron." Blood 93(12): 4406-4417.

Cao, W., et al. (2010). "A case report of spontaneous mutation (C33>U) in the iron-responsive element of L-ferritin causing hyperferritinemia-cataract syndrome." Blood Cells Mol Dis 44(1): 22-27.

Casarrubea, D., et al. (2013). "Abnormal body iron distribution and erythropoiesis in a novel mouse model with inducible gain of iron regulatory protein (IRP)-1 function." J Mol Med (Berl) 91(7): 871-881.

Casey, J. L., et al. (1989). "Iron regulation of transferrin receptor mRNA levels requires iron-responsive elements and a rapid turnover determinant in the 3' untranslated region of the mRNA." EMBO J 8(12): 3693-3699.

Cavadini, P., et al. (2007). "RNA silencing of the mitochondrial ABCB7 transporter in HeLa cells causes an iron-deficient phenotype with mitochondrial iron overload." Blood 109(8): 3552-3559.

Cavadini, P., et al. (2002). "Assembly and iron-binding properties of human frataxin, the protein deficient in Friedreich ataxia." Hum Mol Genet 11(3): 217-227.

Chappell, S. L., et al. (2011). "The role of IREB2 and transforming growth factor beta-1 genetic variants in COPD: a replication case-control study." BMC Med Genet 12: 24.

Chen, C. Y., et al. (2008). "Messenger RNA half-life measurements in mammalian cells." Methods Enzymol 448: 335-357.

Chen, G., et al. (2007). "Overexpression of iron regulatory protein 1 suppresses growth of tumor xenografts." Carcinogenesis 28(4): 785-791.

Chen, O. S., et al. (1997). "Dietary iron intake modulates the activity of iron regulatory proteins and the abundance of ferritin and mitochondrial aconitase in rat liver." J Nutr 127(2): 238-248.

Chen, T. T., et al. (2005). "TIM-2 is expressed on B cells and in liver and kidney and is a receptor for H-ferritin endocytosis." J Exp Med 202(7): 955-965.

Chiabrando, D., et al. (2012). "The mitochondrial heme exporter FLVCR1b mediates erythroid differentiation." J Clin Invest 122(12): 4569-4579.

Chollangi, S., et al. (2012). "Hemerythrin-like domain within F-box and leucine-rich repeat protein 5 (FBXL5) communicates cellular iron and oxygen availability by distinct mechanisms." J Biol Chem 287(28): 23710-23717.

Chung, B., et al. (2009). "Hepcidin decreases iron transporter expression in vivo in mouse duodenum and spleen and in vitro in THP-1 macrophages and intestinal Caco-2 cells." J Nutr 139(8): 1457-1462.

Cianetti, L., et al. (2005). "Expression of alternative transcripts of ferroportin-1 during human erythroid differentiation." Haematologica 90(12): 1595-1606.

Clarke, S. L., et al. (2006). "Iron-responsive degradation of iron-regulatory protein 1 does not require the Fe-S cluster." EMBO J 25(3): 544-553.

Cmejla, R., et al. (2006). "A novel iron responsive element in the 3'UTR of human MRCKalpha." Biochem Biophys Res Commun 341(1): 158-166.

Cohen, L. A., et al. (2010). "Serum ferritin is derived primarily from macrophages through a nonclassical secretory pathway." Blood 116(9): 1574-1584.

Coon, K. D., et al. (2006). "Preliminary demonstration of an allelic association of the IREB2 gene with Alzheimer's disease." J Alzheimers Dis 9(3): 225-233.

Cooperman, S. S., et al. (2005). "Microcytic anemia, erythropoietic protoporphyria, and neurodegeneration in mice with targeted deletion of iron-regulatory protein 2." Blood 106(3): 1084-1091.

Cotter, P. D., et al. (1992). "Enzymatic defect in "X-linked" sideroblastic anemia: molecular evidence for erythroid delta-aminolevulinate synthase deficiency." Proc Natl Acad Sci U S A 89(9): 4028-4032.

Cox, L. A., et al. (1993). "Posttranscriptional regulation of chimeric human transferrin genes by iron." Biochemistry 32(18): 4738-4745.

Cozzi, A., et al. (2013). "Human L-ferritin deficiency is characterized by idiopathic generalized seizures and atypical restless leg syndrome." J Exp Med 210(9): 1779-1791.

Craig, J. E., et al. (2003). "Hereditary hyperferritinemia-cataract syndrome: prevalence, lens morphology, spectrum of mutations, and clinical presentations." Arch Ophthalmol 121(12): 1753-1761.

Cremonesi, L., et al. (2003a). "Identification of two novel mutations in the 5'-untranslated region of H-ferritin using denaturing high performance liquid chromatography scanning." Haematologica 88(10): 1110-1116.

Cremonesi, L., et al. (2003b). "Scanning mutations of the 5'UTR regulatory sequence of L-ferritin by denaturing high-performance liquid chromatography: identification of new mutations." Br J Haematol 121(1): 173-179.

Crooks, D. R., et al. (2012). "Tissue specificity of a human mitochondrial disease: differentiation-enhanced mis-splicing of the Fe-S scaffold gene ISCU renders patient cells more sensitive to oxidative stress in ISCU myopathy." J Biol Chem 287(48): 40119-40130.

Culling, C. F. A., et al. (1985). Cellular pathology technique. London ; Boston, Butterworths.

Curtis, A. R., et al. (2001). "Mutation in the gene encoding ferritin light polypeptide causes dominant adult-onset basal ganglia disease." Nat Genet 28(4): 350-354.

Daher, R., et al. (2015). "Heterozygous Mutations in BMP6 Pro-peptide Lead to Inappropriate Hepcidin Synthesis and Moderate Iron Overload in Humans." Gastroenterology.

Darshan, D., et al. (2011). "Reduced expression of ferroportin-1 mediates hyporesponsiveness of suckling rats to stimuli that reduce iron absorption." Gastroenterology 141(1): 300-309.

Dautry-Varsat, A., et al. (1983). "pH and the recycling of transferrin during receptor-mediated endocytosis." Proc Natl Acad Sci U S A 80(8): 2258-2262.

De Domenico, I., et al. (2007). "Ferroxidase activity is required for the stability of cell surface ferroportin in cells expressing GPI-ceruloplasmin." EMBO J 26(12): 2823-2831.

Deck, K. M., et al. (2009). "Evidence that phosphorylation of iron regulatory protein 1 at Serine 138 destabilizes the [4Fe-4S] cluster in cytosolic aconitase by enhancing 4Fe-3Fe cycling." J Biol Chem 284(19): 12701-12709.

Delatycki, M. B., et al. (1999). "G130V, a common FRDA point mutation, appears to have arisen from a common founder." Hum Genet 105(4): 343-346.

DeMeo, D. L., et al. (2009). "Integration of genomic and genetic approaches implicates IREB2 as a COPD susceptibility gene." Am J Hum Genet 85(4): 493-502.

DeRusso, P. A., et al. (1995). "Expression of a constitutive mutant of iron regulatory protein 1 abolishes iron homeostasis in mammalian cells." J Biol Chem 270(26): 15451-15454.

Deshmane, S. L., et al. (2009). "Monocyte chemoattractant protein-1 (MCP-1): an overview." J Interferon Cytokine Res 29(6): 313-326.

Devireddy, L. R., et al. (2005). "A cell-surface receptor for lipocalin 24p3 selectively mediates apoptosis and iron uptake." Cell 123(7): 1293-1305.

Devireddy, L. R., et al. (2010). "A mammalian siderophore synthesized by an enzyme with a bacterial homolog involved in enterobactin production." Cell 141(6): 1006-1017.

Devireddy, L. R., et al. (2001). "Induction of apoptosis by a secreted lipocalin that is transcriptionally regulated by IL-3 deprivation." Science 293(5531): 829-834.

Di Nardo, A., et al. (2000). "Alternative splicing of the mouse profilin II gene generates functionally different profilin isoforms." J Cell Sci 113 Pt 21: 3795-3803.

Donovan, A., et al. (2005). "The iron exporter ferroportin/Slc40a1 is essential for iron homeostasis." Cell Metab 1(3): 191-200.

dos Santos, C. O., et al. (2008). "An iron responsive element-like stem-loop regulates alpha-hemoglobin-stabilizing protein mRNA." J Biol Chem 283(40): 26956-26964.

Duce, J. A., et al. (2010). "Iron-export ferroxidase activity of beta-amyloid precursor protein is inhibited by zinc in Alzheimer's disease." Cell 142(6): 857-867.

Dupic, F., et al. (2002). "Duodenal mRNA expression of iron related genes in response to iron loading and iron deficiency in four strains of mice." Gut 51(5): 648-653.

Dupuy, J., et al. (2006). "Crystal structure of human iron regulatory protein 1 as cytosolic aconitase." Structure 14(1): 129-139.

Dycke, C., et al. (2008). "A role for lysosomes in the turnover of human iron regulatory protein 2." Int J Biochem Cell Biol 40(12): 2826-2832.

Epsztejn, S., et al. (1997). "Fluorescence analysis of the labile iron pool of mammalian cells." Anal Biochem 248(1): 31-40.

Farhan, S. M., et al. (2014). "Exome sequencing identifies NFS1 deficiency in a novel Fe-S cluster disease, infantile mitochondrial complex II/III deficiency." Mol Genet Genomic Med 2(1): 73-80.

Faucheux, B. A., et al. (2002). "Lack of up-regulation of ferritin is associated with sustained iron regulatory protein-1 binding activity in the substantia nigra of patients with Parkinson's disease." J Neurochem 83(2): 320-330.

Fehringer, G., et al. (2012). "Association of the 15q25 and 5p15 lung cancer susceptibility regions with gene expression in lung tumor tissue." Cancer Epidemiol Biomarkers Prev 21(7): 1097-1104.

Fernandes, A., et al. (2009). "The molecular basis of hepcidin-resistant hereditary hemochromatosis." Blood 114(2): 437-443.

Ferreira, C., et al. (2000). "Early embryonic lethality of H ferritin gene deletion in mice." J Biol Chem 275(5): 3021-3024.

Ferring-Appel, D., et al. (2009). "Cell-autonomous and systemic context-dependent functions of iron regulatory protein 2 in mammalian iron metabolism." Blood 113(3): 679-687.

Fillebeen, C., et al. (2003). "A phosphomimetic mutation at Ser-138 renders iron regulatory protein 1 sensitive to iron-dependent degradation." Mol Cell Biol 23(19): 6973-6981.

Finberg, K. E., et al. (2008). "Mutations in TMPRSS6 cause iron-refractory iron deficiency anemia (IRIDA)." Nat Genet 40(5): 569-571.

Fleming, M. D., et al. (1998). "Nramp2 is mutated in the anemic Belgrade (b) rat: evidence of a role for Nramp2 in endosomal iron transport." Proc Natl Acad Sci U S A 95(3): 1148-1153.

Fleming, R. E. (2007). "Hepcidin activation during inflammation: make it STAT." Gastroenterology 132(1): 447-449.

Fosset, C., et al. (2006). "RNA silencing of mitochondrial m-Nfs1 reduces Fe-S enzyme activity both in mitochondria and cytosol of mammalian cells." J Biol Chem 281(35): 25398-25406.

Franke, K., et al. (2013). "Erythrocytosis: the HIF pathway in control." Blood 122(7): 1122-1128.

Friedlich, A. L., et al. (2007). "The 5'-untranslated region of Parkinson's disease alpha-synuclein messengerRNA contains a predicted iron responsive element." Mol Psychiatry 12(3): 222-223.

Galy, B., et al. (2013). "Iron regulatory proteins control a mucosal block to intestinal iron absorption." Cell Rep 3(3): 844-857.

Galy, B., et al. (2008). "Iron regulatory proteins are essential for intestinal function and control key iron absorption molecules in the duodenum." Cell Metab 7(1): 79-85.

Galy, B., et al. (2010). "Iron regulatory proteins secure mitochondrial iron sufficiency and function." Cell Metab 12(2): 194-201.

Galy, B., et al. (2005a). "Generation of conditional alleles of the murine Iron Regulatory Protein (IRP)-1 and -2 genes." Genesis 43(4): 181-188.

Galy, B., et al. (2005b). "Altered body iron distribution and microcytosis in mice deficient in iron regulatory protein 2 (IRP2)." Blood 106(7): 2580-2589.

Galy, B., et al. (2006). "Iron homeostasis in the brain: complete iron regulatory protein 2 deficiency without symptomatic neurodegeneration in the mouse." Nat Genet 38(9): 967-969; discussion 969-970.

Ganz, T. (2011). "Hepcidin and iron regulation, 10 years later." Blood 117(17): 4425-4433.

Gareus, R., et al. (2006). "Mouse profilin 2 regulates endocytosis and competes with SH3 ligand binding to dynamin 1." J Biol Chem 281(5): 2803-2811.

Gehring, N. H., et al. (1999). "Inactivation of both RNA binding and aconitase activities of iron regulatory protein-1 by quinone-induced oxidative stress." J Biol Chem 274(10): 6219-6225.

Gerard, C., et al. (2001). "Chemokines and disease." Nat Immunol 2(2): 108-115.

Gerber, J., et al. (2003). "An interaction between frataxin and Isu1/Nfs1 that is crucial for Fe/S cluster synthesis on Isu1." EMBO Rep 4(9): 906-911.

Ghosh, M. C., et al. (2008). "Tempol-mediated activation of latent iron regulatory protein activity prevents symptoms of neurodegenerative disease in IRP2 knockout mice." Proc Natl Acad Sci U S A 105(33): 12028-12033.

Ghosh, M. C., et al. (2013). "Deletion of iron regulatory protein 1 causes polycythemia and pulmonary hypertension in mice through translational derepression of HIF2alpha." Cell Metab 17(2): 271-281.

Giansily-Blaizot, M., et al. (2013). "Homozygous mutation of the 5'UTR region of the L-Ferritin gene in the hereditary hyperferritinemia cataract syndrome and its impact on the phenotype." Haematologica 98(4): e42-43.

Gieselmann, R., et al. (1995). "Distinct biochemical characteristics of the two human profilin isoforms." Eur J Biochem 229(3): 621-628.

Girelli, D., et al. (2001). "Clinical, biochemical and molecular findings in a series of families with hereditary hyperferritinaemia-cataract syndrome." Br J Haematol 115(2): 334-340.

Girelli, D., et al. (1995). "Molecular basis for the recently described hereditary hyperferritinemia-cataract syndrome: a mutation in the iron-responsive element of ferritin L-subunit gene (the "Verona mutation")." Blood 86(11): 4050-4053.

Goetz, D. H., et al. (2002). "The neutrophil lipocalin NGAL is a bacteriostatic agent that interferes with siderophore-mediated iron acquisition." Mol Cell 10(5): 1033-1043.

Goldschmidt-Clermont, P. J., et al. (1991). "Regulation of phospholipase C-gamma 1 by profilin and tyrosine phosphorylation." Science 251(4998): 1231-1233.

Goldschmidt-Clermont, P. J., et al. (1990). "The actin-binding protein profilin binds to PIP2 and inhibits its hydrolysis by phospholipase C." Science 247(4950): 1575-1578.

Goldwurm, S., et al. (2000). "Biochemical and genetic defects underlying human congenital hypotransferrinemia." Hematol J 1(6): 390-398.

Goswami, T., et al. (2006). "Hereditary hemochromatosis protein, HFE, interaction with transferrin receptor 2 suggests a molecular mechanism for mammalian iron sensing." J Biol Chem 281(39): 28494-28498.

Gout, I., et al. (1993). "The GTPase dynamin binds to and is activated by a subset of SH3 domains." Cell 75(1): 25-36.

Gouya, L., et al. (2006). "Contribution of a common single-nucleotide polymorphism to the genetic predisposition for erythropoietic protoporphyria." Am J Hum Genet 78(1): 2-14.

Grabs, D., et al. (1997). "The SH3 domain of amphiphysin binds the proline-rich domain of dynamin at a single site that defines a new SH3 binding consensus sequence." J Biol Chem 272(20): 13419-13425.

Graham, R. M., et al. (2007). "Liver iron transport." World J Gastroenterol 13(35): 4725-4736.

Gray, N. K., et al. (1996). "Translational regulation of mammalian and Drosophila citric acid cycle enzymes via iron-responsive elements." Proc Natl Acad Sci U S A 93(10): 4925-4930.

Gray, N. K., et al. (1993). "Recombinant iron-regulatory factor functions as an iron-responsive-element-binding protein, a translational repressor and an aconitase. A functional assay for translational repression and direct demonstration of the iron switch." Eur J Biochem 218(2): 657-667.

Green, R., et al. (1968). "Body iron excretion in man: a collaborative study." Am J Med 45(3): 336-353.

Guo, B., et al. (1995). "Characterization and expression of iron regulatory protein 2 (IRP2). Presence of multiple IRP2 transcripts regulated by intracellular iron levels." J Biol Chem 270(28): 16529-16535.

Guo, B., et al. (1994). "Iron regulates cytoplasmic levels of a novel iron-responsive element-binding protein without aconitase activity." J Biol Chem 269(39): 24252-24260.

Guo, K., et al. (2006). "Characterization of human DHRS6, an orphan short chain dehydrogenase/reductase enzyme: a novel, cytosolic type 2 R-beta-hydroxybutyrate dehydrogenase." J Biol Chem 281(15): 10291-10297.

Gutierrez, L., et al. (2009). "Iron speciation study in Hfe knockout mice tissues: magnetic and ultrastructural characterisation." Biochim Biophys Acta 1792(6): 541-547.

Haack, T. B., et al. (2013). "Homozygous missense mutation in BOLA3 causes multiple mitochondrial dysfunctions syndrome in two siblings." J Inherit Metab Dis 36(1): 55-62.

Haile, D. J., et al. (1992). "Cellular regulation of the iron-responsive element binding protein: disassembly of the cubane iron-sulfur cluster results in high-affinity RNA binding." Proc Natl Acad Sci U S A 89(24): 11735-11739.

Hansen, H. M., et al. (2010). "Fine mapping of chromosome 15q25.1 lung cancer susceptibility in African-Americans." Hum Mol Genet 19(18): 3652-3661.

Hanson, E. S., et al. (2003). "Oxygen and iron regulation of iron regulatory protein 2." J Biol Chem 278(41): 40337-40342.

Hare, D., et al. (2013). "A delicate balance: Iron metabolism and diseases of the brain." Front Aging Neurosci 5: 34.

Harrison, P. M., et al. (1996). "The ferritins: molecular properties, iron storage function and cellular regulation." Biochim Biophys Acta 1275(3): 161-203.

Harrold, S., et al. (1991). "A comparison of apparent mRNA half-life using kinetic labeling techniques vs decay following administration of transcriptional inhibitors." Anal Biochem 198(1): 19-29.

Hausmann, A., et al. (2005). "The eukaryotic P loop NTPase Nbp35: an essential component of the cytosolic and nuclear iron-sulfur protein assembly machinery." Proc Natl Acad Sci U S A 102(9): 3266-3271.

Henderson, B. R., et al. (1996). "Iron regulatory proteins 1 and 2 bind distinct sets of RNA target sequences." J Biol Chem 271(9): 4900-4908.

Henderson, B. R., et al. (1993). "Characterization of a second RNA-binding protein in rodents with specificity for iron-responsive elements." J Biol Chem 268(36): 27327-27334.

Hentze, M. W., et al. (1996). "Molecular control of vertebrate iron metabolism: mRNA-based regulatory circuits operated by iron, nitric oxide, and oxidative stress." Proc Natl Acad Sci U S A 93(16): 8175-8182.

Hentze, M. W., et al. (2004). "Balancing acts: molecular control of mammalian iron metabolism." Cell 117(3): 285-297.

Hentze, M. W., et al. (2010). "Two to tango: regulation of Mammalian iron metabolism." Cell 142(1): 24-38.

Hernandez Martin, D., et al. (2008). "[Hereditary hyperferritinemia and cataract syndrome: a de novo mutation]." An Pediatr (Barc) 68(4): 408-410.

Hetet, G., et al. (2003). "Molecular analyses of patients with hyperferritinemia and normal serum iron values reveal both L ferritin IRE and 3 new ferroportin (slc11A3) mutations." Blood 102(5): 1904-1910.

Hirling, H., et al. (1994). "Mutational analysis of the [4Fe-4S]-cluster converting iron regulatory factor from its RNA-binding form to cytoplasmic aconitase." EMBO J 13(2): 453-461.

Hubert, N., et al. (2002). "Previously uncharacterized isoforms of divalent metal transporter (DMT)-1: implications for regulation and cellular function." Proc Natl Acad Sci U S A 99(19): 12345-12350.

Hvidberg, V., et al. (2005). "Identification of the receptor scavenging hemopexin-heme complexes." Blood 106(7): 2572-2579.

Invernizzi, R., et al. (2013). "Effects of mitochondrial ferritin overexpression in normal and sideroblastic erythroid progenitors." Br J Haematol 161(5): 726-737.

Itkonen, O., et al. (2012). "Binding of hepcidin to plasma proteins." Clin Chem 58(7): 1158-1160.

Iwai, K., et al. (1995). "Requirements for iron-regulated degradation of the RNA binding protein, iron regulatory protein 2." EMBO J 14(21): 5350-5357.

Jabara, H. H., et al. (2016). "A missense mutation in TFRC, encoding transferrin receptor 1, causes combined immunodeficiency." Nat Genet 48(1): 74-78.

Jeong, S. Y., et al. (2011). "Iron insufficiency compromises motor neurons and their mitochondrial function in Irp2-null mice." PLoS One 6(10): e25404.

Joshi, R., et al. (2012). Cellular Iron Metabolism – The IRP/IRE Regulatory Network. Iron Metabolism, InTech.

Kamei, A., et al. (2010). "Dietary iron-deficient anemia induces a variety of metabolic changes and even apoptosis in rat liver: a DNA microarray study." Physiol Genomics 42(2): 149-156.

Kannengiesser, C., et al. (2009). "A new missense mutation in the L ferritin coding sequence associated with elevated levels of glycosylated ferritin in serum and absence of iron overload." Haematologica 94(3): 335-339.

Kanwar, P., et al. (2013). "Diagnosis and treatment of hereditary hemochromatosis: an update." Expert Rev Gastroenterol Hepatol 7(6): 517-530.

Kato, J., et al. (2001). "A mutation, in the iron-responsive element of H ferritin mRNA, causing autosomal dominant iron overload." Am J Hum Genet 69(1): 191-197.

Kautz, L., et al. (2014). "Identification of erythroferrone as an erythroid regulator of iron metabolism." Nat Genet 46(7): 678-684.

Kautz, L., et al. (2008). "Iron regulates phosphorylation of Smad1/5/8 and gene expression of Bmp6, Smad7, Id1, and Atoh8 in the mouse liver." Blood 112(4): 1503-1509.

Keel, S. B., et al. (2008). "A heme export protein is required for red blood cell differentiation and iron homeostasis." Science 319(5864): 825-828.

Kerenyi, M. A., et al. (2008). "Stat5 regulates cellular iron uptake of erythroid cells via IRP-2 and TfR-1." Blood 112(9): 3878-3888.

Kidane, T. Z., et al. (2006). "Release of iron from ferritin requires lysosomal activity." Am J Physiol Cell Physiol 291(3): C445-455.

Kim, S., et al. (2004). "S-nitrosylation of IRP2 regulates its stability via the ubiquitin-proteasome pathway." Mol Cell Biol 24(1): 330-337.

Kispal, G., et al. (1997). "The ABC transporter Atm1p is required for mitochondrial iron homeostasis." FEBS Lett 418(3): 346-350.

Kohler, S. A., et al. (1999). "Molecular cloning of mouse glycolate oxidase. High evolutionary conservation and presence of an iron-responsive element-like sequence in the mRNA." J Biol Chem 274(4): 2401-2407.

Kohn, M., et al. (2010). "Near-infrared (NIR) dye-labeled RNAs identify binding of ZBP1 to the noncoding Y3-RNA." RNA 16(7): 1420-1428.

Kozyraki, R., et al. (2001). "Megalin-dependent cubilin-mediated endocytosis is a major pathway for the apical uptake of transferrin in polarized epithelia." Proc Natl Acad Sci U S A 98(22): 12491-12496.

Kramer, A., et al. (2014). "Causal analysis approaches in Ingenuity Pathway Analysis." Bioinformatics 30(4): 523-530.

Krause, A., et al. (2000). "LEAP-1, a novel highly disulfide-bonded human peptide, exhibits antimicrobial activity." FEBS Lett 480(2-3): 147-150.

Kristiansen, M., et al. (2001). "Identification of the haemoglobin scavenger receptor." Nature 409(6817): 198-201.

Kulaksiz, H., et al. (2008). "Pancreatic beta-cells express hepcidin, an iron-uptake regulatory peptide." J Endocrinol 197(2): 241-249.

Kulaksiz, H., et al. (2005). "The iron-regulatory peptide hormone hepcidin: expression and cellular localization in the mammalian kidney." J Endocrinol 184(2): 361-370.

Laemmli, U. K. (1970). "Cleavage of structural proteins during the assembly of the head of bacteriophage T4." Nature 227(5259): 680-685.

Lambrechts, A., et al. (2000). "Profilin II is alternatively spliced, resulting in profilin isoforms that are differentially expressed and have distinct biochemical properties." Mol Cell Biol 20(21): 8209-8219.

Lambrechts, A., et al. (1997). "The mammalian profilin isoforms display complementary affinities for PIP2 and proline-rich sequences." EMBO J 16(3): 484-494.

Lamoril, J., et al. (1991). "Human erythropoietic protoporphyria: two point mutations in the ferrochelatase gene." Biochem Biophys Res Commun 181(2): 594-599.

Lane, R. S. (1966). "Changes in plasma transferrin levels following the adminstration of iron." Br J Haematol 12(3): 249-258.

Lassing, I., et al. (1985). "Specific interaction between phosphatidylinositol 4,5-bisphosphate and profilactin." Nature 314(6010): 472-474.

LaVaute, T., et al. (2001). "Targeted deletion of the gene encoding iron regulatory protein-2 causes misregulation of iron metabolism and neurodegenerative disease in mice." Nat Genet 27(2): 209-214.

Le, N. T., et al. (2002). "The role of iron in cell cycle progression and the proliferation of neoplastic cells." Biochim Biophys Acta 1603(1): 31-46.
Lee, P., et al. (2009). "Severe iron overload with a novel aminolevulinate synthase mutation and hepatitis C infection. A case report." Blood Cells Mol Dis 42(1): 1-4.
Leimberg, M. J., et al. (2008). "Macrophages function as a ferritin iron source for cultured human erythroid precursors." J Cell Biochem 103(4): 1211-1218.
Levy, J. E., et al. (1999). "Transferrin receptor is necessary for development of erythrocytes and the nervous system." Nat Genet 21(4): 396-399.
Li, J. Y., et al. (2009). "Scara5 is a ferritin receptor mediating non-transferrin iron delivery." Dev Cell 16(1): 35-46.
Li, K., et al. (2008). "Iron-dependent regulation of frataxin expression: implications for treatment of Friedreich ataxia." Hum Mol Genet 17(15): 2265-2273.
Lill, R., et al. (2008). "Maturation of iron-sulfur proteins in eukaryotes: mechanisms, connected processes, and diseases." Annu Rev Biochem 77: 669-700.
Lim, S. C., et al. (2013). "Mutations in LYRM4, encoding iron-sulfur cluster biogenesis factor ISD11, cause deficiency of multiple respiratory chain complexes." Hum Mol Genet 22(22): 4460-4473.
Lin, E., et al. (2001). "Regulation of the 75-kDa subunit of mitochondrial complex I by iron." J Biol Chem 276(29): 27685-27692.
Liu, G., et al. (2013). Novel heterozygous missense mutations in GLRX5 gene of a chinese patient affected by sideroblastic anemia. Fifth Congress of the Internation BioIron Society (IBIS). London.
Liu, Q., et al. (1995). "Identification of a new acute phase protein." J Biol Chem 270(38): 22565-22570.
Liu, W., et al. (2005). "Hemochromatosis with mutation of the ferroportin 1 (IREG1) gene." Intern Med 44(4): 285-289.
Liu, Z., et al. (2012). "Siderophore-mediated iron trafficking in humans is regulated by iron." J Mol Med (Berl) 90(10): 1209-1221.
Lovell, M. A., et al. (1998). "Copper, iron and zinc in Alzheimer's disease senile plaques." J Neurol Sci 158(1): 47-52.
Lu, J., et al. (2001). "Profilin binding to poly-L-proline and actin monomers along with ability to catalyze actin nucleotide exchange is required for viability of fission yeast." Mol Biol Cell 12(4): 1161-1175.
Luscieti, S., et al. (2013). "Novel mutations in the ferritin-L iron-responsive element that only mildly impair IRP binding cause hereditary hyperferritinaemia cataract syndrome." Orphanet J Rare Dis 8: 30.
Maffettone, C., et al. (2010). "Tumorigenic properties of iron regulatory protein 2 (IRP2) mediated by its specific 73-amino acids insert." PLoS One 5(4): e10163.
Mastrogiannaki, M., et al. (2009). "HIF-2alpha, but not HIF-1alpha, promotes iron absorption in mice." J Clin Invest 119(5): 1159-1166.
Mayr, R., et al. (2010). "Ferroportin disease: a systematic meta-analysis of clinical and molecular findings." J Hepatol 53(5): 941-949.
McKie, A. T., et al. (2000). "A novel duodenal iron-regulated transporter, IREG1, implicated in the basolateral transfer of iron to the circulation." Mol Cell 5(2): 299-309.
McLeod, J. L., et al. (2002). "Mutation spectrum in Australian pedigrees with hereditary hyperferritinaemia-cataract syndrome reveals novel and de novo mutations." Br J Haematol 118(4): 1179-1182.
Meehan, H. A., et al. (2001). "The hairpin loop but not the bulged C of the iron responsive element is essential for high affinity binding to iron regulatory protein-1." J Biol Chem 276(18): 14791-14796.
Meilinger, M., et al. (1995). "Removal of lactoferrin from plasma is mediated by binding to low density lipoprotein receptor-related protein/alpha 2-macroglobulin receptor and transport to endosomes." FEBS Lett 360(1): 70-74.
Melis, M. A., et al. (2008). "A mutation in the TMPRSS6 gene, encoding a transmembrane serine protease that suppresses hepcidin production, in familial iron deficiency anemia refractory to oral iron." Haematologica 93(10): 1473-1479.

Merkofer, M., et al. (2006). "Fenton chemistry and iron chelation under physiologically relevant conditions: Electrochemistry and kinetics." Chem Res Toxicol 19(10): 1263-1269.
Merle, U., et al. (2007). "The iron regulatory peptide hepcidin is expressed in the heart and regulated by hypoxia and inflammation." Endocrinology 148(6): 2663-2668.
Meynard, D., et al. (2009). "Lack of the bone morphogenetic protein BMP6 induces massive iron overload." Nat Genet 41(4): 478-481.
Meyron-Holtz, E. G., et al. (2004). "Genetic ablations of iron regulatory proteins 1 and 2 reveal why iron regulatory protein 2 dominates iron homeostasis." EMBO J 23(2): 386-395.
Mochel, F., et al. (2008). "Splice mutation in the iron-sulfur cluster scaffold protein ISCU causes myopathy with exercise intolerance." Am J Hum Genet 82(3): 652-660.
Mok, H., et al. (2004). "Disruption of ferroportin 1 regulation causes dynamic alterations in iron homeostasis and erythropoiesis in polycythaemia mice." Development 131(8): 1859-1868.
Morales, M., et al. (2000). "Actin-dependent regulation of neurotransmitter release at central synapses." Neuron 27(3): 539-550.
Morgan, E. H., et al. (1983). Synthesis and secretion of transferrin. Plasma Protein Secretion by the Liver, Academic Press, New York. 4**:** 96-101.
Moroishi, T., et al. (2011). "The FBXL5-IRP2 axis is integral to control of iron metabolism in vivo." Cell Metab 14(3): 339-351.
Mosmann, T. (1983). "Rapid colorimetric assay for cellular growth and survival: application to proliferation and cytotoxicity assays." J Immunol Methods 65(1-2): 55-63.
Muckenthaler, M., et al. (1998). "IRP-1 binding to ferritin mRNA prevents the recruitment of the small ribosomal subunit by the cap-binding complex eIF4F." Mol Cell 2(3): 383-388.
Muckenthaler, M., et al. (2003a). "Relationships and distinctions in iron-regulatory networks responding to interrelated signals." Blood 101(9): 3690-3698.
Muckenthaler, M., et al. (2003b). "Regulatory defects in liver and intestine implicate abnormal hepcidin and Cybrd1 expression in mouse hemochromatosis." Nat Genet 34(1): 102-107.
Muckenthaler, M., et al. (2011). A High Through-Put Screen Identifies MCP-1 (CCL2) As a Novel Regulator of Iron Homeostasis and a Modifier of Hereditary Hemochromatosis Disease Severity. 53rd ASH Annual Meeting and Exposition. San Diego.
Muckenthaler, M. U., et al. (2008). "Systemic iron homeostasis and the iron-responsive element/iron-regulatory protein (IRE/IRP) regulatory network." Annu Rev Nutr 28: 197-213.
Mueller, S. (2005). "Iron regulatory protein 1 as a sensor of reactive oxygen species." Biofactors 24(1-4): 171-181.
Muhlenhoff, U., et al. (2003). "Components involved in assembly and dislocation of iron-sulfur clusters on the scaffold protein Isu1p." EMBO J 22(18): 4815-4825.
Muhlenhoff, U., et al. (2002). "The yeast frataxin homolog Yfh1p plays a specific role in the maturation of cellular Fe/S proteins." Hum Mol Genet 11(17): 2025-2036.
Mullner, E. W., et al. (1989). "A specific mRNA binding factor regulates the iron-dependent stability of cytoplasmic transferrin receptor mRNA." Cell 58(2): 373-382.
Mumford, A. D., et al. (1998). "Hereditary hyperferritinemia-cataract syndrome: two novel mutations in the L-ferritin iron-responsive element." Blood 91(1): 367-368.
Munoz-Munoz, J., et al. (2013). "Hereditary hyperferritinemia cataract syndrome in four patients with mutations in the IRE of the FTL gene." Clin Genet 83(5): 491-493.
Navarro-Sastre, A., et al. (2011). "A fatal mitochondrial disease is associated with defective NFU1 function in the maturation of a subset of mitochondrial Fe-S proteins." Am J Hum Genet 89(5): 656-667.
Neilands, J. B. (1995). "Siderophores: structure and function of microbial iron transport compounds." J Biol Chem 270(45): 26723-26726.
Nemeth, E., et al. (2004). "Hepcidin regulates cellular iron efflux by binding to ferroportin and inducing its internalization." Science 306(5704): 2090-2093.
Neonaki, M., et al. (2002). "Down-regulation of liver iron-regulatory protein 1 in haemochromatosis." Biochem Soc Trans 30(4): 726-728.

Nicolas, G., et al. (2001). "Lack of hepcidin gene expression and severe tissue iron overload in upstream stimulatory factor 2 (USF2) knockout mice." Proc Natl Acad Sci U S A 98(15): 8780-8785.

Nilsson, R., et al. (2009). "Discovery of genes essential for heme biosynthesis through large-scale gene expression analysis." Cell Metab 10(2): 119-130.

Ohgami, R. S., et al. (2005). "Identification of a ferrireductase required for efficient transferrin-dependent iron uptake in erythroid cells." Nat Genet 37(11): 1264-1269.

Ohgami, R. S., et al. (2006). "The Steap proteins are metalloreductases." Blood 108(4): 1388-1394.

Okamoto, P. M., et al. (1997). "Role of the basic, proline-rich region of dynamin in Src homology 3 domain binding and endocytosis." J Biol Chem 272(17): 11629-11635.

Oliveira, S. J., et al. (2009). "ER stress-inducible factor CHOP affects the expression of hepcidin by modulating C/EBPalpha activity." PLoS One 4(8): e6618.

Olsson, A., et al. (2008). "Myopathy with lactic acidosis is linked to chromosome 12q23.3-24.11 and caused by an intron mutation in the ISCU gene resulting in a splicing defect." Hum Mol Genet 17(11): 1666-1672.

Ordway, G. A., et al. (2004). "Myoglobin: an essential hemoprotein in striated muscle." J Exp Biol 207(Pt 20): 3441-3446.

Oudit, G. Y., et al. (2003). "L-type Ca2+ channels provide a major pathway for iron entry into cardiomyocytes in iron-overload cardiomyopathy." Nat Med 9(9): 1187-1194.

Pak, M., et al. (2006). "Suppression of hepcidin during anemia requires erythropoietic activity." Blood 108(12): 3730-3735.

Pantopoulos, K., et al. (1998). "Activation of iron regulatory protein-1 by oxidative stress in vitro." Proc Natl Acad Sci U S A 95(18): 10559-10563.

Paradkar, P. N., et al. (2009). "Regulation of mitochondrial iron import through differential turnover of mitoferrin 1 and mitoferrin 2." Mol Cell Biol 29(4): 1007-1016.

Park, C. H., et al. (2001). "Hepcidin, a urinary antimicrobial peptide synthesized in the liver." J Biol Chem 276(11): 7806-7810.

Parkinson, M. H., et al. (2013). "Clinical features of Friedreich's ataxia: classical and atypical phenotypes." J Neurochem 126 Suppl 1: 103-117.

Patel, B. N., et al. (2002). "Ceruloplasmin regulates iron levels in the CNS and prevents free radical injury." J Neurosci 22(15): 6578-6586.

Patel, P. I., et al. (2001). "Friedreich ataxia: from GAA triplet-repeat expansion to frataxin deficiency." Am J Hum Genet 69(1): 15-24.

Peslova, G., et al. (2009). "Hepcidin, the hormone of iron metabolism, is bound specifically to alpha-2-macroglobulin in blood." Blood 113(24): 6225-6236.

Petrat, F., et al. (2003). "Reduction of Fe(III) ions complexed to physiological ligands by lipoyl dehydrogenase and other flavoenzymes in vitro: implications for an enzymatic reduction of Fe(III) ions of the labile iron pool." J Biol Chem 278(47): 46403-46413.

Peyssonnaux, C., et al. (2006). "TLR4-dependent hepcidin expression by myeloid cells in response to bacterial pathogens." Blood 107(9): 3727-3732.

Peyssonnaux, C., et al. (2007). "Regulation of iron homeostasis by the hypoxia-inducible transcription factors (HIFs)." J Clin Invest 117(7): 1926-1932.

Pietrangelo, A. (2004). "The ferroportin disease." Blood Cells Mol Dis 32(1): 131-138.

Pigeon, C., et al. (2001). "A new mouse liver-specific gene, encoding a protein homologous to human antimicrobial peptide hepcidin, is overexpressed during iron overload." J Biol Chem 276(11): 7811-7819.

Pilo Boyl, P., et al. (2007). "Profilin2 contributes to synaptic vesicle exocytosis, neuronal excitability, and novelty-seeking behavior." EMBO J 26(12): 2991-3002.

Pinilla-Tenas, J. J., et al. (2011). "Zip14 is a complex broad-scope metal-ion transporter whose functional properties support roles in the cellular uptake of zinc and nontransferrin-bound iron." Am J Physiol Cell Physiol 301(4): C862-871.

Pondarre, C., et al. (2006). "The mitochondrial ATP-binding cassette transporter Abcb7 is essential in mice and participates in cytosolic iron-sulfur cluster biogenesis." Hum Mol Genet 15(6): 953-964.

Ponka, P. (1997). "Tissue-specific regulation of iron metabolism and heme synthesis: distinct control mechanisms in erythroid cells." Blood 89(1): 1-25.

Puccio, H., et al. (2002). "Friedreich ataxia: a paradigm for mitochondrial diseases." Curr Opin Genet Dev 12(3): 272-277.

Puccio, H., et al. (2001). "Mouse models for Friedreich ataxia exhibit cardiomyopathy, sensory nerve defect and Fe-S enzyme deficiency followed by intramitochondrial iron deposits." Nat Genet 27(2): 181-186.

Qian, Z. M., et al. (2011). "Divalent metal transporter 1 is a hypoxia-inducible gene." J Cell Physiol 226(6): 1596-1603.

Qiao, B., et al. (2012). "Hepcidin-induced endocytosis of ferroportin is dependent on ferroportin ubiquitination." Cell Metab 15(6): 918-924.

Rajagopal, A., et al. (2008). "Haem homeostasis is regulated by the conserved and concerted functions of HRG-1 proteins." Nature 453(7198): 1127-1131.

Ramos, E., et al. (2011). "Evidence for distinct pathways of hepcidin regulation by acute and chronic iron loading in mice." Hepatology 53(4): 1333-1341.

Richardson, D. R., et al. (2010). "Mitochondrial iron trafficking and the integration of iron metabolism between the mitochondrion and cytosol." Proc Natl Acad Sci U S A 107(24): 10775-10782.

Riddick, D. S., et al. (2013). "NADPH-cytochrome P450 oxidoreductase: roles in physiology, pharmacology, and toxicology." Drug Metab Dispos 41(1): 12-23.

Robbins, A. H., et al. (1989). "The structure of aconitase." Proteins 5(4): 289-312.

Rodriguez-Manzaneque, M. T., et al. (2002). "Grx5 is a mitochondrial glutaredoxin required for the activity of iron/sulfur enzymes." Mol Biol Cell 13(4): 1109-1121.

Rogers, J. T., et al. (2002). "An iron-responsive element type II in the 5'-untranslated region of the Alzheimer's amyloid precursor protein transcript." J Biol Chem 277(47): 45518-45528.

Rouault, T. A., et al. (1992). "An iron-sulfur cluster plays a novel regulatory role in the iron-responsive element binding protein." Biometals 5(3): 131-140.

Roux, A., et al. (2006). "GTP-dependent twisting of dynamin implicates constriction and tension in membrane fission." Nature 441(7092): 528-531.

Roy, A., et al. (2003). "A novel eukaryotic factor for cytosolic Fe-S cluster assembly." EMBO J 22(18): 4826-4835.

Ruiz, J. C., et al. (2013). "F-box and leucine-rich repeat protein 5 (FBXL5) is required for maintenance of cellular and systemic iron homeostasis." J Biol Chem 288(1): 552-560.

Salahudeen, A. A., et al. (2009). "An E3 ligase possessing an iron-responsive hemerythrin domain is a regulator of iron homeostasis." Science 326(5953): 722-726.

Sanchez, M., et al. (2006). "Iron regulation and the cell cycle: identification of an iron-responsive element in the 3'-untranslated region of human cell division cycle 14A mRNA by a refined microarray-based screening strategy." J Biol Chem 281(32): 22865-22874.

Sanchez, M., et al. (2007). "Iron-regulatory proteins limit hypoxia-inducible factor-2alpha expression in iron deficiency." Nat Struct Mol Biol 14(5): 420-426.

Sanchez, M., et al. (2011). "Iron regulatory protein-1 and -2: transcriptome-wide definition of binding mRNAs and shaping of the cellular proteome by iron regulatory proteins." Blood 118(22): e168-179.

Santambrogio, P., et al. (2007). "Mitochondrial ferritin expression in adult mouse tissues." J Histochem Cytochem 55(11): 1129-1137.

Schipper, H. M. (2012). "Neurodegeneration with brain iron accumulation - clinical syndromes and neuroimaging." Biochim Biophys Acta 1822(3): 350-360.

Schmidt, A., et al. (1999). "Endophilin I mediates synaptic vesicle formation by transfer of arachidonate to lysophosphatidic acid." Nature 401(6749): 133-141.

Schranzhofer, M., et al. (2006). "Remodeling the regulation of iron metabolism during erythroid differentiation to ensure efficient heme biosynthesis." Blood 107(10): 4159-4167.

Seyda, A., et al. (2001). "A novel syndrome affecting multiple mitochondrial functions, located by microcell-mediated transfer to chromosome 2p14-2p13." Am J Hum Genet 68(2): 386-396.
Shah, Y. M., et al. (2009). "Intestinal hypoxia-inducible transcription factors are essential for iron absorption following iron deficiency." Cell Metab 9(2): 152-164.
Shan, Y., et al. (2012). "HSC20 interacts with frataxin and is involved in iron-sulfur cluster biogenesis and iron homeostasis." Hum Mol Genet 21(7): 1457-1469.
Shaw, G. C., et al. (2006). "Mitoferrin is essential for erythroid iron assimilation." Nature 440(7080): 96-100.
Sheftel, A., et al. (2010a). "Iron-sulfur proteins in health and disease." Trends Endocrinol Metab 21(5): 302-314.
Sheftel, A. D., et al. (2010b). "Humans possess two mitochondrial ferredoxins, Fdx1 and Fdx2, with distinct roles in steroidogenesis, heme, and Fe/S cluster biosynthesis." Proc Natl Acad Sci U S A 107(26): 11775-11780.
Sheftel, A. D., et al. (2012). "The human mitochondrial ISCA1, ISCA2, and IBA57 proteins are required for [4Fe-4S] protein maturation." Mol Biol Cell 23(7): 1157-1166.
Sheftel, A. D., et al. (2007). "Direct interorganellar transfer of iron from endosome to mitochondrion." Blood 110(1): 125-132.
Shi, Y., et al. (2012). "Both human ferredoxins 1 and 2 and ferredoxin reductase are important for iron-sulfur cluster biogenesis." Biochim Biophys Acta 1823(2): 484-492.
Shi, Y., et al. (2009). "Human ISD11 is essential for both iron-sulfur cluster assembly and maintenance of normal cellular iron homeostasis." Hum Mol Genet 18(16): 3014-3025.
Shindo, M., et al. (2006). "Functional role of DMT1 in transferrin-independent iron uptake by human hepatocyte and hepatocellular carcinoma cell, HLF." Hepatol Res 35(3): 152-162.
Shu, C., et al. (2012). "The structural basis of iron sensing by the human F-box protein FBXL5." Chembiochem 13(6): 788-791.
Shupliakov, O., et al. (2002). "Impaired recycling of synaptic vesicles after acute perturbation of the presynaptic actin cytoskeleton." Proc Natl Acad Sci U S A 99(22): 14476-14481.
Silvestri, L., et al. (2008). "The serine protease matriptase-2 (TMPRSS6) inhibits hepcidin activation by cleaving membrane hemojuvelin." Cell Metab 8(6): 502-511.
Slepnev, V. I., et al. (1998). "Role of phosphorylation in regulation of the assembly of endocytic coat complexes." Science 281(5378): 821-824.
Smith, S. R., et al. (2004). "Severity of neurodegeneration correlates with compromise of iron metabolism in mice with iron regulatory protein deficiencies." Ann N Y Acad Sci 1012: 65-83.
Smith, S. R., et al. (2006). "Complete loss of iron regulatory proteins 1 and 2 prevents viability of murine zygotes beyond the blastocyst stage of embryonic development." Blood Cells Mol Dis 36(2): 283-287.
Song, D., et al. (2009). "Human ISCA1 interacts with IOP1/NARFL and functions in both cytosolic and mitochondrial iron-sulfur protein biogenesis." J Biol Chem 284(51): 35297-35307.
Spiegel, R., et al. (2013). "Deleterious mutation in FDX1L gene is associated with a novel mitochondrial muscle myopathy." Eur J Hum Genet.
Spiegel, R., et al. (2014). "Deleterious mutation in FDX1L gene is associated with a novel mitochondrial muscle myopathy." Eur J Hum Genet 22(7): 902-906.
Srinivasan, G., et al. (2012). "Lipocalin 2 deficiency dysregulates iron homeostasis and exacerbates endotoxin-induced sepsis." J Immunol 189(4): 1911-1919.
Stangl, G. I., et al. (1998). "Different degrees of moderate iron deficiency modulate lipid metabolism of rats." Lipids 33(9): 889-895.
Synowiec, E., et al. (2012). "Genetic polymorphism of the iron-regulatory protein-1 and -2 genes in age-related macular degeneration." Mol Biol Rep 39(6): 7077-7087.
Tacchini, L., et al. (1997). "Induction of ferritin synthesis in ischemic-reperfused rat liver: analysis of the molecular mechanisms." Gastroenterology 113(3): 946-953.
Takei, K., et al. (1999). "Functional partnership between amphiphysin and dynamin in clathrin-mediated endocytosis." Nat Cell Biol 1(1): 33-39.

Takenawa, T., et al. (2001). "Phosphoinositides, key molecules for regulation of actin cytoskeletal organization and membrane traffic from the plasma membrane." Biochim Biophys Acta 1533(3): 190-206.

Tanno, T., et al. (2007). "High levels of GDF15 in thalassemia suppress expression of the iron regulatory protein hepcidin." Nat Med 13(9): 1096-1101.

Tanno, T., et al. (2009). "Identification of TWSG1 as a second novel erythroid regulator of hepcidin expression in murine and human cells." Blood 114(1): 181-186.

Taylor, M., et al. (2011). "Hypoxia-inducible factor-2alpha mediates the adaptive increase of intestinal ferroportin during iron deficiency in mice." Gastroenterology 140(7): 2044-2055.

Thompson, J. W., et al. (2012). "Structural and molecular characterization of iron-sensing hemerythrin-like domain within F-box and leucine-rich repeat protein 5 (FBXL5)." J Biol Chem 287(10): 7357-7365.

Thorstensen, K., et al. (1990). "The role of transferrin in the mechanism of cellular iron uptake." Biochem J 271(1): 1-9.

Thurlow, V., et al. (2012). "Two novel mutations in the L ferritin coding sequence associated with benign hyperferritinaemia unmasked by glycosylated ferritin assay." Ann Clin Biochem 49(Pt 3): 302-305.

Torrance, J. D., et al. (1968). "A simple technique for measuring storage iron concentrations in formalinised liver samples." S Afr J Med Sci 33(1): 9-11.

Torti, F. M., et al. (2002). "Regulation of ferritin genes and protein." Blood 99(10): 3505-3516.

Trenor, C. C., 3rd, et al. (2000). "The molecular defect in hypotransferrinemic mice." Blood 96(3): 1113-1118.

van der Bliek, A. M., et al. (1993). "Mutations in human dynamin block an intermediate stage in coated vesicle formation." J Cell Biol 122(3): 553-563.

Vanoaica, L., et al. (2010). "Intestinal ferritin H is required for an accurate control of iron absorption." Cell Metab 12(3): 273-282.

Vashisht, A. A., et al. (2009). "Control of iron homeostasis by an iron-regulated ubiquitin ligase." Science 326(5953): 718-721.

Vecchi, C., et al. (2009). "ER stress controls iron metabolism through induction of hepcidin." Science 325(5942): 877-880.

Viatte, L., et al. (2009). "In vivo role(s) of the iron regulatory proteins (IRP) 1 and 2 in aseptic local inflammation." J Mol Med (Berl) 87(9): 913-921.

Vidal, R., et al. (2004). "Intracellular ferritin accumulation in neural and extraneural tissue characterizes a neurodegenerative disease associated with a mutation in the ferritin light polypeptide gene." J Neuropathol Exp Neurol 63(4): 363-380.

Waheed, A., et al. (1999). "Association of HFE protein with transferrin receptor in crypt enterocytes of human duodenum." Proc Natl Acad Sci U S A 96(4): 1579-1584.

Walden, W. E., et al. (2006). "Structure of dual function iron regulatory protein 1 complexed with ferritin IRE-RNA." Science 314(5807): 1903-1908.

Wallander, M. L., et al. (2008). "Iron-independent phosphorylation of iron regulatory protein 2 regulates ferritin during the cell cycle." J Biol Chem 283(35): 23589-23598.

Wang, C. Y., et al. (2012). "ZIP8 is an iron and zinc transporter whose cell-surface expression is up-regulated by cellular iron loading." J Biol Chem 287(41): 34032-34043.

Wang, J., et al. (2008). "Insights on regulation and function of the iron regulatory protein 1 (IRP1)." Hemoglobin 32(1-2): 109-115.

Wang, J., et al. (2004). "Iron-mediated degradation of IRP2, an unexpected pathway involving a 2-oxoglutarate-dependent oxygenase activity." Mol Cell Biol 24(3): 954-965.

Wang, J., et al. (2005a). "Nitric oxide inhibits the degradation of IRP2." Mol Cell Biol 25(4): 1347-1353.

Wang, J., et al. (2002). "Conditional derepression of ferritin synthesis in cells expressing a constitutive IRP1 mutant." Mol Cell Biol 22(13): 4638-4651.

Wang, R. H., et al. (2005b). "A role of SMAD4 in iron metabolism through the positive regulation of hepcidin expression." Cell Metab 2(6): 399-409.

Wardrop, S. L., et al. (1999). "The effect of intracellular iron concentration and nitrogen monoxide on Nramp2 expression and non-transferrin-bound iron uptake." Eur J Biochem 263(1): 41-49.
Whatley, S. D., et al. (2008). "C-terminal deletions in the ALAS2 gene lead to gain of function and cause X-linked dominant protoporphyria without anemia or iron overload." Am J Hum Genet 83(3): 408-414.
White, K., et al. (1988). "Induction of ferritin subunit synthesis by iron is regulated at both the transcriptional and translational levels." J Biol Chem 263(18): 8938-8942.
Whitnall, M., et al. (2012). "Identification of nonferritin mitochondrial iron deposits in a mouse model of Friedreich ataxia." Proc Natl Acad Sci U S A 109(50): 20590-20595.
Wilkinson, N., et al. (2013). "IRP1 regulates erythropoiesis and systemic iron homeostasis by controlling HIF2alpha mRNA translation." Blood 122(9): 1658-1668.
Wilkinson, N., et al. (2014). "The IRP/IRE system in vivo: insights from mouse models." Front Pharmacol 5: 176.
Wingert, R. A., et al. (2005). "Deficiency of glutaredoxin 5 reveals Fe-S clusters are required for vertebrate haem synthesis." Nature 436(7053): 1035-1039.
Wish, J. B. (2006). "Assessing iron status: beyond serum ferritin and transferrin saturation." Clin J Am Soc Nephrol 1 Suppl 1: S4-8.
Witke, W. (2004). "The role of profilin complexes in cell motility and other cellular processes." Trends Cell Biol 14(8): 461-469.
Witke, W., et al. (1998). "In mouse brain profilin I and profilin II associate with regulators of the endocytic pathway and actin assembly." EMBO J 17(4): 967-976.
Witke, W., et al. (2001). "Profilin I is essential for cell survival and cell division in early mouse development." Proc Natl Acad Sci U S A 98(7): 3832-3836.
Wu, K. J., et al. (1999). "Coordinated regulation of iron-controlling genes, H-ferritin and IRP2, by c-MYC." Science 283(5402): 676-679.
Yang, J., et al. (2002). "An iron delivery pathway mediated by a lipocalin." Mol Cell 10(5): 1045-1056.
Yang, X. R., et al. (2010). "Associations of 9p21 variants with cutaneous malignant melanoma, nevi, and pigmentation phenotypes in melanoma-prone families with and without CDKN2A mutations." Fam Cancer 9(4): 625-633.
Ye, H., et al. (2010). "Glutaredoxin 5 deficiency causes sideroblastic anemia by specifically impairing heme biosynthesis and depleting cytosolic iron in human erythroblasts." J Clin Invest 120(5): 1749-1761.
Youdim, M. B. (2008). "Brain iron deficiency and excess; cognitive impairment and neurodegeneration with involvement of striatum and hippocampus." Neurotox Res 14(1): 45-56.
Zanella, I., et al. (2008). "The effects of frataxin silencing in HeLa cells are rescued by the expression of human mitochondrial ferritin." Biochim Biophys Acta 1782(2): 90-98.
Zhang, D. L., et al. (2009). "A ferroportin transcript that lacks an iron-responsive element enables duodenal and erythroid precursor cells to evade translational repression." Cell Metab 9(5): 461-473.
Zhang, D. L., et al. (2011). "Hepcidin regulates ferroportin expression and intracellular iron homeostasis of erythroblasts." Blood 118(10): 2868-2877.
Zheng, J., et al. (1996). "Identification of the binding site for acidic phospholipids on the pH domain of dynamin: implications for stimulation of GTPase activity." J Mol Biol 255(1): 14-21.
Zimelman, A. P., et al. (1977). "Effect of iron saturation of transferrin on hepatic iron uptake: an in vitro study." Gastroenterology 72(1): 129-131.
Zimmer, M., et al. (2008). "Small-molecule inhibitors of HIF-2a translation link its 5'UTR iron-responsive element to oxygen sensing." Mol Cell 32(6): 838-848.
Zumbrennen-Bullough, K. B., et al. (2014). "Abnormal brain iron metabolism in Irp2 deficient mice is associated with mild neurological and behavioral impairments." PLoS One 9(6): e98072.
Zumbrennen, K. B., et al. (2009). "Cysteine oxidation regulates the RNA-binding activity of iron regulatory protein 2." Mol Cell Biol 29(8): 2219-2229.

6. APPENDIX

6.1 Supplementary Figures

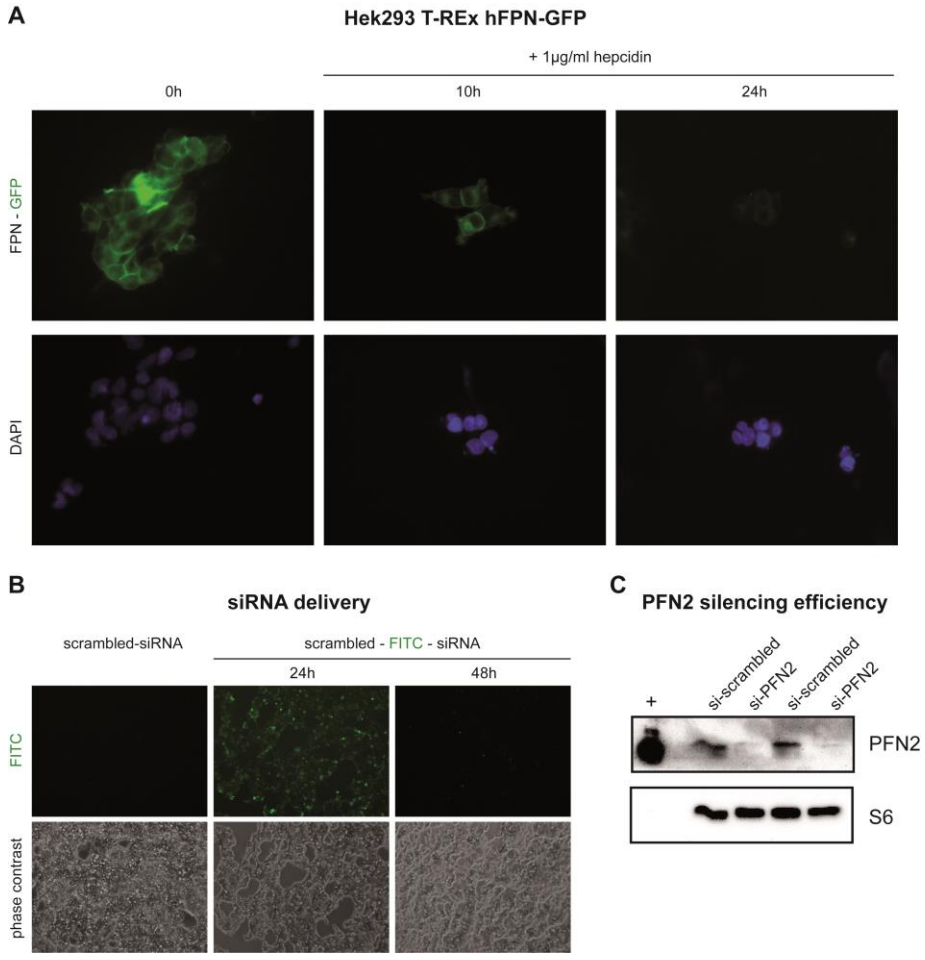

Supp. Figure 6.1 T-REx hFPN-GFP Hek293 reporter system and hPFN silencing efficiency. (A) This Hek293 cell clone (kind gift of Prof. Elizabeta Nemeth, University of California) (Qiao *et al.* 2012) stably expresses a human Ferroportin-green fluorescent protein (hFPN-GFP) fusion protein under the control of a tetracycline-dependent promoter (T-REx Tet-on system, Clontech). Cells were kept in Tet-free culture medium and hFPN-GFP expression was induced by 5-20ng/ml Doxycycline treatment for 16h. hFPN-GFP fusion protein shows cytoplasmic and cell membrane localization as the endogenous FPN protein (left panel). When cells are exposed to 1µg/ml recombinant hepcidin treatment, hFPN-GFP undergoes internalization and degradation, as occurs to the endogenous protein, and the process can be followed by fluorescent microscopy observation. hFPN-GFP internalization starts to be appreciable 5h after hepcidin treatment and it is more evident at 10h after treatment (central panel) as reduced membrane localization and the appearance of an intracellular punctuate pattern. 24h after hepcidin exposure we observe complete internalization and ~80% degradation of hFPN-GFP as shown by the almost total loss of fluorescence (right panel). Images were acquired using a Leica DMI6000B microscope. hFPN-GFP is visible in the green channel and cellular nuclei by DAPI staining in the blue channel. **(B)** The efficiency of siRNA delivery was checked in Hek293 hFPN-GFP cells using a FITC-labeled scrambled-siRNA. Optimal conditions were obtained by transfecting 20pmol siRNA with the X-tremeGENE siRNA reagent (Roche), according to manufacturer's protocol. Images were acquired using a Leica DMI6000B microscope. The efficiency of siRNA delivery is appreciable in the green channel and cells are visualized by phase contrast. **(C)** For the silencing of human PFN2, Hek293 hFPN-GFP cells were subjected to two subsequent transfections (on day 1 and day 3) with 20pmol of human PFN2-specific siRNA (Silencer® Select, Ambion) or a control scrambled siRNA. The efficiency of the silencing was evaluated by Western blotting 48h after the second transfection. A mouse brain sample was loaded as positive control for PFN2 detection (+). S6 protein was monitored in parallel as loading control.

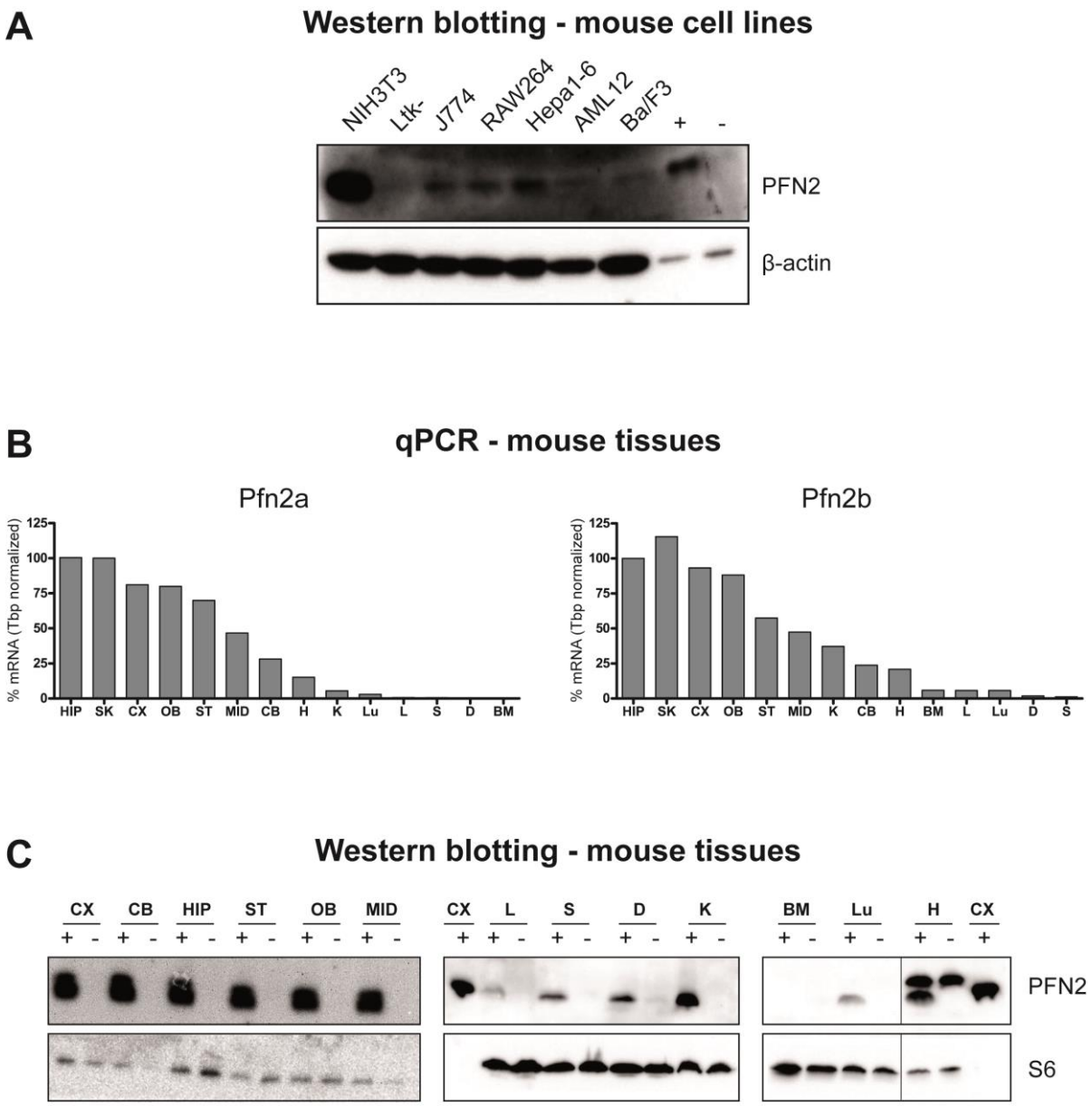

Supp. Figure 6.2 Profilin2 expression levels in different mouse cell lines and mouse tissues. (A) Analysis of endogenous Pfn2 protein levels in different mouse cell lines. 50µg total extracts of NIH3T3, Ltk- (fibroblasts), J774, RAW264 (macrophages), Hepa1-6, AML12 (hepatocytes) and Ba/F3 (B lymphocytes) cells were analyzed by Western blotting. As control of the specificity of the band detected, 5µg of Hek293T cells transfected with a mouse Pfn2 plasmid (+) together with 5µg HeK293T untransfected cells (-) were loaded in parallel. Expression of β-actin was monitored as loading control. Endogenous Pfn2 is low-expressed in the different mouse cell lines tested with the exception of NIH3T3 cells that show high levels of Pfn2. **(B)** The expression of Profilin2 main mRNA isoforms (Pfn2a and Pfn2b) was analyzed by qPCR in different mice tissues. Data were normalized to TATA box binding protein (Tbp) and compared to the levels detected in the hippocampus (set as 100%). **(C)** Profilin2 expression in mouse tissues was also analyzed at protein level by Western blotting. 5µg of total extracts were loaded for brain samples and 50µg were loaded for the other tissues. The specificity of the band corresponding to Pfn2 was ensured by loading samples from wild type mice (+) and samples from Pfn2 knockout mice (-). Expression of S6 ribosomal protein was monitored as loading control. In line with published data, Pfn2 is highly expressed throughout the brain and at lower levels in peripheral tissues. The following abbreviations were used: HIP: hippocampus; SK: skeletal muscle; CX: cortex; OB: olfactory bulb; ST: corpus striatum; MID: midbrain; CB: cerebellum; H: heart; K: kidney; Lu: lung; L: liver; S: spleen; D: duodenum; BM: bone marrow.

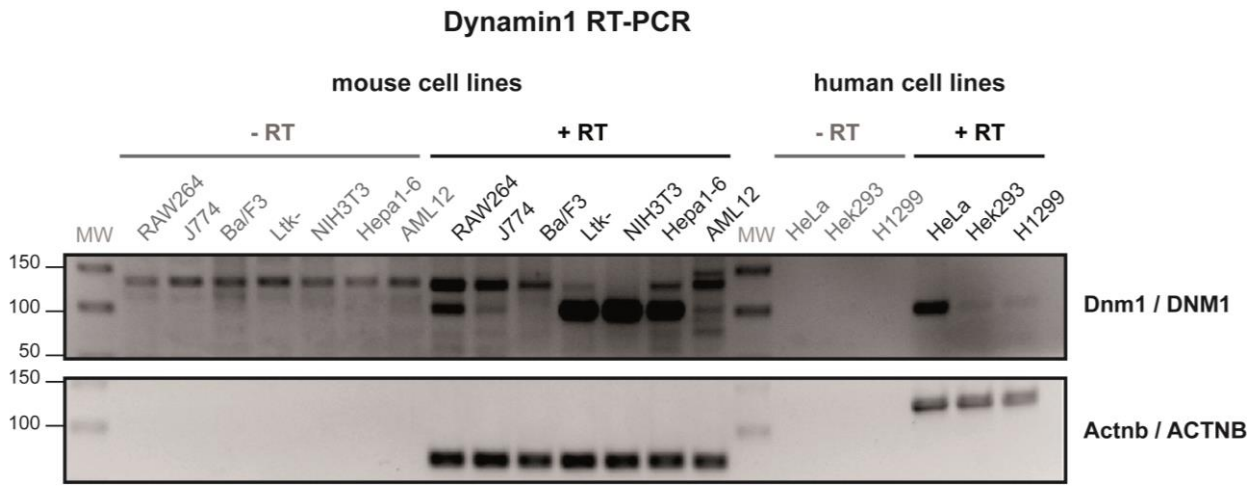

Supp. Figure 6.3 Dynamin1 expression in cell lines. The expression of Dynamin1 mRNA was tested by RT-PCR in different mouse and human cell lines: RAW264 and J774 (mouse macrophages), Ba/F3 (mouse B lymphocytes), Ltk- and NIH3T3 (mouse fibroblasts), Hepa1-6 and AML12 (mouse hepatocytes), HeLa (epithelial cells), Hek293 (human embryonic kidney cells) or H1299 (human lung carcinoma cells). β-actin was analyzed in parallel for calibration and RNA quality control. RT-PCR were performed with specific primers: Dnm1 (102 bp), DNM1 (113bp), Actnb (76bp) and ACTNB (125bp) at 28 PCR cycles for Dnm1/DNM1 and 25 PCR cycles for Actnb/ACNTNB. Dynamin1 showed positive expression in almost all the cell lines tested, with higher levels in RAW264, Ltk-, NIH3T3, Hepa1-6 and HeLa cells. The following abbreviations were used: Dnm1/DNM1: mouse and human Dynamin1; Actnb/ACTNB: mouse and human β-actin: -RT/+RT: minus/plus reverse transcriptase reaction.

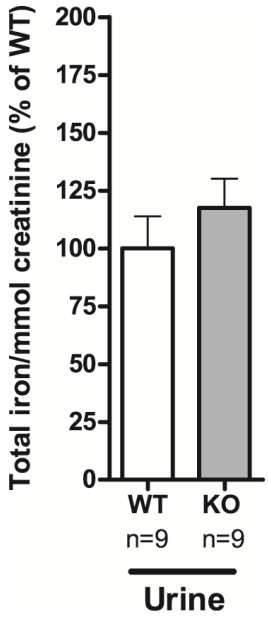

Supp. Figure 6.4 Determination of total iron content in the urines of Pfn2 KO and wild type mice. Atomic emission spectrometry determination of total iron content in urine samples from 7-9 months old male Pfn2 KO and WT mice. Urinary creatinine concentration was also measured for normalization in order to correct for differences in urine dilution. Data are expressed as µg iron/mmol creatinine. Means ± SEM compared to wild type mice, set as 100%. The sample size (n) is indicated.

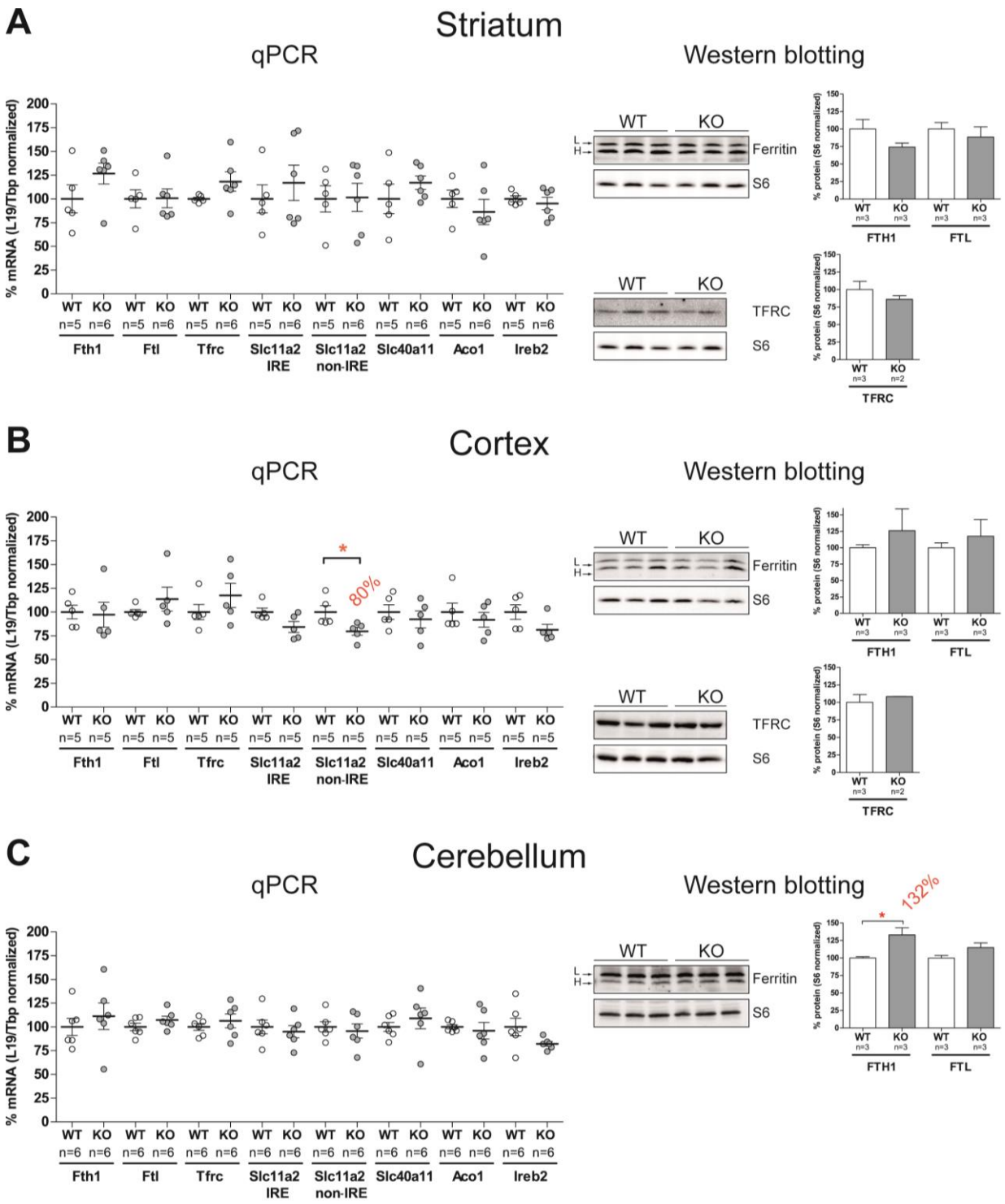

Supp. Figure 6.5 Brain expression of iron-related genes. The expression of iron-related genes was analyzed at mRNA level by qPCR (left panels) and protein level by Western blotting (right panels) in different brain areas from WT and Pfn2 KO 7-9 months old mice: corpus striatum **(A)**, cortex **(B)** and cerebellum **(C)**. For qPCR experiments, Fth1, Ftl, Tfrc, Slc11a2-IRE and non-IRE isoforms, Slc40a11, Aco1 and Ireb2 mRNAs expression was normalized against L19 ribosomal protein and TATA box binding protein (Tbp) expression and compared to wild type mice (set as 100%). Means ± SEM are shown. Sample size (n) is indicated. For Western blotting experiments, H- and L-ferritin and, in some cases transferrin receptor expression was monitored. S6 ribosomal protein levels were used for normalization. Bands intensity was analyzed using the AlphaEaseFC software (Alpha Innotech). Graphs represent quantified data, compared to the signal of WT mice samples (set as 100%). Means ± SEM are shown. The samples size (n) is indicated. The following abbreviations were used: Fth1: H-ferritin; Ftl: L-ferritin; Tfrc: transferrin receptor C; Slc11a2 (Dmt1): divalent metal transporter 1; Slc40a11 (Fpn1): ferroportin; Aco1 (Irp1): iron regulatory protein 1; Ireb2 (Irp2): iron regulatory protein 2; WT: wild type mice; KO: Pfn2 knockout mice; L: L-ferritin subunit; H: H-ferritin subunit.

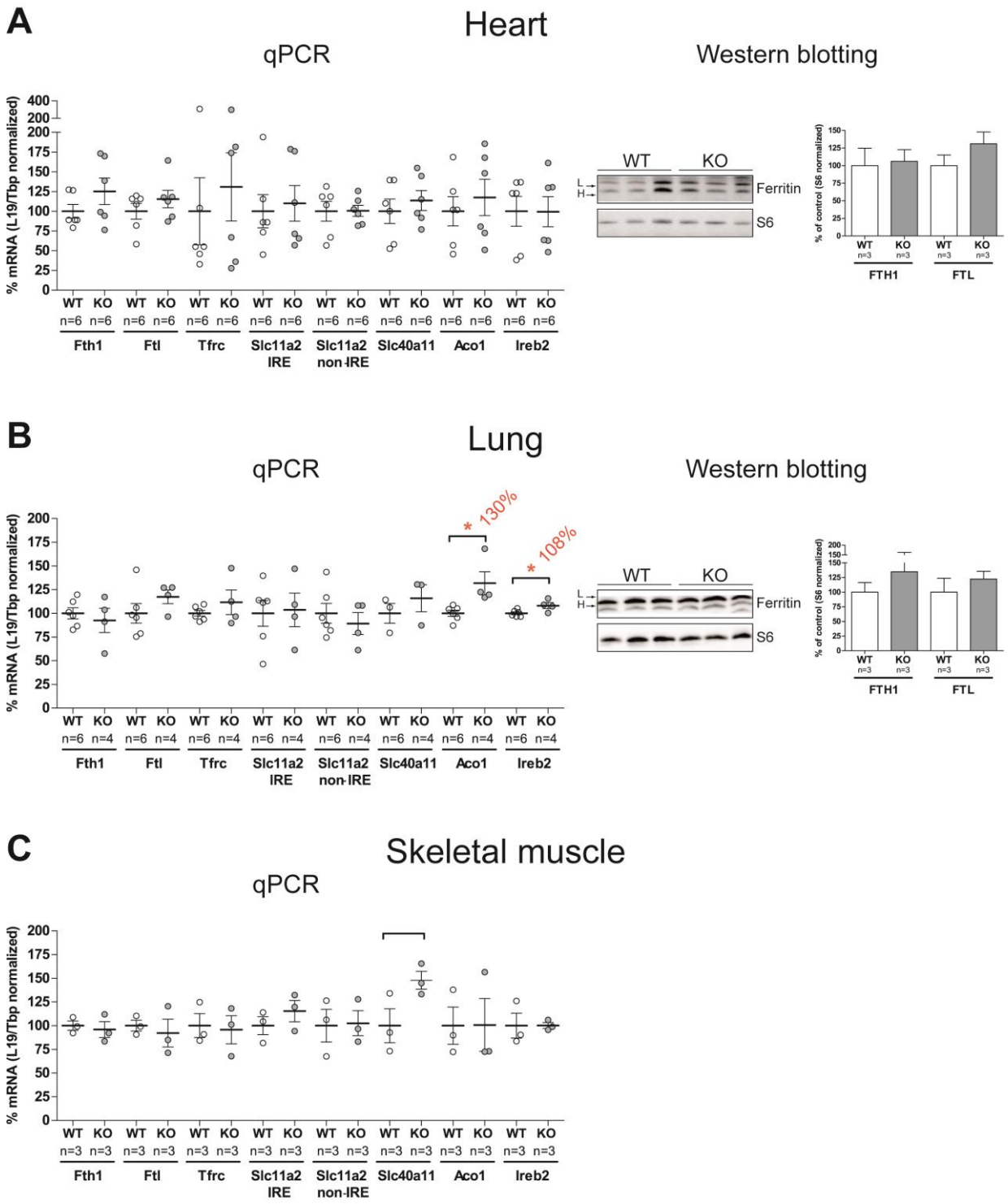

Supp. Figure 6.6 Tissue expression of iron-related genes. The expression of iron-related genes was analyzed at mRNA level by qPCR (left panels) and protein level by Western blotting (right panels) in heart **(A)**, lung **(B)** and skeletal muscle **(C)** tissues from WT and Pfn2 KO 7-9 months old mice. For qPCR experiments, Fth1, Ftl, Tfrc, Slc11a2-IRE and non-IRE isoforms, Slc40a11, Aco1 and Ireb2 mRNAs expression was normalized against L19 ribosomal protein and TATA box binding protein (Tbp) expression and compared to wild type mice (set as 100%). Means ± SEM are shown. Sample size (n) is indicated. For Western blotting experiments, H- and L-ferritin were monitored. S6 ribosomal protein levels were used for normalization. Bands intensity was analyzed using the AlphaEaseFC software (Alpha Innotech). Graphs represent quantified data, compared to the signal of WT mice samples (set as 100%). Means ± SEM are shown. The samples size (n) is indicated. The following abbreviations were used: Fth1: H-ferritin; Ftl: L-ferritin; Tfrc: transferrin receptor C; Slc11a2 (Dmt1): divalent metal transporter 1; Slc40a11 (Fpn1): ferroportin; Aco1 (Irp1): iron regulatory protein 1; Ireb2 (Irp2): iron regulatory protein 2; WT: wild type mice; KO: Pfn2 knockout mice; L: L-ferritin subunit; H: H-ferritin subunit.

6.2 International congress presentations and publications

6.2.1 Congress presentations

"NOVEL IRP-TARGET GENES"
Luscieti S, Galy B, Hentze MW, Sánchez M.
European Iron Club, Nijmegen 15-17 September 2010. Poster presentation.

"PFN2 AS A NOVEL IRP−TARGET MRNA"
Luscieti S, Galy B, Hentze MW, Sánchez M.
International BioIron Society, Vancouver 22-26 May 2011. Poster presentation by Dr. Sánchez M.

"PFN2 AS A NOVEL IRP−TARGET MRNA"
Luscieti S, Galy B, Hentze MW, Sánchez M.
European Iron Club, Louvain-la-Neuve 8-11 September 2011. Poster presentation.

"PFN2 AS A NOVEL IRP−TARGET MRNA"
Luscieti S, Galy B, Hentze MW, Sánchez M.
III IMPPC Annual Conference: RNA biology in cancer and other diseases, Barcelona 3-4 May 2012. Poster presentation.

"NOVEL MUTATIONS IN THE FERRITIN-L IRON-RESPONSIVE ELEMENT THAT ONLY MIDLY IMPAIR IRP BINDING CAUSE HEREDITARY HYPERFERRITINAEMIA CATARACT SYNDROME"
Luscieti S, Tolle G, Aranda J, Benet-Campos C, Risse F, Moran E, Muckenthaler MU, Sánchez M.
International BioIron Society, London 14-18 April 2013. Poster presentation.

"TOWARD A THIRD VARIANT OF ERYTHROPOIETIC PROTOPORPHYRA"
Ducamp S, Gazal S, Sánchez M, **Luscieti S**, Manceau H, Lamoril J, Kannengiesser C, Simonin S, Robréau AM.
Annual Assembly of the Swiss Society of Clinical Chemistry & International Congress of Porphyrins and Porphyrias, Lucerne 16-18 May 2013. Oral presentation by Dr. Ducamp S.

"PROFILIN2 IS CONTROLLED BY THE IRON REGULATORY PROTEINS AND MODULATES IRON HOMEOSTASIS"
Luscieti S, Boyl PP, Galy B, Gutiérrez L, Shvartsman M, Morales MP, Hentze MW, Witke W, Sánchez M.
European Iron Club, Verona 11-14 September 2014. Oral presentation.

"PROFILIN2 IS CONTROLLED BY THE IRON REGULATORY PROTEINS AND MODULATES IRON HOMEOSTASIS"
Luscieti S, Boyl PP, Galy B, Gutiérrez L, Shvartsman M, Morales MP, Hentze MW, Witke W, Sánchez M.
56th American Society of Hematology Annual Meeting, San Francisco 6-9 December 2014. Oral presentation by Dr. Sánchez M.

"PROFILIN-2, A NEW PLAYER IN IRON METABOLISM"
Luscieti S, Boyl PP, Galy B, Gutiérrez L, Shvartsman M, Couso J, Negro A, Morales MP, Hentze MW, Witke W, Sánchez M.
International BioIron Society, Hanghzou 6-10 September 2015. Poster presentation by Dr. Sánchez M.

"A MUTATION IN THE IRON-RESPONSIVE ELEMENT OF ALAS2 IS A MODIFIER OF CLINICAL SEVERITY IN ERYTHROPOIETIC PROTOPORPHYRIA"
Luscieti S, Ducamp S, Manceau H, Kannengiesser C, Hureaux M, Nicolas G, Karim Z, Deybach JC, Gouya L, Puy H, Sánchez M.
International BioIron Society, Hanghzou 6-10 September 2015. Oral presentation by Dr. Sánchez M.

"PROFILIN-2, A NEW PLAYER IN IRON METABOLISM"
Luscieti S, Boyl PP, Galy B, Gutiérrez L, Shvartsman M, Couso J, Negro A, Morales MP, Hentze MW, Witke W, Sánchez M.
RNA Biology in Cancer and other Diseases 2nd Congress RNAREG Consortium-Josep Carreras Leukaemia Research Institute (IJC), Barcelona 24-26 November 2015. Poster presentation by Couso J.

6.2.2 Publications

Results presented in this dissertation (Results and Discussion sections 3.1 and 3.3) are part of the following published manuscripts:

"NOVEL MUTATIONS IN THE FERRITIN-L IRON-RESPONSIVE ELEMENT THAT ONLY MILDLY IMPAIR IRP BINDING CAUSE HEREDITARY HYPERFERRITINAEMIA CATARACT SYNDROME"
Luscieti S, Tolle G, Aranda J, Campos CB, Risse F, Morán É, Muckenthaler MU, Sánchez M.
Orphanet J Rare Dis. 2013 Feb 19;8:30. doi: 10.1186/1750-1172-8-30. PMID: 23421845
(see Annex I)

"SIDEROPHORE-MEDIATED IRON TRAFFICKING IN HUMANS IS REGULATED BY IRON"
Liu Z, Lanford R, Mueller S, Gerhard GS, **Luscieti S**, Sanchez M, Devireddy L.
J Mol Med. 2012 Oct;90(10):1209-21. doi: 10.1007/s00109-012-0899-7. PMID: 22527885
(see Annex II)

Results presented in this dissertation (Results and Discussion sections 3.2 and 3.4) are in preparation for publication. Some text passages of those manuscripts have been adapted in this dissertation.

Annex I: Luscieti *et al.* 2013 OJRD

Luscieti *et al. Orphanet Journal of Rare Diseases* 2013, **8**:30
http://www.ojrd.com/content/8/1/30

ORPHANET JOURNAL OF RARE DISEASES

RESEARCH Open Access

Novel mutations in the ferritin-L iron-responsive element that only mildly impair IRP binding cause hereditary hyperferritinaemia cataract syndrome

Sara Luscieti[1], Gabriele Tolle[2,3], Jessica Aranda[1], Carmen Benet Campos[4], Frank Risse[5], Érica Morán[1], Martina U Muckenthaler[2,3] and Mayka Sánchez[1*]

Abstract

Background: Hereditary Hyperferritinaemia Cataract Syndrome (HHCS) is a rare autosomal dominant disease characterized by increased serum ferritin levels and early onset of bilateral cataract. The disease is caused by mutations in the Iron-Responsive Element (IRE) located in the 5′ untranslated region of L-Ferritin (FTL) mRNA, which post-transcriptionally regulates ferritin expression.

Methods: We describe two families presenting high serum ferritin levels and juvenile cataract with novel mutations in the L-ferritin IRE. The mutations were further characterized by *in vitro* functional studies.

Results: We have identified two novel mutations in the IRE of L-Ferritin causing HHCS: the Badalona +36C > U and the Heidelberg +52 G > C mutation. Both mutations conferred reduced binding affinity on recombinant Iron Regulatory Proteins (IPRs) in EMSA experiments. Interestingly, the Badalona +36C > U mutation was found not only in heterozygosity, as expected for an autosomal dominant disease, but also in the homozygous state in some affected subjects. Additionally we report an update of all mutations identified so far to cause HHCS.

Conclusions: The Badalona +36C > U and Heidelberg +52 G > C mutations within the L-ferritin IRE only mildly alter the binding capacity of the Iron Regulatory Proteins but are still causative for the disease.

Keywords: Serum ferritin, Iron metabolism, IRP/IRE regulatory system, Bilateral cataracts

Background

Ferritin is the protein responsible for the storage and intracellular distribution of iron [1]. It is composed of 24 subunits of two types named H- and L-Ferritin, encoded by two different genes. The H subunit generates ferroxidase activity to incorporate iron into the protein shell and the L subunit facilitates iron-core formation. The synthesis of these two proteins is controlled post-transcriptionally by the Iron Regulatory Proteins (IRPs) that bind to the Iron Responsive Element (IRE), a conserved hairpin-like motif, located in the 5′ untranslated region (UTR) of ferritin mRNAs [2]. The binding of the IRPs to IREs occurs under iron-deficient conditions and results in translational repression of both ferritins. Mutations in the IRE of Ferritin L (FTL) mRNA cause reduced IRP binding with concomitant up-regulation of FTL synthesis in the Hereditary Hyperferritinaemia Cataract Syndrome (HHCS). HHCS (ORPHA163, OMIM # 600886) was first described in 1995 as an autosomal dominant disease characterized by a combination of high serum ferritin levels with congenital bilateral nuclear cataract and the absence of iron overload [3-6]. Differential diagnosis with hereditary hemochromatosis, a genetic iron-overload disease, is achieved by genetic analysis and biochemical measures of serum iron and transferrin saturation indices, which are not increased in HHCS. In this work we describe two families of Spanish and German origin with HHCS caused by novel mutations in the FTL IRE. Unexpectedly for an autosomal dominant disease, one of the mutations was detected in the homozygous state in some affected members of the Spanish family. *In vitro* studies indicate a minor disturbance of the IRP-IRE binding by these mutations.

* Correspondence: msanchez@imppc.org
[1]Institute of Predictive and Personalized Medicine of Cancer (IMPPC), Ctra. de Can Ruti, Camí de les Escoles s/n, 08916, Badalona, Barcelona, Spain
Full list of author information is available at the end of the article

Luscieti *et al. Orphanet Journal of Rare Diseases* 2013, **8**:30
http://www.ojrd.com/content/8/1/30

Methods

Patients

Pedigree 1

Proband (III:2, Figure 1A and Table 1) is a 54 year old woman of Spanish origin presenting a 10-year history of hyperferritinaemia with no sign of iron overload. Serum iron, transferrin saturation and liver functional tests were normal. The patient presents no evidence of hepatitis, cirrhosis, diabetes, inflammatory diseases, metabolic syndrome or neoplasia and genetic testing for HFE hereditary hemochromatosis was negative. She has suffered from bilateral cataracts since she was 18 years old and underwent surgery at the age of 39. The proband has one sister (III:4) and a cousin (III:9) presenting similar clinical features with hyperferritinaemia and juvenile bilateral cataract (Table 1). No evidence of elevated serum ferritin was found in four other sisters of the proband. A deceased maternal uncle (II:4) had suffered from hyperferritinaemia and cataract reported as an adult. Notice that the proband's parents (II:1 and II:2) were first cousins; the mother died from acute myeloid leukemia and the father from senile dementia and he had suffered from cataracts which required surgical correction in adult age. The proband's mother was never diagnosed with cataracts but she suffered from severe myopia. The proband's daughter (IV:1), aged 27, shows no cataracts, but she has moderately elevated serum ferritin levels above 200 ng/ml and low transferrin saturation (to be considered with a concomitant hypermenorrhea) (Table 1). The two sons (IV:2 and IV:3) of the other affected sister also have moderately elevated serum ferritin levels and subject IV:2 also shows early signs of cataracts (Table 1).

Pedigree 2

The proband (IV:1, Figure 1B and Table 1) is a 19 year old man originating from Germany, who was referred to the medical doctor due to fatigue and difficulties in concentrating. He showed high serum ferritin levels with normal serum iron and transferrin saturation. He presented with cataracts since the age of 16 and has not undergone surgery. He does not present any other clinical signs. No evidence for acute or chronic inflammation was detected and his liver functional tests and abdominal morphology at echography medical inspection were normal. The test for Hereditary Hemochromatosis type 1 (HFE) was negative and Hereditary Hemochromatosis type 4 (ferroportin disease) was excluded, with no evidence of pathological mutations in the SLC40A1 gene. The father (III:2) presents with similar biochemical findings showing elevated serum

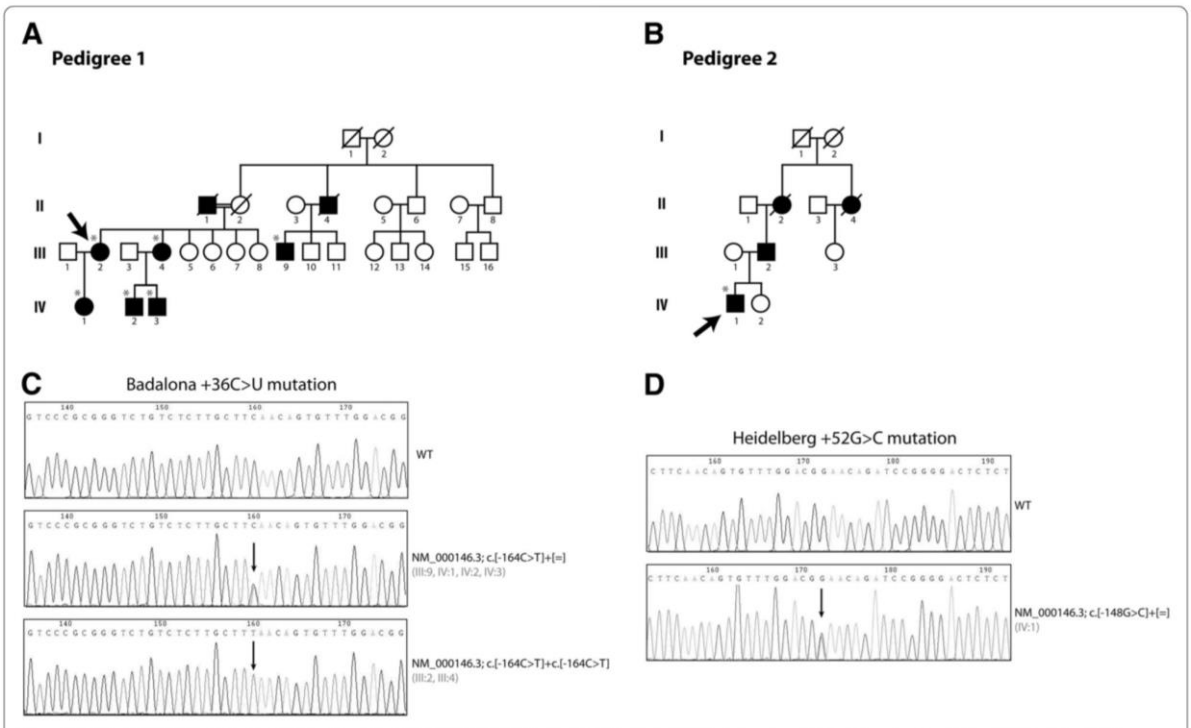

Figure 1 (A, B) Pedigree trees of the two families with HHCS studied. Squares indicate males, circles females and rhombus subjects of unknown sex. Filled symbols indicate affected members and barred symbols indicate deceased subjects. Asterisks indicate subjects characterized at the molecular level. (**C**, **D**) Chromatograms of partial FTL IRE sequences where mutations are located. Arrows indicate the nucleotide position that is altered by the pathological mutation. WT denotes wild type sequence according to reference sequence [NCBI:NM_000146.3]. Traditional and conventional HGVS nomenclatures are shown.

Luscieti et al. Orphanet Journal of Rare Diseases 2013, 8:30
http://www.ojrd.com/content/8/1/30

Table 1 Biochemical and clinical parameters of the affected members of the two pedigrees studied

	Pedigree 1						Pedigree 2		
Characteristic	**III:2 (proband)**	**III:4**	**III:9**	**IV:1**	**IV:2**	**IV:3**	**IV:1 (proband)**	**III:2**	**Normal values**
Age at diagnosis (years)	54	53	48	27	27	25	19	40	
Sex	F	F	M	F	M	M	M	M	
Hb (g/dl)	13.2	13.1	15.3	13.4	14.3	14.7	15.6	15	♂ 13,8–18 ♀ 12,1–15,1
MCV (fl)	92.3	96	94.1	91.3	85.1	83.4	80.9	80,6	79–99
CRP (mg/L)	<5	-	4	<5	<5	-	4	-	5–10
Serum iron (μg/dl)	74	56	79	37	124	243	127	111	37–170
TIBC (μg/dl)	361	-	342	372	327	424	-	-	250–450
Serum ferritin (ng/ml)	719	534	952	239	303	447	1290	1260	♂ 12–300 ♀ 12–200
Transferrin (mg/dl)	252	-	-	260	229	296	291	300	200–360
Transferrin saturation (%)	20	-	23.1	10	38	57	31	25	20–55
ALT (mU/ml)	28	17	35	21	38	14	-	-	14–36
AST (mU/ml)	35	20	40	20	30	30	27	33	9–52
Cataract diagnosis (years)	20	17	20	-	27	-	16	16	
Cataract surgery (years)	39	-	-	-	-	-	-	-	
HFE gene mutation	H63D+/–, S65C –/–, C282Y–/–	H63D–/–, S65C –/–, C282Y–/–	H63D+/+, S65C –/–, C282Y–/–	H63D–/–, S65C –/–, C282Y–/–	H63D–/–, S65C +/–, C282Y–/–	H63D–/–, S65C –/–, C282Y–/–	H63D–/–, S65C –/–, C282Y–/–	-	
Mutation IRE L-ferritin	c.[–164C > T] + c.[–164C > T]	c.[–164C > T] + c.[–164C > T]	c.[–164C > T] + [=]	c.[–164C > T] + [=]	c.[–164C > T] + [=]	c.[–164C > T] + [=]	c.[–148 G > C] + [=]	c.[–148 G > C] + [=]	
	Badalona +36C > U	Badalona +36C > U	Badalona +36C > U	Badalona +36C > U	Badalona +36C > U	Badalona +36C > T	Heidelberg +52 G > C	Heidelberg +52 G > C	

Reference values are indicated in the last column. The following abbreviations were used: Hb, hemoglobin; MCV, mean corpuscular volume; CRP, C-reactive protein; ALT, alanine aminotransferase; AST, apartate aminotransferase. HFE gene mutations refer only to C282Y, H63D and S65C mutations.

ferritin and clinical symptoms with cataracts detected also at the age of 16 (Table 1). The paternal grandmother (II:2) and a great-aunt (II:4) had also suffered from cataracts (Figure 1B).

Written informed consent for genetic analyses was obtained from the probands and relatives of the two families according to the guidelines of the institution and the study protocol conforms to the ethical guidelines of the 2002 Helsinki Declaration.

PCR amplification and DNA sequencing

Genetic studies were performed with minor differences for the two pedigrees.

Genomic DNA was extracted from peripheral blood using the FlexiGene DNA kit or QIAamp DNA Blood Mini kit (Qiagen) according to manufacturer's instructions. PCR amplification of exon 1 of L-ferritin was performed with 50 ng of genomic DNA using primers reported in Additional file 1: Table S1. For pedigree 1 the cycling conditions were: denaturation at 94°C, annealing ranging from 66 to 60°C, and extension at 72°C, each step for 30 - seconds and for 30 cycles while for pedigree 2 were: denaturation at 95°C, annealing at 58°C, and extension at 72°C, step 1 and 2 for 30 seconds, step 3 for 45 seconds and for 38 cycles. The resulting amplification product was verified on a 2% agarose gel. The PCR product was processed to remove excess dNTPs and unincorporated primers: for pedigree 1, 8 μl of PCR product were treated with 10U Exonuclease I and 10U Antarctic Phosphatase (New England Biolabs) at 37°C for 30 min and the reaction was inactivated by heating at 80°C for 15 min. For Pedigree 2, 40 μl of PCR product were cleaned up using the NucleoSpin Gel and PCR Clean-up Kit (Machery-Nagel) according to manufacturer's instructions. The purified PCR product was sequenced using conventional Sanger method [7] by GATC BIOTECH company (Konstanz, Germany). Sequencing results were analyzed using Mutation Surveyor software (SoftGenetics LLC) or Chromas software (Technelysium Pty Ltd).

Plasmid construction

Plasmids for generating EMSA probes were constructed based on the I-12.CAT plasmid [8] by replacing H-ferritin IRE with annealed synthetic oligonucleotides corresponding to the sequences of L-ferritin wild type (WT) or the mutated versions: +39ΔC, Badalona +36 C > U, Milano +36 C > G, Heidelberg +52 G > C or Torino +29 C > G; oligonucleotide sequence are reported in Additional file 1: Table S1. DNA templates were linearized with XbaI and used for *in vitro* transcription.

Electrophoretic mobility shift assay (EMSA)

EMSAs were performed with a new non-radiolabeled method ([9], and manuscript in preparation) using fluorescently labeled probes with Aminoallyl-UTP-ATTO-680 (Jena Bioscience). For direct and competitive EMSAs we include proper controls such as the +39ΔC deletion construct (positive control), the Milano +36 C > G mutation [10], a variation at the same position as the Badalona +36C > U mutation and the Torino +29C > G mutation [11], the counterpart of the Heidelberg +52 G > C change. In competitive EMSAs unlabeled competitors were *in vitro* transcribed using MEGAscript T7 kit (Life Technologies) according to the manufacturer's instructions. Experimentally for both assays, 100 ng of labeled probe (plus increasing molar excess of unlabeled competitor probes in the competitive EMSAs), were heated 3 min at 95°C and then incubated with 120 ng of recombinant His-tagged IRP1 or IRP2 protein for 15 min at room temperature. Non-specific RNA-protein interactions were displaced by adding 50 μg of sodium heparin for 10 min. Samples were loaded on a 5% native acrylamide gel in 1x TBE buffer. RNA-protein complexes were visualized using Odyssey Infrared Imager (LI-CORE Bioscience).

RNA folding predictions

RNA folding analysis of IRE motifs was performed using SIREs Web Server (http://ccbg.imppc.org/sires/, [12]) and RNAfold Web Server (http://rna.tbi.univie.ac.at/cgi-bin/RNAfold.cgi, University of Vienna).

Statistical analysis

Values were compared using Student's t-test for unpaired data. Differences were defined as statistically significant for P values less than 0.05.

Results and discussion

Molecular genetic studies

Sequencing of exon 1 of L-ferritin (FTL) in two families with HHCS revealed the presence of two previously undescribed sequence variations.

In pedigree 1, a C > U change was detected at position +36 of the upper stem of FTL IRE ([NCBI:NM_000146.3]; c.-164C > T, HGSV nomenclature). Interestingly, the mutation was found to be present in the homozygous state in two members of this Spanish family (the proband, III:2 and her sister, III:4), while other affected members carry the change in heterozygosity (Figure 1A and C). To exclude that homozygosity of the mutation may arise from a "drop of allele mechanism" we have sequenced the FTL exon 1 using two independent sets of primers and identical results were obtained (data not shown). Moreover, possible in *trans* deletions were assessed with gene dosage studies by qPCR demonstrating that all studied patients from pedigree 1 carry two copies of the FTL gene (data not shown).

Sequencing analysis in pedigree 2 showed a G > C change at position +52 of the IRE lower stem ([NCBI:

Luscieti *et al. Orphanet Journal of Rare Diseases* 2013, **8**:30
http://www.ojrd.com/content/8/1/30

NM_000146.3]; c.-148 G > C) in a heterozygous state (Figure 1B and D).

Following the traditional nomenclature for FTL IRE mutations we refer to these mutations as the "Badalona +36C > U" and "Heidelberg +52 G > C" mutations, respectively. The presence of either the Badalona or Heidelberg variation was further validated by PCR-Restriction Fragment Length Polymorphism, as the +36C > U and +52 G > C changes introduce a MseI and a HgaI recognition site, respectively (data not shown). Both changes were absent in 50 control subjects, which rules out their being neutral polymorphisms and supports their causative role for the disease. Additionally, the sequencing of the complete FTL gene (coding region and exon-intron boundaries) revealed no other changes.

The Badalona +36C > U and the Heidelberg +52 G > C variants show reduced binding of IRP1 and IRP2

The substitution of guanine by cytosine at position +52 (mutation Heidelberg) is predicted to affect base pairing with the cytosine +29 (Figure 2). However, this is not obvious for the Badalona +36C > U variation because, in theory, the presence of cytosine or uracil at position +36 is not expected to alter base pairing with the guanine at position +47 in the IRE structure (Figure 2), as both C-G or U-G pairing are possible matching pairs within RNA structures. For this mutation we performed folding prediction analysis of the wild-type (WT) and the mutated sequences, using the SIREs and RNAfold Web Servers and the result shows that the Badalona +36C > U substitution increases the folding free energy and opens the structure of the mutated FTL-IRE, when compared to the wild-type IRE (Additional file 1: Figure S1).

For both mutations we next examined the ability of the mutated IRE to bind recombinant IRP1 or IRP2 by electrophoretic mobility shift assays (EMSAs). As expected little IRP binding occurs to the non-functional IRE structure (+39ΔC, Figure 3A and B, lanes 3), which was used as a positive control. Importantly, the Badalona +36C > U and Heidelberg +52 G > C mutations show a reduction of up to 30-40% in the binding to both IRPs (Figure 3A and B, lanes 4 and 6); a similar level of reduction was observed for the Torino +29C > G mutation ([11], Figure 3A and B, lanes 7), while the Milano +36C > G mutation [10] reduces its binding to both IRPs more drastically (Figure 3A and B, lanes 5). Next, we checked the Badalona +36C > U and Heidelberg +52 G > C changes by a more stringent assay, a competitive EMSA. The Badalona +36C > U mutation shows a mild but significant reduction in the efficiency of competition when compared to wild type unlabeled competitor (Figure 4A and C, lanes 17–22 compared to 3–8), while its corresponding control, the Milano +36C > G mutation, is

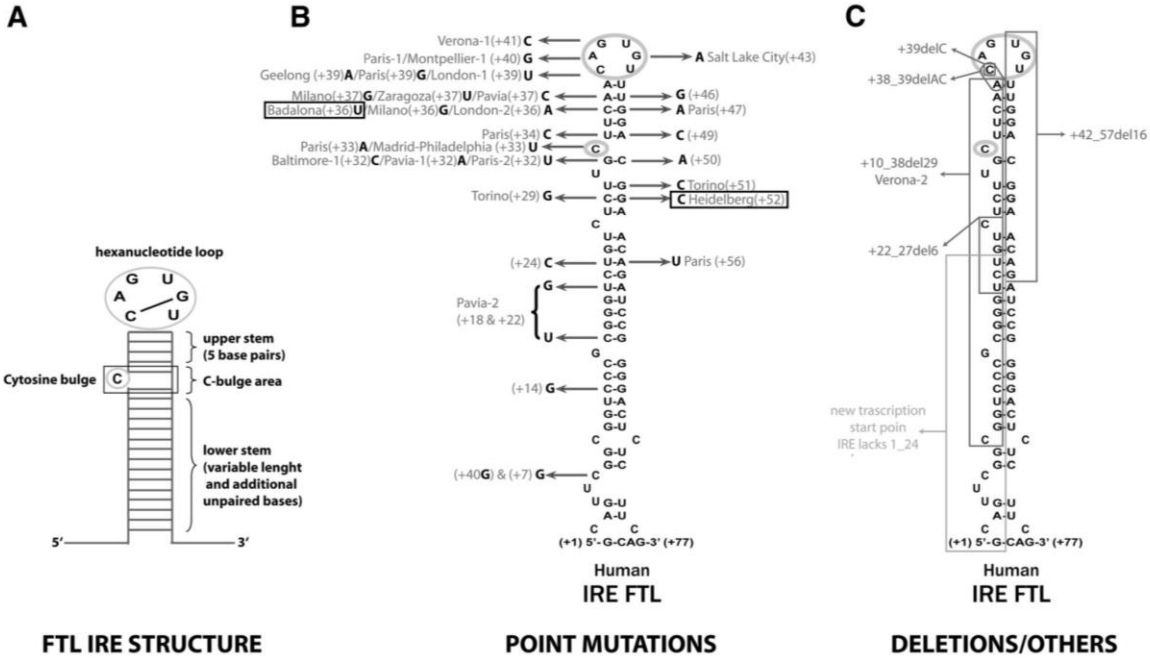

Figure 2 (A) Schematic representation of the canonical structure of FTL IRE depicting important structural parts: the hexanucleotide apical loop, the cytosine bulge and the upper and lower stems. (**B**) Picture of the FTL IRE indicating all known causative point mutations in HHCS. The two new mutations described here (Badalona +36C > U and Heidelberg +52 G > C) are boxed. (**C**) Picture of FTL IRE showing the known deletions causing HHCS.

Luscieti *et al. Orphanet Journal of Rare Diseases* 2013, **8**:30
http://www.ojrd.com/content/8/1/30

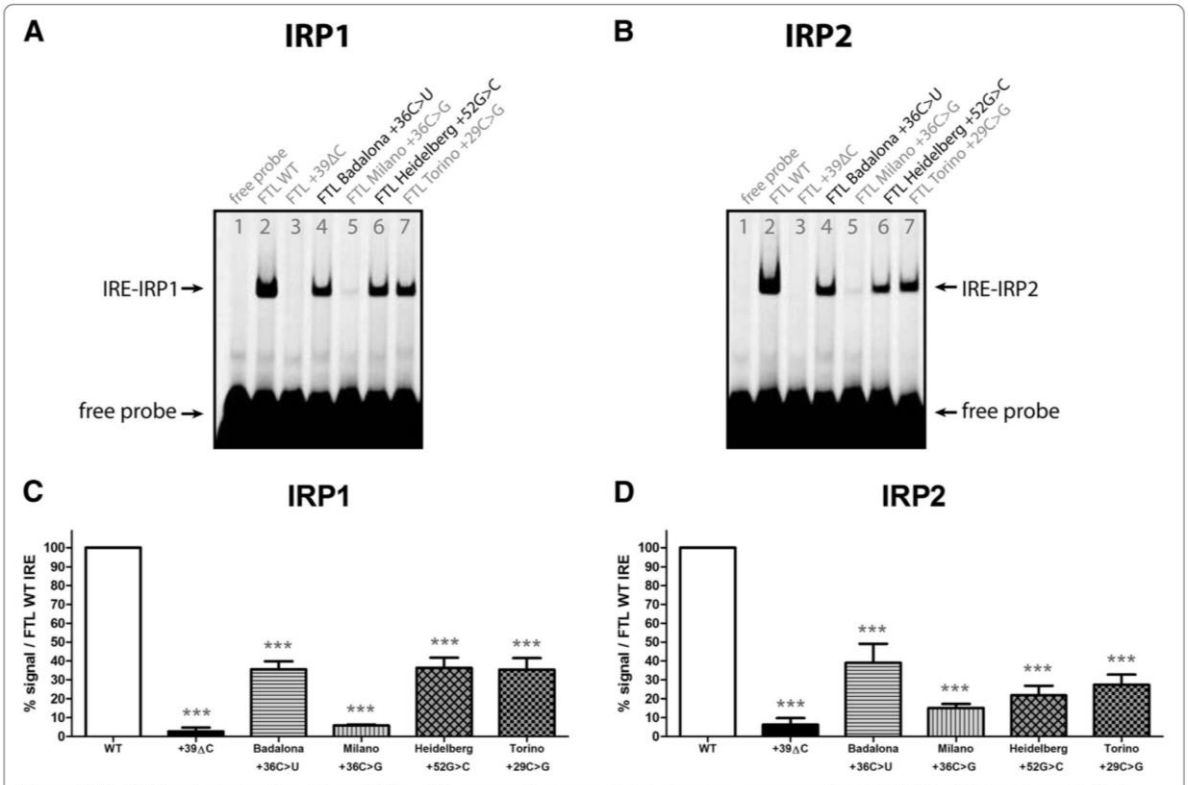

Figure 3 (A, B) Direct electrophoretic mobility shift assays. Fluorescent labeled probes corresponding to FTL IRE wild type (lanes 1–2), the mutations +39ΔC (lane 3), Badalona +36C > U (lane 4), Milano +36C > G (lane 5), Heidelberg +52 G > C (lane 6) and Torino +29C > G (lane 7) were incubated with either rIRP1 (panel **A**) or rIRP2 (panel **B**) and the IRP-IRE complex resolved on acrylamide gels. One representative gel is shown. (**C**, **D**) Quantification of the signals in direct EMSAs compared to the wild type FTL IRE signal that was set to 100%. Means ± SD (standard deviation) of at least three independent experiments are shown. *** $p < 0.001$.

inefficient in displacing the wild type probe; for this mutation a small degree of competition is only appreciable at 20x and 40x molar excess of competitor (Figure 4A and C, lanes 27–28). The Heidelberg +52 G > C mutation also shows a reduced capacity to compete with the FTL WT probe and behaves similarly to its corresponding control, the Torino +29C > G mutation (Figure 4A and C, lanes 31–36 and 37–42). Results obtained for IRP2 were comparable and consistent with previous data showing that IRP1 and IRP2 bind to the L-ferritin IRE with similar affinity (Figures 3 and 4).

Update on HHCS mutations

Hereditary Hyperferritinaemia Cataract Syndrome (ORPHA163, OMIM #600866) was first described in 1995 by two independent groups in Italy and France [3-6]. Additional file 1: Table S2 summarizes all 37 reported mutations causing HHCS, including the two novel mutations reported here. 31 of these are point mutations and 6 are deletions of different sizes. The majority of the causative mutations are located in the hexanucleotide loop, followed by the C-bulge region, the upper stem and the lower stem of the IRE structure (Figure 2). Other occurrences of inherited unexplained hyperferritinaemia but without cataracts or cataracts diagnosed in adult age have been attributed to mutations in the promoter region, coding region or outside the IRE motif of FTL [10,13-15].

Several authors have attempted to correlate the clinical severity of the disease with the position of the IRE mutation [16,17]. An extensive analysis of all described cases in the literature demonstrates that serum ferritin levels correlate with key IRE substructures (Figure 5). Mutations affecting the most important IRE structural elements, such as the hexanucleotide loop or the C-bulge area are detected in patients with more elevated serum ferritin levels compared to those patients with mutations affecting the base pairing of the upper or lower stem of the IRE (Figure 5). Consistently, our cases with mutations in the upper (Badalona mutation) and lower (Heidelberg mutation) IRE stem also show intermediate serum ferritin levels (<1300 ng/ml).

Luscieti *et al. Orphanet Journal of Rare Diseases* 2013, **8**:30
http://www.ojrd.com/content/8/1/30

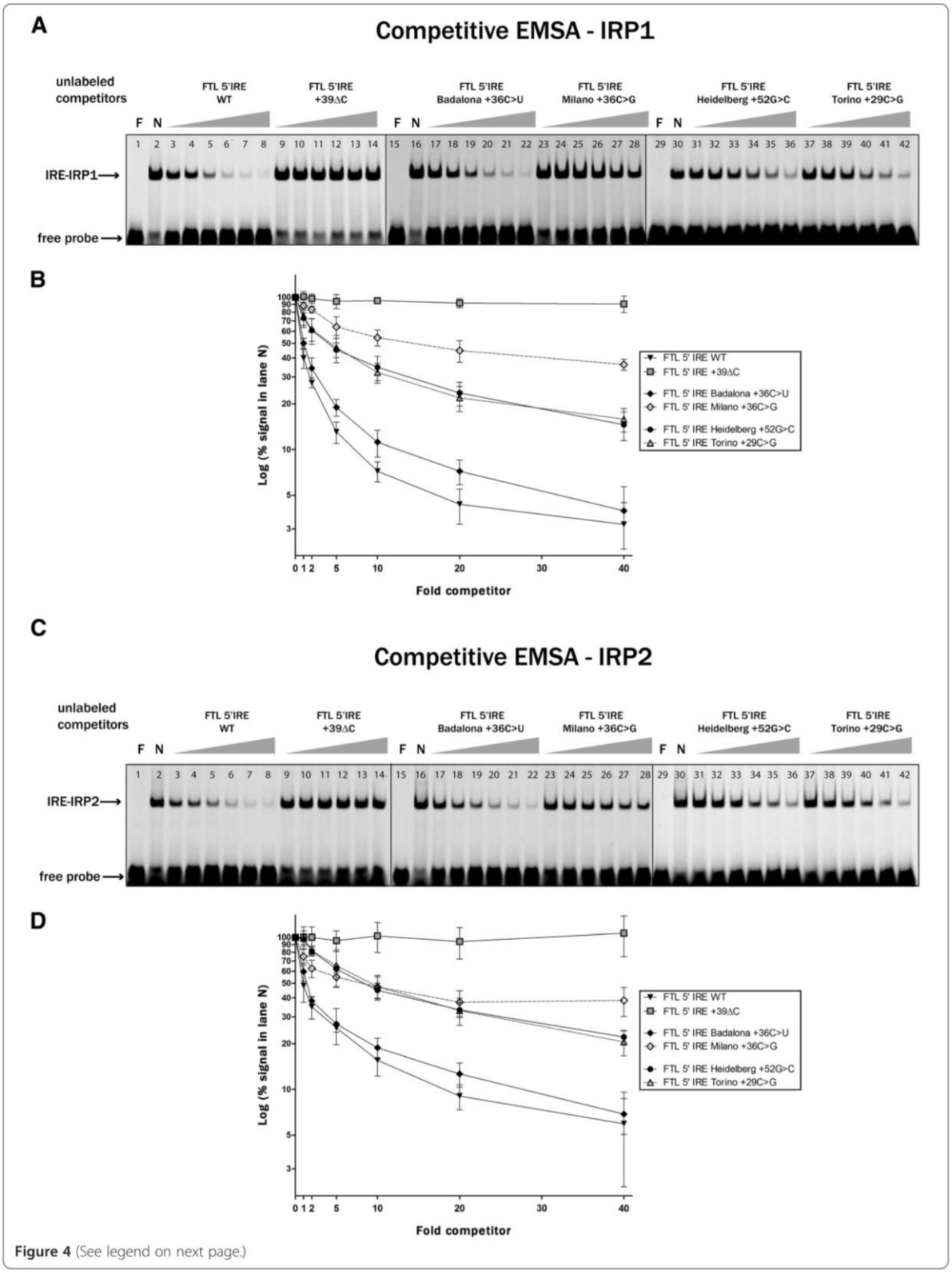

Figure 4 (See legend on next page.)

(See figure on previous page.)
Figure 4 (A, C) Competitive EMSAs. Fluorescent labeled FTL wild type probe was incubated with increasing molar excess concentration (1x, 2x, 5x, 10x, 20x and 40x) of unlabeled competitors corresponding to the FTL IRE wild type sequence (lanes 3–8) or the mutants +39ΔC (lanes 9–14), Badalona +36C > U (lanes 17–22), Milano +36C > G (lanes 23–28), Heidelberg +52 G > C (lanes 31–36) or Torino +29C > G (lanes 37–42). Samples were then incubated with either rIRP1 (panel **A**) or rIRP2 (panel **C**) and resolved on acrylamide gels. One representative gel is shown. F indicates free probe and N indicates no competitor added. (**B**, **D**) Quantification of the signals in competitive EMSAs compared to the signal in lane N (taken as 100%) are represented in logarithmic scale. Means ± SD of at least three independent experiments are shown.

HHCS is inherited as an autosomal dominant trait in all reported families and few cases have been described with *de novo* mutations [18-24]. Homozygous mutations are very unusual in HHCS. Indeed, apart from the case we report here, only one other patient has been reported [25].

The geographical distribution of HHCS patients is worldwide although most cases have been identified in Europe and the USA; most probably due to the localization of specialized laboratories [26]. Global prevalence of the disease has not been clearly defined. In an attempt to screen more than 3000 blood donors and almost 13000 patients with cataract [27] no mutations were detectable in the L-ferritin IRE, suggesting that HHCS is a rare disease. Its prevalence has been estimated to be 1 in 200000 in the Australian population [19].

Conclusions

In this report we describe two families who have HHCS due to two novel mutations in the L-ferritin IRE. Unexpectedly for an autosomal dominant disease, one of these families carries the mutation in a homozygous state in some affected subjects. Within this family there is a tendency for correlation between the genotype of the subjects and the clinical severity of the disease. However, this correlation is not perfect due to associated factors (age, sex, particular clinical history) that make difficult comparison between subjects. Therefore, we confirm that, as previously reported, a phenotype/genotype correlation in HHCS is difficult to establish due to concomitant pathologies, clinical penetrance and the fact that serum ferritin levels are influenced by sex and age and are subjected to inter and intra-individual variability. By *in vitro* assays we show that these mutations mildly impair IRP-IRE binding; however this minor disturbance is sufficient for biochemical and clinical symptoms to occur in the patients. As previously demonstrated by others we also confirm a tendency for a correlation between the position of the IRE mutation and the ferritin levels in this disease.

Moderate hyperferritinaemia is a common feature found in the adult population and it can be attributed to different factors including metabolic disease, liver

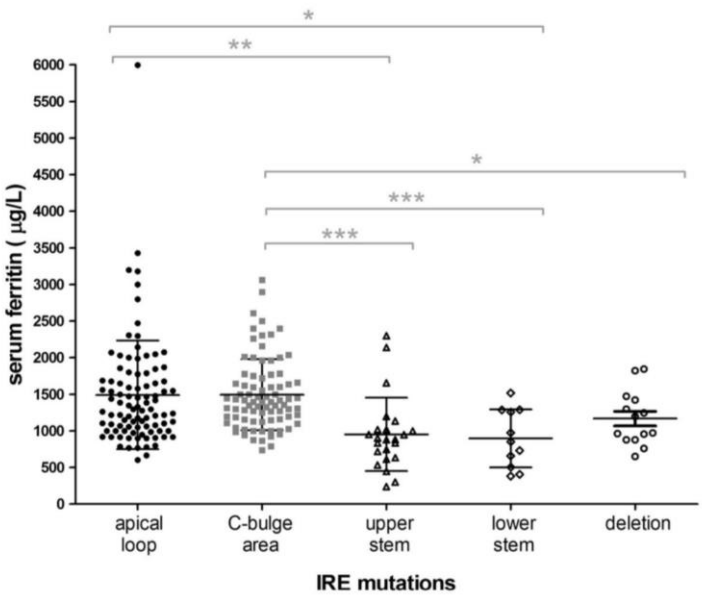

Figure 5 Phenotype-genotype correlation in all described HHCS patients. Serum ferritin levels (y-axis) are reported against the position of the IRE mutation in FTL IRE (x-axis). Patients with mutations affecting the apical loop or the C-bulge area present higher serum ferritin levels compared to the ones with mutations in the upper or lower stems. *p < 0.05; **p < 0.01; ***p < 0.001.

dysfunction, neoplasia, infection and inflammation [28]. Some of these cases could be due to the rare genetic disease HHCS. Therefore, proper tests are important for a correct diagnosis for hyperferritinemia and to avoid unnecessary phlebotomy treatment in the case of HHCS.

Additional files

Additional file 1: Table S1. Primer sequences used for genetic diagnosis and for vector construction in EMSAs. **Figure S1.** (A, B) Structure of the IRE motif of the wild type (panel A) or Badalona +36C > U mutation (panel B). (C, D) RNAfold Web Server folding predictions of the FTL IRE wild type (panel C) or the Badalona +36C > U change (panel D). Colored scale indicates the probability of base pairing from 0 (low, blue) to 1 (high, red). **Table S2.** Table summarizing all HHCS mutations described up to now in the literature. The table shows for each mutation, the conventional nomenclature according to HGVS (corresponding to [NCBI:NM_000146.3] reference sequence), the traditional nomenclature, the position in the IRE structure, the number of families and patients described, the patients' ancestry and the corresponding published report. In bold is indicated the first time a mutation was described; § indicates *de novo* mutations; NA (not available).

Abbreviations

IRP: Iron regulatory protein; IRE: Iron responsive element; UTR: Untranslated region; FTL: Ferritin L; HHCS: Hereditary Hyperferritinaemia cataract syndrome; EMSA: Electrophoretic mobility shift assay; PCR: Polymerase chain reaction; TBE: Tris-borate-EDTA; WT: Wild-type; SD: Standard deviation; NA: Not available; Hb: Hemoglobin; MCV: Mean corpuscolar volume; CRP: C-reactive protein; ALT: Alanine aminotransferase; AST: Apartate aminotransferase.

Competing interests

The authors declare that they have no competing interests.

Authors' contributions

MS is the principal investigator and takes primary responsibility for the paper. CBC and FR recruited the patients. SL, JA, EM and GT performed the laboratory work for this study. MS and MUM co-coordinated the research. SL, MS and MUM wrote the paper. All authors read and approved the final manuscript.

Acknowledgments

The authors would like to thank all patients and their family members for their participation in the study and Harvey Evans for her help in the editing of the manuscript.

This work was supported by the grant PS09/00341 from "Instituto de Salud Carlos III", Spanish Health Program, grant SAF2012-40106 from Ministry of Economy and Competitiveness (MINECO) and grant CIVP16A1857 "Ayudas a proyectos de Investigación en Ciéncias de la Vida Fundación Ramón Areces" to M.S. M.S. held a research contract under the Ramón y Cajal program from the Spanish Ministry of Science and Innovation (RYC-2008-02352). J.A. held a technician support contract under the "Contratos de Técnicos de apoyo a la investigación en el SNS" program from the "Instituto de Salud Carlos III", Spanish Health Program (CA10/01114). M.U.M. acknowledges funding from the E-RARE/BMBF project 01GM1005 and the Dietmar Hopp Stiftung as well as support from the Center For Rare Diseases, Medical Center University of Heidelberg.

Author details

[1]Institute of Predictive and Personalized Medicine of Cancer (IMPPC), Ctra. de Can Ruti, Camí de les Escoles s/n, 08916, Badalona, Barcelona, Spain. [2]Molecular Medicine Partnership Unit (MMPU) EMBL, University of Heidelberg, Heidelberg, Germany. [3]Department of Pediatric Oncology, Hematology, and Immunology, University Hospital of Heidelberg, Heidelberg, Germany. [4]Servicio de hematología y hemoterapia, Hospital Arnau de Vilanova, Valencia, Spain. [5]Praxis für Hämatologie- Onkologie Rhein Ahr, Remagen, Germany.

Received: 23 October 2012 Accepted: 14 February 2013
Published: 19 February 2013

References

1. Arosio P, Ingrassia R, Cavadini P: **Ferritins: a family of molecules for iron storage, antioxidation and more.** *Biochim Biophys Acta* 2009, **1790:**589–599.
2. Hentze MW, Muckenthaler MU, Andrews NC: **Balancing acts: molecular control of mammalian iron metabolism.** *Cell* 2004, **117:**285–297.
3. Girelli D, Olivieri O, De Franceschi L, Corrocher R, Bergamaschi G, Cazzola M: **A linkage between hereditary hyperferritinaemia not related to iron overload and autosomal dominant congenital cataract.** *Br J Haematol* 1995, **90:**931–934.
4. Beaumont C, Leneuve P, Devaux I, Scoazec JY, Berthier M, Loiseau MN, Grandchamp B, Bonneau D: **Mutation in the iron responsive element of the L ferritin mRNA in a family with dominant hyperferritinaemia and cataract.** *Nat Genet* 1995, **11:**444–446.
5. Girelli D, Corrocher R, Bisceglia L, Olivieri O, De Franceschi L, Zelante L, Gasparini P: **Molecular basis for the recently described hereditary hyperferritinemia-cataract syndrome: a mutation in the iron-responsive element of ferritin L-subunit gene (the "Verona mutation").** *Blood* 1995, **86:**4050–4053.
6. Bonneau D, Winter-Fuseau I, Loiseau MN, Amati P, Berthier M, Oriot D, Beaumont C: **Bilateral cataract and high serum ferritin: a new dominant genetic disorder?** *J Med Genet* 1995, **32:**778–779.
7. Sanger F, Nicklen S, Coulson AR: **DNA sequencing with chain-terminating inhibitors.** *Proc Natl Acad Sci U S A* 1977, **74:**5463–5467.
8. Gray NK, Quick S, Goossen B, Constable A, Hirling H, Kuhn LC, Hentze MW: **Recombinant iron-regulatory factor functions as an iron-responsive -element-binding protein, a translational repressor and an aconitase. A functional assay for translational repression and direct demonstration of the iron switch.** *Eur J Biochem* 1993, **218:**657–667.
9. Sanchez M, Galy B, Dandekar T, Bengert P, Vainshtein Y, Stolte J, Muckenthaler MU, Hentze MW: **Iron regulation and the cell cycle: identification of an iron-responsive element in the 3′-untranslated region of human cell division cycle 14A mRNA by a refined microarray-based screening strategy.** *J Biol Chem* 2006, **281:**22865–22874.
10. Cremonesi L, Paroni R, Foglieni B, Galbiati S, Fermo I, Soriani N, Belloli S, Ruggeri G, Biasiotto G, Cazzola M, *et al:* **Scanning mutations of the 5′UTR regulatory sequence of L-ferritin by denaturing high-performance liquid chromatography: identification of new mutations.** *Br J Haematol* 2003, **121:**173–179.
11. Bosio S, Campanella A, Gramaglia E, Porporato P, Longo F, Cremonesi L, Levi S, Camaschella C: **C29G in the iron-responsive element of L-ferritin: a new mutation associated with hyperferritinemia-cataract.** *Blood Cells Mol Dis* 2004, **33:**31–34.
12. Campillos M, Cases I, Hentze MW, Sanchez M: **SIREs: searching for iron-responsive elements.** *Nucleic Acids Res* 2010, **38:**W360–W367.
13. Kannengiesser C, Jouanolle AM, Hetet G, Mosser A, Muzeau F, Henry D, Bardou-Jacquet E, Mornet M, Brissot P, Deugnier Y, *et al:* **A new missense mutation in the L ferritin coding sequence associated with elevated levels of glycosylated ferritin in serum and absence of iron overload.** *Haematologica* 2009, **94:**335–339.
14. Thurlow V, Vadher B, Bomford A, DeLord C, Kannengiesser C, Beaumont C, Grandchamp B: **Two novel mutations in the L ferritin coding sequence associated with benign hyperferritinaemia unmasked by glycosylated ferritin assay.** *Ann Clin Biochem* 2012, **49:**302–305.
15. Faniello MC, Di Sanzo M, Quaresima B, Nistico A, Fregola A, Grosso M, Cuda G, Costanzo F: **Bilateral cataract in a subject carrying a C to A transition in the L ferritin promoter region.** *Clin Biochem* 2009, **42:**911–914.
16. Allerson CR, Cazzola M, Rouault TA: **Clinical severity and thermodynamic effects of iron-responsive element mutations in hereditary hyperferritinemia-cataract syndrome.** *J Biol Chem* 1999, **274:**26439–26447.
17. Cazzola M, Bergamaschi G, Tonon L, Arbustini E, Grasso M, Vercesi E, Barosi G, Bianchi PE, Cairo G, Arosio P: **Hereditary hyperferritinemia-cataract syndrome: relationship between phenotypes and specific mutations in the iron-responsive element of ferritin light-chain mRNA.** *Blood* 1997, **90:**814–821.
18. Arosio C, Fossati L, Vigano M, Trombini P, Cazzaniga G, Piperno A: **Hereditary hyperferritinemia cataract syndrome: a de novo mutation in the iron responsive element of the L-ferritin gene.** *Haematologica* 1999, **84:**560–561.

19. Craig JE, Clark JB, McLeod JL, Kirkland MA, Grant G, Elder JE, Toohey MG, Kowal L, Savoia HF, Chen C, *et al*: **Hereditary hyperferritinemia-cataract syndrome: prevalence, lens morphology, spectrum of mutations, and clinical presentations.** *Arch Ophthalmol* 2003, **121:**1753–1761.
20. Hetet G, Devaux I, Soufir N, Grandchamp B, Beaumont C: **Molecular analyses of patients with hyperferritinemia and normal serum iron values reveal both L ferritin IRE and 3 new ferroportin (slc11A3) mutations.** *Blood* 2003, **102:**1904–1910.
21. Hernandez Martin D, Cervera Bravo A, Balas Perez A: **[Hereditary hyperferritinemia and cataract syndrome: a de novo mutation].** *An Pediatr (Barc)* 2008, **68:**408–410.
22. McLeod JL, Craig J, Gumley S, Roberts S, Kirkland MA: **Mutation spectrum in Australian pedigrees with hereditary hyperferritinaemia-cataract syndrome reveals novel and de novo mutations.** *Br J Haematol* 2002, **118:**1179–1182.
23. Cao W, McMahon M, Wang B, O'Connor R, Clarkson M: **A case report of spontaneous mutation (C33 > U) in the iron-responsive element of L-ferritin causing hyperferritinemia-cataract syndrome.** *Blood Cells Mol Dis* 2010, **44:**22–27.
24. Munoz-Munoz J, Cuadrado-Grande N, Moreno-Carralero MI, Hoyos-Sanabria B, Manubes-Guarch A, Gonzalez AF, Tejada-Palacios P: *Del-Castillo-Rueda A.* Moran-Jimenez MJ: Hereditary hyperferritinemia cataract syndrome in four patients with mutations in the IRE of the FTL gene. Clin Genet; 2012.
25. Alvarez-Coca-Gonzalez J, Moreno-Carralero MI, Martinez-Perez J, Mendez M, Garcia-Ros M, Moran-Jimenez MJ: **The hereditary hyperferritinemia-cataract syndrome: a family study.** *Eur J Pediatr* 2010, **169:**1553–1555.
26. Millonig G, Muckenthaler MU, Mueller S: **Hyperferritinaemia-cataract syndrome: worldwide mutations and phenotype of an increasingly diagnosed genetic disorder.** *Hum Genomics* 2010, **4:**250–262.
27. Bozzini C, Galbiati S, Tinazzi E, Aldigeri R, De Matteis G, Girelli D: **Prevalence of hereditary hyperferritinemia-cataract syndrome in blood donors and patients with cataract.** *Haematologica* 2003, **88:**219–220.
28. Crook MA: **Hyperferritinaemia; laboratory implications.** *Ann Clin Biochem* 2012, **49:**211–213.

doi:10.1186/1750-1172-8-30
Cite this article as: Luscieti *et al.*: Novel mutations in the ferritin-L iron-responsive element that only mildly impair IRP binding cause hereditary hyperferritinaemia cataract syndrome. *Orphanet Journal of Rare Diseases* 2013 **8**:30.

Annex II: Zhuoming *et al.* 2012 J Mol Med

Published in final edited form as:
J Mol Med (Berl). 2012 October ; 90(10): 1209–1221. doi:10.1007/s00109-012-0899-7.

Siderophore-mediated iron trafficking in humans is regulated by iron

Zhuoming Liu[1], **Robert Lanford**[2], **Sebastian Mueller**[3], **Glenn S. Gerhard**[4], **Sara Luscieti**[5], **Mayka Sanchez**[5], and **L. Devireddy**[1,*]

[1]Case Comprehensive Cancer Center and Department of Pathology, Case Western Reserve University, Cleveland, OH 44106, USA

[2]Texas Biomedical Research Institute, San Antonio, TX 78227, USA

[3]Center for Alcohol Research, University of Heidelberg, Heidelberg, Germany

[4]Geisinger Clinic, Weis Center for Research, Danville, PA, 17822

[5]Cancer and Iron group, Institute of Predictive and Personalized Medicine of Cancer (IMPPC), Cancer and Iron group, Crta Can Ruti, Camí de les Escoles s/n, 08916 Badalona, Barcelona, Spain

Abstract

Siderophores are best known as small iron binding molecules that facilitate microbial iron transport. In our previous study we identified a siderophore-like molecule in mammalian cells and found that its biogenesis is evolutionarily conserved. A member of the short chain dehydrogenase family of reductases, 3-OH butyrate dehydrogenase (BDH2) catalyzes a rate-limiting step in the biogenesis of the mammalian siderophore. We have shown that depletion of the mammalian siderophore by inhibiting expression of *bdh2* results in abnormal accumulation of cellular iron and mitochondrial iron deficiency. These observations suggest that the mammalian siderophore is a critical regulator of cellular iron homeostasis and facilitates mitochondrial iron import. By utilizing bioinformatics, we identified an iron-responsive element (IRE; a stem-loop structure that regulates genes expression post-transcriptionally upon binding to iron regulatory proteins or IRPs) in the 3′-untranslated region (3′-UTR) of the human *BDH2 (hBDH2)* gene. In cultured cells as well as in patient samples we now demonstrate that the IRE confers iron-dependent regulation on *hBDH2* and binds IRPs in RNA electrophoretic mobility shift assays. In addition, we show that the *hBDH2* IRE associates with IRPs in cells and that abrogation of IRPs by RNAi eliminates the iron-dependent regulation of *hBDH2* mRNA. The key physiologic implication is that iron-mediated post-transcriptional regulation of *hBDH2* controls mitochondrial iron homeostasis in human cells. These observations provide a new and an unanticipated mechanism by which iron regulates its intracellular trafficking.

Keywords

Mammalian siderophore; IRE-IRP regulation; hemochromatosis

Introduction

Iron (Fe) is indispensable for almost all living organisms with the exception of Lactobacilli and Borrelia, which utilize manganese and cobalt for redox reactions (1). The acquisition

*Contact: lxd59@case.edu; Phone 216-368-1513; Fax 216-368-0494.

and transport of Fe is a challenge to all organisms because of its low solubility and high toxicity. To overcome these problems, organisms such as bacteria and fungi synthesize "siderophores" or iron-specific chelating agents. The role of these compounds is to scavenge iron from the environment (1, 2). In contrast, mammalian cells acquire iron from carrier proteins and the newly acquired iron then enters into a cytosolic "labile" iron pool from which it is distributed among various cellular compartments. This pool of iron is postulated to associate with proteins and low-molecular weight compounds such as siderophores and is a key factor in the cell iron-sensing machinery (3, 4, 5, 6).

We have previously identified a mammalian siderophore and found that it is chemically similar to the *E. coli* Enterobactin – the classical bacterial siderophore (7, 8). Interestingly, the mammalian siderophore is biosynthesized by an evolutionarily conserved pathway and BDH2 (3-hydroxy butyrate dehydrogenase) – a homologue of bacterial EntA catalyzes a rate-limiting step. In this regard, inhibition of *bdh2* expression, which subsequently leads to siderophore depletion, alters intracellular iron homeostasis (8). In addition, siderophore depleted mammalian cells, zebrafish, and yeast fail to synthesize heme – an iron-dependent mitochondrial process (8). These results also suggest that siderophore is a regulatory entity but it is not clear if the expression of mammalian siderophore itself is regulated by iron.

Intracellular iron regulates expression of genes involved in cellular iron metabolism, energy metabolism, cell cycle control and oxygen sensing by altering the interaction of iron regulatory proteins (IRPs) with RNA motifs called iron-responsive elements (IREs). These are stem loop structures present in the untranslated regions of a variety of genes that regulate iron uptake, storage, utilization and transport, as well as other cellular processes such as cell cycle, oxygen sensing and energy metabolism (9 – 12). Genes containing an IRE in the 5′-UTR are translationally inhibited when bound by IRPs, whereas mRNAs containing IREs in 3′-UTR are stabilized when bound by IRPs. Intracellular iron negatively regulates interaction of IRE-IRP complexes, by inhibiting association of IRP with IRE. Hence, intracellular iron promotes the translation of messages containing a 5′ IRE, for example ferritin mRNA. Conversely, low intracellular iron levels have the opposite effect – promoting protein synthesis by stabilizing 3′ IRE-containing mRNAs such as transferrin receptor 1 (*TfR1*) mRNA (9, 11, 13, 14).

IREs are evolutionary conserved hairpin structures of 25–30 nucleotides (15). A typical IRE stem consists of variable sequences that form base pairs of moderate stability ($\Delta G \approx -7$ kcal/mol), and folds into an α-helix that is slightly distorted by the presence of a small bulge in the middle (an unpaired C residue or an asymmetric UGC/C bulge/loop). The loop contains a conserved 5′-CAGUGH-3′ sequence (H denotes A, C or underlined C and G residues form a base pair. The *TfR1* mRNA contains multiple IREs within its long 3′ UTR, while the mRNAs encoding *ferritin-H* and *ferritin-L* contain a single IRE in their 5′ UTRs.

Mice lacking IRPs die *in utero*, thus highlighting the critical importance of the IRE-IRP network (reviewed in refs. 10 and 16). Moreover, mutations in IREs are implicated in human iron disorders (17, 18). Recent studies have also identified non-canonical IREs, which deviate from the above-mentioned sequence, yet confer iron-dependent regulation and in addition they bind IRPs both *in vitro* and *in vivo* (12, 19 – 25). In addition, base substitutions in the pseudotriloop region or in the stem structure of a canonical IRE element also confers iron-dependent regulation (25 – 27). For example, human *ferritin-H* IRE bearing mutations in the 6-nucleotide apical loop sequence that results in conversion of CAGUG(A/C/U) to CAGGG(A/C/U), retains its affinity to IRPs (25).

Mutations in the *HighFe* (*HFE*) gene, which encodes a cell surface, atypical major histocompatibility complex I molecule, cause the most common type of hereditary

hemochromatosis (HH). The specific mutation that leads to amino acid substitution (C282Y), affects the ability of HFE to interact with its chaperone that facilitate its intracellular processing and transport to the surface (28).

Mitochondria are the major site of iron utilization and imported iron is utilized for the synthesis of heme, iron/sulfur clusters (ISCs; refs. 29, 30). Mitochondrial iron import and heme export are coordinated as alterations in these two processes manifest in abnormal mitochondrial iron homeostasis. Alterations in mitochondrial iron homeostasis lead to changes in cellular iron metabolism, suggesting communication between these two compartments (30).

Given the importance of the mammalian siderophore in intracellular iron homeostasis and heme biogenesis (8), it is important to define the mechanisms that regulate the expression of the mammalian siderophore. We have identified a putative IRE in the 3′-UTR of *hBDH2* gene, whose product catalyzes a rate-limiting step in the biosynthesis of the mammalian siderophore. Our studies also demonstrate that this element confers iron-dependent regulation on the expression of *hBDH2* and that it associates with IRPs both *in vitro* and in cells. The iron-dependent regulation of siderophore expression is restricted to hominidae family members. Taken together, our studies show siderophore regulation controls mitochondrial iron import.

Materials and Methods

Cell lines, culture conditions, treatments and transfections

Cells were cultured in Dulbecco's modified Eagle's medium (293T; MIMCD), Minimal essential medium (HeLa), Iscove's modified DMEM (K562), DMEM:F12 (MCF-10 A), Williams E medium (human and primate liver cells) or Medium 200 (HUVEC) supplemented with 10% fetal bovine serum (FBS) or 5% horse serum, 2 mM L-glutamine, 100 units of Penicillin, and 100 μg Streptomycin (Invitrogen). MCF-10 A culture medium contained additional supplements such as insulin, EGFα, cholera toxin B, and hydrocortisone (Sigma). Cells were treated with 100 μM Desferrioxamine (DFO; Calbiochem), or 100 μM Ferric Ammonium Citrate (FAC; Sigma), or 100 μM Hemin (Sigma) for indicated periods of time. Cells were transfected with Lipofectamine (Invitrogen) or X-tremeGENE HP DNA transfection reagent (Roche) as per the manufacturer's recommended procedure.

Bioinformatics approach to identify putative IRE in hBDH2 mRNA

We utilized SIREs (searching for IREs) program available at http://ccbg.imppc.org/sires/index.html to predict iron-response elements in *hBDH2* mRNA (31). Multispecies alignment was performed using CLUSTALW program.

Plasmids and molecular cloning strategy

For iron-dependent regulation studies of *hBDH2* 3′-UTR, a Luciferase reporter containing the *hBDH2* 3′-UTR was constructed as indicated below. A PCR generated ~2 kb fragment containing *hBDH2* 3′-UTR was inserted downstream of the *Luciferase* gene (*luc2*) in pGL4.13 vector (Promega) to generate the Luc - *hBDH2* wt IRE vector. A SV40 early enhancer/promoter drives the expression of the *luc2* gene. We also derived a mutant with nucleotide substitutions within the IRE region of *hBDH2* 3′-UTR (Luc - *hBDH2* mut IRE, also see Fig. 5 B) by site-directed mutagenesis. Additionally, we also generated a series of Luciferase reporter plasmids containing either a 100bp oligomer encompassing the wt *hBDH2* IRE (Luc - WT 100 *hBDH2* IRE) or with nucleotide substitutions in the pseudotriloop region (to convert to a consensus IRE loop sequence; Luc-MT-1 100 *hBDH2*

IRE) or in the stem structure of the *hBDH2* IRE (Luc-MT-2 100 *hBDH2* IRE; also see Fig. 5 B) into pGL4.13 vector. The IRE sequences were inserted downstream of the *luc2* gene as described above. Finally, we also derived Luciferase reporter plasmids bearing wt *hBDH2* IRE (WT-100 5′-LUC) or with nucleotide substitutions in the pseudotriloop region (to convert to a consensus IRE loop sequence; MT1-100 5′-LUC) upstream of the *luc2* gene for iron-dependent translational control analysis (Fig. S3 A). All reporter plasmids were sequence verified.

Luciferase assays

MCF-10 A cells at 50 to 60% confluency cultured in a 6-well plate were transiently transfected with the indicated Luc-IRE reporter plasmids along with a control Renilla Luciferase plasmid (pGL4.74). An empty vector (pGL4.13) served as a negative control. Following the removal of DNA complexes cells were replated in a 24-well plate and treated for 16 hours with 100 μM solutions of Desferrioxamine (DFO, Calbiochem), Hemin (Sigma), or FAC (Sigma). Firefly and Renilla luciferase activities of lysates were assayed using a Dual Luciferase Assay kit from Promega as per the suggested procedure. All Luciferase measurements were normalized to the Renilla Luciferase expression in order to correct for differences in transfection efficiency.

RNA isolation and gene expression analysis

Total RNA was isolated from naïve or treated cells using Trizol method (Invitrogen). DNase I (Promega) treated RNA was then reverse transcribed using Superscript III RT from Invitrogen as per manufacturer's recommendations. The resulting cDNAs were subjected to real time PCR analysis using SYBR Green master mix (Promega) following the manufacturer's recommendations. The fold-change was calculated using ΔΔCT method.

Electrophoretic mobility shift assay (EMSA)

Recombinant His-tagged IRPs (His-IRP-1 and His-IRP-2) were purified from *E. coli* as described in ref. 21. A 100 bp region containing the *hBDH2* wt IRE or with nucleotide substitutions in the pseudotriloop or in the stem structure was (Fig. 5 B) inserted into the pcDNA3.1+ vector (Invitrogen). Similarly, a 60 bp region encompassing the *TfR1* B IRE was subcloned from pUC18-*TfR* B-GH (ref. 32) into the pCDNA3.1+ vector. Radiolabeled wt or mutant *hBDH2* IREs, and *TfR1* B IRE probes were synthesized by *in vitro* transcription using T7 polymerase (New England Bio-labs). Briefly, linearized DNA was transcribed in a 20 μl reaction with 1 U of polymerase at 37°C for 1 hr in the presence of 100 μCi of ^{32}P-GTP (Perkin-Elmer) and 2.5 mM each of ATP, CTP, and UTP (Roche). The labeled cRNA was purified in a Sephadex G-50 column (Roche) following the manufacturer's instructions. Labeled RNA probes had a specific activity of 1–4 × 10^{10} cpm/μg of RNA. The purified labeled probes were stored at −80°C until further use.

EMSAs were performed as previously described in refs. 21 and 33. Concisely, 2–10 × 10^4 cpm of radio labeled RNA probes were initially heat denatured prior to incubation with either 10 ng of purified IRPs for 30 min at room temperature (RT) in a reaction volume of 15μl made up with a binding buffer (25 mM Tris-HCl, pH 7.5; 40 mM KCl; 1% Triton-X 100). Subsequently, RNase T1 (1 unit) was added to the reaction for 10 min at RT, followed by heparin (10 μg/μl; Roche) for an additional 10 min at RT. RNA loading dye was added to each sample and the RNA:protein complexes were resolved for 45 min at 100 v in 0.5 x TBE on a 1.5 mm 4% polyacrylamide gel (GIBCO-BRL) using 0.5 x TBE. Gels were vacuum dried and subjected to autoradiography.

Immunopurification of mRNPs

Immunoprecipitation of IRP-RNA complexes was previously described (34). Briefly, 10 μg of anti-IRP-1 or IRP-2 specific antibody was conjugated to prewashed Protein G-Sepharose (PGS, Invitrogen) in the presence of 200 units each RNAsin (Promega) and Protector RNAse inhibitor (Roche) at 4°C for 1 hour with gentle agitation. The beads were then washed with PBS to remove unbound Ab.

Cells were treated with 100 μM each DFO or hemin for 16 hours at 37°C. Cytoplasmic extracts were prepared by adding 250 μl of lysis buffer (20 mM Hepes, pH 7.6, 25 mM KCl, 0.5% NP-40 and 1 mM PMSF) to the 60-mm dish and incubated at 4°C for 30 min. The clarified supernatants were then incubated with PGS beads coated with anti-IRP antibodies or with uncoated PGS beads (as a control) in binding buffer (20 mM Hepes, pH 7.9, 150 mM NaCl, 0.05% Triton X-100 and 200 units of RNAsin) at 4°C for 1 hour with agitation. The beads were washed twice with the binding buffer and twice with the wash buffer (20 mM Hepes, pH7.9, 150 mM NaCl, 1% Triton X-100, and 200 units of RNAsin). The beads were resuspended in 100 μl of RNase free water, and the bound RNA was recovered by phenol-chloroform extraction and ethanol precipitation. The immunoprecipitated RNA was then subjected to quantitative real time PCR as described above.

In a related set of experiments IRP-RNA complexes from 293T cells stably expressing FLAG-IRPs (35) were precipitated using beads coated with anti-FLAG Ab. Precipitated RNA was recovered as described above.

RNAi knockdown of IRP-1 and IRP-2 genes

The shRNAs specific for IRP-1 and IRP-2 were obtained from Susy Torti (Wake Forest University). HeLa or MCF-10 A cells were transfected with IRP-1 or IRP-2 specific shRNA expressing plasmids and selected for Neomycin resistance (400μg/ml). To achieve a complete knockdown of IRP-1 or IRP-2, the shRNA expressing cells were further transfected with siRNA oligomers specific for IRP-1 or IRP-2 or control siRNA oligomers (Dharmacon). The efficiency of the knockdown was assessed by RT-PCR using gene-specific primers or with IRP-1 and IRP-2 specific antibodies (Santa Cruz biotechnology).

Analysis of hBDH2 mRNA stability

The stability of *hBDH2* mRNA was analyzed by following the procedure described in ref 36. Briefly, Actinomycin D (5 μg/ml) was added to untreated (mock) cells and to cells that were prior treated with 100 μM each DFO or hemin for 16 hours at 37°C. Cells were collected at various times points and the relative levels of *hBDH2* mRNA was quantified by quantitative real time PCR as described above. The *hBDH2* and *TfR1* mRNA levels were normalized to *rlp13a*, a ribosomal gene. Data were plotted on a semi logarithmic graph and the first order decay slope was calculated using lineal regression. Half-lives of *hBDH2* and *TfR1* mRNA were calculated using the equation: $t_{1/2} = \ln 2/(\ln 10 \times$ the slope of the regression line). The slope is $\log_{10} (N_0/N)/t$, where N_0 is the initial amount of mRNA, N is the amount of mRNA at time *t*, and *t* is the elapsed time. Half-lives was calculated from values of three independent experiments.

Assessment of intracellular iron levels

Labile iron pools were measured using the iron-sensitive probes Calcein Green (CALG; Molecular Probes) and rhodamine B-[(1,10-phenanthrolin-5-yl)aminocarbonyl]benzyl ester (RPA) or rhodamine B-[(phenanthren-9-yl)aminocarbonyl]benzyl (RPAC; Axxora), for cytosolic and mitochondrial compartments, respectively. The fluorescent mitochondrial iron indicator RPA contains a rhodamine moiety for mitochondrial targeting and a 1,10-phenanthroline moiety for iron chelation; iron binding quenches the fluorescence of RPA

(37). As a control, we used a structurally similar compound, RPAC, which contains the same fluorophore and linker as RPA but lacks iron-chelating properties and thus its fluorescence is not responsive to iron (37).

Histological procedures

BDH2 or TfR1 levels in paraffin embedded human liver samples from Dr. Gretta Jacobs (Case Western Reserve University) were analyzed using validated anti-human BDH2 (http://www.origene.com/antibody/ab_short.mspx?product=TA501293;Origene) or TfR1 (Invitrogen; ref. 38) antibodies as per the manufacturer's instructions. The nuclei were counterstained with methylene blue. Non-heme iron in human liver tissues was visualized by diaminobenzidine(DAB)-enhanced Perls Prussian blue staining. Non-heme iron stains blue. Hematoxylin and Eosin staining was performed utilizing a kit from Sigma as per the manufacturer's procedure.

Statistical analysis

Statistical analyses were performed by one-way analysis of variance and Tukey HSD (honestly significant difference) test was performed for multiple comparisons using SAS/STAT software. *p* values of less than 0.05 were considered statistically significant. Error bars shown in figures represent SD.

Results

Iron-dependent regulation of human bdh2 expression

We have previously shown that 2,5-dihydroxy benzoic acid (2,5-DHBA) is a component of the mammalian siderophore, which is similar to 2,3-DHBA, the Fe-binding moiety of *E. coli* Enterobactin (7, 8). We also found that BDH2, a homolog of bacterial EntA is responsible for 2,5-DHBA synthesis (8). Depletion of the siderophore from mammalian cells, yeast, and zebrafish embryos caused abnormal accumulation of cytoplasmic Fe and mitochondrial Fe deficiency. Thus, these results suggest that the mammalian siderophore is a critical regulator of cellular iron homeostasis.

Based on these findings, we hypothesize that the siderophore may be in turn regulated by iron. To test this prediction, we assessed *hBDH2* expression in liver samples obtained from hemochromatosis patients. Quantitative real-time PCR analysis with specific primers (Table S1) demonstrated a decrease in *hBDH2* expression in liver samples from hemochromatosis patients compared with liver samples from normal controls (Fig. 1 A). Further, the reduction in *hBDH2* expression inversely coincides with iron indices as well as the genetic status of the disease (Figure 1 A and Table S2). The mRNA levels of *TfR1*, a well characterized iron regulated gene was also decreased in these samples (Fig. 1 B). Transcript levels were normalized to *rlp13a* mRNA, which is not iron regulated.

We next asked if a decrease in *hBDH2* expression is also reflected at the protein level. To address this question, we analyzed hBDH2 expression by immunohistochemistry in frozen liver sections from hemochromatosis patients and from controls (Table S3). Iron overloading in hemochromatosis samples (HH1 -HH5) was confirmed by Perls prussian blue staining (Fig. 1 C). As expected, TfR1 protein levels are decreased in these samples (Fig. 1 C). In accordance with the real-time PCR data, immunohistochemical staining using an anti-hBDH2 antibody also demonstrated less expression of hBDH2 in liver cells from hemochromatosis patients (Fig. 1 C). Finally, in support of these findings, microarray analysis of liver tissues derived from hemochromatosis patients also demonstrated a decrease in *hBDH2* expression (Table S4 and ref. 39). In summary, these results demonstrate that *hBDH2* expression is iron regulated.

To study the generality of iron-dependent regulation of *hBDH2*, we next assessed its mRNA levels under iron-replete or iron-deficient conditions in cultured human cells. Specifically, we utilized adherent non-hematopoietic, immortalized cells (MCF-10 A or HUVEC) or transformed cells (HeLa) and non-adherent hematopoietic cells (K562). Cells were either treated with 100 μM DFO or 100 μM each hemin or FAC as iron sources to achieve iron-deficient or iron-replete conditions, respectively. *HBDH2* and *TfR1* mRNA levels were quantified by qRT-PCR using gene-specific primers (Table S1). As expected, *TfR1* mRNA expression increases upon addition of DFO and decreases following iron supplementation in above-mentioned cultured human cells (Fig. 2 A). Similarly, *hBDH2* mRNA levels are increased under iron-deficient conditions and decreased under iron-replete conditions in all cells (Fig. 2 A). Transcript levels were normalized to *actin* mRNA, which is not iron regulated (Fig. 2 A). In addition, immunoblot analysis with a BDH2 specific antibody further confirmed iron dependent regulation of hBDH2 expression in MCF-10 A cells (Fig. S1). A time course analysis indicated *hBDH2* mRNA levels accumulated progressively in DFO treated MCF-10 A cells (Fig. 2 B). If *hBDH2* mRNA levels were indeed stabilized by iron-delete conditions, then iron supplementation should reverse this process. To test this prediction, we added graded doses of FAC to DFO treated MCF-10 A cells and find that iron supplementation blunted the DFO-induced stabilization of *hBDH2* mRNA (Fig. 2 C). Taken together these studies show that iron regulates the expression of *hBDH2* mRNA in cultured human cells as well as in patient liver.

Identification of an IRE motif in hBDH2 mRNA

Intracellular iron regulates gene expression post-transcriptionally by IRE-IRP network. To determine whether *hBDH2* mRNA contains an IRE-like element, we utilized the SIREs program, which identified a single, IRE-like motif in the 3′-UTR of *hBDH2* mRNA (Figs. 3 A, B & C). The IRE sequence of *hBDH2* mRNA shares several common features with the previously identified 3′-UTR IRE sequence of the *TfR1* gene (Fig. 3 B; ref. 15). For instance, it contains a 6-nucleotide apical loop sequence, CAGGGC, which shares similarities to the canonical IRE sequence of CAG**W**G**H** ('W' stands for A or U and 'H' for A, C, or U). The first C could form a base pair with the fifth G to form an AGG pseudotriloop structure, which may be recognized by the IRPs (25 -27). The IRE of *hBDH2* mRNA also contains an upper stem of 4 paired nucleotides and is separated from the lower stem by a single unpaired cytosine (Figs. 3 B & C). A similar motif was found in *bdh2* homologues in chimpanzee and orangutan but not in other simian primates (Fig. 3 C & D). Since only members of the hominidae family contain an IRE-like sequence in the 3′-UTR of *bdh2*, we suggest that iron-dependent regulation of *bdh2* is a recent evolutionary acquisition. Thus, IRE-like sequences in the 3′-UTR of *bdh2* mRNA is specific to members of the hominidae family, highlighting the adaptation of these species to impose additional mechanisms to regulate the expression of the siderophore.

Iron-dependent regulation of the mammalian siderophore is restricted to hominidae

We assessed iron-dependent regulation of *bdh2* mRNA in transformed liver cells derived from various non-human primates and - as a reference - in transformed human liver cells (Fig. 3 E). Liver is appropriate for these studies since *bdh2* is abundantly expressed in this organ (8). We found that *bdh2* mRNA levels were decreased by hemin and increased by DFO in liver cell lines from chimpanzee and human, but not in baboon, vervet, marmoset and tamarin cells (Fig. 3 E). We evaluated *bdh2* mRNA levels in cultured rodent cells and found that iron does not regulate *bdh2* mRNA. As expected, *TfR1* levels changed based on iron content in all cell types (Fig. 3 E and Fig. S2). Collectively, the results of Figure 3 suggest that the presence of an IRE-like motif determines the iron-dependent regulation of *bdh2*. These results further confirm the prediction that the IRE motif in *bdh2* mRNA is restricted to hominidae family (Fig. 3).

J Mol Med (Berl). Author manuscript; available in PMC 2013 February 08.

Recruitment of IRPs on to hBDH2 IRE-like motif in vitro

Our data suggest that the IRE-like motif in the *hBDH2* mRNA confers iron-dependent regulation. To examine the association between *hBDH2* IRE and IRPs in cells, two sets of co-immunoprecipitation experiments were performed.

In the first set of experiments, we immunoprecipitated endogenous IRP-1 and IRP-2 complexes from naïve cells or cells treated with DFO or hemin using antibodies specific for IRP-1 and IRP-2. Anti-IRP antibodies effectively immunoprecipitated endogenous *hBDH2* mRNA in cytosolic extracts of naïve MCF-10A cells (Fig. 4 A). DFO treatment enhanced immunoprecipitation between IRPs and *hBDH2* mRNA, whereas hemin treatment markedly reduced co-immunoprecipitation of *hBDH2* mRNA with IRPs (Fig. 4 A). *TfR1* also co-immunoprecipitated with IRPs (Fig. 4 A). Together, these data suggest that *hBDH2* mRNA associates with IPRs in cells. In complementary experiments, we immunoprecipitated endogenous *hBDH2* mRNA from 293T cells stably expressing FLAG IRPs (ref. 35) with an anti-Flag antibody and confirm the association of *hBDH2* mRNA with IRPs in cells (Fig. 4 B).

In a second set of experiments, we immunoprecipitated IRP-1 and IRP-2 complexes from cells transfected with a *hBDH2* 3′-UTR reporter plasmid. In these experiments we utilized 293T cells stably expressing FLAG IRP-1 or FLAG IRP-2 (ref. 35). These cells were transfected with reporter plasmids containing either *hBDH2* wt IRE (luc-*hBDH2* wt IRE-3′-UTR) or *hBDH2* mutant IRE (luc-*hBDH2* mutant IRE-3′-UTR). The mutant *hBDH2* 3′-UTR reporter plasmid contains 2 mutations in the IRE that are known to disrupt IRE-IRP interactions (Fig. 5 A for description of these plasmids). An empty Luciferase reporter plasmid served as a negative control. Ectopically expressed *hBDH2* wt IRE 3′-UTR was enriched significantly by immunoprecipitation in both IRP-1 and IRP-2 expressing cells (Fig. 4 C). The mutant reporter plasmid was expressed normally as judged by Luciferase expression (Fig. 5) but failed to associate with either of IRPs (Fig. 4 C). As expected, the empty Luciferase reporter plasmid lacking the *hBDH2* 3′-UTR did not associate with IRP-1 and IRP-2 (Figure 4 C). Together, these data show that *hBDH2* mRNA contains a functional IRE-like motif, which associates with IRPs in cells and is required for iron-dependent regulation of *hBDH2* mRNA expression.

hBDH2 3′-UTR IRE is required for iron-dependent regulation

The results presented so far suggest that IRPs interact with the *hBDH2* 3′-UTR IRE. A Luciferase reporter system was used to directly confirm iron-dependent post-transcriptional regulation by the *hBDH2* 3′-UTR. HeLa cells were transiently transfected with a *Luciferase* reporter gene containing the ~2 kb *hBDH2* 3′-UTR (Fig. 5 A). The control plasmid contained the same promoter but lacked the *hBDH2* 3′-UTR. Following overnight transfection, cells were then treated with FAC or DFO. Luciferase expression was increased by DFO and decreased by FAC in cells expressing *hBDH2* wt IRE 3′-UTR (Fig. 5 C). Mutation of the IRE in the *hBDH2* 3′-UTR abrogated iron-dependent regulation of Luciferase expression (Fig. 5 C).

To further rigorously test the functional importance of IRE in the iron-dependent regulation of *hBDH2*, we placed sequences encompassing *hBDH2* IRE downstream of *Luciferase* coding sequences and assessed the Luciferase expression under iron-replete or iron-deficient conditions (Fig. 5 C). DFO addition led to an increase in Luciferase expression in the wt-100 *hBDH2* IRE-luc and MT1-100 *hBDH2* IRE-luc transfectants compared with MT2-100 *hBDH2* IRE-luc transfectants (Fig. 5 C). To additionally confirm these results, we placed sequences encompassing *hBDH2* IRE upstream of *Luciferase* coding sequences and assessed the Luciferase expression under iron-replete or iron-deficient conditions (Fig. S3

A). Again, *hBDH2* IRE presence conferred iron-dependent expression of Luciferase activity (Fig. S3 C). Collectively, the results of Figs. 5 & S3 indicate that *hBDH2* 3′-UTR or *hBDH2* IRE confers iron-dependence to a heterologous gene.

Abrogation of IRPs blunts the iron-dependent regulation of hBDH2 mRNA

To further assess the role of the IRPs in the regulation of *hBDH2* expression, we abrogated expression of IRP-1 or IRP-2 or both by shRNA and siRNA transfection and determined the expression of *hBDH2* under iron-replete or iron-deficient conditions. We initially assessed the efficacy of siRNA transfection by analyzing the expression levels of IRP-1 and IRP-2 by quantitative real time PCR analysis, which demonstrated the near complete knockdown of these two genes (Fig. S4 A). Loss of both IRP-1 and IRP-2 eliminated the iron-dependent regulation of *hBDH2* or *TfR1* expression as assessed by real time PCR analysis (Fig. S4 B). The effects of IRP reduction were additive, as *hBDH2* mRNA expression was greatly reduced in double knockdown cells (Fig. S4 C). Thus, IRPs are required for iron-dependent regulation of *hBDH2* expression.

hBDH2 3′-UTR IRE is required for iron-dependent destabilization of hBDH2 mRNA

Binding of IRPs to IREs present in the 3′-UTR prolongs the half-life of mRNA by protecting against endonucleolytic cleavage (ref. 14). IRP-1 is dual function protein that can act as an aconitase under iron-replete conditions or binds IRE when iron levels are low. IRP-2 activity is regulated by proteosomal degradation (reviewed in ref. 13). Thus, iron-replete conditions prevent the binding of IRPs to IREs in the target genes, resulting in degradation of mRNAs with 3′-UTR IREs. Conversely, under iron-deficient conditions IRPs bind and prolong the half-life of mRNAs containing 3′-UTR IREs.

We therefore studied the functional importance of the *hBDH2* IRE for mRNA stability. We depleted both IRP-1 and IRP-2 proteins in MCF-10 A cells by RNAi. Data presented in Fig. S5 F confirms the knockdown of IRPs as judged by an immunoblot analysis. Next, we assessed the stability of *hBDH2* and *TfR1* mRNAs under iron-deficient or iron-replete conditions in control shRNA expressing cells as well as in IRP depleted cells. As expected, iron supplementation destabilized the *hBDH2* mRNA, and in contrast, iron scarcity stabilized *hBDH2* mRNA levels in control cells (Fig. S5 A & B). Depletion of IRPs decreased the stability of *hBDH2* and *TfR1* mRNAs (Fig. S5 C & D). Taken together the combined results of Fig. S5 suggest that the iron regulates *hBDH2* mRNA stability through IRP proteins.

As noted in Fig. 3, murine *bdh2* mRNA does not possess an IRE. To test the prediction that *bdh2* mRNA is regulated by iron via IRE-independent mechanisms, we assessed the stability of *bdh2* mRNA in a murine pro-B lymphocytic cell line (FL5.12) under iron-deficient or iron-replete conditions. Data presented in Fig. S5 E shows that *bdh2* mRNA levels are impervious to iron levels. Thus, the observed *hBDH2* regulation is secondary to the IRE (Figs. 1 to 5 and Figs. S3 to S5).

Human BDH2 IRE binds IRPs in vitro

We next examined the binding characteristics of the *hBDH2* IRE-like stem-loop to IRP-1 and IRP-2 by RNA electrophoretic mobility shift assays (EMSAs). A radio labeled RNA oligomer encompassing the *hBDH2* IRE was incubated with increasing amounts of purified recombinant IRP-1 or IRP-2 or a combination of both IRPs (ref. 21) and the complexes were resolved on non-denaturing polyacrylamide gels and the RNA-protein complexes were visualized by autoradiography. *TfR1* B IRE was used as a positive control in these experiments. As expected, *TfR1* B IRE binds to both IRPs (Fig. S6 A). The radiolabeled *hBDH2* IRE also binds to IRP-1 and IRP-2 proteins (Fig. S6 A). To further confirm the

specificity of the binding of IRPs to *hBDH2* IRE, we performed EMSA competition assays. Addition of unlabeled wt *hBDH2* IRE RNA oligomer efficiently inhibited the binding of IRP-1 or IRP-2 to radiolabeled *hBDH2* IRE in a dose-dependent manner (Fig. S6 B). Nucleotide substitutions in the loop region (MT-1; Fig. 5 A), which did not compromise the ability of *hBDH2* IRE to confer iron-dependent regulation also abolished the binding of IRPs to radio labeled *hBDH2* IRE (Fig. S6 B). However, substitutions at positions in the stem region (MT-2; Fig. 5 A), which blunted the iron responsiveness to *hBDH2* IRE is unable to compete (Fig. S6 B). The observation that higher amounts of unlabeled competitor are required to abolish the binding suggests that *hBDH2* IRE binds IRPs with lower affinity. As expected, addition of *TfR1* IRE efficiently inhibited the binding.

In summary, the *in vitro* binding experiments suggest that the *hBDH2* IRE binds purified recombinant IRPs and is consistent with the association of IRPs to *hBDH2* IRE in cells.

Depletion of the siderophore due to increased cytoplasmic iron suppresses iron accumulation in mitochondria

Our data thus far suggest that the *hBDH2* IRE confers iron-dependent regulation upon *hBDH2*. What are the physiological implications of this observation for iron regulation of the siderophore? In our prior study, we showed that depletion of the siderophore led to mitochondrial iron deficiency in yeast, fish and cultured mammalian cells. These studies suggest that siderophore is a major facilitator of mitochondrial iron import (8). Based on these findings, we hypothesize that under iron-replete conditions, down regulation of siderophore via the IRE-IRP network prevents mitochondrial iron overload (Fig. 6 A). We tested this prediction in cultured mammalian cells.

We first asked whether suppression of siderophore by increased cytoplasmic iron changes mitochondrial iron content. We tested this idea using a panel of liver cells from great apes some of which lack a functional IRE in the 3′-UTR of *bdh2* mRNA (Fig. 3 E). Iron-replete conditions were achieved by treatment with hemin. Cytosolic and mitochondrial iron content was quantified using subcellular iron-specific dyes as outlined in methods section (also see refs 8 & 37). If our hypothesis is correct, mitochondrial iron content should not rise upon an increase in cytoplasmic iron in cells with a functional IRE in the 3′-UTR of *bdh2* mRNA. Data presented in Fig. 6 B demonstrate that the mitochondria of liver cells of species with the IRE (human and chimpanzee) are relatively iron deficient despite increased cytoplasmic iron. In contrast, the mitochondrial iron content of cells from a species that does not have the IRE (tamarin) mirrored that of cytoplasmic iron (Fig. 6 B). Thus, the presence of a functional IRE in the *hBDH2* mRNA is necessary for regulation mitochondrial iron levels.

Discussion

Most genes involved in the regulation of cellular iron metabolism are in turn regulated by Iron. This group includes the genes involved in cellular iron uptake, storage, and utilization. All are regulated post-transcriptionally via the IRE-IRP network. As indicated by gene knockout studies, this control is vital for the proper maintenance of cellular iron homeostasis (10, 16). It is not known, however, whether such control also regulates expression of genes implicated in intracellular iron trafficking. Mitochondria are the principal consumers of iron yet the precise mechanisms by which iron is imported into the mitochondria remain elusive (22). Iron in the free form is reactive. It therefore must be shielded and chaperoned to the sites of utilization. In our preceding study, we demonstrated that the mammalian siderophore binds and trafficks iron from cytosol into mitochondria. Further, siderophore depletion results in mitochondrial iron deficiency in a variety of model systems (8). Normally, mitochondrial iron import and heme export are in equilibrium and perturbations in this process leads to abnormal mitochondrial iron homeostasis. Since the mammalian

siderophore is an important facilitator of mitochondrial iron import, this process must be finely regulated to prevent accidental mitochondrial iron overload. However, the molecular basis by which this regulation is achieved remains to be demonstrated. We hypothesize that the mammalian siderophore is regulated by iron via IRE-IRP network to control the siderophore-dependent iron trafficking into the mitochondria.

Siderophore in human cells is regulated by iron

To examine the above-mentioned hypothesis, in this report, we explored the iron-dependent regulation of the siderophore. In cultured cells and in patient samples, *hBDH2* expression is controlled by iron and this regulation is conferred by a single IRE-like motif located in its 3′-UTR. Mutations in the *hBDH2* 3′-UTR IRE resulted in loss of iron responsiveness. Additionally, *in vitro* and *in vivo* experiments found that *hBDH2* IRE associates with IRPs and this association is important for the iron-dependent regulation of *hBDH2* expression. Finally, *hBDH2* IRE also conferred iron responsiveness to a heterologous reporter gene thus, further confirming its functionality.

Human *BDH2* belongs to an evolutionarily conserved family of proteins collectively termed short chain dehydrogenases/reductases (SDRs). Interestingly, the presence of IRE is restricted to *bdh2* genes of members of the hominidae family, and this finding may suggest that it is a newly acquired regulatory mechanism for iron control of *bdh2* genes. Thus, the *hBDH2* IRE adds to a growing list of IREs with a restricted phylogenetic distribution. For instance, *Cdc14a*, succinate dehydrogenase, MRCKα, and AHSP genes although present in all vertebrates, their IREs are restricted to certain species (19 – 21, 24). Thus, the restricted presence of *BDH2* IRE to humans and higher order primates further highlight the importance of the *bdh2* gene in iron trafficking and cellular iron metabolism and the existence of additional mechanisms necessary to regulate the siderophore-mediated iron trafficking in these species.

Iron-regulated expression of the siderophore controls mitochondrial iron content

What are the physiological implications of the regulation by iron of the expression of mammalian siderophore? Based on gene-ablation studies, we found that the mammalian siderophore facilitates mitochondrial iron import. For instance: 1) siderophore-depleted zebrafish embryos and yeast are heme-deficient; and 2) siderophore suppression results in marked elevation of cytoplasmic iron as a consequence of impaired mitochondrial iron import. Thus, changes in mammalian siderophore levels affect cellular iron metabolism (8). In support of this notion, our studies reveal that under iron-replete conditions, down regulation of siderophore via the IRE-IRP network prevents mitochondrial iron overload. Thus, the presence of a functional IRE in the *bdh2* mRNA is necessary for regulation mitochondrial iron levels. In conclusion, based on the previous findings as well as those presented in this report, we hypothesize that iron regulates the siderophore-dependent iron trafficking into the mitochondria.

Supplementary Material

Refer to Web version on PubMed Central for supplementary material.

Acknowledgments

We thank Elizabeth Leibold, Matthias Hentze, Kostas Pantopoulos and Susy Torti for providing reagents, Gretta Jacobs for human hemochromatosis liver sections, Joe Willis for normal human liver sections, Sebastian Mueller for providing RNA samples of normal and hemochromatosis liver, Robert Lanford for providing transformed liver cells of human and apes, and Alan Tartakoff for editorial assistance. This work is supported by K01CA113838, R01DK081395, and Case Western Reserve University start up funds to L.R.D and by PS09/00341 from Spanish

Health Program (Instituto de Salud Carlos III) and RYC-2008-02352 research contract (Spanish Ministry of Science and Innovation) to M.S. L.R.D. is also a recipient of career developmental awards from March of Dimes and American Society of Hematology.

References

1. Guerinot ML. Microbial iron transport. Annu Rev Microbiol. 1994; 48:743–772. [PubMed: 7826025]
2. Nielands JB. Siderophores: structure and functions of microbial iron transport compounds. J Biol Chem. 1995; 27:26723–26726.
3. Kakhlon O, Cabantchik ZI. The labile iron pool: Characterization, measurement, and participation in cellular processes. Free Radical Biol & Med. 2002; 33:1037–1046. [PubMed: 12374615]
4. Kruszewski M. Labile iron pool: the main determinant of cellular response to oxidative stress. Mut Res. 2003; 531:81–92. [PubMed: 14637247]
5. Fernandez-Pol JA. Isolation and characterization of a siderophore-like growth factor from mutants of SV40-transformed cells adapted to picolinic acid. Cell. 1977; 14:489–499. [PubMed: 210954]
6. Jones R, Peterson C, Grady R, Cerami A. Low molecular weight iron-binding factor from mammalian tissue that potentiates bacterial growth. J Exp Med. 1980; 151:418–428. [PubMed: 6985950]
7. Raymond KN, Dertz EA, Kim SS. Enterobactin: an archetype for microbial iron transport. Proc Natl Acad Sci USA. 2003; 100:3584–3588. [PubMed: 12655062]
8. Devireddy LR, Hart DO, Goetz DH, Green MR. A mammalian siderophore synthesized by an enzyme with a bacterial homolog involved in enterobactin production. Cell. 2010; 141:1006–1017. [PubMed: 20550936]
9. Eisenstein RS. Iron regulatory proteins and the molecular control of mammalian iron metabolism. Annu Rev Nutr. 2000; 20:627–662. [PubMed: 10940348]
10. Hentze MW, Muckenthaler MU, Galy B, Camaschella C. Two to tango: Regulation of mammalian iron metabolism. Cell. 2010; 142:24–38. [PubMed: 20603012]
11. Muckenthaler MU, Galy B, Hentze MW. Systemic iron homeostasis and the iron-responsive element/iron-regulatory protein (IRE/IRP) regulatory network. Annu Rev Nutr. 2008; 28:197–213. [PubMed: 18489257]
12. Sanchez M, Galy B, Muckenthaler MU, Hentze MW. Iron-regulatory proteins limit hypoxia-inducible factor-2alpha expression in iron deficiency. Nat Struct Mol Biol. 2007; 14:420–426. [PubMed: 17417656]
13. Wallander ML, Leibold EA, Eisenstein RS. Molecular control of vertebrate iron homeostasis by iron regulatory proteins. Biochim Biophys Acta. 2006; 1763:668–689. [PubMed: 16872694]
14. Binder R, et al. Evidence that the pathway of transferrin receptor mRNA degradation involves an endonucleolytic cleavage within the 3′ UTR and does not involve poly(A) tail shortening. EMBO J. 1994; 13:1969–1980. [PubMed: 7909515]
15. Piccinelli P, Samuelsson T. Evolution of the iron-responsive element. RNA. 2007; 13:952–966. [PubMed: 17513696]
16. Rouault TA. The role of iron regulatory proteins in mammalian iron homeostasis and disease. Nature Chem Biol. 2006; 2:406–414. [PubMed: 16850017]
17. Beaumont C. Mutation in the iron responsive element of the L ferritin mRNA in a family with dominant hyperferritinaemia and cataract. Nat Genetics. 1995; 11:444–446. [PubMed: 7493028]
18. Kato J, et al. A mutation, in the iron-responsive element of H ferritin mRNA, causing autosomal dominant iron overload. Am J Hum Genet. 2001; 69:191–197. [PubMed: 11389486]
19. Rogers JT, et al. An iron-responsive element type II in the 5′-untranslated region of the Alzheimer's amyloid precursor protein transcript. J Biol Chem. 2002; 277:45518–45528. [PubMed: 12198135]
20. Cmejla R, Petrak J, Cmejlova J. A novel iron-responsive element in the 3′UTR of human MRCKalpha. Biochem Biophys Res Commun. 2006; 341:158–166. [PubMed: 16412980]

21. Sanchez M, et al. Iron regulation and the cell cycle. Identification of an iron-responsive element in the 3′-untranslated region of human cell division cycle 14 mRNA by a refined microarray-based screening strategy. J Biol Chem. 2006; 281:22865–22874. [PubMed: 16760464]
22. Meehan HA, Connell GJ. The hairpin loop but not the bulged C of the iron responsive element is essential for high affinity binding to iron regulatory protein-1. J Biol Chem. 2001; 276:14791–14796. [PubMed: 11278657]
23. Sierzputowska-Gracz H, McKenzie RA, Theil LC. The importance of single G in the hairpin loop of the iron responsive element (IRE) in ferritin mRNA for structure: an NMR spectroscopy study. Nucleic Acids Res. 1995; 23:146–153. [PubMed: 7870579]
24. dos Santos CO, et al. An iron responsive element-like stem-loop regulates a-hemoglobin-stabilizing protein mRNA. J Biol Chem. 2008; 283:26956–26964. [PubMed: 18676996]
25. Butt J, et al. Differences in the RNA binding sites of iron regulatory proteins and potential target diversity. Proc Natl Acad Sci USA. 1996; 93:4345–4349. [PubMed: 8633068]
26. Barton H, Eisenstein RS, Bomford A, Munro H. Determinants of the interaction between the iron-responsive element-binding protein and its binding site in rat L-ferritin mRNA. J Biol Chem. 1990; 265:7000–7008. [PubMed: 2324109]
27. Henderson BR, Menotti E, Bonnard C, Kuhn LC. Optimal sequence and structure of iron-responsive elements. J Biol Chem. 1994; 269:17481–17489. [PubMed: 8021254]
28. Feder JN, et al. A novel MHC class I-like gene is mutated in patients with hereditary haemochromatosis. Nat Genet. 1996; 13:399–408. [PubMed: 8696333]
29. Napier I, Ponka P, Richardson DR. Iron trafficking in the mitochondrion: Novel pathways revealed by disease. Blood. 2005; 105:1867–1874. [PubMed: 15528311]
30. Richardson DR, et al. Mitochondrial iron trafficking and the integration of iron metabolism between the mitochondrion and cytosol. Proc Natl Acad Sci USA. 2010; 107:10775–10782. [PubMed: 20495089]
31. Campillos M, Cases I, Hentze M, Sanchez M. SIREs: searching for iron-responsive elements. Nucleic Acids Res. 2010; 2010:1–8.
32. Casey JL, et al. Iron responsive elements: regulatory RNA sequences that control mRNA levels and translation. Science. 1988; 240:924–928. [PubMed: 2452485]
33. Hanson ES, Foot LM, Leibold EA. Hypoxia post-translationally activates iron-regulatory protein 2. J Biol Chem. 1999; 274:5047–5052. [PubMed: 9988751]
34. Sanchez M, Galy B, Hentze M, Muckenthaler MU. Identification of target mRNAs of regulatory RNA binding proteins using mRNP immunopurification and microarrays. Nat Protoc. 2007; 2:2033–2042. [PubMed: 17703216]
35. Zumbrennen KB, Wallander ML, Romney SJ, Leibold EA. Cysteine oxidation regulates the RNA-binding activity of iron regulatory protein 2. Mol Cell Biol. 2009; 29:2219–2229. [PubMed: 19223469]
36. Li X-L, Andersen JB, Ezelle HJ, Wilson GM, Hassel BA. Post-transcriptional regulation of RNAse-L expression is mediated by the 3′-Untranslated region of its mRNA. J Biol Chem. 2007; 282:7950–7960. [PubMed: 17237228]
37. Rauen U, et al. Assessment of chelatable mitochondrial iron by using mitochondrion-selective fluorescent iron indicators with different iron-binding affinities. Chembiochem. 2007; 8:341–352. [PubMed: 17219451]
38. Tampanaru-Sarmeslu, et al. Transferrin and Transferrin receptor in human hypophysis and pituitary adenomas. Am J Pathol. 1998; 152:413–422. [PubMed: 9466567]
39. Hagist S, et al. In vitro-targeted gene identification in patients with hepatitis C using a genome-wide microarray technology. Hepatol. 2008; 49:378–386.

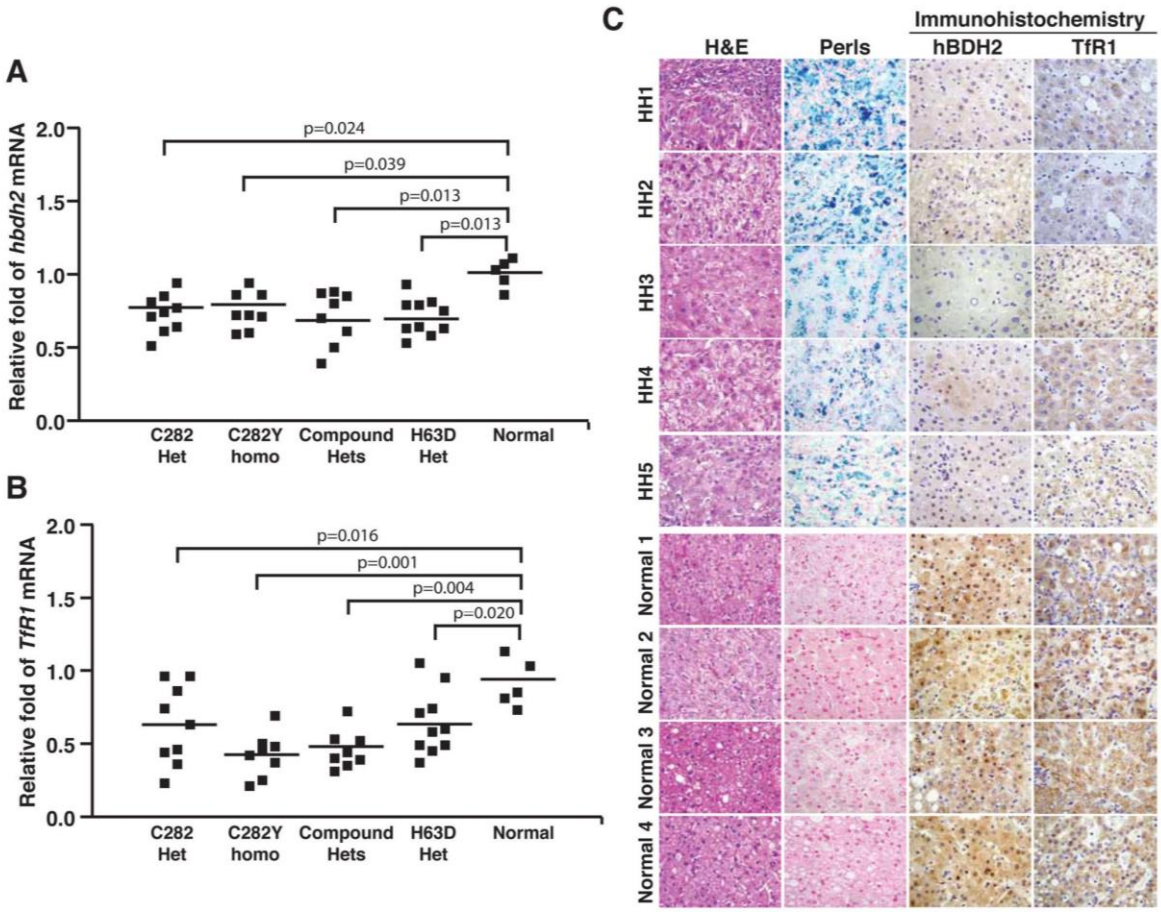

Figure 1.

Human *BDH2* mRNA and protein are down regulated in liver from hemochromatosis patients. (**A**) Total RNA from normal or hemochromatosis liver samples were subjected to quantitative real time PCR using primers specific for *hBDH2* and mRNA levels were normalized to *rlp13a*, a ribosomal gene. (**B**) *TfR1* mRNA levels were analyzed to assess the impact of iron overloading, an iron-regulated mRNA. (**C**) Hemochromatosis (HH1–5) or normal liver sections were immunostained with anti-BDH2 Ab (Origene) and Perls Prussian blue staining to detect iron. Non heme iron stains blue. As a positive control, liver sections were also stained with anti-TfR1 Ab. Hematoxylin-Eosin (H&E) staining was performed to demonstrate the liver architecture.

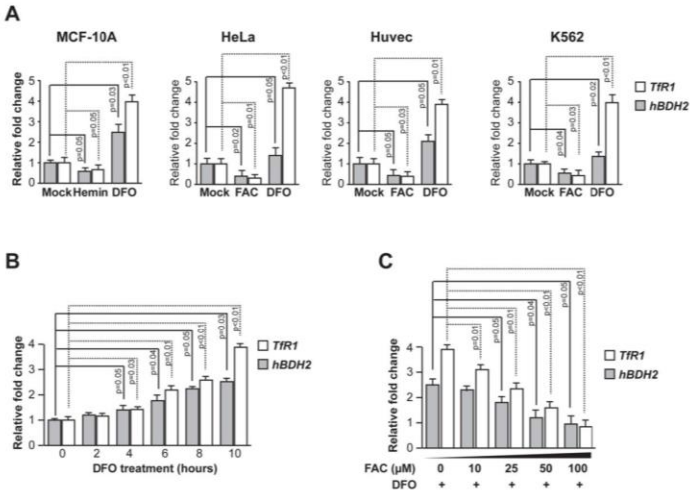

Figure 2. Iron-deficiency leads to increased *hBDH2* mRNA levels

(**A**) Human cell lines were treated with hemin, FAC, DFO or mock-treated for 16 hours and *TfR1* and *hBDH2* mRNAs were quantified by real time PCR analysis 16 hours post treatment. (**B**) MCF-10A cells were treated with DFO for the indicated times and *hBDH2* and *TfR1* mRNAs were quantified as described above. (**C**) Iron supplementation reverses DFO-induced increase in *hBDH2* and *TfR1* mRNAs. MCF-10 A cells were treated with 100 μM of DFO along with increasing amounts of FAC and relative levels of *hBDH2* mRNA were quantified 10 hours post treatment as described above. For A – C, value on y-axis was set at 1.0 for the mRNA levels in untreated cells. The relative mRNA levels in each sample were normalized to *actin* mRNA. Results shown are the average of three independent experiments with error bars depicting SD.

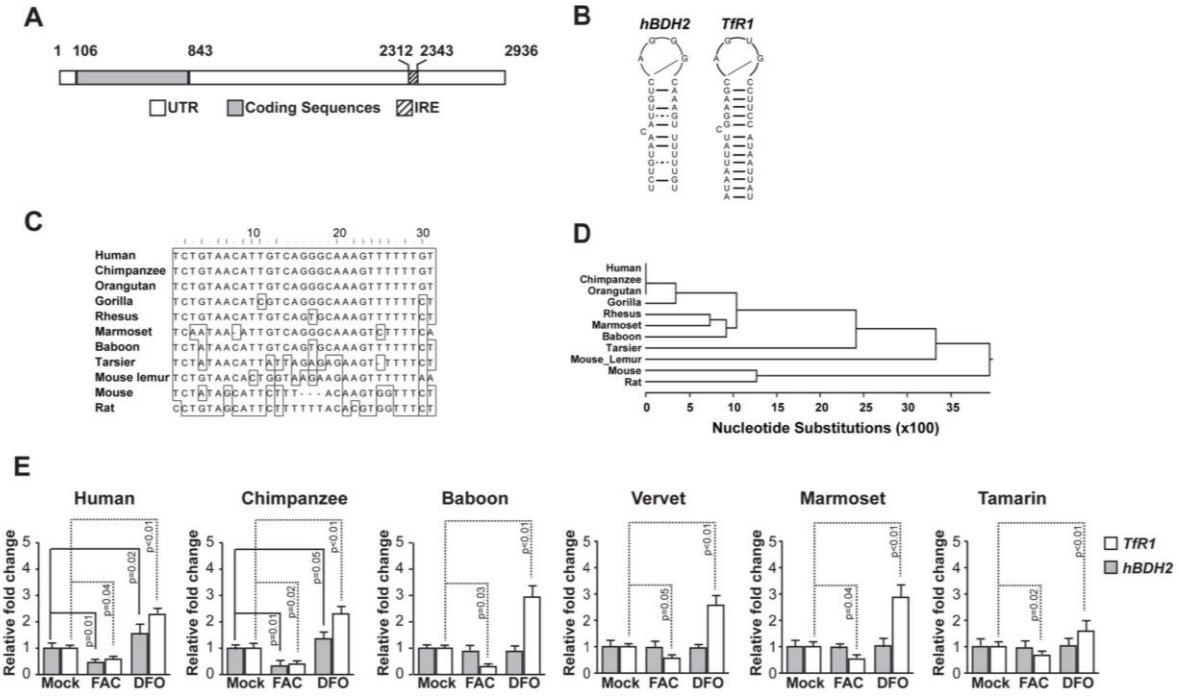

Figure 3. Structure, sequence, and phylogenic conservation of *hBDH2* 3′-UTR IRE

(**A**) Location of the *hBDH2* IRE in the 3′-UTR. IRE. Black boxes indicate exons and the hatched box indicates the location of the IRE. (**B**) Predicated secondary structures of 3′-UTR IREs of *hBDH2* and *hTfR1*. (**C**) Multispecies alignment of *hBDH2* 3′-UTR IRE sequences. (**D**) Phylogenetic distribution of *bdh2* IRE. (**E**) Iron-dependent regulation of *hBDH2* mRNA is restricted to members of the hominidae family. *TfR1* and *hBDH2* mRNAs were quantified by real time PCR in transformed human and primate liver cell lines 16 hours after treatment with FAC or DFO. The value on *y*-axis was set at 1.0 for the mRNA levels in untreated cells. The relative mRNA levels in each sample were normalized to *eif2b2* (an internal standard for RT-PCR analysis of primate mRNA samples). Positive control includes *TfR1*, whose expression is affected by iron. Results shown are the average means of three independent experiments with error bars depicting SD.

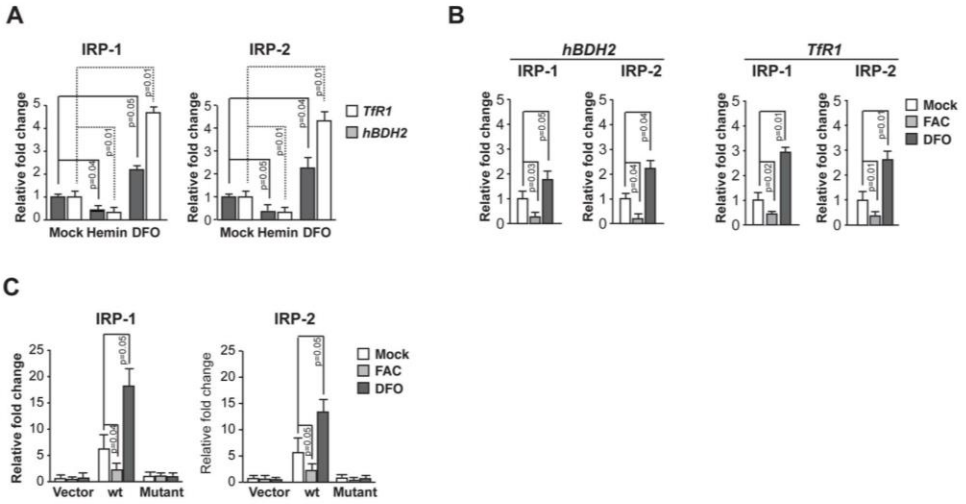

Figure 4. IRP-1 and IRP-2 associate with *hBDH2* mRNA

(**A**) MCF-10 A cells were initially treated with 100 μM each hemin or DFO for 16 hours. Cytoplasmic extracts of naïve or hemin or DFO treated MCF-10A cells were incubated with anti-IRP-1 Ab or anti-IRP-2 Ab and the RNA-protein complexes were precipitated with protein G Sepharose beads and the mRNAs in the immunoprecipitates were quantified in a real-time PCR analysis. (**B**) Co-immunoprecipitation of IRPs with endogenous *hBDH2* mRNA. 293T cells stably expressing FLAG-IRP-1 or FLAG-IRP-2 were initially treated with 100 μM each FAC or DFO for 16 hours. Cytoplasmic extracts of naïve or FAC or DFO treated 293T cells stably expressing FLAG-IRP-1 or FLAG-IRP-2 were incubated with anti-FLAG Ab coated beads and the mRNAs in immunoprecipitates were quantified in a real-time PCR analysis. For A and B, the value on *y*-axis was set at 1.0 for the mRNA levels in naïve cells. The relative mRNA levels in each sample were normalized to the input *hBDH2* mRNA. Results shown are the average means of three independent experiments with error bars depicting SD. (**C**) 293T cells stably expressing FLAG-IRPs were transiently transfected with a Luciferase reporter plasmid or Luciferase reporter plasmids containing *hBDH2* wt IRE or *hBDH2* mutant IRE (also see Figure 5 A). Transfected cells were then treated with 100 μM each hemin or DFO for 16 hours. Cytoplasmic extracts of transfected and treated cells were then incubated with anti-FLAG Ab coated beads and the *luc* mRNAs in immunoprecipitates were quantified in a real-time PCR analysis. The value on *y*-axis was set at 1.0 for the mRNA levels of cells transfected naïve Luciferase reporter plasmid. The relative mRNA levels in each sample were normalized to the input firefly *luc* mRNA. Results shown are the average means of three independent experiments with error bars depicting SD.

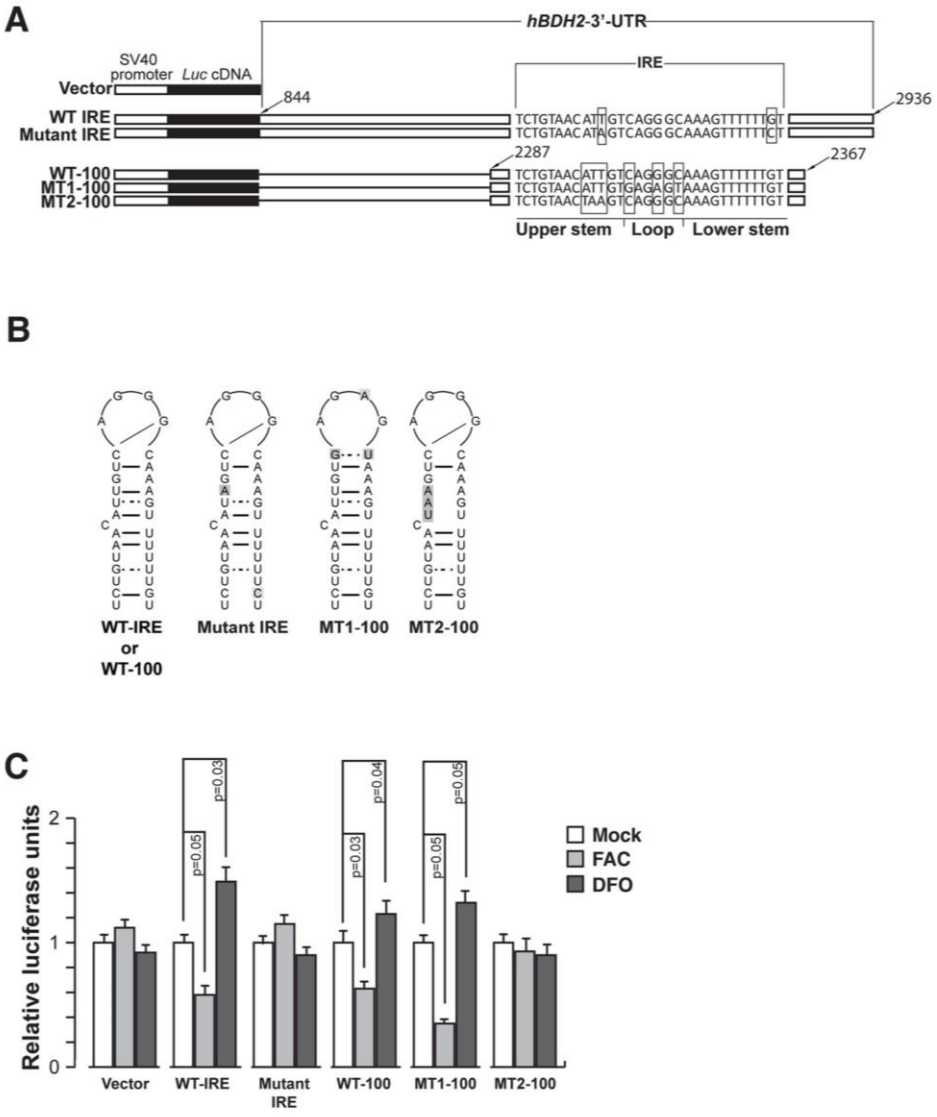

Figure 5. *hBDH2 2*IRE and 3′ UTR confer iron-dependent regulation on to a heterologous gene
(**A**) Schematic of the Luciferase reporter plasmids. (**B**) Secondary structures of wt or mutant *hBDH2* IREs. Mutant nucleotides are shaded. (**C**) MCF-10 A cells were transfected with Luciferase reporter plasmids shown in (A) and subsequently treated with 100 μM each of FAC or DFO. Sixteen hours later, cells were assayed for Luciferase activity. Data presented are arbitrary firefly Luciferase light units that have been normalized using the Renilla Luciferase measurements to account for transfection efficiency. All experiments were performed in triplicate, and error bars represent the SD.

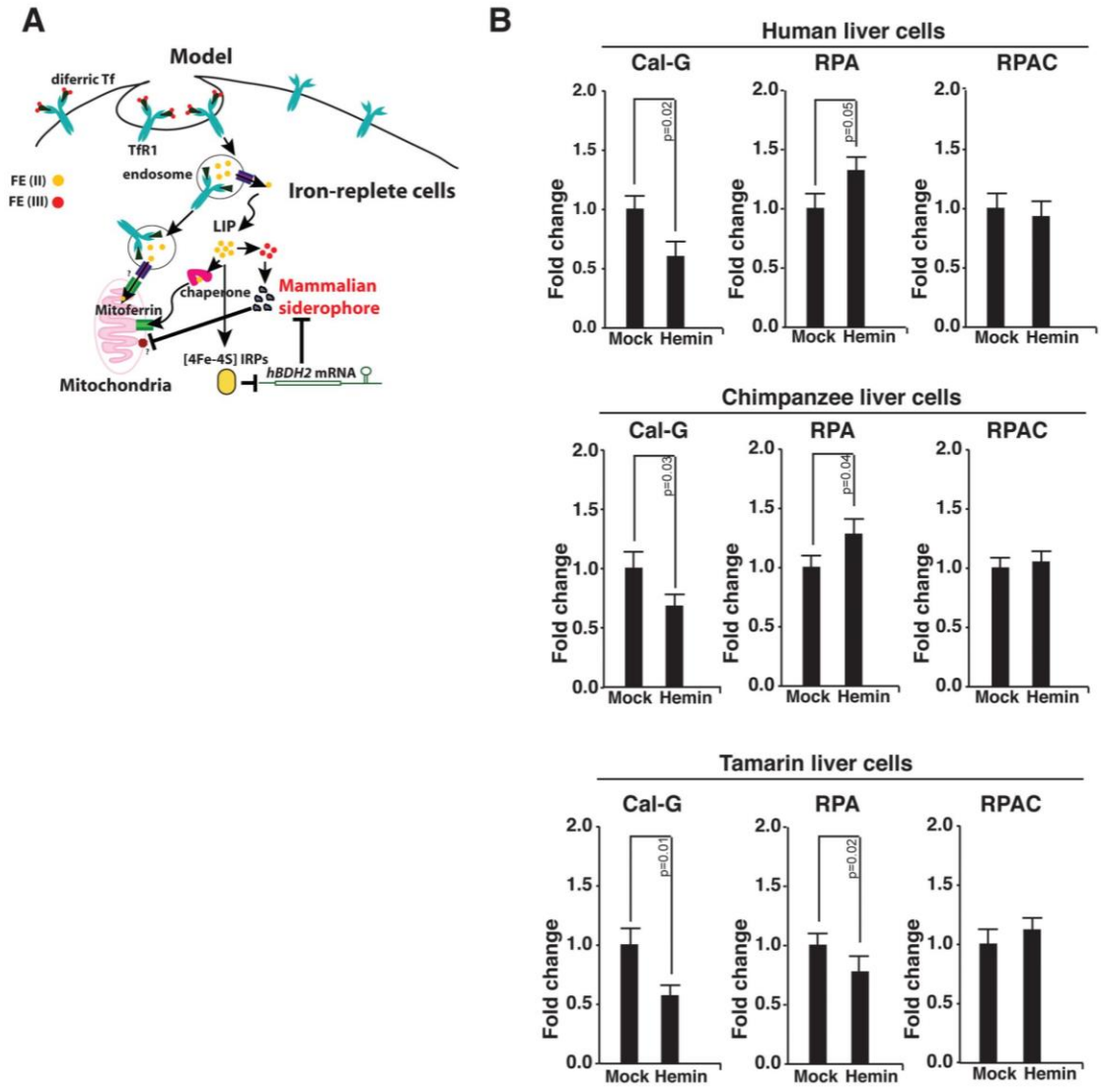

Figure 6. Iron regulation of siderophore controls mitochondrial iron

(**A**) Proposed model for iron regulation of siderophore-mediated iron trafficking. In normal human cells a portion of the cytoplasmic free iron pool is composed of the iron-siderophore complex, which is also the form of iron imported into mitochondria. Iron-replete conditions destabilize *hBDH2* mRNA leading to reduced siderophore levels. As a consequence, mitochondrial iron levels diminish. (**B**) Assessment of mitochondrial iron levels in primate cells with or without *hBDH2* 3′-UTR IRE under replete conditions. RPA or RPAC fluorescence was monitored in control and hemin-treated cells by fluorometry as detailed in methods section. Results shown are the average means of three independent experiments with error bars depicting SD.

7. ACKNOLEDGEMENTS

First of all, I would like to thank Mayka for giving me the opportunity to do my PhD in her laboratory at IMPPC. I want to thank her for her endless faith in my project, her enthusiasm and encouragement over these years. Thanks for all the time you dedicated me, for being a continuous source of ideas, for guiding me and showing me instruments and ways to solve everyday problems but letting me do things my way. Thanks for believing in me and pushing me when it was needed. And especially thanks for the patience, comprehension and great help in these last months.

Thanks to all the current and previous members of the Mayka's lab: Érica and Jessica, Francisco, Anna, Jorge, Antonio, Maya and Ricky. Thanks for your help, the science you shared and but also for the great atmosphere you created in the lab. A special thanks to Jessi, Maya, Antonio y Jorge for their contribution to this work. Jessi y Érica, sois el alma y la alegría del lab, gracias por estar siempre dispuestas a ayudar, por las risas, por los consejos, por hacer que cada día fuera una alegría el ir a trabajar, por ser amigas, os echo de menos!
I also thank people who are not part of Mayka's group but that helped me out, in particular thanks to Bea and Emili for technical support and for sharing all their precious tips and tricks. But also Mar, Vane, Pat, Mel, Neus, Julien, Elvira, Raquel, Berta, Mireia, Quim, Mònica, Miyako, Fumi, Ernest, Josep, Sonia, Violeta, Gaby, Adri y Jose, Juan y Jessica, all wonderful people with great laboratory skills, always prompt to help by giving an advice, showing how machines work, lending a reagent, rescuing your PC or just for a chat in the cell culture room or in the corridor. If I've forgotten anyone, I apologize.
I will always remember my stay at "un" IMPPC with great affection. I arrived when everything started, I've seen the lab and the institute growing, I've learned a lot and I've also grown, as scientist, but most importantly as person.

I want to especially thank our collaborator Prof. Walter Witke, head of the Institute of Genetics at the University of Bonn, for generously sharing with us the so important Pfn2 knockout mice and for making me feel very welcome in his laboratory. Thanks to all the people of the lab in Bonn for their huge help and the time they dedicated me while learning new techniques. I'm extremely indebted to Pietro for his interest and involvement in my work, his suggestions and motivation and for all the time he took for discussion. This project would not have been the same without you! And a very special thank goes to Marina for her support and friendship in and outside the lab. My time in Bonn was a great experience and I mostly owe it to you!

Thanks to our collaborators Bruno Galy, Matthias Hentze, Dunja Ferring-Appel and Daniela Casarrubea from the EMBL in Heidelberg for sharing with us samples from IRPs knockout mice and IRP1* transgenic mice and for the fruitful discussions and suggestions. A special thank goes to Dunja for her assistance with mice blood testing.

Thanks to Mar Mallo from the Affymetrix Microarrays Platform of the Josep Carreras Leukaemia Research Institute (IJC) in Badalona for microarray performance and to Lara Nonell from the Microarray Analysis Service of the Hospital del Mar Medical Research Institute (IMIM) in Barcelona for the support with microarray analysis.

Thanks to Lucía Gutiérrez and M. Puerto Morales from the ICMM-CSIC in Madrid for the atomic absorption iron measurements and TEM analysis. I'm particularly indebted to Lucía, thanks for being such an enthusiastic super-fast collaborator and a wonderful person.

I'm grateful to our collaborators Marina Muckenthaler and Gabriele Tolle (MMPU, University of Heidelberg), Hervé Puy and Sarah Duchamp (INSERM, University Paris Diderot), Lax Devireddy and Zhouming Liu (Case Western Reserve University, Cleveland) and to their colleagues, too numerous to be listed. Thanks for your generous and productive collaboration, I've very pleased to have contributed to these projects.

Grazie a Maura e Patrizia. Sono stata piú che fortunata ad avervi avuto come maestre, non solo per quello che ho appreso da voi a livello tecnico ma specialmente per avermi insegnato quello che é essere un buon ricercatore, rigoroso e obbiettivo, e soprattutto per essere un esempio a seguire di vera passione e dedicazione a questo spesso difficile lavoro.

Grazie a Gaia, Fede e Patty. In tutti questi anni, siete sempre state lì, lontane ma sempre vicine. Grazie per il vostro appoggio, le mille email e messaggi, soprattutto all'inizio della mia avventura spagnola quando tutto sembrava così tragico.

Gracias a Rafa. Lo diré con palabras de otro:

"...Ich war nie gut in Wahrscheinlichkeitsrechnung, aber das hier hab sogar ich kapiert. Die Chance, dass wir beide uns treffen, ging gegen Null und doch stehen wir jetzt hier. So weit gekommen und so viel gesehen, so viel passiert, dass wir nicht verstehen, ich weiß es nicht, doch ich frag' es mich schon, wie hast du mich gefunden? Eine von 80 Millionen..."

Gracias por estar a mi lado en lo bueno y en lo malo. Gracias por tus croquis, por hacerme ver las cosas desde otro punto de vista, por tu paciencia en estos últimos difíciles meses, por animarme siempre y sobre todo por creer en mi más que yo misma.

Grazie a mamma e papà per tutti i sacrifici che avete fatto per me. Grazie per essermi stati sempre vicini in questi anni, per il vostro incondizionato amore, per la pazienza e per l'insistenza, forse la maggiore ragione per cui tutto questo alla fine è arrivato a buon fine.